SALTA, ARGENTINA
28-31 AUGUST 2018

SECOND CIRCULAR

SegemAR
Servicio Geológico Minero Argentino

INTERNATIONAL ASSOCIATION ON THE GENESIS OF ORE DEPOSITS
1964
IAGOD

ASOCIACIÓN GEOLÓGICA ARGENTINA

Co-sponsored by

The Geological and Mining Survey of Argentina (SEGEMAR) and the Geological Association of Argentina (AGA) warmly invite you to the

15th Quadrennial Symposium of the International Association on the Genesis of Ore Deposits (IAGOD)

Ore Deposits:
providing resources for present & future generations

SECOND CIRCULAR

Convention Center of Salta
Salta, Argentina
28-31 August 2018

www.15iagods.org

TABLE OF CONTENTS

LETTER OF INVITATION FROM THE PRESIDENT of the 15th IAGOD Symposium

The Geological and Mining Survey of Argentina (SEGEMAR) and the Geological Association of Argentina (AGA) are proud to organize the forthcoming 15th Quadrennial Symposium of the International Association on the Genesis of Ore Deposits (IAGOD), to be hosted in the city of Salta, Argentina, 28th to 31st August 2018 and give full support for its achievement.

*The focal theme for this Symposium is: «**Ore Deposits: providing resources for present and future generations**».*

It is worthy to highlight that this is the first time for Argentina to host such an important meeting. South America, particularly the Andean region that includes some of the richest metallogenic provinces in the world, such as the richest Cu-Mo province, one of the most extensive and rich Sn and Ag belts, one of the richest Sb belts, the most important concentrations of Li in salars, and one of the richest borates provinces. Also it hosts some of the largest individual ore deposits such as Cerro Rico de Potosí, Llallagua, Chuquicamata and El Teniente mines. South America offers excellent geology hosting world class mineral deposits covering the past 2 billion years of Earth's metallogenic history, encompassing almost every conceivable metallogenic process.

Thus the region offers something that will tempt every economic geologist and metallogenist. The diversity of the geology, mineral resources, and local population invite the world to investigate and discuss our science and enjoy Argentina's renowned hospitality. The chance for Argentina to host this important meeting is a unique opportunity to help create an extraordinary environment for the presentation and exchange of knowledge and research results on the genesis of mineral deposits.

It will also give an invaluable occasion for local scientists to expand upon their training in various aspects related to metallogeny and research tools. The Argentine bid commits to enhance the participation in the IAGOD Symposium of young geoscientists, students, and delegates from less advantaged countries from around the globe. The commitments from the Geological Survey of Argentina and the Geological Association of Argentina, the support from the Ibero-American Geological and Mining Survey Association, as well as from the private natural resources sector, guarantee a successful 15th Quadrennial IAGOD Symposium.

There are five post-symposium field trips planned. Trips are organized in order to visit world class deposits of metals (Ag, Sn, Cu) and nonmetals (B, Li), as well as having the opportunity to discover the cultural aspects of the region and their inhabitants, involving mines from Argentina, Bolivia, and Chile.

There will be a variety of day tours available during the conference within Salta city and nearby areas.

The venue for the event is the Salta Convention Center, a world-class facility which has a record of numerous large national and international meetings.

It is our pleasure to warmly invite you to Salta. We look forward to meeting you at the 15th Quadrennial Symposium of the International Association on the Genesis of Ore Deposits.

Eduardo Zappettini
The President of IAGOD

COMMITTEES

HONORARY COMMITTEE

Daniel Meilán
Secretary of Mining, Ministry of Energy and Mining, Republic of Argentina

Julio Ríos Gómez
President of the Geological and Mining Survey of Argentina (SEGEMAR)

Mario Pereira
National Director of the Geology and Mining National Survey, Chile (SERNAGEOMIN)

Daniel Ricardo Blasco
Secretary of Mining, Provincia of Salta, Argentina

Ricardo Salas
Former Secretary of Mining, Salta, Argentina

Miguel Soler
Secretary of Mining, Jujuy Province, Argentina

Ricardo Alonso
University of Salta, Argentina

ORGANIZING COMMITTEE

President

Eduardo O. Zappettini
Institute of Geology and Mineral Resources, SEGEMAR; Commission for the Geological Map of the World (CGMW); President of IAGOD

Members

Martin Gozalvez
Institute of Geology and Mineral Resources, SEGEMAR

Graciela Marin
Institute of Geology and Mineral Resources, SEGEMAR; Geological Association of Argentina

Susana Segal
Former Institute of Geology and Mineral Resources, SEGEMAR

Carlos Herrmann
Institute of Geology and Mineral Resources, SEGEMAR

Nora Rubinstein
National and Technical Research Research Council-Argentina (CONICET), IGeBA Department, University of Buenos Aires

Diego Guido
National Scientific and Technical Research Council-Argentina (CONICET), University of La Plata, Eploration Vicepresident (AUSTRAL GOLD)

Pablo Caffe
National and Technical Research Research Council-Argentina (CONICET)

José Marcelo Arnosio
University of Salta

Waldo Vivallo Sandoval
Geology and Mining National Survey, Chile (SERNAGEOMIN)

Raúl Lira
National Scientific and Technical Research Council-Argentina (CONICET), Univesity of Córdoba
Coordinator of the 15th IAGOD Symposium Scientific Committee

IAGOD COUNCIL 2016-2020

President: *Eduardo Zappettini* - Argentina - eduardo.zappettini@segemar.gov.ar
Secretary General: *David Lentz* - Canada – dlentz@unb.ca
Chief Treasurer: *Reimar Seltmann* – UK - R.Seltmann@nhm.ac.uk
Publication Manager: *Franco Pirajno* – Australia - franco.pirajno@uwa.edu.au
Promotion Manager: *Xiang Junfeng* – China - xjf2929@163.com
Webmaster: *Evgeniy Naumov* – Russia - naumovevg@gmail.com
Executive Manager: *Alla Dolgopolova* – UK - A.Dolgopolova@nhm.ac.uk

Councillors

Past President: *Mao Jingwen* – China - jingwenmao@263.net
First Vice President: *Nora Rubinstein* – Argentina - nora@gl.fcen.uba.ar
Second VP: *Sergei Cherkasov* – Russia - s.cherkasov@sgm.ru
1st VP at Large: *Alexandra Gomez Escobar* – Colombia - alexagomeze@gmail.com
2nd VP at Large: *Alexey Aleshin* – Russia - aleshin@igem.ru
Past Secretary General: *Sun Xiaoming* – China - eessxm@zsu.edu.cn

Regional Councillors

Africa: *Paul Nex* - South Africa - Paul.Nex@wits.ac.za
Asia: *Batkhishig Bayaraa* – Mongolia - bkhishig@must.edu.mn
Australasia: *Nigel Cook* – Australia - nigel.cook@adelaide.edu.au
Europe: *David Holwell* – UK - dah29@leicester.ac.uk
North America: *Ed Ripley* – USA - ripley@indiana.edu
South America: *Diego Guido* – Argentina - diegoguido@yahoo.com
China: *Xie Guiqing* – China - guiqingxie@sohu.com
India: *Dipak Pal* – India - dipak.pal@gmail.com
Iran: *Seyed Mehran Heidari* – Iran - sm.heidari@gmail.com
SE Asia: *Khin Zaw* – Australia - Khin.Zaw@utas.edu.au

Ex officio Members

Account holder: *Andreas Nägele* – Germany - iagod@schweizerbart.de
President, SGA: *Jorge Relvas* – Portugal - president@e-sga.org
Executive Secretary, SGA: *Jan Pasava* - Czech Republic - jan.pasava@geology.cz

15th IAGOD SYMPOSIUM ORGANIZERS

Geological and Mining Survey of Argentina (SEGEMAR)

Geological Association of Argentina (AGA)

Contact information

secretariat@15iagods.org

IMPORTANT DATES

Abstracts

20th January, 2018	Opening of Online Abstract Submission
15th May, 2018	Deadline for Abstracts Submission
15th July, 2018	Notification of Acceptance of reviewed Abstracts
31st July, 2018	Registration Payment Deadline for submitted Abstracts

Registration

20th January, 2018	Opening of Registration and Online Payment
15th February, 2018	Opening of Payment by bank transfer
15th February, 2018	Opening of Registration and Online Payment for Short Courses
31st March, 2018	Early Bird Registration Deadline
1st August, 2018	Online Registration and Online Payment Deadline

OVERALL STRUCTURE OF THE 15TH IAGOD SYMPOSIUM

August 23th – August 27th 2018
Pre-Symposium field trip

August 26th – August 27th
Short Courses

August 28th
Welcome Party

An opening reception will be held on the first evening of the Symposium and is planned for approximately 750 people. The reception includes a bar and hot and cold hors d'oeuvres and local music and entertainment. This will be located off site and showcases a special place with historical significance.

The ticket for the Opening Reception is included in the Registration price.

August 28 - August 31
Symposium Scientific Programme
Special Sessions
Keynote presentations
Poster sessions

Registration fees cover coffee-breaks and lunch

August 31
Farewell Assembly

A farewell dinner will be held on the last evening of the conference, after the conclusion of the General Assembly.

September 1st onward
Field trips

The field trips will typically be of 3 - 5 days duration. Costs will include land transport from and to Salta, meals and accommodation.

REGISTRATION

(payment portal opens 20th January, 2018)

	Early Bird U$S (before May 15th)	Regular Payment U$S
IAGOD Member	450	500
Non member	550	600
Student*	225	250

*A valid student card will be required to pick up accreditation at the registration desk

To pay as IAGOD Member you have to pay Membership fees before registering to the Symposium .

Discounted registration for IAGOD Members: To be eligible for the discount pay a 3-year term (total €30) that must include 2018.

For joining IAGOD download Membership Application Form http://iagod.org/node/16 and send completed to: IAGOD chief treasurer Prof Reimar Seltmann r.seltmann@nhm.ac.uk and copy to account holder Dr Andreas Naegele mail@schweizerbart.de

For membership payment please use the web shop at: http://www.schweizerbart.de/iagod/membership-payment.

For registering as IAGOD Member you can download the ***Membership application*** (at the Downloads section) and pay IAGOD membership fees before registering to the Symposium (see instructions at www.iagod.org).

For registering to the Symposium you are asked to complete the ***Registration form*** (at the Downloads section) and send it back to the following email address: registration@15iagods.org. For Registration create an account. Use the same account for Registration & Payment, as well as for Abstract submission.

From January 20th, 2018 the online Registration Payment option can be accessed through the IAGOD Symposium web page (www.15iagods.org)

The ticket for the Opening Reception is included in the Registration price. Registration fees cover coffee-breaks and lunch each day.

Please note:

- The early bird registration will be closed on 30th May 2018.
- Online registration closes: 1st August 2018.
- Payment by bank transfer will be available from February 15th until 1st August 2018.
  After 1st August payments will only be on site.
  Details for bank transfer will be provided at the IAGOD Symposium web page (www.15iagods.org).
- There will be no refund after 31 July 2018 if registered participants cancel by personal reasons.

INSTRUCTIONS FOR AUTHORS

Abstracts

There will be a printed symposium programme but only electronic abstract volume.

Information on publication of full papers in Special Issues of IAGOD affiliated journals (Ore Geology Review, Global Tectonics and Metallogeny) and potentially a proceedings volume (IAGOD Quadrennial Symposia, Schweizerbart) wil l be provided on the Symposium website www.15iagods.org and within the Final Programme.

All abstracts must be submitted in English.

They must include sufficient information for reviewers to judge the nature and significance of the topic, the adequacy of the investigative strategy, the nature of the results, and the conclusions. The abstract should summarize the substantive results of the work and not merely list topics to be discussed.

An abstract is an outline/brief summary of your paper and your whole project. It should have an intro, body and conclusion. It is a well-developed paragraph, should be exact in wording, and must be understandable to a wide audience. Abstracts highlight major points of your research and explain why your work is important; what your purpose was, how you went about your project, what you learned, and what you concluded.

If your title includes scientific notation, Greek letters, bold, italics, or other special characters/symbols, do make sure they appear correctly.

Abstracts can be accepted either as poster or oral communication. The Abstract Scientific Committee will select submitted abstracts and determine whether they are accepted for oral or poster presentation. Oral presentations are not guaranteed. If your abstract is accepted as a poster, you will be requested to be available for discussion during the corresponding poster viewing session.

For abstracts submissions please go to the Abstract submission Platform at the IAGOD Symposium web page (www.15iagods.org).

At least one presenter for each accepted abstract must register for the Symposium and **pay the registration fee by 15th July 2018**. Abstracts without presenter paid registration by this date will be removed from the Symposium programme and electronic abstracts volume.

Poster Presentations

General information

All posters must be written in English.

The exhibition of posters of each exhibitor will take place in the halls of the Convention Center.

Posters will be exhibited during one day during the Congress and will be grouped by sessions and by topics. Presenters are expected to be present at the daily poster sessions and requested to attend their posters the day their session is scheduled in the Final Program.

It is important to consult the final program beforehand to know the location of the poster in the panels. Volunteers will offer assistance.

Photographing posters or oral sessions will be prohibited except by authorized agents of the Symposium or by the first author of the presentation.

No chairs and tables will be provided at the exhibition site. If any special items are needed, the staff should be required to assist during the sessions.

Poster dimensions

54 inches high and 36 inches wide

We recommend that you use 72-point bold font for title and a 60-point font for authors and affiliations. The title should be the same as the work of the conference. The texts and illustrations must have enough size to read from a distance of 2 meters.

Oral Presentations

General information

Computers, audio-video equipment and technical assistance will be provided to monitor and test the presentation of each participant.

Format of the oral presentations

Presentations will only be allowed to display in Microsoft PowerPoint (.ppt and .pptx). There will be no projectors or slide carusel. Presenters have the responsibility to ensure the exposure is compatible with Windows and Microsoft office. Letter Arial, Times New Roman, Etc. Common format such as AVI, MPG

The presentations must be in English. There will be no simultaneous translation into Spanish.

Regular Oral presentations will be 20 minutes long, including a couple minutes for questions. It is essential that speakers strictly follow the Final Program and respect the stipulated time.

30 minutes before the session the presenter must go to the corresponding room to receive instructions for use of equipment and control that everything is in order.

Speakers have to bring the presentation in # USB stick #. Speakers will not be allowed to use their own laptop.

Presentations will be deleted from computers after the end of each session.

Abstract Preparation Guidelines

All abstracts must be submitted in English.

Author Name(s): The presenting author of an accepted abstract must attend, register and pay for the Symposium.

An author may present **no more than two** abstracts. More than two submissions can be accepted from an autor if one of his/her co-authors present additional abstracts. If an abstract is accepted, the presenter must be one of the co-authors listed.

If an author's name appears on more than one abstract, it must be identical on each submission. Do not list authors by initials only.

Provide email and affiliation only for the first autor.

Abstract category

Please choose from the abstract categories available (T: Topics and S: Special Sessions): See Plenary talks and Thematic Sessions below.

Data

Abstracts that appear to be replicate versions of a single study will be rejected. Abstracts containing identical or nearly identical data submitted from the same institution and/or individuals will be rejected.

Format

Abstracts of original science – content should be structured into the following four (4) sections: Background, Methods, Results and Conclusions.

Content

Abstracts are limited to 1200 words (or 2 pages A4). This includes the text in type Arial 11 point, plus any graphic/table.

Images/Graphics/Tables – Their use is encouraged if they are relevant to the research submitted. Only one of the following is allowed per abstract:

- Images/Graphics: Images should be pasted under «attachment» in the template in JPG/BMP format, maximum size 9cm x 17cm, and resolution up to 300dpi. Please note that these may be resized to fit in the final printed material. Their inclusion counts as 350 words for the total count of the abstract

- Tables: Tables have to be added as a table and not as an image in the template. The characters used in the table count toward the total words count of the abstract (max 1200)

Clarity of expression will be considered in the review process. The overall quality of language used should assure comprehension by the reader.

Do not include:

References, abbreviations, footnotes, key words, credits, or grant support in your submission.

Proofread abstracts carefully to avoid errors. IAGOD will never edit the scientific content of a submission, after approval by the Scientific Committee. If accepted, the abstract will be published in electronic versions as submitted.

Presentation

All abstracts presented at the Scientific Sessions must conform to the eligibility criteria listed above.

All presentations and question-and-answer periods will be in English. If presenters need assistance in understanding or responding to questions in English, they are encouraged to have a member of their research group assist them.

Any additional or revised guidelines for abstract presentation will be provided to presenting authors of accepted abstracts in their notification email.

Copyright

The submitter acts on behalf of all co-authors and in submitting an abstract, transfers to IAGOD the copyright and all other rights in the material comprising the abstract if the abstract is accepted.

IAGOD, as holder of the copyright of the accepted abstract, reserves all rights of reproduction, distribution, performance, display, and the right to create derivative works in both print and digital formats.

Disclosure

All abstracts submitted are disclosed to members of the peer-review selection committee, as well as to IAGOD staff as necessary in connection with the Scientific Sessions. Those abstracts that are accepted for presentation are made available to the public in advance of the Scientific Sessions. Abstracts not accepted for presentation are not published, and are ordinarily not disclosed outside of IAGOD and persons associated with the selection process (i.e., the peer-review committee). Notwithstanding these policies and procedures, IAGOD is not subject to any confidentiality requirements with respect to submitted abstracts. In addition, compliance with any disclosure or nondisclosure requirements that apply to researchers or research sponsors (whether under federal securities laws, contract agreement, or otherwise) is the sole responsibility of the researcher and/or sponsor, and not IAGOD.

Abstract Withdrawal

If you decide to withdraw your abstract prior to the submission and editing deadline, you should send an email to the following email address: abstracts@15iagods.org

Include your abstract control number, title and the presenting author's name in your email.

NOTE: Before sending an Abstract, You have to Sign In at the web page of the IAGOD Symposium (www.15iagods.org). If you do not have an account sign up. Use the same account for Registration & Payment.

PLENARY LECTURES, THEMATIC AND SPECIAL SESSIONS

PLENARY LECTURES - KEYNOTE SPEAKERS

Eduardo Zappettini (President of IAGOD)
Metallogenic Potential of Argentina

Reimar Seltmann (IAGOD Distinguished Lecturer)
Mineral exploration models from simple fiction to complex reality

Richard Sillitoe
Volcano-tectonic controls on Andean porphyry deposits

Lena Monteiro (SEG Regional VP Lecturer)
Copper deposits in Brazil: geological setting, process and evolution of mineral systems

Fernando Tornos (SGA Keynote speaker)
Microbiology and the formation of ore deposits

Olga Plotinskaya
Paleozoic porphyry Cu (Mo, Au) systems from the Urals

Franco Pirajno
Rare Earth mineral systems associated with alkaline intrussions and carbonatites

Jeffrey Hedenquist
Near-surface features of the epithermal environment: Formation, characteristics and contrasting implications for exploration

THEMATIC SESSIONS

T1: Epithermal gold deposits
T2: Ore deposits in rift environments
T3: Ore deposits related to granites: from ore forming processes to metallogeny
T4: Metallogeny of the Andes
T5: Metallogeny of cratonic areas
T6: Global tectonics and Metallogeny: large to giant ore deposit settings
T7: Non conventional ore sources: Exploration and extraction
T8: Geochemistry of ore forming fluids
T9: Precision Geochronology and isotope geology of ore-forming processes: its importance in exploration and metallogenic modelling
T10: Predictive modelling applied to mineral resources
T11: Ore mineralogy

SPECIAL SESSIONS

S1: *New discoveries and new research on skarn deposits*

Conveners: Zhaoshan CHANG (James Cook University, Townsville), Larry Meinert (Energy & Mineral Resources USGS), Taofa Zhou (Hefei University of Technology, Hefei)

Sponsored by: IAGOD WG on Skarn Deposits

Outline: South America has some of the largest skarn deposits in the world, including Antamina and Las Bambas. This session will focus on recent advances in understanding the geology, geochemistry, and mineralogy of skarn deposits across the globe.

S2: *New developments in magmatic sulfide and oxide deposits in South America and worldwide*

Conveners: Maria Emilia Schutesky Della Giustina (Universidade de Brasília, Brasil), David Holwell (University of Leicester, UK)

Sponsored by: IAGOD CODMUR

Outline: Magmatic ore deposits are the single most important source of Ni, PGE, Cr, Ti and V on the planet. Their formation results from processes that involve major fluxes of metals from the mantle to the crust, through magmatism, and the diversity of the deposits is determined by a range of crustal processes, including chemical fractionation and contamination and increasingly recognised physical processes such as sulfide injection, slumping, brecciation and entrainment in magmas on a range of scales. This session will cover new developments in geological, analytical and exploration models for magmatic Ni-Cu-PGE sulfides and magmatic Cr-Fe-Ti-V deposits. We welcome contributions that cover a broad range of approaches from the field, mineralogical and geochemical studies, through to large scale mineral systems approaches. Within this session, there will be a focus on recent developments in South America, alongside presentations covering deposits worldwide.

S3: *Magmatic-hydrothermal systems and the formation of porphyry type and IOCG deposits*

Conveners: Fernando Tornos (Spanish National Research Council – CSIC) and David Lentz (University of New Brunswick, Economic Geology Chair)

Sponsored by: SGA & IAGOD WG on IOCG-IOA systems

Outline: Magmatic-hydrothermal systems form a wide variety of ore deposits related to the evolution of fluids exsolved from igneous rocks. Cooling, reaction with host rocks, boiling and mixing with other fluids can form large deposits of base, precious and critical metals that are included in the porphyry, epithermal, IOCG, skarn and several other styles of mineralization. The session is focussed to the description, evolution, chronology and geochemistry of the porphry type and IOCG systems with especial emphasis in the evolution of the mineral systems and the mechanism that trigger ore formation.

S4: *High-tech critical metals: Evaluation and deposit models. Meeting the resource demands of the low carbon society*

Conveners: Kenzo Sanematsu (Geological Survey of Japan, AIST), Yasushi Watanabe (Faculty of International Resource Sciences, Akita University, Japan), Jens C. Andersen (Camborne School of Mines, University of Exeter) and Reimar Seltmann (Natural History Museum, London)

Sponsored by: IAGOD WGCM

Outline: Critical metals have the higher supply risk and economic importance than the other metals although this classification changes with time. The supply risk is related to heterogenous distribution or difficulty in economical processing or extraction of the metals (e.g., rare earths, niobium, indium, cobalt, silicon). Some of these critical metals recently attract the attention due to a rapid increase of the price or demand for high technology. Additionally, climate change has led to strong societal demands for the phasing out of fossil fuel in favour of carbon neutral energy resources. If this is to

have significant global impact, this is likely to generate an unprecedented demand for metals that are critical to energy production (Dy, Ga, In, Nd, Se), storage (Li, Co), conversion (Pt, Pd) and efficiency (In, Ga). This session invites contributions to the geology, new deposit models, exploration, evaluation and extraction of these high-tech critical metals as well as how their increased extraction may affect the current mining industry and global economy.

S5: Technical developments and geological applications in remote sensing: from satellites to unmanned aerial vehicles (UAV)

Conveners: Valery Bondur (Presidium RAS, 14 Lewinsky Prospect, Moscow), Sergey Cherkasov (Vernadsky State Geological Museum of Russian Academy of Sciences (SGM RAS) and Marina Diaz-Michelena (National Institute of Aeronautics – INTA)

Sponsored by: IAGOD CTOD WG Remote Sensing Methods for Tectonics & Ore Prospecting

Outline: The session is dedicated to the intensively developing technologies of multispectral and hyper-spectral surveys, aerial magnetometry, and other geophysical methods with UAVs as carriers for the corresponding equipment as well as to the satellite data being used for geological purposes. Presentations on unmanned aircraft systems (UAS) for these data acquisition, methods and software for data processing, as well as results of the surveys are welcome.

S6: Uranium deposits and resources

Conveners: Luis López (Comisión Nacional de Energía Atómica, Argentina), Michel Cuney (French National Centre for Scientific Research) and Mostafa Fajek (University of Manitoba)

Sponsored by: IAGOD IUG (International Uranium Group)

Outline: With increased need for uninterrupted, long-term and sustainable supply of uranium, it has become important to look into augmenting the resource base, and making the mining and extraction more efficient and environmentally friendly. This requires a deeper understanding of the genesis of uranium deposits under various geological environments with complex mineralization processes through analysis of the geochemical and mineralogical characteristics of each deposit. Such information will be helpful in guiding further exploration and optimization of extraction and production, and in effective environmental management.

The proposed session will look into complete metallogenic characterization of uranium and associated critical material deposits where uranium could be recover as main, co- and by-product. The outputs are also expected to enrich the IAEA database on uranium - World Distribution of Uranium Deposits (UDEPO) - and help understand the global distribution of uranium in a consistent manner and thus provide valuable inputs available resources and their sustainable development.

S7. Base Metals in sedimentary sequences

Conveners: Thierry Bineli-Betsi - Botswana International University of Science and Technology, Josefina Pons IIPG-Universidad Nacional del Río Negro-Universidad Nacional del Comahue - CONICET and Joseph Zulu Josrum Enterprises (Pvt) Ltd

Outline: Sedimentary hosted deposits are the most importance source of lead and zinc and totalize the twenty-three percent of the world's copper production. This session covers the broad range of deposits hosted in sedimentary basins, including Sedimentary Exhalative, Mississippi Valley Type, Vein-type and Sedimentary Hosted Copper Deposits.

This session will explore the numerous aspects related to the critical factors involved in the genesis of these sedimentary hosted base metal deposits: 1) large-scale geodynamic setting of mineralization; 2) lithological and structural controls on deposits with special emphasis on the tectono-thermal evolution of the basin; 3) the origin of the metals and sulphur; 4) geochronology 5) the source and geochemistry of the mineralizing fluids; 6) fluid drive mechanisms; 7) the metals transport and precipitation mechanisms and 10) the main factors that help to preserved them.

PRE-SYMPOSIUM SHORT COURSES

Epithermal deposits (1 day)
Diego Guido (sponsored by SEG)
Prices:

Regular attendee:	..... U$S 200
SEG or IAGOD member:	..... U$S 150
Student with University ID:	..... U$S 100

Fluid inclusions (1 day)
Daniel Moncada (sponsored by SGA)
Prices:

Regular attendee:	..... U$S 200
SGA or IAGOD member:	..... U$S 150
Student with University ID:	..... U$S 100

Faults, Veins, Breccias, and related Alteration (1 day)
Anna Fonseca - SRK Consulting (Canada)
Prices:

Regular attendee:	..... U$S 200
IAGOD member:	..... U$S 150
Student with University ID:	..... U$S 100

Non-magmatic mineral systems (2 days)
Franco Pirajno
Prices:

Regular attendee:	..... U$S 300
IAGOD member:	..... U$S 200
Student with University ID:	..... U$S 150

Ore mineralogy of micron- to nanoscale to atomic scale observations (1 day)
Nigel Cook and Cristiana Ciobanu
Prices:

Regular attendee:	..... U$S 200
IAGOD member:	..... U$S 150
Student with University ID:	..... U$S 100

Metallogeny of uranium (2 days)
Michel Cuney
Prices:

Regular attendee:	..... U$S 300
IAGOD member:	..... U$S 200
Student with University ID:	..... U$S 150

Opening of Short Courses Registration payment: 15th February 2018
Cancelation policy: Short Courses will be cancelled and fees refunded if there are less than 10 attendees.
Cancelation deadline: 31st June 2018

PRE- AND POST-SYMPOSIUM FIELD TRIPS

The rich mining history of this part of America that began with the exploitation of Ag in the Cerro Rico de Potosí (Bolivia) continues today with the exploitation of Cu and Au porphyries in the Andean region of Chile and Argentina, as well as Li from the salt lakes in the Puna - Altiplano triangle that comprises Argentina Bolivia and Chile.

Trips will be organized in these three countries in order to visit world class deposits of metals (Ag, Sn, Cu) and nonmetals (B, Li) having the opportunity to discover the cultural aspects of this region and their inhabitants.

Registration and payment of field trips start January 20th, 2018. If any trip is cancelled because of force majeur or not reaching the minimum number of participants, payments will be refunded.

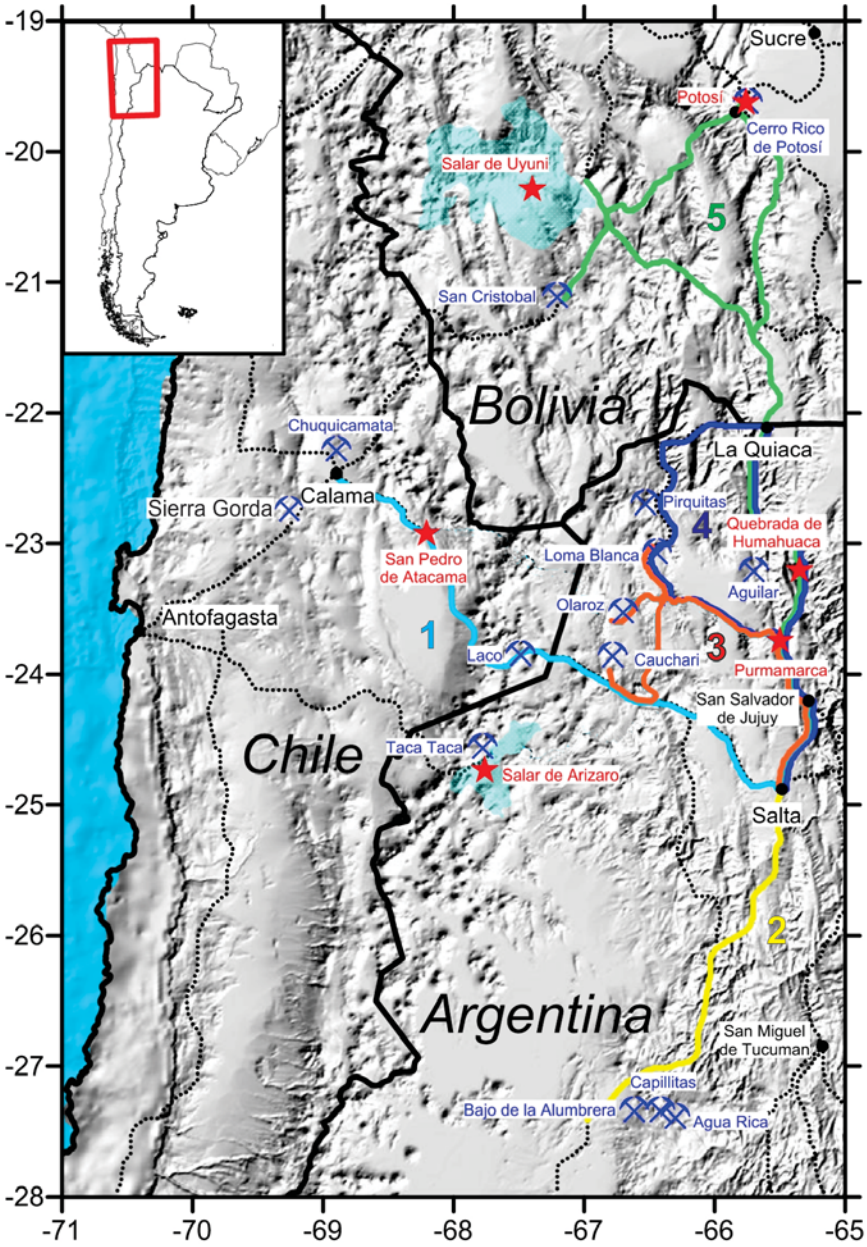

FT1	Wealth in the Andes: Copper and Iron
FT2	Land of the Inca Rose: Farallon Negro District
FT3	Li-rich salt lakes and borates in the Argentine Puna
FT4	Road of Silver in the Argentine Puna: Aguilar and Pirquitas Mine
FT5	The Bolivian Altiplano: in the search of the Silver Land

Pre-symposium field trip

FT1. WEALTH IN THE ANDES: COPPER AND IRON

Sponsored by: SGA

Synthesis: Starting in Calama, Chile the visit includes the world largest porphyy Cu Chuquicamata mine (86 Mt Cu) as well as the Sierra Gorda porphyry Cu-Mo and the volcanogenic El Laco Fe deposit (430 Mt Fe) in Chile. In Argentina drill cores from the Taca Taca porphyry (Cu-Au-Mo) (13 Mt Cu - 180 t Au) will be examined.

Cultural aspects: visits toursitic destinations such as San Pedro de Atacama (Chile), San Antonio of the los Cobres and Santa Rosa de Tastil (Argentina), Atacama salt lake (Chile) and salt lake (Argentina).

Duration: 5 days **PRICE: U$S 1400**

Post-symposium field trips

FT2. LAND OF THE INCA ROSE: FARALLÓN NEGRO DISTRICT

Summary: Visit the world-class mineral deposit Bajo de la Alumbrera (porphyry Cu-Au; 3.9 Mt Cu, 490 t Au), Agua Rica (porphyry Cu-Au-Mo; 4.9 Mt Cu, 193 t Au), the Capillitas polymetallic vein deposit, known for its rhodochrosite production and the epithermal Au-Ag-Mn Farallón Negro Mine. Mineralizations are hosted in a back-arc Miocene volcanic complex and comprise more than 12 Mt Cu and 750 t Au.

Cultural aspects: Capillitas mine is a unique deposit of rhodochrosite for its original and uncommon stalactite-like formations. This beautiful mineral is considered the «national stone» of Argentina. While visiting the region you will enjoy old towns like Cafayate, Santa María and Andalgalá.

Duration: 4 days **PRICE: U$S 1000**

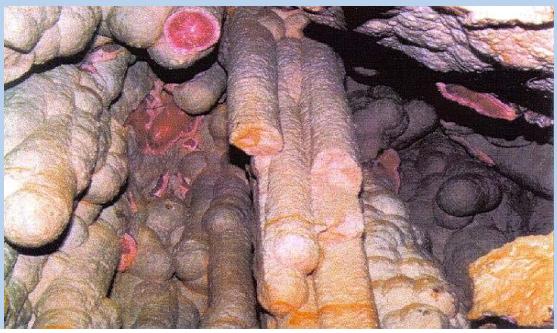

FT3. LI-RICH SALT LAKES AND BORATES IN THE ARGENTINE PUNA

Summary: Visit the Tertiary fourth largest borate deposit in the world: Loma Blanca (12.7 Mt borates) and an active boratiferous geyser, as well as lithium brine deposits in the salt flats of Olaroz (1.5 Mt Li carbonate), Cauchari (4.9 Mt Li carbonate) and Rincón (7.4 Mt Li carbonate). This region of the Argentine Puna is one of the main global reserves of Li and B.

Cultural aspects: visit the typical Puna towns Purmamarca, San Antonio de los Cobres and Susques.

Duration: 3 days **PRICE: U$S 750**

FT4. ROAD OF SILVER IN THE ARGENTINE PUNA: AGUILAR AND PIRQUITAS MINES

Summary: Visit the Ordovician SEDEX type world class Ag-Zn-Pb Aguilar deposit (2.75 Mt Pb, 4.35 Mt Zn, 6,000 t Ag) and discuss its genesis. See the newly open Pirquitas Sn-Ag-Zn open pit (3,250 t Ag, 0.4 Mt Zn), the southern end of the Bolivian Tin belt.

Cultural aspects: visit the Quebrada de Humahuaca (Cultural and Natural Heritage, UNESCO).

Duration: 4 days **PRICE: U$S 1000**

FT5. BOLIVIAN ALTIPLANO: IN THE SEARCH OF THE SILVER LAND

Summary: Visit the world-class Ag-Sn Cerro Rico deposit (0.1 Mt Ag, 2.4 Mt Sn) and the Ag-Zn-Pb San Cristobal epithermal mine (4 Mt Zn, 1,4 Mt Pb, 20,000 t Ag), Bolivia.

Cultural aspects: Travel through the Quebrada de Humahuaca (Cultural and Natural Heritage, UNESCO) and visit Potosi, with the world known Royal Mint and the Uyuni world largest salt lake.

Duration: 5 days **PRICE: U$S 1600**

SPONSORSHIP AND EXHIBITION

The IAGOD was established in September 1963 with the objective of promoting international co-operation in the study of the genesis of ore deposits and furthering the growth of knowledge in this field. IAGOD is a member of IUGS. These tasks are achieved in several ways. This quadrennial international symposium is the most important one. The 15th IAGOD Symposium, with the theme « *Ore Deposits: providing resources for present and future generations*», covers all aspects of currently hot topics in economic geology that will lead to an enhanced understanding of the genesis of mineral deposits and important practical issues of improved exploration concepts and discoveries in economic geology.

It is worth highlighting that this is the first time for Argentina to host such important meeting.

We expect a mix of industry, government, and academia, with a strong student component, attending the Quadrennial Symposium. This four days symposium will be supplemented by field trips, workshops, and short courses. The symposium will provide a great opportunity to promote mining companies through sponsorship and participation as exhibitors.

Join us, to reach for the peak of the understanding of ore deposits and the concepts of exploration, having a chance to reach a broad international audience through this Symposium.

Sponsors have the opportunity to have their sponsorship promoted in various ways:

	Platinum U$S 10,000	Gold U$S 6,000	Silver U$S 3,000	Bronze U$S 2,000
Acknowledgement with logo on conference web site	•	•	•	•
Acknowledgement with logo on abstract book	•	•	•	
Exhibition space (in order of sponsorship level)	•	•	•	•
Company banner/logo displayed in venue (level dependent)	•	•	•	•
Acknowledgement at opening/closing conference	•	•		
Promotional material included in registration package	•	•	•	
Complementary registration for up to 3 delegates	•			
Complementary registration for up to 2 delegates		•		
Complementary registration for up to 1 delegate			•	•
Acknowledgement at opening/closing one session (of choice)			•	•

ACCESSIBILITY AND TRANSPORT

INTERNATIONAL AIRPORT M. MIGUEL DE GÜEMES.

76 weekly flights from Salta to Buenos Aires, Córdoba, Mendoza, and Iguazú; connecting to international destinations in America and Europe.

SALTA/BUENOS AIRES FLIGHTS

ANDES - 3 flights a week
AEROLINEAS ARGENTINAS - 23 flights a week
LAN - 21 flights a week

DIRECT FLIGHTS TO SALTA

Buenos Aires, Córdoba, Mendoza, Iguazú.

INTERNATIONAL FLIGHTS

From Santa Cruz, Bolivia > Salta
From Rio de Janeiro > Iguazú > Salta
From Santiago de Chile > Mendoza > Salta
From Lima / Montevideo / Panamá / Santiago de Chile / Porto Alegre / Rio de Janeiro > Córdoba > Salta11

EZEIZA INTERNATIONAL AIRPORT (BUENOS AIRES)

It has around 30 air carriers with many direct flights from New York, Miami, Dallas, Atlanta, Toronto, Auckland, Sydney, Houston, Rome, Madrid, Paris, Amsterdam, Frankfurt, London, Barcelona, Dubai, Doha and all South American main cities.

Operating air carriers: Aerolíneas Argentinas, Aeromexico, Air Canada, Air Europa, Air France, Alitalia, American Airlines, Austral, Avianca, Boliviana de Aviación, BQB Líneas Aéreas, British Airways, Conviasa, Copa Airlines, Delta Airlines, Emirates, Gol, Iberia, KLM, LAN, Lufthansa, Qatar Airlines, SKY Airlines, TAM, TAME, Turkish Airlines, United Airlines.

AEROLINEAS ARGENTINAS

The main airline in Argentina offer the followings discounts:
10% live for attendees, 15% direct to speakers; 25% direct commission of the association

INTERNATIONAL LAND CONNECTIONS

ACCESS BY LAND

Nationals

- From Buenos Aires: NR 34 / NR 9
- From Iguazú: NR 16
- From Córdoba: NR 9
- From Tucumán: NR 9 / NR 40
- From Jujuy: NR9 / NR 34

Internationals

From Bolivia through the border crossing points:
- Yacuiba (Salvador Mazza)
- Bermejo (Aguas Blancas)

From Chile through the border crossing points:
- Sico: (San Pedro de Atacama - San Antonio de los Cobres - Salta)
- Jama: (San Pedro de Atacama - Jujuy - Salta)

From Paraguay through border crossing points:

- National Route NR 81

NATIONAL DISTANCES

PROVINCE	ROUTES	KM FROM SALTA	TRAVEL TIME IN MINUTES
Buenos Aires	34	1.605	21
Cataratas del Iguazú (Misiones)	16	1.464	17
Córdoba	9	903	12
Humahuaca (Jujuy)	9	245	4
La Quiaca (Jujuy)	9	410	7
La Rioja	9/38	772	10
Mendoza	9/38/40	1.506	16
Mendoza (via Córdoba)	9/5	1.609	17
Paso de Jama (Jujuy)	9/52	473	6 1/2
Purmamarca (Jujuy)	9	157	3
Ruinas de Quilmes	68/40	241	4 1/4
Salinas Grandes	9/52	222	5
Salinas Grandes (via Quebrada del Toro)	51/40	265	4
San Fernando del Valle de Catamarca	9/38	555	7
San Miguel de Tucumán	9	311	4
San Miguel de Tucumán (via Cafayate)	68	420	8
San Salvador de Jujuy	34	124	1 1/2
San Salvador de Jujuy (through cliffside road)	9	92	2
Santiago del Estero	34	460	6
Tafí del Valle (Tucumán)	68	310	6
Termas de Río Hondo (Santiago del Estero)	9	400	5
Tilcara (Jujuy)	9	176	3 1/4

PUBLIC TRANSPORTATION SYSTEM

Bus – Taxi - Car service - Car rental

VENUE AND ACCOMMODATION

SALTA HOST CITY

NIGHTS ON BALCARCE STREET

Folklore peñas (pubs), regional food restaurants, bars, arranged along the traditional Balcarce Street: night in "La Balcarce" is characterized by good folk music, the sound of the guitars, drums, the zambas and chacareras (both traditional dances), friends gather to enjoy asado (roasted meet) and empanadas (pasty), topped with the flavors of the exquisite wines from Salta.

Peñas are a must for tourists who want to have fun and dance, enjoy music and traditional food. There are also bars where live bands from different genres play, restaurants that serve regional and international food.

ARTISANS FAIR

On Sundays from 10:00 to 09:00 more than 200 artisans gather, on both sides of Balcarce Street which dresses in colors, shapes, sounds and smells that convey images from afar as much as vivid present images. The number of visitors grows every Sunday as not only people visiting from around the world assist but salteños that have prolonged the magic of gathering with friends at night to the point of becoming a family ride, they enjoy the afternoons, our traditions and fun with music and shows for both grownups and children. There are many different crafts; the ones made in alpaca are typical, fabrics, embroidery, ceramics, sweets, etc.

CONVENTION CENTER

Salta does not only mean culture, tradition, beauty and landscape diversity; it is also the ideal framework for Business Tourism. That is why the Convention Center of Salta is waiting for you to offer you the best place for your event.

Convention Center of Salta was opened on August 11, 2007; its main objective is to satisfy the growing demand of the business tourism segment that includes the organization of conferences, trade fairs, exhibitions, sporting events, corporate and incentive trips.

This majestic work is considered as one of the most significant of the interior of the country, not only because of its infrastructure, but also for its capacity and leading technology.

The Convention Center Salta S.E. was established in May, 2012, to positions Salta province within Argentina and Mercosur, as a destination for Meetings, Conventions and Events, offering the highest quality at the forefront of modernity requirements, offering visitors and clients the best result.

FLOOR PLAN

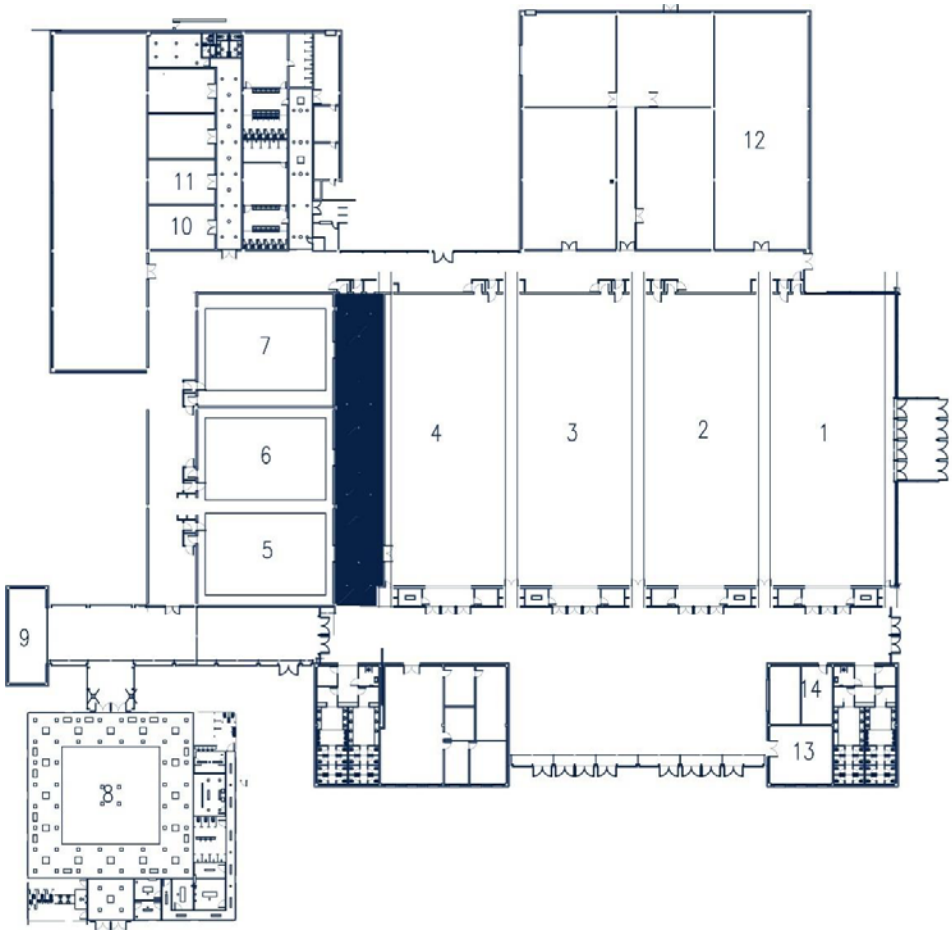

N°	HALL	CAPACITY IN AUDITORIUM
1	Nogales	600
2	Algarrobo	600
3	Cardones	600
4	Lapacho	600
5	Los Ceibos	220
6	Jacaranda	220
7	Tipal	220
8	Álamos	200
9	Sala Computación	10
10	Aula Escuela 1	25
11	Aula Escuela 2	25
12	Deposito RIVA	450
13	Sala VIP	15
14	Sala de Prensa	8

THE CONFERENCE CENTER






LOCATION

The Convention Center of Salta is located at the entrance of the city on the route to the International Airport Martin Miguel de Güemes - Limache roundabout, Kennedy Avenue-5 minutes from the airport and 10 minutes from downtown. Excellent conditions of accessibility and connection.

Salta City

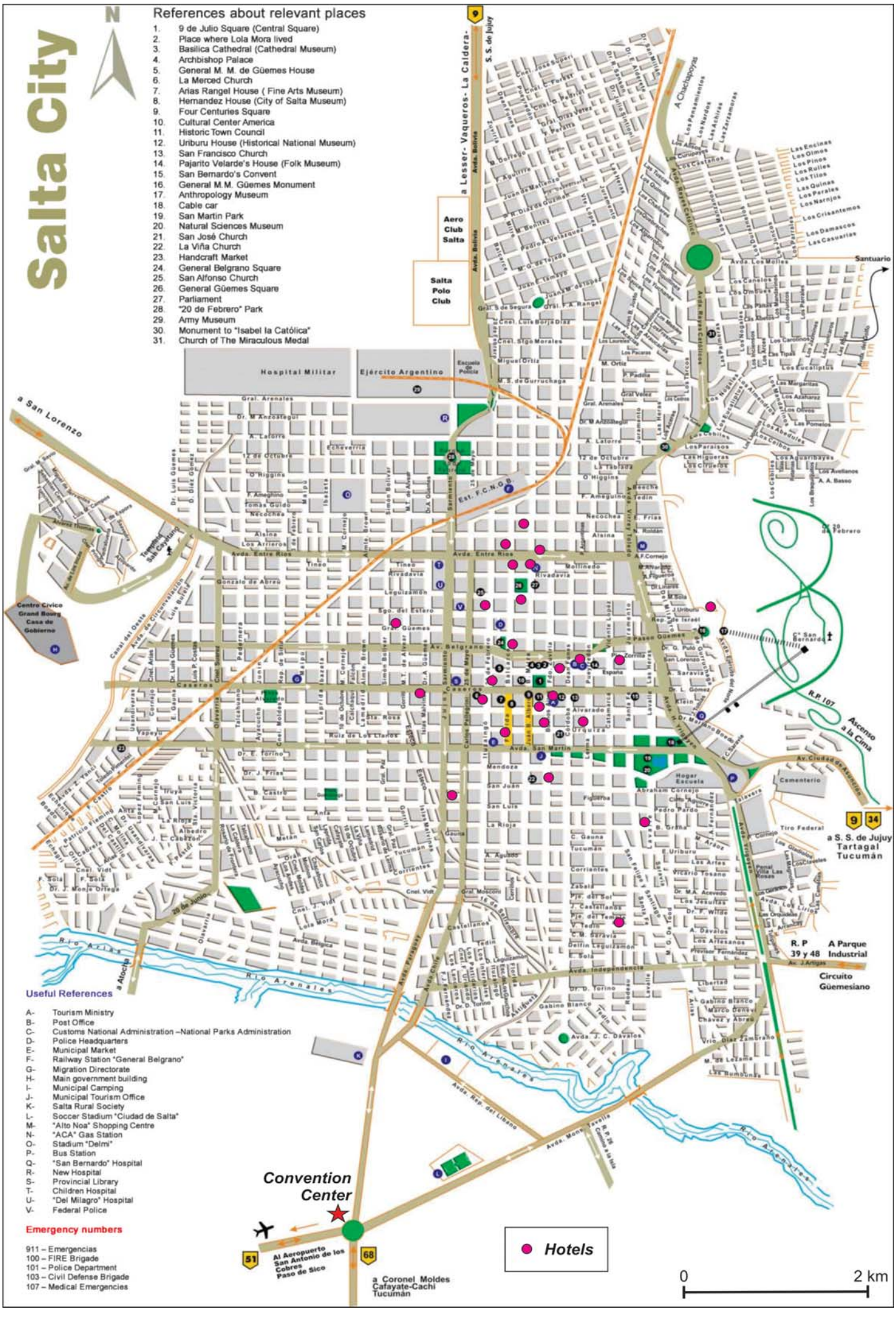
N
References about relevant places
1. 9 de Julio Square (Central Square)
2. Place where Lola Mora lived
3. Basilica Cathedral (Cathedral Museum)
4. Archbishop Palace
5. General M. M. de Güemes House
6. La Merced Church
7. Arias Rangel House (Fine Arts Museum)
8. Hernandez House (City of Salta Museum)
9. Four Centuries Square
10. Cultural Center America
11. Historic Town Council
12. Uriburu House (Historical National Museum)
13. San Francisco Church
14. Pajarito Velarde's House (Folk Museum)
15. San Bernardo's Convent
16. General M.M. Güemes Monument
17. Anthropology Museum
18. Cable car
19. San Martin Park
20. Natural Sciences Museum
21. San José Church
22. La Viña Church
23. Handcraft Market
24. General Belgrano Square
25. San Alfonso Church
26. General Güemes Square
27. Parliament
28. "20 de Febrero" Park
29. Army Museum
30. Monument to "Isabel la Católica"
31. Church of The Miraculous Medal
a Lesser- Vaqueros- La Caldera-
S.S. de Jujuy
Aero Club Salta
Salta Polo Club
Hospital Militar
Ejército Argentino
Escuela de Policía
a San Lorenzo
Santuario
Centro Cívico Grand Bourg Casa de Gobierno
Convention Center
Hotels
Useful References
A- Tourism Ministry
B- Post Office
C- Customs National Administration –National Parks Administration
D- Police Headquarters
E- Municipal Market
F- Railway Station "General Belgrano"
G- Migration Directorate
H- Main government building
I- Municipal Camping
J- Municipal Tourism Office
K- Salta Rural Society
L- Soccer Stadium "Ciudad de Salta"
M- "Alto Noa" Shopping Centre
N- "ACA" Gas Station
O- Stadium "Delmi"
P- Bus Station
Q- "San Bernardo" Hospital
R- New Hospital
S- Provincial Library
T- Children Hospital
U- "Del Milagro" Hospital
V- Federal Police
Emergency numbers
911 – Emergencias
100 – FIRE Brigade
101 – Police Department
103 – Civil Defense Brigade
107 – Medical Emergencies
Al Aeropuerto San Antonio de los Cobres Paso de Sico
a Coronel Moldes Cafayate-Cachi Tucumán
a S. S. de Jujuy Tartagal Tucumán
A Parque Industral
Circuito Güemesiano
R.P 39 y 48
R.P 107
Ascenso a la Cima
0
2 km

HOTEL ACCOMMODATION

The province's current hotel capacity is 19.000 beds. This includes 4 and 5 star hotels as well as boutique hotels. Besides, Salta as four venue auditoriums and 110 conference rooms, prepared to accommodate meetings and conventions which call for different magnitude and technology.

HOTELS IN THE CITY

FIVE STARS HOTELS (U$S 120 - 220)

- Alejandro I
- Sheraton Salta

FOUR STARS HOTELS (U$S 90 - 160)

- Amerian
- Design Suites
- Portezuelo Hotel
- Provincial Plaza

THREE STARS HOTELS (U$S 70 - 100)

- Posada del Sol
- Shauard
- Wilson
- El Colonial
- Las Moras (Villa San Lorenzo)

BOUTIQUE HOTELS (U$S 100 - 120)

- Aldaba Hotel
- Del Vino Boutique
- Hotel Legado MÃ-tico
- House of Jasmines (La Merced chica)
- Patios de Lerma
- Solar de la Plaza
- Las Chirimoyas

ONE AND TWO STARS HOTEL FOR STUDENTS (U$S 25 - 50)

TOURISM INTERESTS

MOVITRACK - SHORT TRIP - 1 DAY

SAFARI TO THE CLOUDS

Aboard vehicles specially designed for maximum enjoyment of the landscape and the difficulties of the Puna, wind, sun, cold and heat, are inevitable partners in this adventure. 4x4 Trucks with comfort of a motor home , have onboard bathroom and ceilings that open on certain sections of the circuits, open on certain sections of the circuits, this feature allows not only have a complete panoramic view, but also a forced oxygenation leaving with no effect altitude sickness. They seat 18 and 20 people and are ideal vehicles to travel in small groups given the distribution of its interior.

CAFAYATE SHORT TRIP - 1 DAY

The road to Cafayate has a particular geography that has been carved by wind and sun. Surprising rock formations seen in gorges and multicoloured mountains surprise the traveller. Some of these formations are the Garganta del Diablo or Devil's Throat, El Anfiteatro or Amphitheatre, El Sapo or Frog, El Fraile or Friar, Los Castillos or Castles, among many.

THE VINE AND WINE MUSEUM - 1 DAY

In the Calchaquí- Valleys, a region noted for its viticulture, valleys, mountains and gorges, one finds The Vine and Wine Museum. It is a live space, full of visual and sound effects that are interactive and entertaining, presenting all visitors with a chance to learn.

CACHI – SHORT TRIP – 2 DAYS

Surrounded by coloured mountains and blessed by the Calchaqui River, Cachi remains a restful town, as well as protecting more than one hundred archaeological sites. Located at 2.280 metres above sea level, this Calchaqui town is recognized by visitors for its particular essence. The Cachi snow capped massif, is one of the treasures that give special characteristics to this town of six thousand inhabitants.

IRUYA – SHORT TRIP – 2 DAYS

Surrounded by an incredible landscape, Iruya is a magic town, literally hanging in the mountains in the north of the province of Salta. Its steep stone streets seem to be from another time. As if out of a postcard, Iruya invites to rest and meditate.

TOLAR GRANDE – 2 DAYS

The small town of Tolar Grande is set in the high altitude Puna desert from where the volcanoes found in the province can be visited (Llullaillaco, Socompa, Arizaro, Aracar and Guanaquero), as well as the incredible water holes in the salt flats, and the most unforgettable landscape. The Arita Cone is a perfect cone of a black lava, 147 metres high and one of the most outstanding geographical features in Salta. It is found at the Arizaro Salar, in the high plateau or Puna, 80 kilometres away from Tolar Grande.

CREATING HANDS		
Duration Days	**Circuit description day by day**	**Region and main tourist attractions**
6	**Day 1:** *Reception at the Airport, Transfer to the Hotel. In the afternoon, Themed City Tour (Museum de Fine Arts, Museum of Contemporary Arts, House of Culture, Historical Centre).* **Day 2:** *Leaving for Cafayate. Quebrada de las Conchas. Accommodation and lunch. Pictorial Workshop under the supervision of a professor of visual arts at the town of Cafayate. End of the activity. Visit to a crafts workshop. Night in Cafayate.* **Day 3:** *Workshop day and country lunch. Return to Cafayate, Afternoon off. Night in Cafayate.* **Day 4:** *Continuing the Workshop day and country lunch. Return to Cafayate.Afternoon off. Night in Cafayate.* **Day 5:** *Return to Salta, Night in Salta, Reunion dinner* **Day 6:** *Transfer to Salta Airport*	*Salta and its outskirts.* *Lerma Valley.* *Puna: Santa Rosa de Tastil (archeology and crafts), town of San Antonio de los Cobres.* *Province of Jujuy:* *Salinas Grandes* *(salt pools, arts and crafts)* *Purmamarca (Cerro de los Siete Colores, arts and crafts).* **Quebrada: gorge; cuesta: winding road.*

THE INCA TRAIL AND SACRED SNOW PEAKS		
Duration Days	**Circuit description day by day**	**Region and main tourist attractions**
5	**Day 1:** *Salta - San Antonio de los Cobres. Salta, Quebrada del Toro, Puerta de Tastil, San Bernardo de las Zorras, Laguna del Toro, Palomar, Pie del Nevado de Chañi, Andean Spiritual Ceremony. Salinas Grandes, San Antonio de los Cobres. Dinner. Night in San Antonio de los Cobres.* **Dia 2:** *San Antonio de los Cobres - Cachi. La Polvorilla Viaduct, Abra del Acay, Andean Spiritual Ceremony, La Poma, Inca Barns. Payogasta, Cachi. Accommodation in cabins. Dinner.* **Day 3:** *Cachi - Las Pailas - Cachi. Vivencial Workshops - Tinku – sharing perceptions and feelings aroused from Ceremonies. Interpretation of the messages of the Apus with Pusak-Nuna Andean Spiritual Guide.Visit Cachi*	*Lerma Valley.* *Quebrada del Toro: C-14 Branch, Tren a las Nubes.* *Puna: Santa Rosa de tastil (archeology), Nevado de Chañi, Salinas Grandes, San Antonio de los Cobres (La Polvorilla Viaduct).* *Calchaqui Valleys: La Poma (Incas' Barns, Devil's Bridge), Payogasta, cachi (church, museum, crafts mar-*
	and Las Pailas with a local guide. Dinner and accommodation in Cachi. **Day 4:** *Cachi - Corralito. NR40, Las Pailas. Molinos. Camino de los Artesanos, Seclantás, Angastaco, San Carlos, Animaná, Corralito. Dinner and accommodation in peasant-based tourism Network.* **Day 5:** *Corralito - Cafayate - Salta* *Trekking and lunch in the community. Visits around Cafayate, visit around the town. At Punilla, NR 68, Ceremony of Gratitude. Visiting the incredible Geological formations in the Calchaqui Valley and in Quebrada de las Conchas. Lerma Valley, Arrival to Salta.* **Observations:** *Circuit available throughout the year.*	*ket, archeological ruins), Inca Trail, Molinos (crafts), Seclantás, Angastaco, Quebrada de las Flechas, San Carlos, Animaná, Corralito, Native communities.* *Quebrada de las Conchas.* *Lerma Valley.* **Quebrada: gorge; cuesta: winding road.*

GOLDEN FISH FLY FISHING AND WINE EXPERIENCES		
Duration Days	**Circuit description day by day**	**Region and main tourist attractions**
9	-*Fly fishing of gold fish in ,wild and clear waters in the middle of the yungas forest. A programme prepared for people with adventurous spirit, and who are fond of fishing. Accommodation in boutique Hotels, 3* 4* 5* (stars)* *Camping.* *Meals at camping and winery.* *Tastings.* *Full days of fly fishing activities.* • *All transfers on double-cabin 4x4 truck or similar with A/C.* • *03 nights of accommodation in Salta.* • *04 nights in lodge next to the river.* • *01 night in camping.* • *01 lunch in winery.* • *04 lunches* • *06 dinners.* • *01 tasting.* •*Traveler's Assistance Insurance.*	*Salta City and outskirts.* *Observations: From March 15th through December 15th. This programme can be modified regarding the number of days, according to the travelers' preferences.*

CALCHAQUI ROADS		
Duration Days	**Circuit description day by day**	**Region and main tourist attractions**
6	**Day 1**: *Salta – Amblayo.* *Excursion to Amblayo located between Lerma Valley and the Calchaquí Valleys. Cuesta del Obispo. Descent to the town of Amblayo. According to the season, participation in agricultural activities (milking cows, cheese making). Night in a family home.* **Day 2**: *Horseback riding in Amblayo – Mountain refuge. Horse-riding expedition through the Amblayo Valley along an old horse trail. (Duration: 5 hours). Arrival at the mountain refuge. Night.* **Day 3**: *Mountain refuge horseback Riding – Quebrada de las Conchas – Cafayate (surroundings). Midday horse riding towards the Quebrada de las Conchas, ascending to a wonderful panoramic view. Cafayate. Meeting with a family from the Rural Tourism Network. Night in a family home.* **Day 4**: *Cafayate - Quebrada de las Flechas - Molinos – Seclantás. In the morning, a walk around the surroundings with the hosts and participation in the preparation of a regional lunch. In the afternoon, visit to a craft winery and a tour to the Quebrada de las Flechas. Visit to the town of Molinos. Night in Seclantás in a famiy home.* **Day 5**: *Seclantás – Trek to Acsibi – Cachi.* *Reaching closer to the starting point in off-road vehicles. Trekking day towards the caves of Acsibi. At the end of the day, return to Cachi. Night.* **Day 6**: *Cachi - Los Cardones National Park– Salta.* *In the morning, walk to the Algarrobal visiting crop areas. In the afternoon, return to Salta through the Los Cardones National Park.* **quebrada: gorge; cuesta: winding road; camino: road.*	*Lerma Valley.* *Calchaquí Valleys:* *Amblayo, Quebrada de las Conchas (geological formations), Cafayate, (gastronomy, rural tourism, winery, wines), Quebrada de las Flechas, Angastaco, Molinos, Seclantás (Acsibi caves), Cachi (Los Cardones National Park, Algarrobal), Cuesta del Obispo, Quebrada de Escoipe)*

VALLEYS, SUBTERRANEAN RIVERS, CAVES AND MYSTERIES		
Duration Days	**Circuit description day by day**	**Region and main tourist attractions**
5	**Day 1:** *Transfer to the hotel. Tour around the city. Dinner with the whole tour group and guide. Accommodation in Salta.* **Day 2:** *Salta - La Poma - Cachi -Seclantás.* *Escursion to the Calchaquí Valleys through the Cuesta del Obispo. Los Cardones National Park. National Road N. 40 heading towards the town of La Poma. Circuit around one of the stretches of the Calchaqui river within the caves. A small trek through the Graneros incaicos. Picnic. Return to Cachi taking NR N. 40. Visit to the Archeological Museum. Leaving for Seclantás through "el Camino de los Artesanos". Night in Seclantás.* **Day 3:** *Seclantás - Molinos - Angastaco.* *Excursion to the Caves of Acsibi. Trekking. Visit to a vicuña farm and a church in the town of Molinos. On the way to Angastaco visit and lunch at El Carmen Farm. Entrance and snacks in Angastaco. Small trek in Los Colorados. Camping in La Quebrada de las Flechas.* **Day 4:** *Quebrada de las Flechas - San Carlos - Animaná - Cafayate - Quebrada de Cafayate - Salta.* *Excursion to San Carlos through some small villages located by the roadside. Visit to an ancient church. Animaná. Cafayate. Visit to a traditional winery and tasting of wines. Lunch at a high altitude bar. Return to Salta city through the Qubrada de las Conchas. Stops at natural attractions such as Los Castillos, Anfiteatro, the Garganta del Diablo, etc. Night in Salta.* **Day 5:** *Transfer to Salta city airport.*	*Salta City and its outskirts: Historical city center, churches, museums, San Bernardo Hill, Balcarce Street, San Lorenzo.* *Calchaquí Valleys:* *Quebrada de Escoipe, Cuesta del Obispo, Cachi, Los Cardones National Park, Recta del Tin Tin), Amblayo, Isonza, Payagasta, Seclantás, (Camino de los Artesanos), Molinos (vicuña farm, church), Angastaco, Los Colorados, Quebrada de las Flechas, San Carlos (church, arts and crafts), Animaná, Cafayate (winery, wines), Quebrada de las Conchas (geological formations).* **quebrada: gorge; cuesta: winding road; recta: stretch; camino: road; vicuña: Andean camelidae.*

BIRDWATCHING SALTA

Duration Days	Circuit description day by day	Region and main tourist attractions
8	1. Huaico Reserve, San Lorenzo Birdwatching walk at Huaico Reserve in search of Huaico Tinamou, Cream-backed Woodpecker, Alder Amazon, Red-tailed Comet... We then visit San Lorenzo in search of Red-legged Seriema... two nights accommodation at Selva Montana Lodge, San Lorenzo. Night outing for Hoy´s Screech Owl, Scissor- tailed Nightjar... 2. Mountain pass and Yala river, San Lorenzo Full day excursion for Torrent Duck, Rufous-throated Dipper, Red-faced Guan... 3. Palomitas and J. V. Gonzales Full day exploring transitional cloudforest and dry woodland in search of Toco Toucan, Black-legged Seriema... Two nights accommodation at hotel in J.V. Gonzales 4. J.V. Gonzales Full day exploring dry chaco forest looking for Quebracho Crested-Tinamou, Spot-winged Falconet, Turquoise-fronted Amazon, Brown Cacholote, Scimitar-billed Woodcreeper... 5. El Tunal, Juramento, San Lorenzo Full day trip in search of Rheas, Tinamous, Crowned Eagle, Andean Condor... Overnight at Selva Montana Lodge 6. Toro Canyon, San Antonio de los Cobres Ful day exploring the canyon, cactus fields and lagoons looking for Horned and Giant Coots, Andean Goose, Giant Hummingbird... two nights at Hosteria de las Nubes, S.A.C 7. Gallo Mount pass, Pocitos saltflat, S.A.C High Andes birding full day in search of Andean and Puna Flamingoes, Rufous-bellied and Gray-breasted Seedsnipes, Puna Plover... 8. Abra Blanca, Salta We drive back to Salta with several birding stops at different altitudes. End	*Lerma valley, San Lorenzo* *Birds of Huaico Reserve* *Santa Laura mountain pass, Yala* *Birds of Yungas forest* *Chaco forest* *Birds of Yungas and Chaco woodland.* *Dry Chaco brushland.* *Birds of semidesert chaco habitat* *Chaco Salteño* *Birds of chaco habitat* *Puna, lagoons and canyons* *Birding the Puna* *High Andes, saltflats, rivers and lakes.* *Birds of the High Andes* **Quebrada: gorge; Guaipos: birds from the area; Yungas: Aymaran for "warm lands"; pava de monte alisero: a bird from the family of Cracids; hoteria: guest house.*

THE INHOSPITABLE PUNA

Duration Days	Circuit description day by day	Region and main tourist attractions
3	**Day 1:** *Salta - Quebrada del Toro - San Antonio de los Cobres - Pocitos -Tolar Grande. Departure from Salta. Circuit through the route of the Train to the Clouds (via the Quebrada del Toro). Arrival in San Antonio de los Cobres. Crossing through Salar de Pocitos and the Desierto del Diablo. Arrival in Tolar Grande. Night in Tolar Grande* **Day 2:** *Tolar Grande - Salar de Arizaro - Tolar Grande. Outing. Circuit through the Salar de Arizaro. Arrival at the rare formation "Cono de Arita" (Arita's Cone). Trek. Return. Visit to the Tunel del Hombre Muerto and Ojo de Mar. Night in Tolar Grande.* **Day 3:** *Tolar Grande - San Antonio de los Cobres - Quebrada del Toro - Salta. Return to Salta. Visit to the archeological ruins of Santa Rosa de Tastil. End of excursion.*	*Puna: Santa Rosa de Tastil (archeological place), San Antonio de los Cobres (town, arts and crafts), Salar de Pocitos, Desierto del Diablo, Salar de Arizaro, Tolar Grande, Ojos de Mar, Cono de Arita, Tunel del Hombre Muerto.* *Quebrada del Toro: Railways of the Tren a las Nubes.* **Quebrada: gorge; salar: salt flat; cono: cone.*

WINE ROUTE TOUR

Duration Days	Circuit description day by day	Region and main tourist attractions
6	**Dia 1:** *Reception and transfer to the hotel. Night in Salta.* **Day 2:** *Visit to the City and surroundings. Night in Salta.* **Day 3:** *Full day excursion to Cafayate visiting a winery and the Vine and Wine Museum (tickets included). Accommodation.* **Day 4:** *Visit to two wineries. Excursion to Molinos, visiting places where the "Patero" wine is elaborated in a traditional fashion. Night in Molinos.* **Day 5:** *Excursion to Cachi and Cachi Adentro. Continuation of trip through the Cuesta del Obispo. Arrival in Salta. Night in Salta.* **Day 6:** *Transfer to Salta city airport.* **quebrada: gorge; cuesta: winding road; recta: stretch; camino: road; Patero: a wine made by stepping on grapes.*	*Salta City and its outskirts: Historical Center, churches, museums, San Bernardo Hill, Monuments, Balcarce Street, San Lorenzo.* *Calchaquí Valleys: Quebrada de Escoipe, Cuesta del Obispo, Payogasta (wines), Cachi (Los Cardones National Park, recta del Tin Tin, church, museum), Cachi Adentro: (wineries, Seclantás (Camino de los Artesanos, "Salta's poncho"), Molinos (winery, "Patero" wine, museum), Angastaco, Quebrada de las Flechas, San Carlos (church, arts and crafts), Animaná, Cafayate (winery, wines, Vine and Wine Museum, goat cheese factory), Quebrada de las Conchas (geological formations).*

HIGH ALTITUDE NORTHERN WINES

Duration Days	Circuit description day by day	Region and main tourist attractions
4	**Day 1:** *Salta. Reception and transfer to the hotel. City tour around 9 de julio Square, Basilica Cathedral, Cabildo (Town Council), Convent of San Francisco, San Bernardo Hill Summit, the Monument to General Güemes, the 20 de Febrero Monument, Quebrada de San Lorenzo and Crafts Market. Night in Salta.* **Day 2:** *Salta - Cachi. (Tour around the Valleys). Circuit: Quebrada de Los Laureles. Quebrada de Escoipe. Cuesta del Obispo. Enchanted Valley. Piedra del Molino (3348 meters above sea level.). Recta del Tin Tin. Los Cardones National Park, Nevado de Cachi. Stops and treks along the circuit to enjoy the beauty of the gorgees. Lunch. Visit to a winery. Night in Cachi.* **Day 3:** *Cachi - Cafayate. (Tour around the Valleys). Leaving for Cafayate taking National Road N. 40*	*Salta City and its outskirts: Historical Center, churches, museums, San Bernardo Hill, Monuments, Balcarce Street, San Lorenzo.* *Calchaquí Valleys: Quebrada de Escoipe, Cuesta del Obispo, Payogasta (wines), Cachi (Los Cardones National Park, recta del Tin Tin, church, museum), Seclantás (Camino de los Ar-*
	along the Calchaquí River, Historical towns such as Seclantás (Camino de los Artesanos) and Molinos (ancient Spanish Hacienda and National Historical Museum). Quebrada de Las Flechas (a 25-minute light trekking tour) wine-producing area of remarkable towns such as Animaná, San Carlos and Cafayate. Visit to the wineries Nanni (organic wines), El Esteco and Domingo Hermanos. **Day 4:** *Cafayate - Salta Airport. Leaving for the archeological place of Quilmes (Province of Tucumán). Return to Cafayate. Lunch at Finca "Las Nubes" with tasting of wines of Bodega Mounier. Return to Salta through the Quebrada de Las Conchas (Garganta del Diablo, Anfiteatro and Los Castillos among others). Arrival in Salta. Night in Salta.* **Quebrada: gorge; cuesta: winding road; recta: stretch; nevado: a snowcapped mountain; camino: road.*	*tesanos, Salta's poncho), Molinos (Colomé winery, museum), Angastaco, Quebrada de las Flechas, San Carlos (church, arts and crafts), Animaná, Cafayate (winery, wines, Vine and Wine Museum, goat cheese factory), Quebrada de las Conchas (geological formations).* *Province of Tucumán: Ruinas de Quilmes.*

CONTACT INFORMATION OF LOCAL TRAVEL AGENCIES

If you are interested in hiring a tour you may contact any of the following Travel Agencies, members of the Salta Convention & Visitors Bureau:

Agencia del Peregrino
info@agenciadelperegrino.com.ar
www.agenciadelperegrino.com.ar
Phone +54-387-4229440

Tastil Viajes
info@tastil.com.ar
http://www.turismotastil.com.ar
Phone +54-387-4311223

UMA Travel
promocion@umatravel.tur.ar
www.umatravel.tur.ar
Phone +54-387-4228317

Servicio Geológico Minero Argentino
www.segemar.gov.ar

Asociación Geológica Argentina
www.geologica.org.ar

CONTACT INFORMATION

15th Quadrennial IAGOD Symposium
secretariat@15iagods.org
www.15iagods.org

International Association
on the Genesis of Ore Deposits
www.iagod.org

SALTA, ARGENTINA
28-31 AUGUST 2018

15th Quadrennial International Association on the Genesis of Ore Deposits Symposium

SYMPOSIUM PROCEEDINGS

SegemAR
Servicio Geológico Minero Argentino

INTERNATIONAL ASSOCIATION ON THE GENESIS OF ORE DEPOSITS
1964
IAGOD

ASOCIACIÓN GEOLÓGICA ARGENTINA

SPONSORS

PLATINUM SPONSORS

SegemAR
Servicio Geológico Minero Argentino

GOLD SPONSORS

GOLDCORP
CERRO NEGRO

Mansfield Minera S.A.
Compañía de Fortuna Silver Mines Inc.

SALES DE JUJUY

YAMANAGOLD

SILVER SPONSORS

Pan American SILVER CORP.

GROSSO GROUP

SOUTH AMERICAN SALARS

ADVANTAGE LITHIUM

CERRO VANGUARDIA

ANGLOGOLDASHANTI

GRUPO AGV

BRONZE SPONSORS

Bayton
GRUPO EMPRESARIO

FOMICRUZ

ENERGOLD GROUP™

GOLDEN MINERALS COMPANY
SILEX Argentina
COLQUE EXPLORACIONES

MINERA SANTA CRUZ
AFILIADA A HOCHSCHILD MINING

PATAGONIA GOLD

SOUTHERN COPPER
EXPLORACIONES ARGENTINA

Enaex

COPPER SPONSORS

ATA
HOTELERÍA & ALIMENTACIÓN INSTITUCIONAL

Co-sponsored by

ASGMI
Asociación de Servicios de Geología y Minería Iberoamericanos

FUNDACION EMPREMIN

SOCIETY OF ECONOMIC GEOLOGISTS
FOUNDED 1920

SOCIETY for GEOLOGY APPLIED to MINERAL DEPOSITS

SALTA, ARGENTINA
28-31 AUGUST 2018

15th Quadrennial International Association on the Genesis of Ore Deposits Symposium

SYMPOSIUM PROCEEDINGS

SegemAR
Servicio Geológico Minero Argentino

SCIENTIFIC COMMITTEE

EDITED BY

Daniel Rastelli, Dolores Álvarez, Noelia Iannizzotto, Ines Korzeniweski, Cintia Marquetti, Feliciano Pagnanini, Javier Peroni, Susana Segal – (Institute of Geology and Mineral Resources, SEGEMAR)

Proceedings of the 15th Quadrennial International Association on the Genesis of Ore Deposits Symposium
ANALES 56 - SEGEMAR
ISSN 0328-2325

BUENOS AIRES - 2018

15TH QUADRENNIAL IAGOD INTERNATIONAL ASSOCIATION ON THE GENESIS OF ORE DEPOSITS SYMPOSIUM, SALTA, ARGENTINA

HONORARY COMMITTEE

Honorary President
Julio Ríos Gómez
President of the Geological and Mining Survey of Argentina (SEGEMAR)

Members
Diana Carolina Sánchez
Secretary of Mining, Ministry of Production, Argentina
Mario Pereira
National Director of the Geology and Mining National Survey, Chile (SERNAGEOMIN)
Daniel Ricardo Blasco
Secretary of Mining, Salta Province, Argentina
Ricardo Salas
Former Secretary of Mining, Salta Province, Argentina
Miguel Soler
Secretary of Mining, Jujuy Province, Argentina
Ricardo Alonso
University of Salta, Argentina

ORGANIZING COMMITTEE

President
Eduardo O. Zappettini
Institute of Geology and Mineral Resources, SEGEMAR;
Commission for the Geological Map of the World (CGMW); President of IAGOD

Members
Martín Gozalvez
Institute of Geology and Mineral Resources, SEGEMAR
Graciela Marin
Institute of Geology and Mineral Resources, SEGEMAR; Geological Association of Argentina
Eduardo Marquina
Institute of Geology and Mineral Resources, SEGEMAR
Susana Segal
Former Institute of Geology and Mineral Resources, SEGEMAR
Carlos Herrmann
Institute of Geology and Mineral Resources, SEGEMAR
Nora Rubinstein
National and Technical Research Research Council-Argentina (CONICET),
IGeBA Department, University of Buenos Aires
Diego Guido
National Scientific and Technical Research Council-Argentina (CONICET),
University of La Plata, Eploration Vicepresident (AUSTRAL GOLD)
Pablo Caffe
National and Technical Research Research Council-Argentina (CONICET)
José Marcelo Arnosio
University of Salta
Waldo Vivallo Sandoval
Geology and Mining National Survey, Chile (SERNAGEOMIN)
Raúl Lira
National Scientific and Technical Research Council-Argentina (CONICET),
Univesity of Córdoba Coordinator of the 15th IAGOD Symposium Scientific Committee

IAGOD COUNCIL 2016-2020

President: Eduardo Zappettini - Argentina - eduardo.zappettini@segemar.gov.ar
Secretary General: David Lentz - Canada - dlentz@unb.ca
Chief Treasurer: Reimar Seltmann - UK - R.Seltmann@nhm.ac.uk
Publication Manager: Franco Pirajno - Australia - franco.pirajno@uwa.edu.au
Promotion Manager: Xiang Junfeng - China - xjf2929@163.com
Webmaster: Evgeniy Naumov - Russia - naumovevg@gmail.com
Executive Manager: Alla Dolgopolova - UK - A.Dolgopolova@nhm.ac.uk

Councillors

Past President: Mao Jingwen - China - jingwenmao@263.net
First Vice President: Nora Rubinstein - Argentina - nora@gl.fcen.uba.ar
Second VP: Sergei Cherkasov - Russia - s.cherkasov@sgm.ru
1st VP at Large: Alexandra Gomez Escobar - Colombia - alexagomeze@gmail.com
2nd VP at Large: Alexey Aleshin - Russia - aleshin@igem.ru
Past Secretary General: Sun Xiaoming - China - eessxm@zsu.edu.cn

Regional Councillors

Africa: Paul Nex - South Africa - Paul.Nex@wits.ac.za
Asia: Batkhishig Bayaraa - Mongolia - bkhishig@must.edu.mn
Australasia: Nigel Cook - Australia - nigel.cook@adelaide.edu.au
Europe: David Holwell - UK - dah29@leicester.ac.uk
North America: Ed Ripley - USA - ripley@indiana.edu
South America: Diego Guido - Argentina - diegoguido@yahoo.com
China: Xie Guiqing - China - guiqingxie@sohu.com
India: Dipak Pal - India - dipak.pal@gmail.com
Iran: Seyed Mehran Heidari - Iran - sm.heidari@gmail.com
SE Asia: Khin Zaw - Australia - Khin.Zaw@utas.edu.au

Ex officio Members

Account holder: Andreas Nδgele - Germany - iagod@schweizerbart.de
President, SGA: Jorge Relvas - Portugal - president@e-sga.org
Executive Secretary, SGA: Jan Pasava - Czech Republic - jan.pasava@geology.cz

15th IAGOD SYMPOSIUM ORGANIZERS

Geological and Mining Survey of Argentina (SEGEMAR)
Geological Association of Argentina (AGA)

Contact information

secretariat@15iagods.org

CONTENT

SESSIONS

PLENARY LECTURES

CHAPTER 1
EPITHERMAL GOLD DEPOSIT

Convenor: Diego Guido

IGNEOUS ACTIVITY AND TECTONIC SETTING FOR LOW-SULPHIDATION EPITHERMAL GOLD MINERALIZATION IN JAPAN

Keiko Hattori[1], Kenichi Kano

[1]*University of Ottawa, Shizuoka University - khattori@uottawa.ca*

INTRODUCTION

Japan contains numerous epithermal vein-type Au deposits where Au occurs as electrum in dark sulphide-rich bands (ginguro-bands) in quartz+adularia±carbonate veins. The majority of deposits are low-sulphidation-type (Sillitoe & Hedenquist, 2003) hosted by Miocene submarine volcanic rocks, the Green Tuff belt (Fig. 1). The mineralization took place at shallow depths (< 300 m) by fluids of predominantly meteoric water origin based on low salinity and D/H ratios of the fluids, and alteration mineral assemblage (e.g., Hattori & Sakai, 1979; Shikazono, 1985). The evidence suggests the mineralization under subaerial conditions after the uplift of host submarine rocks. This paper presents the timing of Au mineralization in three representative districts; Izu Peninsula in south-central Japan, Sado island in northwestern Japan, and Hokusatsu area in southern Japan (Fig. 1).

IZU DEPOSITS (>47 T Au, >1230 T Ag)

The Izu block contains many past Au producers, including the Toi (18.4 t Au) and Seigoshi mines (16 t Au). The Izu block represents the northern end of the Izu-Mariana island arc and started as submarine volcanoes on the eastern margin of the Philippine Sea plate above the Pacific Plate. NW move of the Philippine Sea plate resulted in the collision of the volcanic chain with Honshu at ~2 Ma, uplift of the Izu block to subaerial conditions and anticlockwise rotation, and subsequent east and westward double subduction (e.g., Tani *et al.*, 2011). The double subduction produced an extensional regime where numerous tholeiitic mafic dyke swarms and monogenetic volcanic fields formed. The available K-Ar ages of Au veins, <2 Ma (Shikazono & Tsunakawa, 1982; MITI, 1987a), suggest the mineralization after the collision of the Izu block where a rearc volcanic activity started. Au veins strike NW- SE in the western part and EW in the eastern part of the peninsula, and are parallel to tholeiitic mafic dykes in the region (Nakamura *et al.*, 1984), suggesting the mineralization during crustal extension related to the double subduction (Fig. 1).

SADO MINE (>77 T Au, >2400 T Ag)

Sado Au deposits occur in EW trending veins on Sado island (Fig. 1). Mineralization was closely linked with the development of the Japan Sea, which started as a back-arc basin at ~25 Ma, separating Japan from Eurasia. The basin development is followed by oceanic mafic volcanism, and injection of mafic dyke swarms (e.g., Jolivet *et al.*, 1994). Available K-Ar ages for adularia from Au veins show two events; 22-24.4 Ma and 13-14 Ma (Shikazono and Tsunakawa, 1982; MITI, 1987b). The early event corresponds to the start of mafic magmatism at Sado and major rifting in the eastern Japan Sea. The later event corresponds to the start of mafic dyke swarms on the island. The Au veins are sub-parallel to the mafic dykes, indicating that mineralization took place under the same extension regime.

HOKUSATSU DISTRICT (>440 T Au)

Au veins in this district formed at <1.56 Ma including the Okuchi (22 t Au), Yamagano (28.4 t Au) and Hishikari deposits (> 440 t Au). The Hishikari deposit has veins striking N50E where most formed <0.7 Ma with the oldest 1.3 Ma (Tohma *et al.*, 2010). Host rocks are volcanic rocks at the northern end of the Ryukyu arc. Oblique subduction of both the Pacific and Philippines Sea plates below Japanese islands causes the southward movement of southern Kyushu and northwestward move of the northern Kyushu (Mashima, 2016). The disparity of crustal motion created crustal extension in the area where Au deposits form. This extension is reflected by the change in igneous rocks. The Shishimano group rocks, contemporaneous with the Au mineralization at Hishikari, records an increased mafic contribution since 1.0 Ma, which is consistent with the upwelling of asthsnospheric mantle in an extension regime

DISCUSSION AND CONCLUSIONS

Although the ages of the mineralization in these Au districts in Japan are different, all have common features; Au mineralization occurred during extension after cessation of volcanic- front magmatism. The extensional regime for the Au mineralization formed in response Japan-scale tectonic activity, and is reflected by asthenospheric mantle-driven magmatism. The geological setting of low-sulphidation epithermal Au deposits in Japan is similar to that in

northern Nevada (John, 2001), where Au mineralization coincided with continental rifting and tholeiitic mafic magmatism. The data from these Au camps suggest that although epithermal Au mineralization occurs at shallow depths, it is a product of large-scale lithospheric evolution.

REFERENCES

Hattori, K., Sakai, H., 1979. Ore fluids for Neogene veins and Kuroko. Econ Geol. 74:535-555.

John, D.A., 2001. Epithermal deposits in the Northern Great Basin. Econ. Geol. 96:1827-1853.

Jolivet, L., Tamaki, K., Fournier, M., 1994. Japan Sea. J. Geophys. Res. 99: 22,237-22,259.

Mashima, H., 2016. Tectonic of the Kumamoto earthquakes. Kumamoto earthquake workshop.

MITI, 1987a. Report on the Izu area, Ministry Internat. Trade & Industry (In Japanese).

MITI, 1987b. Report on the Sado area, Ministry Internat. Trade & Industry (In Japanese).

Nakamura, K., Shimazaki, K., Yonekura, N., 1984. Philippine Sea plate. Bull., Soc. Geol. Fr. 26: 221-243.

Shikazono, N., 1985. The Seigoshi Au-Ag district, Izu. Chem. Geol. 49: 213-230. Shikazono, N, Tsunakawa, H., 1982. K-Ar ages of deposits. Mining Geol. 32: 479-482.

Sillitoe, R.H., Hedenquist, J.W., 2003. Linkages between volcanotectonic setting, ore-fluid compositions, and epithermal precious –metal deposits. Soc. Econ. Geol. Sp. Pub. 10: 315-343.

Tani, K, Fiske R. S., Dunkley, D. J., Ishizuka O., Oikawa, T., Isobe, I., Tatsumi, Y., 2011. The Izu Peninsula, Japan: Zircon geochronology reveals a record of intra-oceanic rear-arc magmatism in an accreted block of Izu–Bonin upper crust. Earth Planet. Sci. Lett. 303: 225-239.

Tohma, Y., Imai, A., Sanematsu, K., Yonezu, K., Takahashi, R., Koyama, M., Sekine, R., Duncan, R., Watanabe,, K., 2010. Characteristics and Mineralization Age of the Fukusen N° 1 Vein, Hishikari Epithermal Gold Deposits, Southern Kyushu, Japan. Res Geol. 60: 348-358

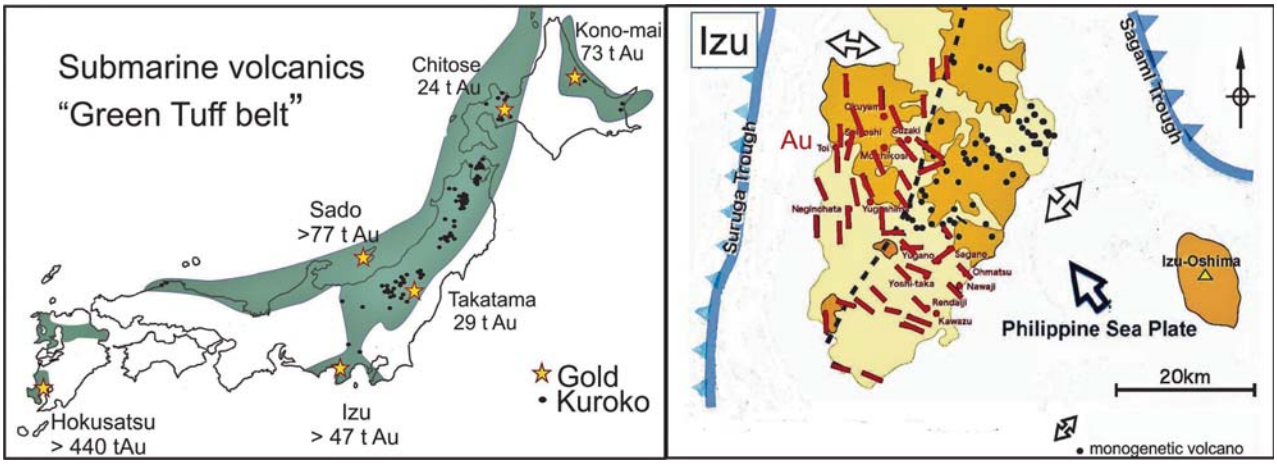

Figure 1. Location of major gold districts and distribution of submarine volcanic belt (Left) and geological setting of epithermal gold veins in Izu peninsula (Right).

TRIDIMENSIONAL MODELLING OF EPITHERMAL PULSES AT CENTRAL VEIN, AMANCAYA MINE, II REGION, CHILE

López Paola[1], López Luciano, Guido Diego, Páez Gerardo

[1]CONICET-Austral Gold S.A., Instituto de Recursos Minerales (INREMI-FCNyM-UNLP) Street 64 and 120, (1900) La Plata, Argentina - paolalopez.lp@gmail.com

INTRODUCTION

Identification and classification of quartz textures and the mineralization pulses is an efficient and economical exploration tool in epithermal systems. This technique provides valuable information and allows the time/space location of gold-silver mineralization along the vein. In this contribution, different observation scales are used to determine the correlation between Au-Ag mineralization and the hydrothermal pulses distribution to use this as an exploration tool for the Amancaya Mine.

GEOLOGICAL BACKGROUND

The Amancaya Mine is included within the Paleocene-Eocene metallogenetic belt of northern Chile. It is located at 215 km of Antofagasta city and 70 km east of Taltal in the western border of Central Depression near the limit with the Coastal Range (25°32' S- 69°49' W). The deposit is a large structurally controlled quartz-carbonate epithermal system with 42 linear kilometers of veins in N-S, NNE and NW trending structures with steep dips to the East. The main structure is the Central vein system studied here.

THE CENTRAL VEIN

The Central vein gathers two main structures (North and South veins) and a significant number of branches and second-order structures. The North vein is a NNE-SSW trending vein dipping 70-80° to the east, while the South vein has a NW-SE azimuth and a steeper dip to the east. These veins join to form an obtuse angle with a "boomerang" shaped morphology.

The veins infill is the same in both segments and consists of four hydrothermal events discriminated according to their mineralogy and texture. The first (EvA) is represented by a barren chalcedonic massive pulse.

The second event (EvB) is divided into five pulses, from which Pulse 3 and 4 (P3 and P4) add economic metals to the vein. P3 is characterized by recrystallized quartz and adularia forming a massive texture with scarce drussy cavities, containing disseminated coarse grains of base metal sulfides and pyrite associated with native Au. P4 is characterized by colloform-crustiform textures, with chalcedony, fine grain quartz, sulfides, clays and adularia, with disseminated fine grain native Au and electrum.

The third stage (EvC), is represented by barren crystalline quartz with coarse amethyst crystals in a crustiform banding with comb textures, and minor breccias.

Finally, there is a late event (EvD), characterized by carbonate-rich pulses with colloform banding and breccias.

METHODS

The vein was modelled combining explicit and implicit techniques with Leapfrog Geo 4.0 software. The first step was the digitalization of the hanging and footwall limit lines from a pre-mining map, and plan maps from six open pit levels. Combining polylines from surface mapping (explicit) with a selection of vein intervals from drill-holes (implicit), a final model for Central vein was created.

Using these geological limits as interpolation boundaries, Au-Ag geochemical values were modelled. The veins and the geochemical interpolation was performed using a Radial Basin Function (RBF) algorithm.

Using the same method, the relative amounts of each hydrothermal pulse was modelled using information from 34 vein drill-cores. An empiric scale, ranging from 0 (absent) to 4 (very abundant), was defined to highlight the presence of each event.

MODELLING

The Au and Ag isovalue surfaces (Fig. 1) show the geometry of the Central vein ore shoots. Au distribution in the North vein has a north-trending shoot with a 20° plunge that outcrops close to the South vein intersection. This shoot has a vertical extension averaging 130 m. The South vein ore-shoot exhibits a 45° plunge to the south, with an approximately 54 m vertical extension. The Ag shows a distribution clustered toward the surface, close to the outcropping Au ore-shoot (Fig. 1).

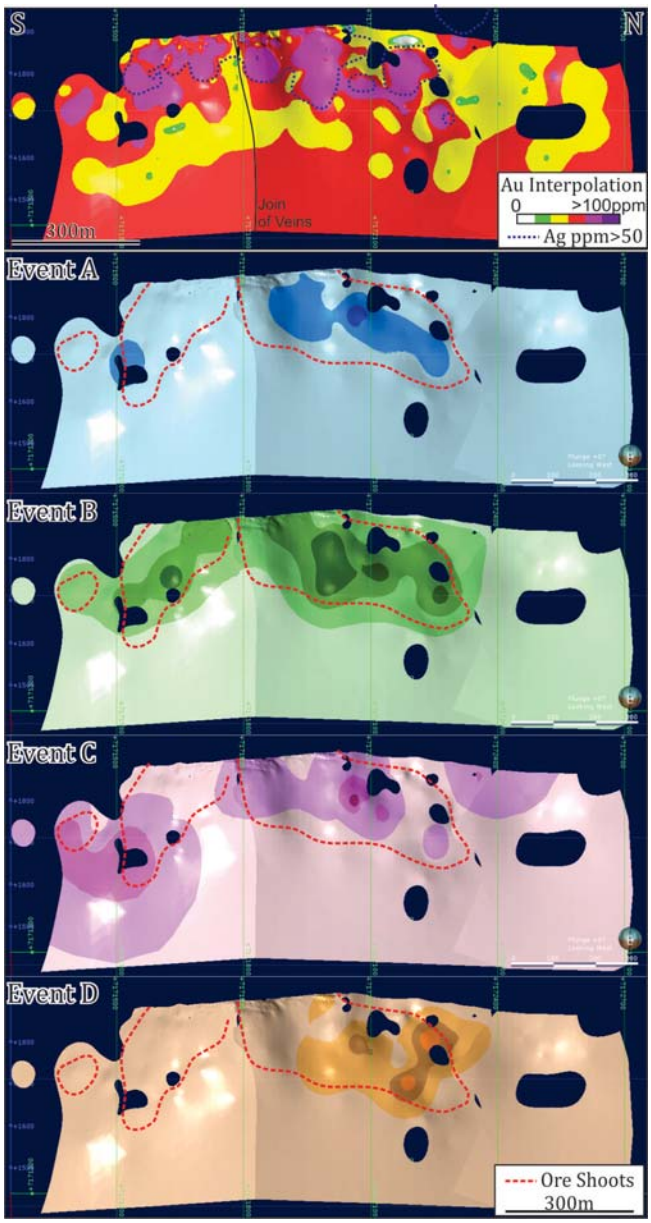

Figure 1. Numeric model of different parameters of Central Vein system. In the events the most abundant is in dark colors.

When considering the distribution of the epithermal infill, it can be observed that EvA is poorly represented and almost limited to the North Vein. EvB has a large distribution along both veins, is the main filling event considering its relative volume, and shows similar morphology to Au ore-shoots. EvC shows different distribution in both veins; in the North vein it has a shallow distribution, whereas in the South vein it shows a deeper distribution. EvD is only present in the central portion of the North vein (Fig. 1).

As EvB was proved to be the mineralizing event with mineralogy and this 3D modelling, a detailed analysis of the distribution of each pulse was done, showing that P3 is better represented in the deeper zones, whereas P4 is better represented toward the shallow portions of the veins.

CONCLUSIONS

The distribution of both ore-shoots and hydrothermal infill probably indicate that the main opening of the structures was following a WNW orientation, although this hypothesis must be confirmed with a detailed structural analysis.

Modelling of epithermal pulses confirms that EvB has the best correlation with Au distribution, controlling the geometry of the ore-shoots. The EvA, EvC and EvD show little, to no correlation with the Au and Ag grade distributions (Fig. 1). The 3D modelling technique has proven to be a powerful tool to analyze different kind of controls on the geometry of ore-shoots in epithermal environments.

GEOLOGY AND HYDROTHERMAL ALTERATION OF THE SIERRA INESPERADA LITHOCAP, GUANACO DISTRICT, CHILE

Conrado Permuy Vidal[1], Laura Maydagán, Gerardo N. Páez, Diego M. Guido, Jorge Osorio.

[1]*Instituto de Recursos Minerales, Facultad de Ciencias Naturales y Museo, Universidad Nacional de La Plata, La Plata, Argentina*

conradopermuyvidal@gmail.com

INTRODUCTION

The Sierra Inesperada hill is situated about 7 km southwestward direction of the Guanaco Mine, a high-sulfidation structurally controlled deposit formed during the Paleocene to early Eocene (~45 Ma; Puig *et al.*, 1988; Guido *et al.*, 2014). The mineralization at Guanaco is hosted in ENE-WSW to E-W trending structures composed of gold-bearing vuggy-silica with minor quartz-enargite veins (Guido *et al.*, 2014). The Sierra Inesperada is a N-S elongated topographic high composed of Paleocene volcanic rocks interpreted as part of a maar- diatreme complex (Páez *et al.*, 2015). The whole volcanic pile is affected by prominent advanced argillic alteration corresponding to an extensive lithocap (1 km^2). Lithocaps are volumetrically significant domains of hypogene silicic (>1 km thick), advanced argillic and argillic-altered rocks that can form above and to the side of shallow intrusions. Lithocaps can be particularly challenging for exploration because may host high-sulfidation epithermal mineralization in their fracture-controlled roots (feeders) and some overlie and partially overprint porphyry deposits (Sillitoe, 1995, 2010). Chang *et al.* (2011) demonstrated that a combination of SWIR analyses, focusing on spatial changes in the alunite 1,480 nm peak positions, coupled with whole rock geochemistry, can provide effective tools for vectorization towards the heat and fluid source responsible for lithocap formation. This works shows preliminary exploration results on geological and alteration features in the Sierra Inesperada for vectorization towards mineralized structures within the lithocap.

METHODOLOGY

Geologic and hydrothermal alteration mapping, core logging of diamond drill holes from the area were integrated with available geochronological determinations to establish the volcanic stratigraphy and temporal framework of volcanism and alteration within the district in Sierra Inesperada (Figure 1). A total of 41 chip rock samples were collected along a 5- km traverse of the advance argillic alteration zones for portable SWIR analyses to complement mapping. Spectral analysis of all samples were made using a TerraSpec 4 Hi-Res Mineral Spectrometer (Analytical Spectral Devices, Inc.) provided by Austral Gold Ltd. The spectral range varies from 350–2,500 nm of both visible-to-near infrared electromagnetic radiation. At least two analyses were performed for each sample to avoid differences in the intensity of absorption features and heterogeneities within the rock. Spectra and spectral parameters were obtained and calculated using The Spectral Geologist (TSG) software (www.thespectral geologist.com.au). Spectral parameters corresponding such as wavelength position of an absorption feature were calculated using scalers in TSG for both reflectance and hull quotient corrected spectra.

RESULTS AND CONCLUSIONS

The geology of the Sierra Inesperada is mostly composed of Paleocene volcanic rocks assigned to the Chile-Alemania Formation. Basal units are andesitic-dacitic porphyritic lava flows overlaid by a thick stratified pyroclastic sequence. The last includes several pyroclastic surge deposits intercalated with massive pumiceous ignimbrites and lenses of lithic-rich breccias with clasts that can reach up to 1 m diameter at the northern part of the hill. Fine grained lapilli size surge deposits show high flow regime structures such as cross- stratified stratification, antidunes, and ballistic impacts. These features accompanied with accretional lapilli and slumping structures are interpreted to be formed as a consequence of water-magma interaction (Páez *et al.*, 2015). At the northern side of the hill, two intrusive breccia bodies (Brecha Inesperada and Brecha Medialuna) were mapped. These are 1.5 to 0.5 km diameter outcrops composed of massive to stratified matrix supported breccias with polymictic porphyritic clasts of rounded to subangular shape up to ten meters diameter. The matrix is fine grained with cavities. The sequence is topped by a rhyodacitic flow dome cropped in the Cerro Chancho, in the southern Sierra Inesperada. Páez *et al.* (2015) interpreted that the pyroclastic sequence and the two intrusive bodies are part of a maar- diatreme volcanic edifice.

The geology of Sierra Inesperada is completed by small dioritic stocks of Eocene age intruding paleocene units and late olivine basaltic lava flows of the Catalina Formation (Espinoza *et al.*, 2011).

The Sierra Inesperada has prominent advance argillic alteration affecting the paleocene units, mapped as pervasive silicification blankets, quartz alunite + argillic zones which give place to an extensive lithocap of 1 km^2 (Figure 1). Pervasive silicification occurs in the south and eastern part of the hill typified by strong silica replacements

of volcanic rocks that preserve primary volcanic textures. NNO-trending silicified structures are preserved with locally residual quartz and vuggy silica textures. These structures locally host strongly silicified matrix supported breccias with fluidized matrix interpreted as phreatic breccias.

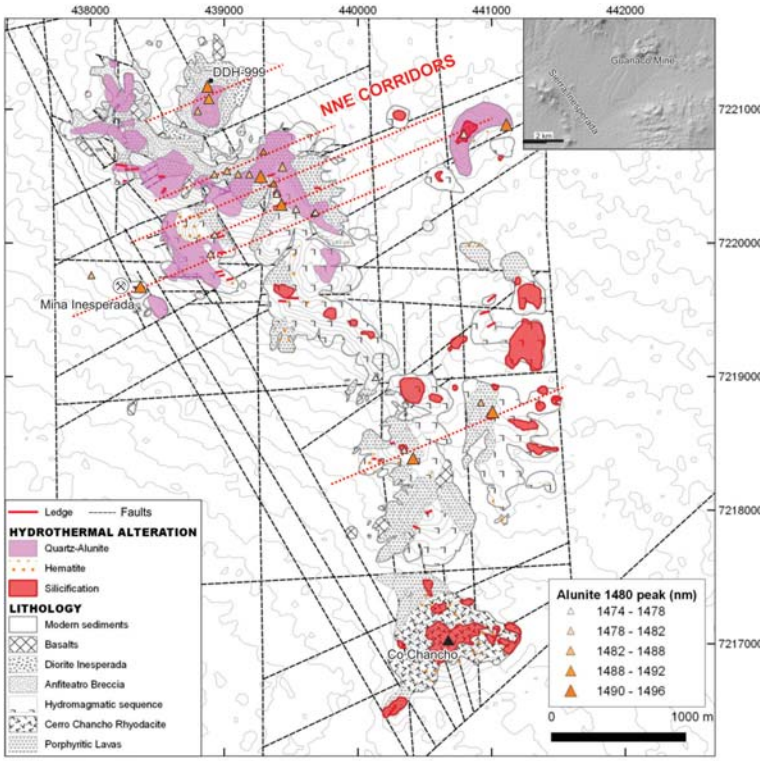

Figure 1– Geological and alteration map of the Sierra Inesperada with the alunite SWIR analyses.

LATE FAULTS ARE FILLED WITH SILICA AND HEMATITE

In the northern part of the Sierra Inesperada, volcanic units show a bleached appearance due to kaolinite, "limonite", goethite and a regular pattern of jarosite veinlets. Discontinuous outcrops of NNE trending silicified structures can be traced along 1 km length. These are composed of coarse grained alunite fillings with locally residual quartz, and vuggy silica textures and pyrite boxworks. Some structures are affected by late barite breccias and some of them contain Cu oxides. In the western portion of the hill, a vertical shaft is placed with significant dumps of the Mina Inesperada old gold mine. Sulphide-bearing (pyrite and enargite) breccias with intense altered porphyritic volcanic clasts are observed. Breccias with Cu oxide minerals (brochantite-atacamite) seems to be the main ore minerals for miners.

Results of collected samples for SWIR analyses drops alunite, jarosite, gypsum, kaolinite, goethite, dickite, pyrophyllite, siderite, illite-smectite and muscovite. In SWIR spectra, K-Na alunites have a strong absorption feature at about 1,480 nm wavelength. The position of this feature shifts related to the Na/(Na+K) ratio (Chang *et al.*, 2011). For the Sierra Inesperada alunite samples, the 1,480 peak reveals that the highest Na contents (~1,490-1,495) drop in the center-northern portion of the hill within quartz-alunite zone and related to NNE corridors. The sample from Mina Inesperada shielded the highest 1,499 value corresponding to calcic (huangite) alunite composition. This sample also registered pyrophyllite representing the highest temperature within NNE corridors. These corridors and corresponding cropping structures represent the conduits or feeder zones of the lithocap and display the same ENE-WSW orientation that mineralized structures in Guanaco Mine which makes them attractive for encouraging exploration.

REFERENCES

Chang, Z., Hedenquist, J.W., White, N.C., Cooke, D.R.., Roach, M., Deyell, C.L., Garcia, J., Gemmell, J.B., McKnight, S., Cuison, A.L., 2011. Exploration tools for linked porphyry and epithermal deposits: Example from the Mankayan intrusion-centered Cu-Au district Luzon, Philippines. Economic Geology 106: 1365-1398.

Espinoza, F., Matthews, S., Cornejo, P., Venegas, C., 2011. Carta Catalina, Región de Antofagasta. Servicio Nacional de Geología y Minería, Carta Geológica de Chile, Serie Geología Básica. 129 (63 p. Santiago).

Guido, D., Jovic, S., Galina, M., Peralta, C., Mendiz, C., Sastre, L., Kasaneva, S., 2014. Caracterización del depósito epitermal de alta sulfuración El Guanaco, Antofagasta, Chile. Actas Del XIX Congreso Geológico Argentino. Córdoba, Argentina. CD–ROM.

Páez, G., Permuy Vidal, C., Jovic, S., Guido, D., Osorio, J., Kasaneva, S., 2015. Depósitos hidromagmáticos en la Faja Paleocena de la Región de Antofagasta: Ejemplos del Distrito

Minero El Guanaco. XIV Congreso Geológico Chileno, Actas. Servicio Nacional de Geología y Minería, Chile, La Serena, Chile. CD–ROM.

Puig, A., Diaz, S., Cuitino, L., 1988. Sistemas hidrotermales asociados a calderas en el arco volcánico paleógeno de la region de Antofagasta, Chile: Distritos El Guanaco, Cachinal de La Sierra y El. Andean Geol. 15 (1), 57-82.

Sillitoe R.H., 1995. Exploration of porphyry copper lithocaps. AUSIMM Publication Series 9:527"532.

Sillitoe R.H., 2010. Porphyry copper systems. Economic Geology 105: 3-41.

GEOCHEMICAL STUDY ON EPITHERMAL GOLD MINERALIZATION OF SESAME VEIN, SANGILO MINE, BAGUIO MINERAL DISTRICT, PHILIPPINES

Kotaro Yonezu[1], Akira Imai, Jillian Aira S. Gabo-Ratio, Eric S. Andal

[1]*Kyushu University, Japan - yone@mine.kyushu-u.ac.jp*

BACKGROUND

The Baguio mineral district is a major gold copper mining area in the Philippines. The district is located in northern Luzon and about 200 km to the north of Manila. In terms of tectonic setting, two subduction zone surrounding Luzon island. Topography is high and rugged. The district comprises diverse deposit types: high to low sulfidation epithermal gold deposits, porphyry copper deposits and skarn gold/ base metal deposits. Especially, gold production is one of the most plentiful area in the Philippines. For example, Acupan mine had been mined more than 200 tonnes of gold from at least 40 individual narrow epithermal gold veins and splays. In this research, samples were collected from Sesame quartz vein in Sangilo mine. Sangilo mine is located at vicinity of Acupan mine. In addition, some quartz veins such as Sesame vein and Taka Barr vein are running in both mines. Acupan mine has been well studied about geology, mineralization, alteration and thermochemical environment. However, Sangilo mine has been limited study about these. Therefore, the objective of this study is to characterize geochemical environment based on ore mineralogy. In addition, comparison of geochemical environment between Sangilo mine and Acupan mine was also conducted.

METHODS

Methods are composed of ore mineral observation, gangue mineral observation, alteration mineral observation and SEM-EDS analysis. These methods were conducted for quartz vein samples and adjacent host rock at two locations of Sesame quartz vein: underground face and outcrop. At first, underground samples and outcrop samples were divided into parts based on megascopic characteristics. Ore mineral and gangue mineral were observed to clarify spatial relationship to gold mineral. Moreover, ore mineral and gangue mineral in barren zone were also confirmed to emphasis difference between gold mineralized zone and not. Alteration mineral was analyzed to infer hydrothermal fluid condition which caused hydrothermal alteration of host rock. Sphalerite and Electrum were analyzed to decide FeS (mol%) and Ag/(Ag+Au) (at%). These parameters were used to deduce sulfur fugacity and temperature of gold mineralized zone.

RESULTS

Samples were collected from two locations of Sesame quartz vein having orientation of N37oE and dipping 68oSE: underground face and outcrop. The vein was hosted by Dark diorite (hornblende diorite) in Sangilo mine and Virac Granodiorite in Acupan mine. Structure of Sesame quartz vein is massive vein having 3.35 m at underground face. Vein material are composed of quartz zone, fault gouge zone and clay zone. Alteration mineral of dark diorite are chlorite and illite. Quartz color have white, light gray and gray. Quartz contain variable ratio of breccia of dark diorite. Quartz texture are composed of colloform, comb, mosaic, feather, flamboyant and bladed texture. Grain size of quartz zone also have variety. Sesame vein was divided into thirteen parts from V1 to V13 in underground face and five parts from OV1 to OV5 in outcrop samples based on megascopic characteristics. Gold mineralized zones were confirmed two parts of quartz zones: V2 and V11 in underground and three parts of quartz zones: OV2, OV4 and OV5 in outcrop. As a result of ore mineral observation, typical mineral assemblage was confirmed for each auriferous zone. Electrum was only observed as gold mineral. In V2, electrum was confirmed in dark diorite breccia and associated with pyrite although occurrence of gold is relatively rare among auriferous parts. In V11, electrum was confirmed in dark quartz and associated with pyrite, arsenopyrite, marcasite and covellite. In OV2, electrum was confirmed in white quartz zone and associated with pyrite, chalcopyrite, marcasite, sphalerite, galena and acanthite. In OV4, electrum was confirmed in white quartz zone and associated with pyrite, sphalerite and galena. In OV5, Electrum was confirmed in calcite zone and associated with pyrite and galena. Result of gangue mineral observation also indicates distinct characteristics of gangue mineral. In V11, quartz grains were classified into two zones: fine- grained and coarse-grained quartz zone based on grain size. Electrum exist in fine-grained quartz zone. In OV4 quartz grains were classified into three zones: fine-grained, middle- grained and coarse-grained quartz zone. Electrum exist in coarse-grained quartz zone. Previous study shows Au-Ag ratio and mole percent FeS of Sphalerite are variable depending on the environment of formation. Based on these previous researches, sulfur fugacity and temperature were deduced in V11 and OV4. Selection of these two zones are because of relatively higher abundance

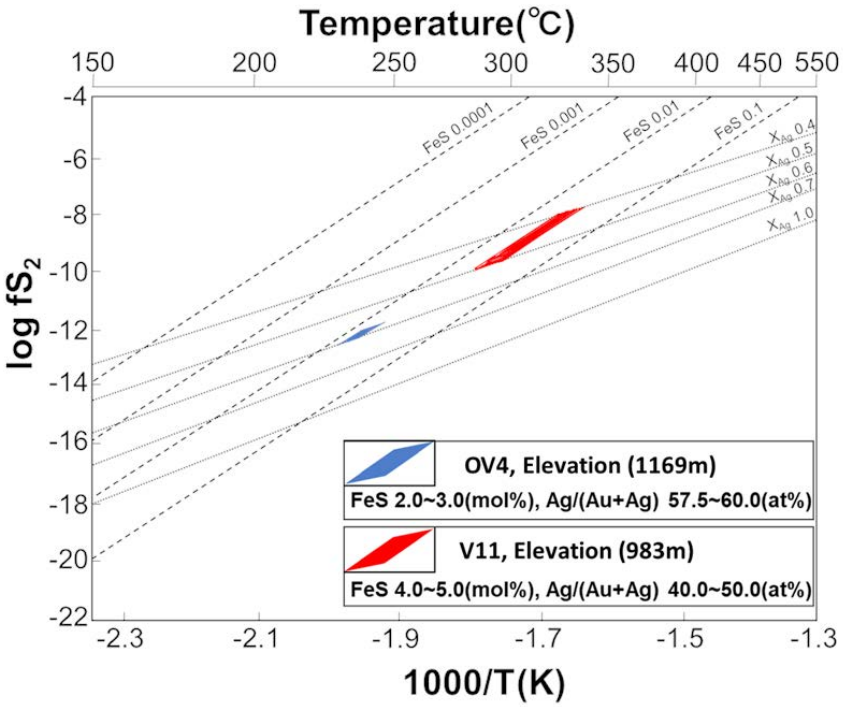

of electrum and sphalerite. These dedications show difference of temperature and sulfur fugacity in V11 and OV4. Based on result of observation and analysis, three different hydrothermal activities cause different occurrence of gold mineral. According to previous research of mineral observation in Acupan mine, auriferous veins were classified into three stages: Stage III, Stage IVa and Stage IVb. These three stages have similar characteristics with gold mineralizaed zone classification of this research with regards to mineral occurrence and temperature range.

CONCLUSIONS

This research clarified three different gold occurrences based on result of mineral observation and mineral composition analysis. These data have similarity to classification of previous research on adjacent mine. Three different hydrothermal activity might form each auriferous vein with different physicochemical properties.

MESOTHERMAL TO EPITHERMAL MINERALIZATION VEIN SYSTEM AT THE MARMATO GOLD DEPOSIT, COLOMBIA

Leonardo Santacruz Reyes[1], Stewart Redwood, Massimo Matteini, Nilson Botelho, Alessandro Cecchi, Julian Ceballos, Juan Carlos Molano

[1]*Geologist, National University of Colombia, Bogotá*

The Marmato epithermal to mesothermal vein gold deposit is located in the late Miocene Middle Cauca Gold Belt in the Western Cordillera of the northern Andes. Exploration work by Gran Colombia Gold Corp. has defined total underground resources in the Upper and Deeps Zones in the measured, indicated and inferred categories (NI 43-101) of 93.2 Mt containing 8.1 Moz Au and 37.6 Moz Ag. Past production is estimated to have been between 1.9 and 2.4 Moz Au over two and a half millennia. Underground mining is currently carried out by Mineros Nacionales S.A., a subsidiary of Gran Colombia Gold Corp., which produced 25,162 oz. of gold in 2017, and by artisanal miners.

Mineralization is hosted almost entirely by the Marmato Porphyry which comprises intrusions P1 to P5 formed by hornblende-bearing dacitic to andesitic hypabyssal porphyry intrusions, with ilmenite and minor magnetite and an adakite-like signature, and the Arquía Complex of graphitic and minor chlorite schists of probable Late Jurassic to Cretaceous age. The porphyry intrusions have been dated between 6.576 ± 0.075 Ma and 5.75 ± 0.11 Ma by LA-ICP-MS 206Pb/238U zircon. The age of mineralization was determined by 40Ar/39Ar analyses of adularia in an epithermal vein and a mesothermal veinlet which indicates plateau ages between 6.95 ± 0.02 Ma to 5.96 ± 0.02 Ma, closely related to the magmatism.

The Marmato gold deposit comprises an epithermal system hosted by R-type and R'-type shears, located in the Upper Zone (1,600 to 1,000 mamsl) (Figure 1), associated with illite- smectite and kaolinite alteration and sulfide-rich veins with pyrite, arsenopyrite, marmatite (Fe-rich sphalerite), galena, silver sulfosalts and electrum. Sulfur isotopes indicate sulfur of magmatic origin and a sulfur fugacity between -9.2 to -11 log fS2 is shown by sphalerite analyses. A mesothermal quartz veinlet system hosted by T-type fractures occurs in the Deeps Zone (1,000 to <200 mamsl) (Figure 1), with inferred and indicated resources of 30.2 Mt containing 2.20 Moz Au and 2.9 Moz Ag, which is associated with biotite and albite- muscovite-sericite alteration, and quartz veinlets with pyrrhotite,

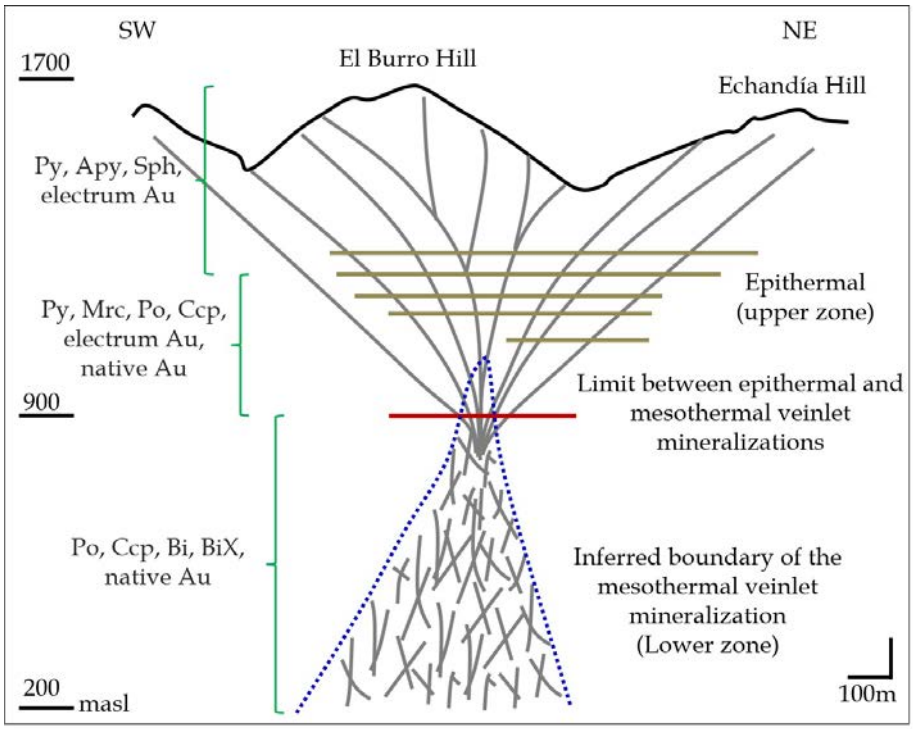

Figure 1 Schematic cross section of the Marmato deposit (modified from Gran Colombia Gold Corp.) showing the two principal zones. The Upper Zone is characterized by epithermal sulfide veins and the Deeps (Lower) Zone with mesothermal veinlets, each with 700 meters of vertical extension. The sulfides are zoned from the Upper to the Lower Zone accompanied by an increase in the fineness of gold. Horizonal lines in the Upper Zone show the mine levels for gold extraction by Mineros Nacionales. Abbreviations: Py - Pyrite; Ccp - Chalcopyrite; Po - Pyrrhotite; Apy - Arsenopyrite; Sph - Sphalerite (Marmatite); Mrc - Marcasite; Bi - Bismuth; BiX - Bismuth minerals; Au - Gold.

chalcopyrite, bismuth and native gold. Alteration is superimposed on pervasive epidote-chlorite-carbonate alteration in the Upper Zone and biotite alteration in the Deeps Zone. Analyses of fluid inclusions in quartz related to gold mineralization show that homogenization temperatures and salinity vary from the top to the bottom of the system from 305.4°C to 395.4°C and 4.96 to 11.93 wt%-NaCleq., respectively. Eutectic temperatures indicate a mineralizing fluid with a H_2O–NaCl chemistry. Quartz is strongly zoned in the veinlets and veins and exhibits zones of amorphous silica in the epithermal zone indicating high fluid flows and rapid variations in the fluid conditions.

Mineralization at the Marmato gold deposit is structurally controlled and potentially influenced by the presence of graphitic schists, which are a good source of bismuth and could also reduce the mineralizing fluids in the mesothermal Deeps Zone, where pyrrhotite is dominant. Mineralization formed at temperatures of approximately 400°C to 300°C and, along with the Riedel structural control, lithological influence, mineralogy and fluid properties, generated a favorable setting for the occurrence of the "liquid bismuth collector model" and the generation of a vertical continuity and zonation of >1,400 meters. We propose that the interaction of these factors generated a distinctive deposit model that could be termed "Marmato Type", and that other similar deposits may occur within the late Miocene arc of the northern Andes.

FLUID CHARACTERISTICS AND EVOLUTION OF THE DETACHMENT-HOSTED EPITHERMAL Au-Ag-Pb-Zn-Cu DEPOSIT BANSKÁ HODRUŠA, SLOVAKIA

Alexander Kubač[1], Peter Koděra, Peter Uhlík, Rastislav Vojtko, Martín Chovan, Jaroslav Lexa, Anthony E. Fallick

[1]*Department of Economic Geology, Faculty of Natural Sciences, Comenius University in Bratislava, Slovakia*

alexander.kubac@gmail.com

INTRODUCTION

The Banská Hodruša intermediate-sulfidation Au-Ag±Pb-Zn-Cu deposit at the Rozália mine represents an unusual subhorizontal multi-stage vein system, hosted by a low-angle normal fault zone (LANF). The deposit is hosted by the central zone of the Middle Miocene Štiavnica Stratovolcano in the Central Slovakia Volcanic field, located on the inner side of the Carpathian arc. The stratovolcano includes an extensive caldera, a late stage resurgent horst in the caldera centre and an extensive subvolcanic intrusive complex. The eastern part of the deposit is currently mined and recently it was characterised in terms of mineralogy (Kuba *et al.*, 2018). This contribution ties up on this work with data on genesis of the deposit, including an evaluation of the likely sources and nature of the mineralizing fluids.

THE BANSKÁ HODRUŠA DEPOSIT

The epithermal gold vein system at the Rozália mine occurs in 400–650 m depth, hosted by pre-caldera andesite, near to the flat roof of a pre-mineralization subvolcanic granodiorite pluton. The shear zone (LANF), hosting the subhorizontal vein system, is related to processes of underground cauldron subsidence and exhumation of the subvolcanic granodiorite pluton, probably accompanied by a sector collapse of the hosting stratovolcano. The veins are dismembered by a set of quartz-diorite porphyry sills and later steeply-dipping mineralized faults of the resurgent horst. The ore deposit consists of two parts, separated by a thick sill of quartz-diorite porphyry.

The epithermal vein mineralization originated during several stages. The Stage 1 is related to hydraulic fracturing along subhorizontal structures resulting from vertically-oriented extension and corresponds to the origin of low-grade silicified hydrothermal breccia at the base of the deposit. The major productive Stage 2 is related to the early evolution of the LANF with southward movement of the downthrown block and represented by a stockwork of steep veins with rhodonite-rhodochrosite (Stage 2a) and quartz-sulphide-carbonate (Stage 2b) assemblages with sphalerite, galena, chalcopyrite, pyrite, gold, rare hessite, petzite. Locally, they are accompanied by quartz-gold veins resulting from complementary sinistral strike-slip movements (Stage 2c). Stage 3 is related to a renewed motion of the downthrown block towards SE, represented by thin quartz-gold veins located on tension cracks inside the shear zone (Stage 3a), and complementary detachment hosted quartz-base metals-gold veins (Stage 3b). Stage 4 includes rare barren post-ore quartz veins. The ore mineralization is accompanied by strong adularization, silicification and illite, that dominates along the upper plane of the shear zone.

METHODS

Representative samples from the recent mining works of the Rozália mine were studied by fluid inclusion microthermometry and stable isotope analyses. The $^{18}O/^{16}O$ and $^{13}C/^{12}C$ isotopic compositions were analysed at SUERC (Glasgow, UK), D/H at the Earth Sciences Institute of SAS in Banská Bystrica (Slovakia). The XRD analyses of clay fraction were used to estimate the illite crystallinity (Kubler index) and illite crystallization temperatures (Ji and Browne, 2000). For interpretations, fluid inclusion and stable isotope data from the western part of the deposit were also used (Kodra *et al.*, 2005).

FLUID INCLUSIONS

According to fluid inclusion microthermometry, quartz, sphalerite and carbonates crystallized from fluids of low salinity (~1–4 wt% NaCl eq.) and moderate temperatures (~250–310°C) that have experienced an extensive boiling. This temperature range corresponds well to temperatures of illite crystallization from the vicinity of most of the veins (270–290°C). However, data from sphalerite show apparently lower mean homogenization temperatures (Th) than quartz (~250–280°C vs. ~270–310°C), but salinity is similar, so the changes in temperature are probably invoked by boiling which is an endothermic process. Sometimes carbonates from various stages show lower Th values. No apparent differences occur between data from both parts of the deposit, neither individual stages except of Stage 1 silicified hydrothermal breccias which show slightly higher temperatures. The highest fluid pressure was determined for Stage 1 inclusions (~85 bars), while the Stage 2 and Stage 3 inclusions showed very variable pressure

estimates (45–80 bars). Highest pressure corresponds to initial opening of host fractures, when the hydrothermal system was governed by suprahydrostatic conditions, probably with a lack of connection to the surface. The probable paleodepth (~550 m) can be derived from the lowest pressure value (47 bar).

STABLE ISOTOPES

Oxygen isotope data from vein quartz, carbonates and illites associated with gold mineralization show that the source fluid was isotopically homogeneous for all stages of veins and both parts of the deposit. There is a little variation in $^{18}O_{fluid}$ values (mostly -2 to 1 ‰), and in illite crystallinity (0.4 to 0.6), except of Stage 1 silicified hydrothermal breccias and associated illites that are isotopically slightly heavier. Carbonates showed slightly lower $^{18}O_{fluid}$ values (-1.9 to -2.7 ‰), indicating more meteoric component in the fluid. Isotopically homogeneous fluid indicates a deep-convecting source of meteoric fluids that mixed with magmatic fluids during their ascent from the source magma chamber.

Isotopic composition of fluids in equilibrium with alteration minerals of the disseminated- stockwork base metal mineralization show an apparent mixing trend, related to a relatively shallow convection of meteoric water in the vicinity of the apical part of the granodiorite pluton. The mixing trend points to a similar meteoric water isotopic composition as the epithermal gold vein system. This indicates that there was no time to significantly change the isotopic composition of meteoric water by changes in climate, which is consistent with the assumed quick exhumation of the pluton, followed by granodiorite unroofing and detachment shear zone evolution hosting the Au-Ag veins.

Interestingly, the oxygen isotope and illite crystallinity data from clays from the roof of the gold deposit are nearly constant, which indicates that there was no apparent thermal gradient along the upper plane of the shear zone. The large-scale alteration here probably results from condensation of vapour escaping from boiling fluids migrating within the shear zone. This horizon worked as a collector of hydrothermal fluids flowing along the shear zone (and producing the Stage 3 veins), as well as a collector of vapor escaping from boiling fluids in the entire thickness of the shear zone. Thus, this horizon is quite important for future exploration as it marks areas with extensive boiling (and possibly associated gold mineralization) in the footwall of the horizon.

CONCLUSIONS

Fluid inclusion and stable isotope data from the Banská Hodruša deposit show that the palaeofluids were of low salinity and moderate temperature in both parts of the deposit. Variable pressures determined from boiling fluid inclusion assemblages indicate suprahydrostatic conditions with local decompression in dilatational structures. Opening of dilatational structures enabled an active suction of fluids and their boiling resulting in precipitation of gold. Isotopically homogeneous fluid indicates the presence of a deep- convecting source of meteoric fluids that mixed with magmatic fluids during their ascent from the subvolcanic magma chamber.

REFERENCES

Kodra P., Lexa J., Rankin A.H., 2005. Epithermal gold veins in a caldera setting: Banská Hodruša, Slovakia. Miner Deposita 39:921–943

Kuba A., Chovan M., Kodra P., Kyle J.R., •itHan P., Lexa J., Vojtko R., 2018. Mineralogy of the epithermal precious and base metal deposit Banská Hodruša at the Rozália mine (Slovakia). Miner Petrol (in press).

Ji J., Browne P.R.L., 2000. Relationship between illite crystallinity and temperature in active geothermal systems of New Zealand. Clays Clay Miner 48: 139–144.

Support by grants APVV-15-0083 and VEGA-1/0560/15 is acknowledged.

NEW EXPLORATION MODELS FOR LOW SULFIDATION EPITHERMAL Au-Ag DEPOSITS: A NEW ZEALAND PERSPECTIVE

Anthony B. Christie[1], Mark P. Simpson

[1]*GNS Science - t.christie@gns.cri.nz*

INTRODUCTION

Low sulfidation epithermal Au-Ag deposits of the Hauraki Goldfield produced >7 Moz Au between 1861 and 1952 from ~50 quartz vein deposits associated with Miocene-Pliocene volcanism. Exploration from the 1970s led to new Au-Ag mining beginning at Martha, and later at Favona, Trio and Corenso (all at Waihi), and at Golden Cross and Broken Hills, that combined, have produced ~3.7 Moz Au since 1988. The proximity of geothermal systems in the nearby Taupo Volcanic Zone, where Au-Ag is being deposited, has helped develop local process-based exploration models from existing international descriptive epithermal models. These, together with the cumulative exploration and research information developed from the 1980's has led to a better understanding of the characteristics of the deposits and improved exploration models.

REGIONAL AND DISTRICT SCALES

From the 1970s, area selection at regional and district scales was assisted by aeromagnetic surveys and stream sediment geochemical surveys. The magnetic surveys highlighted areas of potential hydrothermal alteration in the volcanic rocks by magnetic "lows" resulting from demagnetisation due to the replacement of magnetite by pyrite. The stream sediment surveys provided geochemical anomalies of pathfinder elements for follow-up exploration. This work, together with regional mapping, identified several structurally controlled corridors of hydrothermal alteration and mineral deposits. In the 1990s, the availability of the geological, geochemical and geophysical data in digital form, enabled GIS, and later GIS-based prospectivity analysis, to highlight target areas. Useful data themes have included: host rock lithology and age, lineaments identified in digital elevation models and satellite imagery, anomalies in aeromagnetic, electromagnetic and gravity geophysical data, distribution of known mineral deposits, mapped areas of hydrothermal alteration, and stream sediment and rock geochemical anomalies.

From the late 2000s, more detailed ground based gravity surveys and helicopter-borne EM surveys were used in the southern part of the goldfield to assist targeting on a district scale using an exploration target model of magnetic lows, gravity highs and linear resistive zones. Recent research on structural controls on the localisation of known deposits has highlighted the importance of deep regional structure in the Mesozoic basement greywacke rocks underlying the Tertiary volcanic rocks. Radiometric dating of many of the deposits has shown that the northern deposits were formed during an extended period between ca. 16 and 10 Ma, in contrast to the southern deposits, which mostly formed over a short period between ca. 7 and 6 Ma, suggesting a fundamental difference in tectonic control on deposit formation between the two areas.

Until recently, andesitic and dacitic stratigraphic units have been considered more prospective for hosting large gold deposits than rhyolitic units in the Hauraki Goldfield. This was based on empirical evidence that most of the historic gold production was for veins hosted in andesite and dacite, with generally small production from deposits hosted in rhyolitic rocks. Initial exploration at the rhyolite-hosted Wharekirauponga deposit confirmed this general observation, with gold present in thin sheeted and stockwork quartz veins. However, recent drilling has intersected some much wider and continuous mineralised veins, more typical of the larger andesite hosted deposits, thus providing a new exploration target type for the goldfield and increasing the area of prospective ground in the region.

DEPOSIT SCALE

During the 1980s and 1990s, in addition to the standard geological logging and assays, many diamond drilling programmes included petrographic and XRD analyses of the hydrothermally altered rocks, as well as fluid inclusion homogenisation temperature measurements of quartz veins. These additional parameters were to identify spatial trends in the paleotemperature of the former hydrothermal fluid potentially enabling modelling of the epithermal system architecture and vectoring to zones of mineralization. Based on research of the geothermal systems, the main hydrothermal mineral indicators sought were the clay mineral sequence of smectite, interlayered illite/smectite and illite, corresponding to increasing temperature. Also sought were the occurrence of adularia as an indicator of high permeability, and the occurrence of bladed calcite or quartz pseudomorphed bladed calcite in veins as indicators of boiling of the fluid. The occurrence of vapour rich and vapour filled fluid inclusions were also used as evidence of

boiling. Boiling is significant because it is a very efficient mechanism for depositing gold from the hydrothermal fluid. Multiple hydrothermal events indicated by vein textures such as multi-banded veins and multiple brecciation events (especially breccias containing clasts of mineralised breccia) were considered good signs for potential gold deposition in the hydrothermal system. Because of their cost, routine fluid inclusion analyses went out of favour in exploration in the 1990s but have continued to be used in research, particularly for providing paleodepth information for deposits. From the 2000s, short wave infrared reflectance spectral analyses (SWIR, e.g. PIMA and TerraSpec) have generally been adopted as an alternative to XRD analyses because of their lower cost, enabling a much larger number of drill core analysis points down a drill hole. Researchers have continued using XRD analyses to calibrate the SWIR analyses. From the mid-2010s, portable XRF geochemical analyses have increasingly been applied to complement traditional assay and ICP-MS multi-element geochemical analyses, especially for analyses of drill core. Geochemical proxies for adularia and illite are used to identify hydrothermal alteration trends, to vector to mineralization.

The discovery of the Favona vein system at Waihi in 2000, and subsequent extensive drilling and underground mining of the deposit has shown that it has a classic epithermal model profile with a major thick vein fanning or horsetail-branching upward. Some of the branch veins further split into smaller veins, most eventually pinching out near the top of the system. A large upward-opening cone of hydrothermal breccia is present in the upper 100 m of the deposit, and silica blanket and sinter deposits have recently been recognised in the upper part. Future research on the structural architecture, and vein and breccia textures at Favona is likely to provide valuable information on features that will be useful for calibrating paleodepth and mineral potential of other deposits. This is particularly important in the Hauraki Goldfield because many prospects were explored in the 1980s and early 1990s as open-pit, low grade, high tonnage targets and drilled only to shallow depths (~150 m). Mining at Waihi and Golden Cross shows potential for mineralization to extend to much deeper levels. Therefore, many of the previously drilled deposits should be re-evaluated with the new information and drilled to greater depth.

CONCLUSIONS

Exploration of Taupo Volcanic Zone geothermal systems for hot water, provided information from the 1970s to develop process-based exploration models for epithermal gold mineralization of the Hauraki Goldfield. More than 40 years of modern gold exploration and 29 years of mining in the goldfield has provided a wealth of new information in the form of geochemical and geophysical exploration data, drill core and underground exposures available for research. This has enabled the development of new exploration concepts and models. Particularly significant for future exploration of the Hauraki Goldfield is the recognition of the potential for larger producing rhyolite-hosted deposits. Furthermore, there is potential for significant veins at depth beneath areas only shallowly drilled and abandoned as open pit targets in the 1980s and early 1990s. These deposits require deeper drilling to investigate their potential as underground mining targets. This exploration should utilise the new geochemical, mineralogical and descriptive tools to vector to mineralization.

HIGH-GRADE EPITHERMAL GOLD MINERALIZATION AT DVOINOYE, CHUKOTKA, RUSSIAN FEDERATION

Andreas Dietrich[1], Carlos Tellez, Brian Thomson, Vyacheslav Akinin, Jeff Benowitz, Paul W Layer.

[1]*Dietrich Consulting E.I.R.L.,LLC Northern Gold, Anadyr, Chukotka AO, Russian Federation - an_dietrich@yahoo.com*

INTRODUCTION

The Dvoinoye district is located in the Chukotka Autonomous Okrug in far eastern Russia, north of the Arctic Circle. The epithermal "Zone 37" vein is the largest deposit in the district. High grade Au-Ag vein mineralization was initially mined in the period 1996 to 2007 via small pits.Underground development of the Zone 37 vein started in 2011, with production from 2013. The small "September" vein and breccia orebody, located 15 km northwest of Zone 37, was mined as open pits in 2017. The paper presents results of exploration work including geological mapping, ore petrography, and geochronological data, to showcase this emerging epithermal vein district.

GEOLOGICAL SETTING

The Dvoinoye district is located in the Tytylveem volcanic belt, a remnant of Lower Cretaceous (Aptian) volcanism overlying deformed Triassic passive margin sedimentary rocks of the Arctic Alaska – Chukotka terrain, and in turn overlain to the east by the much more extensive Albian to Campanian Okhotsk-Chukotka Volcanic Belt (e.g. Akinin & Miller 2011, Goryachev & Yakubchuk 2008, Nokleberg et al 2000, Sidorov *et al.* 2009, Tikhomirov et al, 2012, Yabuchuk 2009).

The volcanic sequence of the Dvoinoye district starts with dacitic to rhyolitic ignimbrites of the Pycheveemskaya suite that are followed by volcanic and epiclastic rocks of the Tytylveem suite. The lower Tytylveem Formation is an intercalation of andesitic lava flows, hyaloclastites, peperites and subaqueous mass flow deposits. It is followed by the middle Tytylveem Fm. of felsic pyroclastic horizons including ignimbrites, tuffs, and epiclastic deposits. Local fault-controlled basins deposited thick (>1,000m) sequences of epiclastic agglomerates, conglomerates and sandstones of volcanic provenance. The upper Tytylveem Formation comprises massive andesite lava flows and agglomerates.

STRUCTURE

The main regional structures strike north-northeast, manifested in a series of valleys with strike lengths of up to tens of kilometres. Vein mineralization and the development of breccia corridors is preferentially controlled by trans-tensional jogs and splays along these north-northeast-striking fault systems. Locally observed left-stepping jogs and low angle slickenline rakes indicate sinistral strike-slip component. Late normal faulting and listric fault geometries result in a 25° rotation of tectonic blocks of the formerly subhorizontal stratigraphic sequence during regional extension.

A less prominent set of north-northwest-striking faults (N150°-160°E,dips 70°-80°NE) also controlled mineralization and the emplacement of dikes and breccias. The north-northwest and north-northeast striking faults enclose an inter-plane angle of ~60° and can be interpreted as a conjugate shear pair that formed in a N-S oriented stress field (ì1~N000°E).

A roughly orthogonal set of structures of north-northeast- (N010°-020°E) and SE- strike(N110°-135°E) controlled the emplacement of a granitoid intrusive complex.

MAGMATISM

Early subvolcanic units intruded only the lower Tytylveem Fm. Local clusters of andesite- diorite stocks are associated with halos of disseminated pyrrhotite-pyrite and sub-economic Cu-Au anomalies. A thick dacite porphyry unit (U-Pb Zircon 120.4 ± 1.0 Ma), interpreted as a cryptodome, partially hosts the Zone 37 vein and is in turn cut by a series of rhyolite sills (U-Pb Zircon 118 ± 3Ma) and a rhyolite dike (U-Pb Zircon 118.0 ± 1.2Ma). A different group of flow-banded rhyolite flow-dome complexes intruded the lower and middle Tytylveem Fm.

A later generation of chiefly granitoid plutons and related subvolcanics intruded the entire stratigraphic sequence including the upper Tytylveem Fm. The emplacement of this intrusive complex is represented by a U-Pb zircon age of a rhyolite dated at 94.0 ± 0.1Ma. Granite intrusions cross-cut epithermal vein mineralization.

MINERALIZATION

The epithermal Zone 37 vein developed along a north-northeast-striking fault and has a strike length of 800m with widths reaching 35m. The ore shoot has a slightly southwest- plunging, well defined top, and is mineralized over a vertical interval of up to 250m. It is characterized by colloform to crustiform banded quartz-chalcedony-adularia with

millimeter-wide bands of sulphosalts-sulphides and native gold or gold-rich electrum (Ag:Au of 1). Towards lower levels mineralization passes into crustiform banded coarse quartz with spotty bands of pyrite-galena-chalcopyrite-sphalerite (Ag:Au of 5-10). Adularia gangue from the vein is dated with 117.1 ± 3.9Ma (40Ar/39Ar plateau age), whereas another set of adularia samples returned ages of 97.4 ± 1.8Ma and 91.0 ± 1.4Ma (40Ar/39Ar plateau age).

At Zone 1, sets of up to 2m wide veins and vein breccias developed along a north-northwest- striking corridor over a total structural width of up to 20m. Mineralization comprises massive to vaguely banded coarse white quartz with early K-feldspar. An early phase of semi-massive to spotty banded Pb-, Zn- and Cu-sulphides is associated with chlorite, hypogene hematite and high gold grades with visible gold mineralization.

The September Northeast deposit is located 15 km west-northwest of Dvoinoye Zone 37. The system developed along a prominent north-northeast-striking structural corridor that has controlled rhyolite dikes, as well as phreato-magmatic to phreatic breccia bodies. Mineralization consists of a set of sheeted vein lenses and veinlet stockwork with polymetallic (galena, sphalerite, chalcopyrite) sulphide and Ag-sulphosalt (freibergite) mineralization. Gangue mineralogy and textures comprise fine-grained quartz with sulfide bands, occasionally with cockade ore ring textures, as well as coarse crystalline quartz ±adularia-carbonate-chlorite gangue. Exceptionally high gold grades are associated with telluride mineralization plus native gold. Ore petrography identified hessite (Ag_2Te), altaite (PbTe), in paragenesis with chalcopyrite, accessory galena, pyrite, chalcocite, and traces of sphalerite, arsenopyrite, and acanthite (Ag_2S). Vein mineralization is disrupted by rhyolite dikes, phreatomagmatic breccias with juvenile rhyolite clasts and by phreatic breccias. Some breccias carry high amounts of mineralised vein clasts in a milled rock-flour matrix with abundant sulphide fragments (pyrite, galena, sphalerite, local tellurides). It remains unclear if the vein matrix was mineralized by hydrothermal fluids or if sulphide (and Au) mineralization was inherited from milled mineralized wall rock.

The Ilirney intrusive complex developed geochemical halos with systematic anomalies in B- Bi-Sn-W, Cu-Pb-Zn, As-Sb and local Te. Mesothermal gold-base metal mineralization with spotty high-grade Au-Ag-As-Sb anomalies occurs disseminated, in veinlet stockworks, or in generally narrow and short vein lenses of coarse quartz±orthoclase around the cupolas of individual intrusions.

DISCUSSION

We suggest that magmatism and mineralization of the Dvoinoye district reflect an evolving magmatic arc environment. Lower Tytylveem magmatism, with partially subaqueous andesitic volcanism together with andesitic-dioritic stocks suggests an early island arc setting that evolved into a terrestrial volcanic arc until the middle Tytylveem Fm.. Epithermal mineralization appears to have been intimately related to shallow subvolcanic magmatism with dacite domes, rhyolite sill and dikes. The later emplacement of a batholitic intrusive complex demonstrates a burial of the stratigraphic sequence to deeper erosion levels. The granitoid intrusions cross-cut epithermal vein mineralization and generate their own geochemical anomalies with local mesothermal mineralization. The thermal event of batholitic emplacement around 94Ma may have reset the 40Ar/39Ar ages of epithermal adularia gangue.

A recurrent discussion during exploration of the district was the co-existence of epithermal mineralization, granitoid plutons, and mineralization styles that are more typical of deeper intrusion-related environments. Mapping of cross-cutting relationships together with geochronology indicate evolution from shallow subvolcanic-epithermal conditions to a deeper plutonic environment. The co-existence of epithermal and mesothermal mineralization does not indicate contemporaneity but rather is a result of overprinting. Pulses of late mesothermal mineralization might have locally overprinted and added to pre- existent epithermal mineralization.

REFERENCES

Akinin, VV and Miller, EL., 2011. Evolution of calc-alkaline magmas of the Okhotsk-Chukchi volcanic belt. - Petrology 19-3: 237-277

Goryachev, N and Yakubchuk, A., 2008. Gold deposits of Magadan Region, Northeast Russia: Yesterday, today, and tomorrow. SEG Newsletter 74

Nokleberg, W.J., Parfenov, L.M., Monger, J.W.H., Norton, I.O., Khanchuk, A.I., Stone, D.B., Scotese, R.C., Scholl, D.W., Fujita, K., 2000. Phanerozoic tectonic evolution of the Circum-North Pacific. USGS Professional Paper 1626, 133p

Sidorov, A.A., Belyi, V.F., Volkov, A.V., Savva, N.E. Kolova, E.E., 2009. Gold-silver deposits and ore assemblages of the Okhotsk-Chukchi volcanic belt. Doklady Earth Sciences Vol 427A, No 6, p 950-955

Tikhomirov, P.L., Kalininina, E.A., Monguti, T., Makishima, A., Kobayayashi, K., Cherepanova, I.Y., Nakamura, E.,2012. The Cretaceous Okhotsk–Chukotka Volcanic Belt (NE Russia): Geology, geochronology, magma output rates, and implications on the genesis of silicic LIPs. J Volcanology Geothermal Research 221-222: 14-32

Yabubchuk, A.S., 2009. Revised Mesozoic-Cenozoic orogenic architecture and gold metallogeny in the northern Circum-

INFLUENCE OF STRUCTURAL AND LITHOLOGICAL CONTROLS IN ORE-SHOOTS FORMATION AND MORPHOLOGY FROM JULIETA VEIN, CASPOSO DISTRICT, CORDILLERA FRONTAL, SAN JUAN, ARGENTINA

Sebastian Jovic[1], Diego Palma, Conrado Permuy Vidal, Luciano Lopéz, Diego Guido, Mariano Mongan, GustavoSotarello

[1]*CONICET - Austral Gold Argentina - s.jovic@fcnym.unlp.edu.ar*

The Casposo district is located in the Cordillera Frontal, in the centre-west of the San Juan province, Argentina (Fig. 1a). It is characterized by the presence of low sulfidation epithermal veins, hosted in volcanic rocks of the Choiyoi Group (Sotarello *et al.* 2002). The structural trend that controls the Au-Ag mineralization has a main NW-SE direction, with Kamila and Mercado as the main mineralized sectors (mined by open pits, and actually by underground mining). In Kamila sector, 3 structures with different orientations were recognized, 2 subparallel structures, Inca and B-vein with a NW-SE orientation and a SW dip, and Aztec vein with N-S orientation and W dip, between B-vein and Inca, developing a dextral jog. Julieta is one of the most important targets of Casposo district and will be in production at the end of 2018. The vein is located 5 kilometres to the NW of the operations zone (Kamila/Mercado), within the same NW regional structural corridor (Fig. 1b). The target was discovered by Intrepid Minerals in 2005 and explored by Troy Resources until 2013. Austral Gold resumed exploration of the target since the end of 2016 until the middle of 2017, performing tasks of geological mapping, mineralization mapping, surface sampling, logging of drill survey. The mineralization is hosted within volcanic rocks composed of two thick crystaloclastic ignimbrite sequences with andesitic (lower section) to dacitic (upper section) compositions, intruded by a series of pre- and post-mineralization subvolcanic intrusions including dykes, and cryptodomes.

Julieta vein is composed of carbonate and quartz with banded and brecciated textures, which participate in the filling of the vein in different proportions. Nine pulses of mineralization are summarized in 4 events: a barren initial carbonate hydrothermal event, a siliceous hydrothermal event that provides Au and Ag to the system, a new barren carbonate hydrothermal event, and a final tectonic-hydrothermal event that remobilized metals (Palma *et al.* 2017).

Julieta has an extension of approximately 1 km, an average width of 1.7 m, reaching up to 4 m maximum thickness. The vein can be divided in 6 different segments according to their orientation: North and North extension segments both with NW orientation, East-West segment, Central segment that vary between N-S to NW orientation, North-South segments, and South segment with NW attitude (Fig. 1c). The structure dips 70° to the SW in the North and South segments, in the Central segments dips 50° to the SW, E-W segments dips to the S, while N-S segments are vertical. The North and South segments represent continuous segments while the Central, E-W, and North Extension

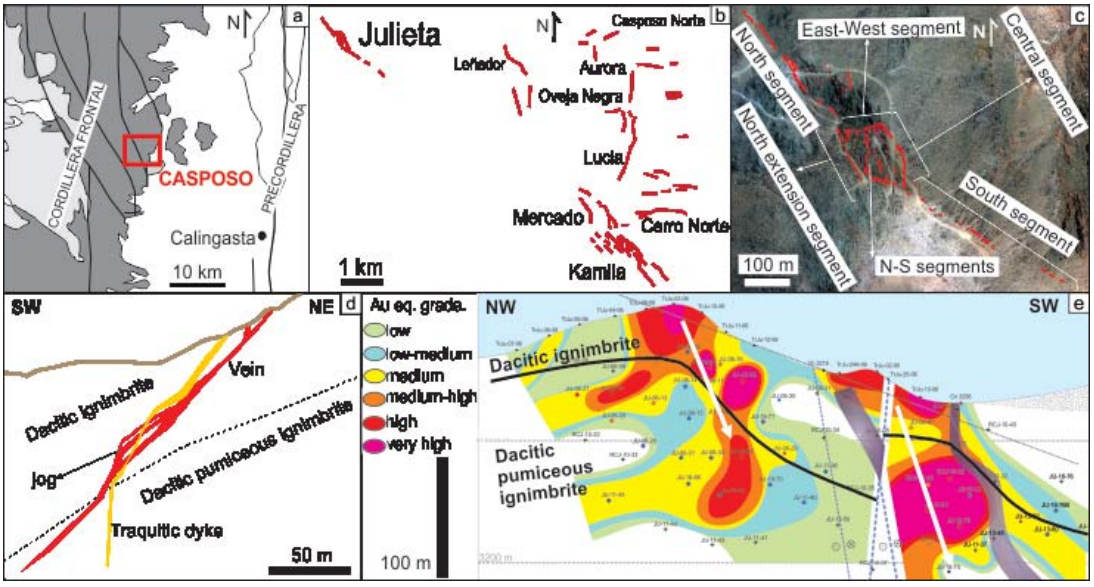

Figure 1 a) Casposo district location map. b) Mineralization map of Casposo district with Julieta vein location. c) Julieta vein map. d) Schematic cross section of Julieta vein. e) Longitudinal section of Julieta vein. cores with study of mineralizing events, reprocessing of previous geophysical data and detailed magnetometric

segments form an extensional jog where N-S segments represent tensional veins (Fig. 1c). The cross sections show that in depth the vein presents a dip change generating an inflection and the development of several subparallel branches forming a jog or curvature in the vertical (Fig. 1d). The change of dip and morphology of the fault/vein with the consequent formation of a vertical jog, corresponds to the contact between two levels of dacitic ignimbrites with different rheological behaviours, where the lower level could be more competent with respect to the upper level (Fig. 1 d). The longitudinal section shows two ore-shoots, one in the North segment and the other in the North extension segment, both with ~60° SW plunge (white arrows in Fig. 1e). The highest Au values are related with the contact between the dacitic pumiceous ignimbrite and the dacitic ignimbrite (Fig. 1e).

The analysis of the structural and lithological controls at vein scale, allows us to determine the orientations with greater permeability and greater development of ore-shoots, their morphology and sizes, and the relation with lithologies, thus generating an optimization in the exploration of this type of structures.

REFERENCES

Sotarello, G., Belvideri, I., Machuca, E., and Castro de Machuca, B., 2002. Low sulfidation epithermal system in the Casposo-Villa Corral área, Calingasta, San Juan, Argentina. Argentina Mining 2002 conference, Mendoza, Argentina, 16 p.

Palma D., Jovic S., Guido D. M., Ruiz R., Páez, G., Permuy Vidal C., Sotarello G., López, L., 2017. Evolución de eventos mineralizantes en la veta Julieta, Distrito Casposo, Cordillera Frontal, San Juan Argentina. XX Congreso Geológico Argentino, Tucumán. Actas: ST9-92-98.

EPITHERMAL MINERALIZATION IN CASTRO BASIN, SOUTHERN BRAZIL: STRATIGRAPHY, TECTONIC CONTEXT AND MINERAL POTENTIAL

Felipe Brito Mapa[1], Ivan Pereira Marques, Monica Mazzini Perrotta, Bruno Boito Turra, Luis Carlos Melo Palmeira

[1]*Geological Survey of Brazil - felipe.mapa@cprm.gov.br*

BACKGROUND

This work presents the results obtained during the geological mapping carried out in the Castro Basin, southern Brazil, by the Geological Survey of Brazil (CPRM). The Castro Basin is a tectonostratigraphic unit located at the west edge of the Southern Ribeira Belt (S and SE Brazil) comprising hydrothermally-altered volcanic (intermediate to acidic), pyroclastic and sedimentary rocks, assembled in the Castro Group. Some authors state that Castro Basin was formed on a transtensional event, during the collapse of the Gondwana Orogenic Belt. Others suggest that the basin was developed in a rift system during the Ediacaran throughout southeastern South America. Previous studies indicate an age of 549.6 Ma for the rhyolites (zircon U-Pb) and the occurrence of gold in epithermal quartz veins. There are at least three gold targets: Torre (deposit), São Daniel and Iapó (prospects).

METHODS

Detailed studies were performed in the basin and its surroundings, focused on gold and base metals targets. Additional analytical data comprised lithogeochemistry, geochronology and mineral reflectance spectrometry. Furthermore, a surface geochemical survey, geophysical-geological integration were also conducted in the area. The geophysical data (radiometric and magnetometric) were obtained on Paraná-Santa Catarina high resolution airborne geophysical acquisition project of CPRM. A geochemical surface survey was carried out to collect stream sediment, and heavy-mineral concentrate samples at active drainage system (10 to 20 km² area). These samples were prepared and analyzed by the SGS-GEOSOL laboratory using aqua-regia digestion (54 elements) and fire-assay (Au, Pt and Pd) methods with ICP-OES readout. The heavy-mineral concentrates were analyzed using a semi-quantitative mineralogical method. Six rock samples were analyzed using the zircon U- Pb geochronology in LA-ICP-MS. Seventy rock samples were sent to the SGS-GEOSOL laboratory for preparation, analysis and determination of major, trace, rare earth and noble elements concentrations. The major elements were determined using X-ray fluorescence method. Trace and rare earth elements were determined using lithium metaborate fusion and multi-acid digestion methods with ICP-AES and ICP-MS readout. The elements Au, Pd and Pt, were determined using the fire-assay method with ICP-OES readout. Spectroscopic mineral reflectance analyses were performed in eighty-five

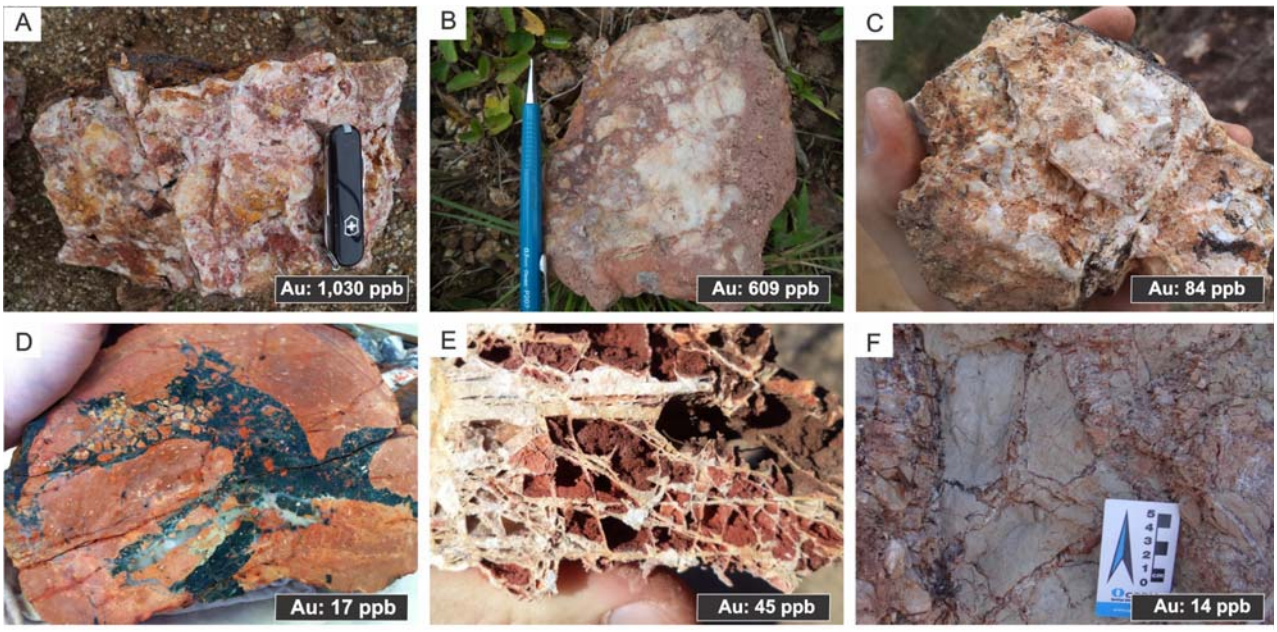

Figure 1: Gold bearing silicified zones in Castro Basin (Au-rates information on bottom). (A) Silicified breccia at São Daniel prospect. (B) Silicified breccia at Torre deposit; (C) Silicified breccia at Iapó target. (D) Lithophysa-rhyolite (orange) with chalcedony-sericite infill (white- green) and brecciated texture. (E) Fine quartz veins and veinlets with boxwork and stockwork textures. (F) Illite-smectite hydrothermal alteration halos surrounding stockwork quartz veins.

hydrothermally-altered samples to determine hydrothermal mineral assemblages using the ASD-FieldSpec-3 Hi-Resolution Spectroradiometer.

RESULTS

The dataset integration allowed a significant update of the available geological map. Moreover, metallogenetic information such as mineral occurrences distribution and the indication of favorable areas for gold mineralization were added to the map. Castro units segmentation exhibit a NE-SW trend, which is well observed in airborne geophysical data. The volcanic rocks show intermediate to acidic composition with strong alkaline affiliation. The bimodal magmatism, with high potassium calcium-alkaline or shoshonitic affinity, suggests intra-continental rift setting. Geochronological data showed two volcanic formations, the lowermost Tronco (intermediate), and the uppermost Tirania (acidic), presenting a minimum interval of 6.2 Ma between both volcanic episodes, with the acidic volcanism lasting until the Early Cambrian (532.6 Ma). Thus, the lithostratigraphic column was updated with the insertion of a new unit, the Aparição Formation, which represents a pyroclastic-volcanoclastic-sedimentary hydrothermally-altered facies, located between the two volcanic units. Gold anomalies were identified in stream sediments geochemistry (up to 80 ppb), and heavy-minerals concentrates (up to 9 grains). Higher concentrations of gold in rock samples (up to 1,030 ppb) were found in silicified zones composed of quartz, chalcedony, iron and manganese oxides and sulfides (FIGURES 1A, B, C). The silicified zones present variable thickness (meters to kilometers) with brecciated, stockwork and boxwork textures. They have tabular structure dipping sub-horizontally to sub-vertically. Two types of gold mineralized structures were recognized in the basin: (1) stratiform layers with spherules and lithophysae infilled by quartz, chalcedony, agate and sericite, associated with the base of rhyolitic flows and sin-volcanic processes (FIGURE 1D); (2) veins and veinlets of quartz, chalcedony and sulfides, related to faults and synchronous hydrothermalism (FIGURE 1E). The three main mineralized targets (São Daniel, Torre and Iapó) show gold bearing quartz veins striking to NE-SW, NNW-SSE and ENE-WSW, respectively. These veins show hydrothermal alteration halos composed mostly by illite- smectite (FIGURE 1F), and locally by smectite, illite, sericite (white mica) and adularia. These hydrothermal mineral assemblages suggest temperature range between 160 to 260°C for their crystallization. Airborne gamma-spectrometry data revealed high K areas strongly associated with extensive hydrothermalism. This feature can be used as a guideline for alteration and mineralization targetting. The magnetometric data are widely affected by the Mesozoic NW-SE-striking Ponta Grossa dyke swarm. However, the data show structural features that may be associated with the pathways and possible sources of mineralized fluids (E-W and NE-SW shallow magnetic lineaments).

CONCLUSION

The Castro Basin mineral system analysis indicates that favorable areas for gold mineralization are related with the occurrence of quartz veins and silicified zones, illite- sericite hydrothermal alteration halos, gold surface geochemistry anomalies and high K geophysical anomalies. The Aparição Formation is the main unit of the illite-sericitic alteration and represents a useful prospectivity guide for the mapping of silicified zones with potential gold mineralization. NE-SW-striking faults indicate a high association with the mineralized and hydrothermally-altered areas and can be related to ore migration and deposition. The styles and types of hydrothermal alteration show halos and mineral assemblages compatible with a low-sulfidation epithermal model. The hydrothermal alteration halos surrounding the mineralized zone are divided into five zones, from the center to the border: (a) quartz-adularia, (b) sericite, (c) illite-sericite, (d) illite-smectite, (e) propylitic. The conceptual model of the hydrothermal alteration types and associated mineralization developed for the basin suggests that smectite-illite mineral assemblage is related to a shallow erosive level, and the mineralized veins found in this work are located in low-grade ore zones. The occurrence of illite and sericite halos associated with gold silicified zones indicate higher temperature (260°C) and depth that may fit to higher-grade ore. Finally, the area still shows prospectivity potential for the occurrence of undiscovered Au-Ag low-sulfidation epithermal deposits. Additionally, the metallogenetic and geotectonic models (rift-basin), the bimodal magmatism and the occurrence of iron, copper, zinc and uranium minerals, may suggest the possibility of deeper mineral systems, which increases the economic potential of the area.

EVOLUTION OF MINERALIZING EVENTS IN THE ARMADILLO VEIN EPITHERMAL SYSTEM, MARTINETAS DISTRICT, EASTERN DESEADO MASSIF, SANTA CRUZ, ARGENTINA

Facundo Julián De Martino[1], Horacio J. Echeveste, Sebastián M. Jovic, Mario O.R. Tessone, Remigio Ruiz, Raúl E. de Barrio, Silvio Franco

[1]*Instituto de Recursos Minerales (INREMI), Facultad de Ciencias Naturales y Museo. UNLP. Calle 64 y 120 (1900), La Plata*

facundodemartino@yahoo.com

INTRODUCTION

Martinetas mining district is located in the eastern Deseado Massif, Santa Cruz province, Argentina. It is characterized by the presence of Au-Ag low sulfidation epithermal veins system, hosted by volcanic and sedimentary rocks of the Bahía Laura Volcanic Complex. The mineralization is distributed in three sectors: Armadillo, Choique and Central Vein Zone all of them in production. Armadillo is composed by WNW-ESE quartz veins, with subvertical to high dip to the north, with 1 to 3 meters thick. The veins are characterized by banded colloform, filling textures and replacement of carbonate with "lattice bladed" texture. These veins are associated with minor sheeted veins.

MINERALIZATION STAGES

In basis on the analysis of DDH core samples, two mineralizing events were determined (Figure 1): E1, hydraulic-hydrothermal stage and E2, tectono-hydrothermal stage. The E1 comprises four replacement and filling pulses; P1 is formed by white silica with lattice bladed texture (possibly replacement of calcite by quartz), P2 is represented by massive silica breccia with P1 vein and host rock fragments. The P3 cuts the previous pulses and corresponds to a silica-adularia colloform banded texture with specks of organic matter, spatially associated with gold. The P4, associated with a new hydraulic fracturing event, shows breccia texture with fragments of the previous pulses, silica, organic matter and native gold. Finally, a tectonic-hydrothermal event is represented in the P5 by a breccia with small holes and cavities filled with silica and iron oxides that cuts off the previous pulses and the host rock. Gold values are associated with pulses P3 and P4, corresponding to E1.

Under reflected light microscope, it was determined that the ore minerals are restricted to stages with presence of organic matter. The chemical composition of the mineral assemblage have been established by electron probe microanalysis (EPMA) with wavelength-dispersive X-ray spectroscopy (WDS). This analysis determined the presence of native gold, native silver and electrum.

The maceral constituents of the organic matter (kerogens) identified in pulses P3 and P4 were determined by optical methods under oil inmersion in a microscope of white light, where the color and reflectance of the macerals

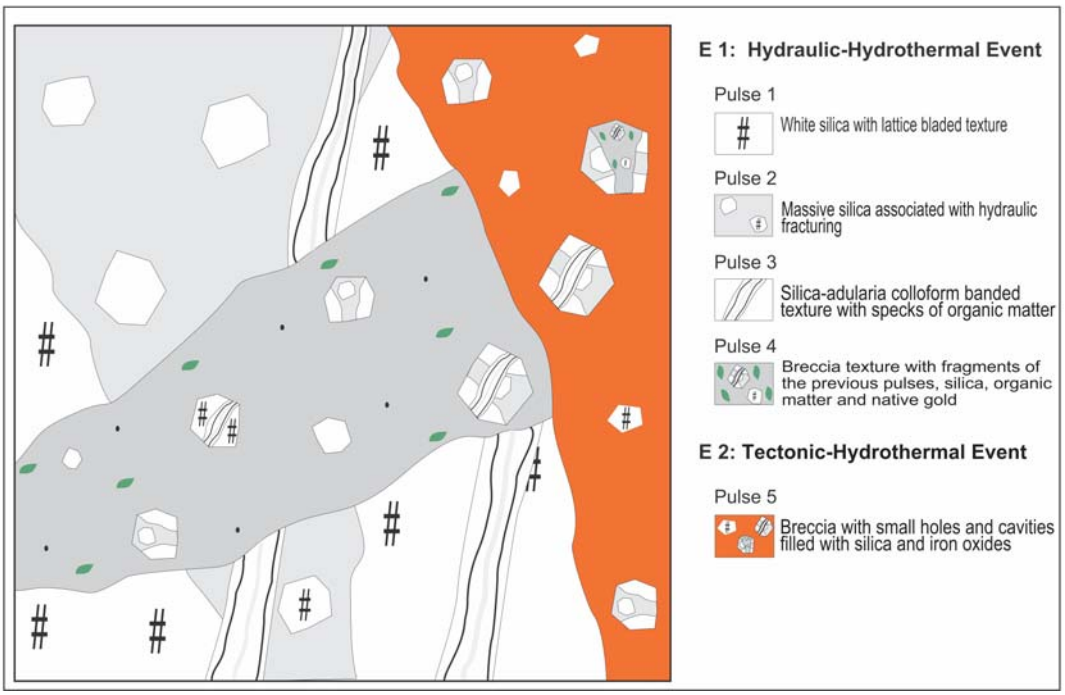

allowed us to define them as vitrinite and inertinite. Vitrinite macerals are derived from parenchymatous and woody tissues of roots, stems, barks and leaves composed of cellulose and lignin (ICCOP, 1998). As regards Inertinite, it is considered to derived from vegetable material that has been strongly altered and degraded in oxidizing conditions (Falcon and Snyman, 1986). Many authors associate these conditions with wildfire (Cope and Chaloner, 1985; Cohen *et al.*, 1987; Jones, 1993; Guo and Bustin, 1998; Glasspool, 2000). This fact may be evidence of a previous carbonization or carbonization during deposition of the beds that contain the plant remains. A possible explanation of its origin is a pyroclastic event, represented in the area by the base surge deposits and associated thin massive black clayed layers (De Martino et. al., 2017).

CONCLUSIONS

(a) There is a strong spatially correlation between the anomalous gold-silver and the presence of pulses P3 and P4 and (b) gold is observed as minute grains associated with the motes of organic matter under a reflected light microscope, therefore a genetic relationship between gold and organic matter can be inferred.

The macerals would be directly responsible (fixation of the Au by part of the lignite) or indirect (reduction by bacteria or thermochemically induced by changes in the Eh and Ph of the fluid by part of the organic matter) of the precipitation of the ore minerals. This would involve the circulation of hydrothermal fluid by carbonaceous beds and uptake of the kerogens they contain, causing the subsequent reduction and precipitation of gold, silver and electrum.

The importance of defining the mineralizing events that make up the Armadillo vein system lies in identifying the sectors and pulses that bring economic mineralization, allowing optimization of the exploitation of this sector and planning of exploration in the district.

STRUCTURAL CONTROLS ON THE LOCALISATION OF LOW-SULFIDATION EPITHERMAL MINERALISATION - WEST JAVA, INDONESIA

Michael Cunningham

WITHDRAWN BY THE AUTHOR

A | 13

EVOLUTION OF THE MINERALIZING EVENTS IN THE INCA VEIN, CASPOSO DISTRICT, CORDILLERA FRONTAL, SAN JUAN, ARGENTINA

Diego Palma[1], Sebastián M Jovic, Diego M. Guido, Conrado Permuy, Remigio Ruiz, Facundo De Martino

[1]CONICET- YTEC - diegopalma90@yahoo.com

INTRODUCTION

The Casposo district is located in the Cordillera Frontal, in the center-west of the San Juan province, Argentina. It is characterized by the presence of low sulfidation epithermal veins, hosted in volcanic rocks of the Choiyoi Group. The structural trend that controls the Au-Ag mineralization has a main NW-SE direction, and Kamila and Mercado are the main mineralized sectors (mined in the past with open pits, and actually underground at Kamila). In Kamila sector, 3 structures with different orientations predominate (Inca, Aztec, and B Vein). Kamila and Mercado areas form an epithermal Au and Ag-bearing quartz vein system, mainly represented by colloform banded and brecciated textures, and minor lattice bladed replacements. The ore includes native Au and Ag, electrum, acanthite, tetrahedrite and silver sulfosalts, which are associated with pyrite, chalcopyrite, sphalerite, galena and digenite (Sotarello *et al.* 2002).

GEOLOGICAL SETTING

The stratigraphic sequence at Casposo mine started with marine sedimentary rocks (Cb sup –Pm inf) defined by Caballé (1986) as La Puerta Formation. This formation is overlain by a thick intrusive and volcanic sequence assigned to the Permian-Triassic Choiyoi Group. Basal andesitic volcanic flows, tuffs and breccias are the main subsurface unit at Casposo and are overlain by rhyolite, rhyolite-dacite flows and dacitic ignimbrite flows. The volcanic units dip 15 to 20° to the east, and is affected by N-S, E-W and NW-SE-trending structures, filled by the epithermal quartz veins, and dacitic, rhyolitic, and andesitic dikes of different ages, but most of them post-mineralization (Hedenquist, 2012) .

METHODOLOGY

From the cross and longitudinal sections interpretation, 120 drill cores of Inca vein were selected for further study. We worked with drill holes samples, which have an average perforated length of 300m from the surface. In each hole, the mineralized section was studied, carrying out a characterization on a macroscopic scale of the different mineralizing pulses, from their relative temporal relationship, determining the textures, morphologies, mineralogy assemblages and alterations.

RESULTS

A sequence of 8 mineralizing pulses (P1-P8) was defined. These were grouped into six main events:

E1 Event, Carbonatic

P1: Banded colloform calcite, pink bands with visible crystals, gray bands with a lattice bladed texture and white bands. Sometimes it creates cockade textures, and in others it looks massive.

E2 Event, Siliceous

P2: Milky silica with massive to banded texture, replacement of lattice bladed type. It usually presents hollows due to the leaching of a preexisting mineral.

P3: Banded colloform milky silica, bands with fine adularia crystals and a mineral with needle habit (probably zeolites). Ginguro bands -sometimes forming thick patches of fine grained sulfides- and green clays.

P4: Gray massive silica with specks of fine disseminated sulfides. It also has visible crystals of chalcopyrite, galena, sphalerite, red silvers and electrum, which shows a thick grain size. As in P2, this pulse has a lattice bladed replacement texture.

E3 Event, Clayish

P5: Brownish-green tone clays accompanied with calcite, forming brecciated textures with previous pulses clasts. Occasionally, it has thick grained pyrite crystals.

E4 Event, Siliceous

P6: Gray massive silica with thick quartz crystals, a needle mineral (probably zeolites) and pink adularia.

E5 Event, Tectonic-Hydrothermal

P7: Breccia with a black silicified matrix, different angular clasts of the host rock and the previous pulses. When it has abundant clasts of P3 and P4 pulses, an increase of Au-Ag values is recognized.

E6 Event, Carbonatic

P8: Fine white massive calcite veinlets, cutting the P7 pulse.

FINAL CONSIDERATIONS

From the study of the mineralizing events in the Inca vein, a multi stages vein system was recognized. This is formed by 8 pulses, 7 of them hydrothermal and 1 tectonic- hydrothermal.

These pulses are characterized by the presence of massive, banded and breccia textures, together with lattice bladed replacement textures. The mineralogy is mainly dominated by Au-Ag sulfides and base metals (chalcopyrite, galena, sphalerite) along with pyrite, in a gangue of quartz, adularia, clays and calcite.

These pulses were grouped into 6 main events; E1 which begins with a carbonatic fluid, followed by E2 of siliceous nature. This event initially only deposits quartz, and then Au and Ag minerals in fine ginguro bands, finally base metals sulfides. The fluid develops in to a green clays dominated composition, together with breccia textures in the E3 Event. Then, a siliceous event appears again, but barren this time. After this, an event with both tectonic and hydraulic components is recognized, acting simultaneously, generating a breccia with a black matrix that sometimes can have associated precious metals, because of the Tectonic- Hydrothermal event. Finally a minor event is recognized, which forms fine veinlets of carbonatic nature (E6).

BIBLIOGRAPHY

Caballé, M.F. 1986. Geological study of the Cordillera Frontal eastern sector, between the Manrique and Calingasta rivers (San Juan Province). Doctoral Thesis of the Natural Sciences Faculty, La Plata University (Unpublished), La Plata., 205 p.

Hedenquist, J.W., 2012. Observations on epithermal mineralization in the Casposo and Castano Nuevo districts, San Juan, Argentina. Final report for Troy resources limited.

Sotarello, G., Belvideri, I., Machuca, E., and Castro de Machuca, B. 2002. Low sulfidation epithermal system in the Casposo-Villa Corral área, Calingasta, San Juan, Argentina. Argentina Mining 2002 conference, Mendoza, Argentina, 16 p.

A | 14

THE SANTA CRUZ CENTRAL CALDERA FIELD: A NEW FRONTIER IN THE EXPLORATION FOR GOLD AND SILVER IN CONCEALED JURASSIC CALDERAS OF THE CHON AIKE VOLCANITES OF SOUTHERN PATAGONIA, ARGENTINA ?

Carlos Jorge Chernicoff[1], Flavia Maria Salani

[1]CONICET-SEGEMAR, CONICET-UBA - jorge.chernicoff@segemar.gov.ar

The Patagonian region of Argentina hosts an extensive volcanic field of mainly acidic character referred to as the Chon Aike Volcanic Province (Kay *et al.*, 1989; Pankhurst *et al.*, 1998; Sruoga *et al.*, 2010). Its genesis is related to the extensional context that preceded, and eventually caused, the breakup of the Gondwana supercontinent. The effusion of the acidic volcanites and pyroclastics is thought to be related to the combination of calderas and large fractures.

In the Deseado Massif, southern Patagonia, this volcanism contains gold and silver epithermal deposits, on account of which it has been defined as an Au-Ag metallogenic province (Schalamuk *et al.*, 1999).

Among the main caldera structures identified by other authors in the Deseado Massif (e.g. Férnandez *et al.* 1996; Guido, 2004; Echavarría *et al.* 2005; Sruoga *et al.* 2008 y 2010; Ruiz *et al.* 2011) are the La Josefina, the Cerro 1º de Abril, the El Dorado-Monserrat and the Cerro Torta Calderas, all of them in the extra-Andean zone, as well as the La Peligrosa Caldera located in the Andean region.

The present authors have identified a caldera field –Santa Cruz Central Caldera Field (Salani and Chernicoff, 2018a, 2018b)– on the basis of the geological interpretation of the aeromagnetic survey of the Deseado Massif (SEGEMAR, 1998). Although this caldera field is covered by Neogene and Quaternary deposits, it is clearly bound to be related to the surrounding volcanites and pyroclastics of the Chon Aike Formation, particularly the nearby outcrops exposed at the río Seco (ca. 48°42´S/68°15´W).

The newly defined caldera field needs to be viewed in the context of the Au-Ag metallogenic province defined by Schalamuk *et al.* (1999) in the Deseado Massif, this being the reason why we propose the relatively nearby Chon Aike calderas of La Josefina, Cerro 1ro de Abril, El Dorado-Montserrat and Cerro Tortas, as analogous examples. An average depth estimate of 350-550 m to the floor of the newly defined caldera field was calculated using the Euler module of the Oasis Montaj (TM) software package.

The Santa Cruz Central Caldera Field is formed by four calderas –and a number of associated lava domes– which extend in a roughly latitudinal corridor for at least 150 km (Fig. 1). Three of these calderas are larger than 20 km wide, the whole caldera field being controlled by NNE-SSO and ENE-OSO regional structural lineaments (herein detected as magnetic features) well known elsewhere in the exposed portion of the Deseado Massif, where they have been assigned to a transtensional context (e.g. Sruoga *et al.*, 2008, and references therein).

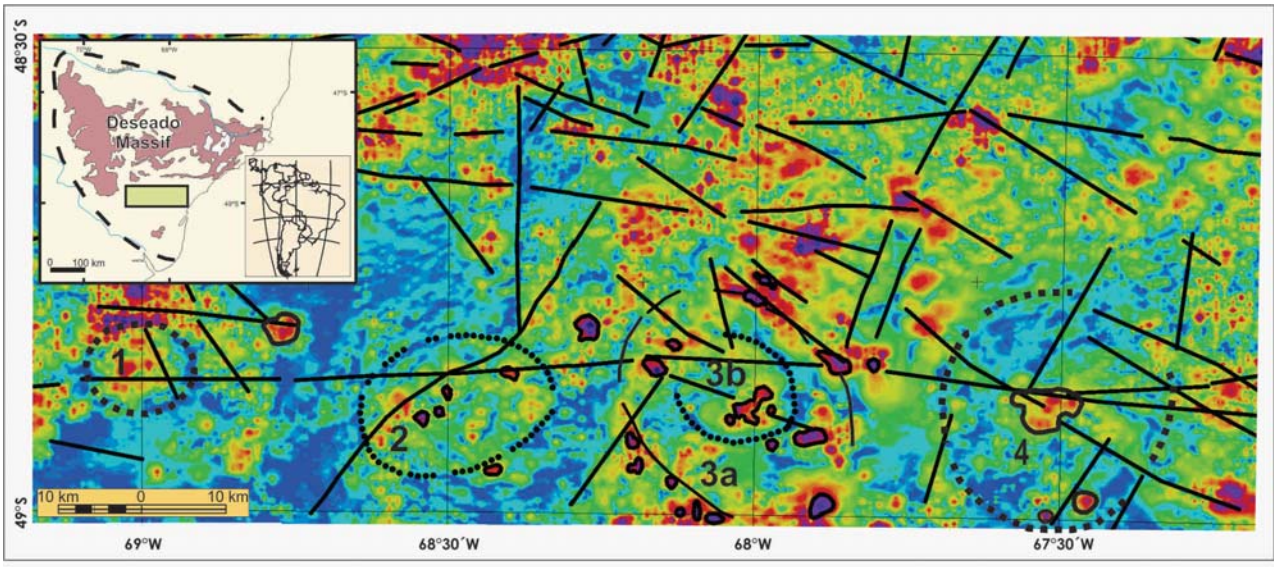

Figure 1. Analytic signal of the total magnetic field of the Santa Cruz Central Caldera Field, Santa Cruz province, Argentina. Numbers 1 to 4: individual calderas. Ring structures indicated as dotted/solid lines; magnetic lineaments indicated as solid lines.

Numbered 1 to 4 from west to east, the calderas comprising the Santa Cruz Central Caldera Field are: 1) The smallest caldera, centered at 49°S/69°W, with a maximum diameter of 14 km. In the immediate proximity of this caldera there is a 4 km-wide lava dome centered at 48°53'S/67°30´W located at the intersection of two fractures. 2) A 23 km wide caldera, centered at 48|53'S/ 68°29'W, hosting 1-2 km wide eruptive bodies inside it. 3) The largest caldera (3a), centered at 48°52'S/68|02'W, has a maximum diameter of 30 km, with aligned, 1 to 3.5 km-wide, domes following the circular pattern of the ring fractures. Internally, there also occurs a concentric nested structure of 14 km in diameter (3b), with 600 m-wide igneous bodies in its interior. 4) A 25 km wide caldera, centered at 48°47'S/68°46'W, hosting a 5 km-wide igneous body in its interior plus two lava domes ranging in size 1-2 km in the southern caldera rim.

Given the known occurrence of gold and silver mineralization associated with calderas and large fractures elsewhere in the Deseado Massif, our identification of the Santa Cruz Central Caldera Field may well open a new frontier in the exploration for Au-Ag mineralization in this region.

REFERENCES

Echavarría, L.E., Schalamuk, I.B. and R.O. Etcheverry, 2005. Geologic and tectonic setting of the Deseado Massif epithermal deposits, Argentina, based on El Dorado-Montserrat. Journal of South American Earth Sciences, 19: 415–432.

Fernández, R.R., Echeveste, H., Echavarría, I. and I.B Schalamuk, 1996. Control volcánico y tectónico de la mineralización epitermal del área de La Josefina, Macizo del Deseado, Santa Cruz, Argentina. XIII Cong. Geol. Arg. y 3° Congreso Exploración de Hidrocarburos, 3: 41–54.

Guido, D., 2004. Subdivisión litofacial e interpretación del volcanismo jurásico (Grupo Bahía Laura) en el este del Macizo del Deseado, provincia de Santa Cruz. RAGA, 59 (4): 727–742. Kay, S. M., Ramos, V. A., Mpodozis, C. and P. Sruoga, 1989. Late Paleozoic to Jurassic silic magmatism at the gondwana margin: analogy to the Middle Proterozoic in North America? Geology 17, 325-328.

Pankhurst, R.J., Leat, P.T., Sruoga, P., Rapela, C.W., Márquez, M., Storey, B.C. and T.R. Riley, 1998. The Chon Aike province of Patagonia and related rocks in West Antarctica: A silicic large igneous province. Journal of Volcanology and Geothermal Research 81: 113-136.

Ruiz, R., G.N. Páez, D.M. Guido, S.M. Jovic and I.B. Schalamuk, 2011. La caldera Cerro 1º de Abril: evolución geológica e implicancias en el estilo eruptivo del volcanismo Jurásico del Macizo del Deseado. XVIII Congreso Geológico Argentino (CD).

Salani F.M. and C.J. Chernicoff, 2018a.The Santa Cruz Central Caldera Field: concealed Jurassic calderas of the Chon Aike volcanism in southern Patagonia, Argentina. COV10.

Salani F.M. and C.J. Chernicoff, 2018b. Calderas jurásicas asociadas a las volcanitas de la Formación Chon Aike en las inmediaciones del Puesto Salado, sector oriental de la provincia de Santa Cruz, Argentina. Geoacta 42: 61–70.

Schalamuk, I., de Barrio, R., Zubia, M., Genini, A. and H. Echeveste, 1999. Provincia Auroargentífera del Deseado, Santa Cruz. In: Zappettini, E. (Ed.), Recursos Minerales de la República Argentina. IGRM,SEGEMAR, Anales 35, 1177-1188.

SEGEMAR, 1998. Levantamiento geofísico aéreo (magnetometría y espectrometría de rayos gamma) Bloque Macizo del Deseado. Servicio Geológico-Minero Argentino.

Sruoga, P., Busteros, A., Giacosa, R., Martínez, H., Kleiman, L., Japas, S., Maloberti A. and M. R. Gayone, (2008). Análisis litofacial y estructural del Complejo Volcánico Bahía Laura en el área el Dorado-Monserrat, provincia de Santa Cruz, Argentina. RAGA 63(4): 653-66. Sruoga, P, Japas, María S., Salani, F. M., Kleiman, L E. and N. A. Rubinstein, 2010. Caldera La Peligrosa (47° 15´S, 71° 40´O): Un Evento Clave en La Provincia Silicea Chon Aike. RAGA, 66(3): 368-379.

A | 15

CENTRAL VEIN FLUID INCLUSIONS FROM THE AMANCAYA EPITHERMAL DISTRICT, PALEOCENE- EOCENE METALLOGENIC BELT, II REGION, NORTHERN CHILE

López Paola[1], Salvioli Melisa, Curci Marcela, Páez Gerardo, Guido Diego

[1]CONICET-Austral Gold S.A., Instituto de Recursos Minerales (INREMI- FCNyM-UNLP) Street 64 and 120, (1900) La Plata, Argentina - paolalopez.lp@gmail.com

INTRODUCTION

Fluid inclusions (FI) allow to determine the initial conditions of the fluid as temperature and salinity. On epithermal systems, this could be a good exploration guide. In this preliminary study we characterize two different stages of the hydrothermal infill of the Central Vein system, the main structure of the Amancaya District, a large epithermal system located in the II Region of Chile.

GEOLOGICAL BACKGROUND

The Amancaya District is located within the Central Depression of the Antofagasta Region, Northern Chile. The deposit is hosted in volcanic rocks from Chile-Alemania Formation and is composed of an extensive structurally controlled vein field. The main mineralized structure is Central Vein system characterized by two large veins that defines a "boomerang" shaped structure, from a NNE-SSW trending northern vein to a NW-SE oriented south vein.

The hydrothermal filling is the same in both veins and consists of four hydrothermal events according to the quartz textures and mineralogy. This study focuses on two stages of hydrothermal filling, one representing the main Au-Ag mineralizing event (EvB) and the other represent a late barren event (EvC).

METHODS

Petrographic studies were performed in an Olympus BX53 microscope, while microthermometric studies were performed using a Linkam THM600 plate, both located at the Instituto de Recursos Minerales (INREMI-UNLP).

From the temperature of ice fusion (T°f) we estimated the salinity of fluids (expressed as % wt. NaCl), whereas homogenizaton temperatures (T°h) were obtained heating the sample up to 300°C.

PETROGRAPHIC ANALYSIS

While analyzing EvB, we only considered FI in primary quartz (not recrystallized) and sphalerite crystals. The FI in quartz were grouped in two fluid inclusions assemblages (FIA) following their relief and filling degree (F=VL/(VL+VV)). Inclusions in FIA1 are high relief randomly distributed inside quartz crystals and have irregular to pseudo tabular shapes from 4 to 30µ. The F factor is variable between 0.6 and 0.8, this group contains a little proportion of monophasic FI of vapor. The FIA2 contains abundant low relief FI from 3 to 7µ with globose and irregular shapes, and F values close to 0.9. They are arranged randomly or partially aligned and can be classified as pseudo-secondary. Additionally, two high relief FI were analyzed in translucent sphalerite (FIsph). They range from 15 to 25µm and the F values are near to 0.7, showing a regular shape resembling negative crystals.

The EvC is represented by amethyst. We also recognized two FIAs in primary quartz based on their relief and F factor. The FIA1 is represented by irregular to pseudo tabular FI from 6 to 40µ, whit high relief and F values mostly around 0.5, although it can vary from 0.1 to 0.5. This group is represented in the growth zones or in the center of crystals. The FIA2 is represented by low relief FI with F around 0.95. The dominant shape is globous but some tabular forms are also recognized. This group is in the growth zones of crystals or forming short alignments within the crystals, suggesting a primary to pseudo-secondary origin.

MICROTHERMOMETRY

All samples were cooled below -100°C without evidence of CO_2 presence within the system, although small concentrations cannot be completely ruled out.

In EvB, the T°h ranges between 245° and 270°C for FIA1, and 170°-190° in the case of FIA2, while T°f vary from -1.5° to -2°C and -1.8°C to -2°C, respectively. Two eutectic temperatures were measured for FIA1 of EvB: -24° and -28°C (Fig. 1c). In the FIsph the T°h is 236°C and the T°f is -1.4°C.

For EvC, the obtained T°h ranges from 200° to 262°C for FIA1, and 160°-190°C for FIA2, while T°f varies from -0.9° to -1.4°C and -0.9° to -1.1°C respectively. The eutectic point for EvC could not be determined (Fig. 1c).

CONCLUDING REMARKS

The measured T°h and salinities of the mineralization hydrothermal fluid at Central Vein system is compatible with the range of an epithermal environment. Salinities do not show significant variations among the different FI assemblages; however, Fig.1d shows that lower salinities were recorded in EvC (1.4 to 2.4 % wt. NaCl) when compared with EVB (2.5 to 3%wt. NaCl) (Bodnar, 1993). The eutectic temperature measurements in EvB suggests a CO_2 poor fluid within the H_2O-NaCl-KCl compositional system (Linke, 1965).

Finally, petrographic studies evidence boiling conditions during mineral deposition, as is supported by different degrees of F factors in most studied assemblages (Fig. 1a and 1b). Following these observations, we estimate a depth the boiling level to be between 400 and 600m below the paleo-water table for EvB, and between 160 and 500m of depth below the paleo-water table for EvC (Haas 1971, Fig. 1e).

REFERENCE

Bodnar, R.J., 1993. Revised equation and table for determining the freezing point depression of H20-NaCl solutions. Geochim. Cosmochim. 57, 683-684.

Haas, Jr., J.L., 1971. The effect of salinity on the maximum thermal gradient of hydrothermal system at hydrostatic pressure. Econ. Geol. 66, 940-946.

Linke, W. F., 1965. Solubilites of inorganic and metal organic compounds. Amer. Chem. Soc., pp. 1914.

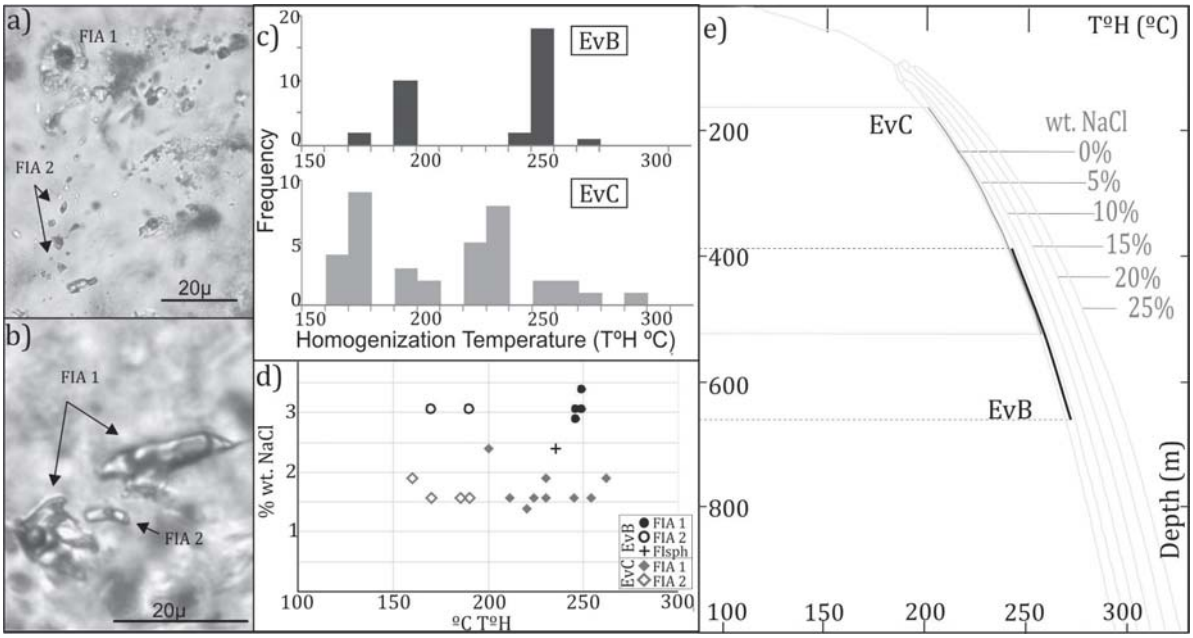

Figure 1 a) Microphotography of FI in EvB. b) Microphotography of FI in EvC. c) Frequency histograms of FI of different events in Central Vein system. d) Distribution diagrams of homogenization temperature vs. salinity in % wt. NaCl. e) Estimated depth of boiling level in different stages of hydrothermal filling according to Haas (1971).

A | 16

HYPOGENE AND SUPERGENE ALTERATION AT THE FARALLÓN NEGRO INTERMEDIATE- SULFIDATION DEPOSIT, NW ARGENTINA

Herzog Michael Alexander[1], Hagemann Steffen Gerd, Gilg Hans Albert, Fogliata Ana Silvia, Montenegro Nicolás

[1]*Department of Earth and Environmental Sciences, Ludwig Maximilian University of Munich, Germany*

mi.herzog@campus.lmu.de

The Miocene Farallón Negro Volcanic Complex (FNVC) comprises, amongst others, the world-class Bajo de la Alumbrera Cu-Au porphyry, and the Farallón Negro intermediate sulfidation epithermal deposits (e.g. Malvicini and Llambías, 1963; Gutiérrez *et al.*, 2006; Salado Paz *et al.*, 2011; Márquez-Zavalía and Heinrich, 2016). The latter is a structurally- controlled, Au-Ag-Mn-bearing quartz-carbonate vein deposit with the Farallón Negro and Alto de la Blenda vein systems representing the main ore bodies.

This study aims to decipher supergene and hypogene alteration minerals and zonation specifically focusing on clay minerals in both the Farallón Negro and Alto de la Blenda vein systems. In order to better understand the mineralogy, chemistry and distribution of clay minerals key vein segments of both vein systems were logged and sampled and detailed petrography, paragenesis and X-ray diffraction (XRD) analyses were performed. XRD analyses of clay alteration minerals are based on two sampled diamond drill holes (DDHs) intersecting vein segments in volcaniclastic-andesitic breccia and monzonite host rock lithologies.

The NW portion of the Farallón Negro and Alto de la Blenda vein systems are located in andesite lava flows and breccias, whereas the SE portions are hosted in a monzonite stock (7.5±0.2 Ma: 40Ar-39Ar on hornblende; Sasso, 1997). The Farallón Negro vein system contains, in the monzonite, the Veta Farallón Negro Ramo Norte, Veta Encuentro and Veta Cecilia, whereas the Alto de la Blenda vein system contains, in the andesitic lava and breccias, the Veta Laborero and, in the monzonite, the Veta Chica, Veta Esperanza, Veta Esperanza Sureste and Veta Portezuelo.

Both vein systems display similar mineralogy and textures. The veins consist of > 85 vol.% quartz and Mn-carbonates and sulfide-sulfosalt mineral assemblages of pyrite-chalcopyrite- sphalerite-galena and pyrite-galena-penzhinite-jalpaite-mckinstryite-polybasite-tennantite- tetrahedrite. Gold occurs as electrum and penzhinite ($(Ag,Cu)4AuS_4$). Characteristic textures include colloform-banded, pseudo-acicular, growth zone, massive, comb grains and vug infill. The veins are locally brecciated with early and late quartz-carbonate matrices and angular fragments of strongly-altered andesite and monzonite fragments wallrocks.

Paragenetically, six distinct stages of vein formation, five hypogene and one supergene stage, are defined (Figure 1). The first stage consists of brecciated, hydrothermally altered wallrock clasts in a matrix of quartz, Mn-rich calcite and minor pyrite and chalcopyrite. The second stage is characterized by colloform alternating bands of manganese carbonates with pyrite-chalcopyrite-sphalerite-galena. The third stage contains Au-Ag-bearing sulfosalts such as polybasite and tennantite, which are located within a quartz-carbonate matrix. Stage four comprises clear comb quartz and only minor Ca-rich carbonates. Stage five consists of mm- sized subhedral clear quartz and calcite crystals in open vugs. The final, sixth supergene stage consists mostly of various Mn-oxides including pyrolusite and todorokite that replaced hypogene Mn-bearing carbonates (mostly Mn-rich calcite, kutnahorite and rhodochrosite), gypsum and anhydrite that form in local wallrock cavities. Another common late stage feature observed in all vein segments is the local oxidation of sulfide phases such as sphalerite, into smithsonite, and pyrite into Fe-hydroxides.

Hydrothermal alteration minerals and assemblages define distinct alteration zones that can extend up to 35 m away from the veins and breccias. Due to the deep and highly irregular weathering, in some vein segments down to 450 m depth, the hydrothermal alteration zones comprise a mixture of hypogene and supergene minerals. The major proximal hypogene alteration assemblages in the monzonite are quartz-Mn-rich carbonate-pyrite-illite-chlorite, whereas in the andesitic breccia quartz-pyrite-illite-chlorite dominate. The transition to the intermediate alteration zone, in the monzonite stock, is characterized by quartz-pyrite- calcite-interstratified illite-smectite. In the andesitic wallrock, quartz-pyrite-chlorite-illite defines the indistinct distal alteration zone.

Detailed XRD analyses in andesitic breccias bordering the Veta Laborero vein system revealed R3 illite-smectite, chlorite and dioctahedral smectite. In contrast, hydrothermal alteration minerals in monzonite, approximately 23 m from the Veta Cecilia vein displays various interstratified clay minerals such as R1 and R3 illite-smectite, R0 chlorite-smectite and chlorite. Furthermore, the possible supergene modification of initial hypogene illite or chlorite and subsequent conversion of illite or chlorite layers into smectite layers, resulting in a R1, R3 illite-smectite or R0 chlorite-smectite structure, locally overprints the primary hypogene nature of some clay minerals. The distinction between hypogene and supergene clay minerals in near-surface samples is still possible due to the increase in dioctahedral smectite and, to lesser extent, kaolinite towards the surface.

Future work on the carbonate chemistry (carbon and oxygen isotopes) and fluid inclusion analyses will constrain the P-T-X-t conditions of the hydrothermal system, thereby provide further constraints on a robust alteration model for the Farallón Negro deposit. This can then be used for the exploration of concealed gold-bearing veins.

REFERENCE LIST

Gutiérrez, A.A., Chong, G.D., and Espinoza, S.R., 2006, Niveles de exposición de yacimientos del distrito minero Agua de Dionisio (YMAD), Catamarca: Revista de la Asociación Geológica Argentina, v. 61, p. 269-278.

Malvicini, L., and Llambías, E.J., 1963, Mineralogía y orígen de los minerales de manganeso y sus asociados en Farallón Negro, Alto de la Blenda y Los Viscos, Hualfín, Catamarca: Revista de la Asociación Geológica Argentina, v. 18, p. 77-202.

Márquez-Zavalía, M.F., and Heinrich, C.A., 2016, Fluid evolution in a volcanic-hosted epithermal carbonate-base metal-gold vein system: Alto de la Blenda, Farallón Negro, Argentina: Mineralium Deposita, v. 51, p. 873-902.

Salado Paz, N., Fogliata, A.S., Avila, J.C., and Montenegro, N., 2011, Veta Esperanza Sudeste, un caso particular de enriquecimiento supergénico en el yacimiento Alto de la Blenda, distrito minero Agua de Dionisio, Provincia de Catamarca: Revista de la Asociación Geológica Argentina, v. 68, p. 185-194.

Sasso, A.M., 1997, Geological evolution and metallogenetic relationships of the Farallón Negro Volcanic Complex, NW Argentina: Unpublished Ph.D thesis, Queen's University, Kingston, Canada, 540 p.

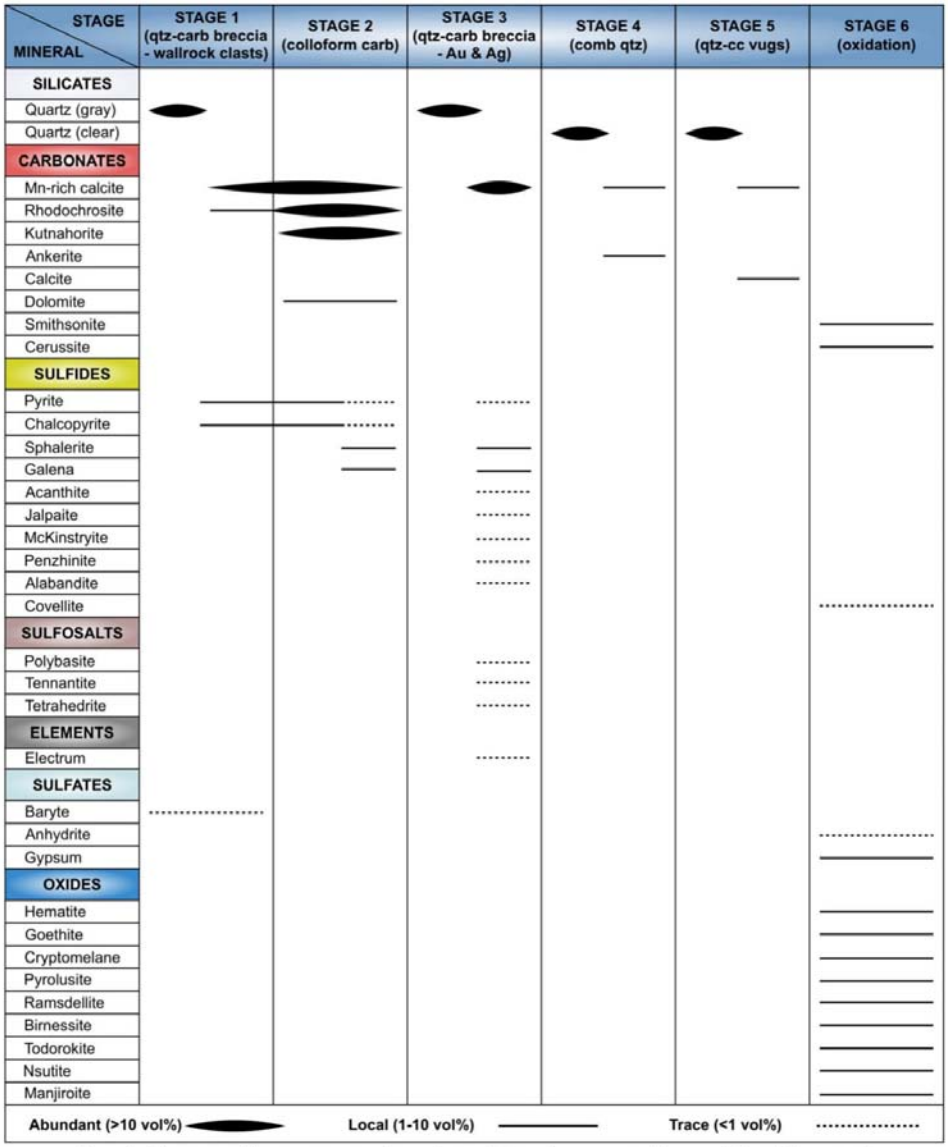

Fig. 1. Paragenetic sequence based on internal cross-cutting relationships, and mineral assemblages, epithermal textures and weathering features (e.g., the oxidation of Mn carbonated to oxides) in both the Farallón Negro and Alto de la Blenda veins.

A | 17

ADVANCED ARGILIC ALTERATION RELATED TO HIGH GRADE GOLD MINERALIZATION AT PAULA ANDREA PROSPECT, DESEADO MASSIF, SANTA CRUZ

Débora Godoy Prieto[1], Janet Sarapura Martinez

[1]*Minera Don Nicolas SA, National Route N3, km 2085, Santa Cruz Province, Argentina - dgodoyprieto@gmail.com*

BACKGROUND

Paula Andrea prospect is an early-stage exploration prospect located in the northeast sector of the Deseado Massif, in Santa Cruz Province. It is situated 3.5 km southeast of La Paloma Mine (Resource 1,460 kT @ 5.55 g/t Au, 260,566 Oz Au Measured), a low sulphidation gold deposit, hosted by volcanic Jurassic rocks from the Bajo Pobre Formation.

Detail mapping and trenching programs conducted in the area define several targets of interest, being Chulengo and Baritina those of greater potential, displaying high grade gold surface anomalies up to 75.2 ppm Au. Perforation campaigns also validate the continuity of the mineralization at depth and establish that the geometry of ore bodies appears to be discontinuous, isolated breccias, following NW and EW regional lineaments related to a rhyolitic dome margen. The irregular clusters consist in a few meters thick silica-sulfide cemented hydrothermal breccias and faults, or intensely leached silicic altered rocks.They collectively form weak to moderate zones of hydrothermal brecciation and faulting, typically between 1-5m wide.This epithermal structures are predominantly hosted by strongly altered andesitic volcaniclastic units and lesser flow-banded rhyolitic lava.

In order to achieve a better understanding of mineralization controls, a detail grid based alteration spectroscopy study (SWIR) was performed in the area, to accurately map out hydrothermal alteration mineral distribution, temperature gradients and it relations to gold anomalies. Advanced argillic alteration mineral assemblages; zunyite + dickite + barite+ silica ± high-cristalinity kaolinite ± pyrophillite ± alunite, were recognized associated with high grade gold mineralization. This association is indicative of a specific temperature range between 250°C to 300°C and ph<2.

METHODS

The alteration spectroscopy study included a total of 1758 surface samples, covering an area of approximately 33 km^2. Seven samples were selected to conduct petrographic studies. Alteration minerals were identified using oreXpress spectrometer and the USGS digital spectral library as reference. Thermal gradients were established based on reported temperature stability fields for hydrothermal minerals common in the epithermal environment (Corbett and Leach,1998).

RESULTS

In addition to the minerals recognized by spectrometry studies, ganga and ore minerals were integrated compiling surface mapping information. The resulting mineral assemblages allowed to define six main alteration zones (Simmons *et al.*,2005);

1 Silicification Zone consists of quartz infilling fractures, open-space cavities and intense replacement and leaching of host rocks. Silicification halos range from a few centimeters up to 1m wide, closely related to mineralized structures.

2 Advanced Argillic Zone is characterized by the mineral assemblage; zunyite + dickite + barite+ silica ± high-cristalinity kaolinite +hematite± pyrophillite ± alunite± jarosite; reflecting a temperature range between 250°C to 300°C and ph<2.

Diagnostic minerals such as zunyite and crystalline alunite were recognized by SWIR survey, and also in thin sections.

Advanced argilic alteration occurs dominantly along NW-striking regional lineament, parallel to the SW edge of a rhyolitic dome intrusion that cuts the lower volcaniclastic andesitic sequence. The principal alteration halo had a strike length of 1.3 km, with its higher temperature focus centered over Baritina Target, where high-grade gold surface anomalies up to 75.2 ppm Au were reported.

3 Intermediate Argillic Zone forms an asymmetrical halo surrounding advanced argillic alteration zone. The alteration assemblage extends out laterally up to 2.25 km to the NE and 1.7 km to the SE from the advanced argillic zone. It is defined by the presence of dickite+ illite+ illite-smectite + high-cristalinity kaolinite; indicating a temperature range between 170° to 200°C and intermediate ph conditions. This zone is typically associated with moderate to high grade gold anomalism, when affecting andesitic volcaniclastic units, for example at Chulengo Target.

4 Argilic Zone occurs adjacent to the intermediate argilic halo at the NE sector of the prospect. It is defined by the presence of illite-smectite +kaolinite ± smectite; reflecting a temperature around 150° C and intermediate ph conditions.

5 Propylitic Zone is concentrated along a NE regional fault zone (Atrevida Fault) at the west end of the prospect, locally overprinting the prior argillic alteration zones. It comprises the mineral assemblages, smectite + chlorite ± smectite-illite ± calcite ± zeolites; characteristic of temperature range <150°C and basic ph conditions.

6 Sub Propylitic zone is characterized by the presence of smectite+ chlorite± zeolites. This alteration marks the limit of the system towards S and SW edge of the prospect.

CONCLUSIONS

The spectroscopy analyses carried out at Paula Andrea prospect effectively mapped an extensive, asymmetrical alteration zonation pattern that reflects progressive increases in temperature and a decrease in pH, from the NE end of the area towards the high-grade Au zone, centered over Baritina Target.

There is a strong correlation between high grade gold anomalies and advanced argillic alteration mineral assemblages.

The alteration zonation, combined with mineralogical and textural evidences indicates that the style of mineralization at Paula Andrea does not correspond to a typical low sulphidation deposit. The association between intense, leached silicic alteration (i.e. vuggy silica) and high-temperature acid-stable minerals, such as zunyite + dickite + hypogene alunite strongly suggests acidic, oxidized fluid conditions formed in the magmatic-hydrothermal environment.

Spectral study had proven an effective, relatively low cost exploration technique in mapping out hydrothermal alteration minerals associated with major fluid pathways, and had provide excellent vectoring information for follow up investigation.

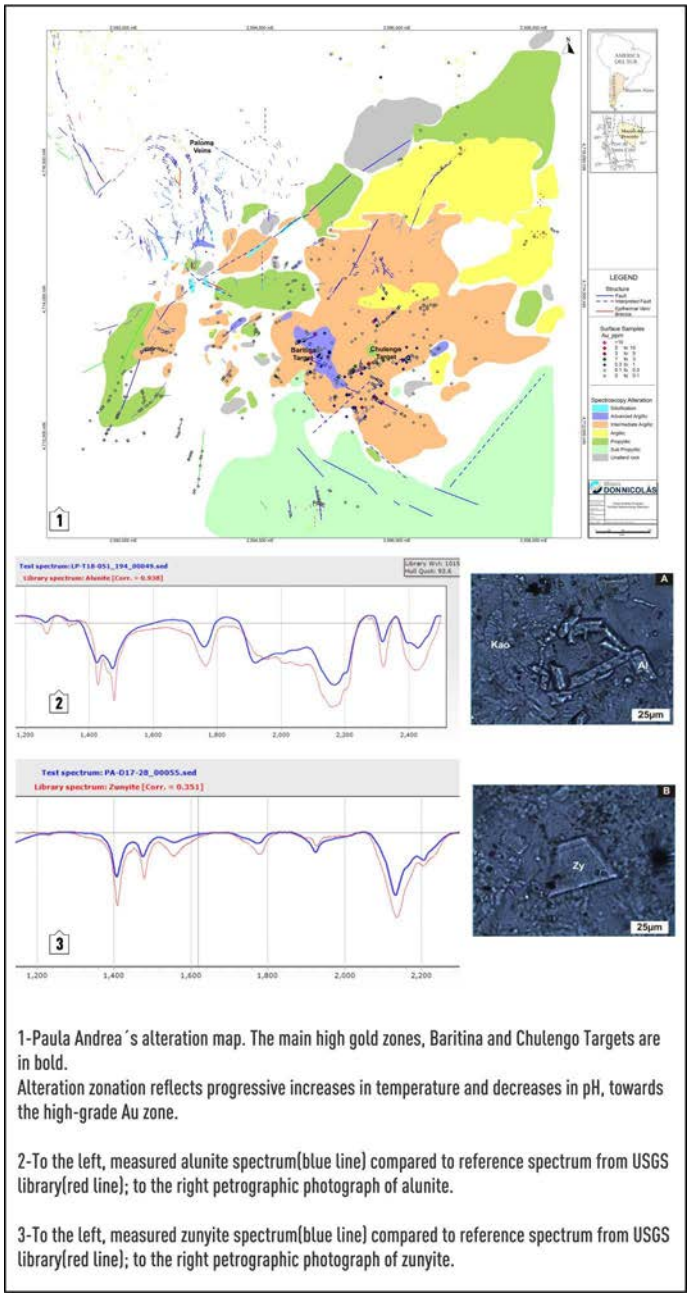

1-Paula Andrea´s alteration map. The main high gold zones, Baritina and Chulengo Targets are in bold.
Alteration zonation reflects progressive increases in temperature and decreases in pH, towards the high-grade Au zone.

2-To the left, measured alunite spectrum(blue line) compared to reference spectrum from USGS library(red line); to the right petrographic photograph of alunite.

3-To the left, measured zunyite spectrum(blue line) compared to reference spectrum from USGS library(red line); to the right petrographic photograph of zunyite.

A | 18

CHARACTERIZATION OF MINERALIZED FLUIDS FROM CHANCÓN MINING DISTRICT; APPLICATIONS IN ENERGY-RELATED TECHNOLOGIES

Daniel Moncada[1], Bastián Muñoz, Alexis Valenzuela

[1]*Department of Geology, University of Chile, Plaza Ercilla 803, Santiago, Chile - dmoncada@ing.uchile.cl*

Critical and strategic minerals do change with time. To develop new technologies, some elements are needed to produce, transmit, store and conserve energy. In recent years a wide variety of rare metals, including indium, selenium and tellurium, have found important applications in energy-related technologies such as advanced photovoltaic solar cells (Jaffe *et al.*, 2011). These metals are produced commercially as a byproduct in the refining of porphyry copper and similar ores, and from indium- selenium- and tellurium-rich epithermal deposits. The Chancón mining district is located within the Coastal Range of Central Chile and shows characteristics and mineralization that can be produced as by-product from the gold mineralization (e.g. tellurium or selenium) to the base metal mineralization zinc (e.g. Indium). The proposed study will involve analyses of In, Se, and Te from well-characterized fluid inclusions from the La Leona vein to identify differences in fluid chemistry, including metal contents, which may help to better understand metal transport and deposition in the Coastal Range systems. The La Leona vein shows a mineral zonation from the surface to beneath the deepest levels sampled. The shallow part has minerals assemblages quartz- calcite, and pyrite, with gold and silver mineralization. While in the deepest levels sampled shows chloride-epidote, chalcopyrite, sphalerite and galena. Three stages of mineralization have been defined: (1) pre-ore stage is characterized by pyrite and chalcopyrite, (2) Au-Ag and base metal stage; characterized by pyrite, chalcopyrite, sphalerite, galena and Au-Ag in quartz, pyrite and chalcopyrite, (3) post-ore stage; characterized by rhombic calcite, chlorite and epidote. Samples were assayed by 62 elements include indium mineralization range from 0.04 to 12.5 ppm, selenium range from 3.7 to 22.8 ppm and tellurium range from 2.2 to 11 ppm.

A detailed petrographic study of fluid inclusion shows primary and secondary Fluid Inclusion Assemblages (FIAs) hosted in quartz and were classified as containing: (1) coexisting liquid-rich and vapor-rich fluid inclusions shows a homogenization temperatures (Th) ranges from 250 to 245 °C and final ice melting temperature (Tm) ranges from -4.8 to -3.7 °C; (2) secondary assemblages consisting of only vapor-rich inclusions, (3) liquid-rich inclusions with consistent liquid-to-vapor ratios hosted in sphalerite shows the Th ranges from 240 to 235 °C and Tm ranges from -6.5 to -6.1 °C. Laser ablation ICMPS in fluid inclusions shows enrichment of critical elements in sphalerite. The In range from 0.2 to 276.8 ppm, Se range from 37.1 to 482.5 ppm, Te range from 0 to 99.5 ppm, Au range from 0.1 to 8.1 ppm and Ag range from 13.1 to 1640.6 ppm. Secondary fluid inclusions in quartz only shows enrichment in Ag range from 2.8 to 9 ppm. These suggest that some critical elements might be important in this area

REFERENCES

Jaffe, J., Price, G., Ceder, R. G., Eggert, T. E., Graedel, K., Gschneidner, M., Hitzman, F., Houle, A., Hurd, R., Kelley, A., King, D., Milliron, B. J., Skinner, F., Slakey, 2011. Energy Critical Elements: Securing Materials for Emerging Technologies. American Physical Society, Materials Research Society, Washington, DC, 28p

CHAPTER 2
ORE DEPOSITS IN EXTENSIONAL TECTONIC SETTINGS

Convenor: Silvia Lagorio

MINERALIZATION OF NATIVE COPPER IN SERRA GERAL BASALTS (PARANÁ MAGMATIC PROVINCE), MESOPOTAMIA REGION (ARGENTINA): NEW EVIDENCE FROM BOREHOLES SUPPORTING RESULTS OF SURFACE LAVAS

Silvia Leonor Lagorio[1], Susana Segal, Carlos Herrmann, Abel Pesce, Guillermo Cozzi

[1]*Instituto de Geología y Recursos Minerales (IGRM) SEGEMAR; Parque Tecnológico Miguelete (San Martín - Buenos Aires)*

silvialagorio@gmail.com

BACKGROUND

Volcanic rocks covering the Argentine Mesopotamia belong to the southern region of the Paraná Magmatic Province. The latter corresponds to a major tholeiitic event constituting a large igneous province (LIP) of Early Cretaceous age that covers an extensive region of Brazil, Paraguay, Uruguay and northeastern Argentina (e.g. Lagorio *et al.*, 2016). Rocks belong to the Serra Geral Formation that in the studied region is essentially composed by basalts and basaltic andesites, in which the occurrence of native copper has been mentioned for several decades.

In previous works the results of the investigations in the mineralization of the Serra Geral lavas were presented both concerning surface lavas from Corrientes province (Monte Caseros, Curuzú Cuatiá, Jofre localities; Herrmann *et al.*, 2011, 2013) as well as those from boreholes (Curuzú Cuatiá; Pesce *et al.*, 2016). For this contribution results from other three boreholes are presented, that are located in Villaguay (Entre Ríos province), Cerro Azul and Oberá (Misiones province), along with data from surface lavas of the latter province (Posadas city, transect between Eldorado and Bernardo de Irigoyen towns).

METHODS

Research was essentially based on microscopic studies of the transparent and opaque minerals and the geochemical features of the lavas. Materials from the boreholes were small rock chips (0.1-1.0 cm in size) that were carefully handpicked under optical magnification and washed with distilled water in an ultrasonic bath prior to carrying out the chemical analyses

RESULTS

The predominant opaque minerals of these rocks are iron oxides, by far being magnetite the most abundant phase, that intergrowths with the transparent minerals conforming the groundmass of these lavas. In lesser amounts ilmenite and hematite are present, both partially associated with magnetite or scattered in the groundmass. Also in some sectors profuse limonite is formed by alteration of iron oxides.

Native copper from both surface lavas and material from boreholes always appears in small grains, frequently related to the alteration products (celadonite, smectites) of olivine, also as an inclusion in plagioclase or as interstitial grains in the groundmass of the rocks. Also, very fine veins of native copper in transparent minerals occur. Noteworthy, in the material from Villaguay and Cerro Azul boreholes as well as in some oxidized surface samples from Corrientes and Misiones, native copper is mostly replaced by cuprite. Some amygdaloidal surface lavas from the province of Corrientes bear zeolites (clinoptilolite and heulandite) associated with celadonite and smectites as well as scarce cuprite filling the small voids, constituting a paragenesis comparable to stage I (zeolite facies) of Vista Alegre district (Brazil), studied by Pinto *et al.* (2010), as pointed out by Herrmann *et al.* (2011, 2013). However, native copper in the amygdules has not been reported, only scarce cuprite as its alteration product, showing a substantial difference with respect to what has been reported from Vista Alegre district (Brazil).

Sulfides have also been identified in lavas from the Argentine Mesopotamia region. The predominant phase in the material of all the studied areas is disseminated granular pyrite. Chalcopyrite and rhombic chalcocite also occur, along with digenite and covellite as supergene enrichment products of those sulfides and native copper, in material from the Curuzú Cuatiá borehole as well as in some surface samples.

Occurrence of native gold and electrum was found in the material from the Curuzú Cuatiá borehole, as was also previously reported in the basalts that crop out in the province of Corrientes (Herrmann and Segal 2005, Herrmann *et al.*, 2013). Native gold was also identified in the Vista Alegre district (Pinto *et al.*, 2010) and Realeza (Da Rosa Arena *et al.*, 2014) in Brazil. As it is known from the literature, presence of native copper along with native gold and silver has been described in continental basalts of several large igneous provinces.

In the analyzed samples, Cu contents are variable, up to 320 ppm. No relationship was found regarding the geochemical lithotype (e.g., high-Ti or low-Ti varieties), or texture of the rock (massive or amygdaloidal samples) or in relation to its surface location or its position in depth.

CONCLUSIONS

The association of native copper with smectite and celadonite as well as cuprite replacing native copper along with the latter phyllosilicates and zeolites found in some of the studied samples is consistent with an epigenetic genesis, but it is clearly poorly developed. There is no evidence of significant mobilization and subsequent precipitation of copper in these rocks, pointing out a remarkable difference respect to what was reported in Vista Alegre district and Realeza (Brazil). There the mineralization is completely epigenetic, as a consequence of the action of hydrothermal solutions at low temperatures (< 150º C) related to the Guaraní aquifer (Pinto *et al.*, 2010, Da Rosa Arena *et al.*, 2014). Instead, mineralization of native copper in the lavas of Argentine Mesopotamia region is mainly hypogene, according to what was found until today. This is reinforced by the occurrence of sulfides, absent in the above mentioned Brazilian localities.

Data from Curuzú Cuatiá borehole reveal that the base of the lava pile that overlies a significant level of sandstones carrying thermal fluids must be at a depth between 670 and 800 meters. Besides, thermal fluids have a temperature of 38º C and a pH=7.5, typical of sodium-chloride waters (Pesce *et al.*, 2016). As can be inferred from low–temperature Eh-pH stabilities for the system Cu-O-H-S-Cl (Brown, 2006), at pH 7.5 native copper is stable along with sulfides under negative Eh values. Solutions seem not to have moved upwards enough to attain the positive Eh conditions suitable for significantly remove copper from the basalts. Probably, the lack of important faults as those present in southeastern Brazil (e.g. Río Uruguay, Río Iguazú, Río Piquiri) would not have allowed a significant circulation of hydrothermal solutions capable to leach and redeposit native copper in the lavas of this part of the Paraná Magmatic Province.

REFERENCES

Brown, A.C., 2006. Genesis of native copper lodes in the Keweenaw district, northern Michigan: a hybrid evolved meteoric and metamorphogenic model. Economic Geology,101, 1437-1444.

Da Rosa Arena, K., Hartmann, L.A, Baggio, S.B., 2014. Geology and mineralization of native copper, gold and silver in Realeza, Paraná, Brazil, in: Hartmann L.A., Baggio, S.B. (Eds.), Metallogeny and crustal evolution of the Serra Geral Group. IGEO/UFRGS, Porto Alegre, pp. 335-368.

Herrmann, C., Lagorio, S., Segal, S., 2011. Mineralización de Cu en los basaltos de Serra

Geral de la provincia de Corrientes, Argentina. Su caracterización en el contexto regional. 18º Congreso Geológico Argentino. Neuquén.

Herrmann, C., Lagorio, S., Segal, S., Cozzi, G., 2013. Caracterización de la mineralización de cobre en los basaltos de la provincia de Corrientes. 10º Congreso Argentino de Geología Económica, San Juan.

Lagorio, S., Vizán, H., Geuna, S., 2016. Early Cretaceous volcanism in central and eastern Argentina during Gondwana break-up. SpringerBriefs in Earth System Sciences, DOI 10.1007/978-3-319-29593-0_1. Springer, Switzerland.

Pesce, A., Segal, S., Lagorio, S. 2016. El recurso geotérmico y la metalogénesis de los basaltos mesozoicos en Curuzú Cuatiá, Mesopotamia Argentina. 11º Congreso Argentino de Geología Económica, Salta.

Pinto, V.M., Hartmann, L.A., Wildner, W., 2011. Epigenetic hydrothermal origin of native copper and supergene enrichment in the Vista Alegre district, Parana basaltic province, southernmost Brazil. International Geology Review 53, 1163-1179.

FORMATION OF EPITHERMAL Ag-Au DEPOSIT AND DISPLACEMENT-LENGTH SCALING OF NORMAL FAULTS AS AN EXPLORATION TOOL: PALMAREJO MINE, CHIHUAHUA MEXICO

Joseph Ruffini

Coeur Mining - jruffini@live.com

The Palmarejo mining district is comprised of various low sulfidation Ag-Au epithermal quartz vein breccia deposits in the Sierra Madre Occidental mountain range in Northwest Mexico, which represents one of the major epithermal Ag-Au systems globally. The system is hosted in Basin and Range normal faults as a product of arc extension and associated volcanism that formed throughout the Oligocene to Miocene (28 to 18 Mya). This occurred after a prolonged period of convergence related to subduction, which reversed to an extensional regime as the subducting plate began to rollback with time. The deposit is defined by multi-stage quartz vein breccias with sphalerite-pyrite-galena, hosted in normal faults that have accommodated between 50 to 300 m of dip-slip displacement.

The idea of displacement-length scaling is well established in the structural literature. It details the concept that the strike length of a fault can be related to the displacement by an approximate ratio, which diminishes away from the center of the fault. This varies depending on hosting lithology, fault linkage, among other factors. In this study, the focus is on the mineralized portion of a fault, or the section that is of current economic significance. Measurement of previously well-defined systems provides the general local ratio that can be applied to exploration targets. Displacement and fault dimensions have been collected using surface and underground geologic maps, diamond drill core, sectional interpretation, and resource estimation domains. The ratio has been useful in revisiting previous deposits that were considered fully defined, but with the help of the displacement- length ratio, a significant amount of new resource potential was discovered. It can also help in a system with few drillholes to understand the potential dimensions of a system before extensive investment in drilling.

A | 22

LEAD ISOTOPIC SIGNATURE OF THE RIFT-RELATED PARAMILLOS DE USPALLATA Pb-Ag-Zn VEINS, ARGENTINA

Ana Paula Orellano Ricchetti[1], Nora A. Rubinstein

[1]Instituto de Geociencias Básicas, Aplicadas y Ambientales de Buenos Aires, Universidad de Buenos Aires-CONICET - anapaula.orri@gmail.com

INTRODUCTION

The Paramillos de Uspallata Pb-Ag-Zn vein deposit is located in the northern part of the Cuyo rift basin, developed in the Triassic (~235 Ma) and linked to the collapse of the Permian regional orogen and the beginning of the Gondwana supercontinent breakup (Figure 1a). Rifting is controlled by a large-scale NNE mechanical anisotropy and NW crustal-scale faults originated in Permian. The basin infill consists of continental sediments with locally interbedded alkaline basaltic lavas and rhyolitic tuffs and minor basaltic dykes unconformably overlying a Paleozoic volcano-sedimentary basement. The geochemistry of the basaltic magmatism suggests crustal contamination by interaction with underlying Permian volcanic rocks. During the Tertiary, the Andean orogeny inverted the basin, reactivated previous structures and produced arc volcanism.

The Paramillos de Uspallata deposit includes thirty-three subvertical veins emplaced along dextral and oblique-normal faults with NE-SW directions, coincident with Permian orogeny structures, and less E-W-trending ones (Figure 1a). The veins are up to 2 meters thick and up to 2.5 km in length and have banded, crustiform, cockade, and breccia textures. They are composed of sphalerite, galena, chalcopyrite, pyrite, marcasite, and freibergite-tetrahedrite with minor boulangerite, pyrargyrite, and owyheeite in a siderite with minor quartz gangue. Fluid inclusions and isotopic analyses revealed that the ore fluids had low temperatures, low to moderate salinity and resulted from the mixing between magmatic/metamorphic and meteoric fluids. Initially, these veins were considered as related with the Miocene Cu- porphyry deposits outcropping in the area; however, recent studies show that the Paramillos de Uspallata vein deposit is genetically linked to the extensional tectonics that followed the collapse of the Permian orogen and resulted in the rift formation and the consequent diastathermal metamorphism, which would have triggered the hydrothermal system.

METHODS

Two galena and three sphalerite samples from different veins were analyzed for lead isotopes at the Geochronological Research Centre of the University of São Paulo. Clean grains were carefully selected and Pb concentrates were prepared following standard methods. The isotopic analyses were carried out on a multicollector micromass spectrometer. The results were compared with previous lead isotopic data from the more likely sources of lead that are the basalts host rocks of the deposit and Permian arc volcanic that from the basement of the Cuyo basin rift.

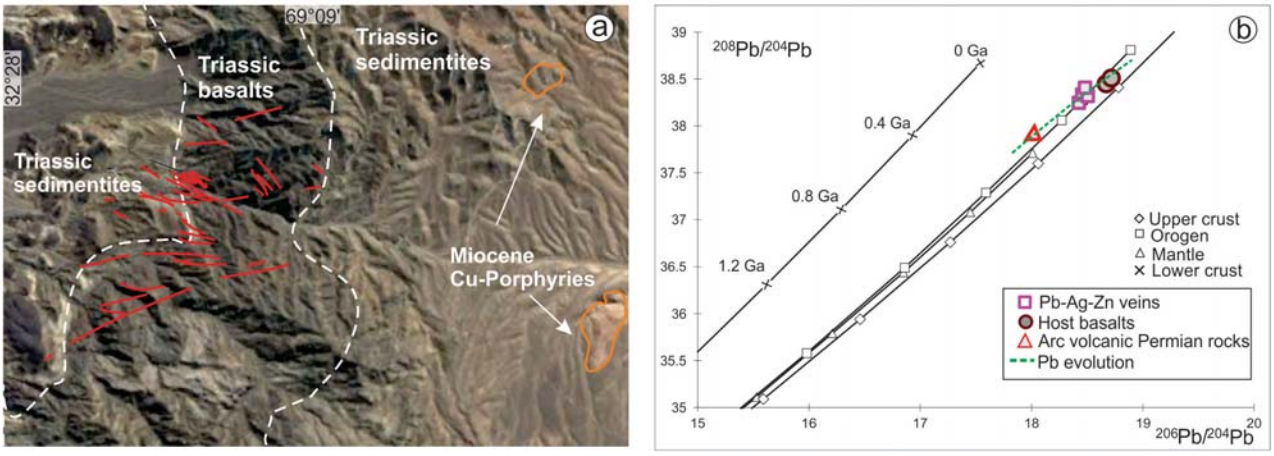

Figure 1: a) Veins location (in red) and outcropping distribution of Triassic and Miocene rocks in the area. b) Thorogenic diagram showing plumbotectonic curves (black), galena and sphalerite of the Paramillos de Uspallata veins (squares) and the Permian volcanic rock (triangle) composition.

RESULTS

The lead isotope composition of galena is slightly variable in 207Pb/204Pb and 206Pb/204Pb, and is distinctly lower than those of the host basalts, what point out the involvement of an older source for this m*etal.* Likewise, in the plumbotectonic diagrams, the vein samples plot close to the orogen curve defining a roughly linear array with the basalts and the Permian volcanic (green dashed line, Figure 1b).

CONCLUSION

The lead isotopic signature of the Paramillos de Uspallata Pb-Ag-Zn vein deposit suggests that the lead was sourced not only by the basaltic magmatism linked to the rifting but also by the Permian volcanic rocks that form the basement of the rift basin. This is consistent with the genetic model of the rift-related ore deposits in which Pb derives from a mixture of rocks with a long period of residence in the upper crust and rocks deformed during repeated orogenic cycles. In this context, reactivated crustal-scale faults would have acted as the main conduits for metals transport from the basement upward.

En la T2 (que ya pasé) en el ID 74, la autora me contestó los nombres completos, no se si los querés agregar.

A | 23

GENESIS OF THE LOMA GALENA DEPOSIT, NAVIDAD DISTRICT, PATAGONIA ARGENTINA

Bouhier Verónica[1], Franchini Marta, Tornos Fernando, Rainoldi Ana Laura, Patrier Patricia and Beaufort Daniel

[1]*Consejo Nacional de Investigaciones Científicas y Técnicas. Centro Patagónico de Estudios Metalogenéticos, Argentina - vbouhier@gmail.com*

Loma Galena (6410.8 t Ag, 997,130 t Pb) is one of the eight deposits of the world class Ag + Pb ± (Cu, Zn) Navidad district (19.670 t Ag and 1.32 Mt Pb) located in the west of the North Patagonian Massif of Argentina. The deposit was formed in an active continental rift basin during the Middle Jurassic, when subaerial volcanic activity was contemporaneous with lacustrine sedimentation. The normal faults that delimited the horsts and grabens in the deposit and the Sauzal fault, a detachment fault, acted as the main conduits for the upflow of hydrothermal fluids (Fig. 1). The deposit has a lithologic control and the highest metal anomalies are found in highly permeable and reactive autobrecciated mafic volcanoclastic rocks interbedded in the volcano-sedimentary Cañadón Asfalto Formation (Fig. 1).

The volcanic rocks are high-K basaltic andesite to dacite in composition and they have yielded LA-ICPMS U-Pb zircon ages of 173.9 ± 1.9 Ma and 170.8 ± 3.0 Ma. Lava flows surrounded by autobrecciated carapace were dominantly extruded in subaerial conditions whereas hyaloclastite and peperite facies suggest contemporaneous subaqueous volcanism synchronous with sedimentation. Lacustrine sedimentation represented by calcareous mudstone with pisolithic and laminated limestone, sandstone, chert and coal overlies the volcanic rocks. A Sr-rich evaporite layer interbedded in the sedimentary succession indicates intermittent drying out of the lake and hypersaline conditions.

The mineralization occurs in veins and hydrothermal breccias that lie on the structural hanging wall and footwall of the main faults, in mineralized autobreccia and chaotic breccia at the contact between volcanic and sedimentary rocks, and disseminated in the organic- rich sedimentary rocks. The earliest mineral infill of veins and breccias consists of calcite I and siderite with crustiform, cockade and platy textures, followed by two main episodes of mineralization. During the first mineralization stage precipitated framboidal pyrite and colloform pyrite, marcasite, galena and sphalerite. During the second stage chalcopyrite, bornite and tennantite-tetrahedrite with minor amounts of covellite and digenite replaced the early sulfides. Colloform bands of pyrite and marcasite show the highest Ag contents, although all sulfides and sulfosalts carry Ag. Sulfides are rarely observed in situ, on the walls of veins; they are usually found as transported fragments cemented by several pulses of chalcedony deposition with minor barite. Late infill consists of calcite II, barite II, quartz and strontianite. Hydrothermal breccias present voids with a geopet al infilling with detrital material of sand-silt size and variable composition (chalcedony, quartz, calcite, ankerite, barite, sulfides, rock fragments) with parallel lamination.

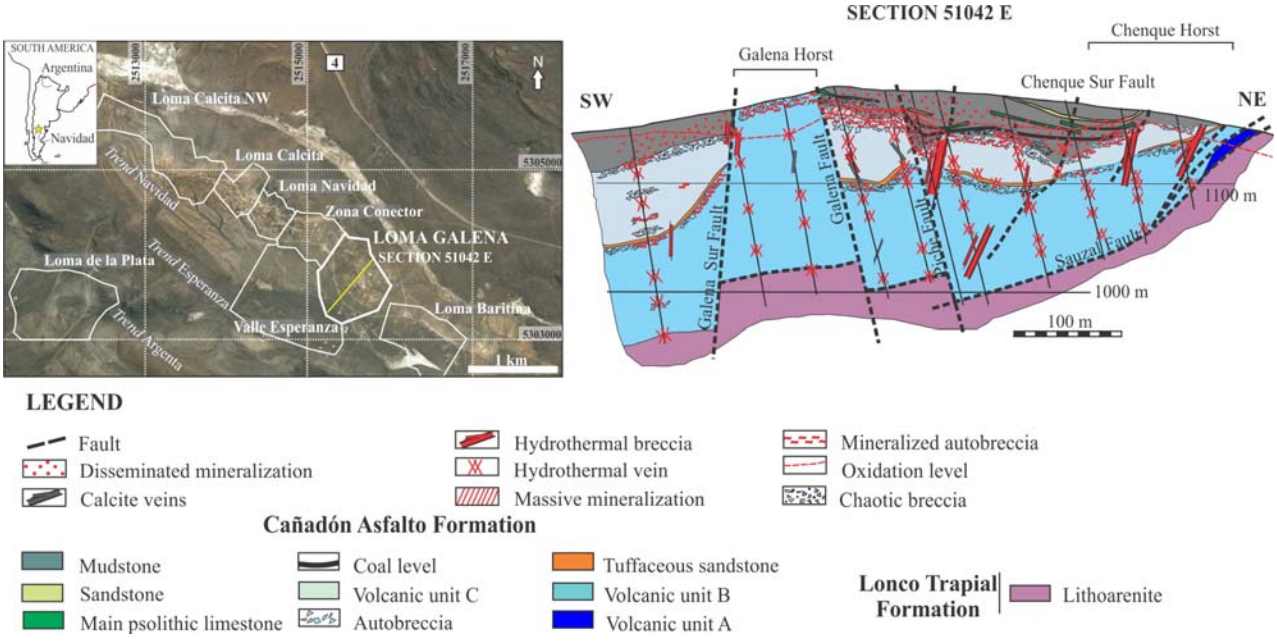

Volcanic rocks next to veins and breccias are altered and replaced by albite, adularia, calcite, celadonite, quartz, chlorite, sulfides, chalcedony, several types of clay minerals (kaolinite and smectite with illite-smectite mixed layers and traces of tosudite), Fe-Mg-Mn carbonates and calcite II. In the sedimentary rocks, the clasts are replaced by chalcedony, kaolinite and carbonates. Calcite and chalcedony also fill micro-veinlets.

The sulfur isotopic signatures of sulfides hosted in veins and hydrothermal breccias (δ34S -0.9 to +8.3‰) are more restricted than the δ34S of sulfides hosted in the autobreccia, chaotic breccia and sedimentary rocks (δ34S -15.4 to +12.9). The sulfur isotopic signature of hydrothermal barite varies between +15.7 and +22.0‰. The isotopic composition of celestite from the evaporite layer in the sedimentary rocks is 35.3‰.

Calcite I from veins has $\delta^{13}C$ values between -4.4 and -0.3‰ and a $\delta^{18}O$ of +19.7 to +22.1‰. Calcite 2 also from veins and breccias displays $\delta^{13}C$ values between -3.5 and -1.7‰ and $\delta^{18}O$ values of +11.2 to +15‰. Chalcedony II infill of veins and breccias has $\delta^{18}O$ between +16.2‰ and +18.4‰. Late quartz infill of veins and breccias has a $\delta^{18}O$ of +12.4‰.

Calcite I hosts aqueous fluid inclusions with a salinity close to 16.4 wt.% NaCl equiv. that homogenize between 165.8 and 208.3°C. Barite hosts aqueous fluid inclusions that homogenize to liquid in the range of 111-169°C. Fluid inclusions in calcite II have lower salinity (0 to 4.2 wt.% NaCl equiv.) and homogenization temperatures (58 to 95°C) than calcite I.

Early calcite I (siderite?) precipitated in veins and breccias from fluids with high salinity (~16.4% wt. NaCl eq.), temperatures (Th) <208 °C, and isotopic compositions of $\delta^{18}O$ fluid= 7.4‰ to 11.6 ‰ and $\delta^{13}C$ CO_2-6.4 to -2.3 ‰. Calcite I, albite, adularia, celadonite, and chlorite formed during the interaction of deeply derived chloride-rich fluid with the host volcanic rocks. The system intermittently boiled, as evidenced by platy texture in the calcite infill of veins and breccias. The steam generated during boiling at depth could condense in the overlying sedimentary rocks, forming H_2S and CO_2 -rich steam-heated waters. The abundance of black shale and the sulfur isotope values suggest that the bottom waters of the lake were anoxic and the loci of abundant biogenic sulfate reduction.

Mixing of the upflow chloride-rich fluid with H_2S-rich steam-heated water efficiently precipitated Ag bearing pyrite, marcasite, sphalerite and galena and dissolved some early formed hydrothermal phases in the altered volcanic rocks followed by the precipitation of tosudite and abundant kaolinite. The subsequent stage introduced Cu with Ag through fluids of limited circulation from the north and channeled by the Sauzal fault, and replaced some previous sulfides. Evidences that support the sulfide formation by fluid mixing are the following: a) the sulfur isotopic signatures of sulfides indicate a mixed source, with sedimentary sulfur derived from the biogenic reduction of the sulfate from the evaporite interbedded in the lacustrine sedimentary rocks and deep hydrothermal sulfur; b) the textures of sulfides such as framboids of pyrite and colloform pyrite-marcasite that are indicative of quick supersaturation, and, c) the high metal contents in sulfides and sulfosalts.

Once the H_2S was consumed, the diluent was CO_2-rich steam-heated water. Gradual cooling and dilution of chloride fluids by mixing with descending CO_2-rich steam-heated water may also account for the successive formation of illite-smectite, smectite, chalcedony, barite, carbonates rich in Fe and Mn, and calcite II in veins and breccias, in the volcanic and overlain sedimentary rocks at Loma Galena.

CHAPTER 3
ORE DEPOSITS RELATED TO GRANITES: FROM ORE FORMING PROCESSES TO METALLOGENY

Conveners: Jingwen Mao, Shao-Yong Jiang, Xiaoming Sun

THE GEOCHEMISTRY OF THE TOPS OF MINERALISED VARISCAN GRANITE SYSTEMS: EVIDENCE OF Li-Cs-F-Tl FROM SW ENGLAND

Charlie Moon

Moon Geology, Rose Cottage, Calstock, Cornwall, PL18 9QQ, Camborne School of Mines, CEMPS, University of Exeter, TR10 9EZ, UK - cjm@moongeology.co.uk

Tin and tungsten mineralization are well known from SW England. However the nature of the controlling composite granites has more recently been established by geochemical and, geophysical surveys.

The relatively late stage intrusives are also Li and F-rich as well as containing trace Nb and Ta. Enrichment of Cs in these Li- and F-rich granites, as well as basal Permian breccias has been known for some time. However data were very limited and the regional TellusSW data (TellusSW, 2014) (soils, stream sediments and waters) for the first time provide information on the spatial distribution of Cs, as well as Li and F in waters, which can be compared with more well- known Sn, W and Ta distribution.

The occurrence in high Cs in latest granites and earliest Permian breccias, coupled with the known volatile behaviour of Cs in Li-Cs-Ta systems, suggest that enrichment in basal breccias may be due to reworking of acid volcanic material, removed from the intrusive cover, or geothermal output. In the SE Devon these Cs anomalies have a regional spatial relationship with Sb mineralization.

Fluoride in water data highlight the Li and F-rich granites in the St Austell area. Other major F anomalies reflect U-Cu rich Permian sediments and probably lamprophyres. Fluorite-rich veins are well known in the area, mainly associated with Permo-Triassic Pb- rich mineralization and the data indicate F may be derived from a deep source.

Regional surveys for low abundance elements such as Nb, Ta, Cs, and Tl are now readily possible with advances in XRF and ICP-MS sensitivity. These enable detection of zoning of mineralised systems and of buried mineralization.

REFERENCE

[dataset] TellusSW, 2014. Tellus GB Website. http://www.tellusgb.ac.uk

A | 25

GEOCHEMICAL CHARACTERISTICS AND U-Pb ZIRCON AGES OF GRANITES IN A TUNGSTEN- MINERALIZED DISTRICT OF CATAMARCA PROVINCE IN SIERRAS PAMPEANAS, ARGENTINA

Kenzo Sanematsu[1], Yoshiaki Kon, Martín R. Gozalvez, Dolores Alvarez, Facundo Cecenarro, Noelia F. Iannizzotto, Yuki Tsunazawa, Takaomi D. Yokoyama, Carlos Herrmann, Eduardo O. Zappettini

[1]*Geological Survey of Japan, AIST - k-sanematsu@aist.go.jp*

BACKGROUND

The Sierras Pampeanas in northwest of Argentina are located in the proto-Andean margin of southwest Gondwana and consist of Paleozoic metamorphic rocks and granitic rocks. Ordovician and Late Devonian – Early Carboniferous granites were widely found in Sierras Pampeanas, northwest of Argentina. The granitic rocks consist mainly of pearluminous biotite granite and muscovite granite with lesser amounts of metaluminous granitic rocks. We studied granitic rocks in the Sierras Pampeanas of Catamarca Province in order to constrain geochemistry and emplacement ages of granitic magma that was related to tungsten (W) mineralization. Small W and/or Sn deposits were mined in the studied area and they consist of wolframite- and/or scheelite-bearing quartz veins hosted in granitic rocks and low-grade metamorphic rocks. Greisen alteration proximal to the quartz veins is found and distal alteration is rarely recognized. Skarn type W mineralization is rarely found in the studied area.

METHODS

Granitic rock samples for geochemical analyses and age dating were sampled in Fiambalá, Belén, Ambato and Ancasti ranges of Catamarca Province, Argentina. Whole-rockgeochemical compositions and U-Pb zircon ages were determined at Geological Survey of Japan. Granitic rock samples were dried at room temperatures and crushed by a jaw crusher. Individual 50 g fractions of the crushed samples were pulverized using a rod mill with alumina containers and rods.

Fused glass beads were prepared from a mixture of 0.5 g of the pulverized sample and 5 g of lithium tetraborate for whole-rock chemical analyses. The sample mixture was fused at 1200 °C in a Pt crucible using a high-frequency fusion instrument and cooled on a Pt disk. Major elements in the glass beads were analyzed by X-ray fluorescence Spectrometer (Rigaku ZSX Primus III+). Calibration curves of the major elements were established using the GSJ geochemical reference samples of igneous rock series.

Trace elements of the glass beads were analyzed with an inductively coupled plasma-mass spectrometry (ICP-MS) system (Agilent 7500cx) equipped with a femtosecond laser-ablation system. Abundances of trace elements were calculated by calibration lines prepared by GSJ geochemical reference samples of igneous rock series. Before the elemental analysis, flow rates of the carrier gas and the ion-lens settings were optimized to minimize the production ratio of $^{232}Th16O/^{232}Th$.

Zircon grains were separated from the granite samples by rough grinding, magnetic separation and hand picking. The zircon grains were mounted on epoxy disks, polished to expose cross-sections of the grains, and then coated with carbon. Backscattered electron and cathodoluminescence (CL) images of the polished zircon grains were obtained before U- Pb dating to visualize their internal textures. In situ zircon U-Pb dating was conducted by LA-ICP-MS (Agilent 7500cx). Reference zircons were also measured to check if the ages are consistent with their recommended values within analytical uncertainties. "Isoplot" was used to draw concordia plots and a relative probability plot and to calculate weighted means.

RESULTS AND DISCUSSIONS

Studied granitic rocks are classified as granite by a normative albite-orthoclase-anorthite ternary diagram and as shoshonitic series or high-K series in a K_2O-SiO_2 plot. Alumina saturation index [molar $Al_2O_3/(CaO+Na_2O+K_2O)$] of the granites show strongly to weakly peraluminous compositions with the exception of syenite from the El Portezuelo Pluton (Fig. 1a). The peraluminous granites consist of biotite granite and muscovite-biotite granite with a small amount of garnet-bearing granite. The granites are geochemically and petrographically classified into I-type and S-type granites and most of them have geochemical characteristics of A-type (e.g., high Ga/Al ratios). Low magnetic susceptibilities show that all the granites are ilmenite-series that can be related to W-Sn mineralization. Tungsten contents of unaltered granites tend to be high with the increase of SiO_2 andrelatively high (>~10 ppm W) in some samples of the Mudadero, Los Ratones, Cerro Colorado and Quimivil Granites (Fig. 1b). However, the elevated W contents do not necessarily correspond to granite related to W mineralization because no W deposit was found in the Mudadero Granite.

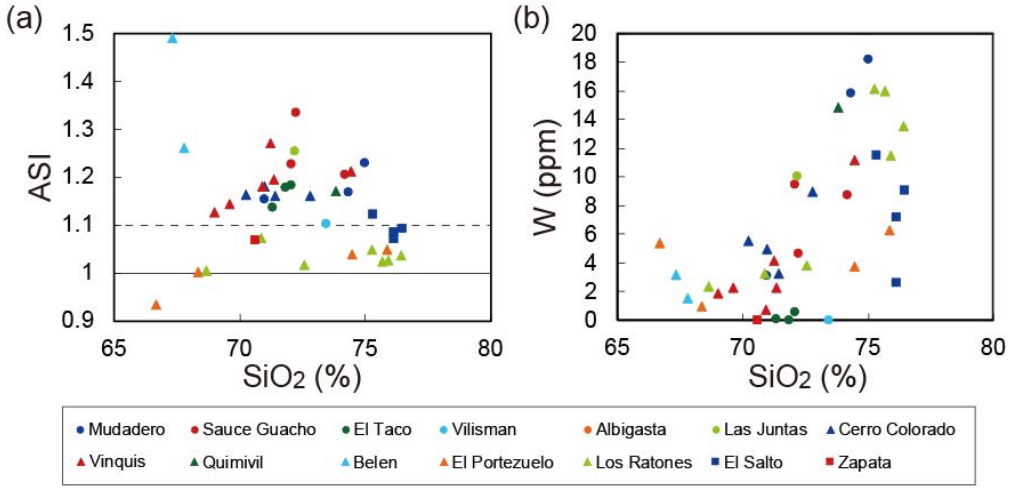

Fig 1 (a) Alumina saturation index (ASI) versus SiO_2 plot and (b) W versus SiO_2 plot of the unaltered granite samples.

U-Pb zircon ages of the Los Ratones Granite (319 Ma) and Vinquis Granite (353 Ma) related to W mineralization are consistent with a range of previously-reported zircon ages from 380 to 320 Ma. The results suggest the possibility of multiple events of W mineralization in the studied area. No significant difference was recognized between the Devonian-Carboniferous granites related to W mineralization and barren granites although the Ordovician granites have no W or Sn mineralization (e.g., Albigasta and Belén Granites).

ACKNOWLEDGEMENT

This study is a part of the fiduciary obligation project of Heisei 29 years supported by Ministry of Economy, Trade and Industry (METI) of Japan.

A | 26

EARLY PALEOZOIC VEINS OVERPRINTED BY LATE MESOZOIC GOLD MINERALIZATION IN THE JIANGNAN OROGEN: CONSTRAINTS FROM AR-AR GEOCHRONOLOGICAL, FLUID INCLUSION AND SIMS OXYGEN ISOTOPE STUDIES OF GOLD DEPOSITS IN NORTHEASTERN HUNAN, SOUTH CHINA

Teng Deng[1], Deru Xu, Guoxiang Chi

[1]East China University of Technology - dengteng2015@126.com

A number of gold deposits, totaling over 970 t Au, have been discovered in the Jiangnan Orogen which refers to a Neoproterozoic collisional zone in the Southeastern Yangtze block, South China. The Wangu and Huangjindong gold deposits in northeastern Hunan are the two representative gold deposits in the Jiangnan Orogen (Fig. 1). Each of the two deposits has a reserve of over 80 t Au and average grades of 4 – 10 g/t Au. The gold deposits were located near Late Mesozoic granites and NE-trending faults, but the ore bodies were hosted by Early Paleozoic WNW-trending faults. Previous research indicate that gold mineralization may occurred at Late Neoproterozoic, Early Paleozoic and Late Mesozoic, and the metamorphic-sourced ore fluids are characterized with low-medium temperatures and salinities. However, due to the lack of reliable geochronological work and systematic petrographic work, the mineralization ages, fluid sources and characters of gold mineralization fluids remain to be unclear.

To solve these problems, detailed petrographic work was conducted to establish the paragenesis sequence in the gold deposits. One muscovite sample crosscutting the pre-ore veins in the Huangjindong deposit and another muscovite sample crosscutting the syn-ore veins of the Dayan gold occurrence in Wangu area were used for Ar-Ar dating. Zircons from the Lianyunshan granite cut through by the syn-ore veins in the Dayan gold occurrence were used for laser ablation inductively coupled plasma-mass spectrometry (LA-ICP-MS) U- Pb dating. Arsenopyrite from the ore veins were used for electron microprobe analysis (EMPA) analysis to evaluate ore-forming temperature. Fluid inclusions research was conducted on quartz, scheelite and sphalerite to study fluid characteristics from each stage, and secondary ion mass spectrometry (SIMS) oxygen analysis was used on quartz to figure out the fluid sources of different stages.

Five generations of quartz veins were distinguished based on field and specimen observations, i.e., the pre-ore barren quartz (Q1) and quartz (Q2)-scheelite stages, syn-ore quartz (Q3)-pyrite-arsenopyrite and quartz-(Q4)-gold-polysulfide stages, and post-ore quartz (Q5)-calcite stage. The muscovite crosscutting the pre-ore barren quartz (Q1) veins yielded the Ar-Ar age of ca. 400 Ma, and the Q1 veins were hosted by Early Paleozoic faults, indicating the Q1 were formed during Early Paleozoic. The muscovite crosscutting the syn- ore quartz (Q3)-pyrite-arsenopyrite veins yielded the Ar-Ar age of ca. 130 Ma, and the zircons in the Lianyunshan granites yielded the LA-ICP-MS U-Pb age of ca. 142 Ma, suggesting the quartz (Q3)-pyrite-arsenopyrite veins were formed during Late Mesozoic (ca. 142 – 130 Ma). Arsenopyrite geothermometry indicate that the quartz (Q3)-pyrite- arsenopyrite stage was formed at 243 ± 20. In addition, fluid inclusions in the pre-ore veins are characterized by the H_2O-NaCl-CO_2 system, homogenization temperatures of 266 – 276 °C and salinities of 5 – 5.4 wt.% NaCl equivalent, whereas those in the syn-ore veins overprinting the barren veins have a H_2O-NaCl composition system, homogenization temperatures of 169 to 256 °C, and salinities from 8.7 to 15.2 wt.%. In addition, the $^{18}O_{fluids}$ and $^{18}O_{quartz}$ values the pre-ore veins were both higher than those from some syn-ore veins, indicating metamorphic origin for the pre-ore veins and involvement of magmatic water in the syn-ore veins.

Based on these studies, it is proposed that both the Early Paleozoic and Late Mesozoic veining events are controlled by the same fracture systems, with the former being formed in a relatively deep, orogenic deformation-metamorphic environment, and the latter in a relatively shallow, extensional environment accompanied by extensive granitic magmatism. Reactivation of the Early Paleozoic structures during the Late Mesozoic orogeny, together with availability of sulfur and gold, possibly associated with granitic intrusions, played a key role in the formation of the gold deposits in northeastern Hunan and possibly elsewhere in the Jiangnan Orogen.

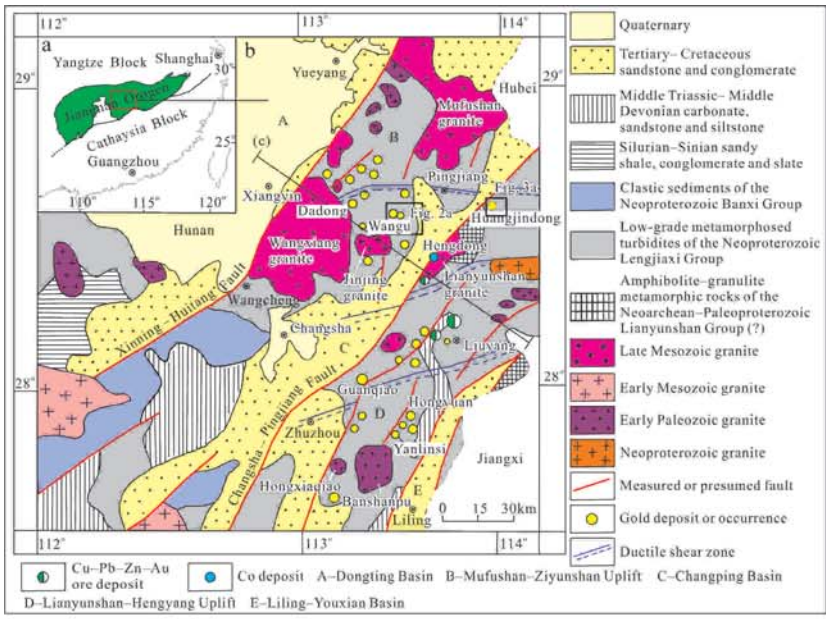

Fig. 1. (a) Location map of the Jiangnan Orogen, South China and (b) simplified map of Northeastern Hunan.

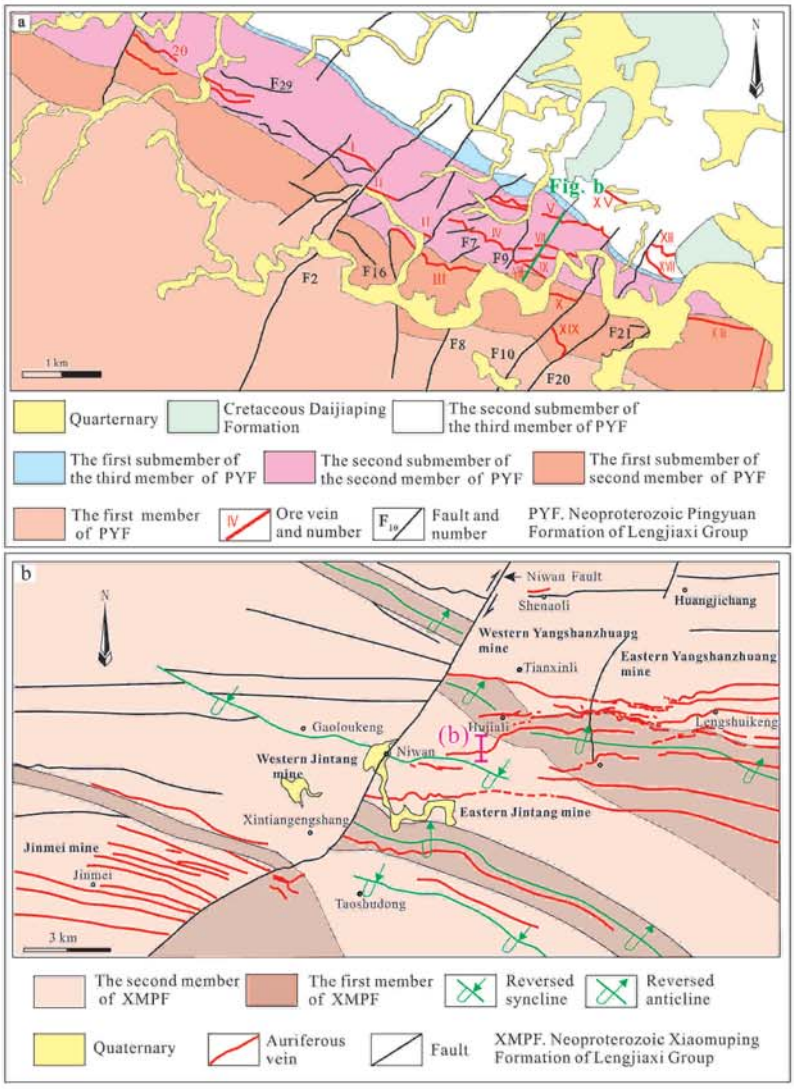

Fig. 2. Geological map of the (a) Wangu and (b) Huangjindong gold deposits.

A | 27

TANTALUM-NIOBIUM MINERALIZATION IN GRANITOID INTRUSIONS: EXPERIMENTAL STUDY

Chevychelov Vitaly

IEM RAS, Chernogolovka, Russian Federation - chev@iem.ac.ru

BACKGROUND

Problem of the origin of rare-metal deposits in granites is considered as taking into account the results of experiments that can provide geologists with some new criteria and limitations in interpreting geological data and assessing the reliability of a genetic hypothesis. At crystallization of a granite melt, the concentrations of rare elements can increase substantially. The main factor controlling the accumulation of these elements in the residual melt is the compatibility of these elements with minerals and melt, as well as the solubility of accessory minerals in the melt and in the coexisting high-temperature fluid. This solubility is determined by the temperature, pressure and composition of the melt. Niobium and tantalum are high field strength elements (HFSE). They cannot be integrated in the structural lattice of most rock-forming minerals and therefore are concentrated at fractional crystallization in silicate melts prior to saturation of the melt by accessory minerals, for example, columbite-tantalite or pyrochlore-microlite series.

METHODS

Rock samples and analytical data on the geochemistry and geology of typical Ta-Nb deposits were used directly in experiments, as well as for correction of experiments and applying results to natural objects. The experiments were carried out with alkaline, subaluminous and alumina-rich granitoid melts at temperatures of 600-850 °C, and pressures of 100-400 MPa in internally heated pressure vessels (IHPV). At studying of the dissolution of tantalum- niobium minerals in the magmatic melts, the crystals of these minerals were placed inside glass powder with the addition of fluoride aqueous solution. Method of approach to equilibrium on both sides was used in the experiments on the study of the partitioning of components between the melt and the fluid. After the experiments, the melts and mineral phases were examined by optical and electron-scanning microscopy, and their chemical composition was determined by microprobe analysis (EDS and WDS). Analytic methods of X- ray diffractometry and ICP-MS, ICP-AES were also used.

RESULTS

Experimental data show that the change in alkalinity and alumina-rich melt most significantly affects the effective solubilities of Ta and Nb in the melts. These solubilities are maximal in the alkaline melt. The contents of Ta and Nb significantly decrease (by an order of magnitude or more) in subaluminous melt, and, finally, the contents reduce several times more in alumina-rich melt. Simultaneously the Nb/Ta ratio decreases, since the Nb content decreases faster than Ta.

At tantalite solubility the effective solubility of Ta in the melt is higher than the solubility of Nb at all the studied melts and temperatures, so the Nb/Ta ratio in the melt is always less than unity and it varies from ~0.8-0.7 to ~0.1. The Nb/Ta ratio in alumina-rich melt decreases to a minimum of ~0.1 at reduced temperature 650 °C. Therefore, it is likely that the decrease in temperature can lead to the significant separation of Ta and Nb in alumina-rich granite melts. At the melt crystallization, Nb will partially escape in the mineral phases, and Ta will remain in the melt until the last. As is known, tantalum deposits are associated with similar alumina-rich granites.

The temperature dependence of the effective solubility of Ta and Nb is positive, but it is less pronounced, compared with the dependence on the alkalinity-alumina in the melt. With decreasing temperature from 850 to 650°C, the Ta content in the melt decreases by 2-3 times, and Nb in aluminous melts reduces up to 6-10 times. The solubility reduction is much better off manifested in subaluminous melt.

It is shown that the effective solubility of Ta in the melt is practically independent on the composition of the dissolved mineral at the columbite-tantalite series (Mn,Fe)(Nb,Ta)$2O_6$. Simultaneously the effective solubility of Nb changes significantly: it is maximal at columbite dissolution, decreases at tantalite dissolution and becomes minimal at pyrochlore dissolution (Fig. 1). It is found that pyrochlore $(Ca_{1.1}Na_{0.8}Ce_{0.05})(Nb_{1.8}Ti_{0.2})O_{5.9}F_{1.1}$ becomes unstable in alumina-rich melt. Na_2O, F, and CaO are removed from mineral, and the same time SiO_2, Al_2O_3, and probably K_2O are incorporated to the mineral from the melt. At the same time pyrochlore can crystallize from the alkaline residual magmatic melt more likely than columbite-tantalite, since the crystallization of pyrochlore requires a significantly lower saturation concentration of the melt in Nb.

The obtained data on the rate of diffusion transport of Ta and Nb in magmatic melts (DH∼n•10^{-9}- n•10^{-11} cm^2/s) allow us to evaluate the processes of these metals transport and the possible crystallization of tantalum-niobium minerals in connection with ore formation in granites. Strong effect of the melt composition and pressure on the diffusion of these metals in melts, especially in alkaline melts, is established.

CONCLUSIONS

Our experimental data on the effective solubilities, partitionings and diffusions of Ta and Nb in granitoid melts, as well as comparison of these data with the results of the investigation of natural deposits, allow us to evaluate the physical-chemical conditions for the formation of tantalum and niobium mineralization at the magmatic stage. The obtained data confirm the leading importance of crystallization fractionation of granitic magma in providing stepwise concentration in the melt of rare metals in albitite and others deposits associated with calc-alkaline granites, including lithium-fluorine granites.

ACKNOWLEDGEMENTS

The work was supported by the RFBR grant N° 18-05-01001A.

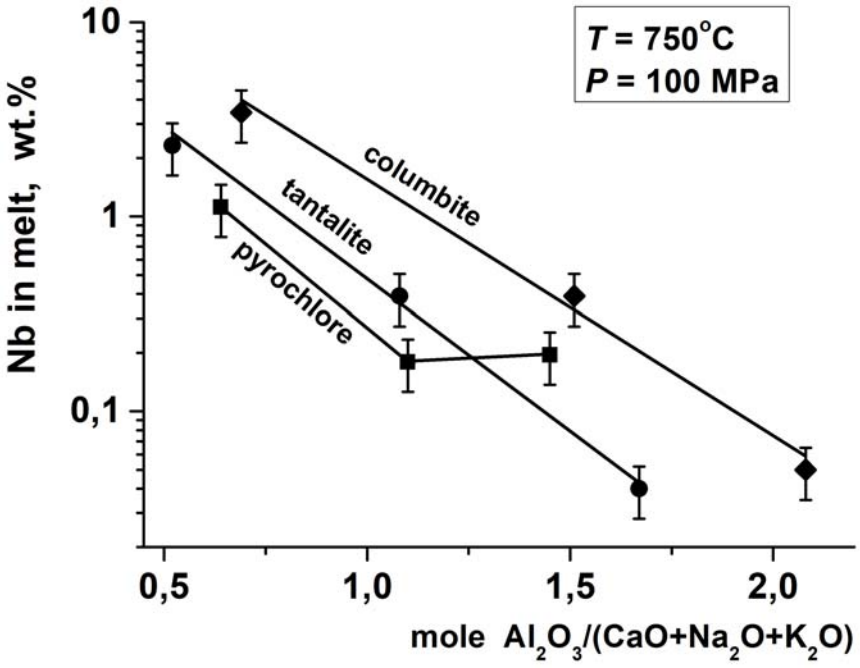

Fig. 1. The contents of Nb in aluminosilicate melts with different alkalinity-alumina content at the dissolution of columbite, tantalite and pyrochlore

A | 28

GOLD DEPOSITS OF THE ALTAY-SAYAN FOLD AREA (RUSSIA) RELATED TO CAMBRIAN AND ORDOVICIAN GRANITOIDS

A.I. Chernykh[1], E.V. Vetrov

[1]Central Research Institute of Geological Prospecting for Base and Precious Metals - chernykh@tsnigri.ru

Within the Altay-Sayan fold area (Central Asia, Russia) granitoids of different ages (from Early-Cambrian to Triassic) are widely spread. These magmatic complexes reflect main stages of geodynamic evolution of the region. The most extensive are Cambrian and Ordovician granitoids in the central and eastern parts of the Altay-Sayan, which originated in island-arc, accretionary and collisional settings. Many gold deposits of low-sulphide Au- quartz, skarn and gold-bearing copper-porphyry types are associated with these particular magmatic complexes. The authors studied gold mineralization and ore-forming Cambrian and Ordovician granitoids in order to update metallogenic division and create exploration criteria for reliable forecasting of new prospects in underexplored remote areas. The study is focused on the Tannuolsky ore district located at the southern Altay-Sayan near Mongolian border.

The Tannuolsky district is composed of Early-Cambrian volcanic-sedimentary rocks associated with island-arc settings (Kadvoiskaya, Serligskay, Irbiteiskaya series). These rocks are cut by Cambrian and Ordovician gabbro, diorite, granodiorite, granite and plagiogranite composing the major Ugneshskiy pluton and numerous minor massifs. Within the region gold and gold-bearing polymetallic, copper and iron mineralization are located.

The comprehensive study of the Tannuolsky district granitoids includes: review of existed maps and literature, field observation, petrographic and X-ray fluorescence study, isotopic geochronology (U-Pb by SHRIMP-II) and geochemistry (Rb-Sr and Sm-Nd by ICP-MS). Ores and host rocks have been studied by petrographic and mineragraphic methods complimented by SEM (JSM 6510 LV) and EPMA (Camebax-Micro) techniques.

Cambrian and Ordovician granitoids of the Tannuolsky district vary in their age, formation conditions, composition and metallogenic profile. Based on the complex investigations and previous study results three magmatic complexes have been recognized: Mainsky, Tannuolsky and Argoliksky.

The oldest Mainsky complex (534-518 Ma, U-Pb) initially discovered at the Tannuolsky district is presented by few small intrusives of gabbro-plagiogranite composition. By the chemical composition plagiogranite belongs to M-type and reveals similarity with island-arc plagiogranite. Trace element distribution pattern together with Sm-Nd and Rb-Sr isotopic signatures imply formation of the Mainsky complex plagiogranite happened due to partial melting of the Neoproterozoic (0.82 Ga) metamafics located at the basement of the island- arc system. Positive Pb-anomaly, relatively increased (for M-plagiogranite) initial $^{87}Sr/^{86}Sr$ and $\varepsilon_{Nd}(T)$=+5.02 show possible addition of an ancient crust component into the area of magma generation.

Formation of the minor lenses of the magnetite-bearing garnet-pyroxene skarn and low- sulphide Au-quartz veins is genetically linked to plagiogranite of the Mainsky complex. Gold- bearing quartz veins are less than 1 m thick with gold content below 1 g/t. Gold mineralization of this stage is hard to separate from more extended mineralization of the Late Cambrian stage.

Late Cambrian (508-492 Ma, U-Pb data) Tannuolsky complex is represented by diorite- granodiorite-plagiogranite rocks composing numerous major and minor massifs cutting Early Cambrian volcanic-sedimentary units and Mainsky complex rocks. Petrochemically granitoids of the Tannuolsky complex correspond to I-type granite and significantly differ from the Mainsky complex magmatic rocks. The trace-element distribution pattern and Sm-Nd and Rb-Sr isotopic signatures infer their composition is similar to granitoids formed from partially melted Neoproterozoic (0.72 Ga) metamafic-rocks contaminated by ancient continental crust material. The rocks of Tannuolsky complex have been formed during accretion stage of the Tannuolsky district evolution.

Most of the gold mineralization indicators of the Tannuolsky district are related to exo- and endo-contacts and roof pendants of the Tannuolsky complex. The gold-skarn mineralization is associated with diorite and quartz-diorite intrusion of the first phase. Garnet-pyroxene skarn form lenses up to 5-10 m thick and hundreds meter long. Besides magnetite skarn contain chalcopyrite-bornite, quartz and gold mineralization. Intrusion of the second phase granitoids caused formation of the gold-bearing skarn lenses and numerous low-sulphide Au-quartz veins. Extended scale of Late Cambrian ore-forming processes is, firstly, a result of the larger volume of magmatism occurred. On the other hand, rocks dislocated intensively during accretion of the island-arc volcanic and intrusive complexes are characterized by high-permeability.

Based on spatial distribution of the gold mineralization three ore clusters have been recognized within the Tannuolsky ore district: Elegetsky, Aptarinsky and Shiviligsky.

Volcanic-sedimnetary rocks of the Aptarinsky ore cluster host vein zones with gold content 1-4 g/t in ore bodies 3 to 20 m thick. High gold content is confined to the zones of extensive silicification, sulphide-quartz veins and sulphidization. Quartz veins are 1 to 3 m thick. The maximum gold contents up to 30-90 g/t occur when sulphide-quartz mineralization is localized within calcareous garnet-pyroxene skarn. Sulphides are represented by chalcopyrite, bornite, and pyrite. Skarn rocks often contain magnetite and gematite. Malachite, chalcosine, covelline, and limonite are typical for the oxidation zone of crushed veins.

Gold was discovered in quartz veins, silicified skarns and heavy-mineral concentrate of diluvial deposits and crushed samples. The extracted gold particles vary in size from 0.01 to 3-4 mm. Typical is a wide range of gold fineness from 790 up to 1000 ‰. The most widespread is gold with fineness of 820-840 ‰ and 870-920 ‰. This gold is associated with formation of gold-bearing quartz veins, and fineness changes possibly show different stages of their formation and different erosion level of the ore-forming system. The gold with higher fineness of 990-1000 ‰ may represent the earlier formed gold affected by thermal influence of numerous Devonian dykes. Silver is most common admixture (0.1 to 19%), mercury (0.1-0.4% up to 2.7%) and copper (.1-0.3% up to 0.77%) are less typical. Correlation of gold with copper and silver occurs in the primary and secondary geochemical fields of the crushed veins.

Besides gold-bearing skarn and low-sulphide Au-gold veins copper-porphyry mineralization is associated with small granitoid bodies of the Tannuolsky complex second phase. A number of ore fields with disseminated and vein sulphide mineralization have been described. Sulphides are represented by pyrite, chalcopyrite, bornite and molibdenite. Mineralized zones are 20-80 m thick and up to 2 km long with Cu content 0.1-0.4%, Mo – 0.001-0.01% and Au - 0.1-0.4 g/t. This type of mineralization is similar to the Late-Cambrian gold-bearing copper-porphyry Ak-Soug deposit located in comparable geological settings to the north-east from Tannuolsky district.

Late-Ordovician granite-leucogranite massifs (451-447 Ma, U-Pb) of the Argoliksky complex have been formed during the collision stage in relatively lesser extent. Petrochemical characteristics of Argoliksky granite are close to A-type granite rocks. Isotopic and chemical signatures allow to suggest that formation of these granitoids happened in upper parts of the collision structures. These low-alumina melts could be generated from mafic Neoproterozoic (0.17-0.78 Ga) protolith contaminated by crustal material.

Geochemical anomalies and secondary dispersion halos and trains of Cu, Mo and Au are spatially associated with Argoliksky granitoids depleted in ore components. This implies that intrusion of Late-Ordovician Argoliksky complex caused partial reworking of ore matter within existed ore fields.

Complex study of the Tannuolsky district gold mineralization indicates its high potential for ore deposits discovery. Aptarinsky ore cluster was suggested as a first priority prospecting area for exploration. Revealed features of gold mineralization distribution, geological structure, age and composition of rocks are a solid base to resolve problems of gold prospecting in comparable ore clusters of the Altay-Sayan – Martayginsky, Kommunarsky, Mrassky, Olkhov-Chibizheksky and Kaakhemsky. Investigation on distribution and localization patterns of gold mineralization associated with Cambrian and Ordovician magmatism allows to identify prospectivity of ore districts and clusters and direct exploration work.

A | 29

HIGHLY EVOLVED XIANGHUALING A-TYPE GRANITIC ROCKS: INSIGHTS INTO MULTI-STAGE SN-POLYMETALLIC MINERALIZATION IN SOUTH CHINA

Huan Li

WITHDRAWN BY THE AUTHOR

GENESIS OF THE MOUNT PLEASANT W-MO-BI (FIRE TOWER ZONE) AND SN-ZN-CU-IN (NORTH ZONE) DEPOSITS, NB CANADA: EXAMINATION OF CONTRASTING MINERALIZATION TYPES POSSIBLY LINKED TO REDOX EVOLUTION DURING EPISODIC DEVOLATILIZATION OF AN EXTREMELY FRACTIONATED LEUCOGRANITE

David R. Lentz

Dept of Earth Sciences, University of New Brunswick, Fredericton, NB E3B5A3 Canada - dlentz@unb.ca

INTRODUCTION

The two Late Devonian Mount Pleasant granophile deposits are hosted in the southwestern margin of the Mount Pleasant Caldera complex, NB, Canada (McCutcheon *et al.*, 1997; Dostal and Jutras, 2016). The Fire Tower zone W-Mo-Bi deposit (North & West) is reported have Indicated resources of 13.5 Mt of 0.33% WO_3 0.21% MoS2 and 0.06% Bi (Dunbar *et al.*, 2008) and the adjacent North zone deposit has Sn-In resources (with Zn, Cu) of 4.9 Mt with 0.43% Sn, 67.8 g/t In, 0.67% Zn, and 0.11% Cu (Indicated) and inferred resources of 7.6 Mt of 0.22% Sn, 74.6 g/t In, 0.99 % Zn, and 0.09 % Cu (McCutcheon *et al.*, 2012).

GRANITES AND MINERALIZATION

The W-Mo-Bi system is associated with the 1st phase granite (leucogranite GI) and the Sn-In deposits are associated with the second granite (GII) (see Sinclair *et al.*, 1988; Yang *et al.*, 2003; Inverno and Hutchinson, 2006; Zhang *et al.*, 2017). The 3rd granite phase does not seem to be directly associated with mineralization at Mount Pleasant. The age of both deposit systems is well constrained at 370 Ma by molybdenite Re-Os (Thorne *et al.*, 2013) and U-Pb monazite (Charnley *et al.*, 2017). The differences between the two ore systems are somewhat perplexing, although the GI is a fine-grained porphyry that represents a subvolcanic system with a diatreme with W-Mo-Bi mineralization at the base above the G1 porphyry (Kooiman *et al.*, 1986; Samson, 1990). The GII tuffisitic dykes are derived from the biotite-bearing GII granites at depth, and are associated with the North zone Sn-In mineralization (Yang *et al.*, 2003; Inverno and Hutchison 2004, 2006); these granites did not crystallize in the same way, with the early GI possibly pressure quenching (& oxidizing, Lentz, 2016) explaining the changes in mineralization systems. The reduced Sn-In mineralization locally overprints W-Mo-Bi, which is particularly evident in the Fire Tower Zone. In contrast to the Fire Tower zone, the North Zone has endogranitic contact, and exogranitic styles of tin and base-metal mineralization (Inverno and Hutchinson, 2004; Sinclair *et al.*, 2006), including lode style that are detailed in the McCutcheon *et al.* (2012) report. The degree of alteration in the GI and GII granites limits further petrophysical or mineral-chemical analysis of the redox relations.

EXTREME FRACTIONATION - MAGMATIC EVOLUTION AND HYDROTHERMAL ENRICHMENT

The three phases of high level (subvolcanic, at pressures less than 100 MPa), high silica granites are very highly evolved (Sinclair *et al.*, 1988; Yang *et al.*, 2003; Inverno and Hutchinson, 2006) with high F, flat REE patterns, high REE contents, very pronounced negative Eu anomalies, with very low Zr/Hf and Nb/Ta; they typically plot in the fractionated crustal A-type granite field. Lentz (2014) postulated that the high degree of fractionation of these granites was due to extreme fractionation due to thermal anomalies associated with other magmatism in the region (see Dostal and Jutras, 2016). Petruk and Owen (1975) noted considerable monazite and xenotime in the W concentrate that NRCan CANMET studied, with moderate middle REE. They report that the 70% wolframite concentrate had 15% monazite and 2% xenotime with an average grain size of 20 microns. Assadzadeh *et al.* (2017) also note high total REE up to 10% in fluorite associated with Sn- or W-rich mineralization and provide a detailed analysis of the REE+Y enrichment processes. However, there are generally no bulk analyses of REE and Y in these mineralization types, except for the two CANMET certified reference materials MP-1b (Zinc- Tin- Copper- Lead Ore) and MP-2a (W-Mo ore), which are incomplete; further work is needed to assess the REE+Y potential in these two separate ore systems. We anticipate that the REE+Y associated with monazite-xenotime are directly associated with the highest grades of W-Mo- Bi and Sn mineralization. Although W, Mo, and Bi are hydroxide complexes and Sn is dominantly a chloride complex in these types of systems, combinations of OH, Cl, and F were likely responsible for the significant enrichment of REE+Y in the mineralization and that decreasing T, as well as fixation of F in mica and saturation of fluorite, was responsible for saturation of REE+Y phases (cf. Assadzadeh *et al.*, 2017).

CONCLUSIONS

The GI, GII, and GIII granites are highly specialized, and produce notable mineralization of two very different types. The two granites associated with mineralization are geochemically indistinguishable, although they are invariably altered to some degree. Differential degassing of H_2 may help explain the change in redox that would affect the redox sensitive elements, in particular Mo and Sn.

REFERENCES

Assadzadeh, G.E., Samson, I.M., Gagnon, J.E., 2017. The trace element chemistry and cathodoluminescence characteristics of fluorite in the Mount Pleasant Sn-W-Mo deposits: Insights into fluid character and implications for exploration. Journal of Geochemical Exploration, 172, 1-19.

Charnley, B.E., Lentz, D.R., Mcfarlane, C.R.M., 2017. Hydrothermal monazite and xenotime related to granites associated with the North Zone Mount Pleasant Sn-Zn-Cu-In (& W) deposits, NB, Canada: preliminary studies. SGA Quebec 2017, 4 p.

Dostal, J., Jutras, P., 2016. Upper Paleozoic mafic and intermediate volcanic rocks of the Mount Pleasant caldera associated with the Sn–W deposit in southwestern New Brunswick (Canada): Petrogenesis and metallogenic implications. Lithos, 262, 428-441.

Dunbar, P., El-Rassi, D., Rogers, J.S., 2008. A technical review of the Mount Pleasant Property, including an updated mineral resource estimate on the Fire Tower zone, southwestern New Brunswick. Technical Report for Adex Mining Inc.

Inverno, C.M.C., Hutchinson, R.W., 2004. The endogranitic tin zone, Mount Pleasant, New Brunswick, Canada and its metallogenesis. Applied Earth Science: IMM Transactions Section B., 113, 261–288.

Inverno, C.M.C., Hutchinson, R.W., 2006. Petrochemical discrimination of evolved granitic intrusions associated with Mount Pleasant deposits, New Brunswick, Canada. Applied Earth Science: IMM Transactions Section B. 115, 23–39.

Kooiman, G.J.A., McLeod, M.J., Sinclair, W.D., 1986. Porphyry tungsten-molybdenum orebodies, polymetallic veins and replacement bodies, and tin-bearing greisen zones in the Fire Tower Zone, Mount Pleasant, New Brunswick. Economic Geology 81, 1356-1373.

Lentz, D.R., 2014. The role of magma advection and regional thermal evolution in prolonging fractionation in spatially & temporally associated magmatic systems: examining conditions for extreme differentiation & formation of granophile ore deposits. IMA 2014 Johannesburg, SA.

Lentz, D.R., 2016. Differential degassing of H_2 causes redox changes affecting multivalent element partitioning during volatile phase saturation of crystallizing magmas. IGC 2016, Cape Town, SA.

McCutcheon, S.R., Anderson, H.E., Robinson, P.T., 1997. Stratigraphy and eruptive history of the Late Devonian Mount Pleasant Caldera Complex, Canadian Appalachians. Geological Magazine 134, 17–36.

McCutcheon, S., Reddick, S, McKeen, T., Scott, S., Kociumbas, M., 2012. Technical report Mount Pleasant Property, including an updated mineral resource estimate on the North zone, southwestern New Brunswick. Technical Report for Adex Mining, 212 p.

Petruk, W., Owen, D., 1975. Monazite from the Mount Pleasant Deposit, New Brunswick. Canadian Mineralogist 13, 298-299.

Samson, I.M., 1990. Fluid evolution and mineralization in a subvolcanic granite stock: the Mount Pleasant W-Mo-Sn Deposits, New Brunswick, Canada. Economic Geology 85, 145-163.

Sinclair, W.D., Kooiman, G.J.A., Martín, D.A., 1988. Geological setting of granites and related tin deposits in the North Zone, Mount Pleasant, New Brunswick. In Current Research, Part B, Geological Survey of Canada, Paper 88-1B, 201-208.

Sinclair, W.D., Kooiman, G.J.A., Martín, D.A., Kjarsgaard, I.M., 2006. Geology, geochemistry and mineralogy of indium resources at Mount Pleasant, New Brunswick, Canada. Ore Geology Reviews 28, 123–145.

Thorne, K., Fyffe, L.R., Creaser, R.A., 2013. Re-Os geochronological constraints on the W- Mo mineralizing event in the Mount Pleasant Caldera Complex: implications for the timing of subvolcanic magmatism and caldera development. Atlantic Geology 49, 131 – 150.

Yang, X.M., Lentz, D.R., McCutcheon, S.R., 2003. Petrochemical evolution of subvolcanic New Brunswick, Canada: comparison of Au versus Sn-W-Mo-polymetallic mineralization systems. Atlantic Geology 39, 97–121.

Zhang, W., Lentz, D.R., Charnley, B.E., 2017. Petrogeochemical assessment of rock units and identification of alteration/mineralization indicators using portable X-ray fluorescence measurements: Applications to the Fire Tower Zone (W-Mo-Bi) and the North Zone (Sn-Zn- In), Mount Pleasant deposit, New Brunswick, Canada. Journal of Geochemical Exploration 177, 61-72.

THE CONTRIBUTION OF BISMUTH (TELLURIUM) MELTS TO GOLD MINERALIZATION: A CASE STUDY FROM THE BAOLUN GOLD ORE DEPOSIT IN HAINAN PROVINCE OF SOUTH CHINA

Deru Xu[1], Qiang Shan, Qinyi Huang, Guoxiang Chi, Teng Deng

[1]*School of Earth Sciences, East China University of Technology - xuderu@gig.ac.cn*

The contribution of bismuth (tellurium) melts (Melt means high temperature (＞600°C) and relatively low water content (＜ 10 wt.%). After go through this abstract, I found the «melt» that the authors proposed-bismuth (tellurium) melt is actually a fluid rich in bismuth and tellurium. So, I think the word «melt» is not a suitable term that can be used in this abstract.) to gold mineralization: a case study from the Baolun gold ore deposit in Hainan Province of South China.

The Baolun gold (Au) deposit, with a proven reserve of ＞80 t Au at an average grade of 10.3 g/t Au, is a large-scale, high-grade Au deposit located in Hainan Island, South China (Fig. 1). The mineralization occurs mainly as sheeted Au-quartz veins, with a minor amount in altered cataclasite. The orebodies are developed within a swarm of NNW-trending fracture zones in Lower Silurian meta-volcaniclastic sedimentary rocks of greenschist to lower-amphibilite facies, which were intruded by Triassic granitoids (Fig. 1). Gold mainly occurs as native Au, which is associated with a variety of Au- and Bi (Te)-bearing minerals. However, there has been debate on ore genesis of the Baolun deposit, with respect to the contribution of either magmatic-hydrothermal or metamorphic fluids to the Au mineralization.

To elucidate the issue, fifty-two sheeted Au-quartz vein samples from the Baolun deposit were selected for the present study. Bulk-rock analyses on ore-forming elements of the collected samples were performed by Perkin-Elmer Elan 6000 inductively coupled plasma mass spectrometer (ICP-MS). Polished thin-sections of the samples were investigated by optical microscopy and back-scattered electron (BSE). *In-situ* chemical compositions of the representative ore- and gangue minerals were carried out through spot analysis and X-ray elemental mapping using SHIMADZU EPMA-1720 electron microprobe analysis (EMPA) equipped with four wavelength-dispersive spectroscoies (WDS).

The hydrothermal system is divided into six stages (Fig. 2), including a pre-mineralization stage (stage-I) characterized by barren quartz, four syn-mineralization stages with different Au-Bi (Te) ore mineral assemblages (stage-II: native Au; stage-III: native Au – pyrrhotite – arsenopyrite – pyrite – chalcopyrite; stage-IV: maldonite – native Bi – Au-Bi symplectite (native Au + native Bi); stage-V: bismuthinite – native Au – jonassonite – joséite-B – galenobismuthite), and a post-mineralization stage (stage-VI) characterized by barren quartz, calcite and pyrite. The occurrence of auriferous Bi-rich blebs in stage-IV and stage-V ores, together with the positive correlations between Au and Bi (and Te), suggests that Bi melt may have played an important role in the formation of the Baolun Au deposit.

Based on the spatial-temporal relationship between the deposit and granitic intrusions and temperature – fO_2 – fS_2 conditions deduced from mineral assemblages, we propose that the deposit formed from a magmatic-hydrothermal system (with potential contributions from metamorphic and other fluid sources). In the early stages of mineralization (stage II and III), Au was oversaturated whereas Bi and Te was undersaturated, and so native gold was precipitated without Bi- and Te-bearing minerals (Why Au becomes oversaturated in stage II and III?). In the later stages (IV and V), Bi and Te become oversaturated and Bi melt was developed (Why Bi and Te become oversaturated in stage IV and V?). Bi melt scavenged Au from the hydrothermal solution which was undersaturated with Au (due to precipitation in the early stages), thus contributing to Au mineralization by preventing total loss of the remaining Au with the spent fluid.

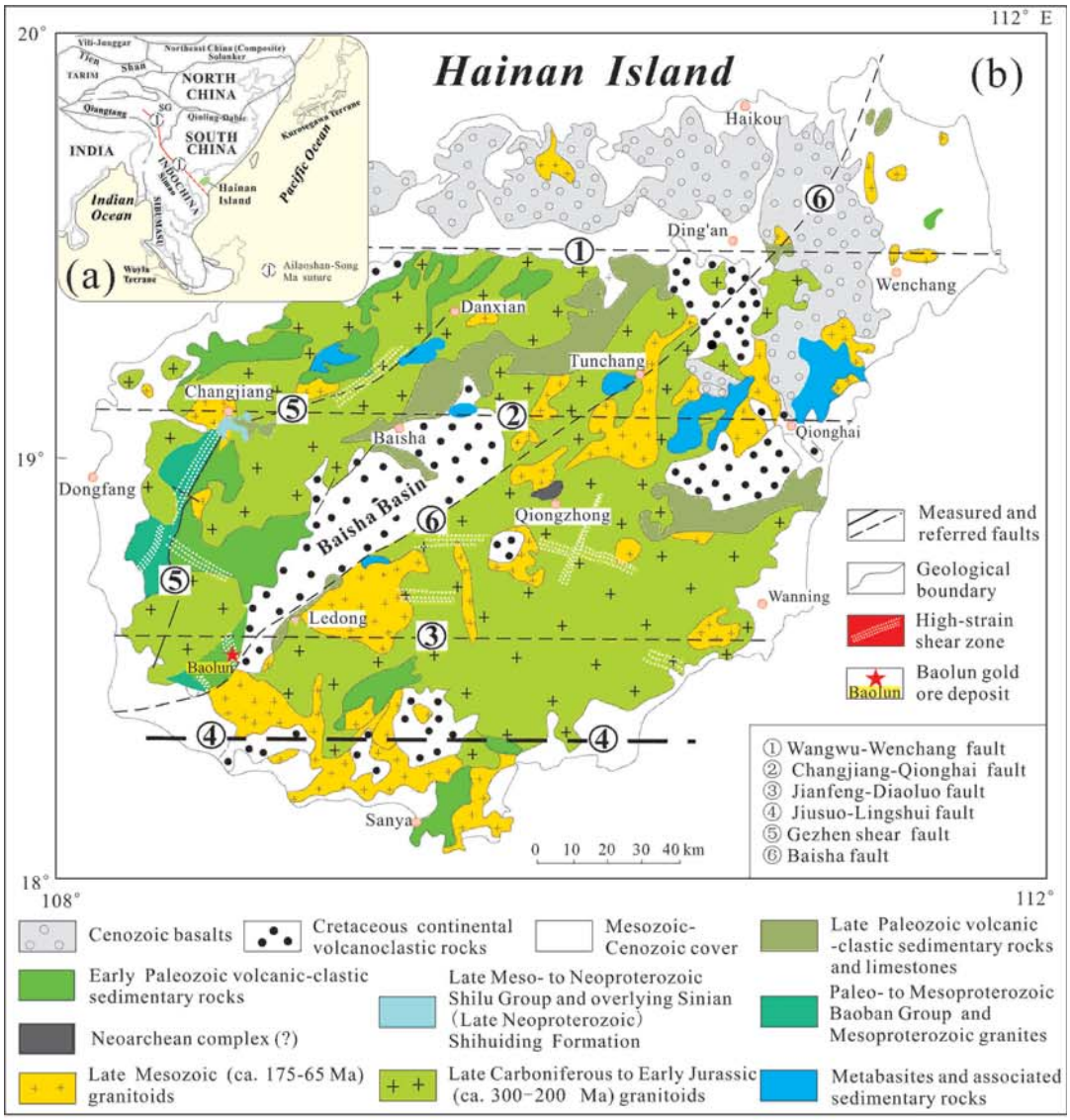

Fig. 1. (a) Location map and (b) simplified map showing the main stratigraphic and magmatic units, and the Baolun gold ore deposit in Hainan Island, South China.

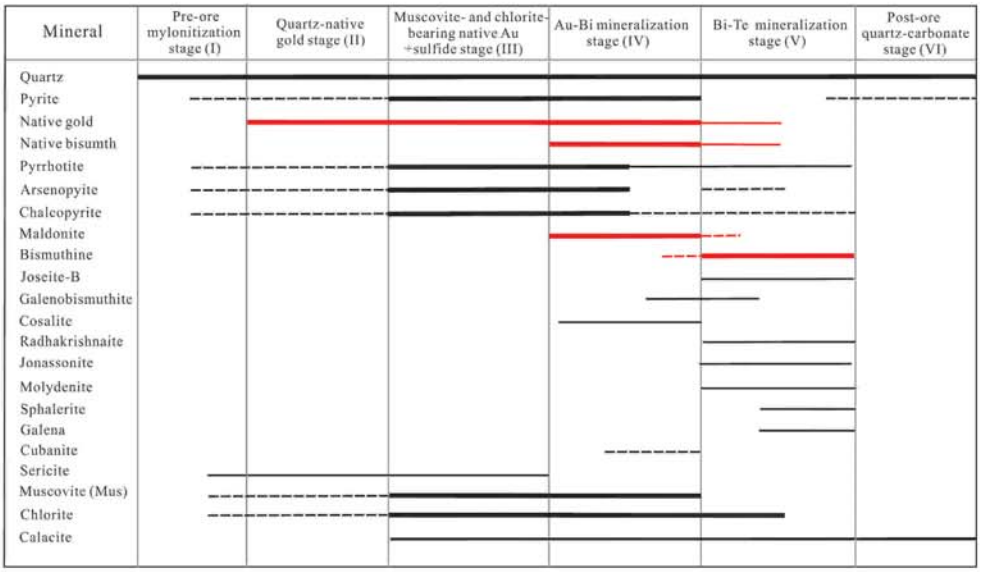

Fig. 2. Paragenesis of ore- and gangue minerals in the Baolun Au ore deposit.

GEOLOGY AND METALLOGENY OF TUNGSTEN AND TIN DEPOSITS IN CHINA: AN OVERVIEW

Jingwen Mao[1], Hegen Ouyang, Shiwei Song, M. Santosh, Shunda Yuan, Zhenhua Zhou, Wei Zheng, Huan Liu, Yanbo Cheng, Maohong Chen, Junfeng Xiang

[1]MLR Key Laboratory of Metallogeny and Mineral Assessment, Institute of Mineral Resources, Chinese Academy of Geological Sciences, Beijing, 100037, China; Hebei GEO University, Shijiazhuang, 050031, China - jingwenmao@263.net

Tungsten and tin deposits in China are widely distributed in the South China Block, Himalayan-Tibetan-Sanjiang and Kunlun-Qilian-Qingling-Dabie-Sulu orogens, and North Orogenic Belt. Among these, the South China Block hosts the major mineralization with about 78 % (9.126 Mt WO_3) and 88 % (7.684 Mt Sn) of the country's total tungsten and tin resources, respectively. The tungsten resources occur within three hydrothermal ore types: skarn (62 %), quartz-vein (19 %), and porphyry (17 %); whereas the tin deposits are in skarn (81 %), (tourmaline-) quartz-vein (8 %), (quartz-) sulfide (4 %), greisen (4 %), and porphyry (3 %) types.

The tungsten and tin mineralization formed during multiple events ranging from Neoproterozoic to Early Tertiary with a peak in the Middle Jurassic to Early Cretaceous, with an uneven spatial and temporal distribution pattern. The Neoproterozoic tin deposits occur in the southern and western margins of the Yangtze Craton; the Early Paleozoic tungsten deposits are mainly distributed in the North Qilian and the westernmost part of the Eastern Kunlun orogens; the Late Paleozoic tin and tungsten deposits are mainly developed in the western part of the North China Orogen; the Middle to Late Triassic tungsten and tin deposits are sporadically distributed over the whole country; the Early Jurassic to Early Cretaceous tungsten and tin deposits mainly occur in East China; and the Late Cretaceous to Early Tertiary tin deposits developed in the Himalayan-Tibetan-Sanjiang Orogen.

The petrological characteristics of tungsten- and tin-related granitoids in China vary with the associated ore elements and can be divided into Sn-dominant, W-dominant, W-Cu, and W-Mo groups. The granitoids associated with Sn- and W-dominant hydrothermal systems are highly fractionated S- and I-type high-K calc-alkaline and/or shoshonite intrusions which show metaluminous to peraluminous nature, with enrichment in F, B, Be, Rb, Nb, Ta, depletion in Ti, Ca, Sr, Eu, Ba, Zr, and strongly negative Eu anomalies. The granitoids associated with W-Cu and W-Mo deposits are of high-K calc-alkaline to shoshonitic nature, metaluminous, depleted in Nb and Ta, and display weakly negative Eu anomalies. Granitoids associated with Sn- and W-dominant deposits are reduced whereas the granitoids linked to W-Cu and W-Mo deposits are relatively oxidized. The magma sources of W-dominant granitoids are ancient crust whereas those connected with Sn, W-Mo, and W-Cu deposits are from variable mixing of ancient and juvenile crustal components.

The spatial and temporal distribution pattern of tungsten and tin deposits in China is intimately related to the regional geodynamic evolution. The Neoproterozoic (850-790 Ma) tin deposits are associated with peraluminous, highly fractionated, and volatile enriched (boron and fluorine) S-type granites sourced from melting of ancient crust under a post- collisional setting related to the assembly of Rodinia supercontinent. The Early Paleozoic (450-410 Ma) tungsten and tin deposits are genetically associated with highly fractionated S-type granites formed during post-collisional stage and were derived from partial melting of a thickened continental crust in the context of Proto-Tethyan assembly. Granitoids associated with Late Paleozoic (310-280 Ma) tungsten deposits were derived from the melting of ancient and juvenile crust with I-type affinity associated with the closure of the Paleo-Asian Ocean. The Middle to Late Triassic (250-210 Ma) tungsten and tin deposits are related to the assembly of the Pangea supercontinent although their geological setting shows variations. Those in South China and the Himalayan-Tibetan-Sanjiang belt are associated with collision with magma derivation through partial melting of a thickened continental crust, whereas in the Qin-Qi-Kun and North China orogens, a post-collisional extensional setting dominates. The Early Jurassic (198-176 Ma) tungsten deposits, located in the northern part of northeast China, are associated with highly fractionated I-type granites derived from juvenile lower continental crust with minor input of mantle materials during the subduction of the Mongol-Okhotsk oceanic plate. The extensive Middle Jurassic to Cretaceous tungsten and tin mineralization involves two stages at 170-135 Ma and 135-80 Ma. The former stage is associated with highly fractionated S- and I-type granites which are products of partial melting of thickened crust with heat input possibly induced by a slab window associated with the Paleo-Pacific oceanic plate subduction beneath the Eurasian continent. The later stage is closely associated with NNE-trending strike-slip faults along the Eurasian continental margin and coeval with the formation of rift basins, metamorphic core complexes, and porphyry-epithermal Cu-Au-Ag deposits. These processes, which were instrumental for the formation of a wide range of mineral deposits, can be ascribed to regional lithospheric thinning and delamination of the thickened lithosphere and thermal erosion in a post-subduction extensional setting. The Late Cretaceous to Early Tertiary (121-56 Ma) tin deposits in southwest China are associated with S-type granite or I-type granodiorite in a back-arc extensional setting of Neo-Tethys plate subduction.

A | 33

TRACE-ELEMENT COMPOISTION OF LI-BEARING MICAS FROM JIANFENGLING W-NB-TA BEARING GRANITE, HUNAN PROVINCE, SOUTH CHINA: IMPLICATION OF MAGMATIC-HYDROTHERMAL PROCESS IN HIGHLY FRACTIONATED GRANITE

Xu Zhao, Jianjun Lu

Nanjing University - zhaoxu3033@gmail.com

ORE GENESIS OF THE GIANT SHAPINGGOU PORPHYRY MO DEPOSIT: CONSTRAINTS FROM THE ORE-RELATED GRANITE PORPHYRY, FLUID INCLUSION, H-O-S-Pb ISOTOPES AND MOLYBDENITE RE-OS GEOCHRONOLOGY

Wang Guo- Guang[1], Ni Pei, Yu Wen, Chen Hui

[1]*State Key Laboratory for Mineral Deposits Research, Institute of Geo-Fluids, School of Earth Sciences and Engineering, Nanjing University - ggwang@nju.edu.cn*

BACKGROUND

Porphyry deposits are the world's most important sources of Cu and Mo, and account for approximately 50 to 60% of the world's Cu production and more than 95% of the world's Mo production. Most porphyry deposits occur in oceanic-continental subduction-related magmatic arc setting. In recent years, continental-continental collision belts have also proven to be favorable sites for porphyry Mo deposits. The Qinling-Dabie Orogen is a Mesozoic continental-continental collisional belt between the North China Block and the South China Block, and it is estimated to contain a total of approximately 8.6 Mt of Mo metal, accounting for 66% of China's Mo metal resources. Compared with porphyry deposits in arc setting, the porphyry mineral systems in collisional belt are lack of well constrained.

The Shapinggou porphyry Mo deposit, located in the easternmost zone of the Qinling-Dabie Mo belt, was discovered in 2009 with a proven reserve of 2.37 Mt of Mo m*etal.* The Shapinggou Mo deposit is one of the largest Mo deposits in Asia. Given its theoretical and practical significance, the newly discovered Shapinggou deposit deserves detailed research on its ore genesis.

ORE DEPOSIT GEOLOGY

The Dabie Orogen is the central part of the Triassic Qinling-Dabie–Sulu Orogen. The Shapinggou porphyry Mo deposit is in close proximity to the EW-trending Xiaotian-Mozitan fault in the Dabie Orogen. Several NNE- and NW-trending second-order faults developed in the deposit. The Yanshanian igneous rocks occur in most part of the ore deposit and nearby region. Field cross-cutting relationships and previous dating data from the igneous rocks in the Shapinggou deposit indicate that the Yanshanian magmatism dominantly happened in the Early Cretaceous and can be further divided into two stages. The early-stage rocks are widespread and can be further divided into two subgroups of acidic and intermediate rocks. The late-stage rocks are of two types, quartz syenite and granite porphyry.

At the surface, the mineralization displays a distinct metal zoning, characterized by the Shapinggou porphyry Mo deposit surrounded by several Pb–Zn deposits. Molybdenum orebodies are hosted in the granite porphyry. The Mo orebodies typically take the form of an inverted cup approximately 1000 to 1300 meters in diameter. In addition, the Mo orebodies range from 140 m to -940 m depth, with the biggest thickness being 945 m. The proven molybdenum reserves are up to 220 Mt, with an average grade of Mo=0.14 wt.%. The mineral compositions are simple and molybdenum is the primary commodity in the whole deposit. The ore minerals include molybdenite and pyrite, with minor sphalerite, chalcopyrite, magnetite, and galena. Molybdenite mainly occurs as radial coarse-grained aggregates in quartz veinlets along open-space fissures and is occasionally spotted, scaly, and disseminated in the ore-related granite porphyry and wallrocks. The gangue minerals are quartz, K-feldspar, sericite, and chlorite, with lesser amounts of biotite, calcite, and epidote.

Four stages of wallrock alterations developed in the Shapinggou Mo deposit, i.e., stage 1 silicic-sodic alteration, stage 2 potassic alteration, stage 3 phyllic alteration, and stage 4 propylitic alteration. Spatially, these hydrothermal alteration types show well-defined silicic- sodic, potassic, phyllic, and propylitic alteration zones from the center zone outward (Fig. 3). Both the silicic-sodic and potassic alteration are genetically tied to the crystallization of ore-related granite porphyry.

METHODS AND RESULTS

We present systematic LA ICP-MS zircon U-Pb dating and Hf isotopes, whole rock elemental and isotopic compositions, combined with fluid inclusions and H-O-S-Pb isotopes and molybdenite Re-Os isotopic results to constrain ore genesis of the Shapinggou porphyry Mo deposit.

Two stages of Early Cretaceous magmatism, 138-128 Ma and 116-114 Ma, took place at Shapinggou in a post-collisional setting. These granitoids can be divided into four groups, including the early-stage granites (134-129 Ma, SiO_2=62.33 to 76.27%) and intermediate rocks (129-128 Ma, SiO_2=52.41 to 60.72%) and the late-stage quartz syenite (116 Ma, SiO_2=64.09 to 65.12%) and Mo-bearing granite porphyry (114 Ma, SiO_2=74.95 to 77.26%). The

early-stage granites have high Sr contents, Sr/Y and LaN/YbN ratios, but low Y, Yb and MgO contents, showing low-Mg adakitic chemical features. They were possibly generated by partial melting of the thickened mafic lower continental crust. The early-stage intermediate rocks have relatively high MgO contents (2.71 to 4.84%) and Mg# values (46 to 60), but low Sr/Y and LaN/YbN ratios, which were likely derived from a hybrid mantle metasomatized by melts from foundered eclogitic lower continental crust and subsequent fractional crystallization. The late-stage quartz syenite shows chemical features of metaluminous A- type granites, including high abundances of alkalis, HFSE (Zr, Nb), and trivalent REE. The late-stage Mo-bearing granite porphyry displays high SiO_2, alkalis, Zr, Ce contents, and A/CNK ratios, but low Ba, Sr, P and Ti, showing affinity to highly fractionated I-type granites. The late-stage quartz syenite and granite porphyry were possibly produced by partial melting of intermediate compositions of middle crust. The giant Shapinggou porphyry Mo deposit was most likely formed by effective transport of volatiles and Mo in a convecting granitic magma column, rather than by direct melting of Mo-enriched sources.

Hydrothermal quartz mainly contains three types of fluid inclusions, namely, two-phase liquid-rich (type I), two- or three-phase gas-rich CO_2-bearing (type II) and halite-bearing (type III) inclusions. The last two types of fluid inclusions are absent in stages 1 and 4. Type I inclusions in the silicic-sodic zone (stage 1) display homogenization temperatures of 340 to 550 °C, with salinities of 7.9-16.9 wt.% NaCl equivalent. Type II and coexisting type III inclusions in the potassic zone (stage 2), which hosts the main Mo orebodies, have homogenization temperatures of 240–440 °C and 240–450 °C, with salinities of 34.1–50.9 and 0.1–7.4 wt.% NaCl equivalent, respectively. Type II and coexisting type III inclusions in the phyllic zone (stage 3) display homogenization temperatures of 250–345 °C and 220–315 °C, with salinities of 0.2–6.5 and 32.9–39.3 wt.% NaCl equivalent, respectively. Type I inclusions in the propylitization zone (stage 4) display homogenization temperatures of 170 to 330 °C, with salinities lower than 6.5 wt.% NaCl equivalent. The abundant CO_2-rich and coexisting halite-bearing fluid inclusion assemblages in the potassic and phyllic zones highlight the significance of intensive fluid immiscibility of a NaCl-CO_2-H_{2O} system in deep environments (up to 2.3 kbar) for giant porphyry Mo mineralization. Hydrogen and oxygen isotopic compositions indicate that ore-fluids were gradually evolved from magmatic to meteoric in origin. Sulfur and lead isotopes suggest that the ore-forming materials at Shapinggou are magmatic in origin. Re-Os dating of molybdenite gives a well-defined 187Re/187Os isochron with an age of 112.7±1.8 Ma, suggesting a post-collisional setting.

CONCLUSIONS

The giant Shapinggou porphyry Mo deposit is generated in a post-collisional extensional setting.

It was most likely related to a long-term run mamga system and was formed by effective transport of volatiles and Mo in a convecting granitic magma column.

It is featured by intensive fluid immiscibility of a NaCl-CO_2 -H_2O system in deep environments.

Response to the reviewer

Comment 1: It is quite uncommon that in a porphyry deposit, the potassic alteration postdate silicic alteration.

Reply: Many thanks for your comments. We have carefully checked the samples collected beneath the ore-related potassic zone. Those samples not only show clearly silicification, but also pervasive albitization. The photos of the hand samples and under microscopy are shown in Figs.1 and 2, respectively. In this abstract, we would like to use the term "silicic-sodic alteration" instead of "silicic alteration"

Fig.1 the photos of the gray hand samples collected beneath the pink ore-related potassic alteration zone. The gray color results from the strong silicic-sodic alteration, which is easily identify from potassic alteration just based on the color.

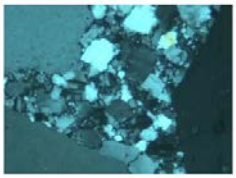

Fig.2 the microphotographs of in the silicic-sodic alteration zone. The picture shows that the hydrothermal micro albitite and quartz as matrix minerals occur the large magmatic Kf and quartz minerals.

Comment 2: Climax-type porphyry molybdenum deposits are associated with A-type granites but not highly fractionated I-type granites.

Reply: Many thanks for your reminding. We have deleted the descriptions about the comparison between the Shpinggou ore-related intrusion and the ore-related intrusions in Climax-type porphyry molybdenum deposits.

Comment 3: It is also quite unusually for the main Mo orebodies in the Shapinggou deposit occur in the potassic zone.

Reply: It is true that the main Mo orebodies are primarily confined within the potassic alteration zone, with minor in the phyllic zone. The relevant photos are shown in the following:

Fig.3 the typical photos of the pink ore-related potassic alteration.

TIN AND TUNGSTEN DEPOSITS IN NORTHEAST QUEENSLAND, AUSTRALIA: PAST, PRESENT, AND PROSPECTIVITY

Yanbo Cheng[1], Zhaoshan Chang, Jaime Poblete, Kairan Liu, Carl Spandler, Gavin Clarke, Paul Dirks

[1]Economic Geology Research Centre (EGRU) and Department of Geoscience, James Cook University, 1 James Cook Dr, Douglas, QLD 4811, Australia - yanbo.cheng1@jcu.edu.au

Northeast Queensland of Australia is an important Sn-W-Mo-Au mineralized province in Australia, particularly for Sn and W, which includes ~10% of Australia's Economic Demonstrated Resources (EDR) of Sn and ~13% of the country's EDR of tungsten (Chang et al, 2017). Sn-dominant deposits mainly occur in three districts: the Kangaroo Hills, Herberton and Cooktown districts. The W-dominant deposits occur only in the northeast Mt Carbine-Watershed area. W-Mo deposits have been found in both the Herberton (e.g., Wolfram Camp) and Kangaroo Hill districts.

To discern differences between "fertile" and "non-fertile" igneous rocks associated with Sn- W-Mo mineralization and reveal the genetic links between coeval intrusive and extrusive rocks, we integrate whole rock geochemistry, geochronology and Hf isotope signatures of igneous zircons from contemporaneous plutonic and volcanic rocks from the Herberton Sn and W-Mo mineral field. The 310-300 Ma intrusive rocks and associated intra-plutonic W-Mo mineralization formed from relatively oxidized magmas after moderate degrees of crystal fractionation. The geochemical and isotopic features of the coeval volcanic succession are best reconciled utilizing the widely-accepted volcanic-plutonic connection model, whereby the volcanic rocks represent fractionated derivatives of the intrusive rocks. The volcanic rocks of 335-310 Ma (Sn formation stage) are compositionally less evolved than the coeval intrusive rocks. In this case, we propose that the most fractionated magmas were not lost to volcanism, but instead were effectively retained at the plutonic level, which allowed further localized build-up of volatiles and lithophile metals in the plutonic environment. Given the common occurrence of volcanic and plutonic rocks associated with Sn-W-Mo mineralization worldwide, we suggest that a proper understanding of plutonic-volcanic connections can assist in assessment of regional-scale mineralization potential, which in turn can aid strategies for future ore deposit exploration.

The Wolfram Camp Mine deposit is a greisen type W-Mo deposit. The host rock of the deposit is Late Carboniferous James Creek granite and which has locally intruded Hodgkinson Formation sandstone. The orebodies contain wolframite and molybdenite occur as pipe-like bodies of quartz in the roof zone of the intrusion. Alteration associated with the Wolfram Camp mineralization is mainly greisen type. The alteration can be divided into quartz-rich greisen zones, muscovite-rich greisen zones and greisenized granite zones with decreasing alteration levels. The mineralization in the study area are closely related to post- intrusive hydrothermal events and can be divided into several stages. The major ore minerals, wolframite and molybdenite, formed during the greisen stage, and base metal sulphide minerals and scheelite formed in later sulphide and calcite stages. Fluid inclusion studies was conducted on the ore bearing quartz crystals in the pipes. The homogenization temperatures of the fluid inclusions quartz containing wolframite are about 410 °C. Results from a stable isotope study suggest that the source of the hydrothermal fluid related to the formation of the wolframite, molybdenite and base metal sulphides is purely magmatic. However, the fluid responsible for the introduction of the calcite is a combination of magmatic water and meteoric water.

The Mt Carbine quartz-wolframite-scheelite sheeted vein deposit is hosted in Ordovician to Devonian Hodgkinson Formation metasedimentary rocks. Field observation and drill core logging have provided evidence for a five stage paragenetic sequence of mineralization and veining, with two of the stages having significant W mineralization. Wolframite is typically euhedral and occurs in quartz veins, while scheelite occurs as (1) euhedral grains in quartz vein and, (2) pseudomorphing wolframite grains or cutting across wolframite grains as veinlets. This observation is consistent with the scheelite CL images and in-situ composition variation. The LA-ICP-MS zircon U-Pb dating results reveal the magmatic activities occurred during 300-265 Ma. Molybdenite Re-Os age and muscovite 40Ar-39Ar ages are between 285-275 Ma. Fluid inclusion studies reveal that most of the inclusion are primary and distributed in assemblages or isolated, with homogenization temperatures ranging from 290 to 210 °C. Laser Raman analysis identified CH_4 in vapour bubbles. Together with H-O-S isotopic compositions, our data indicate that both magmatic fluid and metamorphic water contributed the formation of Mt Carbine W deposit.

The Watershed scheelite deposit lies within the Mossman Orogen, which comprises deformed Silurian-Ordovician metasedimentary rocks of the Hodgkinson Formation by Carboniferous and Permian granites of the Kennedy Igneous Association. Multiple felsic dykes cut cross the metasedimentary rocks at Watershed including: (a) monzonite dyke (~350 Ma); and (b) dioritic, granitic plutons and dykes (281-271 Ma). A first non-economic

mineralization event corresponds to the crystallization of disseminated scheelite in monzonite dykes. The bulk of the scheelite mineralization formed during a second event in shear-related quartz multi-staged veins and vein halos. The vein stages occurred synchronously with three retrograde stages in calc-silicate conglomerate. The retrograde minerals in calc-silicate comprises clinozoisite after garnet, quartz, plagioclase, scheelite and phlogopite with minor sodium-rich amphibole. The principal control on scheelite mineralization at Watershed are: (a) early monzonite dykes enriched in scheelite (W source); (b) shear zone that acted as fluid conduits transporting tungsten; (c) calc-silicate conglomerate that provide a source for calcium to form scheelite; and (d) an extensional depositional environment characterized by vein formation and normal faulting, which provide trapping structures for fluids, with fluid decompression being a likely control on scheelite deposition.

Based on metal commodities, the mineral deposits of the northeast Queensland Sn-W-Mo-Au province can be classified into five types: Sn-dominant, W-dominant, W-Mo, porphyry-skarn Au-Cu and the traditionally recognized intrusion related gold deposits (IRGDs). Based on geological characteristics and our high precision geochronological results, Sn-dominant deposits and associated igneous rocks in northeast Queensland formed in three episodes: ~265 Ma, 330-310 Ma and ~345 Ma. The W-dominant mineralization only formed during 285-250 Ma, and W-Mo mineralization occurred during 310-300 Ma and 345-335 Ma. The porphyry-skarn type Au-Cu deposits in Chillagoe District formed during 335-295 Ma, and the Au-dominant deposits in Georgetown and Cape York Peninsula formed in two episodes: 350-335 Ma and 285-280 Ma. Overall, the combined results from dating both magmatic and hydrothermal activities show a younging trend from southwest to northeast in the northeast Queensland Sn-W-Mo-Au province.

REFERENCE

Chang, Z., Clarke, G., Cheng, Y., Poblete, J., Liu, K. 2017. Sn-W-Mo mineralization in north- east Queensland. In: Phillips, G N (ed) Australian Ore Deposits, The Australasian Institute of Mining and Metallurgy: Melbourne, pp. 681-688.

NEW GRANITE-RELATED TUNGSTEN DEPOSITS IN NORTHERN JIANGXI PROVINCE OF SOUTH CHINA: ORE-FORMING PROCESS AND GENETIC MODEL

Shao-Yong Jiang[1], Ning-Jun Peng, Suo-Fei Xiong, Dao-Hui Pi

[1]*China University of Geosciences - shyjiang@cug.edu.cn*

INTRODUCTION

South China hosts a number of world-class granite-related tungsten deposits and most of them are located in southern Jiangxi Province, southeastern Hunan and northern Guangxi, and northern Guangdong provinces. The Dahutang tungsten deposit, located in northern Jiangxi Province, is a newly found world-class deposit with an estimated WO_3 reserve of 2 million tones. It consists of the Shimensi, Dalingshang and Shiweidong ore sections that are currently mined and a number of ore prospect areas such as Dawutang, Yikuangdai, Pingmiao and Dongdouya. Tungsten mineralization in the deposit occurs as quartz vein, veinlet and hydrothermal breccia. The Dahutang deposit is unique because abundant scheelite orebodies of veinlet occur in the host rock of Neoproterozoic granite near the Mesozoic granites, which is different from those scheelite orebodies (as skarn) occurred within the carbonate host rocks near the granites.

SAMPLES AND METHODS

Samples for dating include zircon from the granites, molybdenite from the veinlets and hydrothermal breccias, scheelite from the veinlets. The fluid inclusion samples include quartz, scheelite, apatite and calcite from different hydrothermal stages. The geochemical and Sr-Nd-Pb-S-H-O isotope samples include both the granites and the ores. Detailed field investigation and petrographical observation, together with zircon U-Pb, molybdenite Re-Os and scheelite Sm-Nd isotope dating, mineral chemistry, fluid inclusion study, and major and trace elements and Sr-Nd-Pb-S-H-O isotope analyses are carried out in this study for the Dahutang deposit.

RESULTS

The tungsten mineralization in the Dahutang deposit is genetic related to the Mesozoic S- type granitic rocks with zircon U-Pb ages of ca.150-130 Ma (Huang and Jiang, 2012, 2013, 2014; Jiang *et al.*, 2015). Integrated geochemical and Sr-Nd-Hf isotope studies have provided unambiguous evidence of an anatectic sedimentary origin of possibly Neoproterozoic sediments with intercalated volcanic rocks for these granitic rocks (Huang and Jiang, 2014). The molybdenite Re-Os dating results reported by various researches reveal slightly different ages, but in the range of ca.150-140 Ma, and the scheelite Sm-Nd dating shows an age of 142 Ma (Jiang *et al.*, 2015). Generally, the time scale for the formation of a large-scale deposit is no longer than 5 Ma, therefore it is possible multiple mineralization stages may occur in the Dahutang deposit (Jiang *et al.*, 2015).

Fluid inclusion microthermometric studies (Peng *et al.*, 2018) of wolframite and scheelite indicate similar temperatures of ca. 340-330 °C, which are generally 70 °C higher than those in coexisting quartz (~270 °C). Both CH_4 and CO_2 are indentified in variable stages of fluid inclusions by Laser Raman analysis. The ore-forming fluids are characterized by high- to medium-temperature, low-salinity, CH_4, and/or CO_2-bearing aqueous fluids. Chalcopyrite and sphalerite are the most abundant solids recognized in fluid inclusions of quartz from different ores. The geological, geochemical and isotope evidences suggest a dominantly magmatic source for the ore metals and fluids but with variable amounts of component (such as Ca) from host rocks (possibly released from plagioclase via water-rock interaction) and mixing of meteroic water in the ore-forming fluids.

CONCLUSIONS

The Dahutang tungsten deposit is a S-type granite-related magmatic-hydrothermal deposit. It may involve multiple stages of mineralization. The ore materials are mainly derived from the Mesozoic granites that possibly originated from the partial melting of Neoproterozoic sediments with intercalated volcanic rocks in the region. The ore precipitation mechanism includes an early cooling process, a major fluid mixing and fluid-rock interaction process.

REFERENCES

Huang L.C., Jiang S.Y., 2012. Geochroronology, geochemistry and petrogenesis of the porphyric like two-mica granite in the Dahutang tungsten deposit, Jiangxi Province. Acta Petrologica Sinica, 28, 3887-3900 (in Chinese with English abstract).

Huang L.C., Jiang S.Y., 2013. Geochronology, geochemistry and petrogenesis of the tungsten- bearing porphyritic granite in the Dahutang tungsten deposit, Jiangxi Province. Acta Petrologica Sinica, 29, 4323-4335.

Huang L.C., Jiang S.Y., 2014. Highly fractionated S-type granites from the gaint Dahutang tungsten deposit in Jiangnan Orogen, Southeast China: Geochronology, petrogenesis and their relationship with W-mineralization. Lithos, 202-203, 207-226.

Jiang S.Y., Peng N.J., Huang L.C., Xu Y.M., Zhan G.L., Dan X.H., 2015. Geological characteristic and ore genesis of the giant tungsten deposits from the Dahutang ore-concentrated district in northern Jiangxi Province. Acta Petrologica Sinica, 31, 639-655.

Peng N.J., Jiang S.Y., Xiong S.F., Pi D.H., 2018. Fluid evolution and ore genesis of the Dalingshang deposit, Dahutang W-Cu ore field, northern Jiangxi Province, South China. Mineralium Deposita, https://doi.org/10.1007/s00126-018-0796-2.

W-Nb-Pb-Zn MINERALIZATION IN EARLY CRETACEOUS I-TYPE GRANITOIDS IN THE LIZIKENG VOLCANIC BASIN OF JIANGXI PROVINCE, SOUTH CHINA

Hui-Min Su[1], Shao-Yong Jiang, Ming-Yu Cao

[1]*China University of Geosciences - suhuimin1984@163.com*

INTRODUCTION

W-Sn-Nb-Ta deposits are widespread in South China in close association with Mesozoic granitoid rocks, and mainly occur in two regions: the Nanling Range areas and the Northern Jiangxi-Southern Anhui regions. However, the W-Sn-Nb-Ta mineralization has rarely been found in the volcanic basins, although a number of Mesozoic volcanic basins occur in South China which hosts many important Pb-Zn-Ag and U deposits that are genetically related to volcanic and subvolcanic rocks.

The Lizikeng basin, located at the eastern part of the North Wuyi area, is a representative volcanic basin with occurrence of both volcanic rocks and accompanying subvolcanic and plutonic rocks. In this basin, only several small to medium-sized Pb-Zn deposits (e.g., Caijiaping, Lizikeng, Huangbaikeng, Jiaotang, and Zhoujia) are previously reported. In this study, we report our new finding of W-Nb bearing minerals in the granitoid rocks from the Lizikeng basin, which shed new light on discovery of rare-metal mineralization potential in the volcanic basin.

SAMPLES AND METHODS

Samples for this study include porphyric quartz monzonite, granite porphyry and biotite monzogranite, and ore veins from the Lizikeng basin. Zircons are separated from all these three rocks and dated by LA-ICP-MS method. Thin sections are made both for fresh and altered granitiods, and mineral morphology are observed by SEM and chemical compositions of selected minerals are analyzed by EMPA. Whole rock powders are prepared and analyzed for their Sr-Nd isotopes. Quartz, fluorite and carbonates from the altered rocks and ore veins are prepared for fluid inclusion studies.

RESULTS

The Cretaceous porphyric quartz monzonite and granite porphyry in this study widely outcrop within the Lizikeng basin, whereas the highly evolved biotite monzogranite is a concealed granitic pluton exposed only by recent drilling. Zircon U-Pb dating reveals an age of 133 ± 2 Ma for the porphyric quartz monzonite, 132 ± 1 Ma for the granite porphyry, and 129 ± 2 Ma for the biotite monzogranite, corresponding to the early Cretaceous volcanic-intrusive activities in the area.

The whole-rock geochemistry indicates that the three granitic rocks belong to I-type granites, for example, in the plots of Y vs Rb, Th vs Rb, all the data fall in the I-type granite trend. These rocks also show highly evolved characteristic and most of the data plot in the fractionated granite field in the diagram of Zr+Nb+Ce+Y vs (K_2O+Na_2O)/CaO. The biotite monzogranite contains typical rare metal minerals, such as W-bearing rutile, niobium rutile, ferberite, and columbite group minerals. In the discriminant diagrams of Ba vs Rb, Nb vs GCL, all of the biotite monzogranite data plot in the tungsten granite field. The porphyric quartz monzonite and granite porphyry, having consistent low whole-rock $\varepsilon_{Nd}(t)$ values of -10.36 to -9.64 and zircon $\varepsilon_{Hf}(t)$ values of -14.15 to -8.20, were derived from Proterozoic mafic-intermediate lower crust sources without any significant contribution of mantle- derived material. The biotite monzogranite, which shows also negative but slightly higher $\varepsilon_{Nd}(t)$ and higher $\varepsilon_{Hf}(t)$ values of -7.61 to -7.06 and -9.32 to -7.00 respectively, might also be derived from a major Proterozoic infracrustal source, but may have a small contribution of mantle-derived material. Our analyses show that the early Cretaceous highly evolved biotite monzogranite in the basin may show potential for W-Nb-Pb-Zn mineralization in depths. The high degree of fractionation of the monzograntic melt and the subsequent multi-stage hydrothermal activities are the key factors controlling the W-Nb-Pb-Zn mineralization in the Lizikeng Basin.

CONCLUSIONS

The discovery of the early Cretaceous granitic rocks with the W-Nb mineralization potential indicates that the North Wuyi area is also prospective not only for Cretaceous Pb-Zn but also for rare metal mineralization, which open a new window for rare metal prospecting in the volcanic basins in South China.

A | 38

AGE AND GEOCHEMISTRY OF THE ORE-BEARING GRANITOIDS OF THE PORPHYRY Mo DEPOSITS IN THE LESSER XING'AN–ZHANGGUANGCAI RANGE METALLOGENIC BELT, NE CHINA: PETROGENESIS AND TECTONIC IMPLICATIONS

Xiaofei Yu

Development and Research Center of China Geological Survey - xfyu@jlu.edu.cn

BACKGROUND

Porphyry type Mo deposits represent the world's primary sources of this commodity, and their mineralization is closely associated with subduction-related calc-alkaline magmatism. However, there is another important type of Mo deposit in NE China, i.e., high- grade, rift-related deposits associated with fluorine-rich, highly evolved rhyolite magmas. In recent years, several medium to super large porphyry Mo deposits have also been discovered in the region (e.g. Chalukou, Huojihe, Luming, Jidetun, Daheishan, etc.), making NE China the second most important Mo province in China. It attracts more and more researchers' attentions. However, there remains significant potential for the further discovery of Mo deposits. Compared with the Eastern Qinling and Yanliao Mo ore belts, research on the Zhangguangcai Range Mo metallogenic belt is relatively limited. As a result, Mo exploration remains limited.

On the basis of previous work, we focus on its geologic characteristics, using precise geochronological data obtained from SIMS zircon U-Pb and petrology, element geochemistry as well as isotopic geochemistry for the ore-bearing granitoids of the porphyry Mo deposits in the Lesser Xing'an–Zhangguangcai Range metallogenic belt. This work also contributes to a better understanding of the timing of the ore system, the regional metallogenic regime, and the geodynamic setting of Early–Middle Jurassic large-scale ore mineralization in the Lesser Xing'an–Zhangguangcai Range metallogenic belt.

METHODS

Representative granitoids samples from the Jidetun, Daheishan, Luming and Fu'anpu porphyry Mo deposit were collected for geochemical analyses, Sr–Nd isotopic analyses and SIMS zircon U–Pb analyses. Sample crushing and zircon separation were conducted at the mineral separation laboratory of the Earth Science Exploration Technology Services Ltd. of Hebei Province at Langfang. The sites for zircon U–Pb age analysis were selected on the basis of the cathodoluminescence (CL) images as well as transmitted and reflected light micrographs to reveal their internal structures, which were acquired using a Cameca IMS-1280 SIMS at the Institute of Geology and Geophysics, Chinese Academy of Sciences in Beijing. Major and trace elements were analyzed at the Science Experiment Center of Jilin University Testing. Sr–Nd isotope compositions of samples were determined on a VG Axiom HR–MC–ICP–MS at the Beijing Research Institute of Uranium Geology.

RESULTS

Spot analyses from 15 grains (sample 3DHSTJ02-B25) yield concordant results with a weighted mean $^{206}Pb/^{238}U$ age of 168.3±1.4 Ma and a mean square weighted deviation of 0.06, which is interpreted as the crystallization age of the Daheishan granodiorite porphyry and consistent with an Middle Jurassic magmatic event. A total of 15 zircon U–Pb analyses of a porphyritic monzogranite (sample FAP-N) from the Fuanpu Mo deposit have ages ranging from 165.2 Ma to 172.6 Ma and the concordia intercept is 169.4±1.3 Ma. In comparison, 15 analyses of a granodiorite (sample JDT-N) from the Jidetun Mo deposit yielded $^{206}Pb/^{238}U$ ages of 160.5 to 170.9 Ma, with a weighted mean age of 160.48 ±0.82 Ma. Zircon U–Pb dating of a granodiorite (sample HJH-yx-B1) from the Huojihe Mo deposit yielded $^{206}Pb/^{238}U$ ages of 179.8 to 188.3 Ma, with a weighted mean age of 184.2 ±1.4 Ma. The studied rocks are monzogranite to granodiorite, metaluminous, and high-K calc- alkaline to shoshonitic series. Chondrite-normalized REE patterns are characterized by significant light rare earth element (LREE)/heavy rare earth element (HREE) fractionation, and have weakly negative to no Eu anomalies. These granites are also enriched in large ion lithophile elements (LILEs; e.g. Rb, Th, U, and K), and strongly depleted high field strength elements (HFSE) such as Nb, Ta, Ti, HREEs. These results are in accordance with the features of rocks formed in a subduction zone tectonic setting. The Sr–Nd isotopic compositions of the studied rocks from the porphyry Mo deposits (Daheishan, Fu'anpu, Huojihe and Jidetun) almost are homogeneous.

CONCLUSION

In the past ten years a number of precise rock and ore ages have been obtained for the granitoids-related porphyry Mo deposits in NE China. These ages indicate that Mo mineralization occurred during the Early–Middle

Jurassic (197–161 Ma), coinciding with the contemporary magmatic activities in the Lesser Xing'an–Zhangguangcai Ranges. Based on the whole-rock geochemistry of the ore-bearing granitoids from the porphyry Mo deposits in the the Lesser Xing'an–Zhangguangcai Range metallogenic belt, we conclude that the granitoids are characterized by high-K, calc-alkaline, pronounced fractionation of LREE/HREE, enrichment in large ion lithophile elements and depletion in high field strength elements, which are in accordance with the geochemical characteristics of the magmatism in typical continental margin tectonic setting. The granitoids were generated in an arc setting, which is further confirmed by trace element variation diagrams, in which all the samples plot within the volcanic arc granite (VAG) fields. Combined with regional tectonic evolution, whole-rock geochemical, and isotopic studies, we proposed that the formation of the ore-bearing granitoids from the porphyry Mo deposits in the the Lesser Xing'an–Zhangguangcai Range metallogenic belt was related to the westward subduction of the Paleo-Pacific Plate in the Early–Middle Jurassic, under which accreted crust was melted and the compression impeded magma ascent through the upper crust. Through the study on the ore-bearing granitoids from the porphyry Mo deposits in the Lesser Xing'an–Zhangguangcai Range metallogenic belt, we conclude that the Early-Middle Jurassic hydrothermal activity and mineralization in this region were associated with magmatism triggered by the subduction of the Paleo-Pacific Plate.

A | 39

STUDY ON THE EXPLORATION AND RESOURCES ESTIMATION OF RARE EARTH ELEMENTS, NORTHERN VIETNAM

Jaeho Lee

KIGAM - jhlee@kigam.re.kr

This study was conducted to secure overseas mineral resources throughout mineral exploration and potential evaluation of REE occurrences within the Nghe An province, Northern Vietnam. The exploration tools for the first and second survey areas (Quy Chau and Quy Hop) were the geological mapping, soil geochemical, pitting, and geophysical surveys. Also the test drilling survey was designed to the insurance of the potential resources. The geology of the study area are mainly consisted of Ban Chieng biotite granite complex and Dai Loc gneissic granite complex intruding Bu Khang formation comprising of schist, gneiss and limestone. Main mineralization have the characteristics of occurrence with tin and ruby, and minerals that contain REEs, monazite and xenotime, are thought as occurring in the alteration zone of granite complex. In order to elucidate the source rock of monazite and xenotime confirmed from heavy sand, the soil geochemical survey was carried out and an analysis result with ICP-MS on the soil samples collected typically on an exploration grid lines indicated that total REE oxide content(TREO) was about 1.4 times of crustal abundance. The pitting survey was conducted on the grid point with high TREO, and the pits with higher TREO of more than 1,000 ppm were identified. It was considered that ore bodies with REE anomaly might develop in the NW direction. The result of geophysical survey suggested the detailed survey on the boundary between high and low resistivity zones. Based on the above results, the drilling survey have been carried out to estimate REE resources on the survey areas. The 30 drillholes was completed for 660 m. The core samples were collected at intervals of 1 m. TREO ranges from 126 ppm to 2,738 ppm, and the inferred mineral resources was estimated approximately 148,000 t under the cut-off grade of TREO 300 g/t and the average grade of 660 g/t.

IMPLICATIONS OF Sn ISOTOPE FRACTIONATION IN ORES AND ROCKS ASSOCIATED WITH Sn MINERAL DEPOSITS

Ryan Mathur[1], Wayne Powell

[1]*Juniata College - mathur@juniata.edu*

Sn isotope variations in ores and rocks is a relatively new field for geochemistry. This presentation will focus on how the data can provide insight into ore formation and what potential exploration applications the data possess. Sn isotope values are presented for cassiterite, stannite and igneous rocks. Analytical techniques for the separation of Sn from these different chemical matrices can be found in (Mathur *et al.*, 2017).

Systematic variations of Sn isotope values in ores occur in all types of Sn deposits where cassiterites are approximately 2 ‰ heavier than later formed stannite in 6 different deposits analyzed. We highlight redox reactions as the most likely cause for the isotopic shift along with new experimental data that support fractionation associated with SnCl vapor. Sn isotope compositions of igneous rocks associated with mineralization have lower Sn isotope values (d124Sn=-1.2 to -1.8 ‰) than published rock standards (d124Sn= +0.1 to +0.6‰) not associated with mineralization. These general observations have both genetic and exploration importance.

REFERENCE

Mathur, R., Powell, W., Mason, A., Godfrey, L., Yao, J., and Baker, M. E., 2017, Preparation and Measurement of Cassiterite for Sn Isotope Analysis: Geostandards and Geoanalytical Research, 41,4, 701-707.

A | 41

Ta-Sn-Nb PARAGENESIS IN COMPLEX PEGMATITES: A CASE STUDY FROM PRESQUEIRA DYKE. GALICIA, NW SPAIN

Mercedes Fuertes-Fuente[1], Antonia Cepedal, Ana Roza Llera, Agustín Martín-Izard

[1]*Department of Geology, University of Oviedo, Spain - mercedf@uniovi.es*

BACKGROUND

Tantalum and tin are currently consider as high-technology metals due to its use in capacitors for wireless technology and in touch-screen displays. These metals can occur in high concentrations in pegmatites and occasionally form ore deposits. In Galicia, NW Spain, there are several occurrences of pegmatites such as the Presqueira dyke, which has been explored recently by a mining company. This work focuses on the Sn-Ta(Nb) paragenesis of this complex pegmatite.

The pegmatite is located in the Galicia Trás-os-Montes Zone (GTMZ) (Farias *et al.* 1987), one of the zones in which the NW Iberian Variscan Massif was divided. The GTMZ comprises a pile of units thrusted over the autochthonous Central Iberian Zone (Fig. 1a). The pegmatite is in one of these units, the Schistose Domain. The metamorphism is in greenschist facies. The GTMZ shows two deformation events associated with nappe emplacement, with recumbent folds. Subvertical axial-plane folds and shear zones typify a last deformation event. At the same time, synkinematic granitoids were emplaced being the pegmatite related to them.

METHODS

Samples were taken from exploration adits in the Presqueira dyke. Thin-sections were studied by optical microscopy, SEM-EDAX, EPMA (Cameca SX100) at Oviedo University.

RESULTS

The Presqueira dyke is a non-outcropping main dyke that forks into branches, with 700 meters in length and up to 15 meters in width (NI 43-101 Technical Report, 2014). The pegmatite strike is coincident with the regional schistosity. The body has a layered internal structure with coarse-grained and fine-grained albite-rich bands. It is mainly composed of albite, spodumene, quartz, muscovite and K-feldspar. The main accessory minerals are Ta- Sn-Nb bearing oxides, phosphates and pet alite.

Ta-Sn-Nb-bearing oxides are cassiterite and members of the columbite-tantalite group. These minerals usually are disseminated in the albite-rich bands of the body. Cassiterite is mainly enriched in Ta and Nb (Ta+Nb up to 4.5 wt. %), having lower contents of Fe (0.1-0.75 wt. %) and Ti (0.06-0.12 wt. %). Under transmitted light optical microscopy, this oxide commonly reveals colour zoning, with clear and dark bands in accordance with content variations of the above mentioned trace elements. Moreover, cassiterite sometimes presents columbite-tantalite inclusions or is intergrown with this mineral.

Columbite-tantalite forms fine-grained crystals with prismatic and tabular habits. Uraninite is present as inclusions (Fig. 1b). SEM-BSE images of crystals show a normal zoning with a euhedral core enriched in niobium and a rim enriched in tantalum (Fig. 1b). Cores and rims present fine oscillatory zoning. In addition, the rims are sometimes irregular, resulting in a sub-euhedral to anhedral crystal with a euhedral prismatic core. On other occasions, the contact of these Ta-rich rims with the Nb-rich cores is lobate, giving rounded corners, and embayments (Fig. 1b). Sometimes, the oscillatory zonation of Nb-rich cores is partially disrupted by a patchy Ta-richer zonation. These growth textures may indicate episodes of Nb-rich core dissolution previous to Ta-rich rim formation. The composition of cores corresponds to ferrocolumbite with Ta/(Ta + Nb) = 0.12-0.47 and Mn/(Mn + Fe) = 0.37-0.52. Rim composition varies between ferrocolumbite and ferrotantalite with Ta/(Ta + Nb) = 0.37-0.62 and Mn/(Mn + Fe) = 0.20-0.49. Superimposed upon the described zonation patterns, ferrotapiolite occurs at the margins of the grains or along microfractures (Fig. 1c), which leads us to interpret it as evidence of this phase representing the last Ta-Nb oxide formed in the paragenesis.

CONCLUSIONS

From this study we conclude that the trend followed by the Ta-Nb bearing oxides in the columbite-tantalite quadrilateral supports that fractionation progressed from ferrocolumbite to ferrotantalite. This trend is thought to be in accordance with low fluorine activity (e.g. Tindle & Breaks 2000). The Presqueira pegmatite may represent a fluorine-poor system, which it is also supported by the lack of lepidolite, as the Li-bearing phase. We interpret that the ferrotapiolite represents a later event superimposed on the earlier columbite- tantalite. The replacement of an

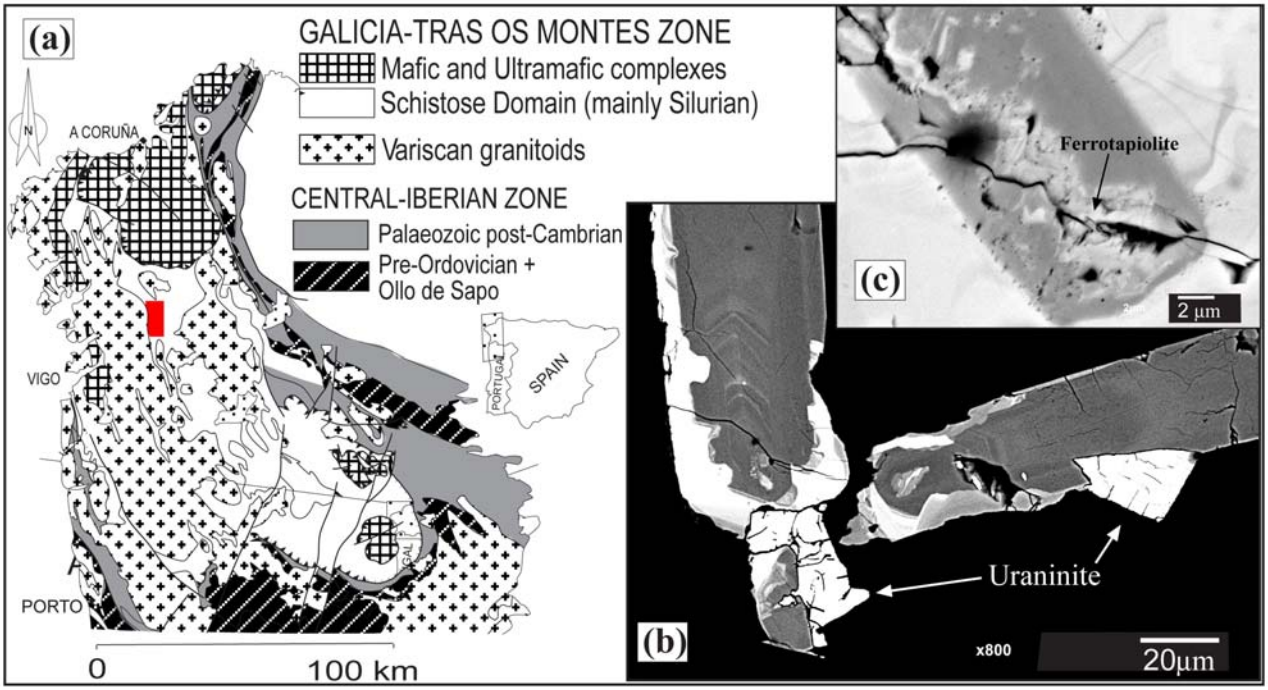

Figure 1. A) Location of the studied area (red rectangle). B) SEM-BSE images of columbite-tantalite with uraninite showing a fine-oscillatory zoned core (ferrocolumbite) and a lobulated rim (ferrotantalite). C) Ferrotapiolite filling a microveinlet that crosscuts a columbite-tantalite grain.

early columbite-tantalite by late Ta-richer generations has been described in rare-element granitic pegmatites (e.g. Chudík *et al.* 2011). Reactive fluids that separate from evolved residual albitic melts in the last stages of pegmatite crystallization may be involved in these replacements. In the studied pegmatite, the re- equilibration of the earlier columbite-tantalite with a late fluid could have produced its partial resorption followed by the later crystallization of the Ta-Fe-richer oxide (ferrotapiolite).

REFERENCES

Chudík, P., Uher, P., Gadas, P., Škoda, R,. PrseK, J., 2011. Niobium-tantalum oxide minerals in the Jezuitské Lesy granitic pegmatite, Bratislava Massif, Slovakia: Ta to Nb and Fe to Mn evolutionary trends in a narrow Be,Cs-rich and Li,B-poor dike Mineralogy and Petrology, 102, 15–27.

Farias, P., Gallastegui, G., González Lodeiro, F., Marquínez, J., Matin Parra, L.M., Pablo Macia, J.G., Rodríguez Fernández, L.R., 1987. Aportaciones al conocimiento de la litoestratigrafia y estructura de Galicia Central. Memoria Facultad de Ciencias Universidad de Porto I, 411-431. NI 43-101 TECHNICAL REPORT (2014). Alberta-1 rare metals project Galicia.

Tindle, A. G., Breaks, F. W. (2000) Columbite-tantalite mineral chemistry from rare-element granitic pegmatites: Separation Lakeh area, N.W. Ontario, Canada. Mineralogy and Petrology, 70, 165-198.

A | 42

SKARN EVOLUTION OF A GIANT SANGDONG W- MO DEPOSIT, SOUTH KOREA: GENETIC IMPLICATIONS

Jeonggeuk Kang[1], Seon-Gyu Choi, Jieun Seo, Sang-Tae Kim, Gyoo-bo Kim, Jonghyun Lee, Chang Seong Kim

[1]*Department of Earth and Environmental Science, Korea University, Seoul - rkdwjdrmr@korea.ac.kr*

BACKGROUND

The Sangdong deposit, one of the giant W-Mo skarn deposits in the world, is located in Taebaeksan mineralized province, eastern South Korea. The skarns are hosted in interbedded limestone within the Myobong slate and the Pungchon limestone, in the lower part of the Choseon Supergroup. The Sangdong skarn is characterized by multi-stage mineralization that has distinct distribution of skarn zones (central quartz-mica zone surrounded by amphibole-biotite skarn zones, and finally outer pyroxene-garnet skarn zones) with fluorite. Previously, some researchers have classified the Sangdong W deposits with diverse redox environment - such as reduced W-skarn (Einaudi *et al.*, 1981), moderately reduced W-skarn (Newberry, 1983), and distal oxidized W-skarn (Kawk, 1987). We present physicochemical conditions of the Sangdong deposits through petrological, mineralogical, and stable isotopic evidence.

METHODS

Whole-rock and rare earth elements concentrations were determined using inductively coupled plasma-optical emission spectrometry (Thermo Jarrell-Ash ENVIRO II), inductively coupled plasma-mass spectroscopy (Perkin Elmer Sciex ELAN 6000), instrumental neutron activation analysis, and ion selective electrode at Activation Laboratories Ltd., Canada. Mineral chemistry of the skarn was determined using JEOL JXA-8600 SX electron microprobe at Korea University. Carbon and oxygen isotope compositions of carbonate minerals collected from skarns were determined. The stable isotope analyses were conducted using Gas Bench II and Thermo Finnigan Delta plus XP isotope ratio mass spectrometer at McMaster University.

RESULTS

Sangdong granite occurs about 1 km below the surface. It is reported Cretaceous in age (87.5 Ma, Kim, 1986) that is similar to the mineralization age (86.6-87.2 Ma, Seo *et al.*, 2017). Sangdong granite corresponds to a highly evolved, peraluminous, high-K calc-alkaline granite. The contents of Rb and Sr correspond to reduced W-skarns to low F-B-Sn skarns that is similar to other giant W deposits such as the Cantung, the Pine Creek, and the Mactung deposits. N-S fault zones were found by drillings near the Sangdong granites. This structure would have transported ore-forming fluid repeatedly to the Myobong and Pungchon formation and contributed to make distribution of skarn zones in Sangdong. Slate in the Myobong formation induced the ore-forming fluid to flow through reservoir.

Development of skarn is the result of multistage skarn mineralization. Four stages of skarn evolution has been determined from cross-cutting, replacement texture and mineral assemblages. During stage I (prograde I skarn), skarn formation began with calcic a assemblage represented by intermediate-Fe pyroxene (1-74 mole % hedenbergite) + andraditic garnet (8-99 mole % andradite) + wollastonite. These were replaced by pyroxene with 58-95 mole % hedenbergite and garnet with at least 35 mole % almandine + spessartine component, respectively in stage II (prograde II skarn). This indicates prograde II skarn was formed under a relatively reduced environment (Fig. 1). During stage III (retrograde skarn), hydrous alteration occurred and pre-existing skarn minerals were altered to amphibole and biotite. Stage IV (vein stage) represents the formation of veins that overprinted previous skarns. This stage is the latest phase of skarn evolution that have quartz, muscovite, and chlorite mineral assemblages. Scheelites were enriched in stage III and IV that show zoning pattern with high molybdenum contents in back scattered electron images. However, scheelites in stage I and II have relatively homogeneous composition that have low molybdenum contents. The bleached limestone shows the most enriched average carbon and oxygen isotope compositions (δ^{13}CV-PDB = -0.53 ‰, δ^{18}OV-SMOW = 14.95 ‰) relative to the vein calcite (δ^{13}CV-PDB = -3.97 ‰, $\delta^{18'}$18OV-SMOW = 12.26 ‰), whereas the skarn calcite (δ^{13}CV-PDB = -5.82 ‰, δ^{18}OV-SMOW = 11.38 ‰) has the most depleted isotopic composition. Theoretical models of carbon and oxygen isotope covariation proposed by Zheng and Hoefs (1993) indicate that calcites precipitated within only a small temperature variation (350-450°C) and this is concordant with the homogenization temperatures of fluid inclusions in the pyroxene (366-476° C, Moon, 1985). The CO_2 mole fraction (XCO_2) was estimated as 0.1 from the best fit of the theoretical models and this indicates skarn mineralization occurred in an open system rather than a closed system.

CONCLUSION

Several evidences support fluorine is associated with Sangdong deposits. Abundance of fluorite reflects that F-rich ore-forming fluids were generated from the Sangdong granite. Sn/Mo and W/Sn ratios from the prograde and retrograde skarns correspond to W-F skarns (Newberry, 1998). REE patterns of skarn show negative Eu anomalies and this indicates REE were transported as REE-F complexes under hydrothermal conditions (Haas *et al.*, 1995). However, amphibole and biotite compositions with higher chlorine contents than fluorine indicate that fluorine activity was not high as much as the greisen deposits. According to the physicochemical condition of the Sangdong deposit determined from the geochemical data, we present the genetic model of Sangdong deposit. F-bearing hydrothermal fluids were generated from highly evolved, and peraluminous Sangdong granite. This fluids moved along the fault zone repeatedly, and formed multi-stage skarn mineralization in the interbedded limestone of the Myobong and Pungchon formation. Primary prograde skarns occurred widely under oxidized environment (Prograde I), and these were replaced under reduced environment (Prograde II), after that overprinted to later retrograde skarns. Lastly, the vein stage occurred by injection of late fluids.

REFERENCES

Einaudi, M.T., Meinert, L.D., Newberry, R.J., 1981. Skarn Deposits, in: Skinner, B.J. (Ed.), Seventy-Fifth Anniversary Volume. Economic Geology, 317-391.

Haas, J.R., Shock, E.L., Sassani, D.C., 1995. Rare earth elements in hydrothermal systems: Estimates of standard partial molal thermodynamic properties of aqueous complexes of the rare earth elements at high pressures and temperatures. Geochimica et Cosmochima Acta, 59(21), 4329-4350.

Kim, K.H., 1986. Petrology and petrochemistry of Sangdong granite. Unpub. M.S. Thesis, Kyungbuk National University, pp. 80.

Kwak, T.A.P., 1987. W-Sn skarn deposits and related metamorphic skarns and granitoids, first ed. Elsevier Science, Amsterdam.

Moon, K.J., 1985. Fluid Inclusion Study of the Sangdong Tungsten Skarn Deposits. Jour. Korean Inst. Mining Geol. 18(3), 205-216.

Newberry, R.J., 1983. The Formation of Subcalcic Garnet in Scheelite-Bearing Skarns. Canadian Mineralogist, 21, 529-544.

Newberry, R.J., 1998. W- and Sn-skarn deposits: A 1998 Status Report, in: Lentz, D.R. (Ed.), Mineralogical Association of Canada Short Course Series, Mineralized Intrussion-Related Skarn Systems. Mineralogical Association of Canada., Quebec, pp. 289-336.

Seo, J.H., *et al.*, 2017. Magmatic-hydrothermal processes in Sangdong W-Mo deposit, Korea: Study of fluid inclusions and 39Ar-40Ar geochronology. Ore Geology Reviews, 91, 316-334.

Zheng, Y.-F., Hoefs, J., 1993. Carbon and oxygen isotopic covariations in hydrothermal calcites. Mineralium Deposita, 28, 79-89.

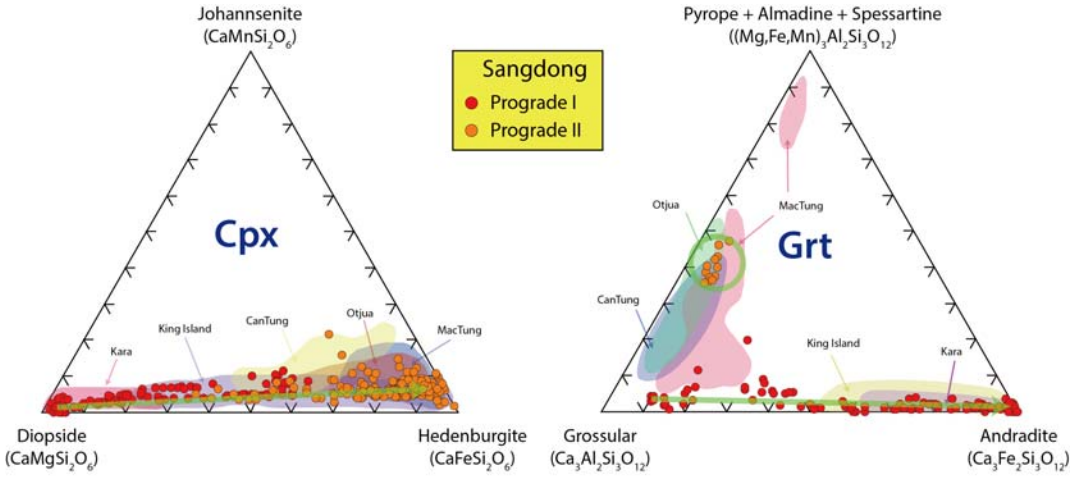

Figure 1. Evolution trend of garnet and clinopyroxene composition from Sangdong

A | 43

THE GEOCHEMISTRY OF THE CRETACEOUS GRANITOIDS SUITES ASSOCIATED WITH THE TUNGSTEN POLYMETALLIC DEPOSITS IN THE HWANGGANGRI PROVINCE, SOUTH KOREA

Jonghyun Lee[1], Seon-Gyu Choi, Chang Seong Kim, Jieun Seo

[1]*Department of Earth and Environmental Science, Korea University, Seoul - jongdol@korea.ac.kr*

INTRODUCTION

In the Hwanggangri province, located in central part of the southern Korean peninsula, many magmatisms were accompanied by W-Mo and polymetallic(Cu-Pb-Zn-Au-Ag) mineralization. There are more than twenty W-Mo deposits such as proximal vein type deposit (Jungbo and Weolak), proximal skarn deposit (Geumseong), and distal polymetallic deposit (Boksu, Dangdu, Useok, and Kwangsin). With W-Mo mineralization, abundance of fluorite is reported in these deposits, and mineralization ages are all concentrated in the Cretaceous at 89.6 Ma (Jungbo), 89.8 Ma (Weolak), and 96.5 Ma (Geumseong). The Hwanggangri province consists of four Cretaceous biotite granites as like the Muamsa, Susan, Weolaksan, and Sokrisan granite which have similar ages of 91 ± 2 Ma, 89 ± 2 Ma, 91 ± 2 Ma and 88 ± 2 Ma, respectively. These characteristics are similar to the Sangdong, one of the giant W-Mo skarn in the world. However, the Sangdong deposit is associated with hidden Sangdong two mica granite (87.5 ± 4.5 Ma). We reviewed geochemical and mineralogical data of these five granites to find the relationship of the characteristics of granites with W-Mo mineralization.

ANALYTICAL METHODS

Analyses for chemical compositions of major and minor components including REE were carried out by Activation Laboratories. Ltd, Ancaster, Canada. Whole-rock and REE concentrations were determined using inductively coupled plasma-mass spectroscopy (Perkin Elmer Sciex ELAN 6000).

RESULTS

All of the granites are medium- to coarse-grained granites. Except for the Sokrisan granite, most of granites show porphyritic and graphic textures. Magnetic susceptibility values of the Muamsa, Susan, Weolaksan, and Sokrisan granite are 0.02-4.21, 0.01-0.05, 0.02-2.52, and 1.01-1.95 (x10-3 SI), respectively. This wide range of values indicates fractional crystallization of magma in magnetite series granites. Magnetic susceptibility value tends to decrease with degree of differentiation of magma increases. These granites are classified as sub-alkaline, high-K, calc-alkaline, and metaluminous to peraluminous granites. In particular, A/CNK (molar ratio) value of the Sangdong granite is 1.0 to 1.5 and corresponds to the peraluminous characteristic which is caused by hydrothermal alteration. In Y+Nb versus Rb diagram, the Cretaceous granites in the Hwanggangri province are classified volcanic arc granite and within plate granite but Rb is enriched by evolving process of magma. The Muamsa, Susan, Weolaksan and Sokrisan granite are plotted in boundary between I-type and A-type granite characteristics on the (Na2O+K2O)/CaO versus (Zr+Nb+Ce+Y) discrimination diagram (*Whalen et al., 1987)*. All the granites are related to the W and Mo mineralization, which correspond to nearby deposits (Figure. 1a). The Muamsa, Susan, Weolaksan, and Sokrisan granite are fractionated felsic granites. The Rb/Sr versus SiO2 diagram suggests that the Muamsa, Susan, Weolaksan, Sokrisan, and Sangdong granite have more evolved feature. They show high Rb and lower Sr which indicated that more evolved and associated mainly with low F-B-Sn skarns in the Sr versus Rb diagram. It indicates that they are related to relatively high F activity. The Sangdong granite is characterized by reduced W skarn deposits. All the granites have low Sr/Y and high Y island- arc andesite-dacite-rhyolite field characteristics. The Muamsa, Susan, Weolaksan, Sokrisan, and Sangdong granite have similar strong negative Eu anomaly with HREE enrichments and LREE depletions (Figure. 1b). The Muamsa, Susan, Weolaksan, and Sokrisan granite have strong depletion of Ba, K, Sr, P and Ti in primitive-mantle normalized trace elements patterns (Figure. 1c). It indicates that these granites are highly evolved granites. In diagram of Nb/Ta versus Zr/Hf, the Muamsa, Susan, and Weolaksan granite have similar characteristics while the Sokrisan granite has higher Nb/Ta value than the others (Figure. 1d).

CONCLUSION

We represent the relationship of granites and W-Mo mineralization using mineralogical and geochemical data. The Muamsa, Susan, Weolaksan and Sokrisan granite have similar mineralogical characteristics like major mineral assemblages, texture, magnetic susceptibility, and geochemical feature. All the granites were emplaced at relatively shallow depth. They have high evolved (SiO2 >70 weight %) with oxidized characteristics (magnetite

series). However, the Sokrisan granite is different from other Cretaceous granites in Nb/Ta versus Zr/Hf diagram. Unlike the previous studies, there are some differences between productive granites (Muamsa, Susan and Weolaksan) and barren granite (Sokrisan) in this study. Many W-Mo deposits like Geumseong, Jungbo and Weolak occured around the Muamsa, Susan, and Weolaksan granite, but there is no deposit around the Sokrisan granite because all the deposits near the Sokrisan granite had been eroded out. Abundance of fluorite in the Sangdong deposit and the Hwanggangri province is associated with W dominant mineralization than Mo mineralization. We consider that fluorite is a criterion for determining W dominant mineralization than Mo mineralization.

A | 44

FERTILE MAGMA GENERATION DURING THE OROSIRIAN ON THE SOUTHERN AMAZONIAN CRATON: AN EXAMPLE FROM THE TAPAJÓS MINERAL PROVINCE, NORTHERN BRAZIL

Lucas Villela Cassini[1], Jean-François Moyen, Caetano Juliani

[1]University of São Paulo - lucascassini72@gmail.com

INTRODUCTION AND GEOLOGIC CONTEXT

It's axiomatic that the generation of mineral deposits, porphyry systems in particular, require the presence of fertile rocks. These lithotypes will provide ligands, fluids, volatiles and the metal content necessary to form a mineral occurrence. That's the main reason why porphyry deposits are preferentially, but not only, found in arc-related tectonic settings. Arc-related magmas tend to be metaluminous, calc-alkaline, hydrous and slightly oxidized, conditions that confer them their metallogenetic favorability. Hence, the geochemistry characteristics of a given rock suite is essential in order to establish whether it's fertile or not. The importance of geochemistry is particularly augmented on the context of southern Amazonian Craton, one of the most important gold producing regions in Brazil which still lack detailed studies.

This region of the craton, also known as Tapajós Mineral Province (TMP), is characterized by Orosirian igneous suites of calc-alkaline affinity. The classic tectonic model treats this magmatism as a consequence of the paleoproterozoic orogenic events responsible for the coalescence of the craton. An alternative tectonic model suggests that the craton was amalgamated through E-W well marked lineations installed on ancient archean continental crust. Later A-type granitic intrusions mark the transition towards an anorogenic tectonic setting. Most recent papers show the dominance of magmatic-hydrothermal deposits such as porphyry (Au, Au-(Cu) and Cu-Mo-(Au) and epithermal (quartz-alunite) systems genetically related to the calc-alkaline units. On the first case the mineralization is most commonly found within the potassic alteration zone and consists in gold-bearing quart+pyrite veins and veinlet sets.

With the intention of establishing prospecting criteria, we use simple whole-rock geochemistry succeeded by geochemical modelling in order to determine the metallogenetic potential of the different rock suites identified on the central TMP.

TYPOLOGY AND GEOCHEMISTRY FEATURES OF THE LITHOTYPES

The central TGP shows the predominance of granitic rocks with subordinated volcanic units. Among the main intrusive bodies are: i) the Creporizão Suite (CRP, 1.99-1.95 Ga); ii) the Parauari Suite (PAR, 1.89 Ga); and iii) the Maloquinha Suite (MLQ, 1.87 Ga). Volcanic units, both explosive and effusive examples, are most commonly attributed to the Iriri Group (ca.1.87 Ga) and these will be addressed from this point forward as VLC-A. A few older examples of extrusive lithotypes (ca. 1.97 Ga) were also described on the TMP, and these will be denominated VLC-B hereinafter.

The CRP suite is composed by granites, granodiorites, monzonites and syenites. Hydrothermal alteration is ubiquitous, most commonly potassic alteration, where the primary igneous plagioclase is progressively substituted by secondary K-feldspar. Furthermore, shallow level porphyry intrusions are often related to the CRP suite. VLC-B is essentially rhyolitic, flow-banded, fine grained, and is frequently found on topographic domes. MLQ is essentially granitic, leucocratic, porphyritic and non-magnetic. PAR shows a wider compositional range and varies between granodiorite, tonalite, quartz-monzonite and granite. The rocks are porphyritic, grey colored, with plagioclase phenocrysts distributed on a biotite and hornblende rich matrix. VLC-A varies from basaltic-andesite, andesite, dacite and rhyolite.

Invariably, all rocks from the CRP suite are either calc-alkalic or alkali-calcic. The most primitive units are described as metaluminous granodiorites and tonalites and, as differentiation occurs, get more strongly peraluminous. An identical behavior is verified for the synchronous VLC-B. Intermediate VLC-A and PAR are metaluminous and fractionates towards more peraluminous compositions. Such trend contrasts with acid VLC-A and MLQ, which are essentially peraluminous. With respect to their trace element contents, most units present low La/Yb ratios and tend to cluster around 20. Using this ratio it's possible to separate two different types of granodiorites related to the CRP suite, one with moderate La/Yb (~40), the other with low La/Yb (~10), both considered as potential initial liquids from which the other lithotypes were differentiated.

Geochemical modelling starting from the low La/Yb granodiorites reveal that these rocks evolved to alkali-granite compositions, with an increase of the La/Yb ratio, through the fractionation of albite, labradorite, K-feldspar and amphibole, with minor magnetite and titanite/ilmenite. The degree of crystallization falls within the interval

0.43-0.57 and generate a cumulate with monzonitic composition. An identical result was modeled for the moderate La/Yb granodiorites, however, fractionation tends to increase the ratio and shift the trend away from the sample cluster. The modelling results for the 1.88 Ga sequence reveals the presence of amphibole as the main phase of the cumulate (up to 43%) for VLC-A and PAR, which is accompanied by the crystallization of labradorite and albite, with magnetite and apatite as the main accessories. MLQ apparently shows a distinct and shorter petrologic evolution, characterized by the fractionation of calcic plagioclase, biotite, clinopyroxene and ilmenite, for a very small degree of crystallization (between 0.09 and 0.12).

DISCUSSION

Our results demonstrate that whole-rock geochemistry and particularly aluminosity are important parameters in discussing the petrogenesis of granites. Accordingly, the trend defined by the CRP suite and synchronous VLC-B (both varying from metaluminous to mildly peraluminous) indicates the presence of mafic rocks on their petrologic evolution and strongly suggests a mantelic heritage with minor or negligible crustal contribution. An identical behavior is observed for PAR and the more primitive facies of VLC-A (both 70 million years younger than CRP). A different story is told by MLQ and the acid facies of VLC- A, which are clearly more peraluminous, indicating a genetic link with felsic sources and most likely the reworking of preexisting continental crust.

The presence of moderate and low La/Yb CRP granodiorites suggests a slightly diachronic magmatic evolution on the TMP. In fact porphyry systems are not related to one big pluton, rather they are most commonly found on a context of multiple intrusions, a consequence of the continuous input of magma provided by melting of the mantle wedge. Geochemical modelling reveals that within the age range of CRP (from 1.99 to 1.95 Ga) the rocks evolved mainly though fractional crystallization. The presence of amphibole and magnetite on the petrologic evolution of the CRP suite should be highlighted. These minerals are also present on the 1.88 Ga sequence, which reinforces the metallogenetic potential of these suites and the diachronic character of the magmatic-hydrothermal system on the central TMP. The modelling results for the anorogenic and peraluminous MLQ suite don't show relevant concentrations of hydrous minerals on its evolution, and as a consequence, this unit is understood as less fertile from a metallogenetic perspective.

CONCLUSIONS

When coupled with geochemical modelling, a simple whole-rock geochemistry has been proven to be an important tool to identify economically potential igneous suites. In this context, the fertility of igneous rocks on the TMP was verified mainly through their petrologic evolutions which involves, most importantly, the fractionation of amphibole and magnetite, indicating the hydrous and slightly oxidized characteristics of the magmas attributed to the CRP and PAR suites. The results point to a diachronic and complex magmatic-hydrothermal system, responsible for the generation of many mineral occurrences (porphyry and epithermal systems) that still need a better understanding. Regardless, our results highlight the importance of further investigation on the southern Amazonian Craton and extend the economic potential of the Orosirian calc-alkaline magmatism.

CHAPTER 4
METALLOGENY OF THE ANDES

Convenor: Nora Rubinstein

COPPER-GOLD-SILVER MINERALIZED TOURMALINE BRECCIA PIPES AT SOLEDAD, PERU

Steven Park

Chakana Copper Corporation - spark@chakanacopper.com

Chakana Copper Corporation's Soledad property hosts numerous quartz-tourmaline-sulfide breccia pipes exposed at surface containing high-grade gold, copper and silver. Chakana has completed over 17,000 meters of DDH drilling since August 2017. Geochemical data and geological observations from drill core and surface mapping have led Chakana geologists to support a genesis of breccia pipe formation related to degassing of a deep magma source. The mineralized tourmaline breccias at Soledad represent a gold-rich end member of intrusion-related polymetallic pipes that do not appear to be associated with a porphyry copper system.

The Soledad project is located in central Peru in the prolific Miocene metallogenic belt 35 km south of Barrick's Pierina Au-Ag mine. The project is in the Ticapampa-Aija Mining District of the Cordillera Negra where sub-epithermal polymetallic (Pb-Ag-Zn) veins have been mined since the 17th century. The Soledad breccia pipes are hosted predominantly in andesitic volcanic rocks of the Lower Calipuy Group, early Tertiary in age. Recent geologic mapping on the project identified additional breccia pipes located near contact zones between Cretaceous clastic sediments and Lower Calipuy volcanics.

Drilling to-date has focused on Breccia Pipe #1, where previous drilling confirmed a vertical extent of mineralized breccia from surface to a depth of 490m at which point the deepest drill hole exited the pipe structure. Interpretation of geophysical data (IP and CS/NS-AMT) suggests the pipes extend much deeper. Highlights from the most recently released drill results are 119.0m @ 3.36 g/t Au and 1.14% Cu from Breccia Pipe #1 and 164.0m @ 1.84% CuEq from Breccia Pipe #5.

Mineralized quartz-tourmaline veins related to Breccia Pipe #1 have returned >1,000 g/t Ag over several one meter sample widths.

The breccias have dimensions of 50 – 100 m diameter at surface with separation between the pipes of 300 – 500 m. The breccia is predominantly monomictic with clasts derived from the host andesite volcanic rocks. These clasts are generally tabular, or "shingle" shaped, and are strongly altered by quartz-sericite-tourmaline. The breccia – wall rock contact is generally defined by vertical quartz- tourmaline-sulfide sheeted veining. An alteration halo of quartz-sericite has been recognized in wall rock outboard from the breccia for several meters.

Quartz-tourmaline-sulfide mineralization is hosted primarily within breccia matrix; in high grade zones, sulfides also replace breccia clasts. Based on petrography studies, the sulfide assemblage includes an early stage of pyrite, arsenopyrite, sphalerite, chalcopyrite, tetrahedrite-tennantite and bismuthinite followed by bournonite, galena and silver sulfosalt. Supergene chalcocite commonly rims chalcopyrite with minor covellite; hypogene chalcocite has also been tentatively identified.

Free gold is found on crystal boundaries between chalcopyrite, pyrite, galena and unidentified sulfosalt minerals as a product of a late event; gold formed as bleb inclusions (20-100 mm) within pyrite during an earlier event. Late carbonate minerals (calcite and siderite) are found in breccia voids. Breccia Pipe #1 and Breccia Pipe #5 have distinct geochemical signatures and minor differences in mineralogy. For example, in Breccia Pipe #1 common arsenopyrite occurs as a distinct paragenetic event not intergrown with other sulfide minerals; in Breccia Pipe #5 As values are very low and arsenopyrite is absent. Also, tabular siderite is common in Breccia Pipe #5 and rarely seen in Breccia Pipe #1.

Genesis of these breccia pipes is considered to have been related to degassing of a deep (>5 km) magma source as local vapor pressure exceeded lithostatic pressure resulting in the explosive release of B, H_2O, CO_2, S along sheeted vertical fractures into the overlying volcanic pile. These gasses did not breach the paleosurface resulting in the upward tapering of breccia pipes terminating as small circular ring fractures in the host volcanic rocks. Shingle clasts were the result of brecciation of vertical sheeted fractures and, to a lesser degree, of finely laminated volcanic flows.

Blocky clasts in the breccia are noted where wall rock consists of more competent volcanic units. Close spatial correlation of clast shape with wall rock stratigraphy suggests minimal movement within the pipe structure during breccia formation, although shingle clasts show imbrication and other stacking arrangements suggesting a downward flow of hydrothermal fluids and settling of clasts at some point during breccia formation. In localized zones having a high clast-to-matrix ratio with predominantly shingle-shaped clasts, these clasts tend to pack tightly thus reducing permeability. Where blocky clasts are mixed with shingle clasts, voids were created that later filled with sulfide resulting in high Au-Cu-Ag grades along margins of the breccia pipes.

Exposed breccia pipes on the Soledad project are marked by a conspicuous 'monument' outcrop, generally circular to elliptical in plan and ranging from 20 to 50 meters in height due to the silicified breccia's erosion resistance relative to surrounding country rock. In most cases, these outcrops feature a carapace of altered wall rock enclosing the breccia and hosting vertical quartz-tourmaline sheeted veining that characteristically defines the margins of the breccia pipe structures. Drilling has shown that the pipe structures are vertically oriented at a plunge of less than 10o with diameters increasing with depth. Recent drilling on Breccia Pipe #1 encountered a blind finger of breccia sub- parallel to the main body measuring 20 x 110 meters. Between this blind breccia and the main body is another narrow breccia form that transitions into, and terminates as, a high-grade quartz- tourmaline-sulfide vein carrying grades of >1,000 g/t Ag.

Breccia pipes appear to have structural control, although geologic mapping has yet to demonstrate location of a breccia pipe at a structural intersection seen on surface. Breccia Pipe #1 is located along trend from an ENE-trending strike-slip fault and near the intersection with a prominent NW- trending vein structure. This same strike-slip fault clipped the carapace of two Au-Cu-bearing breccia outcrops 600m WSW of Breccia Pipe #1. Breccia Pipes #5 and #6 are spaced 520m apart along a prominent N-S fault that cuts numerous E-W quartz-tourmaline replacement structures.

Deep major structures may be the primary influence on the location of these breccia pipes.

A NEW HYDROTHERMAL ALTERATION AREA ASSOCIATED TO NEOGENE MAGMATISM IN VALLE HERMOSO DISTRICT, CENTRAL ANDES (35° S)

Martín Gozalvez[1], Patricia Sruoga, Cintia Marquetti, Angel Jara, Marta Godeas, Mario Rosas

[1]*SEGEMAR - Martín.gozalvez@segemar.gov.ar*

Valle Hermoso district (35°S) is located in the Central Andes and it belongs to a ~200 km- long and 20 km-wide belt (34°S-36°S) which includes volcanic-related Fe, Fe-Cu and Cu-(Ag) mineral deposits and hydrothermal alteration areas.

Since 2005, the Instituto de Geología y Recursos Minerales (IGRM) from SEGEMAR has been conducting geological and metallogenetic studies in the 34°-35° Andean segment in order to identify and characterize the mineral resources. The main goal of these studies is to discriminate among the different magmatic events, linking the hydrothermal alteration and mineralization pulses during Mesozoic and Neogene times (Crosta and Palacio, 2015; Sruoga, *et al.*, 2008; 2016).

The study area is located along the río del Cobre, between the río Tordillo and the arroyo Santa Helena. The local stratigraphic record includes sedimentary and volcaniclastic/volcanic rocks of Middle Jurassic to Middle Cretaceous ages and Neogene volcanic/subvolcanic sequences.

Along the eastern margin of the río del Cobre, the so-called manto-type Cu deposits (Adriana, Victoria, Sybil, Anita y El Guanaco) are related to the Río Damas Formation, of Kimmeridgian age and widespread distribution in Chile. The chalcocite, chalcopyrite, bornite and pyrite mineralization is hosted in veins, small pockets and vesicle infills in porphyritic andesitic sills and chloritized volcanic breccias (Crosta and Palacio, 2015). These Cu mineral deposits are spatially and probably genetically related to the Upper Jurassic calcalkaline volcanism.

Along the western margin of the río del Cobre, a large-volume subvolcanic body, dioritic in composition and largely affected by calco-sodic hydrothermal alteration, has been recognized for the first time. In the south, it intrudes gypsum beds from the Yeso Auquilco Formation, whereas in the north, sedimentary rocks from the Lotena Formation are intruded. Petrographically, the diorites vary in texture from coarsely granular to slightly porphyritic and they contain plagioclase and clinopyroxene, with titanite and apatite as accesory phases. U-Pb dating of zircons from a fresh diorite yielded an age of 13.17±0.25 Ma.

The actinolite + apatite + pyrite hydrothermal alteration is well developed on the east slope hill, on the top there is quartz+pyrite+calcite alteration with abundant Fe oxides. Both types of hydrothermal alteration were identified in the ASTER satellite images and is markedly visible in the field.

The hydrothermal alteration has been characterized through mapping, petrography, X-ray diffraction and fluorescence and SWIR spectroscopy in order to determine the mineral assemblages.

The actinolite + apatite + pyrite alteration occurs in net contacts massive veins with north- east strike and thickness between 0.2 and 0.6 m. It also occurs pervasively replacing the dioritic mafic minerals by actinolite. This alteration is overprinted by chlorite+epidote+calcite assemblage and minor secondary biotite. In some actinolitic veins it was observed that the calcite had formed parallel veins systems.

This new alteration area is interpreted as a possible IOCG system with an extended calco- sodic (actinolite+ apatite + pyrite) alteration, overprinted by phyllic (quartz+ pyrite), propylitic (chlorite+epidote+calcite) and potassic alteration (biotite).

A similar model was previously proposed for Las Choicas deposit (Franchini *et al.*, 2007), located 22 km north of the study area.

Based on the Neogene volcanic stratigraphy reported elsewhere (Sruoga *et al.*, 2008, 2016), the radiometric data presented here points out to this magmatic event as unique, in this Andean segment.

Near-future studies will allow to better understand the magma sequence and to refine the metalogenetic model, as well as the relationship between Las Choicas and Valle Hermoso districts.

REFERENCES

Crosta, S., Palacio, M. B., 2015. Carta minero-metalogenética 3569-III –Malargüe, provincia de Mendoza. Servicio Geológico Minero Argentino. Boletín 407, 89 p. Buenos Aires.

Franchini, M., de Barrio, R. E., Pons, M. J., Schalamuk, I., Ríos, F., Meinert, L., 2007. Fe skarn, iron oxide Cu-Au, and manto Cu-(Ag) deposits in the Andes Cordillera of south-west Mendoza province (34°-36°), Argentina. Exploration and Mining Geology, 16 (3-4), 233-265.

Sruoga, P., Rubinstein, N. A., Etcheverría, M. P., Cegarra, M., Kay, S. M., Singer, B., Lee, J., 2008. Estadío inicial del arco volcánico neógeno en la Cordillera Principal de Mendoza, Argentina (35° S). Revista de la Asociación Geológica Argentina 63(3), 454-469.

Sruoga P., Etcheverría M., Cegarra, M., Mescua, J., Crosta, S., 2016. Hoja Geológica 3569-13 Cerro Risco Plateado, provincia de Mendoza. Servicio Geológico Minero Argentino. Boletín 420, 107.

HYDROTHERMAL ALTERATION AND MINERALIZATION IN SANTA CLARA PORPHYRY Cu-Mo DEPOSIT, ARGENTINA

Feliciano Pagnanini[1], Nora Rubinstein, Eduardo Zappettini, Susana Segal

[1]*Servicio Geológico Minero Argentino - feliciano.pagnanini@segemar.gov.ar*

BACKGROUND

The Santa Clara Cu–Mo porphyry deposit is located in the Frontal Cordillera geological province, in north-western Mendoza Province, Argentina. It is hosted by Lower Carboniferous sedimentary rocks (El Plata Formation), and Gondwanan granitic rocks. Also a premineral granodioritic stock crops out in the north-western margin of the prospect area. Two suites of dikes up to 5 meters in thickness are linked to the mineralization. One of them with NNW strike is composed by andesitic and dacitic rocks, the other consists in one andesitic dike with NNE strike. Between them intruded an intermineral dacitic stock. Postmineral volcaniclastic rocks and a dacitic neck which intrudes the granodioritic stock crop out in the project area (fig. 1a).

Exploration of the Santa Clara ore deposit began in the early 1964´s and included regional geological mapping, surface geochemical sampling (analyzing Cu, Mo, Pb and Zn), inductive polarization profiles and a preliminary drilling program which drilled a total of 2,531 m.

METHODS

A cloud-free ASTER image that includes the Santa Clara deposit was analyzed in the Level 3A version. VNIR and SWIR radiance at the sensor data were normalized and converted to relative reflectance using the Flat Field method. The ASTER orthorectified relative reflectance VNIR and SWIR subsystems were processed and analyzed using the VNIR 15 m resolution spatially registered to 30 m of SWIR spatial resolution, thus forming a nine-band image data set VNIR + SWIR in 30 m spatial resolution that can be easily integrated to a geographical information system (GIS). The SWIR spectral range presented by the bands, covers the characteristic absorption zone of phyllosilicates, carbonates and other alteration minerals, which allows its detailed discrimination (fig. 1 b&c).

Petrographic and ore mineralogy studies carried out in surface and drill-hole samples allowed defining the lithologic units (fig. 1a), alteration assemblages and ore parageneses.

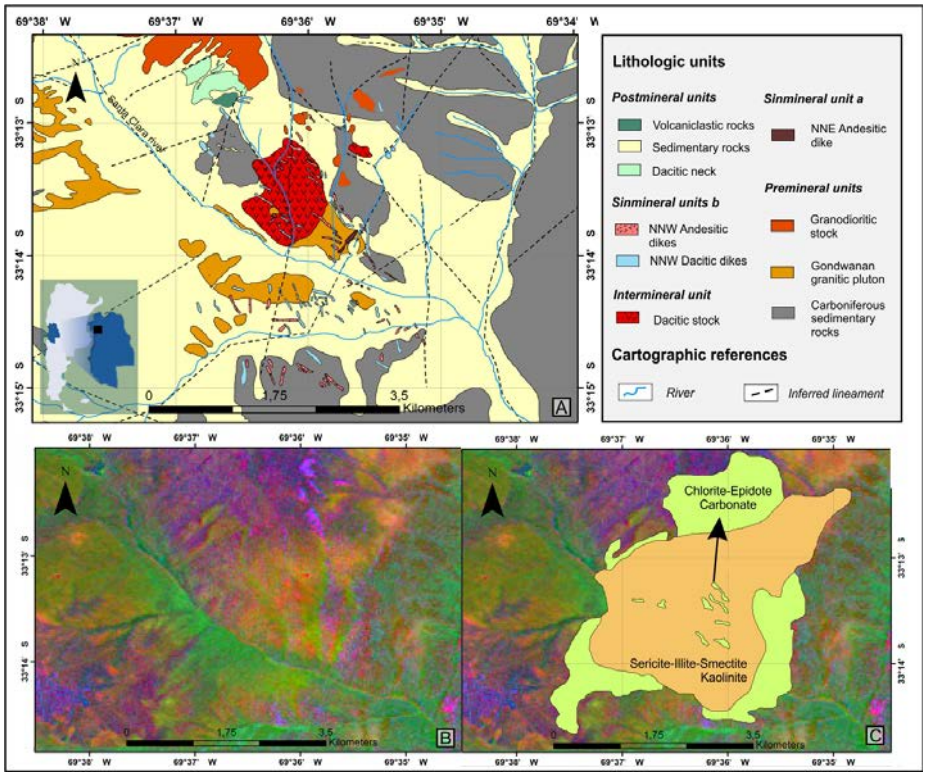

Figure 1. A. Geology of the study area. B. RGB [(5+7)/6; (4+6)/5; (7+9)/8] false color ASTER image. Granitic rocks in green (to west); granodioritic rocks in blue (to north) and Carboniferous sedimentary rocks in brownish green (to east). C. Alteration

RESULTS

On the surface, the alteration halo has an oval shape following a NNE-SSW direction (fig. 1 b). In the Aster image (fig. 1 b&c) it is possible to distinguish an area with high reflectance in band ratios (5+7)/6 and (4+6)/5 (sericite, illite, smectite, kaolinite) surrounded by an area with high reflectance in band ratio (7+9)/8 (calcite, chlorite, epidote). Within the first area, it is possible to distinguish elongated zones 30 m thick with high reflectance in bands (7+9)/8 that are spatially related to andesitic and dacitic dikes (fig. 1a). Affecting these, an assemblage of epidote and fibrous actinolite has been petrographically identified.

Two assemblages of potassic alteration were recognized in the area. The first one consists of pervasive biotite, potassic feldspar, quartz and magnetite, affecting the NNE andesitic dike and the hosting granite. Irregular veinlets up to 7 mm in thickness composed of magnetite- quartz with K-feldspar halos are abundant.

The second assemblage consists of pervasive biotite and potassic feldspar affecting the NNO andesitic and dacitic dikes, with the biotitization less intense than in the NNE andesitic dike. The following veinlet sequence has been observed: a) irregular veins with magnetite-chalcopyrite (A-type), b) regular sutured veins with molybdenite-chalcopyrite (B- type), and c) regular veins with pyrite (D-type).

The ore paragenesis of Santa Clara porphyry consists of chalcopyrite, pyrite, molybdenite, magnetite, digenite and covellite. Pyrite (disseminated and in veins) occurs as anhedral and subhedral grains of variable size (50-400 microns), in aggregates, intergrown with molybdenite and/or intimately associated with chalcopyrite (replacing or being replaced by this). Chalcopyrite (from 220 to 300 microns width) occurs as fissure disseminated aggregates or filling veins. Locally it is replaced by secondary digenite and covellite as rims and/or veinlets. Magnetite (30 to 140 microns) occurs disseminated and in veins occasionally replaced by chalcopyrite. Molybdenite occurs as needles or sheets, both disseminated or in sutured veins. Small inclusions of sphalerite (30 to 45 microns) were identified within some pyrite grains.

CONCLUSIONS

The alteration pattern occurring in Santa Clara deposit is typical of porphyry-type deposits. Moreover the presence of two potassic alteration assemblages spatially associated to different dike suites allow suggesting two stages of porphyry type alteration/mineralization in the genesis of the deposit.

A MIO-PLIOCENE Li-BEARING IGNIMBRITE IN THE RATONES ENDORHEIC BASIN, PUNA PLATEAU, SALTA, ARGENTINA

Walter Rojas[1], Manfred Strecker, Heiko Pingel, Ricardo Alonso

[1]Eramine Sudamerica SA - walrojas40@gmail.com

Lithium (Li)-rich brines in the internally drained sedimentary basins of the Altiplano-Puna Plateau of the Central Andes have increasingly moved into the focus of exploration efforts and economic exploitation. Here we report on a Li-reach volcanic deposit in the Ratones Basin of the Argentine Puna. As most other basins (salars) in this region, the basin is part of a compressional basin-and-range environment, with Cenozoic strata in the basin settings and Paleozoic units in the adjacent ranges. The basement rocks surrounding the Ratones Basin are comprised of crystalline Precambrian rocks and Ordovician flysch units. Neogene rocks, both volcanic and sedimentary units, are widely distributed in the Puna. Paleogene red beds and their fossil content indicate a humid environment (the Eocene Geste Formation) and represent the oldest sedimentary units. In contrast, the Neogene strata comprise thick evaporitic lacustrine sequences (gypsum, borate, and halite-bearing units) interlayered with pyroclastics. Leaching and addition of water by thermal springs are the main mechanisms that feed the salars with alkaline and Earth alkaline elements, such as Li. Li-bearing units, however, are also associated with the volcanic units that outcrop in or in the immediate vicinity of the salars. Ignimbrites, for example, cover about 500.000 km^2 and are thus widely distributed in the Altiplano-Puna region and constitute the largest ignimbrite province in the world. Some of the ignimbrites have clear affinities with giant volcanic calderas, although some ignimbrite bodies are rather isolated, and their origin is still ambiguous. Farallón Catal, an island in the Hombre Muerto salar (13 Ma) host such a deposit. In general, the Puna ignimbrites cover a time interval between Early Miocene and Middle Pleistocene. We analyzed an ignimbrite deposit below the Centenario-Ratones basin that was encountered during exploration drilling at 200 m depth. We determined a preliminary U-Pb zircon age of 5.0 ± 0.2 Ma for this unit. ICP analysis of this deposit detected anomalous Li values with a maximum of 200 ppm. Until now, there is no correlation with other ignimbrite bodies in the region (e.g. Cerro Galan) and the source remains unknown, but the Ratones volcano to the south may have constituted the source. Both, the age and the Li content of the ignimbrite are, however, important, especially in light of the history of mineralized brines in the Ratones Basin and other Puna salars. This is particularly true concerning the presence of Li brines below the ignimbrite in light of further exploration and evaluation of economically viable resources.

A | 49

DISTRIBUTION OF THE HYDROTHERMAL ALTERATION IN THE MORRO DEL COBRE PORPHYRY DEPOSIT, ARGENTINA

María Verónica Bastías Torres[1], Nora A. Rubinstein

[1]Universidad Nacional de San Juan - CONICET (Argentina) - verobastias.geo@gmail.com

INTRODUCTION

The Morro del Cobre deposit is located 45 km southwest from Barreal city (Fig. a) in the Frontal Cordillera of San Juan province. The region includes Miocene porphyry type deposits at advanced exploration stages such as Pachon, Altar and Los Azules (Fig. b). Morro del Cobre was defined in 1960 as a Cu-Mo porphyry deposit and since then to the present it has been explored intermittently.

Field reconnaissance, sampling and relogging of 2,400 drill core meters together with petro- mineralogical studies of 60 thin sections of surface and core samples were performed to assess the lithology and hydrothermal alteration linked to the Morro del Cobre porphyry type mineralization.

RESULTS

The mineralization is linked to a dacitic porphyry composed of plagioclase, quartz, biotite and scarce amphibole phenocrysts in a groundmass consisting of a quartz-feldspar mosaic which intrudes an andesitic porphyry. Both subvolcanic bodies are hosted by dacitic tuffs of Permo - Triassic age (Choyoi Magmatic Cicle). Potassic alteration with an assemblage of K- feldspar + quartz ± biotite ± magnetite was recognized in the deposit area. In the dacitic porphyry the alteration is moderate to strong and has pervasive distribution, in the andesitic porphyry and in the dacitic tuffs it is mild to moderate and localized in veins. In the dacitic porphyry the secondary K-feldspar replaces plagioclase phenocrysts (in the form of patches or rims) and locally invades the groundmass. The secondary biotite occurs in aggregates in the groundmass. There is abundant disseminated magnetite, chalcopyrite and pyrite. Associated to the potassic alteration there are different types of veins in the dacitic tuff and the andesitic porphyry: wavy A-type veins up to 1 cm in thickness composed of quartz+ K- feldspar ± anhydrite ± chalcopyrite + bornite + pyrite with k-feldspar halos (Fig. c); wavy EBT-type veins up to 0.4 cm in thickness composed of quartz + anhydrite ± K-feldspar ± pyrite + chalcopyrite + magnetite with biotite ± K-feldspar halos (Fig d); EB-type veins up to 1.5 cm in thickness composed of biotite ± magnetite ± andalusite ±apatite ± quartz (Fig e) and planar B-type veins up to 0.5 cm in thickness composed of quartz + anhydrite ± molybdenite + chalcopyrite + pyrite. The presence of andalusite in the EB-veins is indicative of high temperature formation (>550°).

The phyllic alteration is moderate and occurs pervasively and in veinlets overprinting the potassic alteration in the andesitic porphyry and the dacitic tuffs with an assemblage of quartz + sericite ± pyrite. Secondary quartz occurs in interstitial patches and filling the vesicles of the tuffs; sericite occurs interstitially, in halos of D-type veins and replacing feldspar and mafic minerals crystalloclasts; pyrite occurs in disseminated form. Associated to the pervasive phyllic alteration there is a set of wavy D-type veins up to 2 cm in thickness (Fig f) composed of quartz + pyrite ± chalcopyrite ± anhydrite with an internal sericite halo and an external calcite halo. A set of late planar veins up to 5 cm in thickness composed of gypsum ± pyrite cut all the aforementioned sets of veins. In the transition between the potassic and phyllic alteration zones there are the highest hypogenic Cu and Mo contents, which reach values of 0.84% and 0.025%, respectively.

CONCLUSION

The Morro del Cobre Cu-Mo porphyry type deposit is linked to a post Gondwanan dacitic porphyry. The mineralizing system started with an early potassic stage that produced pervasive and in veinlets (A, EBT and EB-type) alteration with an ore paragenesis of chalcopyrite - pyrite ± bornite. A late potassic stage resulted in B-type veins with an ore paragenesis of molybdenite + chalcopyrite + pyrite. A phyllic stage which overprints the potassic one led to pervasive and in veinlets (D-type and gypsum ± pyrite veins) alteration.

Due to the characteristics of magmatism and the proximity to Miocene intrusives, it could be inferred that El Morro del Cobre would be part of the Mio-Pliocene metallogenic belt located in the Central Andes of Argentina and Chile.

Figure. a) Location of the Morro del Cobre porphyry deposit; b) Google Earth image showing other porphyry deposits in the area; c) A-type vein with a K-feldspar halo in the andesitic porphyry; d) EBT-type vein with a biotite halo in the dacitic tuff; e) EB-type veins in the dacitic tuff; f) D-type veins with a sericite halo in the dacitic tuff.

A | 50

CHARACTERIZATION OF THE MINERALIZING FLUIDS OF THE QUEBRADA DEL DIABLO LOWER WEST EPITHERMAL GOLD DEPOSIT, ARGENTINA

María Celeste D'Annunzio[1], Nora A. Rubinstein

[1]Universidad Nacional del Sur – CONICET (Argentina) - celeste.dannunzio@gmail.com

BACKGROUND

The Gualcamayo Mining District (GMD) is located in the eastern Precordillera of Argentina. Gold mineralization in the district is hosted by three deposits (Fig. a): Amelia Inés- Magdalena (AIM), Quebrada del Diablo (QDD) Main, and Quebrada del Diablo (QDD) Lower West.

The oldest rocks of the GMD area are Late Cambrian to Early Ordovician marine platform limestones. These rocks are overlain by Middle Ordovician shales and Upper Ordovician siliciclastic conglomerates and sandstones deltaic deposits. These deposits are discordantly overlain by post-glacial transgressive facies and a long-lived sequence of paralic sedimentary facies of Carboniferous to Permian age. The Paleozoic sequence is intruded by the Gualcamayo Igneous Complex, which consists of subvolcanic dacitic intrusives of Late Miocene age (~9 Ma) (Fig. a).

AIM consists of veinlets and breccias with a paragenesis of pyrite, chalcopyrite, sphalerite, arsenopyrite, gold, calcite, and quartz which overprints a skarn mineralization.

QDD Main is a gold deposit hosted in dissolution and collapse carbonatic breccias affected by dolomitization, silicification, and decarbonatization. The gold mineralization consists of free gold in microscopic grains spatially associated to oxidized sulfides (pyrite, marcasite, As-pyrite, chalcopyrite, sphalerite, and pyrrhotite), galena, orpiment, realgar, cinnabar, calcite, quartz, gypsum, and barite.

QDD Lower West is a gold deposit with an ore grade of 2.85 g/t located at ~ 600 m depth and to the west of QDD Main. The mineralization of QDD Lower West is hosted by the cement of tectonic breccias conforming an irregular body elongated in West-East direction of 500 m long, 100 to 150 m wide and ~150 m thick. Three alteration-mineralization stages were recognized in this deposit. The first stage consists of a fine-grained intergrowth of pyrite, arsenopyrite, chalcopyrite, and sphalerite forming the cement of tectonic breccias. This ore paragenesis is spatially associated with sparitic calcite (I) and microcrystalline aggregates of quartz (I). Pyrite and chalcopyrite of the first stage are replaced by hypogene marcasite and covellite, respectively, suggesting an increase in ϕS during this mineralization stage. The second stage is formed by barren calcite veinlets (calcite II). The third stage consists of fine-grained intergrowths of calcite (III), adularia and quartz (II) in veinlets and minor hydrothermal breccias. Spatially associated with these minerals there are realgar, orpiment, calaverite, and coloradoite.

The aim of our research is to establish the physicochemical conditions and the origin of the mineralizing fluids of the QDD Lower West gold deposit based on ore paragenesis, isotopic, LA-ICP-MS and fluid inclusion studies in order to build a genetic model for this deposit.

METHODS

The LA-ICP-MS mapping was performed in one sample at the Chemical Fingerprinting Laboratory of Laurentian University with a Resonetics Resolution M-50 excimer Ar–F laser system with He–Ar carrier gas.

Fluid Inclusion studies included petrographic and micro-thermometric analysis and were performed in calcite II of seven samples. The micro-thermometric analysis were conducted using a Linkam stage calibrated at -56.6 °C, +0.0 °C, and 25 °C. A heating rate of 5 °C/s was used for ice-melting temperatures and 10 °C/s for homogenization temperature measurements. Salinity and density were calculated using the Microsoft Excel spreadsheet for interpreting micro-thermometric data from fluid inclusions HOKIEFLINCS_H_2O-NaCl.

One sample of limestone host-rock and one sample of hydrothermal calcite were analyzed for C and O isotopes and two samples of sulfides were analyzed for S isotopes at Activation Laboratories (Actlabs, Canada).

RESULTS

LA-ICP-MS mapping shows that gold is hosted in pyrite and as submicroscopic inclusions in sphalerite and calcite (Fig. b). Our fluid inclusions results indicate that the barren fluids of the second stage had temperatures between 306.5 and 248.5 °C and low salinity (~1.5 wt.% NaCl eq.). The $\delta^{18}O$ value of the hydrothermal calcite (17.3‰ $\delta^{18}O$ SMOW) is lighter than 2 fluid that obtained for the limestone (20.2‰ $\delta^{18}O$ SMOW), while the $\delta^{13}C$ value of hydrothermal calcite is slightly heavier than that obtained for the limestone (-1.54 ‰ $\delta^{13}C$ VPDB). This could indicate that C and O in hydrothermal calcites come from the limestones by carbonate dissolution process. The $\delta^{34}S$

H S values calculated from the isotopic composition of the first stage pyrite are ~2 ‰ (At 305.5 to 294.8 °C: -1.79 and -1.65 ‰ $\delta^{34}S$. At 248.5 °C -2.09 and -1.95 ‰ $\delta^{34}S$), which is within the magmatic field (generally between -5 and 7‰).

CONCLUSIONS

The ore paragenesis studies performed in QDD Lower West deposit reveals that early mineralizing fluids (that led to gold mineralization hosted in pyrite and as submicroscopic inclusions in sphalerite and in calcite), had intermediate sulfidation conditions with the fS increasing towards the end of the stage. According to fluid inclusion results, the barren fluids of the second stage had low temperature and salinity. The late mineralizing fluids were neutral and had intermediate to high sulfidation conditions. The isotopic results reveal that the limestone host rock was the source of the C and O and that sulfur was of magmatic origin.

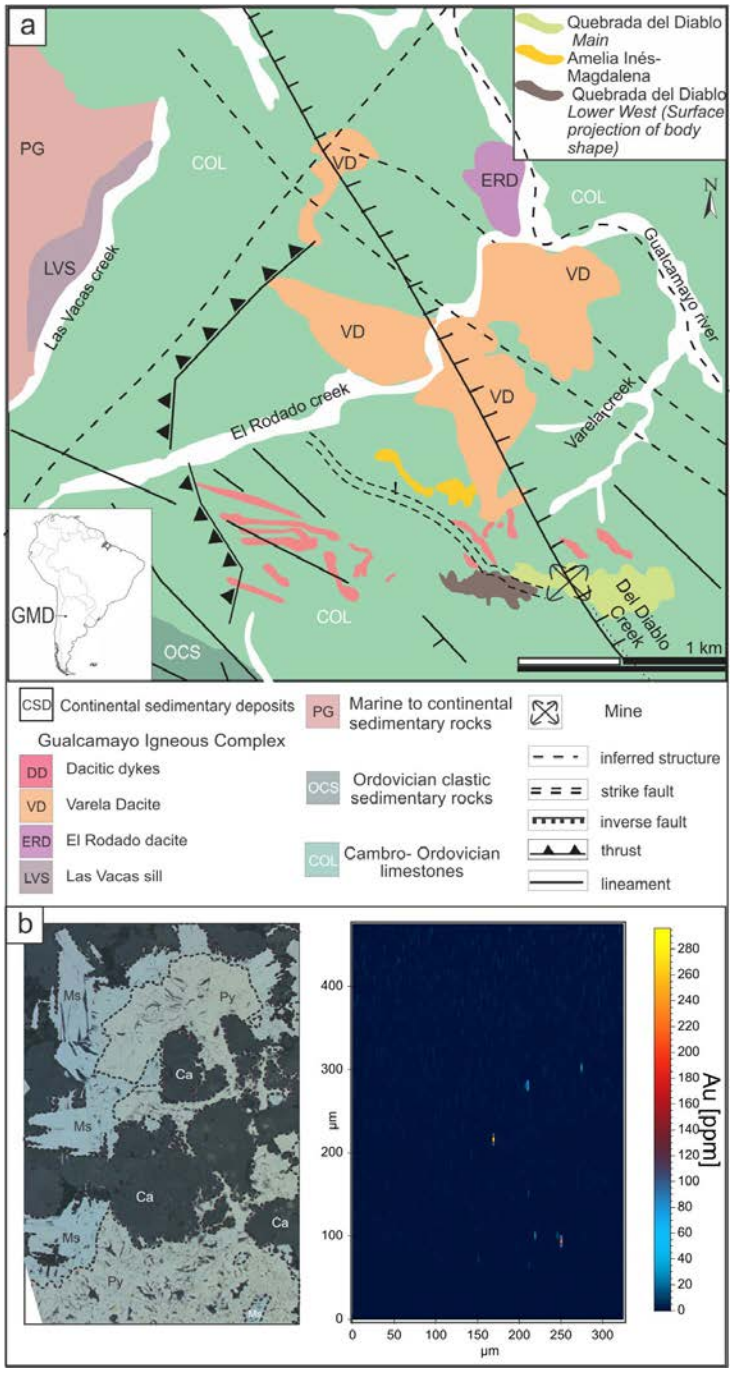

Figure. a) Geology of the GMD showing the location of the mineralized bodies. b) LA-ICP mapping. Left: Mapped sample

A | 51

PERMIAN MAGMATISM RELATED TO PALAEOZOIC PORPHYRY AND EPITHERMAL MINERALIZATION IN AN EARLY ANDEAN METALLOGENIC BELT, CORDILLERA FRONTAL, ARGENTINA

Gregory Poole[1], Steffen Hagemann, Anthony Kemp, Marco Fiorentini, Eduardo Zappettini, Heejin Jeon, Ian Williams, Nora Rubinstein

[1]*Centre for Exploration Targeting, School of Earth Sciences, Australian Research Council Centre of Excellence for Core to Crust Fluid Systems, The University of Western Australia, Perth, Australia - gregory.poole@research.uwa.edu.au*

The South American Andean margin has experienced continuous subduction related processes for over 320 million years and, therefore is the type location for modern "Cordillera-type" arc subduction systems. Across this protracted period of evolution, epochs of porphyry Cu-Au-Mo and epithermal Au-Ag mineral systems have been emplaced in well constrained metallogenic belts. Certain epochs, such as the Miocene-early Pliocene and middle Eocene-early Oligocene, are well endowed with base and precious metals, and form late in the margin's evolution. In contrast, Palaeozoic arc-related magmatic belts formed early in the margins history, are lesser known for mineralization and consequently underexplored. This study aims to understand the factors controlling the formation of Paleozoic mineralization by constraining the temporal evolution of magmatism in an early Andean magmatic belt and investigate the source and composition of magmas related to Paleozoic porphyry and epithermal systems.

The Permian Carrizal (30°S) – Infiernillo (34°S) magmatic belt in the Cordillera Frontal, Argentina, contains several porphyry (e.g., San Jorge) and epithermal (e.g., Casposo) mineral systems. This metallogenic belt developed after a period of subduction on the southwestern margin of Gondwana during the late Carboniferous to early-Permian. In the early Permian a shift in compressional forces saw arc relaxation and has been correlated with the spatially extensive volcanic Choiyoi Group that produced copious felsic volcanism covering most of the Argentinian/ Chilean Andes between 26° and 42°S.

This study analysed the isotopic systems in zircon from intrusions spatially related to 10 mineral occurrences (largely Cu and Au) located within the Permian magmatic belt

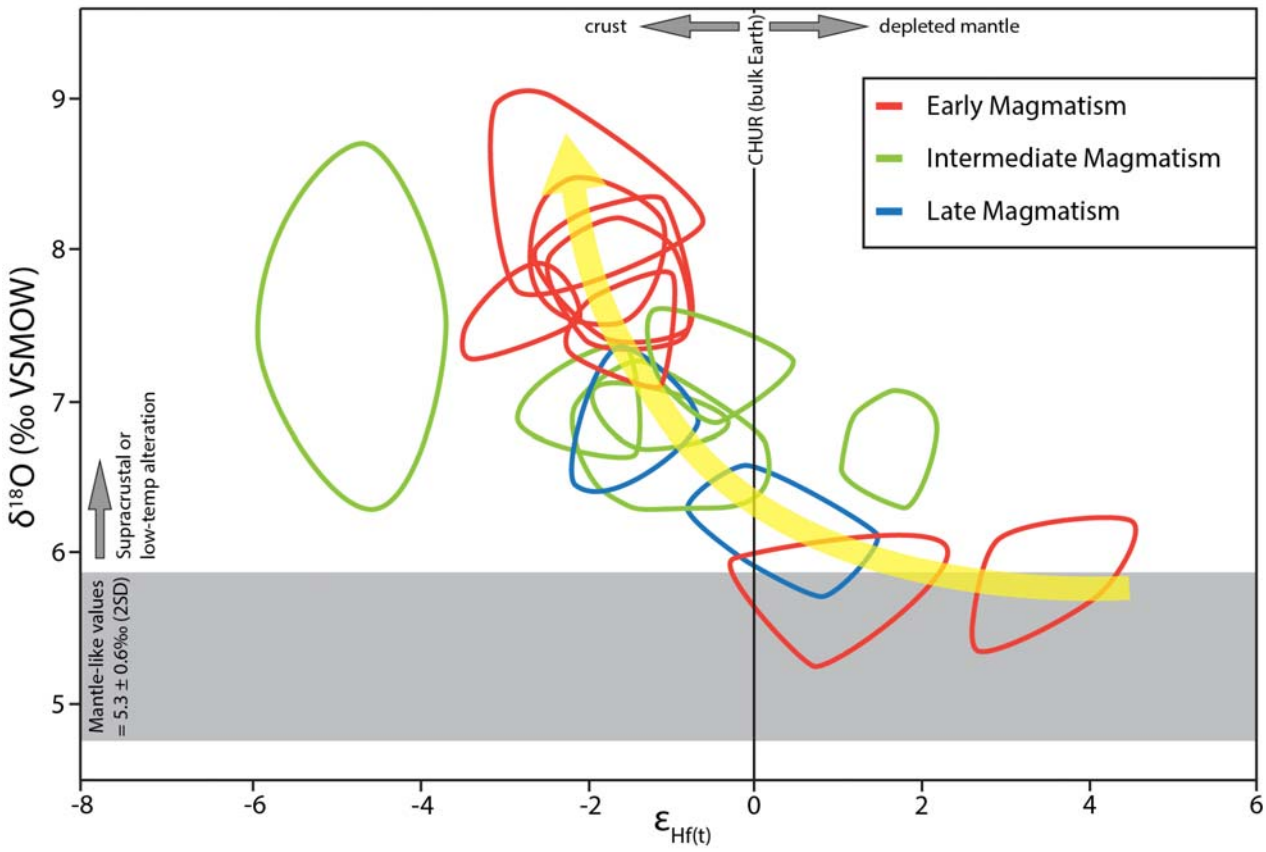

THE CASPOSO GOLD-SILVER DEPOSIT: EVIDENCE FOR PERMIAN, LOW SULFIDATION EPITHERMAL MINERALIZATION IN THE CORDILLERA FRONTAL, SAN JUAN PROVINCE, ARGENTINA

Grignola Sebastian[1], Hagemann Steffen, Fogliata Ana, Miller John, Jourdan Fred, Ford Arianne, Santos Joao. O, Sotarello Gustavo, Belvideri Irma

[1]*The University of Western Australia - sebastiangrignola@hotmail.com*

BACKGROUND AND METHODS

Epithermal gold-silver mineralization in Argentina is well documented in the Miocene and Jurassic. In this study we are presenting new geochronology data, which provides evidence for Permo - Triassic low sulfidation epithermal style mineralization in the Choiyoi Group rocks at the eastern side of the Cordillera Frontal. Careful mapping of the deposit area revealed significant cross cutting relationships between pre-, syn- and post-mineralization dikes and stock and the gold bearing vein system. In addition, adularia in gold-bearing quartz-carbonate and sulfides veins were analysed using 30Ar/39Ar geochronology. Intrusive rocks such granitoids, rhyolites; basalts were analyzed using U-Pb SHRIMP on zircons.

The Casposo gold-silver deposit is located Calingasta Department in San Juan Province, Argentina in the eastern margin of the Cordillera Frontal. The Cordillera Frontal is characterized by polycyclic structures with N-S orientation and structural vengeance to the west (Heredia *et al.*, 2002).

THE CASPOSO GOLD-SILVER DEPOSIT

The Casposo deposit is hosted within the andesitic and rhyolitic volcanic flows and breccias of the Choiyoi Group (Stipanicic *et al.*, 1968). The rhyolitic sequence is stratigraphically overlain by a porphyritic andesitic. The volcanic rocks are intruded by dikes of rhyolitic and andesitic compositions. Two significant plutons are exposed at the eastern side of the Casposo deposit: the Casposo (mainly granodiorites and tonalities) and Colorado plutons (syenogranites).

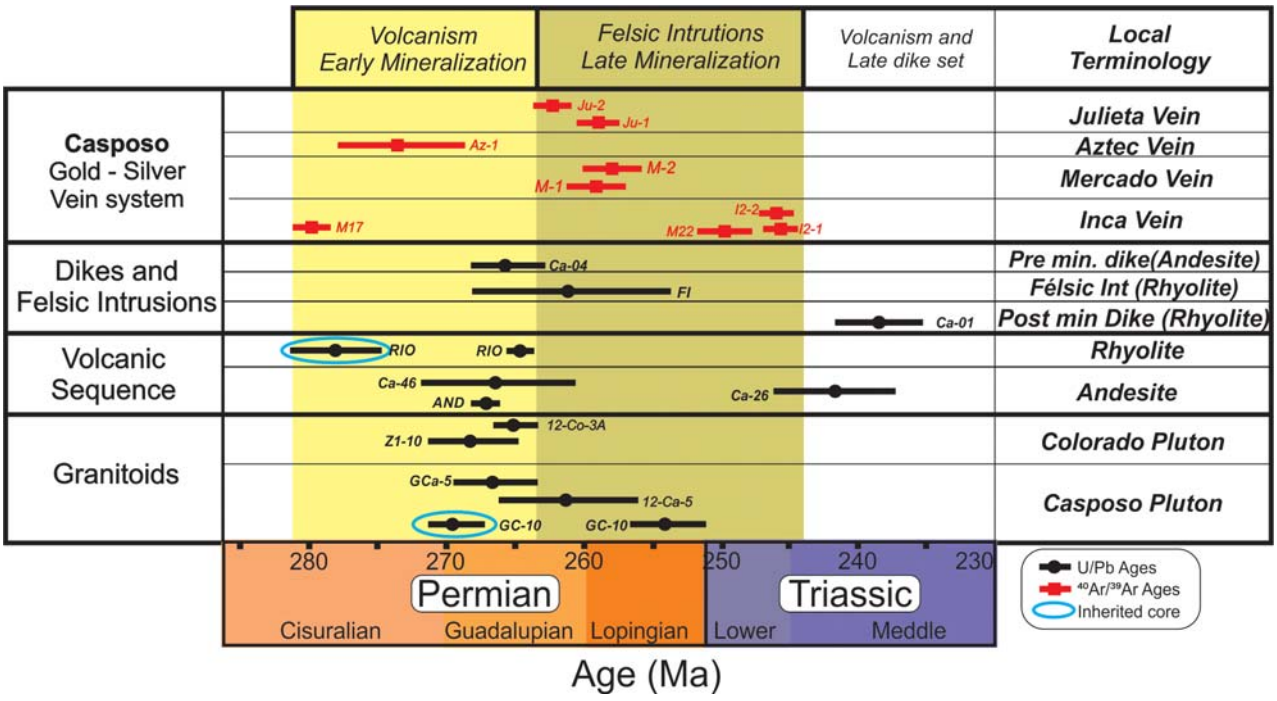

Figure 1: Schematic diagram showing the age ranges (SHRIMP U/Pb on zircons and titanites and 40Ar/39Ar on adularias) for the gold-silver vein system, dikes and felsic intrusions, volcanic sequence and granitoids in the Casposo deposit and surrounding area.

Gold-silver mineralization at Casposo is controlled by NW trending, SW dipping fault zones that are locally filled by massive quartz-carbonate veins and breccias. The NW-trending faults were subsequently reactivated as dextral fault zones that control the geometry of the major gold-silver veins. Later during the Andean orogeny, the NW-trending faults were reactivated as late sinistral faults. A second fault type comprises N-trending thrust faults with dextral reverse kinematics which have segmented north trending veins within the Kamila deposit (Nelson, 2008).

Gold-silver mineralization in the Casposo area is represented by a series of 10 km long N to NW and E-W trending quartz-carbonate veins, including the Kamila area (Inca, Aztec and B- vein veins), Mercado and Julieta veins. The quartz-adularia-calcite veins occur as massive, banded, colloform, lattice-blade or brecciated veins with classic ginguro textures and fine grained black sulfides as well as minor amounts of pyrite-chalcopyrite, and native silver. Local minor quartz stockworks are common.

RELATIVE TIMING OF DIKES AND GOLD-SILVER VEINS

The Kamilla-Mercado area is characterized by several dikes that provide relative timing constraints with respect to dike and vein emplacements. Andesitic porphyritic, tuff and breccia are crosscut by a trachyandesite dike. This pre-mineralization dike is cut by the veins from the Kamila area. The timing relationship between the veins and felsic intrusions is presently unclear but interpreted as broadly synchronous. A post-mineralization rhyolitic dike crosscuts the trachyandesite, the Au-Ag veins and the felsic intrusion.

GEOCHRONOLOGY AND GEOLOGICAL EVOLUTION OF THE CASPOSO DEPOSIT

The combined geochronology and field mapping data suggests that gold-silver mineralization at Casposo can be grouped in two age ranges related to two main pulses of hydrothermal fluid flow within fault zones in the andesite-ryholite host rocks. The first pulse of hydrothermal fluid is related to the period of time between 282 Ma to 263 Ma, rhyolite volcanism, granitoid magmatism at the Casposo Pluton and emplacement of the Aztec (Az-1) and Inca (M17) veins between 284 Ma and 269 Ma. During this event the first set of NW- and N-trending vein systems formed (Inca and Aztec), the E-W trending veins (e.g. Cerro Norte) are part of the later second pulse of hydrothermal fluid. At the end of the first event (<270 Ma to 263 Ma) the rhyolite-andesite, felsic intrusions, andesitic dikes and granitoid magmatism at Colorado and Casposo plutons were emplaced. The second, major pulse of hydrothermal fluid flow is related to the period of time between 263 Ma and 244 Ma, continued rhyolite-andesite volcanism and granitoid magmatism (e.g., the Casposo pluton). The Inca vein crosscuts andesitic dikes (sample Ca-04), whereas both the Kamila- Mercado and the Cerro Norte veins are crosscut by rhyolitic dikes (sample Ca-01). The age dates on these dikes bracket the main mineralization to between 265.7 ± 1.2 and 238.4 ± 1.6 Ma. New NW- and N-trending vein systems formed during this late mineralization event (e.g. at Inca and Aztec), and the E-W trending veins (e.g. Cerro Norte). The 40Ar/39Ar ages on the Julieta and Inca vein systems (see Ju-2 and I2-1) bracket the age of the late mineralization event. The lower age limit of the late mineralization event also corresponds to the age on the pre-mineralization andesitic dike. The period after the second pulse of hydrothermal fluid (<244 Ma to 235 Ma) is characterized by andesite volcanism and emplacement of post-mineralization rhyolite dikes.

The new geochronology data on gold-related adularia provides evidence for Permian gold- silver mineralization at the low-sulfidation epithermal Casposo deposit. These findings potentially 'open the door' for gold exploration in "old" lithotectonic rock units considered, in the past, as less fertile for epithermal style gold-silver mineralization.

REFERENCES

Heredia, N., Rodríguez Fernández, L. R., Gallastegui, G., Busquets P., Colombo F., 2002. Geological setting of the Argentine Frontal Cordillera in the fat-slab segment (30 00'-31 30'S latitude). Journal of South American Earth Sciences, 15, 79–99.

Nelson, E. P., 2008. Structural Geological Analysis of Casposo District, San Juan, Argentina. Report for Intrepid Mines Ltd., Colorado School of Mines.

Stipanicic, P. N., Rodrigo, F., Baulies, O. L., Matinez, C. G., 1968. Las formaciones presenonianas en el denominado Macizo Nordpatagónico y regiones adyacentes. Revista de la Asociación Geológica Argentina, 23, 76-98.

MAGMA OXIDATION CONDITIONS RELATED TO GOLD AND COPPER MINERALIZATION IN THE HUALGAYOC MINING DISTRICT, PERU

Martín Viala[1], Keiko Hattori

[1]*University of Ottawa - mvial044@uottawa.ca*

INTRODUCTION

The Hualgayoc mining district is located in the Andean Cordillera of northern Peru, 30 km north of the Yanacocha high-sulphidation Au deposit. The district hosts many Au ± Cu deposits, including the Cerro Corona Au-Cu porphyry, Tantahuatay high sulfidation Au, and AntaKori Cu skarn/high sulphidation Au-Cu deposits. In addition, the Cerro Jesus and Cerro San Jose intrusions host past-producing mines of Ag-rich intermediate sulfidation veins. The main objective of the study is to evaluate the characteristics of the intrusions associated with various mineralization.

The dominant phase of intrusive rocks in the Hualgayoc mining district is hornblende ± biotite-bearing porphyritic diorite with magnetite micro-phenocrysts. This includes the Cerro Corona complex, the Coymolache sill, the San Miguel diorite, and the San Nicolas, Cerro Quijote, Cerro Jesus, Cerro San Jose, Cerro Caballerisa and Cerro Choro Blanco intrusions. Volcanic rocks include the Hualgayoc rhyodacite north of Cerro Corona, the San Miguel andesite which contains clinopyroxene with rare xenocrysts of blue sapphire, and the andesitic to rhyolitic volcanic rocks of the Calipuy formation, host rocks to some of the AntaKori and Tantahuatay deposits.

All intrusions are hydrothermally altered except for the Coyomolache sill, the San Nicolas intrusion and the Hualgayoc rhyodacite. Variable chlorite ± epidote alteration affects the San Miguel diorite and Cerro Quijote intrusions. Intense alteration of white mica and clay minerals occurs at San Jose, Cerro Jesus, Tantahuatay and AntaKori. Acidic alteration of pyrophyllite ± alunite is present in Cerro Cienaga, Cerro Tantahuatay and AntaKori. Potassic alteration of K-feldspar + biotite + magnetite occurs in the Cerro Corona complex, and locally in the San Jose intrusion.

GEOCHRONOLOGY

We obtained new U-Pb zircon ages of 14 igneous rocks from the district. The data indicate that magmatic activity occurred from 15 to 9 Ma, which is similar to the ages of igneous rocks of the Yanacocha high-sulfidation Au deposit (16-8 Ma; Longo *et al.*, 2010), although most intrusions in the Hualgayoc District were emplaced between 14 and 15 Ma. Some of these intrusions are accompanied by Au-Cu mineralization (i.e., Cerro Corona), whereas

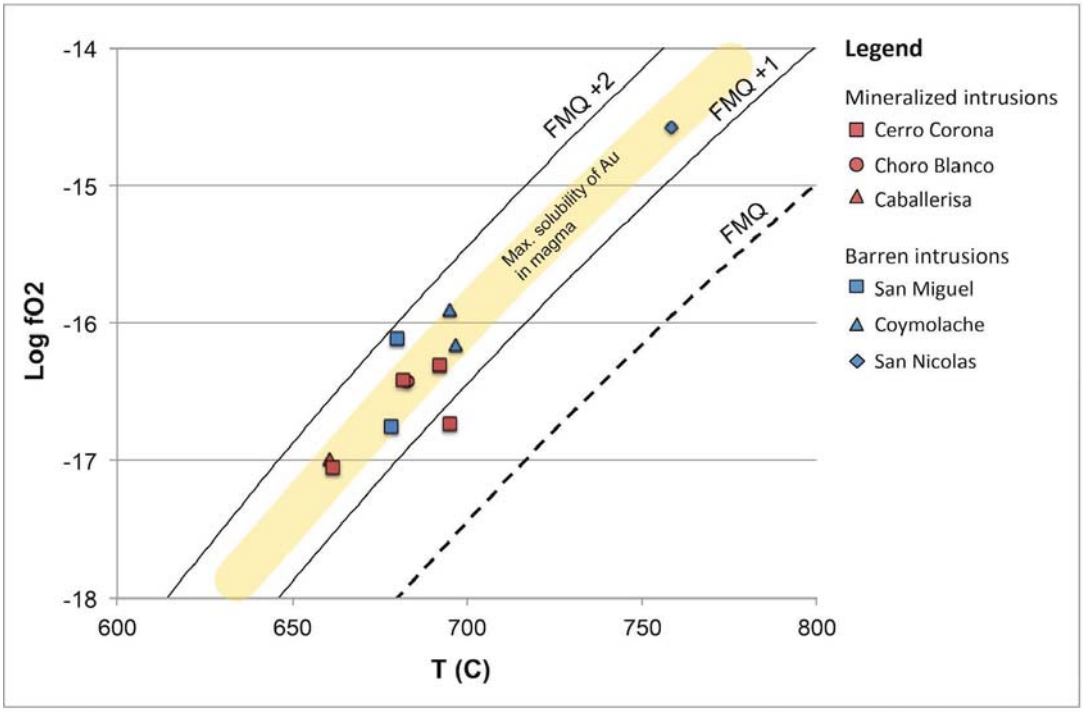

Figure 1. Temperature vs fO_2 relation for several barren and mineralized intrusions in the Hualgayoc District. Temperature was calculated from Ti content in zircon. Band of maximum solubility conditions for Au in hydrous sulfur-rich melt from Botcharnikov *et al.* (2010)

others appear to be barren (Coymolache). The volcanic rocks of the Calipuy formation which host the Tantahuatay high-sulphidation deposit are dated at 13 Ma. Late magmatism consists of barren rhyodacite-rhyolite domes intruded at 9.7 Ma.

BULK ROCK COMPOSITIONS

Igneous rocks in the district show high Sr/Y (40–90), moderately low Y concentration (8-16 ppm) and [La]n/[Yb]n ratio (9–18), and low [Dy] n/[Yb]n ratio (1.4-1.1). The geochemical signature is attributed to water-rich magmas formed by partial melting of an amphibole- bearing source. High water content in the magmas suppressed early crystallization of plagioclase to result in high Sr. Amphibole is responsible for low heavy rare earth elements and Y. All intrusions have relatively low Th content (3-7 ppm), indicating essentially no assimilation of siliciclastic rocks during magma ascent through the thick continental crust.

OXIDATION STATE OF MAGMAS

Using Ce4+/Ce3+ ratios in zircon and bulk rock compositions, fO_2 values of the parental melt for individual intrusions were calculated following the method of Smythe and Brenan (2016). All intrusions are moderately oxidized, FMQ +1 to +2 (logarithmic units above the fayalite-magnetite-quartz buffer) and the values are apparently independent of the association with mineralization (Figure 1). Oxidized melt can dissolve sulphides in the source and transport Au to the upper crust without precipitation of Au- and base metal- bearing sulphide melt (Botcharnikov *et al.* 2010). Au solubility in andesitic melt increases with increasing oxidation conditions and reaches its maximum value at around FMQ +1.5, beyond which the solubility of Au starts decreasing dramatically (Botcharnikov *et al.* 2010). In contrast, the solubility of Cu in andesitic melt increases steadily with increasing oxidation conditions (Zajacz *et al.* 2012). The median fO_2 value of magmas from the Hualgayoc mining district, FMQ +1.48, correspond to high Au solubility and appears to be consistent with the abundant Au mineralization in the district including the high Au/Cu ratio, ~1.7 x10-4, of the Cerro Corona deposit. If the magmas were more oxidized (FMQ e+2) we would expect to observe prevalent Cu mineralizations with minor Au mineralizations

CONCLUSION

Au-(Cu) mineralization in the Hualgayoc mining district is associated with hydrous, moderately oxidized magmas that originate from amphibole-bearing source rocks, with little to no crustal assimilation upon ascent and emplacement. Contemporaneous emplacement of mineralized and barren intrusions in the district suggest that an intrinsically high fO_2 value recorded by magmas does not necessarily imply the presence of Cu and Au mineralization. Other factors include the generation of a significant hydrothermal system upon magma crystallization in order to mobilize metals exsolved from magmas and and concentrate to economic values.

Our results also suggest that although the fO_2 value of magma may be of limited use to differentiate barren from mineralized intrusions across a district, this characteristic may be useful to identify potentially mineralized districts associated with high magmatic oxidation state (FMQ >+1) from barren districts with low magmatic oxidation state (FMQ <+1).

REFERENCES

Botcharnikov, R.E., Linnen, R.L., Wilke, M., Holtz, F., Jugo, P.J., Berndt, J., 2010. High gold concentrations in sulphide-bearing magma under oxidizing conditions. Nature Geoscience 4, 112-115.

Longo, A.A., Dilles, J.H., Grunder, A.L., Duncan R., 2010. Evolution of calc-alkaline volcanism and associated hydrothermal gold deposits at Yanacocha, Peru. Economic Geology 105, 1191-1241.

Smythe, D.J., Brenan, J.M., 2016. Magmatic oxygen fugacity estimated using zircon-melt partitioning of cerium. Earth Planet. Sci. Lett. 453, 260-266.

Zajacz, Z., Candela, P.A., Piccoli, P.M., Walle, M., Sanchz-Valle, C., 2012. Gold and copper in volatile saturated mafic to intermediate magmas: Solubilities, partitioning, and implications for ore deposit formation. Geochim Cosmochim Acta 91, 140-159.

CHAPTER 5
METALLOGENY OF CRATONIC AREAS

Convenor: Martín Gozalvez

ALKALI ELEMENT MOBILITY ASSOCIATED WITH GOLD MINERALIZATION IN THE PILAR DE GOIÁS GREENSTONE BELT, CENTRAL BRAZIL

Rafael Rachid Barbieri Bacha[1], Catarina Labouré Bemfica Toledo, Adalene Moreira Silva

[1]*Universidade de Brasília (UnB), Brazil - bacharachid@gmail.com*

The Archean-Paleoproterozoic Terrane of Goiás is interpreted as an allochthonous exotic fragment of Archean-Paleoproterozoic crust that has been incorporated to the west of the Brasília Belt during the Brazilian Cycle (Jost *et al.*, 2013). It is composed of five gold-bearing greenstone belts surrounded by six TTGs Complexes. The northern area hosts the greenstone belts Pilar de Goiás, Guarinos and Crixás, and the TTG complexes Hidrolina, Moquém, Caiamar and Anta, while the southern area hosts the greenstone belts Faina and Serra de Santa Rita, and the TTG complexes Caiçara and Uvá.

The greenstone belts occur with similar irregular and elongated morphology that range from 40 to 100 km long and approximately 6 km wide. Every greenstone belt has its own geological and metalogenetic evolution, and geochronological data has shown that the evolution of the region is complex with multiple events from Archean to Paleoproterozoic, and Neoproterozoic recycling (Jost *et al.*, 2014).

The Pilar de Goiás greenstone belt is composed of basal metavolcanic rocks with komatiitic and tholeiitic affinity and an upper metavolcanosedimentary sequence with several gold occurrences (Jost *et al.*, 1991). The Pilar mine is placed in the southwestern of Pilar de Goiás greenstone belt and is a mid-tier gold producer with an average of 75,000 ounces per year and 2,300 koz of gold resources. The mineralization of the Pilar mine and other gold occurrences are hosted in quartz veins associated with hydrothermal alteration in a set of intercalated schist of the metavolcanosedimentary sequence (Serra do Moinho Formation). This study experiments the hypothesis proposed by Heath and Campbell (2004) that the fluid flow of gold-bearing hydrothermal systems can be monitored based on alkali element mobility, and therefore provide a geochemical vector to investigate possible new gold prospects.

The hypothesis of this thesis was tested by analyzing 469 samples, adopting ICP-MS method, from two diamond drill holes (JOT_002 and JOT_005) performed in the southern part of the Pilar de Goiás greenstone belt, both located in the metavolcanosedimentary sequence. The drill hole JOT_002 was analyzed from 23.14 to 250.06 m depth and the drill hole JOT_005 from 103.61 to 312.88 m depth, as shown in attachment. The drill holes have intercepted barren and mineralized zones.

In order to quantify the potential mineralized zones based on alkali element mobility, the Upper Continental Crust normalized ratio ((Cs + Rb)/Th)UCC is selected as alteration index. The mobile elements Cs and Rb are efficient indicators in hydrothermal systems due to its tendency of enrichment near mineralized zones and depletion in barren zones. The alkali concentration was divided by the immobile element Th. The reason to divide the index to Th in reverse of using (Cs + Rb) absolute concentration is due to the fact that high incompatible elements such as U, La and Th probably have had similar variations to the alkali elements in unaltered rocks, this Th normalizing compensates the variation (Heath and Campbell, 2004).

The hydrothermal alteration near the mineralized quartz veins is characterized by the presence of sericite, biotite and chlorite, combined with the increase of garnet content. Moreover, the presence of sulphides as pyrite, pyrrhotite and arsenopyrite is noticeable, while visible gold is rarely seen. The alteration index ((Cs + Rb)/Th)UCC has shown great efficiency in discriminating mineralized and barren areas, with ((Cs + Rb)/Th)UCC >3 for potentially mineralized and ((Cs + Rb)/Th)UCC <3 for unmineralized zones. Also, the alteration index increases progressively toward the gold mineralization, providing a geochemical vector to mineralization. The visible alteration halo varies from less than 1 to 5 meters, while the zone of ((Cs + Rb)/Th)UCC >3 may reach up to 80 meters. The mineralized zones in the metavolcanosedimentary rocks of the Pilar de Goiás greenstone belt is surrounded by a zone of ((Cs + Rb)/Th)UCC that is 16 to 100 times larger than visible alteration halo.

The research performed by Heath and Campbell (2004) has shown that the ratio ((Cs + Rb)/Th)N primitive mantle normalized has produced excellent geochemical vectors when applied for the basaltic rocks at Kalgoorlie and Kambalda. The same method adjusted to Upper Continental Crust (Taylor and McLennan, 1995) normalization was applied for the metasedimentary rocks that host the gold mineralization at the Pilar de Goiás greenstone belt, the results are positive and corroborate with the hypothesis proposed by Heath and Campbell (2004).

The hydrothermal fluid penetrated tens of meters into the wall rocks providing an effective vector to mineralization. The alkali enrichment zones are believed to be products of cooling fluid that flowed outward from mineralized quartz veins and the alkali depletion zones are resulted by prograde alteration zones from higher temperature fluid flow (Heath and Campbell, 2004). The ratio has shown great discrepancy between mineralized

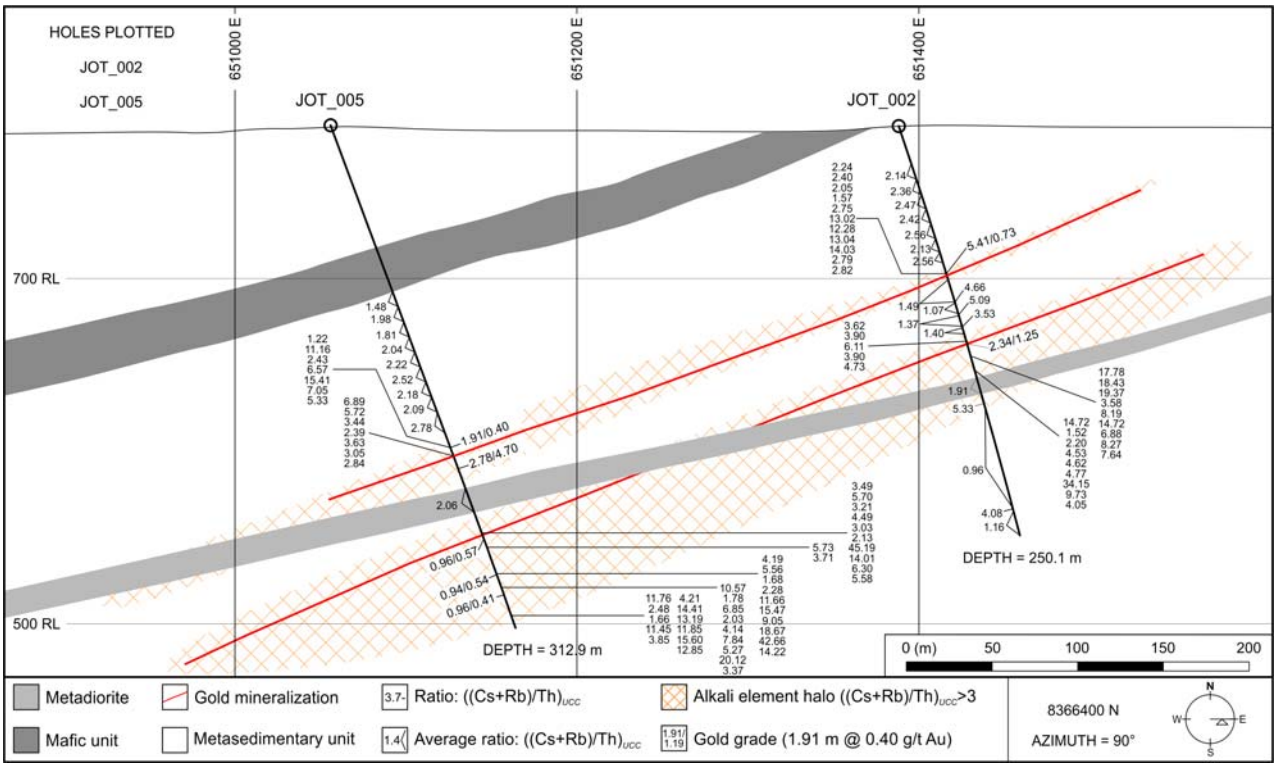

and barren zones: the mineralized are represented by enrichment in alkali elements and non- mineralized zones are depleted. The gold mineralization halo associated with the alkali element enrichment also is extremely larger than the visible alteration, providing a larger geochemical vector when targeting gold exploration. In addition, the alkali concentration of the host rock enriches toward gold mineralization, confirming that the ((Cs + Rb)/Th)UCC is useful when combined with other techniques to explore new gold prospects.

REFERENCES

Heath, C.J., Campbell, I.H., 2004. A New Geochemical Technique for Gold Exploration: Alkali Element Mobility Associated with Gold Mineralization in the West Australian Goldfields. Economic Geology, 99, 313-324.

Jost, H., Carvalho, M.J., Rodrigues, V.G., Martins, R., 2014. Metalogênese dos greenstone belts de Goiás. In: Silva, M.G., Neto, M.B.R., Jost, H., Kuyumjian, R.M. (Orgs.), Metalogênese das províncias tectônicas brasileiras, Belo Horizonte, CPRM, pp. 141-168.

Jost, H., Chemale, J.R.F., Fuck, R.A., Dussin, R.A., 2013. Uvá complex, the oldest orthogneisses of the Archean Paleoproterozoic terrane of central Brazil. Journal of South American Earth Sciences, 47, 201-212.

Jost, H., Oliveira, A.M., 1991. Stratigraphy of the greenstone belts, Crixás region, Goiás, Central Brazil. Journal of South American Earth Sciences, 4, 201-214.

Taylor, S.R., Mclennan, S.M., 1995. The geochemical evolution of the continental crust. Reviews in Geophysics, 33, 241-265.

PRECAMBRIAN CONGLOMERATE-HOSTED GOLD DEPOSITS IN BRAZIL: A REVIEW

Evandro Klein

Geological Survey of Brazil - evandro.klein@cprm.gov.br

Conglomerate-hosted gold mineralization is an important and ubiquitous feature of Precambrian cratons worldwide (e.g., deposits of the Archean Witwatersrand basin, South Africa, and Tarkwa, in the West-African Craton), and respond for about one third of global gold resources/production. In Brazil, conglomerate-hosted gold deposits (Table 1, Fig. 1) are also distributed throughout Precambrian terranes, occurring in cratonic areas and in more or less reworked Archean-Paleoproterozoic basement segments within Neoproterozoic mobile belts. The reported ore resources (plus past production) associated with this deposit class are about 465 t Au (15 Moz), and most of these are contained in deposits of the Jacobina basin/goldfield. As observed elsewhere, the long-standing debate concerning to the age and tectonic setting of sediments and gold deposition, the syngenetic versus epigenetic origin of gold mineralization, the source of gold, and the influence of post-depositional processes on the economic potential of (paleo) placer deposit, also apply to the Brazilian deposits.

The Precambrian auriferous conglomerates in Brazil are mostly part of siliciclastic, quartz- rich basins that were probably deposited in large ancient alluvial plains to sub-aerial braided delta settings and indicate continental erosion and sediment transport in areas lacking vegetation. Greenstone belts, rift and foreland basins are the main settings of depositions, followed by passive margin and cratonic covers. Apparently, there is a difference in the age of the deposits formed in basins from diverse tectonic settings (Table 1, Fig. 1).

The São Francisco Craton hosts the oldest basins/deposits (Siderian to Neoarchean). At Jacobina (rift or foreland), the most significant gold (U, pyrite) mineralization occurs within the matrix of the conglomerates associated with pyrite and fuchsite, and both Witwatersrand-type paleoplacer and extensive fluid flow along a controlling fault system, with subsequent multi-phase hydrothermal alteration, have been invoked to explain the origin of mineralization. Probably, a two-stage, detrital + hydrothermal, model explains better the mineralization. At Moeda (passive margin), the significant correlation of U vs. S is suggestive of a paleoplacer origin for heavy minerals such as

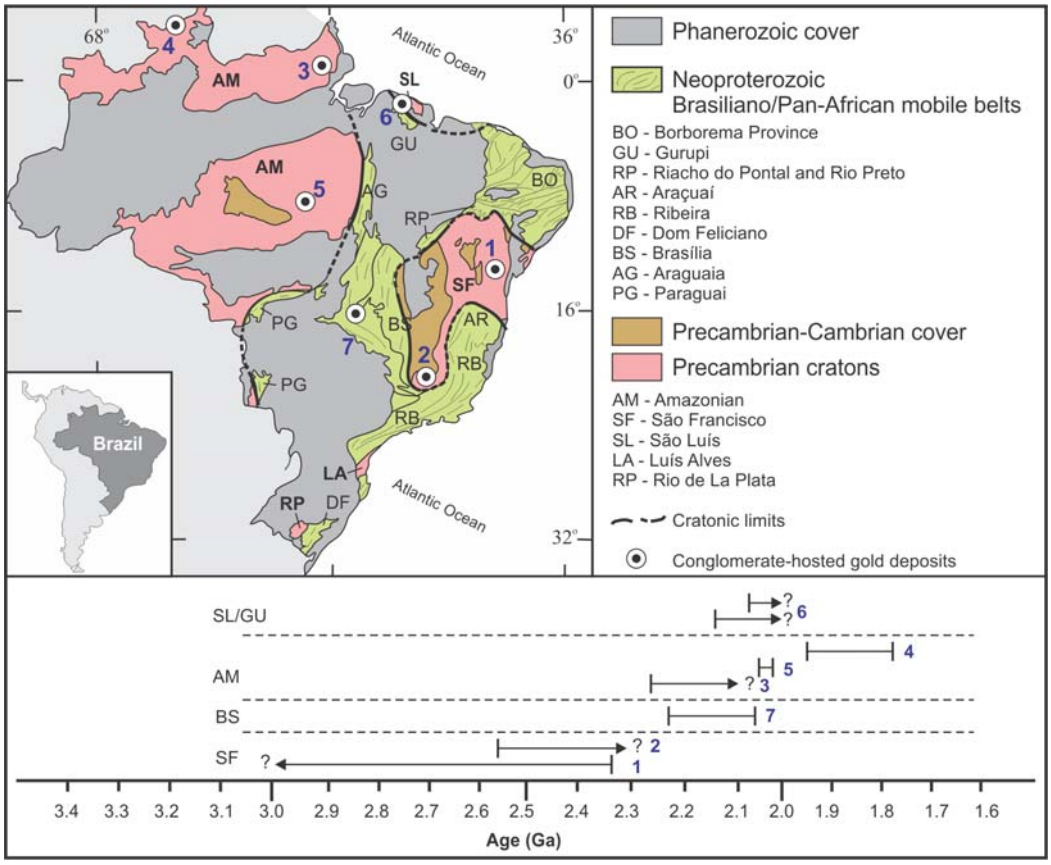

Figure 1 – Major geotectonic framework of Brazil and location of the conglomerate-hosted gold deposits (numbers are those of Table1). The age of sediment deposition is also shown.

pyrite and uraninite, and a paleoplacer origin for gold is the usual interpretation. However, several lines of evidence indicate post-mineralization hydrothermal overprint and/or gold introduction by hydrothermal fluids.

Deposits associated with greenstone belts formed in the Rhyacian. Faina, in the basement of the Neoproterozoic Brasilia Belt, shows gold concentrations in more or less deformed diamictites of the second sedimentary cycle of the hosting greenstone belt, whereas Santa Maria, in the Amazonian Craton, hosts gold in the top sequence of the greenstone belt, which can be either part of its stratigraphic sequence, or a cover sequence of the greenstone.

A modified paleoplacer origin is also suggested for the Orosirian Castelo de Sonhos deposit, which is the most recent discovery in Brazil of this type, and related to a foreland basin. Although lacking detailed studies, this model likely apply to the other two deposits related to foreland basins in the São Luís Craton (Vizeu) and Gurupi Belt (Igarapé de Areia), which also formed at the Rhyacian-Orosirian boundary. The last two deposits correlate in sedimentary, tectonic, and age characteristics with Tarkwa.

The youngest, Orosirian to Statherian, and poorly known in terms of gold mineralization, is the Roraima basin, in northwestern Amazonian Craton, which represents a large cratonic cover, widely known for its uranium potential and the alluvial gold and diamond found in creeks that drain conglomerates.

N°	Tectonic domain/ basin/stratigraphic unit	Tectonic setting	Deposit	Age (Ma)	Au (t): resources + past production (p)
São Francisco Craton					
1	Jacobina/ Serra do Córrego Fm.	Rift or foreland	Jacobina (goldfield)	2320-3200	301 + 70 (p)
2	Gandarela syncline/ Moeda Fm.	Passive margin/rift	Palmital and others	<2563	35
2	Ouro Fino syncline/ Moeda Fm	Passive margin/rift	Ouro Fino	<2563	3
Amazonian Craton					
3	Vila Nova	GB	Santa Maria	<2260	1.1
4	Roraima SG	Cratonic	na	1783-1950	<1
5	Tapajós Province/ Castelo dos Sonhos Fm.		Foreland Castelo de Sonhos	2011-2050	46.5 + 9.3 (p)
São Luís Craton and Gurupi Belt					
6	Igarapé de Areia Fm	Foreland	BoaEsperança and others	<2078	na
6	Vizeu Fm.	Foreland	Vizeu	<2137	na
Brasilia Belt					
7	Faina greenstone belt	GB	Eliseo, Sierra	2060-2220	na

Numbers in the first column refer to those in Figure 1
na: not available, GB: greenstone belt, Fm: Formation, SG: Supergroup

Table 1 – Main characteristics of the conglomerate-hosted gold deposits in Brazil

LITHOLOGICAL AND STRUCTURAL CHARACTERIZATION OF THE ALMAS VOLCANIC SEDIMENTARY SEQUENCE

Caio Bussaglia Ress[1], André Gomes Walczuk, Tiago Angelo Valim, Henrique Araujo Lopes, Felipe Henrique Teles Faria Souza.

[1]*Universidade de Brasilia - caio_ress@hotmail.com*

BACKGROUND

The present study took place in the city of Almas (TO) - Brazil, where important gold occurrences have been explored since the seventeenth century. From the geological aspect, the study area is located within the Almas-Conceição Domain, a Paleoproterozoic terrane inserted in the northern portion of the Brasília Belt (Figure 1 and 2). Companies such as Vale and Rio Novo Mineração estimate the resources for the region in more than 25,000 kg of gold.

The Almas-Conceição Domain is composed of granite-gneisses terrains surrounded by narrow and curvilinear stripes of metavolcano-sedimentary rocks. The archean metavolcano- sedimentary sequence of Almas, named Riachão do Ouro Group, is divided into two units: (I) a basal one, composed of metamorphosed basic and intermediate rocks containing cushioned structure and ultramafic lenses, named Córrego do Paiol Formation; and (II) an upper unit, called Morro do Carneiro Formation, consisting of quartzite, phyllite, metaconglomerate, metachert, tuffs, metavolcanic rocks and banded iron formations (BIF's).

The aim of this study was to do geological and aerogeophysical data association in order to further characterize the Riachão do Ouro Group, using extensive field, petrographic and structural data.

METHODS

This study is a compilation of the data collected for the course completion work (CCW) of the 2016 geology class of University of Brasilia (UnB), entitled «Geology and aerogeophysics of the Almas Greenstone Belt''. The main purpose of the CCW was to present a geological map of an area of 1,600 Km² in a scale of 1:50,000.

This one-year research project was divided into three steps. The first one consisted of a pre-field stage, in which we did bibliography review and processed aerogeophysics data (aeromagnetometric and aerogammaspectrometric data) provided by the Brazilian geological survey (CPRM) and remote sensing images. The second step consisted of the field stage, a 25 straight days campaign. Finally, during the last stage, where 250 thin sections and a series of borehole data to detail the petrographic and stratigraphic characteristics of the Riachão do Ouro Group.

RESULTS

Using the aerogeophysical data, the tonalite-trondhjemite-granodiotite bodies (TTG's) and the volcano-sedimentary sequence were clearly separated in the analytic signal of the magnetic field (Figure 3); also, the TTG subdivision into granodiorite and tonalite, and the volcano sedimentary sequence into volcanic (Córrego do Paiol Formation) and sedimentary members (Morro do Carneiro Formation) were determined using the aerogammaespectometric ternary RGB data.

The Almas-Conceição terrain was deformed by two co-axial deformational events, which yield a general structural trend represented by a N30E foliation. The first event occurred during the Riacian Period and the second one during the Neoproterozoic Era. The Almas- Conceição Domain presents a dome and keels architecture due to these events, with the volcano-sedimentary sequence associated with low topographic areas.

The present work followed the lithological unit division of the Riachão do Ouro Group presented in previous studies. In the study area, the Córrego do Paiol Formation is composed of basalts, granatiferous amphibolites, actinolite-chlorite schists, garnet amphibolites and andesites. In addition, it is observed hydrothermalites associated to the gold mineralization on the basal portion of this formation. The Morro do Carneiro Formation consists of quartizites and pellites with intercalations of conglomerates, BIF's, gondits, cherts, fine amphibolites, and actinolite-chlorite schists. The Riachão do Ouro Group rocks reached facies, represented by iron formations composed by amphibole (cummnigtonite- gunerite) and garnet. However, the majority of rocks were superimposed by low greenschist facies assemblages (Figure 4 and 5).

CONCLUSIONS

From the review of all data gathered in the region of the Almas volcano-sedimentary sequence, we present in this abstract a significant contribution to the geological context of this important segment of the Almas-Conceição domain.

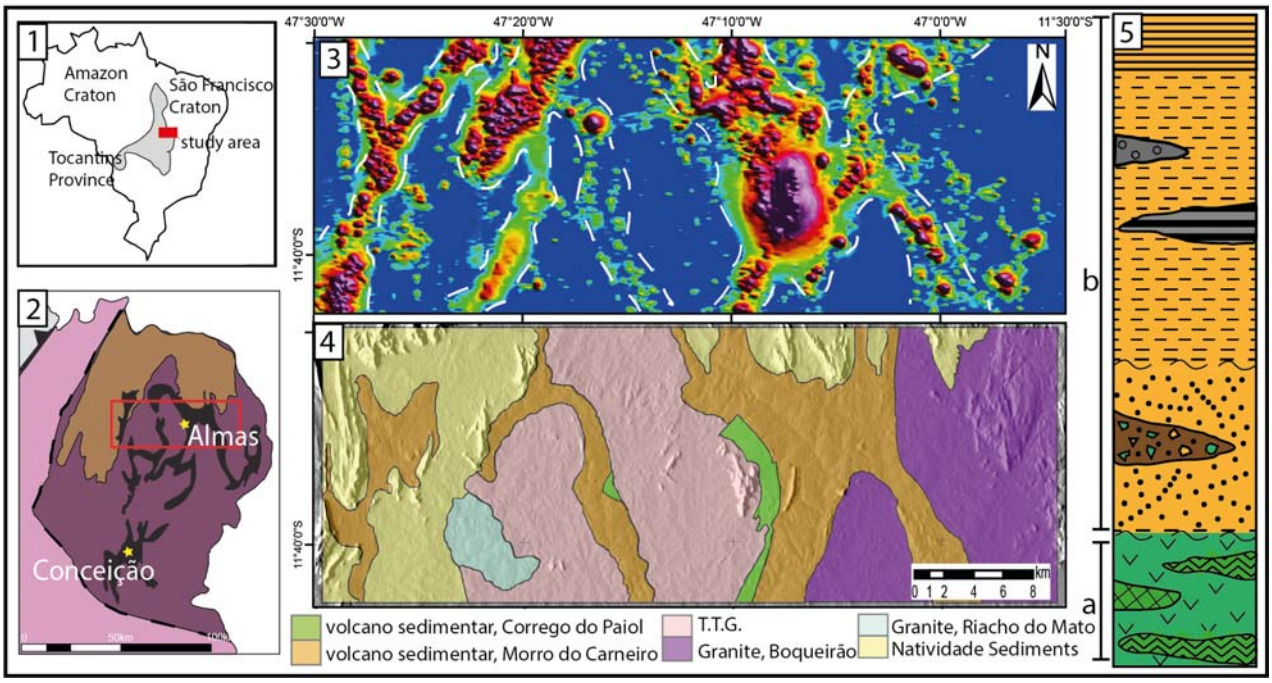

Figure: 1) Tocantins Province and area of study. 2) Almas-Conceição Domain. 3) Analytic signal map; delimitation of volcano sedimentary sequences associated with very strong positive Y-shaped anomalies and TTG domains for magnetic lows anomalies. 4) Simplified lithologic map, showing major lithologies. The volcano sedimentary sequence was divided into Córrego do Paiol and Morro do Carneiro formations for better visualization of this occurrence within the area. 5) Representative stratigraphic column of the Riachão do Ouro Group: a – Córrego do Paiol Formation: basalts and lens of hydrothermalized schists and b – Morro do Carneiro Formation: quartzites and pellites intercalated with conglomerates, BIF's, gondites and schists in amphibolite facies.

The geophysical results were an important tool for delimitation of volcano-sedimentary and TTG's domains, and even for the individualization of these bodies in their internal members, presenting high correspondence with field data, confirming a great reliability of this method.

Previously described as a volcanic sequence formed mostly by volcanic basic rocks intercalated with felsic volcanic lenses and terrigenous and chemical sedimentary materials, we demonstrate that, in fact, in the Almas belt, the sedimentary members are much more expressive, with basic volcanic rocks occurring only at the base, intercalated with schists and volcanic rocks of intermediate and felsic composition.

Concerning the auriferous mineralization, although it might have a strong structural control, its origin is the result of hydrothermalism, which was highly reactive with the basal portions of the Riachão do Ouro sequence, yielding veins of quartz with precipitation of sulfides and gold.

EDIACARAN QUARTZ-GOLD VEIN MINERALIZATION IN THE PALEOPROTEROZOIC BASEMENT, "EL TARUMÁN", PIRARAJÁ, URUGUAY

Felipe Paullier[1], Graciela Sosa, Klaus Wemmer, Alfons van den Kerkhof, Julio Jorge Spoturno, Pedro Oyhantcabal

[1]*Department of Geology, Faculty of Sciences, Universidad de la República. Igua 4225 CP11400, Montevideo, Uruguay*

felipepaullier1709@gmail.com

Gold-bearing quartz veins are a common feature along the western margin of the Neoproterozoic Dom Feliciano Belt, Uruguay. The veins crosscut both upper crustal rocks of the orogenic belt and the basement of the cratonic foreland. Despite the more than 200 km regional extension of the mineralization, the mineralogy, structural controls, PT conditions, age, and character of the of mineralizing fluid have not been studied in detail so far. Our study comprises a gold-bearing area located ca. 8 km west of Pirarajá village. This district with coordinates of ca. 33°45'40"S and 54°50'08"W covers about 9 km^2 and is known as the "El Tarumán gold mineralization".

The quartz veins are hosted in dolomitic marble, which is part of a platform succession composed of meta-conglomerate, quartzite, gneiss, mica-schist and marble, metamorphosed in the amphibolite facies. The deposition age based on detrital zircon data is Paleoproterozoic and is one of the units of the pre-Neoproterozoic foreland basement of the Dom Feliciano Belt. The area shows strong deformation related to at least three main events. The first event (D1) is represented by regional ductile deformation, responsible for the folding and the first foliation. During this stage, an anticlinal fold with an N030° axial plane was generated. The second deformation event (D2) is represented by brittle shearing. D2 is characterized by the generation of conjugate faults and joints striking N110° and N030°, typical of a transpressive environment. The last deformation event (D3) is related to Jura-Cretaceous doleritic dikes.

The gold-bearing quartz veins vary from a few millimeters to metric thickness and have decametric lengths. They include barren quartz as well as quartz veins containing sulfides and oxides (fractures with hematite filling). Gold is commonly associated with the sulfides, but free gold can be observed where the sulfides are oxidized.

The mineralized veins are concentrated in the fold hinges and in the sheared marble bands. The emplacement of the quartz veins postdates the major deformation episode. The veins occur in two predominant strike directions: N030° and N110. The first direction coincides with the main foliation, while the second corresponds to the main faulting in the region.

Alteration processes in the host rock, associated with the mineralization include sericitization, hematitization, carbonation and silicification. The geochemical signature is characterized by the association Au-Ag-Pb-Cu-As-Zn. The most abundant ore mineral is pyrite, with minor galena, chalcopyrite, sphalerite and accessory enargite, chalcocite and tennantite. Weathering and oxidation of sulfides produced free gold besides malachite.

Cathodoluminescence (CL) has been applied in order to better visualize the microfabrics in quartz. The primary quartz shows deep blue CL, whereas secondary textures show shades of brown and orange CL, pointing at lower trace elements and higher OH-related defect centers in the crystal lattice of the secondary quartz. The oldest secondary textures (T1) are represented by a diffusive irregular network linked with subgrain boundaries, optically visible by patchy undulose extinction. T2 is associated with grain boundaries formed during a late stage of the main deformation. The "T1-T2" fluid inclusions principally decorate subgrain and grain boundaries. T3 is characterized by fluid pathways associated with the partial recrystallization or the introduction of external fluids, and T4 by healed microfractures cross cutting all other microtextures. These textures point to deformation in the ductile to brittle transition, assumed in the range of ca. 280-300 °C.

We could establish a clear correlation between the microstructures and the different fluid inclusion assemblages. Primary aqueous-carbonic fluid inclusions were found in relict non- deformed quartz (T0) with blue CL. These early inclusions are relatively rich in CO_2 with only small water volume fractions of ca. 0.3. They have salinities of 11-14 % NaCl and homogenization temperatures (Th) between 330 and 390 °C. The bulk fractions of these fluid inclusions can be estimated as H_2O(.55) CO_2(.40) NaCl(.05) and assumed to correspond with the primary magmatic fluid. Short trails of pseudo-secondary aqueous-carbonic fluid inclusions (water Vol. fracs. 0.75-0.80) are associated with T1 textures. They have salinities of 14-17 wt % NaCl equiv. and Th between 180 and 350 °C. Another set of aqueous-carbonic fluid inclusions is associated with the T2 textures, i.e. essentially decorating grain boundaries. They have water Vol.fracs of ca. 0.90 and salinities of 13-18 wt % NaCl equiv. with Th between 200 and 350 °C. T1 and T2 inclusions are successively enriched in $CaCl_2$ with maximum $CaCl_2$ contents of ca. 5-7 wt%, pointing at changes of the fluid composition during rock alteration. The gas component in all inclusions is pure CO_2 and is successively reduced for inclusions related with T0 to T2. Fluid pathways (T3) do not contain fluid inclusions probably due to the fine grain

size of the recrystallized quartz. Trail-bound aqueous fluid inclusions with lower salinity of 6-7 % NaCl and lower Th (150-220 °C) are associated with late healed microfractures (T4).

Isochore calculations show that the primary CO_2-rich aqueous-carbonic inclusions must have been trapped at ca. 500-550 °C /3 kbar, probably during a thermal event with a temporally higher geothermal gradient during uplift after the peak-metamorphic conditions. This thermal event was followed by a period of about isobaric cooling. During cooling CO_2 may have been lost by carbonation, i.e. the forming of fine-grained secondary carbonate in the vein and the salbands with the host rock. As a result the fluid became water-richer and also became richer in $CaCl_2$, the latter probably as a result of feldspar alteration. These fluids are preserved as fluid inclusions along subgrain and grain boundaries during weak ductile shearing at conditions of ca. 300-350 °C /ca. 2.5-3 kbar (T1) and ca. 260-300 °C /ca. 2-2.5 kbar (T2). Late low-salinity fluids are probably of meteoric origin and were trapped below ca. 280 °C (T4).

Muscovite is associated with the quartz veins and was separated for K/Ar age determination. An age of 592.8 ± 8.7 Ma was obtained and is considered a good estimate of the age of the mineralization taking into account that the temperature obtained from the study of the fluid inclusions is close to the closure temperature of the K-Ar isotopic system (ca. 425 °C).

Despite the Paleoproterozoic age of the host rock, the K-Ar age obtained for the muscovite associated with the quartz veins confirms an Ediacaran age for the vein mineralization. This finding is consistent with the regional framework of a cratonic foreland, which was strongly reworked during the Neoproterozoic Brasiliano Orogeny. The structural data, age dating, fluid compositions and fluid trapping temperature estimates allow us to characterize the "El Tarumán" mineralization as an orogenic gold mineralization related to the Brasiliano orogeny.

PALEOPROTEROZOIC (2.0 TO 1.88 GA) PALEO- MAGMATIC–HYDROTHERMAL SYSTEMS IN THE TAPAJONIC MAGMATIC ARCS AND THE POTENTIAL Cu-Mo-Au PORPHYRY AND AU EPITHERMAL MINERALIZATION IN THE AMAZONIAN CRATON, BRAZIL

Caetano Juliani[1], Carlos Marcello Dias Fernandes, Lena Virgínia Soares Monteiro, Cleyton de Carvalho Carneiro, Carlos Mario Echeverri-Misas, Diego Felipe Gomez-Gutierrez, Lucas Villela Cassini, Geoscience Institute

[1]*University of São Paulo - cjuliani@usp.br*

INTRODUCTION

The Amazon craton is a large (> 4,500,000 km^2) tectonic domain stabilized before the Neoproterozoic. In the southern and western parts, the focus of this study, it is delimited by the N–S trending Neoproterozoic Araguaia belt through thrust shear zones verging to west.

The Amazonian craton was subdivided into six geochronological provinces mainly oriented in NW–SE direction, representing an Archean nuclei with accreted Paleoproterozoic terrains from ca. 2.25 to ca. 0.99 Ga, which are named Central Amazonian (> 2.3 Ga), Maroni–Itacaiúnas (2.2–1.95 Ga), Ventuari–Tapajós (1.95–1.80 Ga), Rio Negro–Juruena (1.8–1.55 Ga), Rondonian–San Ignácio (1.55–1.3 Ga), and Sunsás (1.3–1.0 Ga) by Tassinari and Macambira (1999). New more precise geochronological and geological data (Santos et al, 2000) resulted in the proposition of the following provinces: Carajás (3.0–2.5 Ga), Transamazonas (2.26–2.06 Ga), Tapajós–Parima (2.03–1.86 Ga), Guiana Central (1.95–1.81 Ga), Amazônia Central (1.90–1.86 Ga), Rondônia–Juruena (1.85–1.54 Ga), Rio Negro (1.82–1.52 Ga), and Sunsás (1.45–1.00 Ga). These provinces are considered by all of these authors to result from successive events of B-type subduction, with a collage of magmatic island arcs, developing subsequently into continental magmatic arcs and a huge anorogenic event represented by ca. 1.88 Ga A-type Uatumã volcanic rocks and associated granites. More recently, the integration of these data with new geological, geochronological, geophysical, and metallogenetic data has indicated that the Archean basement continues until at least the Tapajós River, covered by two or three overlapping arcs named the Tapajonic magmatic arcs that are trending approximately W–E, without island arcs. These magmatic arcs are interpreted as the product of a long-lived (ca. 2.2 to 1.88 Ga) subduction of an oceanic crust beneath a mainly Archean continental plate, with variable dip angle and a possible episode of flat-subduction (Bettencourt *et al.*, 2015; Juliani *et al.*, 2016).

THE UATUMÃ MAGMATIC EVENT

The Uatumã unit is recognized in many regions of the Amazonian craton and as defined includes volcanic rocks (predominately rhyolites) and granites that covered more than 2,000,000 km^2. The Uatumã volcanism is considered as being generated in a short intraplate magmatic event with an age close to ca. 1.87 Ga, without potential for Cu–Mo porphyry mineralization. Recent studies, however, have demonstrated that this unit is more complex, constituted by extended calc-alkaline magmatic series (andesites to rhyolites) of different ages (ca. 2.0 Ga, 1.97–1.95 Ga, and 1.89–1.88 Ga), as well ca. 1.88–1.87 Ga A-type rhyolites erupted predominately in several great NE–SW and NW–SE fissures. The calc-alkaline sequences show geochemical characteristics of generation in active continental margins and more frequently are high-K rocks.

The calc-alkaline units are associated with volcanic calderas, stratovolcanoes, post-caldera ring volcanoes and fields of rhyolitic domes. Ignimbrite, fall tuffs, accretionary lapilli tuffs, lahars, volcanic epiclastic and intra-caldera, and inter-volcanic/volcaniclastic lobes lacustrine deposits are common. Remains of Paleoproterozoic (and Mesoproterozoic?) continental sedimentary basins, some of them similar to pull-apart basins are oriented approximately in an E–W direction. Coastal deposits grading upwards to fluvial and desert deposits are present in both the south and northeast part of the studied region.

Calc-alkaline rocks associated with major volcanic structures, such as calderas, appear to be controlled by the continuity of the E–W Archean shear zones extending beneath the volcano- sedimentary cover.

PALEOPROTEROZOIC GOLD MINERALIZATION

Secondary gold mineralization is widespread in the southern part of the Amazonian craton, especially in the Juruena Province (at south of the Cachimbo graben) and in the Tapajós Mineral Province. In the former, it is estimated that more the 850 t. of gold was produced since 70´s years.

Gold mineralization was previously attributed to the orogenic post-Uatumã event, but the hydrothermal alteration and the related structures are not compatible with orogenic gold systems. Instead this hydrothermal alteration is identical to those observed in Mesozoic/Cenozoic high-, intermediate-, and low-sulfidation epithermal

or porphyry systems in intrusive andesitic to rhyolitic porphyries (potassic, propylitic, and sericitic alteration). Primary gold mineralization associated with shallow emplaced magnetite serie-type granitoids and porphyries are associated with many occurrences of chalcopyrite, bornite, covellite, and molybdenite in veins, veinlets, and stockworks, as well sphalerite and galena in some places (Juliani *et al.*, 2016).

HYDROTHERMAL ALTERATION SYSTEMS

In the volcanic rocks, many (some of them large) occurrences of epithermal mineralization have been recognized in the Tapajós, Juruena, Iriri, and Xingu provinces. The better studied of them is the X1 (or V3) high-sulfidation system (Juliani *et al.*, 2005), which represents a very well-preserved system, with a silica cap (formed by vuggy silica) cut by veins of hydrothermal breccia with hematite over an inverted shaped cone of hydrothermal breccia pipe in an older volcanic crater of a ring volcano. The breccia was affected by strongly advanced argillic alteration (with alunite, natroalunite, pyrophyllite, and quartz, and andalusite, corindon, enargite–luzonite, woodhouseite–svanbergite, rutile, hindaslite, topaz, famatinite, tetrahedrite–tennantite, tiemannite, barite, pyrite, chalcopyrite, bornite, covellite, galena, sphalerite, aguilarite, clorargirite, native copper, and silver and gold in small volumes. This zone grades to pyrophyllite-rich advanced argillic alteration in volcanic and volcaniclastic rocks. This one grades to minor zones of intermediated argillic alteration with dickite, an argillic zone, and towards outer typical propylitic alteration. In the deeper part occurs sericitic alteration with pyrite rich zones, suggesting gradation to the porphyry system. Low-sulfidation systems are mainly in faults associated with domes of rhyolites, perhaps with punctual high-grade Ag samples. The Au intermediate-sulfidation mineralization is typically enriched in base-metal sulfides (chalcopyrite, bornite, sphalerite, and galena) and manganiferous carbonates.

The andesitic to rhyolitic intrusive stocks of porphyries are commonly brecciated. They show potassic alteration (secondary K-feldspar and secondary biotite, or predominately biotite in more mafic rocks, locally with sulfides), propylitic alteration in outer parts, zones of sericitic–chloritic that grades to argillic or advanced argillic alteration towards shallower zones, chloritic alteration and sericitic alteration (sericite + quartz + pyrite), as well zones of silicification. Locally sodic alteration (albite and quartz) occurs, especially in more eroded systems. Veins and veinlets similar to A, B, D, and M types are very common. The age of these systems, dated or inferred by geological relationships, indicate three hydrothermal events in ca. 2.0 Ga, ca. 1.97 to 1.95 Ga, and the later one in ca. 1.88 Ga.

CONCLUSIONS

Many occurrences of porphyry-type and epithermal alteration have been identified in recent years in the south Amazonian craton, including some large high- and intermediate- sulfidation systems in the Tapajonic Magmatic arcs. The erosional level preservation of the Paleoproterozoic volcanic/volcanoclastic and subvolcanic units, the calc-alkaline affinity and the oxidation state of the ca. 2.0 to 1.88 Ga magmatic units generated before the ca. 1.88–1.87 Ga A-type magmatism and the new interpreted tectonic setting of these orogenic magmatic events strongly suggest a high potential for the occurrence of calc-alkaline Cu–Mo–(Au) and alkaline Cu–Au porphyry deposits. In fact, a few Au–Cu and Cu–Mo porphyry-type mineralization systems have been characterized in the Tapajós and Juruena mineral provinces. This appears to be an excellent indication, together with the magmatic–hydrothermal systems described here, of notable potential for the existence of economically important copper–molybdenum–gold porphyry deposits in the Amazonian craton. This data suggest a new potential frontier for mineral exploration for large deposits in Brazil.

REFERENCES

Bettencourt, J.S., Juliani, C., Xavier, R.P., Monteiro, L.V.S., Bastos Neto, A.C., Klein, E.L., Assis, R.R., Leite Junior, W.B., Moreto, C.P.N., Fernandes, C.M.D., Pereira, V.P., 2015. Metallogenetic systems associated with granitoid magmatism in the Amazonian craton: an overview of the present level of understanding and exploration significance. Journal of South American Earth Sciences, 68, 22–49.

Juliani C., Rye R.O., Nunes C.M.D., Snee L.W., Correa-Silva, R.H., Monteiro L.V.S., Bettencourt J.S., Neumann R., Neto A.A., 2005. Paleoproterozoic high-sulfidation mineralization in the Tapajós gold province, Amazonian craton, Brazil: geology, mineralogy, alunite argon age, and stable-isotope constraints. Chemical Geology, 215, 95–125.

Juliani, C., Monteiro, L.V.S., Fernandes, C.M.D., 2016. Potencial mineral: Cobre. In: Potencial Mineral do Brasil. Academia Brasileira de Ciências, pp. 134–154.

Santos J.O.S., Hartmann L.A., Gaudette H.E., Groves D.I., Mcnaughton N.J., Fletcher I.R., 2000. A new understanding of the provinces of the Amazon craton based on integration of field mapping and U-Pb and Sm-Nd geochronology. Gondwana Research, 3, 453-488.

Tassinari C.C.G., Macambira M.J.B., 1999. Geochronological provinces of the Amazonian craton. Episodes, 22, 174-182.

CHAPTER 6
GLOBAL TECTONICS AND METALLOGENY: ORE DEPOSIT SETTINGS AND PREDICTIVE MODELLING APPLIED TO MINERAL RESOURCES

Convenor: Martín Gozalvez

NEW PETROGENETIC MODEL FOR MID-MIOCENE ADAKITIC MAGMATISM IN PATAGONIA AND ITS IMPLICATIONS ON PORPHYRY-COPPER DEPOSITS FERTILITY INDICATORS

Gonzalo J. Henriquez[1], Robert R. Loucks, Marco L. Fiorentini

[1]*Centre for Exploration Targeting, School of Earth Sciences, The University of Western Australia, Crawley, WA 6009, Australia*

gonzalo.henriquez@research.uwa.edu.au

The adakites from the Patagonian Cordillera and the Austral Volcanic Zone (AVZ) in the southwest margin of South America have been referred as true slab-melts (Kay *et al.*, 1993; Stern and Kilian, 1996; Ramos *et al.*, 2004). Their steep REE patterns have been interpreted to reflect petrogenesis by partial melting of eclogite in the subducting plate with a substantial role of restite garnet. Their origin has been inferred to be analogous to the compositionally similar "adakites" from Adak Island, in the central Aleutian arc (Kay, 1978). However, further findings at the Aleutians, including: 1) occurrence of xenolith suites reinterpreted as cognate cumulates; 2) presence of a seismically active slab-mantle interface to depths of at least 270 km, which means that slab temperature at this interface is less than 650°C under the volcanic front (Gorbatov and Kostoglodov, 1997); and 3) the occurrence of along-arc variations of tectonic stress, motivates a revision of the slab-melt petrogenesis.

On the other hand, the almost ubiquitous adakitic character of igneous complexes that host major Porphyry Copper Deposits (PCD) has been otherwise associated with high pressure hydrous magmatic differentiation (Loucks, 2014), where the distinguish adakitic features are achieved by amphibole fractionation and plagioclase suppression under tectonic compressive regime (Rohrlach & Loucks, 2005; Loucks, 2014; Chiaradia, 2015). Based on these new concepts, this project aims to explore an alternative non-eclogitic petrogenetic model for the mid-Miocene Patagonian adakites, and additionally, compare these apparently unmineralized suites with igneous complexes that produced giant PCD, in terms of chemical features (i.e. Sr/Y ratios, magmatic hydration and oxidation state) and igneous complex lifespan.

The western margin of Patagonia has experienced the subduction of the Chile Rise since ~22 Ma. As a result, a series of adakitic and non-adakitic igneous complexes in back-arc position are related with the northward-propagating compressive deformation wave, which seems to be associated with the young, warm and buoyant southern part of the subducted Nazca Plate. Zircon U-Pb dating and trace element LA-ICPMS analyses coupled with whole- rock geochemistry and Al-in-hornblende geobarometry (Mutch *et al.*, 2016) and hornblende oxybarometer and hygrometer (Ridolfi *et al.*, 2010) were performed on 4 mid-Miocene Patagonian igneous centres: the adakites from Cerro Pampa, Puesto Nuevo and Chaltén; and a non adakitic andesitic-dacitic centre from Cerro Moyano.

A high-pressure hornblende core was recognised at Puesto Nuevo (7.2 kbar; ~27 km continental depth), whereas the rest of the phenocrysts showed a main magmatic crystallisation stage at 3.4–4 kbar (~13–15 km depth). Slightly higher pressures were obtained from Cerro Pampa hornblende grains, ranging 4–5 kbar (15–18 km depth). Nevertheless, hornblende breakdown textures at Cerro Pampa indicate that final crystallisation stage and magmatic emplacement occurred at shallower crustal levels. Centimetric mafic enclaves were recognised at Cerro Moyano, showing crystallisation pressure of 6.5–7 kbar (~26 km depth). According to petrographic evidence, whole-rock geochemistry and zircon age content, the mafic enclaves are interpreted as cognate cumulates at Cerro Moyano. On the other hand, adakites from Cerro Pampa, Puesto Nuevo and Chaltén yielded fewer autocrystic zircon grains than from Cerro Moyano.

We put forward the hypothesis that Cerro Moyano is an example of a "failed adakite". The existence of mafic cognates cumulates reflects an early stage of high-pressure magmatic differentiation at lower crust to lithospheric mantle levels, however the duration of confining stress was too brief to develop the adakitic signature at this centre. Furthermore, the occurrence of Cerro Moyano matches in space and time with the northward migration of the Chile Rise. This, in addition with the new finding of a second (more mafic) adakitic intrusion at Chaltén (Basaltic andesite, 56.32 wt% SiO_2), are proof that the mid-Miocene Patagonian back-arc igneous centres are the result of magmatic differentiation and not primary slab-melts, due to a fast-compressive tectonic wave produced by the passing southern margin of the Nazca plate.

Empirical evidence suggests that well-endowed igneous complexes in porphyry copper districts are generally associated with adakites with high oxidation state (fO_2 ~ NNO+1 to+2), high magmatic water content (~10 wt%) and emplaced during long lifespans (~7 to 20Myr). Preliminary results indicate that adakitic mid-Miocene magmatism in the study area occurred during a shorter lifespan and was characterized by low-medium dissolved water contents and fO_2 near the FMQ buffer (ie. less oxidized), hence displaying a barren PCD fertility signature.

It is argued that the distinctive chemical features that identify adakitic magmas (e.g. Sr/Y and (Eu/Eu*)/Yb ratios, Figure 1) are not indicative of the fertility of the magmas, but rather simply reflect deep entrapment and

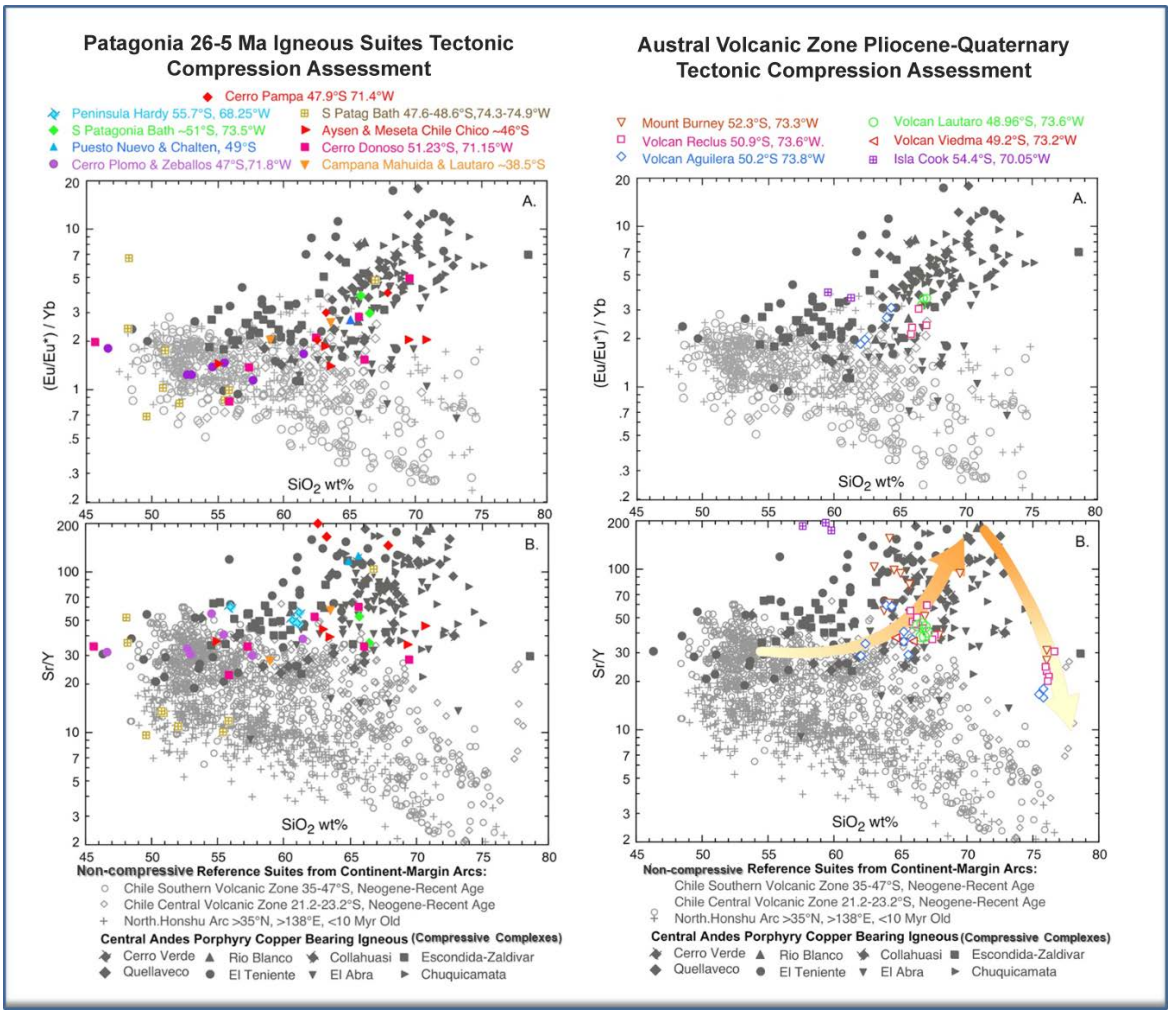

Figure 1. Distinctive Sr/Y and (Eu/Eu*)/Yb ratios developed during high-pressure magmatic differentiation. Compilation of >400 analyses from Patagonia (published literature) compared with world-class PCD and infertile suites.

high-pressure differentiation of arc magmas during tectonic compression. Fractional crystallisation at medium pressure, >3.5 kbar (mid-upper crust level, ~12 km depth), under sub-saturated water conditions (4-6.5 wt% H_2O), are enough requirements to develop the adakitic signature.

REFERENCES

Chiaradia, M., 2015. Crustal thickness control on Sr/Y signatures of recent arc magmas: an Earth scale perspective. Scientific reports. Nature Publishing Group 5.

Gorbatov, A., Kostoglodov, V., 1997. Maximum depth of seismicity and thermal parameter of the subducting slab: general empirical relation and its application. Tectonophysics 277, 165–187.

Kay, R. W., 1978. Aleutian magnesian andesites: melts from subducted Pacific Ocean crust. Journal of volcanology and geothermal research 4: 117-132.

Kay, S. M., Ramos, V.A. y Márquez, M., 1993. Dominant slab-melt component in Cerro Pampa adakitic lavas erupted prior to the collision of the Chile rise in Southern Patagonia. Journal of Geology 101: 703-714.

Loucks, R.R., 2014. Distinctive composition of copper-ore-forming arc magmas: Australian Journal of Earth Sciences, 61: 5-16, doi: 10.1080/08120099.2013.865676.

Mutch, E.J.F., Blundy, J.D., Tattitch, B.C., Cooper, F.J. and Brooker, R.A., 2016, An experimental study of amphibole stability in low-pressure granitic magmas and a revised Al- in-hornblende geobarometer: Contributions to Mineralogy and Petrology, v. 171, p.85.

Ramos, V.; Kay, S.M.; Singer, B.S., 2004. Las adakitas de la cordillera Patagónica: Nuevas evidencias geoquímicas y geocronológicas. Revista de la Asociación Geológica Argentina 59 (4): 693-706.

Ridolfi F, Renzulli A, Puerini M (2010) Stability and chemical equilibrium of amphibole in calc-alkaline magmas: an overview, new thermobarometric formulations and application to subductionrelated volcanoes. Contrib Mineral Petrol 160:45–66.

Rohrlach, B. D. & Loucks, R. R. 2005. Multi-million-year cyclic ramp-up of volatiles in a lower-crustal magma reservoir trapped below the Tampakan copper–gold deposit by Mio–Pliocene crustal compression in the southern Philippines. In: Porter T. M. ed. Super Porphyry Copper & Gold Deposits—A Global Perspective, v.2, pp. 369–407. PCG Publishing, Adelaide.

Stern, C.R., Kilian, R., 1996. Role of the subducted slab, mantle wedge and continental crust in the generation of adakites from

VOLCANOGENIC MASSIVE SULFIDE (VMS) DEPOSITS OF TURKEY

Emin Ciftci[1], Cahit Dönmez, Kurtulus Günay, Nail Yildrim

[1]*Istanbul Technical University - eciftci@itu.edu.tr*

Volcanogenic massive sulfide (VMS) deposits of Turkey occur in three tectonically distinct regions: (I) Kuroko-type deposits in the eastern Pontides Tectonic belt (EPTB); (II) Cyprus- type VMS deposits occur both in Küre area (Kastamonu) and along the Bitlis-Zagros Suture Zone (BZSZ), and (III) Besshi-type VMS deposits in the Hanönü–Tasköprü area (Kastamonu).

The Kuroko type VMS deposits, ranging from a few ten thousand tonnes to a few ten million tonnes in reserve, are all associated with Late Cretaceous felsic volcanics. These consist mainly of dacitic and rhyolitic lavas and pyroclastics that outcrop within a narrow zone running parallel to the Black Sea coast and represent the axial zone of a paleo magmatic arc. Subtypes of the deposits include Cu-, Zn-Cu-, Cu-Zn-, Zn-Pb-Cu metal associations. These deposits are typically mined for Cu, Zn, and Pb. Some of them may also contain significant gold (e.g. Cerattepe deposit) and silver (e.g. Köprübaþý deposit).

The Cyprus type deposits of Turkey occuring along the BZSZ are all allochthonous and associated with mafic volcanics of supra-subduction ophiolites: (I) Middle Eocene Maden Complex – a pile of mafic volcanics, pelagic sediments with limestone blocks and (II) Late Triassic-Late Cretaceous Koçali Complex – a sequence of tectonically imbricated slices of pelagic rock suites, platform carbonates, clastic sediments, serpentinites, and mafic volcanics. Major occurences include Madenköy (Sirvan-Siirt) – currently the largest VMS deposit in Turkey with about 40 Mt reserve and Maden (aka Ergani) (Maden-Elazýð) both hosted by the Maden Complex and Ortaklar (Gaziantep) hosted by the Koçali Complex. The VMS deposits occurring in the Küre area are also allochthonous and are all hosted within mafic volcanics-black shales of Late Triassic Küre Complex, a fairly thick pile of thrust- imbricated deep-sea sediments, intercalated with a dismembered supra-subduction ophiolite. Major past and current producers include Aþýköy, Toykondu, Kýzýlsu, and Bakibaba (Maðaradoruk is a recently discovered ore body in the same area) deposits.

All of these Cyprus-type deposits are mined mainly for Cu, however Zn, Co (e.g. Maðaradoruk) and Au (e.g. Ortaklar) may reach economic grades.

The Besshi-type VMS deposits of Turkey are fairly recent discoveries. They only occur in Hanönü-Tasköprü area (Kastamonu). These are hosted by Akgöl Formation, which consists of low-grade metamorphic siliciclastic sedimentary rocks within the Middle Jurassic Çangaldað Complex comprising ensimatic island arc volcanics and front-arc basin sediments, remnants of oceanic crust, and volcano-clastics, which itself occurs in the Central Pontides. Major examples include Zeybek, Hanönü, Gökýrmak, and past producer Cozoðlu deposits. Deposits of the area are typically low grade but may reach up to 25 Mt (e.g. Gökýrmak deposit).

A | 61

STRUCTURAL EVOLUTION OF THE PATAZ REGION, EASTERN ANDEAN CORDILLERA, NORTHERN PERÚ, AND IMPLICATIONS FOR THE FORMATION OF A CARBONIFEROUS GRANITOID-HOSTED QUARTZ-SULPHIDE-GOLD VEIN-SYSTEM

Daniel Wiemer[1], Steffen G. Hagemann, Nicolas Thébaud, Carlos Villanes

[1]*Centre for Exploration Targeting, School of Earth Sciences, University of Western Australia, 35 Stirling Highway, Crawley, WA 6009, Australia - daniel.wiemer@uwa.edu.au*

Paleogeographic reconstructions of Gondwana display a global distribution of identified Paleozoic gold deposits along the circumferential margin of the supercontinent, indicating a major episode of gold mineralization in the Earth's history. In the Eastern Andean Cordillera of South America, evidence for this global "golden-age" can be found in numerous gold- mining districts that punctuate the NNW-striking remnants of the Gondwana margin. One of these mining districts is the Pataz region, northern Perú, situated immediately east of the prominent NNW-trending Río Marañon Fault that separates the Eastern Andean Cordillera from the younger Western Andean Cordillera. Gold mineralization in Pataz is associated with quartz-sulphide veins hosted by the Carboniferous granitoid Pataz batholith. The batholith intruded strike-parallel to the Río Marañon Fault into deformed greenschist-facies basement rocks, comprising phyllitic schists of the Marañon Complex in the west and metavolcanic and -sedimentary rocks of the Eastern Andean Cordillera Group to the east (Fig. 1a).

Previous studies on the Pataz gold-vein-system led to contrasting formation models, including (i) syn- to post-batholith 'intrusion-related' and (ii) post-batholith 'orogenic-style' end-members. Here, we revisited the Pataz region to shed new light on the formation of the auriferous vein-system. Considering the geological history of the orogenic belt prior to batholith emplacement, we include observations from the basement to investigate the structural framework leading to hydrothermal vein development.

We conducted geological-structural mapping of a N-S-trending corridor of the Pataz district. Structural surface and underground data from regional- to outcrop-/micro-scale observations, including orientations, kinematics and relative timing relationships of structural elements and hydrothermal veins were acquired from: (i) the hydrothermal vein- system and its magmatic host components (Pataz batholith), (ii) volcanic/volcaniclastic rocks forming the volcanic carapace of the batholith, and (iii) semi-pelitic schists of the Marañon Complex and meta-volcanic and -sedimentary rocks of the Eastern Andean Cordillera Group of the basement.

REGIONAL STRUCTURAL GEOLOGY

Three deformation events (D1-D3) can geometrically be correlated between both basement lithotectonic units. Early S1-foliations (D1) developed sub-parallel to bedding planes (S0) and display a dominant NNW-trending strike and medium to steep NE-dip, indicating NE-ward tilt of the basement. In the tectonically lower western unit, S1rotates around the strike- parallel sub-horizontal tilt-axis resulting in both NE- and SW-dips. The tilt-axis correlates with axes of F2folds (D2). The F2folds are mostly observed as decimetre-scale asymmetric S- or Z-type parasitic folds within up- or downward-verging limbs. Locally, close to tight upright transposed first-order F2-rootless fold closures are observed showing local fold axial- planar S2-foliation development. Within more competent metavolcanic rocks of the upper unit, rare D2-related asymmetric shear folds display NE-upward kinematics consistent with SW-ward verging NE-dipping faults.

A D3deformation event is recognized in cm-scale F3-kink-folds within the tectonically lower Marañon Complex and F3-fold-plane-parallel NE-trending faults that cut through the basement. The D3-faulting led to a gentle "kink" of the global D2-strike-direction that also affects the Pataz batholith. The western batholith contact is marked by sub-vertical, NNW- striking faults cutting through D2-structures of the basement. The internal magmatic architecture of the batholith displays intrusive relationships of progressively more felsic components. Magmatic flow directions follow the ~NE-dip of the intruded tilted basement. The supracrustal volcanic carapace of the batholith is affected by a ~NNE-trending horst- and-graben structure, defined by normal fault-bound sections of NW- and SE-dipping beds. The horst structures translate southward into uplifted, late-stage magmatic components of the batholith that display magmatic foliation-orientations indicative of supra-solidus uplift- initiation of the NW-SE extensional horst-and-graben structure.

GOLD-VEIN-SYSTEM

The batholith-hosted veins display three geometric types: (a) steep ENE-dipping arrays, sub- parallel to the western contact of the batholith, (b) medium NE- to ESE-dipping arrays that follow the magmatic-structural grain of

the batholith-interior, and (c) shallow-medium NE-/NNE-dipping veins that are observed in the footwall of the hydrothermal system. All three geometric types display an early paragenetic stage (I) of quartz-pyrite, which shows progressive development from hydraulic breccia into shear-deformed, laminated crack-seal veins, and a later undeformed stage (II) of quartz-pyrite-galena-sphalerite, which forms coarse-grained breccias incorporating fragments of stage-I and/or fill dilatational sites of the earlier stage. Stage-II-mineralization occurred predominantly in the vicinity to conjugate NW- or SE-dipping normal faults. A gentle NW- to NNE-change in strike-direction of the vein-system between domains, separated by NE- and WNW-trending faults is correlated to D3-fault-induced kinking of the basement structures. Hence, the D3deformation event likely occurred syn- to post-vein formation.

Structural data (D1-D2) and inferred semi-pelitic and marginal to arc-related origins of the western and eastern basement units, respectively, suggest E-/NE-directed subduction with associated SW-propagating fault-imbrication of shallow-crustal forearc nappes. Initial bedding-parallel S1-shear deformation progressed into D2-related NE-ward tilt and thrusting of the inner forearc over the outer sub-marine succession. The rheologically weaker and tectonically lower unit experienced F2-fold development. Timing of this basement orogeny remains unclear.

Emplacement of the Carboniferous Pataz batholith occurred through protracted intrusions of progressively fractionated magma batches, following the inherited pre-existing framework of the NE-ward tilted basement. The vein-system initiated in a NE-SW compressional regime during late-stage magmatism, where stage-I veins formed along Andersonian-type footwall-faults, and along medium- to steep-NE-dipping contact faults and energetically-favourable tectonic dispositions determined by the basement-inherited magmatic architecture. A switch to NW-SE-extension-uplift dynamics led to regional horst- and-graben development in the volcanic carapace and facilitated renewed fluid-influx (stage-II) along normal faults. We propose that this transition was controlled by ongoing strike-slip along the Río Marañon Fault (Fig. 1b).

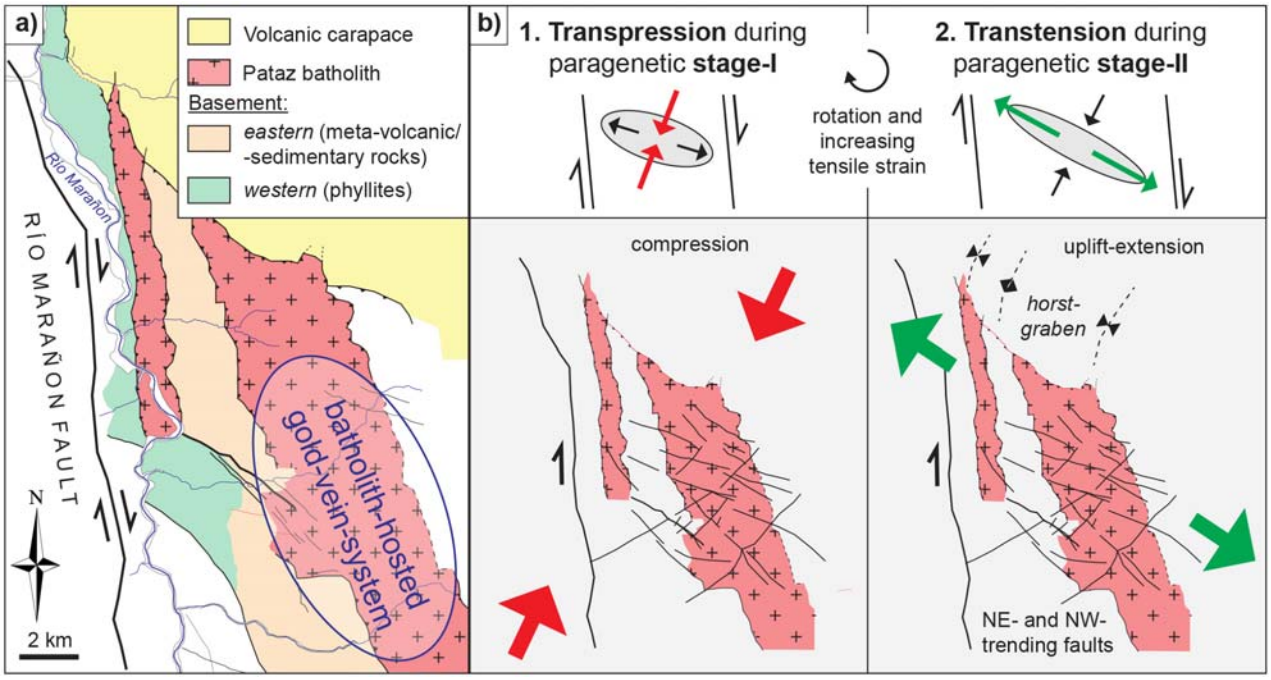

THE GEODYNAMIC SETTING OF THE BUSHVELD IGNEOUS COMPLEX

John Paul Hunt[1], Chris Hatton, Hakundwi Mandende, Michiel de Kock

[1]SRK Exploration Services Limited, University of the Witwatersrand - johnpaulhunt@gmail.com

A number of models have been proposed for the geodynamic setting of the Bushveld Igneous Complex, including meteorite impact (Rhodes, 1975), subduction (Hatton, 1988) and plume-related magmatism (Hatton, 1995; Hatton & Schweitzer, 1995). Whilst the Bushveld Complex has been broadly emplaced sub-concordantly into the Transvaal Supergroup, the transgressive nature of the footwall contact is recognised (Clarke *et al.*, 2009); in the north the footwall is basement granite, increasing upward in stratigraphy to the uppermost unit of the Pretoria Group sediments in the south.

Using a permissible paleomagnetic plate reconstruction of the conceptualised Kenorland supercontinent at 2.45 Ga (Hunt *et al.*, 2017, and references therein), the Kaapvaal is located to the relative southeast of the Kenorland assembly in proximity to Kola-Karelia, Sarmatia, and Siberia each containing Bushveld-aged bimodal intrusions and layered complexes, centred about a hypothesised plume centre to the north of the present day Kaapvaal. Although Bushveld-age intrusions are not known in the Pilbara, geological similarities with the Kaapvaal (de Kock *et al.*, 2009) require its inclusion in this assemblage. Emplacement of the Bushveld plume resulted in rifting of Pilbara-Sarmatia-Kaapvaal. The Zimbabwe craton was not adjacent to the Kaapvaal in the Neoarchean (2.7 Ga) (Rajesh *et al.*, 2014), and it's docking to the Kaapvaal is first recorded during the Limpopo orogeny ~2.05-1.85 Ga (Smirnov et al, 2013).

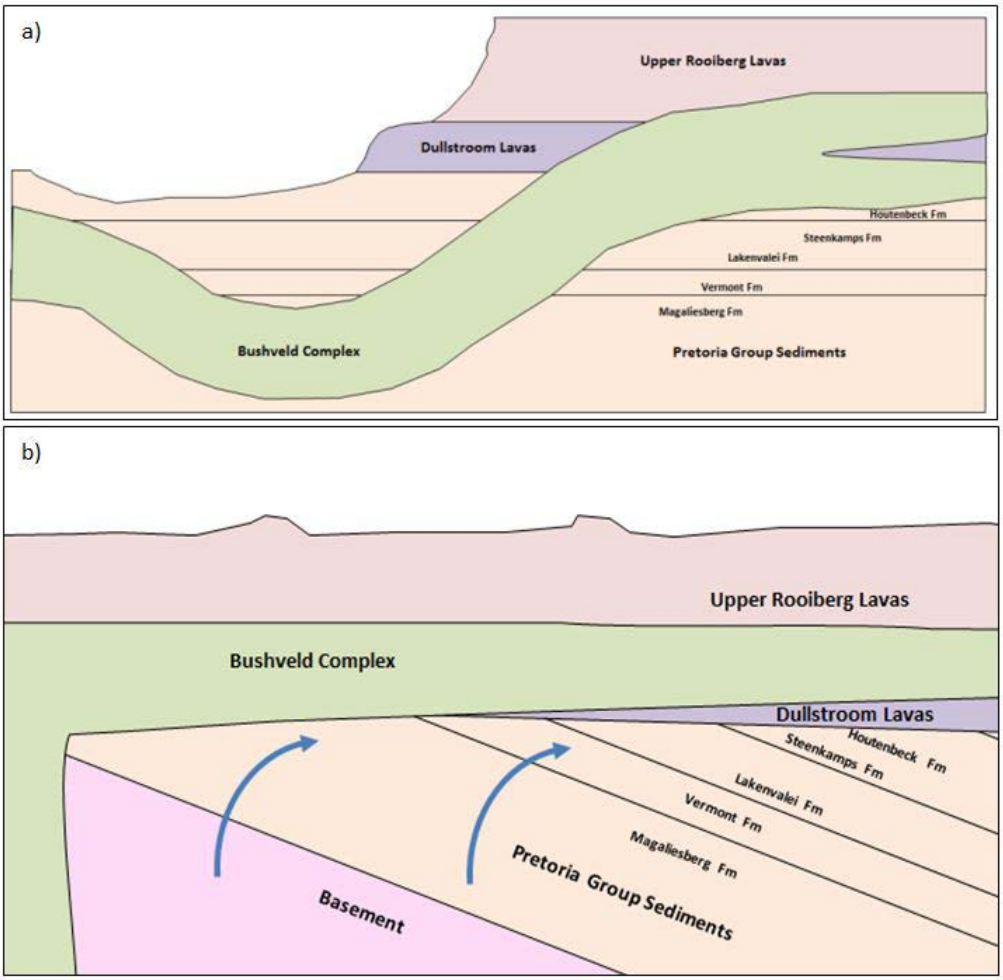

Figure 1. Schematic illustrations (not to scale) of two scenarios with respect to the emplacement of the Bushveld into the Transvaal stratigraphy including a) a dyke-sill-like emplacement model proposed by VanTongeren & Mathez (2015), and b) an alternate model proposed in this paper illustrating tilting (blue arrows) of the regional stratigraphy due to uplift caused by impingement of a plume to the north of the present day Bushveld Complex, such that emplacement of the Bushveld has an essentially horizontal sill-like emplacement, accounting for the upward increasing stratigraphy for the Bushveld footwall contact.

Hunt *et al.* (2017) proposed the positioning of a mantle plume to the present geographical position to the Bushveld Complex, moving initially through the lower crust, propagating perhaps as a deep-level, chonoloith-like structure, but on intersecting the first-order east- west intra-cratonic graben, marked in the north by the Thabazimbi-Murchison Lineament (TML), and to the south by the Spruitfontein-Steelpoort Lineament (SSL), the magmas sequential filled the structure, first with the Lower Zone and Critical Zone magmas, then becoming more sill-like during the emplacement of the Main Zone and Upper Zone magmas, spreading into all four lobes of the complex.

A north to south propagation is evidenced in the distribution of Lower Zone magmas, which are limited to occurring only north of the SSL. Magma chambers did not develop south of the SSL until Lower Critical Zone times. In the eastern Bushveld Complex, near Steelpoort, kilometre-wide fingers of magma were injected towards the SE, with the sense of deformation preserved in the high strain deformation caused in the footwall contact aureole (Clarke et al, 2009).

Van Tongeren & Mathez (2015) suggested that intruding magmas worked their way through the crust. However, an impinging plume to the north of the complex, consistent with Hunt *et al.* (2017), would likely have been responsible for considerable uplift and would have caused rotation of the surrounding regions. It is therefore proposed, that the Bushveld Complex intruded broadly as a horizontal sill on a regional first-order scale, explaining the transgressive footwall contact. It is proposed that these lithological units were initially rotated due to an impacting plume to the north of the present geographic position of the Bushveld Complex, and that the magmas were intruded as broadly horizontal sills following the eruption of the Rooiberg volcanics.

REFERENCES

Clarke, B., Uken, R., & Reinhardt, J. (2009): Structural and compositional constraints on emplacement of the Bushveld Complex, South Africa. Lithos, 111, 21-36.

De Kock, M., Evans, D.A.D., Beukes, N.J. (2009). Validating the existence of Vaalbara in the Neoarchean. *Precambrian Research*, 174, 145-154.

Hatton, C. (1988): Formation of the Bushveld Complex at a plate margin. *Congr. Geol. Soc. S. Afr., 22, 251-254*.

Hatton, C. (1995): Mantle plume origin for the Bushveld Complex and Ventersdorp magmatic province. *J. Afr. Earth Sciences*, 21, 571-577.

Hatton, C. J. and Schweitzer J. K. (1995): Evidence for synchronous extrusive and intrusive Bushveld magmatism. *J. Afr. Earth Sciences*, 21, 579-594.

Hunt, J.P., Hatton, C., de Kock, M.O., & Bleeker, W. (2017). Plume Activity related to the Kaapvaal craton, implications for Rhyacian plate reconstructions and ore deposits. Proceedings SGA Quebec 2017, 20-23 August 2017, Quebec City, Canada.

Rajesh, H.M., Santosh, M., Wan, Y., Liu, D., Liu, S.J., Belyanin, G.A., (2014). Think outside the box: There is no Limpopo orogeny. Precambrian Research 255, 459-466.

Rhodes, R.C. (1975). New evidence for impact origin of the Bushveld Complex, South Africa. Geology 3: 549-554.

Smirnov, A.V., Evans, D.A.D., Ernst, R.E., Söderlund, U., Li, Z.-X., (2013). Trading partners: Tectonic ancestory of southern Africa and western Australia, in Archean supercratons Vaalbara and Zimgarn. Precambrian Research 224, 11–22.

Van Tongeren, J.A., Mathez, E.A. (2015): On the relationship between the Bushveld Complex and its felsic roof rocks, part 2: the immediate roof. Contrib. Mineral Petrol 170:56. DOI 10.1007/s00410-015-1211-y

A | 63

AN OVERVIEW OF FLAKE GRAPHITE – AN EXAMPLE FROM THE LINDI JUMBO GRAPHITE PROJECT, TANZANIA

Michel Cunningham[1], Andrew Cunningham

[1]WSRK Consulting (Australasia) Pty Ltd - mcunningham@srk.com.au

Graphite is a form of pure carbon that normally occurs as black crystal flakes. Its unique physical and chemical properties make it well-suited to many industrial applications, including electronics, lubricants, metallurgy, steelmaking and as anode-material in lithium ion batteries.

Graphite generally forms from high-grade metamorphism of organic matter in sedimentary rocks. The three main types of commercially significant natural graphite are crystalline or disseminated flake, crystalline vein or lump and amorphous or microcrystalline.

The largest graphite deposits tend to be flake but are often relatively low grade. In contrast, vein graphite deposits are smaller but high grade, and amorphous deposits range in size, but are generally lower quality graphite and therefore have restricted use.

Recent exploration has focused on flake graphite mainly in East Africa (e.g. Belama deposit, northeast Mozambique), Canada (e.g. Bissett Creek deposit, eastern Canada) and Australia (e.g. Uley deposit, South Australia), leading to the discovery of approximately 350 million ton (Mt) of graphite in the past 5 years (SNL Database). The largest deposits are in Mozambique and Tanzania, an area noted for large, high purity flake graphite. This increased activity in exploration has resulted in global inferred resources exceeding 800 Mt (USGS, 2018).

Over 80% of graphite demand is still driven by industrial applications with the dominant market, refractories, making up 39% of demand, which in turn is 70% dependent on steel production. Forecasts are that the lithium-ion battery sector may surge about 600% on 2016 consumption levels by 2025 (Benchmark Mineral Intelligence, 2018). Fully electrical vehicles that require batteries of 10 kWh and above are forecast to have a major impact on volume.

Commercially, flake graphite is divided into coarse and fine or super jumbo to fine. Fine flake may be further sub-divided into medium flake, fine flake and powder. Impurities including minerals commonly found in metasedimentary units, usually quartz, feldspar, mica, amphibole, garnet and calcite, with occasional amphiboles, pyrrhotite, pyrite and magnetite.

The value of graphite deposits depends on factors such as grade, purity, size-range of graphite and the presence of impurities, which may have a negative effect on extraction of graphite. Graphite pricing is complex and the main parameters controlling the quality and price are total graphitic carbon (TGC) content and flake size. For content and purity, lithium-ion batteries require anode-quality graphite of 99.9% TGC. The amount of graphite that is included in the anode component is far more than lithium (cathode). For example, it takes 6 carbon (graphite) atoms to bind to a single lithium ion (Source: http://batteryuniversity.com/learn/article/lithium_based_batteries).

In East Africa, several flake graphite deposits are hosted within regionally metamorphosed Neoproterozoic granite-gneiss and metasedimentary units of the transcontinental Mozambique Orogenic Belt, a 240 to 400 km wide belt extending from Mozambique to Kenya. The Lindi Jumbo graphite deposit is a flake-style project located in southeastern Tanzania. The deposit is localised in a high grade metamorphic sequence of graphitic schist, dolomite, quartzite and felsic gneiss. The main deposit is tabular, forming a series of intercalated zones with conformable contacts with the main hosting graphitic units. Within the deposit, there is a high-grade core that is dominated by coarse-grained graphitic schists. The sequences have experienced polyphase deformation resulting in tightly folded re-folds, with a dominant northeast – southwest trend, with moderate dips towards the southeast.

Geological mapping identified a potential 30 km strike length of graphite-bearing units, with potential for repeated graphitic horizons. This work outlined a series of northeast-trending Proterozoic graphite-bearing schists and gneisses in an area previously mapped as Cainozoic and Palaeozoic sedimentary units. Variable thicknesses of graphite-bearing metasedimentary units were mapped across strike with up to 30 m of graphitic schist and 8 m of massive graphite documented.

Enriched graphitic zones generally occur in strongly foliated rocks in which the foliation is defined by the parallel orientation of graphite flakes. The main gangue minerals are quartz, plagioclase and potassium feldspar with subordinate orthopyroxene and biotite. Graphite grains form interstitially between grain boundaries of gangue silicates, and more rarely as inclusions in the silicate minerals.

Vertical Time-Domain Electromagnetic (VTEM), magnetic and radiometric geophysical surveys conducted over two areas delineated thirteen anomalies within the one survey area that were interpreted as graphite targets

for subsequent drill testing with the Lindi Jumbo graphite area highlighted as one of the strongest targets.

Drilling intersected wide zones of high grade graphite with visible jumbo flakes forming multiple bands of continuous graphite over a strike length in excess of 1 km.

Graphite mineralization of the Lindi Jumbo Graphite deposit was modelled into domains based on grade. The existence and continuity of the high-grade domains is well established with confirmed outcrop and three distinct high-grade intervals in the majority of holes intersecting the modelled formation. The graphite flake is dominantly coarse flake of about +80 mesh size particles. Mineral Resource estimates for the deposit is 29.6 Mt averaging 11% TGC for a 3.26 Mt of contained graphite, at a 5 % TGC cut-off (Walkabout Resources ASX Release: 12/2016). Approximately 40% (1.31 Mt TGC) of the resource is in the Measured and Indicated classification, as reported in accordance with the JORC Code (2012) international standards. The application of modifying factors has resulted in over 62% of the graphite contained within the Mineral Resource being converted to Ore Reserve.

A | 64

PROBABILISTIC MINERAL RESOURCE ASSESSMENT OF U.S. TERRITORIES OF THE CARIBBEAN BASIN AND ADJACENT AREAS: PROGRESS REPORT

Lukas Zurcher[1], Floyd Gray, Steve Ludington, Frederic Wilson, Greta Orris, Mark Cocker, Mark Gettings, Tim Hayes

[1]U.S. Geological Survey - lzurcher@usgs.gov

The U.S. Geological Survey (USGS) is partnering with the IberoAmerican Association of Geological and Mining Surveys (ASGMI) to conduct an assessment of undiscovered metallic and non-metallic resources in the Greater Antilles region. The assessment plans to provide science-based information on the geologic availability of these resources for development, land-use planning, and decision making.

The USGS anticipates contributing information generated for the Greater Antilles assessment project to the concurrent ASGMI project "Metallogenetic Map of Central America and the Caribbean". ASGMI, in turn, anticipates contributing expertise on the metallogeny of the region to the USGS assessment project. For this purpose, the USGS plans to conduct a workshop on assessment methodology to support ASGMI's participation in the probabilistic estimation of undiscovered deposits. Both projects stand to benefit significantly from this collaborative effort.

The assessment plans to build on previous USGS assessments in the region. For Puerto Rico, Bawiec (1998) provided mean estimates from different types of undiscovered deposits of 3.5 Mt Cu, 21,000 t Mo, 340 t Au, 2,000 t Ag, 18 Mt Fe, 45,000 t Zn, 55,000 t Pb and 44,000 t Mn. Gray *et al.* (2014) furnished resource estimates for permissive porphyry Cu tracts in Central America and the Caribbean Basin. Undiscovered deposits in a permissive tract in the Greater Antilles were predicted to contain 36 Mt Cu, 210,000 t Mo, 2,700 t Au, and 7,400 t Ag. More recently, Cocker *et al.* (2017), Gass *et al.* (2017), Orris *et al.* (2016; 2017), Wilson *et al.* (2017), and Zürcher *et al.* (2017) presented results on various topics related to this assessment project.

The assessment report plans to include an overview of the geo-tectonic framework of the region, descriptions of delimited permissive tracts, probabilistic estimates of undiscovered resources, references, and GIS databases of tectonic terranes, known mineral deposits and prospects, and mineral-resource assessment tracts.

This study plans to use the USGS three-part assessment methodology (Singer and Menzie, 2010), which consists of descriptive and grade-tonnage mineral deposit models (Cox and Singer, 1986); delineation of permissive tracts; and estimation of numbers of undiscovered deposits. Estimates of undiscovered deposits at different confidence levels are combined with grade-tonnage models in a Monte Carlo simulation to produce probabilistic estimates of resources by tract (Bawiec and Spanski, 2012).

To perform the assessment, the USGS compiled a digital geologic map from sources at 1:100,000 to 1:250,000 scales, as well as a relational database of approximately 750 geochronologic dates, which are expected to be published soon. Geologic, geophysical, geochemical, and mineral occurrence datasets for Puerto Rico and the U.S. Virgin Islands are near completion.

A preliminary data review for Puerto Rico and the U.S. Virgin Islands has permitted delineation of permissive tracts for the occurrence of several deposit types. These include aggregate; barite; limestone and dolomite; epithermal quartz-alunite and adularia-sericite Au-Ag; lateritic and karst bauxite, Ni-Co laterite, and lateritic supergene REE; phosphate; placer Au-PGE and shoreline Ti; podiform Cr; polymetallic vein; porphyry Cu; silica; skarn Cu, Cu-Fe, and Fe; volcanogenic massive sulfide; volcanogenic Mn; and zeolites. It is anticipated that a large part of undiscovered resources will be contributed by tracts for only a few of these deposit types. These are likely to include aggregate, limestone, porphyry Cu- Au, Cu and Fe skarn, epithermal quartz-alunite, polymetallic vein, lateritic supergene REE, and volcanogenic Mn.

The updated information base used for this assessment, and new developments in the understanding of ore forming processes are likely to influence estimates of undiscovered resources in Puerto Rico, and the entire Greater Antilles region. For instance, delineation of permissive areas and/or the estimation of undiscovered porphyry Cu deposits could be affected by consideration of the tectonic changes now recognized as critical in triggering the formation of large porphyry deposits (Cooke *et al.*, 2005; Richards and Holm, 2013); by recognition that porphyry Cu deposits may form in post-subduction as well as arc settings (Ludington *et al.*, 2013; Richards, 2009); and by consideration of the role that post-mineral erosion and cover play in the preservation or concealment of porphyry deposits (Barton, 1996; Kesler and Wilkinson, 2006; Zürcher *et al.*, 2016).

Results from this study are expected to contribute to the understanding of the tectono- magmatic history, evolution of depositional environments, weathering, and related mineralization throughout the Greater Antilles. These will enable better comparisons of the metallogenesis of this region with other parts of the world.

REFERENCES

Barton, M.D., 1996. Granitic Magmatism and Metallogeny of southwestern North America, in Brown, M, Candela, PA, Peck, DL, Stephens, WE, Walker, RJ, and Zen, E, eds., III Hutton Symposium, The Origin of Granites and Related Rocks. Transactions of the Royal Society of Edinburgh, Earth Sciences, vol. 87, pp. 261–280

Bawiec, W.J and Spanski, G.T., 2012. Quick-start Guide for Version 3.0 of EMINERS—Economic Mineral Resource Simulator. U.S. Geological Survey OFR 2009-1057, 26 p.

Bawiec, W.J., 1999. Geology, Geochemistry, Geophysics, Mineral Occurrences and Mineral Resource Assessment for he Commonwealth of Puerto Rico. U.S. Geological Survey OFR 98-038, online version only

Cocker, M.D., Orris, G., Gass, L., Gray, F. and Gettings, M., 2017. Lateritic, Supergene Deposit Potential in Cuba. Geociencias 2017, Havana, MIN1-07

Cooke, D.R., Hollings, P. and Walshe, J.L., 2005. Giant Porphyry Deposits: Characteristics, Distribution, and Tectonic Controls. Economic Geology, vol. 100, N° 5, pp. 801-818

Cox, D.P., and Singer, D.A., 1986. Mineral Deposit Models. U.S. Geological Survey Bulletin 1693, 379 p.

Gass, L., Gray, F. and Orris, G.J., 2017. Maps and Analyses for the USGS Cuban Mineral Resource Assessment. Geociencias 2017, Havana, GEO_4-P3

Gray, F., Hammarstrom, J.M., Ludington, S., Zürcher, L., Nelson, C.E., Robinson, G.R., Miller, R.J. and Moring, B.C., 2014. Porphyry Copper Assessment of Central America and the Caribbean Basin. U.S. Geological Survey SIR 2010–5090–I, 81 p.

Kesler, S.E. and Wilkinson, B.H., 2006. The Role of Exhumation in the Temporal Distribution of Ore Deposits. Economic Geology, vol. 101, N° 5, pp. 919-922

Ludington, S., Hammarstrom, J.M., and Zientek, M.L., 2013. Post-convergent Porphyry Copper Deposits—What, Where, Why. GSA Annual Meeting, Denver, paper 236-4.

Orris, G.J., Cocker, M.D. and Gray, F., 2016. Natural Zeolite Deposits—an Important and Widely-distributed Industrial Mineral Resource in Cuba. GSA Annual Meeting, Denver, paper 318-24.

Orris, G.J., Gray, F., Cocker, M.D., and Gass, L., 2017. Challenges creating Descriptive and Quantitative Deposit Models from Public Information for the U.S. Geological Survey Mineral Resource Assessment of the Republic of Cuba. Geociencias 2017, Havana, GEO_4-P1.

Richards, S.W. and Holm, R.J., 2013. Tectonic Preconditioning and the Formation of Giant Porphyry Deposits, in Colpron, M, Bissig, T, Rusk, BG, and Thompson, JFH, eds., The North American Cordillera and Similar Accretionary Settings. SEG Special Publication, vol. 17, pp. 265-275

Richards, J.P., 2009. Postsubduction Porphyry Cu-Au and Epithermal Au Deposits—Products of Remelting of Subduction-modified Lithosphere. Geology, vol. 37, N° 3, pp. 247-250.

Singer, D.A. and Menzie, W.D., 2010, Quantitative Mineral Resource Assessments—An Integrated Approach. New York, Oxford University Press, 232 p.

Wilson, F.H., Orris, G.J. and Gray, F., 2017. A Geochronological Database for Cuba. Geociencias 2017, Havana, GEO1-O_4.

Zürcher, L., Booksrom, A.A., Hammarstrom, J.M., Mars, J.C., Ludington, S.D., Zientek, M.L., Dunlap, P. and Wallis, J.C., 2016. Relationship between Porphyry Systems, Crustal Preservation Levels, and Amount of Exploration in Magmatic Belts of the Central Tethys Region, in Richards, JP, ed., Tectonics and Metallogeny of the Tethyan Orogenic Belt. SEG Special Publication, vol. 19, pp.213-236.

Zürcher, L., Gray, F., Hayes, T., Orris, G., Gettings, M., Cocker, M., and Gass, L., 2017. Preliminary Assessment of Porphyry Copper Deposits in the Sierra Maestra, Cuba. Geociencias 2017, Havana, GEO_4-P4.

A | 65

THE FORMATION OF THE SORA PORPHYRY Mo-Cu DEPOSIT IN THE KUZNETSK ALATAU TERRANE, RUSSIA: ZIRCON U–Pb AGE, GEOCHEMISTRY AND Sr–Nd ISOTOPIC RESULTS

Anita N. Berzina[1], Adel P. Berzina, Victor O. Gimon

[1]*V.S. Sobolev Institute of Geology and Mineralogy SB RAS, Novosibirsk, Russia - anberzina@gmail.com*

BACKGROUND

The Sora deposit occurs within the Altai-Sayan area in the north-eastern part of Central- Asian Orogenic Belt. It is a large porphyry Mo-Cu deposit but a detailed study is lacking. Especially, absolute geochronology is scarce and the timing of ore-related magmatism has not been well understood. Previous geochronological work was mostly based on Rb-Sr, K–Ar and Ar–Ar systems which yielded ages of mineralization-related granite porphyries ranging from ~467 Ma to 370 Ma (Middle Ordovician–Upper Devonian). In this contribution, we report new data of zircon U–Pb SHRIMP ages, whole rock geochemical and Sr-Nd isotopic data for the magmatic rocks from the Sora deposit in order to constrain the emplacement ages of ore-bearing porphyry association and investigate magma sources, petrogenesis and the genetic relationship between the mafic and intermediate to felsic rocks.

The geodynamic setting of the region is consistent with Early Paleozoic subduction of Paleo- Asian Ocean plate and the continuous accretion of oceanic components to the Siberian continent. The Kuznetsk Alatau island-arc terrane is one of the largest fragments of the Altai-Sayan area. The collision of the terrane with the Siberian continent in the Late Cambrian–Early Ordovician was accompanied with the emplacement of large granitoid plutons. The Sora deposit is hosted in porphyry stocks and dikes associated with the Middle Cambrian-Early Ordovician multi-phase Uibat pluton. The emplacement of the pluton preceded the initiation of the magmatic–hydrothermal system responsible for porphyry Mo- Cu mineralization. Porphyry association consists of pre-ore gabbroic and monzonitic porphyries, mineralization-related granite-porphyries and post-ore dykes of different composition.

METHODS

U–Pb isotopic analyses were performed using the SHRIMP-II at the All Russia Geological Research Institute (St. Petersburg, Russia). Major element compositions of whole-rock samples were determined using X-ray fluorescence; trace elements were analyzed by ICP- MS (Element, Finnigan MAT); strontium isotopic analyses were performed on an MI 1201AT solid mass spectrometer at the Analytical Centre of the Institute of Geology and Mineralogy (Novosibirsk, Russia). Samarium and neodymium isotope analyses were performed at the Laboratory of Geochronology, Geological Institute of Kola Scientific Center of the Russian Academy of Sciences on a multi-collector Finnigan MAT-262 thermal ionization mass spectrometer.

RESULTS

Zircon U–Pb dating of the pre-ore monzodiorite porphyry, ore-bearing granite porphyry, and post-ore granite porphyry yielded ages of 467 ± 2 Ma, 463 ± 2 Ma, and 412 ± 1 Ma, respectively, indicating emplacement of the mineralization-related intrusion took place in the Middle Ordovician. The post-ore dikes represent the most recent Early Devonian magmatic activity in the Sora area. The Middle Ordovician ore-related porphyries are probably related to the transformation in the regional tectonic regime from compression into extension, whereas the emplacement of the younger Early Devonian post-ore dikes are ascribed to extensional setting.

Both plutonic and subvolcanic (porphyry) associations consist of three compositional groups, which include mafic (gabbroic), monzonitic and granitic rocks. The Sora gabbroic rocks, including plutonic (gabbro/monzogabbro) and porphyry dike (gabbro-diorite porphyry) samples, belong to the high-K calc-alkaline series, enriched with MgO and show elevated Mg# values (52-78). They have typical arc magma characteristics such as the enrichment in large-ion lithophile elements and light rare-earth elements, a depletion in heavy rare-earth elements and high-field-strength elements, and negative Nb, Ta, and Ti anomalies, all indicating that magmas parental for these mafic rocks were derived from a mantle that had previously been metasomatised by subduction. High Ba contents relative to Th support mantle enrichment by slab-derived fluids. The Nd model ages of gabbroic samples (0.7-1.1 Ga) indicate that metasomatism probably occurred in Neoproterozoic.

The initial Sr isotopic and ε_{Nd} ratios of the plutonic mafic rocks at Sora range from 0.7038 to 0.7044 and from +1.7 to +2.1, respectively. The mafic samples from porphyry dike series show Sr isotopic compositions similar to those in gabbro/monzogabbro, but yield relatively higher $\varepsilon_{Nd}(t)$ values (+5; +6.5). In summary, geochemical and Sr-Nd isotopic data for the Sora mafic samples suggest that the protolith magmas for mafic rocks from the plutonic series

were sourced from a moderately enriched mantle, while younger mafic porphyry dikes were derived from slightly enriched mantle source. Crustal contamination was not significant during mafic magmas ascent and emplacement. The differences in Sr-Nd isotopic compositions in mafic samples probably suggest compositional heterogenity in the mantle.

The Sora intermediate to felsic (monzonitic and granitic) rocks show positive $\varepsilon_{Nd}(t)$ values and are characterized by a certain similarity in petrogeochemical composition, alkalinity, trace element content, and Sr isotopic composition with gabbroic rocks. These data indicate that a high proportion of mantle-derived material was involved in the generation of monzonitic and granitic rocks.

The monzonitic and gabbroic samples define a linear trend in the K_2O+Na_2O versus SiO_2 diagram, which indicates that the two rock suites share a similar origin. However, the granitic samples do not fall on this linear trend. Furthermore, no rocks compositionally intermediate between the monzonitic and granitic rocks have been identified in the area. This indicates that the granitic rocks were derived from a different source region and/or generated by different petrogenetic process. The most primitive monzonitic samples are characterized by a relatively low SiO_2 (~54%) and high Mg (~8%) content. Initial $^{87}Sr/^{86}Sr$ values range from 0.7043 to 0.7044. The La/Sm ratio of monzonitic plutonic and dike samples is nearly constant, suggesting that their genesis is related to fractional crystallization. These facts indicate that the monzonitic rocks of both plutonic and porphyry associations may have been produced by fractional crystallization of basaltic parental magma. The Sora granitic rocks have low initial $^{87}Sr/^{86}Sr$ ratios (0.7031-0.7040), positive whole rock $\varepsilon_{Nd}(t)$ (+1.6 to +4.1) with young Nd model ages (0.85–1.1 Ga). They show positive correlation between the La and La/Sm, indicating that granitic rocks may have been generated by partial melting of juvenile basaltic lower crust, formed by underplating of mantle–derived mafic magmas similar to Sora mafic rocks in composition. Relatively wide range of $\varepsilon_{Nd}(t)$ in granitic samples most likely reflects the heterogeneity of the juvenile lower crust. Although the Middle Cambrian-Early Ordovician magmatic events, related to the emplacement of the Uibat pluton were not directly related to major mineralization, they may have contributed to the Middle Ordovician mineralization through the storage of significant amounts of metals, sulfur and volatiles in the cumulate zone in the mantle lithosphere.

CONCLUSIONS

The Sora intrusive rocks are composed of plutonic and subvolcanic (porphyry) series, which include mafic (gabbroic), monzonitic and granitic varieties. New zircon U–Pb ages indicate that the mineralization-related porphyry dikes were emplaced in the Middle Ordovician (467-463 Ma). The petrographic, geochemical data and Sr–Nd isotopic compositions indicate that the parental magmas of the Sora mafic rocks were derived from heterogeneous moderately to slightly enriched lithospheric mantle source, metasomatized by fluids. Gabbroic and monzonitic plutonic and subvolcanic rocks may have been produced by fractional crystallization of basaltic parental magma. The granitic plutonic and subvolcanic rocks were likely generated by partial melting of juvenile basaltic lower crust as a result of magma underplating. The ore-bearing magmas of porphyry intrusions were generated during the later stage of magmatic events. The preceding Middle Cambrian-Early Ordovician protracted multiphase igneous activity was not directly related to mineralization, however it is considered vital for the transportation and enrichment of metals at Sora.

This research was funded by the Russian Foundation for Basic Research (grant 16-05-00921).

A | 66

WHITE MICA MINERAL VECTORS TO ORE OBTAINED BY SWIR SPECTROSCOPY MAPPING IN THE ALTAR PORPHYRY Cu-(Au) DEPOSIT, SAN JUAN, ARGENTINA

Luciano Matias Bocanegra
SEG - geobocanegra@gmail.com

BACKGROUND

Altar (31° 29' S, 70° 28' W) is a porphyry Cu-(Au-Mo) deposit with associated epithermal Au- (Ag-Cu) veins located in the Cordillera Principal of San Juan province (Argentina). Mineralization in Altar (995 Mt, 0.35% Cu, 0.083 g/t Au; Marek, 2014) is mainly hosted in a complex stockwork of quartz veinlets and disseminations.

Geochemistry of Cu, Au, and Mo delineates two mineralized centers located in the central ridge (Altar Central) and the east valley (Altar East). Copper-(Au) grades are spatially related with the areas of emplacement of the mineralized subvolcanic stocks and two zones of potassic alteration at depth with chalcopyrite ± pyrite ± bornite, as A veins and disseminations. A subsequent pulse, precipitated the quartz ± molybdenite veinlets (B veins). With progressive cooling of the fluids, the rocks were affected by chloritic alteration (chlorite + hematite ± rutile) as patches at deep, intermediate, and shallow levels. The phyllic alteration at depth is controlled by fractures associated with straight-walled type D veins and at shallow levels forms a continuous halo surrounding the potassic and chloritic alteration types. Kaolinite ± quartz ± rutile occurs at depth in the porphyries and the wall- rocks and forms the halos of type E veins. These late veins are rich in enargite, tennantite, pyrite, relict bornite, and traces of gold. Supergene alteration caused the enrichment of hypogene sulfides and their replacement by covellite ± digenite (Maydagán *et al.*, 2016).

Previous studies (e.g., Cohen, 2011) demonstrated that the wavelength of the 2,200-nm absorption feature corresponding to the Al-OH bond energy of white mica-bearing samples is critical to determinate the pH of hydrothermal fluids in porphyry systems. The wavelength of the 2,200-nm feature of white mica (including both muscovite and illite), shifts from 2,195 nm in muscovite toward 2,220 nm in phengite, as Al is replaced by (Fe, Mg) +Si. Muscovitic white mica (including illite) composition reflects an acidic environment whereas a phengitic composition indicates a more neutral environment (e.g., Cohen, 2011).

METHODS

We performed Short Wave Infrared (SWIR) spectroscopy analyzes on 85 samples from three W-E sections that cut the Altar Central deposit. The objective of this contribution is to identify new mineral vectors towards Cu-rich cores in the deposit and compare the new data with previous microprobe and XRD analyses.

The equipment used for the measurements was an Analytical Spectral Devices, Inc. TerraSpec™ short-wave infrared (SWIR) spectroscopic mineral analyzer. This equipment measures SWIR spectra from 350nm to 2500nm wavelength range, with spectral resolution of 3nm. Raw spectra were processed into The Spectral Geologist V.8.0.2.17 software™ for viewing and extraction of numeric parameters such as the wavelength, width and depth of specific absorption features. Then, spectra was interpreted by comparing the unknown spectra to reference spectra from SPECMIN-PRO 3.1, and The Spectral Geologist™ software.

RESULTS

Alteration zones based on the position of the wavelength of Al-OH absorption (ca. 2200 nm) feature in white micas (WM) were mapped in a section of Altar Central. The results revealed a peripheral zone with phengitic WM (>2209nm) that encompasses an internal zone of normal potassic WM (2200 – 2209nm). At depths between 3550 and 3200 m.a.s.l within the normal potassic WM zone, a hanging level with absorption features <2200nm is interpreted as WM with paragonitic tendency.

The spatial distribution of Cu-Au grades in hypogene zone corresponds to the WM zonation described above, where copper higher grades (>0.7%) correlate to potassic WM even to the transition to phengitic type. In the case of gold, the medium-grade zone (0.1 - 0.2 g/t) correlates with potassic WM and part of the phengitic type to the west. Furthermore, higher gold grades (>0.3 g/t) observed at hole ALD-49, related to D type veins coincides with the transition zone from potassic to paragonitic WM located at shallower levels.

CONCLUSIONS

The normal potassic WM zone recognized herein reflects the main channel of acid fluids during the phyllic-stage. The external halo with phengitic WM (+chlorite) indicates peripheral more neutral fluids. At depth, phengitic

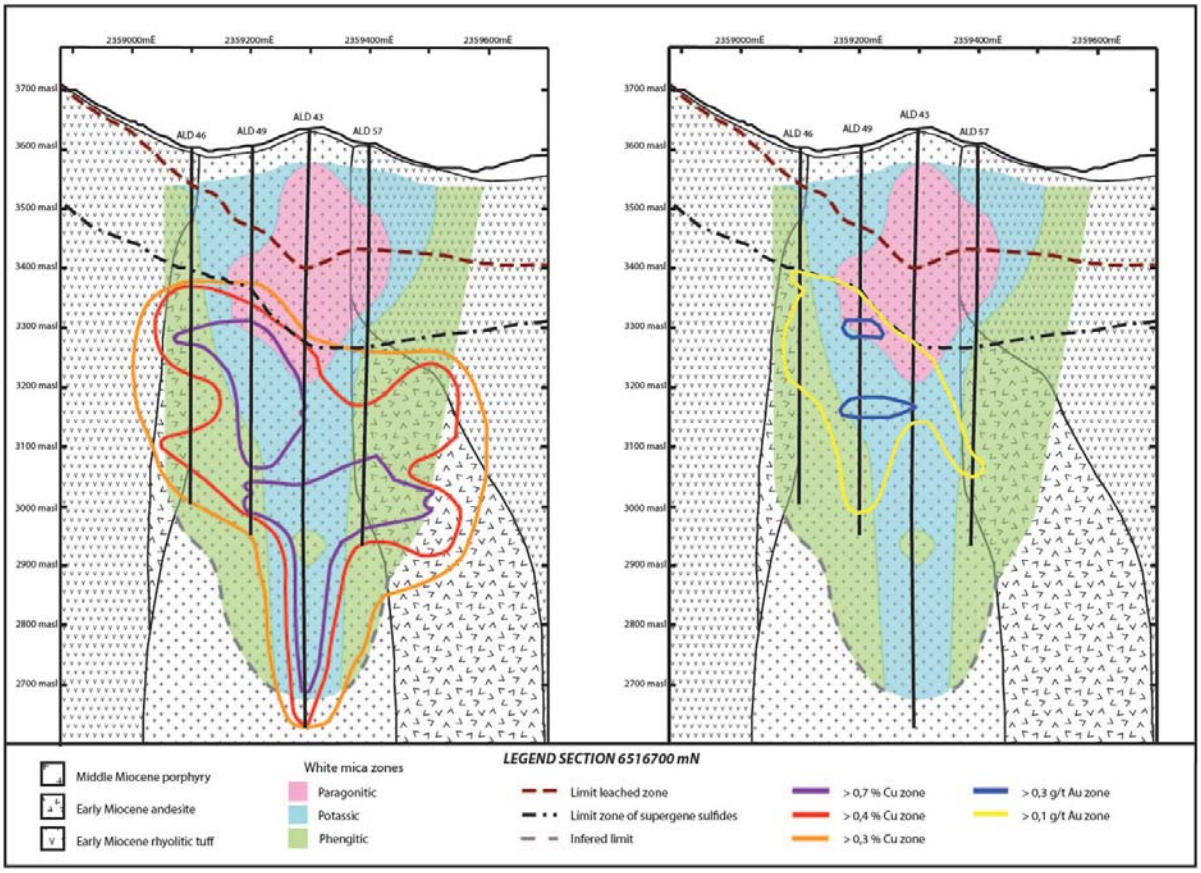

WM + chlorite overprints early potassic (biotitic) alteration. The shallower zone characterized by WM paragonitic tendency (+kaolinite) represent more acidic conditions, suggesting a transition to the epithermal environment (base of lithocap).

Previous studies of the Altar deposit (Maydagán *et al.*, 2016) analyzed the Cu and Au distribution, demonstrating the existence of remobilization and hypogene enrichment zones related to phyllic stage alteration. In this research, we found that the zonation of WM generated during phyllic-stage overprint, determined by drifting in 2200nm wavelength feature, is correlated with Cu and Au grades in the hypogene environment.

Finally, the results obtained support the use of white micas composition by reflectance spectroscopy as a vectoring tool to high-grade mineralization in porphyry systems like the Altar project.

REFERENCES

Cohen, J.F., 2011. Mineralogy and geochemistry of hydrothermal alteration at the Ann- Mason porphyry copper deposit, Nevada: Comparison of large-scale ore exploration techniques to mineral chemistry. Unpublished Master thesis, Oregon State University, Oregon, USA, pp. 111.

Marek J.M., 2014. Estimated mineral resources Altar and Quebrada de la Mina deposits, San Juan Province Argentina (2014) Prepared by Independent Mining Consultants, Inc., for Stillwater Mining Company, Technical Report, pp. 169.

Maydagán, L., Franchini M., Impiccini A., Lentz D., 2016. Phyllosilicates geochemistry and distribution in the Altar porphyry Cu-(Au) deposit, Andes Cordillera of San Juan, Argentina: Applications in exploration, geothermometry, and geometallurgy. Journal of Geochemical Exploration, 167, 83–109.

A | 67

DISTINCTIVE CHEMICAL CHARACTERISTICS, GEODYNAMIC SETTINGS AND PETROGENESIS OF GOLD ORE FORMING ARC MAGMAS

Robert Loucks

University of Western Australia - Robert.Loucks@uwa.edu.au

Low- to high-potassium tholeiitic and calc-alkalic arc magmas that exsolve a gold-ore-forming hydrothermal fluid are distinguished from infertile ordinary arc magmas by higher contents of lithophile elements that partition strongly into melt relative to residues during partial melting of mantle peridotite. Figure 1 shows a compilation of published whole-rock analyses representing magmatic differentiation series in Phanerozoic gold-ore-productive igneous complexes (colours), in comparison with differentiation series in well explored, large arc segments that are apparently barren of significant magmatic-hydrothermal gold mineralization (grey). In these plotting coordinates, Au-fertile magmatic differentiation series are usefully distinct from Au-infertile arc magmas across the low- to high-SiO_2 range.

Lithophile trace-element compositions of primitive mafic magmas (6-12 wt% MgO) that are spatially and temporally associated with major gold-mineralization events are compared in Figure 2A with lithophile-element abundances in unmineralized arc segments. Note the leftward divergence of the slope of Au-fertile parental arc magmas from the slope of Au-infertile arc magmas. The slope of a spidergram array can be represented by the ratio of a highly incompatible element on the left side (e.g., Ba or Nb) to a less incompatible element farther to the right (e.g., Zr or Y). This is the basis of my gold-fertility discriminant ratios in Figure 1, which can be used to identify other gold-fertile igneous complexes and arc segments as potential exploration targets. Figure 2B shows that the lithophile-trace-element abundances in metasomatically "refertilised" average sub-continental lithospheric mantle worldwide differs from the composition of average asthenospheric mantle (NMORB source) in the same sense of leftward-increasing divergence as the difference between gold-fertile mafic arc magmas and gold-infertile mafic arc magmas. This match of divergence trends in Figures 2A and 2B is one of the main lines of evidence that atypical degrees of partial melting of lithospheric mantle are important in the petrogenesis of gold-ore-forming arc magmas.

Published experimental data show that the wet solidus temperature of peridotite is tens of degrees below the solidus temperatures of Fe-Ni(-Cu) monosulfide solid solution (mss) at upper mantle pressures. The experiments show that Au partitions preferentially into hydrous mafic silicate melts relative to mss-bearing restite during low-percentage melting of hydrated mantle peridotite at temperatures below the solidus of mantle mss. The partition coefficient of Au between crystalline mss and hydrous mafic silicate melt is ca. 60, so if the mass fraction of mss in peridotite is <1/60, i.e., < 0.0166 (as is nearly always the case), then the Au content in hydrous mafic silicate melt is greater than in mss-bearing mantle restite. At temperatures above the sulphide solidus, Au partitions into sulphide melt relative to hydrous mafic silicate melt by an enrichment factor of about 10,000, so higher-temperature mafic silicate melts have very low Au content as they segregate from molten-sulphide-bearing mantle restite. Those relatively Au-, Ba, Nb- and K-rich, near-solidus melts of asthenospheric mantle tend to freeze in transit through the cooler lithospheric mantle, producing a long-term accumulation of metasomatic veins and dykes in typical sub-continental lithospheric mantle, as illustrated in Figure 2B.

Metasomatic veins in lithospheric mantle have lower melting temperatures than their refractory peridotite matrix, so they can be selectively re-melted in appropriate tectonic situations, producing magmas that are unusually fertile for magmatic-hydrothermal gold metallogeny. Favorable conditions for selective re-mobilisation of metasomatic veins include (1) hydration of the lower lithospheric mantle during "flat" subduction, which lowers the solidus T, or (2) under-plating by hotter asthenospheric mantle that raises temperatures above the veins' solidus T, or (3) rifting that causes decompression melting of lithospheric mantle, or (4) lithospheric thickening by orogenic shortening, warping its base downward where it is thermally and mechanically ablated by subjacent convecting asthenosphere.

THE METALLOGENIC MAP OF CENTRAL AMERICA AND THE CARIBBEAN

Eduardo O. Zappettini[1], Natalia Amezcua, Gloria Prieto Rincón, Santiago Muñoz Tapia, Xiomara Cazañas Díaz, David Jara, Carolina Maldonado, Fernando Erazo

[1]*Servicio Geológico Minero Argentino - eduardo.zappettini@segemar.gov.ar*

The Metallogenic Map of Central America and the Caribbean is a project carried out by the Asociación de Servicios Geológicos y Mineros de Iberoamérica (ASGMI), under the aegis of the Commission for the Geological Map of the World (CGMW). The Geological Survey of Argentina (SEGEMAR) is in charge of the general coordination, and three regional coordinators are established: Central America, by the Geological Survey of Mexico (SGM); the Caribbean, by the Geological Survey of República Dominicana (SGN) and South America by the Geological Survey of Colombia (SGC). The preparation of the map and related databases is the result of a close cooperation between all the involved countries.

The cartography of the tectonostratigraphic and metallogenic units is based on the Structural Map of the Caribbean, under preparation by CGMW, of which the main elements and formations were updated and adapted following the requirements of the work. The classification of ore deposits are in compliance with the criteria established for recent international metallogenic maps. This map thus will provide the most up-to-date view of the knowledge of the Central America and the Caribbean metallogeny.

The geotectonic base map is being prepared including the most recent geological and geotectonic information available for each country. Magmatic events and sedimentary successions are classified following conventional geotectonic classifications. Metamorphic units are also classified considering the origin of their protolith when known; otherwise, their magmatic or sedimentary origin is indicated.

The mineral deposits classification and representation considers the genesis of the mineral deposit (symbol shape), a simplified classification of paragenetic associations /commodities (symbol color), and size following the international classification used in other international metallogenic maps.

A comprehensive mineral deposit database will be included in the digital version for allowing a better exploitation of the GIS information. This database includes among others the deposit clan or deposits groups, and the deposits models when appropriately defined, following the comprehensive list established by the U. S. Geological Survey.

Typical deposits related to active continental margins, volcanic island arcs and ophiolitic belts are individualized. The most important models include porphyry-type and epithermal deposits associated with arc magmatism, massive sulfides and sedex deposits associated to extensional events, and lateritic Al and Fe-Ni-Co related to ultramafic rocks.

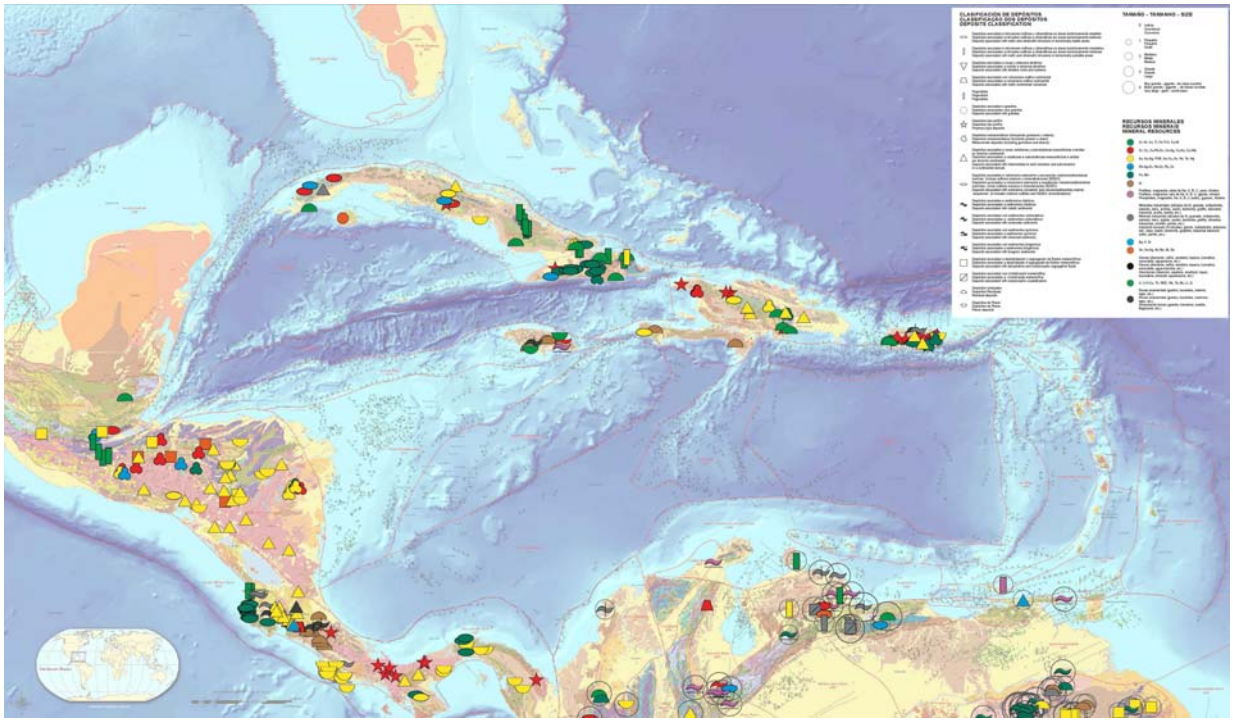

Fig. 1. First draft of the Metallogenic Map of Central America and the

A | 69

CARTOGRAPHY, PETROGRAPGY, GEOCHEMISTRY OF THE MALOUNG MEGA-QUARTZ VEIN (WEST- CAMEROUN): IMPLICATION ON ITS ECONOMIC INTEREST

Kevin Igor Azeuda Ndonfack[1], Jean Pierre Tchouankoue, Josiane Sonmo, Yuling Xie

[1]University of Science and Technology Beijing - kevinazeuda@yahoo.fr

ABSTRACT

The Maloung mega-quartz vein is situated in West Cameroon Region, Foumban and Nde divisions, in Maloung village (5 09' 49" N; 10 51' 55" E). This Maloung mega-quartz vein which is clearly seen on satellite image is located between two mean mega tectonic structures of Cameroon known as the Adamawa Shear Zone (ASZ) in the north and the Sanaga Fault (SF) in the south, both N070 direction. The mega-vein cross-cuts on over 20 km the Precambrian formations constituted of orthogneiss, migmatite, amphibolite and granite. This study that aims to understand the geodynamic setting and economic interest of the Maloung mega-vein is based on, cartography, petrographic studies and geochemical analysis.

Cartography mainly based on DEM (Digital Elevation Model) Image analysis proves that the mega-quartz vein, oriented N55°E with a thickness reaching 100 m, delimits Maloung area in two different morphological units relative to the altitudes: a lower level (750-860 m) at the South East and the higher level (860-1120 m) at the North West of quartz vein. The shift of the Noun river bed by the quartz vein (the upstream toward west and the downstream toward east), the N-S sinistral shear associated with the N080 and N135 fractures observed upon the satellite images and in the field, and the massive, white, euhedral quartz constituting the quartz vein involve a transtensional deformation with sinistral movement. Those data prove the emplacement of the quartz vein in a fault which is compatible with the Riedel fault model composed of P and P' fractures globally oriented E-W and SE-NW respectively. An integration of this fault in the regional lineament is compatible with the Tcholliré-Banyo Shear Zone (TBSZ) situated in the north of Adamaoua Shear Zone.

Petrographically, the mega-quartz vein shows a micropegmatitic texture with quartz as main mineral on which is observed the aqueous brine inclusion. These inclusions, elongated with less than 5 to 10 µm in length, are typically arranged in linear trails indicating a likely secondary origin. Centimetric-metric xenoliths of basement rocks are found in the quartz vein and some xenolith samples present pyrite crystals. The petrographic observation of basement rock has been carry on orthogneiss that contains perthitic orthoclase, microcline, plagioclase, quartz, biotite, green hornblende and accessory minerals such as zircon, sphene, apatite, and with granoblastic hetero-granular to mylonitic texture.

Geochemical analyses of mega-vein samples indicate very high SiO_2 contents with more than 98.68% and that could be used in the industry. The quartz lodes within a shear zone might evidence of an important hydrothermal system deriving from the circulation of large volume of fluid. The origin of quartz vein could be linked to hydrothermal fluids resulting from the dehydration of minerals such as biotite and amphibole in the basement rock during deformation with a contribution of meteoric water however more analyses is required to clarify this hypothesis.

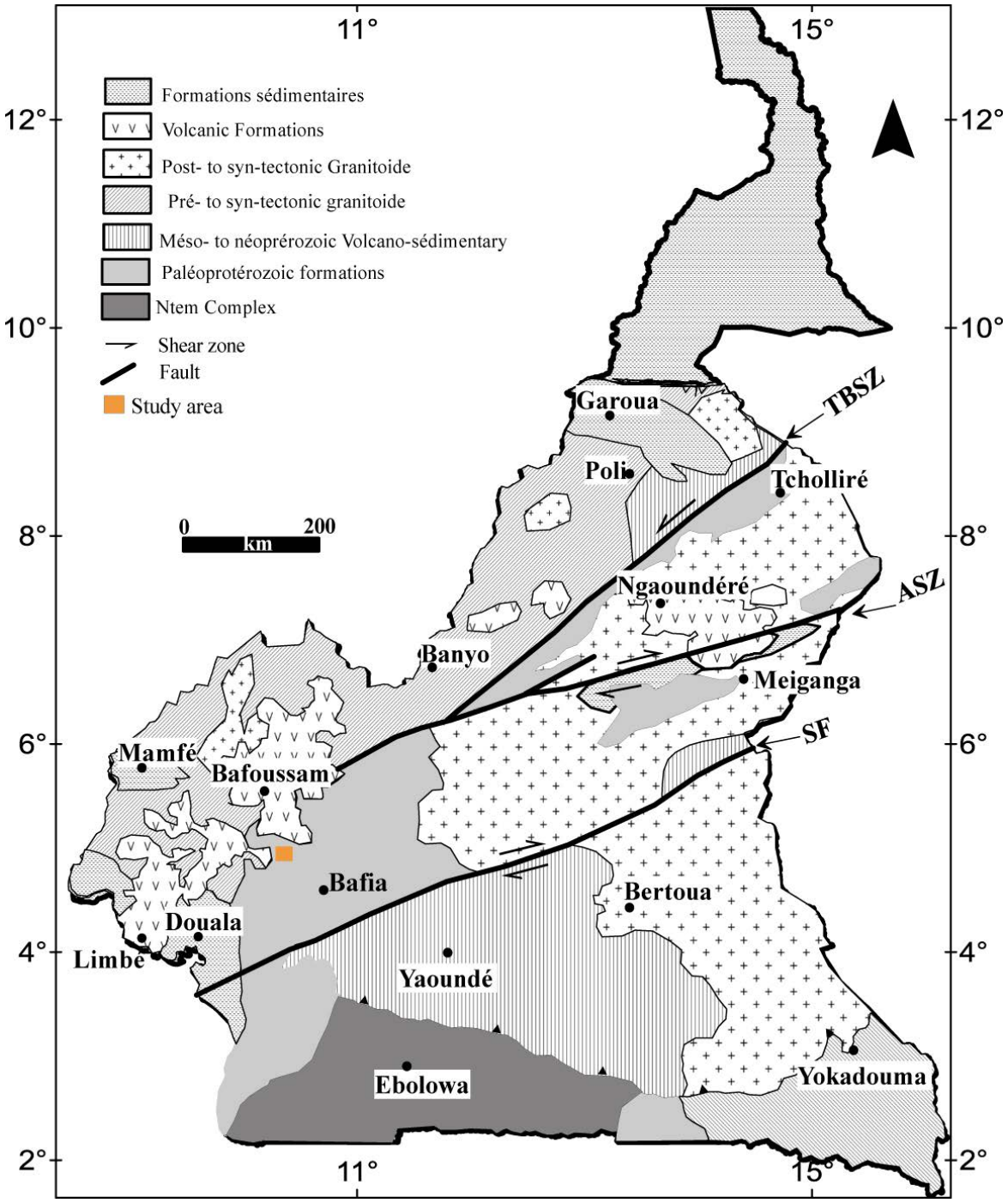
11°
15°
12°
10°
8°
6°
4°
2°
Formations sédimentaires
Volcanic Formations
Post- to syn-tectonic Granitoide
Pré- to syn-tectonic granitoide
Méso- to néoprérozoic Volcano-sédimentary
Paléoprotérozoic formations
Ntem Complex
Shear zone
Fault
Study area
0
200
km
Garoua
Poli
Tcholliré
TBSZ
Ngaoundéré
ASZ
Banyo
Meiganga
SF
Mamfé
Bafoussam
Bafia
Bertoua
Douala
Limbé
Yaoundé
Ebolowa
Yokadouma

A | 70

METALLOGENIC IMPLICATIONS OF REDEFINING THE UPPER PALEOZOIC MAGMATISM IN ARGENTINA: TECTONIC SETTINGS AND RELATED DEPOSIT MODELS

Eduardo O. Zappettini[1], Carlos J. Chernicoff

[1]Servicio Geológico Minero Argentino - eduardo.zappettini@segemar.gov.ar

The Upper Paleozoic Gondwanan magmatic belt extends discontinuously along the western margin of Gondwana in South America, in Argentina stretching from the Puna region to Patagonia.

The recent re-evaluation of the Permo-Triassic Intracratonic Magmatic Belt of La Pampa (ICMB), south-central Argentina (Chernicoff *et al.*, 2018, submitted), allowed to separate this magmatic belt from the peri-Gondwanan magmatism which, on tectonic grounds, in turn was split in two different magmatic belts (figure 1).

The first is the Choiyoi Magmatic Belt (involving arc and back-arc magmatism) extending in Argentina from the north in the Puna region, south into the Frontal Cordillera, San Rafael Block and the basement of the Neuquina Basin (Main Cordillera). The second belt, namely the Norpatagonian Gondwanides, is viewed to be temporally and spatially independent from the Choiyoi Belt due to a contrasting evolution -i.e. accretionary character of the Choiyoi Belt versus collisional character of the Nordpatagonian Gondwanides belt, including different orientation (N-S vs. E-W) and polarity (eastward vs. southward) of the associated paleo-subduction in either case-. This new model differs from the most accepted concept of a transitional evolution between these two belts (e.g. Kleiman and Japas, 2009), and provides a new tectonic framework that allows to better understand the relationship between the different Upper Paleozoic magmatic belts and the genetically related mineralizations in the various stages of their tectonic evolution as well as to define permissive tracts for exploration of new deposit types.

The Choiyoi Magmatic Belt has a prominent N-S orientation. This belt involves magmatic arc rocks of Upper Carboniferous to Lower Permian age with related Porphyry Copper deposits (from North to South: Carrizal, Alcaparrosa, Yalguaraz, San Jorge, Infiernillo, La Voluntad) as well as epithermal Au-rich veins (Castaño Nuevo, Don Sixto). The postorogenic magmatic event that occurs during the Upper Permian to the Lower Triassic has a peraluminous character and related mineralizations include Tungsten veins (La Josefina). A final extensional event is characterized by Pb-Ag-Zn simple veins (Castaño Viejo, Paramillos de Uspallata), five-elements type deposits (Carrizal, Cacheuta) and fluorine deposits (Yaucha, San Rafael district) (Zappettini *et al.*, 2017).

To the south, the Northpatagonian Gondwanides constitutes a mostly E-W belt developed in the North Patagonian Massif, in an arc to collisional tectonic setting involving Tungsten veins (San Martín) related to the

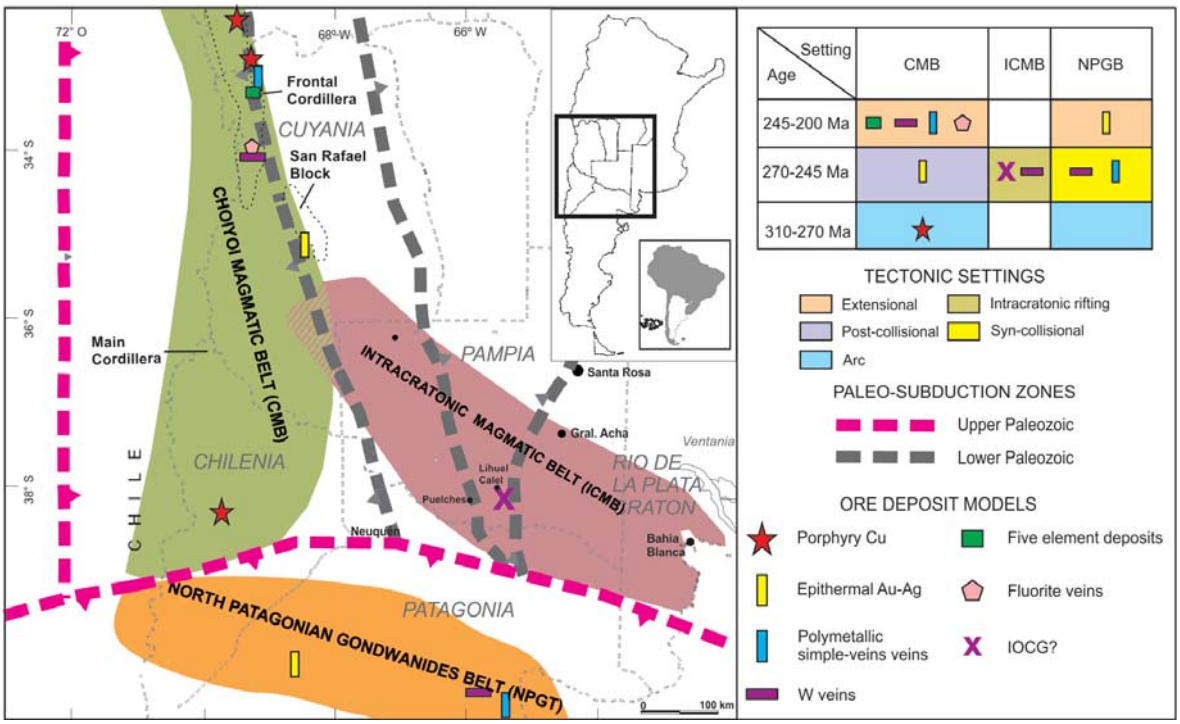

Figure 1. Tectonic context of the Gondwanan magmatic belts of central Argentina (modified after Chernicoff *et al.*, 2018, and references therein), and associated ore deposits.

orogenic stage. Late extensional events during the Triassic is represented by an acidic volcanic activity, with associated Au-rich epithermal veins (Los Menucos, Calcatreu). In this belt unmineralized arc-related intrusions have been identified, which allow to define a permissive tract for porphyry Cu prospection.

A third, mostly unexplored belt has been defined in the La Pampa Province. This has recently been unlinked from the tectonic setting and evolution of the two previously described belts (Chernicoff *et al.*, 2018). An extensive Quaternary cover characterizes the La Pampa province which shows few (less than 5%) rock outcrops. Of these, the exposures of Gondwanan magmatism stands out, and consists of rhyolitic ignimbrites and peraluminous granites generated in an anorogenic to aborted-rift setting. Exposed mineralization is almost unknown, except for an underexplored minor occurrence of a Cu-Fe vein type deposit consisting of hematite and Cu sulfides (Lihue Calel). The tectonic setting and the various geophysical anomalies identified in this area have been interpreted as covered granitic stocks related to the Upper Paleozoic magmatic belt (Chernicoff and Zappettini, 2004), allowing to define a permissive tract for prospecting various deposit models, such as IOCG, Tungsten veins and REE alkaline-related veins. Future multielement geochemical exploration combined with airborne geophysical data interpretation, could improve the definition of exploration targets.

REFERENCES

Chernicoff, C.J. and E.O. Zappettini, 2004. Geophysical evidence for terraneboundaries in south-central Argentina. en Volúmen Especial "Cuyania, an exotic block to Gondwana", Gondwana Research V. 7 N° 4: 1105-1116. ISSN: 1342-937X.

Chernicoff, C.J., E.O. Zappettini, J.O. Santos and N. McNaughton, 2018. El Corredor Magmático Intracratónico Pérmico-Triásico de la provincia de La Pampa, Argentina: nuevas edades U-Pb SHRIMP, composición isotópica de Hf e implicancias geodinámicas. Revista Mexicana de Ciencias Geológicas, submitted.

Kleiman, L.E. and M.S. Japas, 2009, The Choiyoi volcanic province at 34°-36°S (San Rafael, Mendoza, Argentina): implications for the late Paleozoic evolution of the southwestern margin of Gondwana: Tectonophysics, 473, 283-299.

Zappettini, E.O., N. Rubinstein, S. Crosta and S.J. Segal, 2017. Intracontinental rift-related deposits: A review of key models. Ore Geology Reviews 89: 594–608.

A | 71

METALLOGENY OF THE WESTERN PART OF THE YANA-KOLYMA GOLD-BEARING BELT, NORTHEAST RUSSIA

Fridovsky Valery[1], Gamyanin Gennady, Kudrin Maxim

[1]*Diamond and Precious Metal Geology Institute, SB PAS - 710933@list.ru*

The study was conducted in the western part of the Yana-Kolyma gold-bearing belt using the Adycha-Taryn metallogenic zone as an example. The zone is traced northwesterly for 600 km and has a width ranging up to 45 km. It is among the most productive zones of the Yana- Kolyma gold-bearing belt with regard to the number and variety of precious metal deposits. The zone is located at the boundary between the Kular-Nera slate belt and the Verkhoyansk fold-and-thrust belt. The major tectonic structure controlling the zone position is the Adycha-Taryn Fault. It separates tectonic features with different structure and intensity of magmatic rocks, and controls spatial position of deposits. The Adycha-Taryn zone underwent several geodynamic and metallogenic events characteristic of the Late Mesozoic geological history of the outer zone of the Pacific ore belt.

Geological-structural, mineralogical-geochemical and isotopic-geochronological methods of investigation were used.

The Adycha-Taryn zone is specialized for Au-Q (Au-S-Q), Au-Bi, Au-Sb and Ag-Sb mineralizations related to different stages of the tectonic-magmatic development of the area (table).

Gold-quartz and gold-sulfide-quartz types. The commercial gold mineralization of the Adycha-Taryn metallogenic zone belongs to gold-quartz and gold-sulfide-quartz types. Formation of the mineralization is related to accretion and subsequent collision of the Kolyma-Omolon microcontinent against to eastern margin of the North Asian craton. The mineralization is associated with Tithonian-Valanginian granitoids and dikes of the Nera- Bokhapcha Complex. The Ar-Ar age of the deposits formation is 142.7±1.4 – 126.6±2.4. Ma. This is 1-16 Ma later than the emplacement age of granitoids of the Main and Tas-Kystabyt belts and volcanites of the Uyandina-Yasachnaya belt. Distribution of gold-quartz and gold- sulfide-quartz deposits is controlled by high-amplitude extensive thrusts and, less frequently, cross strike-slip faults separating blocks with different geological structure and tectonic history. The ore bodies at the deposits include mineralized fault zones (Bazovskoye, Drazhnoye, Malo-Tarynskoye), quartz vein bodies of simple lens-like form (Sana, Dirin- Yuryakh, Imtachan), and veins in the crests of folds (Pil', Talalakh, Zhdannoye). Gold-quartz low-sulfide mineralization is widespread in the Adycha-Taryn metallogenic zone. Mineral composition of the ore bodies is uniform: 85-95% quartz, 5-15% carbonate (ankerite), and ~1% ore minerals. A successive series of mineral assemblages is recognized in the ores: pyrite-arsenopyrite-sericite-quartz metasomatic, pyrite-arsenopyrite-quartz vein, gold- chalcopyrite-sphalerite-galena, and sulfosalt-carbonate ores.

Table. Characterization of noble metal deposits in the Adycha-Taryn metallogenic zone

Characteristics of deposits	Low-sulfide gold-quartz	Gold-bismuth	Gold-antimony	Silver-antimony
Geodynamic setting	Accretionary		Post-accretionary	
Structural paragenesis	Zones of intense fold and fault deformations of NW strike, concentric folds with subhorizontal hinges, boudinage, fault cleavage	Structures above and near intrusions, mineralized fault zones	Brittle faults, concentric and conical folds of NE strike, including axonoclines, cleavage	Brittle faults, concentric and conical folds of EW strike, including axonoclines
Host rocks	Sandstone and siltstone	Hornfels, granitoids, sandstone, siltstone	Sandstone and siltstone	Dacite, sandstone and siltstone
Morphology of ore bodies	Veins, vein-veinlet, and veinlet-disseminated zones	Quartz, tourmaline, muscovite	Quartz, ankerite, sericite, dickite, paragonite, pyrophyllite	Quartz, dickite, calcite
Ore minerals	Pyrite, arsenopyrite, chalcopyrite, sphalerite, galena, tetrahedrite, meneghinite, boulangerite jamesonite, cholestybite	Wolframite, arsenopyrite, loellingite, donaite, bismuthine, tetradymite, joseite A and B, werlite, tellurobismutite	Antimonite, pyrite, arsenopyrite, berthierite, sphalerite, galena, chalcopyrite, tetrahedrite, jamesonite	Arsenopyrite, pyrite, sphalerite, gudmundite, chalcopyrite, freibergite, pyrarhyrite, berthierite, antimonite
Main productive mineral association	Gold-chalcopyrite- spharelite-galena	Loellingite-glaucodot-arsenopyrite, bismuthine-sulfotelluride	Quartz-antimonite- berthierite	Freibergite-silver-antimony
Geochemical association of elements	Au, As, Sb, Ag, Cu, Zn, Pb, Li	Au, Bi, W, As, Te, Sn, In, Cd	Au, As, Sb, Ag	Ag, As, Sb
Examples of deposits	Bazovskoye, Drazhnoye, Malo-Tarynskoye, Levoberezhnoye, Talalakh	Ergelyakh	Maltan, Sarylakh, Sentachan, Tan	Dichek, Sakhchan, Serp

Gold-bismuth type. These intrusion-related deposits are localized directly in small granitoid stocks or in their hornfels aureoles as well as in dikes of varying composition (granite- porphyry, porphyrite, diabase). In the Adycha-Taryn metallogenic zone, belonging to the gold-bismuth type is the Ergelyakh deposit localized above the cupola of a granitoid pluton. Gold-bismuth mineralizarion is established at polychronous orogenic gold-quartz and gold- sulfide-quartz deposits. The gold-bismuth type is rare in occurrence. Its presence, however, suggests that tectonomagmatic activation of ore-bearing structures occurred repeatedly and that spatial association of various types of mineralization was related to intermediate magma chambers.

Gold-antimony type. Au-Sb mineralization is most widespread in the axial part of the Adycha-Taryn Fault (Sentachan, Sarylakh, Maltan, Tan, Kinyas-Yuryakh and Elgi-Tonor deposits). The presence of this mineralization is a feature that distinguishes the Adycha- Taryn metallogenic zone from other gold-bearing zones in the Yana-Kolyma belt and in the whole of northeast Russia. The antimony mineralization is superposed on the gold-quartz one, which leads to the formation of complex polygenetic gold-antimony deposits. Compositionally, the gold-antimony deposits are characterized by combination of mineral assemblages typical for low-sulfide gold-quartz deposits and a superposed berthierite- antimonite assemblage. Formation of deposits is close in time to Late Cretaceous tectonic- magmatic activation in the Okhotsk-Chukotka volcanic belt.

Silver-antimony type. This type of mineralization is superposed on gold-quartz deposits. Both types of deposits are low-sulfide. Ag concentrations in ore bodies are associated with the occurrence of freibergite-silver-sulfoantimonite assemblage.

A | 72

THE PORTAS DEPOSIT (LUGO, NW OF SPAIN): AN OROGENIC GOLD DEPOSIT RELATED TO PALEOZOIC IRONSTONES

Antonia Cepedal[1], Mercedes Fuertes-Fuente, Agustín Martín-Izard, Daniel Arias, David Aragón

[1]*Department of Geology, University of Oviedo, Spain - mcepedal@geol.uniovi.es*

Gold occurrences are abundant in the Variscan belt of NW Iberian Peninsula and, nowadays, NW Spain and Portugal are extensively prospecting for gold. This work focuses on the Portas Deposit (NW Spain, Fig. 1a), which is associated with quartz-vein systems that crosscuts Ordovician iron-rich metasediments. The aim of this study is the mineralogical characterization of the ore and accompanying minerals to obtain data on ore forming processes.

The Portas deposit is in the Iberian Massif, i.e. the Variscan belt located in the NW Iberian Peninsula. It is in the transition between foreland (West Asturian Leonese Zone, WALZ) and westwards internal areas (Central Iberian Zone) of the belt (Fig. 1a). Local Ordovician sequence is affected by three-coaxial Variscan deformation phases related to E-W shortening (D1-D3, Martínez Catalán *et al.*, 1990). The deposit is in the Sil Syncline, a major D3 structure that represents the limit of the WALZ. The succession that hosts the gold occurrence is an alternation of slates, metasandstones and quartzites, culminating in the Armorican Quartzite. Slates (Llanvirn) overlay the quartzite. Iron-rich metasediments occur in levels transitional to the Armorican Quartzite. Metamorphism is in greenschist facies. Igneous rocks close to the deposit are porphyritic dykes outcropping along Late-Variscan NW–SE faults.

Mineralized samples were taken from 3 drill-cores. Polished-thin sections were studied by optical microscopy, SEM-EDAX, EPMA (Cameca-SX100) at Oviedo University.

Host-rocks and veins. The iron-rich levels are in 5 meters-wide interbedding with quartzite, and mainly consist of chlorite, siderite, apatite and hematite, showing a banded structure outlined by disseminated pyrite (Fig. 1b). Accessory minerals are quartz, muscovite, rutile, organic matter, zircon and REE-phosphates. In addition, hematite occurs impregnating the interbedded quarzitic rocks.

There are highly-deformed quartz veins that appear crosscut by less deformed or undeformed quartz-veins with different orientations. The latter are associated with sulphides (mainly arsenopyrite and pyrite), chlorite and rutile, and produced silicification and chloritization of host-rocks. Sometimes there is a last stage of filling with carbonate and sulphides (pyrite and chalcopyrite). The youngest veins are chlorite-rich with +/- muscovite, rutile, quartz, apatite, REE-phosphates, zircon and sulphides (pyrite and chalcopyrite).

According to the EMPA, chlorite is chamosite (Fetot/(Fe+Mg)= 0.7 to 0.8). Apatite is fluorapatite (up to 3.6 wt% F) and Sr-bearing (up to 1.6 wt% SrO), and the £REE was up to 0.2 wt% (Y_2O_3+SmO+Nd_2O_3).

Metallic paragenesis. The main minerals are arsenopyrite, pyrite and rutile. In smaller proportions, there are marcasite, galena, chalcopyrite, sphalerite, pyrrhotite and gold.

Arsenopyrite occurs within quartz-veins or disseminated in host-rocks. Brittle deformation after arsenopyrite deposition developed microfractures healed by subsequent ore minerals. It composition varies from 43 to 45 wt% As, with trace amounts of Sb.

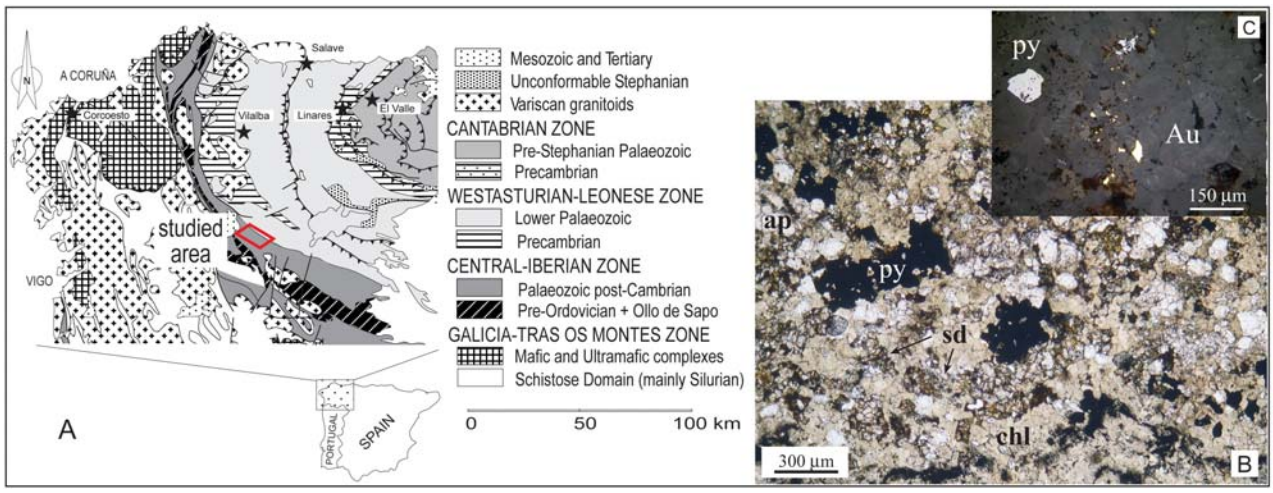

Figure 1. A) Location of the studied area. B) Iron-rich level with chlorite (chl), apatite (ap) and siderite (sd) replaced by pyrite (py). PPL. C) Detail of B), under reflected light, with gold.

Pyrite occurs associated with veins or as disseminations that can be pervasive along S0 (Fig.1b). Within quartz-veins, pyrite overgrows arsenopyrite and heals fractures in it, associated with galena, chalcopyrite, sphalerite and gold. Pervasive pyrite disseminations are related to the replacement of Fe-bearing minerals in the iron-rich levels (Fig. 1b). Siderite replacement produced fine-grained pyrite as pseudomorphs of carbonate aggregates. Replacement of hematite produced aggregates of tiny pyritohedra and prismatic crystals of pyrite, partially recrystallized. This pyrite shows the highest As content (up to 5.4 wt%) and, in two analyses, gold was above the detection limit (0.05 and 0.13 wt% Au, respectively).

Gold (10-16 wt% Ag) occurs as isolated micrograins disseminated in host-rocks (Fig. 1c). However, gold is more abundant as healing microfractures in arsenopyrite or included in pyrite, often associated with galena.

This preliminary work in Portas Deposit suggests that, at least, two main factors played a significant role in the ore deposition: the presence of iron-rich beds in the metamorphic sequence and a significant deformation. The former acted as a chemically favourable rock, and the latter generated dilatational structures that performed as conduits for hydrothermal fluids which could be metamorphic although a magmatic influence cannot be discarded. The spatial vicinity of felsic dykes, probably Late-Variscan, opens the possibility of a magmatic source for metals and fluids. In fact, several gold deposits in NW Iberian were related to Late-Variscan magmatism (e.g. Linares deposit, Cepedal *et al.*, 2013; Vilalba Gold District, Martínez-Abad *et al.*, 2015). Thus, sources of metals and fluids will be a future research in this deposit. The Portas deposit shows a strong similarity with a polymetallic mineralization hosted by Ordovician ironstones from the western French Variscan belt (Gloaguen *et al.*, 2007). The role of the Ordovician iron-rich beds in the formation of the studied gold occurrence provides a new perspective for prospecting gold since Ordovician ironstones are widespread in NW Iberian Massif and, on a large-scale, in the western European Variscan belt.

REFERENCES

Cepedal, A., Fuertes-Fuente, M., Martín-Izard, A., García-Nieto, J., Boiron, M.C., 2013. Journal of Geochemical Exploration 124, 101-126.

Gloaguen, E., Branquet, Y., Boulvais, P., Moëlo, Y., Chauvel, J.-J., Chiappero, P.-J., Marcoux, E. 2007. Mineralium Deposita 42, 399-422.

Martínez-Abad, I., Cepedal, A., Arias, D., Martín-Izard, A., 2015. Ore Geology Reviews 66, 344-365.

Martínez Catalán, J.R., Pérez-Estaún, A., Bastida, F., Pulgar, J.A., Marcos, A., 1990. In: Pre- Mesozoic Geology of Iberia (Dallmeyer, R.D., Martínez-García, E. eds.), 103-114.

GEOCHRONOLOGY OF THE SAREKOUBU GOLD DEPOSIT, SOUTHERN ALTAIDES, CHINA: AR-AR AGES OF FLUID INCLUSIONS IN VEIN QUARTZ

XU Jiuhua[1], ZHANG Hui, CHENG Xihui, BIAN Chunjing

[1]*University of Science and Technology Beijing - jiuhuaxu@ces.ustb.edu.cn*

BACKGROUND

The Sarekoubu gold deposit, located north to Altay city, is one of the vein gold deposits in the southern Altaides, Xinjiang, China. An unusual feature of fluid inclusions in this deposit is abundant for carbonic (CO2-CH4-N2)-bearing composition. Some researchers considered the deposit as a part of volcanic-sedimentary-related system (Wang *et al.*, 2000; Ding *et al.*, 2001; Yan and Chen, 2001; Jiang,2003), while others believed that the deposit was orogenic- related system because of ore-forming stages controlling by shear zones and wall rock alterations (Xu *et al.*, 2008; Qin *et al.*, 2012; Zheng *et al.*, 2013). For many years, the ore- forming ages of the deposit and the origin of the carbonic fluid inclusions have been unclear. This study presents new Ar-Ar age data of fluid inclusions in quartz of main ore stages to discuss ore-forming age and the role of the carbonic fluid inclusions in gold mineralization.

The Sarekoubu gold deposit occurs in the fractured zone which is parallel to the strata of lower Devonian Kangbutiebao Formation (D_1 k_2^2) (Fig.1A). Three hydrothermal mineralizing stages can be distinguished: (I) disseminated pyrite and white quartz vein stage; (II) fine quartz and pyrite veinlet stage cutting stage I vein; and (III) grey quartz stage with polymetallic sulfides. Stages II and III comprise the main gold mineralization stages.

METHODS

The 40Ar–39Ar dating method of fluid inclusions was described by Qiu and Dai (1989), and Qiu *et al.* (2007). The measurement for Ar-Ar age of ore-forming fluids at the Sarekoubu deposit was conducted at the Chinese Academy of Nuclear Energy Sciences (CANES) using the instrument Argus VI. Fluid inclusion thermometry (Roedder, 1984) was done at Fluid Inclusion Laboratory of University of Science and Technology Beijing (USTB).

RESULTS

Three main types of fluid inclusions can be found in the quartz veins: CO2-aqueous fluid inclusions (Type CW), carbonic fluid inclusions (Type C), and salt-aqueous fluid inclusions (Type W). The CO2-rich fluid inclusions (type CW and type C) occur both in the quartz from veins of stage'!and II. Microthermometrhic analyses indicate that the CO2-rich fluid inclusions have been trapped with the minimum temperatures ranging from 243 to 395! for the early vein quartz (stage'!), and 230 to 328! for late polysulfide quartz veins (stage III). Two gold-bearing chalcopyrite-quartz vein samples from stage III were selected for Ar-Ar age study of ore-forming fluids. One sample (SR1005) shows that fluid inclusion in mineralizing quartz has a plateau age of 208.6±3.5Ma and isochronal age of 216.9±6.7Ma (Fig.1E, 1F), and another sample (SR1001), 217.0±3.3 Ma and 218.0 ±6.3 Ma, respectively.

CONCLUSIONS

Previous studies for gold mineralization ages include 40Ar–39Ar age of 320±5Ma of quartz by neutron activation analysis (Ding *et al.*, 2001), and Rb-Sr ages of 395±39Ma of fluid inclusions in quartz (Li *et al.*, 2004). It seems that gold mineralization was related with marine volcano sedimentary event in late Devonian or tectonic deformation in Carboniferous. However, Qin *et al.*(2012) obtained 40Ar–39Ar age of 212Ma of biotite in altered rock from the Sarekoubu deposit, which is very similar with our result. Considering previous geochronology data from adjacent deposits in southern Altaides, we can deduce that the main gold mineralization of the Sarekoubu deposit was a product of regional deformation and metamorphism in the Late Permian and Triassic. The CO2 rich, low salinities, and mesothermal characteristics of the ore forming fluids for the Sarekoubu deposit (Xu *et al.*, 2005, 2015) point to a metamorphic origin.

ACKNOWLEDGEMENTS

This work is funded by National Nature Science Foundation of China (41672070, 41372096).

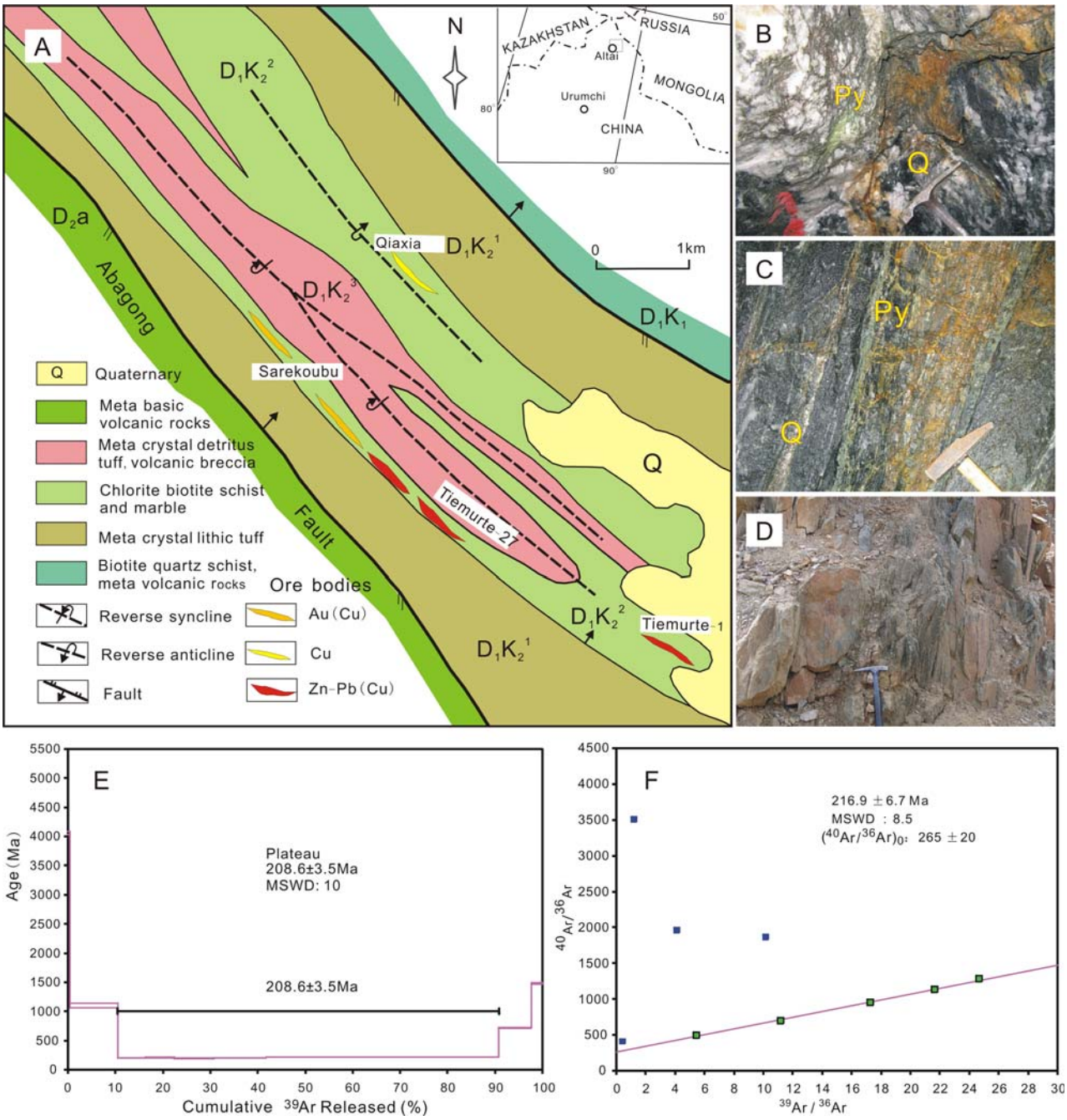

Fig.1 (A) Sketch map of the Sarekoubu area, Altay, Xinjiang, China (Modified after Xu *et al.*,2011); (B) Stage I vein of gold mineralization; (C) Stage II of gold mineralization; (D) Out crop of gold-bearing vein; (E) 40Ar-39Ar Plateau and (F) isochronal ages of fluid inclusions in vein quartz from the Sarekoubu gold deposit. (Three blue square plots are not calculated in (F) because of unreasonable low and high Ar-Ar measurement temperatures).

A | 74

3D MODELING OF STRUCTURAL CONTROLLED ORE-SHOOTS IN A HIGH SULFIDATION EPITHERMAL DEPOSIT GUANACO, NORTHERN CHILE

Luciano López[1], Sebastián Jovic, Conrado Permuy Vidal, Diego Guido, Matías Galina

[1]Consejo Nacional de Investigaciones Científicas y Técnicas, Argentina. 2Instituto de Recursos Minerales, Universidad Nacional de la Plata. Calle 64 y 120, La Plata, (1900), Argentina - lopezluciano@hotmail.com

El Guanaco mine is a high sulfidation epithermal deposit located in the Paleocene - Lower Eocene metallogenetic belt. The deposit is characterized by sub-parallel ledges and veins system formed by vuggy silica and quartz and enargite veins, located in regional ENE-WSW structural trends. The structures have a very discontinuous vein morphology with an important internal segmentation defined by ENE-WSW, E-W, WNW-ESE directions (Fig. 1A). The structural analysis of this deposit, both the tectonic environment and particularly the structural control at deposit scale and mineralized structures, allows us to recognize the different segmentations within trends of structures, defining the sizes, horizontal and vertical continuity, and degree of connection between segments of different orientations, as well as determining the orientations with greater permeability and greater development of mineralized structures and ore shoots (Fig. 1B), thus generating an optimization in the exploration of this type of structures.

METHODOLOGY

The three-dimensional model was produced using Leapfrog Geo 4.2.3. The sources to produce the solids of each ledge were a drill-hole database of the entire project, with information of the spatial position of collar, survey, assay (geochemical analysis of Au, Ag and Cu), lithology and mineralization. More than 100 drill-holes, most of it RC and few DDH, allow to obtain around 2200 samples. 350 channels sampled in underground mine were also used to interpolate the Au values in the ledges.

A lithology-mineralization surface map was used as well as maps of the levels 2610, 2626 and 2650 m of the galleries of the underground mine. To generate the solid of the ledges these maps were used as well as cross section interpretation of the ledges. These sections were uploaded to the software and were used to discriminate the limits and trends of the ledges. Ledge geometries are complex due alteration of host rock. Braided morphologies are common and the interpretation of joining and splits are difficult. Maps of the levels were useful to generate a robust interpretation of the ledges.

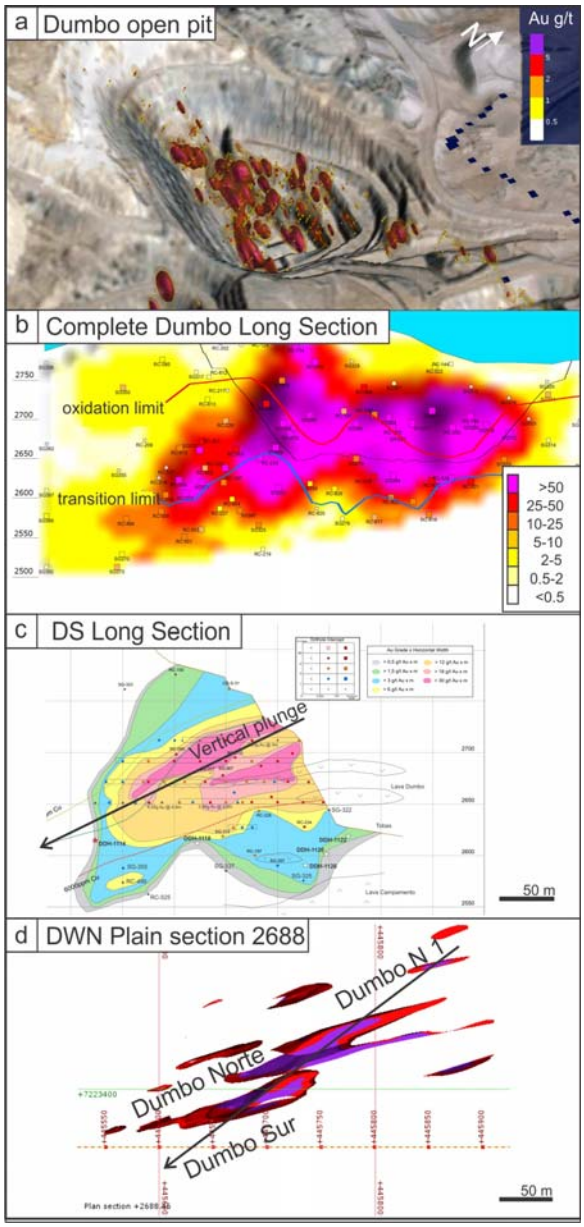

RESULTS

A total of 14 ledges of the Dumbo Oeste Norte sector were modelled, and grouped into three ledge systems, Dumbo Oeste Norte, Dumbo Oeste Norte 1 and Dumbo Sur. These structures were modelled as a vein system due the semi-planar geometry and because the vein system allows to generate geological associations. These ledges were used as hard boundaries for the Au interpolation. The intervals of the interpolation were <0,5, 1, 2, 4 and >4. The spatial distribution of Au exhibits a pattern in each ledge, and a vectorization of the ore-shoots can be established in each ledge.

Dumbo Norte 1 (DN1) gathers 4 ledges and shows a N69 strike and dips 75° N. This system were modelled 600 m in length and about 400 m in a vertical section. Width of the

ledge ranges between 7.5 and 11 m. Even though the ledge splits and joins, the Au highest concentration exhibits a similar arrangement: an ore shoot in the level 2725 masl to the eastern sector of the ledge and a second ore shoot at 2630 masl. The plunge of the ore-shoot of 25° to the SW can be defined along the ledges.

Dumbo Norte (DN) group 4 ledges too, it is sub-parallel to DWN1 with a strike and dip of N74/81N. Three high grade Au zones can be identified in the levels 2770, 2700 and 2625. A general plunge is 27° to the west.

Dumbo Sur system is formed by 6 ledges with strike and dip ranging from N66 to N86 and dips from 80 to 90°. The distribution of the ore shoots in this system is more complex and four high grade zones in the ledges can be assigned at level 2790, 2690, 2650 and 2580. Despite the complex distribution of the high grade zones, a plunge of 26° (Fig. 1C) can be defined in a vertical section.

CONCLUSIONS

The model of the Au intervals in the 14 ledges allow us to define an average ore-shoot for each ledge. Additionally, the possibility to examine the ledges in a 3D environment made possible to define a more general plunge with a strike of N79° and a dip of 29° (Fig. 1D), with the integration of the 14 ledges. The ore-shoots appear deeper to the west along a single ledge and also deeper from north to south when all ledges are analyzed. Gold distribution in the ledges is irregular and extensive zones in the ledges are barren. The exploration of the mine is focused in the identification of these ore-shoots with significantly high gold values.

CHAPTER 7
GEOCHEMISTRY OF ORE FORMING FLUIDS

Convenor: Daniel Moncada

SULFUR AND OXYGEN ISOTOPE CHARACTERISTICS OF TURKISH VMS DEPOSITS

Emin Ciftci[1], Yýlmaz Demir, Abdurrahman Lermi, Gülcan Bozkaya, Nurullah Hanilçi

[1]*Istanbul Technical University - eciftci@itu.edu.tr*

BACKGROUND

Volcanogenic massive sulfide (VMS) deposits occurring in association with the Upper Cretaceous felsic volcanic rocks of the eastern Pontides, considered to be a paleo-arc, are one of the major ore districts of Turkey and subject to numerous studies up to date. These deposits occur in the intra-arc rift zone running parallel to the current coastal line of Black Sea. Although there are various sub-types, the VMS deposits of the region are mainly Cu-Zn- type varying in size (up to a few ten million tonnes) and grades.

In order to characterize the ore forming fluids, sulfur and oxygen isotopic composition of the main ore and associated gangue minerals were studied. These deposits resemble the Kuroko deposits of Japan in many aspects. Thus, these are considered to be "Kuroko-type".

METHODS

Sulfide minerals including pyrite, sphalerite, galena and bornite and sulfate minerals including barite and gypsum were prepared under stereomicroscope for sulfur isotope analyses. Studied samples were acquired from the major VMS deposits of Eastern Pontides belt (northeastern Turkey) . Samples were analyzed at the University of Georgia Department of Geology stable isotope lab (USA) and Iso-Analytical Isotope Lab (UK). To conduct the study, about 50 samples were analyzed. Samples are ground together with V_2O_5, SiO_2, and Cu powders, packed with quartz wool into quartz glass tubes and reacted under vacuum at 1050°C. SO_2 is extracted using a conventional vacuum line equipped with a variable temperature trap. Purified SO_2 is analyzed on a Finnigan MAT 252 mass spectrometer. Laboratory standards are prepared and analyzed with each batch of samples. These standards have been calibrated to reference materials IAEA-S1 ($\delta^{34}S$ = -0.3) and NBS-123 ($\delta^{34}S$ = +17.4). Sample isotopic results are normalized to these standards using a two-point scale, thus $\delta^{34}S$ values are reported relative to VCDT. The 2-sigma of the extraction + analysis is 0.14 for $\delta^{34}S$.2

Oxygen isotope analyses were acquired for quartz gangue that are hand-picked using a twizzer under a stereomicroscope. Samples were analyzed at University of Georgia- Department of Geology stable isotope lab (USA). Samples (1-2mg) are reacted under vacuum with BrF_5 while heated with a variable power CO_2 laser (Synrad, 10510-10650 nm wavelength, 75W max power). Generated O_2 is converted to CO_2 with heated graphite, and the CO_2 is analyzed on a Finnigan MAT 252 mass spectrometer. Sample analyses each day are accompanied by standard mineral analyses. Sample results are adjusted according to the daily average of standard results. Results are reported relative to VSMOW. The 2-sigma of the extraction+analysis is 0.4 for $\delta^{18}O$ for samples yielding over 10 mmol CO . Precision may be diminished for smaller samples.

RESULTS

Data representing the major sulfide minerals vary within a fairly narrow range (-4‰ and +6‰) concentration between –0.5‰ and +4‰. Data representing the major sulfate minerals, on the other hand, range between 17.7‰ and 21.5‰. In general, samples taken from epigenetic stockwork zones within the footwall rocks show values close to zero, while the samples taken from upper zones of the orebodies – zones close to the hangingwall rocks - more oxidized zones, show larger positive values (relatively enriched in heavy sulfur).

Results indicate that magmatic sulfur was the major source however, inorganically reduced seawater sulfate and biogenically reduced sulfate could be considered for some of the deposits as is the case for many Phanerozoic VMS deposits. Sulfate sulfur isotope values are high comparable with the Cretaceous seawater.

Quartz oxygen isotope results were then processed considering the formation temperatures acquired from fluid inclusion studies to convert the data for the fluids that were in equilibrium. Results indicate that the seawater was a dominant component of the VMS mineralizing fluids.

REFERENCES

Valley, J.W., Kitchen, N., Kohn, M.J., Niendorf, C.R., Spicuzza, M.J., 1995. UWG-2, a garnet standard for oxygen isotope ratios: Strategies for high precision and accuracy with laser heating. Geochimica et Cosmochimica Acta, v. 59(24), 5223-5231.

Yanagisawa, F., Sakai, H., 1983. Thermal decomposition of barium sulfate-vanadium pentaoxide-silica glass mixtures for preparation of sulfur dioxide in sulfur isotope ratio measurements. Analytical Chemistry, 55(6), 985-987.

A | 76

FLUID INCLUSIONS FROM ACTIVE AND FOSSIL HYDROTHERMAL SYSTEMS IN CHILE

Daniel Moncada

Department of Geology, University of Chile, Plaza Ercilla 803, Santiago, Chile - dmoncada@ing.uchile.cl

Our understanding of the physical and chemical processes associated with formation of both active terrestrial hydrothermal systems and their fossil equivalents has advanced significantly through a combination of studies of well-characterized deposits. Chile host numerous geothermal, epithermal precious and base metal, polymetallic, and porphyry cooper deposits. Here we describe the fluids and fluid inclusions from the north to the south of Chile. The geothermal systems of Cerro Pabellón, Irruputuncu, and Olca are located between Calama and Iquique (Northern part of Chile) at more than 4,000 meters above sea level. Thin sections from samples of these geothermal systems were examined using a petrographic microscope; fluid inclusion and mineralogical evidence for boiling of the hydrothermal fluids was recorded. Located in the same area the Collahuasi mining district is the Rosario porphyry copper-molybdenum deposit. Preliminary results shows evidence of fluid inclusions assemblages (FIAs) in quartz and were classified at room temperature: (1) Halite-bearing inclusions indicating high salinity fluids; (2) Chalcopyrite daughter mineral; (3) Liquid-rich aqueous inclusions with trapped solid; (4) Coexisting halite-bearing and vapor-rich inclusions with a broad range in liquid-to-vapor ratios indicating fluid-phase separation; (5) Coexisting liquid-rich and vapor-rich inclusions with a broad range in liquid- to-vapor ratios indicating fluid-phase separation; (6) Vapor-rich inclusions indicating flashing of the fluid. The Río-Blanco-Los Bronces porphyry Cu(-Mo) deposit is part of the Central Chilean Mio-Pliocene Metalogenic Belt and the third largest Cu deposit in the world. The petrographic analysis shows (1) Secondary vapour-rich inclusions with solids and (2) Secondary FIAs of coexisting halite-bearing and vapour-rich fluid inclusions and solids. Situated within the Coastal Range of Central Chile, the epithermal precious metal Chancón deposit shows evidence of: (1) coexisting liquid-rich and vapor-rich inclusions with a broad range in liquid-to-vapor ratios indicating fluid phase separation; (2) Vapor-rich inclusions indicating flashing of the fluid. The polymetallic Alhué mining district shows increments in Ag-Cu related to hypersaline fluids (~ 33 wt.% NaCl) in the Lorena vein. The Maqui vein shows Ag-Ba-Cu-Mn-Fe related to low salinity fluids (~ 5% wt. % NaCl). The Tribuna Este deposit shows Ag-Al-Fe-Cd related to intermediate salinities (~18 wt. % NaCl). Finally, the Chilean Patagonia hosts numerous polymetallic and epithermal resource environments, among these the Cerro Bayo District in the Aysén Region. A detailed fluid inclusion petrography, gangue mineral textural characterization and mineralization paragenesis study was conducted on the ore-bearing Fabiola and Dagny vein. Areas of most intense boiling are associated with colloform and bladed calcite textures. These observations were incorporated into a geographical information platform to define potential geospatial correlations between the fluid inclusion characteristics, gangue mineral textures, and ore grades.

FLUID INCLUSIONS CHARACTERISTICS OF TURKISH VMS DEPOSITS

Emin Ciftci[1], Gülcan Bozkaya, Nurullah Hanilçi, Yýlmaz Demir, Abdurrahman Lermi, David Banks

[1]*Istanbul Technical University - eciftci@itu.edu.tr*

ABSTRACT

Turkey sits on an orogenic belt - the Alpine-Himalayan belt. It was formed during the Alpine orogeny, extending from the Alps in Europe to the Himalayan ranges of northern India and southern China. The geological structure of Turkey is the consequence of long-lived subduction, accretion and collision events taken place during the closure of the Tethyan Ocean. Subsequently, many favorable sites for ore deposition developed in Turkey, one of which is the Eastern Pontides Tectonic Belt (EPTB), where all the Kuroko-type VMS deposits are hosted.

The VMS deposits of Turkey have been a major source of copper, to a lesser extent of zinc and lead and made important contributions to the economic development of Turkey over more than half a century. Two of the most recent discoveries, Cerattepe and Hod deposits are exceptionally rich in gold, thus, classified as Cu-Au type, although, majority of the deposits are of Cu-Zn types. Examples include important past producers (e.g. Köprübaþý (Tirebolu-Giresun), Damar, Bognari, Çarkbaþý (Murgul-Artvin), Karaerik, Aðalýk, Karýlar deposits (Espiye-Giresun), and developing producers, e.g., Cerattepe and Hod deposits (Artvin). These deposits are associated with the felsic volcanics of late Cretaceous age without exception and are formed within the axial zone of a paleo-arc environment, the eastern Pontides.

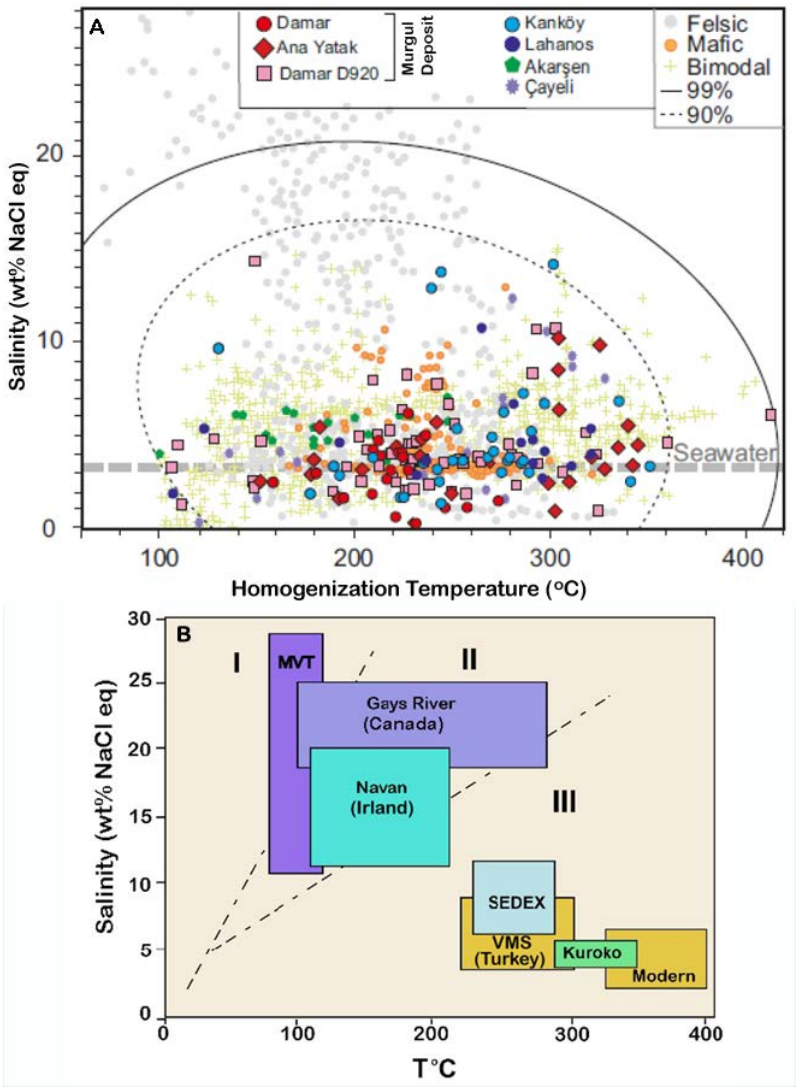

Figure 1. (A) Plot of TH – Salinity (wt% NaCl eq) for the studied Turkish VMS deposits vs. the world renowned VMS deposits (Bodnar *et al.*, 2014); (B) Comparison of the studied deposits with other hydrothermal mineralizations based on the salinity and formation temperatures (R"C).

Samples were acquired from the major volcanogenic massive sulfide (VMS) deposits occurring in northeastern Turkey. For the fluid inclusions study, mapping and measurements were carried out employing a Leica DM2500P polarized optical microscope integrated with a Linkam MDS600 fluid inclusion stage. Chips containing fluid inclusions with adequate size were selected for further LA-ICM-MS analyses. Then individual fluid inclusions in quartz, calcite and baryte were ablated with an ArF excimer laser combined in a Geolas laser ablation system. Laser ablation spot sizes were determined by the size of the inclusions and were normally either 25µm or 50µm in size. The laser was operated at 5 Hz with a fluence (energy on the sample surface) of 10 Jcm-2. The ablated material was analysed in an Agilent 7500c ICP-MS in reaction cell mode where the addition of H2 reduced the interferences on the main isotopes of Ca40 and Fe56. Ablation of inclusions continued until the analytical signal returned to the background value, usually after 15-20 seconds. Calibration of acquired elements used NIST 610 and 612 silicate glass standards and the processing used the SILLS software (Guillong *et al.*, 2008). In fluid inclusions the elements Na, Mg, K, Ca, Mn, Fe Cu, Zn, As, Sr, Sb, Ba, Pb were each analysed with a signal acquisition time of 10ms. An additional analytical program with less elements, Na, Mg, K, Ca, Si Fe, Ag, Au, and increased acquisition times for Ag and Ag was used primarily to acquire data for Ag and Au in fluid inclusions and in the host quartz.

Fluid inclusions study indicates that formation temperatures for the hydrothermals responsible of the formation of the VMS deposits of Turkey range between about 225 and 300 °C, very similar with seawater with respect to the salinity (<10 wt% NaCl eq.). Fluids are found to be prevalently in H_2O-NaCl system and fluids contain significant amount of $CaCl_2$ and $FeCl_2$. Summary of the study is presented in Figures 1a and 1b.

The composition of the fluid inclusions from different locations is dominated by Na, K and Ca with little Mg. The other elements analysed all have concentration in the 10's to a few 100's ppm in solution. There is a considerable variation in the ratio of the three main cations reflecting both the location and the type of inclusions. For Na/K ratios are grouped either around ~1 or ~0.4. Values of Na/K in calcite or baryte are much lower. Ca/K ratios are either ~0.9 or ~0.4, again in calcite and baryte they are lower than these values.

Significant analytical signals for both Au and Ag were recorded for the fluid inclusions in samples from the different locations. The signal coincides with the signal for the major elements in the fluid inclusions, Na, K etc but is not a continuous signal rather it consists of a series of signal spikes of varying intensities. This indicates that the Au and Ag are not in solution but are present as a series of sub-micron sized particles. A similar scenario is observed when the quartz veins that host the inclusions (analysed in areas where no inclusions are present and verified by a lack of significant Na, K, etc. in the quartz) are analysed for Au and Ag. The quartz was analysed for 40 seconds and a series of variable intensity Au and Ag spikes (sub-micron discrete particles) were recorded. These equate to concentration of a few 10's to over 1000 ppm Au and 1 to a few 10's ppm Ag in the quartz veins.

REFERENCES

Bodnar, R.J., Lecumberri Sanchez, P., Moncada, D., Steele MacInnis, M., 2014. Fluid Inclusions in Hydrothermal Ore Deposits. In: Holland, H.D., Turekian K.K., (eds.), Treatise on Geochemistry, Second Edition. Elsevier, Oxford, 13, pp. 119- 142.

Guillong, M., Meir, D.L., Allan, M.M., Heinrich, C.A., Yardley, B.W.D., 2008. SILLS a Matlab-based program for the reduction of laser ablation ICP-MS data of homogeneous materials and inclusions. In Sylvester, P., (Ed.), Laser Ablation ICP-MS in the Earth Sciences: Current Practices and Outstanding Issues. Mineralogical Association of Canada Short Course Series, Vancouver, pp. 328-333.

GEOCHEMICAL CHARACTERISTICS OF RARE EARTH ELEMENTS IN THE CHANGPINGZI Pb-Zn DEPOSIT, GUIZHOU PROVINCE

Ziyong Wang

Kunming University of Science and Technology - chinawangzy@sina.cn

The Changpingzi Pb-Zn deposit is located in the northwestern part of Guizhou province. The exposed strata are mainly carboniferous and also the occurrence position of lead-zinc ores. The ore-bearing rocks are mainly dolomite, biolimestone and bioclastic limestone. This research on the sources of ore-forming fluid has an important significance in understanding the ore genesis and prospecting direction. Rare earth elements (REE) have similar geochemical properties and can be used as good tracers for ore forming fluids. In this abstract, combining with the REE geochemical characteristics, the nature and evolution characteristics of ore-forming fluid are discussed.

The ore samples were analysed at the State Key Laboratory of Continental Dynamics (Northwest University). Trace and REE were determined by inductively coupled plasma mass spectrometry (ICP-MS), and the analytical precission of the method was 2%~5%.

The contents of Total REE in the ore samples range from 4.51×10^{-6} to 18.17×10^{-6} (with an average of 10.02×10^{-6}), LREE/HREE from 4.60 to 6.10, δEu from 0.76 to 3.61 (with a mean of 1.89), δCe from 0.32 to 0.70 (with a mean of 0.56), showing the characteristics of enrichment of LREE, positive anomaly of Eu, and negative anomaly of Ce. The contents of (La/Yb)N range from 4.38 to 7.85 (with a mean of 6.43), showing a distinct differentiation between heavy REE and light REE, and the chondrite-normalized REE patterns all incline to the right.

The δEu and δCe are the reactions of enrichment and depletion of Eu and Ce respectively, which are the redox-sensitive elements. Bau (1991) and Sverjensky (1984) suggested that Eu exists in the form of Eu^{3+} under normal temperature and pressure; under reduced conditions or higher temperature, it mainly exists in the form of Eu^{2+}, due to the large radius of Eu^{2+}, it is not easy to be adsorbed, resulting in relatively enriched Eu in the fluid. The positive δEu anomaly of the ore in the study area shows that it is mainly related to the relatively high temperature and reduction environment of the ore-forming fluid. Under oxidizing environment, Ce mainly exists in the form of Ce^{4+} (Lottermoser, 1992), which is difficult to dissolve, causing Ce loss in the fluid and showing negative anomaly. The northwest region of Guizhou belongs to the basin environment. The Eu and Ce in the surrounding rocks of lead-zinc deposits generally show negative anomalies, the positive anomalies of Eu and the negative anomalies of Ce in the ores in the study area indicate that the fluids with higher temperatures have mixed with seawater with lower temperatures during ore precipitation.

REFERENCES

Bau, M., 1991. Rare-earth element mobility during hydrothermal and metamorphic fluid- rock interaction and the significance of the oxidation state of europium. Chemical Geology, 93, 219-230.

Lottermoser, B.G., 1992. Rare earth elements and hydrothermal ore formation processes. Ore Geology Reviews, 7, 25-41.

Sverjensky, D.A., 1984. Europium redox equilibria in aqueous solution. Earth & Planetary Science Letters, 67, 70-78.

A | 79

STABLE ISOTOPES AND FLUID INCLUSION DATA FROM Ba-Sr ORE DEPOSITS OF THE NEUQUÉN BASIN, WEST ARGENTINA

Raúl E. de Barrio[1], Rodrigo I. Escobar, Melisa A. Salvioli, Clemente Recio, Miguel A. Del Blanco, Ricardo O. Etcheverry

[1]*Instituto de Recursos Minerales, FCNyM-UNLP - debarrio2002@yahoo.com.ar*

BACKGROUND

The Neuquén Basin is located on the eastern side of the Andes in west Argentina, between 67°-71°W and 32°-40°S. It comprises a continuous geological record about 6,000-m-thick that covers an area of approximately 120,000 km^2, near the western edge of the South American Plate, between a volcanic arc to the west and the eastern flank of the foreland.

The lithological sequence consists on clastic, carbonatic, evaporitic, pyroclastic and magmatic rocks, spanning from the Upper Triassic to the Lower Tertiary. The tectonostratigraphic history of the Neuquén Basin involves the development of several alternating marine and continental cycles, mainly during the Jurassic-Cretaceous. An important tectonomagmatic event, the andesitic magmatism represented by the Naunauco Group, developed during the Late Cretaceous-Eocene. This magmatism is represented by intrusive bodies (Colipilli Formation) and extrusive lava series (Cayanta Formation). Later (Oligocene-Miocene; Huantraico volcanics), a new basaltic-andesitic magmatism occurred in the region.

The Neuquén Basin hosts numerous carbonate and evaporite-hosted hydrothermal deposits of barite and celestine, in some cases with very minor amounts of Pb, Zn, Cu and Fe sulfides. Although often stratabound, geological evidence supports an epigenetic origin for these deposits. They are mainly formed by replacement processes of Mesozoic carbonate rocks or evaporites (Tábanos, Auquilco and Huitrín Formations) and infilling of fractures and voids. Thus, they appear in three ways: stratiform ("mantos"), veins and irregular bodies in karstic dissolution cavities.

METHODS

Sulfur and oxygen stable isotope determinations in sulfides and sulfates were performed using conventional methods at the Servicio General de Análisis de Isótopos Estables, Universidad de Salamanca, Spain. Isotope ratios were measured on a VG-Isotech SIRA II dual inlet mass spectrometer. Both internal and international reference standards were run to check accuracy and precision. Results are reported in δ notation relative to the standard Canyon Diable Troilite (CDT) for $\delta^{34}S$ and the Standard Mean Ocean Water (V-SMOW) for $\delta^{18}O$. Long-term reproducibility for repeated determination of reference samples was better than ± 0.2‰ (1δ).

The fluid inclusions were studied by petrography and microthermometry on representative crystals of celestine and barite on stratiform and vein type deposits. The microthermometric study was performed with a Linkam MDS 600 heating-cooling plate. The stage was calibrated using known melting points of solid standards on natural and synthetic fluid inclusions.

RESULTS

Sulfur and Oxygen stable isotope determinations in barite, celestine and galena of the main Ba-Sr ore deposits are listed in Table 1. In general, $\delta^{34}S$ values in sulfates are positive and high (+16/+22‰), while those in galena are negative and low. A bimodal distribution of isotopic values in sulfides (Colipilli, -10.6 / -22.7 ‰; Mallín Quemado, -1.1 / -9.0 ‰) suggest either changing precipitation conditions (Eh, pH, temperature?) or fluid mixing processes (meteoric and magmatic waters).

The $d^{18}O_{SMOW}$ values of barite and celestine from different ore deposits, both stratiform and veins range between +9.9 and +18.7‰, consistent with $d^{34}S$ values of the Jurassic- Cretaceous evaporitic rocks.

Homogenization temperatures obtained in primary fluid inclusions in celestine and barite of Bajada del Agrio and Salado Range areas range from 147° to 243°C distributed in two populations: 147-195°C and 205-247°C. The salinities vary between 0,18 and 16,67 wt% NaCl eq. with an average of 9.80 wt% NaCl eq. On the other hand, Th measured in FI of barite from the Colipilli area also are distributed in two populations: 156-176°C and 223-280°C (stratiform and vein bodies, respectively), with salinities between 0.5 and 8.3 wt% NaCl eq. Probably some low salinities recorded indicate dilution through interaction with fresh water.

CONCLUSIONS

Negative and low d34S isotope values in sulfides (mean –15 ‰) and high values in sulfates (+17/+24‰) discard magmatic sources of S in the origin of the Ba-Sr deposits. Contribution of a magmatic component is only likely at the Mallín Quemado and Loncopué areas.

Probably most of the sulfur in barite and celestine deposits derives from Mesozoic evaporites while the Sr and Ba come from the carbonate-evaporitic and siliciclastic rocks, respectively.

The FI study suggests that the mineralizing fluids were an inorganic aqueous system of calcium chloride composition with an additional organic component, both constituting a polyphase system. The occurrence of methane and cyclohexane further suggests that the evolution of the mineralizing fluids was associated with the migration of basinal waters through the sedimentary sequence and the association of such process with the maturation of hydrocarbon fluids.

Finally, the general geological and geochemical features of the barite-celestine deposits of the Neuquén Basin are similar to those of the Ba-Sr mineralizations of the Coahuila State, NE México which were considered as MVT deposits.

Districts	Mineral	Ore deposit shape	$\delta^{34}S_{CDT}$ (‰) min.	max.	aver.	$\delta^{18}O_{SMOW}$ (‰) min.	max.	aver.
Bajada del Agrio Salado Range	celestine	stratiform n=12	15.0	33.6	22.6	12.0	18.7	15.4
	barite	Vein and remobilization bodies n=21	15.8	29.2	21.5	12.6	17.7	15.9
	galena	vein n=7	-13.8	-16.9	-15.6	-	-	-
Colipilli	barite	stratiform n=8	16.8	24.1	19.6	12.0	16.8	14.3
		vein n=14	14.6	18.4	16.4	9.9	17.0	13.9
	galena	stratiform n=4	-15.6	-22.7	-18.7	-	-	-
		vein n=5	-10.6	-13.2	-11.4	-	-	-
Mallín Quemado, Loncopué Naunauco and others	celestine	stratiform	13.2	34.8	16.7	10.3	16. 8	15.0
	stratiform barite	n=5 n=5	13.8	19.4	16.7	11.4	17.4	14.8
		vein n=6	15.3	21.8	17.6	13.7	18.6	16.1
	sulfides (mainly of Pb)	stratiform n=3	-4.0	-2.8	-3.5			
		vein n=6	-9.0	-1.1	-5.4			

Table 1. $\delta^{34}S$ and $\delta^{18}O$ data of the main Ba-Sr ore deposits of the Neuquén Basin.

A | 80

CHARACTERISTICS OF DEEP-SEA MOUND ORE FORMING FLUIDS IN THE IZENA HOLE SITE, OKINAWA TROUGH, JAPAN

Thomas Tindell[1], Nobuhiro Mukae, Junro Ishibashi, Tatsuo Nozaki, Kotaro Yonezu

[1]*Kyushu University - tindell-tom@mine.kyushu-u.ac.jp*

INTRODUCTION

Japan has the sixth largest exclusive economic zone (EEZ) in the world. The existence of seafloor hydrothermal ore deposits in the area, especially in the Okinawa Trough and Izu- Bonin Arc, has sparked a flurry of exploration activity. The Japan Oil, Gas and Metals National Corporation (JOGMEC) estimates that the amount of ores from seafloor hydrothermal ore deposits, within Japans EEZ, may be more than 50 million tons. The exploration cruise CK16-05 conducted using the drilling ship D/V Chikyu was performed at the Izena Hole in the middle Okinawa Trough, as part of the project of Cross-ministerial Strategic Innovation Promotion Program (SIP), entitled as "Next-generation technology for ocean resources exploration (Zipangu in the Ocean)". A goal of this research project is to narrow down prospects of seafloor hydrothermal ore deposits.

METHODS

Six (6) core samples (C9025A, C9026A, C9027A, C9027B, C9028A and C9032A) were collected on/near the Northern mound during the CK16-05 cruise. The Northern mound location is close to that of Hole C9027A and B. These sampling points are located in a straight line from the center of the mound in an eastward direction. C9027A and B core samples are from the mound, while C9028A, C9026A, C9025A and C9032A core samples are from 50m, 80m, 200m and 250m away from the mound. This study examines cores C9026A and C9027B. Ore petrography was conducted to determine the mineral species. Fluid inclusion microthermometry was carried out to determine the mineralizing fluid characteristics.

RESULTS

(C9026A): Pyrite, marcasite, sphalerite, galena and barite were confirmed in the upper ore body. The layer between ore-bodies are mainly composed of quartz, illite/muscovite, pyrite. In the lower ore-body zone, it has various mineral assemblages: pyrite, marcasite, sphalerite, galena and barite from 46-51 mbsf, pyrite and anhydrite from 51-62 and illite/muscovite, pyrite and kaolinite from 62-65 mbsf. The existence of anhydrite indicates a mixing of seawater and ore-forming fluids and also re-charge zone for this hydrothermal system. Anhydrite may play a role of a caprock for the bottom portion of ore-body zone. Chlorite, pyrrhotite and cubanite were confirmed just below ore-body zone. Silicified rock is composed of quartz, K-feldspar and chlorite.

(C9027): From 0-20 mbsf, pyrite, sphalerite, galena and barite are confirmed. From 20-63mbsf, pyrite and chalcopyrite ± barite are observed. This difference indicates higher ore-forming fluids temperature in deeper portion.

C9026A samples are classified into 3 units as mentioned in sample description. Only pyrite was observed in pumiceous gravel/sand/mud. It mostly occurs as euhedral cubic grains. The upper ore-body zone is characterized by abundant marcasite and pyrite, moderate sphalerite, minor galena and chalcopyrite. Marcasite is often encountered as euhedral crystals or aggregates with sulfide minerals. Pumiceous mud is located between ore-body zones. Framboidal pyrite mostly occurred in the mud. In the lower ore-body zone, it is characterized by abundant pyrite, moderate to minor sphalerite and chalcopyrite, minor marcasite and galena. Euhedral marcasite crystals were not observed in the lower ore-body zone. In the ore-body zone just above silicified rock zone, the limited portion is dominantly composed of pyrrhotite and moderate to minor chalcopyrite and cubanite, minor sphalerite and pyrite. Cubanite is encountered as lamellae texture in chalcopyrite matrix. On the other hand, chalcopyrite was also encountered as lamellae texture in cubanite matrix. This lamellae texture is the result in the decomposition of cubanite into pyrrhotite and chalcopyrite. Marcasite is the dominant mineral in the upper ore-body zone. Euhedral marcasite was observed only in the upper portion of ore-body zone. This probably reflects the difference of ore-forming temperature of the ore-bodies. Moreover, the ore-forming temperature of the upper portion ore-body can be considered as under 260 °C, based on the presence of marcasite.

C9027B ores are mainly composed of dominant pyrite, minor sphalerite, chalcopyrite and galena at 0-20mbsf. Colloform marcasite was observed at only very shallow depth (~1mbsf). Pyrite mostly occurred as subhedral to euhedral grains. Pyrrhotite occurs associated with pyrite at only ~20mbsf. This result is concordant with magnetic susceptibility obtained during the CK16-05 cruise. 20-44mbsf, is mainly composed of pyrite, chalcopyrite, minor sphalerite and galena, in decending order of abundance. Chalcopyrite was mostly observed as anhedral grains, but

occurs as lamellae in a cubanite matrix at around 44mbsf, where cubanite is only observed. Pyrite is dominant in samples C9027B whereas marcasite is dominant in samples C9026B. This result indicates higher formation temperature of sulfide minerals in C9027B samples than C9026B samples.

Fluid inclusion microthermometry was conducted for fluid inclusions in sphalerite which is from 48.6mbsf (in ore-body zone) in C9026A. Fluid inclusions in sphalerite from ore-body zone occur in isolated or parallel crystal planes. All measured fluid inclusions are composed of vapor + liquid phase. Fluid inclusions in sphalerite are 7 to 50 µm in size. The vapor bubbles occupy mostly 20-40 vol.% of the inclusions. Homogenization temperatures range from 300 to 327 °C and the mode shows 300-310 °C. The salinity ranges from 4.5 to 5.3 wt. % NaCl equivalent.

The water depth is about 1600m, corresponding to hydrostatic pressures of about 16.0 MPa. The correction temperature is about 10 °C at the homogenization temperature range of 300-310 °C and salinity of 5 wt. % NaCl equivalent. Therefore, the formation temperature estimated from homogenization temperature of fluid inclusions in sphalerite is from 310-320 °C. The estimated formation temperature of sulfide minerals is much lower than boiling point (350 °C), discounting boiling during the mineralization. The temperature is slightly lower than that of directly measured temperature from active mounds. This is probably the result of lateral flow of ore-forming fluids in the sub-seafloor zone. In addition, measrued samples are located in the pumiceous mud/sand/gravel zone, which exhibits high permeability, contributing to the decreased ore-forming fluid temperature.

CONCLUSIONS

C9026A and C9027B samples are dominated by marcasite and pyrite. This result reflects the difference of formation temperature. The formation temperature of sulfide minerals was 310-320 °C in ore-body zone based on fluid inclusion microthermometry. On the other hand, much lower formation temperature of sulfide minerals can be also considered through microscopic observation.

A | 81

SIMILARITIES AND DIFFERENCES BETWEEN FLUID INCLUSIONS HOSTED BY COLOMBIAN EMERALDS

Javier García Toloza[1], Andrés Felipe González Duran, Juan Carlos Molano Mendoza, Leonardo Santacruz Reyes

[1]CDTEC - geologist@gemlabcdtec.com

INTRODUCTION

Sediment-hosted emerald deposits occur within two parallel and elongated sites (Eastern and Western Emerald Belts) along the NE trending Eastern Cordillera in Colombia. Both belts share similar features: the deposits are located in the external flanks of the Cordillera; emerald is found in hydrothermal breccias and veins hosted by strongly altered (albitized and carbonatized) lower cretaceous marine rocks, and veins are mostly made up of calcite- dolomite, albite and pyrite. Emerald mineralization has been formed by the circulation and mixing of basinal fluids with evolved evaporitic brines. The mineralizing fluids were focused in structurally favorable zones where thermochemical sulfate reactions controlled by the organic-rich wall-rocks took place; these processes led to the releasing of the essential chemical components for the emerald formation.

On the other hand, the most striking differences are about the composition of the host rocks, the age and tectonic setting of the mineralization. On the Eastern belt, the emerald- bearing veins are hosted by a stratiform brecciated level predominantly composed of gray albitites. Mineralization occurred at 65-67 Ma. and it was controlled by an extensional structural style. On the western belt, the mineralized veins and breccias are hosted by organic-rich black shales and were emplaced under the influence of a compressional tectonic phase. There is no agreement on the age of mineralization, there are ages ranging from 12 to 67 Ma.

Furthermore, emerald crystals host abundant fluid inclusions which are widely recognized by their size, complex composition and trapping conditions. As a result, the mineralizing fluids have been subject to numerous studies related to their major geochemical features, still this research has not been undertaken systematically on a regional scale. The purpose of this study was to provide a more detailed information about the physicochemical properties of the emerald-bearing fluids from different districts. A comparative analysis of the results allowed to constrain the relationship between regional events and some mineralization processes.

ANALYSIS AND SAMPLES

Methodology consisted of field work, petrography, Raman and microthermometry analyses of fluid inclusions hosted by emerald crystals. Twelve deposits were visited in order to collect emerald-bearing rock samples. Twelve samples were taken from the Eastern emerald belt in Coliflor, Tigres, Gachalá, Pulpito, Klain and Mirador, whereas ten samples were collected from the Western belt in Cunas, La Pita, Pavas, Cozcuez, Peñas Blancas and Muzo.

Fluid inclusion analyses were carried out on doubly polished emerald chips with thicknesses from 100 µm to 120 µm. Microthermometric measurements were made using a Linkam THMS 600 heating and freezing stage fitted to an Olympus BX41 microscope. All the measured homogenization temperatures were corrected and processed through the software Fluids.exe, Bakker (2003). Raman spectra of the vapour phase and daughter crystals of the inclusions were collected on a Horiba LabRAM HR Evolution microspectrometer using the 532 nm argon ion laser. The presence of CO_2, N_2, and CH_4 in three-phase inclusions was checked referencing the lines 1285, 1388, 2331, and 2917 cm»1, respectively. Daughter crystals were also identified via Raman spectroscopy. CO_2 density variations were determined by measuring the distance separating the Fermi Doublet signals of Raman spectra at 1285 and 1388 cm-1, the higher the separating distance the higher the density.

RESULTS

The average liquid-solid-vapor volume ratio of primary fluid inclusions from the two emerald belts is ~80 % liquid, composed of a complex hypersaline solution H_2O-NaCl-CO_2-(Ca-K-Mg- Fe-Li-SO_4), 12% solids and 8% vapor. The presence of volatile phases like CO_2 and N_2 is ubiquitous, whereas CH_4 is only found in the Western belt. Most of the solid phases correspond to daughter salt crystals (halite and sylvite) and minor carbonates (calcite- dolomite); however, rare earth elements and iron carbonates (parisite and siderite) were found in primary and secondary fluid inclusions in the Western belt.

On the Eastern belt, salinity ranges from 32 - 34 wt% NaCl eq. and the minimum entrapment temperature for the inclusions was approximately 190-200°C; the homogenization temperature of CO2 ranges from 16°C to 17 °C and the average distance between the Fermi doublet of the Raman spectra for CO_2 is ε102.94. On the Western belt, the salinity and the minimum entrapment temperature were higher, 36 - 38 wt% NaCl eq. and 220°C-275°C

respectively; the homogenization temperature of CO2 ranges from 18°C to 29 °C and the average distance between the Fermi doublet of the Raman spectra is ε 103.47. This data indicates there are differences in the CO_2 densities which means the entrapment pressure was different for the two belts.

CONCLUDING REMARKS

There are noticeable differences in the composition, temperature and pressure of the fluids responsible for the emerald mineralization in both Colombian belts. The presence of siderite and parisite as daughter crystals exclusively in the Western belt indicates an input of iron and rare earth elements to the system. This may be in part because of the differences of the host rocks. Since the mineralization at the Eastern belt is hosted by evaporite»bearing rocks, the salinity of the fluids was expected to be higher than in the Western belt; nevertheless, the fluid inclusions from the Western belt displayed higher salinity values. On the other hand, the interaction of the mineralizing fluids and organic- rich black shales was strongly marked at the Western belt by the occurrence of CH4 in the fluid inclusions. These facts reveal substantial differences in the chemical features of the hydrothermal solutions, which may reflect distinct regimes of fluid»rock interaction and sources of elements.

Primary fluid inclusions showed that the minimum entrapment temperature and pressure for the crystallization of emeralds were higher at the Western belt. This plainly indicates that the mineralization took place at different depths in each belt. These physical and geochemical contrasts argue for separated stages of mineralization which were driven by large-scale tectonic events.

REFERENCES

Bakker, R.J., 2003. Package FLUIDS 1. Computer programs for analysis of fluid inclusion data and for modelling bulk fluid properties. Chemical Geology, 194, 3-23.

A | 82

GEOTHERMAL FLUIDS AND MINERAL SCALES AT IRRUPPUTUNCU AND OLCA, CHILE; SEARCHING FOR STRATEGIC MINERALS

Daniel Moncada[1], Gregory De Pascale, Cristian Sprohnle M, Rodrigo Castagno

[1]*Department of Geology, University of Chile, Plaza Ercilla 803, Santiago, Chile - dmoncada@ing.uchile.cl*

Geothermal fluids contain dissolved solids under conditions of elevated temperatures and pressure. The most common components present in geothermal systems are silica, calcium carbonate in some cases precious and base metals. In geothermal systems in the Andes there is little work related to geothermal fluids and associated mineral and their use for strategic mineral exploration. In our research, we focus on two active hydrothermal systems, the Irruputuncu and Olca volcanoes which are located between Chile and Bolivia. Regional mapping shows hydrothermal alteration at the surface associated with a structural trend N-S to NW-SE fractures. The local trend shows E-W structures similar to the Altiplano uplift and deformation of the basement rocks (Reyes *et al.*, 2011).

More than 200 samples were collected from drill cores from these volcanoes. The drill cores PEM 02 and 03 from Olca shows evidence of pyrite and hematite below 400 m. The PGC 02 from Irruputuncu shows evidence of bladed calcite below 350 m and pyrite below 400m. Thin sections from samples of these cores were examined using a petrographic microscope, and fluid inclusion and mineralogical evidence for boiling of the hydrothermal fluids was recorded.This evidence included Fluid Inclusion Assemblages consisting of coexisting liquid- rich and vapor-rich inclusions, and the presence of bladed calcite and/or chalcedonic quartz. Thus, the presence of platy/bladed calcite is strong evidence for boiling in the active hydrothermal systems there. The loss of CO_2 to vapor results in the rapid precipitation of calcite, which favors formation of platy or bladed crystals rather than rhombohedral crystals that form during slower growth.

REFERENCES

Reyes, N., Vidal, A., Ramirez, E., Arnason, K., Richter, B., Steingrimsson, B., Acosta, O., Camacho, J., 2011. Geothermal exploration at Irruputuncu and Olca volcanoes: pursuing a sustainable mining development in Chile. Geothermal Resources Council Transactions, 35, 983–986.

CHAPTER 8
PRECISION GEOCHRONOLOGY AND ISOTOPE GEOLOGY OF ORE-FORMING PROCESSES: ITS IMPORTANCE IN EXPLORATION AND METALLOGENIC MODELLING

Convenor: Carlos Herrmann

THE U-Pb SYSTEMATICS OF HYDROTHERMAL HEMATITE: INSIGHTS FROM THE IOCG SYSTEM AT OLYMPIC DAM, SOUTH AUSTRALIA

Liam Courtney Davies[1], Cristiana L. Ciobanu, Simon R. Tapster, Nigel J. Cook, Kathy J. Ehrig, Allen K. Kennedy, Daniel J. Condon, Max R. Verdugo-Ihl, Benjamin S. Wade, Sarah E. Gilbert

[1]*The University of Adelaide - liam.courtney-davies@adelaide.edu.au*

BACKGROUND

Uranium-bearing minerals that have been isotopically closed since crystallization can be used to accurately constrain geologic events via the coupled U-Pb decay chain. However, the primary isotopic signature of a mineral can be easily modified, through multiple episodes of fluid exsolution, overprinting processes, regional metamorphism and protracted thermal events. Defining a chronology within complex environments such as Proterozoic ore deposits can therefore prove challenging.

The iron-oxide-Cu-Au (IOCG) deposit at Olympic Dam (OD), South Australia, is the largest publicly declared U resource. Located within the ~1.6 Ga Gawler Silicic Large Igneous Province, the deposit is entirely contained within the Olympic Dam Breccia Complex (ODBC); [1, 2], hosted and dominantly derived from the enclosing Roxby Downs Granite (RDG). The magmatic system at OD has been well constrained to ~1593 Ma, however, dating of hydrothermal mineralization has so far yielded low-resolution dates broadly coeval with the magmatism (e.g. uraninite and apatite from altered RDG and pene- contemporaneous volcanic units [3]). We aim to understand if the magmatic-hydrothermal transition can be accurately recorded in minerals that can have only a hydrothermal origin [4, 5], and are closely associated with the ores.

As has been shown at OD [6], hematite is a ubiquitous component of IOCG systems and can contain wt% levels of U, as well as elevated concentrations of W, Mo, Sn, and Pb. The occurrence of primary, often well-preserved oscillatory-zoned, U-W-Sn-Mo-bearing hematite throughout OD provides a mechanism for accurately constraining the timing of hydrothermal mineralization. This type of hematite is present throughout all ore zones and major lithologies at OD (e.g. breccias, sedimentary and volcanic rocks), occurring along the orebody's entire 6 km NW-SE strike [7] and depths of up to ~2 km. There is an intimate association between hematite-rich breccias and primary economic Cu-U-Au-Ag mineralization, which is manifested as concentric zonation with respect to sulphides [2]. Remobilisation of uranium is noted within the ODBC at scales from sub-micron upwards. Deposited as flooding, veinlets and pockets, remobilised uraninite accounts for local U enrichment and is clearly late relative to the widespread disseminations, inferring (probably multiple) processes of dissolution and re-precipitation. Therefore, understanding the principal sources and timing of metal introduction relative to the ~1.6 Ga primary magmatic-hydrothermal event is pivotal in understanding the genesis of OD, as remobilisation or isotopic resetting of minerals may be misinterpreted as new metal influxes and late mineralization events.

The potential of zoned hematite at OD for U-Pb geochronology was first recognised in a reconnaissance geochronological study [6]. Calibration with a non-matrix-matched reference material restricted full assessment of dating accuracy, however, 207Pb/206Pb weighted mean laser-ablation inductively-coupled-plasma mass-spectrometry (LA-ICP-MS) dates broadly tied hematite mineralization as coeval to the RDG. Further LA-ICP-MS studies [8], complemented previous work, but did not critically improve temporal constraints. The biggest obstacle for routine U-Pb hematite dating is the lack of homogeneous reference materials. We have therefore implemented isotope-dilution thermal-ionization-mass- spectrometry (ID-TIMS) to constrain robust ages at OD. Through combined U-Pb isotope- mapping (LA-ICP-MS) and ID-TIMS, targeted grain domains in Proterozoic samples can provide accurate ages down to ~0.05% precision. Data features such as common Pb, discordancy, and reverse discordance are assessed, their mechanisms proposed, and the analytical precision achievable at different resolutions at OD defined.

METHODS

Elevated concentrations of U in hematite can be directly imaged under backscattered electron imaging by scanning electron microscopy, which enables selective targeting of U- rich and inclusion-free domains within grains, ranging from tens of Mm to cm in size. The combination of LA-ICP-MS spot-analysis/mapping, sensitive high-resolution ion microprobe (SHRIMP) and ID-TIMS, allows investigation into the U-Pb systematics of hematite at different analytical and spatial resolutions. Isotopic measurements were collected at Adelaide Microscopy (LA-ICP-MS), Curtin University (SHRIMP) and the British Geological Survey (ID-TIMS). The developing, experimental approach to hematite isotope-dilution required micro-sampling of grains in-situ, by ablating trenches to form ~100 x 100 Mm squares within polished blocks which could be manually extracted under a microscope.

RESULTS AND DISCUSSION

Hematite 207Pb/206Pb weighted mean ID-TIMS ages can be used to interpret ore forming events to a precision of ~0.05%, compared to >1% for microbeam techniques (LA-ICP-MS and SHRIMP). However, as with any mineral, some are subject to chemical overprinting effects yielding lower resolution data. Isotope mapping demonstrates the susceptibility of zoned hematite to overprinting, with low-U, high-common Pb domains affected by fluid- mineral interactions. Potential Pb-diffusion from high- to low-U zones can also be imaged using LA-ICP-MS, where excess, unsupported radiogenic Pb produces reverse discordance.

Nevertheless, in the best-case scenarios, ID-TIMS yields a 207Pb/206Pb hematite weighted mean age of 1592.1 ± 0.88 Ma (MSWD=0.52, n=5), signifying pene-contemporaneous mineralization after RDG crystallization (1593.9 ± 0.4 Ma; [9]), while near-concordant ID- TIMS aliquots point towards negligible disturbance of the U-Pb system. Furthermore, the lifespan of the major mineralizing event is demonstrated to be short when using hematite as a proxy, as there is no robust divergence in age from ~1590 Ma. This does not however rule out mineralization post-dating the oscillatory-zoned hematite but is representative of the bulk of Cu-U mineralization. The ubiquitous presence of hematite within the orebody, and the fact that many subsequent hematite types at OD can be tied to replacement of the zoned type, clearly indicate that the U resource is associated with the magmatic-hydrothermal IOCG system at OD rather than other exotic sources. Dating of zoned hematite in sandstones from a depth of ~1.6 km yields ~1590 Ma dates. Such sediments may be older than the ODBC, and entrapped within the RDG during uplift and brecciation, supporting a deep, rather than shallow granite emplacement.

CONCLUSIONS

The key to robust temporal interpretations, particularly for deposits like OD, is a well- constrained magmatic U-Pb framework combined with a sufficiently large n sample set of hydrothermal grains. This enables interpretation of different, deposit-wide processes, which is rapidly achievable with hematite. Iron-oxide minerals, including magnetite, can become important tools for directly dating mineralization in ore deposits, particularly where other datable minerals are either absent, metamict or not representative of the ore-forming event. The ubiquitous presence of hematite in IOCG deposits, as well as banded iron formation deposits, suggests it has far reaching value in both old, and new, ore deposit research.

REFERENCES

Apukhtina O. B., Kamenetsky V. S., Ehrig, K., Kamenetsky, M. B., Maas, R., Thompson, J., McPhie, J., Ciobanu, C. L., Cook N. J., 2017. Early, deep magnetite-fluorapatite mineralization at the olympic dam cu-u-au-ag deposit, south australia. Economic Geology 112, 1531-1542.

Ciobanua C. L., Wadec B. P., Cook N. J., Schmidt M. A., Giles, D., 2013. Uranium-bearing hematite from the Olympic Dam Cu–U–Au deposit, South Australia: A geochemical tracer and reconnaissance Pb–Pb geochronometer. Precambrian Research, 238, 129-147.

Courtney-Davies, L., Zhu, Z., Ciobanu, C. L., Wade, B.P., Cook, N.J., Ehrig, K., 2016. Matrix-matched iron-oxide laser ablation ICP-MS U–Pb geochronology using mixed solution standards. Minerals, 6 (3), 85.

Ehrig, K., McPhie, J., Kamenetsky, V., 2012. Geology and mineralogical zonation of the Olympic Dam iron oxide Cu-U-Au-Ag deposit, South Australia, In: Hedenquist, J.W., Harris, M., F. Camus (Eds.), Geology and Genesis of Major Copper Deposits and Districts of the World. SEG Special Publication 16, 237-268.

Jagodzinski, E.A., 2016. http://minerals.statedevelopment.sa.gov.au/latest_ updates /mineral_ systems_ drilling_ program _ open_day_presentations.

Krneta, S., Ciobanu, C., Cook, N., Ehrig, K., Kontonikas Charos, A., 2017. Rare Earth Element Behaviour in Apatite from the Olympic Dam Cu–U–Au–Ag Deposit, South Australia. Minerals, 7, 135.

Macmillan, E., Ciobanu, C.L., Ehrig, K., Cook, N.J., and Pring, A., 2016. Chemical zoning and lattice distortion in uraninite from Olympic Dam, South Australia. American Mineralogist, 101, 2351–2354.

Reeve JS, Cross KC, Smith RN & Oreskes N. 1990. Olympic Dam copper-uranium-gold deposit. In: Hughes FE (ed), Geology of the Mineral Deposits of Australia and Papua New Guinea. The Australasian Institute of Mining and Metallurgy, 1009-1035.

Verdugo Ihl, M., Ciobanu, C., Cook, N., Ehrig, K., Courtney-Davies, L., Gilbert, S., 2017. Textures and U-W-Sn-Mo signatures in hematite from the Olympic Dam Cu-U-Au-Ag deposit, South Australia: Defining the archetype for IOCG deposits. Ore Geology Reviews, 10, 1016.

Re-Os AND U-Pb GEOCHRONOLOGY OF Cu-Mo (-W) PORPHYRY-STYLE, ORE-FORMING PROCESSES - AN EXAMPLE FROM THE FORELAND, VARISCAN OROGENIC BELT, POLAND

Mikulski Stanislaw Z.[1], Stein Holly J., Williams Ian S., Markowiak Marek

[1]*Polish Geological Institute-National Research Institute - stanislaw.mikulski@pgi.gov.pl*

GEOLOGIC BACKGROUND OF Cu-Mo (-W) PORPHYRY-STYLE ORE MINERALIZATION

The study area is in southern Poland located along the regional Kraków-Lubliniec Fault Zone (KLFZ), which separates the Upper Silesia Block (part of the Brunovistulian composite Terrane) and Malopolska Block (a thinned marginal part of Baltica), and constitutes the foreland of the Variscan orogenic belt in the central part of Europe. The KLFZ runs parallel to the Trans-European Suture Zone (TESZ), one of the most important composite suture zones in Europe. Here, extensive plutonic and volcanic activity resulted from the amalgamation of the Malopolska and Brunovistulian terranes during the Carboniferous- Permian. In the KLFZ under Mesozoic-Cenozoic platform cover, the Myszków Cu-Mo(-W) porphyry-type deposit and several very prospective areas for other porphyry-, skarn-contact metasomatic, and vein-type deposits have been recognized. All are genetically related to Variscan felsic magmatism and hosted by Ediacaran-Palaeozoic sediments and igneous rocks.

In the Myszków deposit anticipated economic resources of ores down to a depth of 1,000 m are estimated at >550 Mt, with 0.295 Mt of Mo, 0.238 Mt of W, and 0.8 Mt of Cu, with anticipated sub-economic resources at 0.298 Mt of Mo, 0.212 Mt of W, and 0.771 Mt of Cu.

The Myszków deposit has not yet been exploited. Its ore mineralization is mostly as stockwork, forming a system of quartz veins with ore minerals, sulfides (molybdenite, chalcopyrite, and pyrite) and oxides (scheelite, magnetite and/or ilmenite). Geochemically, felsic rocks (granitoids and dacitoids) are peraluminous, calc-alkaline, and medium-K to high-K with moderate Mg (0.39-0.46). The granitoids are classified as I-type magmatic rocks, and were emplaced in a post-collisional environment. Ore-hosting rocks are often strongly altered to varying degrees, mainly by sericitization, carbonatization, chloritization, silicification, feldspathization, epidotization, oxidation, argillitization, and sulfidization. Some intervals are more intensely mineralized with numerous generations of quartz veinlets with molybdenite, pyrite, and chalcopyrite, as well as locally with Pb-Zn-Fe, Au-Ag, and Bi- Te and /or younger REE mineralization. The dominant igneous rocks in the KLFZ are those of felsic composition; granodiorites and dacitoids. Rocks of intermediate to mafic composition, represented by dykes of lamprophyre and/or diabase, are less abundant.

Investigation of magmatic zircon by U-Pb SHRIMP and molybdenite by Re-Os Geochronology for igneous rocks from the KLFZ is sparse using modern U-Pb SHRIMP methods. Until now, age relationships between rocks and mineralization have not been explored. For U-Pb isotopic dating we selected magmatic zircons from 16 different igneous rock samples from the archive boreholes located in mineralized areas in KLFZ. The sensitive high-resolution ion microprobe (SHRIMP) analyses were done at the Research School of Earth Sciences, Australian National University. Re and Os isotopic data for 17 samples of molybdenites from the Myszków deposit and prospective areas in KLFZ were determined by the AIRIE Program, Colorado State University.

Zircon U-Pb isotopic measurements on felsic igneous rocks yields ages from 303.8 ± 2.2 to 294.7 ± 2.3 Ma. Molybdenite from different localities in the KLFZ including the Myszków deposit crystallized during the time interval 300 ± 2 to 296 ± 2 Ma. The majority of molybdenites have moderate Re concentrations ranging from ca. 30 to 90 ppm. A distinctive feature of zircon is the presence of characteristic magmatic oscillatory zoning and minor inherited zircon cores with a wide range of isotopic ages (Paleoproterozoic-Neoproterozoic). Most of the felsic igneous zircon from the magmatic rocks shows concentric zoning and intermediate Th/U in rims (0.30–0.65).

Isotopic results show that igneous and hydrothermal activities in the KLFZ were restricted to a short interval of time, ca. 10 Ma aligned with the Carboniferous-Permian transition. Mineralized porphyry systems, and other types of Cu-Mo(-W) ores within the KLFZ, are closely related to the felsic magmatism in space and time. As an example, molybdenite from different generations of quartz veinlets in the Myszków Mo-Cu(-W) deposit crystallized during the time interval 300 ± 2 to 296 ± 2 Ma. Similarly, molybdenite from quartz veins that cut dacite and granitoid north of Myszków, yields Re-Os ages of 300.0 ± 2 and 299.0 ± 2 Ma, respectively. These are indistinguishable from the zircon U-Pb age for granodiorite from the same borehole, 300.2 ± 3.6 Ma, and zircon ages of 301.0 ± 2.1 – 295.9 ± 2.9 Ma, respectively, from the Myszków-Mrzyglód region. The same is true of Cu-Mo mineralization elsewhere in the KLFZ. The zircon ages of granodiorites from the Pilica region are 295.6 ± 1.9 Ma. Molybdenite from the same region gives an age of 296.3 ± 1.4 Ma. These ages are also consistent with those measured on dacite zircon from the

Bêdkowska Valley. Moreover, Re-Os ages of molybdenite (301 ± 2 Ma) from quartz veinlets cutting rhyolite and Palaeozoic metamudstone in two boreholes near Mysyglów are consistent with the zircon U-Pb ages measured on dacites.

CONCLUSIONS

SHRIMP U-Pb dating of zircons from igneous rocks and Re-Os isotopic studies of molybdenites from the Kraków-Lubliniec tectonic zone, indicate that porphyry-type Mo-Cu(-W) ore mineralization is closely related to the felsic magmatism in space and time. Our U-Pb isotopic studies show that felsic magmatism in the area was a relatively short-lived event (303.8 ± 2.2 to 294.7 ± 2.3 Ma) and is in accordance with Re-Os isotopic ages of molybdenite (300 ± 2 to 296 ± 2 Ma) from the Myszków deposit and other Cu-Mo prospects in the KLFZ. These prospects occur over 60 km from Mys³ów to the Bêdkowska Valley.

We show that felsic magmatism was important to the development of Cu-Mo porphyry ore mineralization in different places beyond the Myszków deposit in the KLFZ, and most probably along another regional NW-trending major shear zones developed in the foreland of the Variscan orogenic belt in central Europe. The KLFZ, like several major NW-trending dextral strike-slip faults parallel to the TESZ, developed in the hinterland and foreland of the Variscan orogenic belt in central Europe. These faults were active in Carboniferous–Permian times as part of mega-shear zones that resulted from the clockwise rotation of the African plate with respect to the European plate. During the Carboniferous- Permian, the eastern part of the European Variscides was the site of rapid continental extension, uplift, and deep fracturing. The transition from a post-collisional to a within-plate setting was favourable for the formation of porphyry and epithermal types of ore mineralization in uplifted areas. However, subsequent Mesozoic and Cenozoic tectonics strongly influenced the rate of erosion, and thus the exhumation or deeper burial of small, individual porphyry systems.

MAGMA SOURCE OF THE ORE-BEARING GRANITOIDS OF THE PORPHYRY Mo DEPOSITS IN THE LESSER XING'AN–ZHANGGUANGCAI RANGE METALLOGENIC BELT, NE CHINA: IN SITU ZIRCON HF-O ISOTOPIC CONSTRAINTS

Yu Xiaofei

Development and Research Center of China Geological Survey - xfyu@jlu.edu.cn

BACKGROUND

Porphyry Mo deposits represent the world's primary sources of this commodity (Sillitoe, 2010). In NE China, many large and super–large porphyry Mo deposits have recently been discovered, and this region has become a globally important source of Mo. Various Mo deposits formed due to intense tectonic–magmatic activities in the region. The Mo deposits in the Lesser Xing'an–Zhangguangcai Range can be classified as porphyry, skarn, and hydrothermal vein types. Porphyry and skarn type are economically the most significant and occurred at the Daheishan, Jidetun, Dashihe, Chang'anpu, Houdaomu, Sanchazi, Liushengdian, and Xinhualong deposits. Hydrothermal vein deposits include the Fu'anpu deposit, while skarn-type Mo deposits include the Dongfeng and Wudaoling deposits. The timing and duration of magmatic–hydrothermal events are significant in understanding ore deposits, from both academic and exploration viewpoints (Stein *et al.*, 1997). In the past ten years a number of precise rock and ore ages have been obtained for the granitoids-related porphyry Mo deposits in the Lesser Xing'an–Zhangguangcai Ranges. These ages indicate that Mo mineralization occurred during the Early–Middle Jurassic (197–161 Ma), coinciding with the contemporary magmatic activities. However, there remains significant potential for the further discovery of Mo deposits in the Lesser Xing'an–Zhangguangcai Ranges.

In situ zircon Hf–O isotopes, in contrast to the traditional whole-rock Sr–Nd isotopes, as they are insensitive to post-magmatic hydrothermal alteration and, therefore, can place robust constraints on the nature and evolution history of the host magma (Li *et al.*, 2013). Moreover, zircons in equilibrium with mantle-derived magma have average $\delta^{18}O$ values of 5.3±0.3‰ (Valley *et al.*, 1998). The zircon $\delta^{18}O$ value is highly retentive and insensitive to modification by differentiation (Valley *et al.*, 2005). Therefore, the zircon $\delta^{18}O$ value can effectively trace the contribution of supracrustal materials to mantle-derived magma (Valley, 2003). In this study, we present new in situ zircon Hf–O isotope data for the ore- bearing granitoids of porphyry Mo deposits in the Lesser Xing'an–Zhangguangcai Ranges, with an aim to constrain the nature of magmatism. This work also contributes to a better understanding of the regional metallogenic regime in northeastern China.

METHODS

Four representative sample of the ore-bearing granitoids of the porphyry Mo deposits (Daheishan, Jidetun, Huojihe and Luming) was used for in situ Hf–O isotopic analyses. Zircon grains were separated from crushed rock using standard heavy liquid and magnetic separation techniques at the mineral separation laboratory of the Earth Science Exploration Technology Services Ltd. of Hebei Province at Langfang. The sites for zircon Hf–O isotope analysis were selected on the basis of the cathodoluminescence (CL) images as well as transmitted and reflected light micrographs to reveal their internal structures. Zircon in-situ oxygen isotopes were analyzed firstly, which were acquired using a Cameca IMS-1280 SIMS at the Institute of Geology and Geophysics, Chinese Academy of Sciences in Beijing. Zircon Hf isotope analysis was carried out in situ using a Newwave UP213 laser-ablation microprobe attached to a Neptune multi-collector ICP–MS at the Institute of Mineral Resources, Chinese Academy of Geological Sciences, Beijing.

RESULTS

The $e_{Hf}(t)$ values and Hf model ages of the Daheishan and Jidetun deposit were both calculated assuming a crystallization age at 168 Ma, while the eHf(t) values of the Huojihe and Luming were calculated at 184 Ma.

All analyzed zircons $\varepsilon_{Hf}(t)$ values from the Daheishan granodiorite porphyry range from 5.6 to 9.9, with the TDM2 ages (582–854 Ma). In situ zircon oxygen isotope analyses indicate that the Daheishan granodiorite has low and uniform $\delta^{18}O_{zircon}$ values, ranging from 5.2 to 6.5‰. The measured $^{176}Hf/^{177}Hf$ ratios from the Jidetun granodiorite vary slightly from 0.282786 to 0.282930, corresponding to ε_{Hf} values from 4.0 to 9.1 and T_{DM2} ages from 625 Ma to 950 Ma.

Fifteen zircons from the Huojihe pluton have been analysed. The measured 176Hf/177Hf ratios vary from 0.282692 to 0.282839, corresponding to $\varepsilon_{Hf}(t = 184\ Ma)$ ranging from 1.0 to 6.2 and two-stage Hf depleted-mantle model ages of 829-1161 Ma. The oxygen zirconHf isotopes ($\delta^{18}O_{Hf}$) range from 5.7‰ to 6.6‰. The measured [(t)

values and the Hf model ages from the Luming pluton vary from 2.0-4.8 and 895 to 1214 Ma, respectively. The oxygen isotope compositions show relatively large variation with $\delta^{18}O$ zircon ranging from 5.7‰ to 6.4‰ (mean at 5.9 ± 0.3‰, n = 20).

DISCUSSION AND CONCLUSIONS

Zircon is a common accessory mineral in granitoids, and its high resistance to alteration and weathering makes it an excellent geochemical tracer of petrogenetic processes and magma source (Vervoort & Blichert-Toft, 1999). Hf isotopic analyses of zircons from the ore-bearing granitoids of the porphyry Mo deposits (Daheishan, Jidetun, Huojihe and Luming) yield consistent results, thus indicating a uniform magma source. The $\varepsilon_{Hf}(t)$ values of all zircons from the ore-bearing granitoids are spread between the chondrite uniform reservoir (CHUR) and the values expected for depleted mantle, which implies a depleted mantle source for the ore-bearing rocks. However, the extensive Mesozoic granites in the area are lack of mantle- source characteristics, and this excludes the possibility that they formed directly from the mantle (Wu *et al.*, 2000). An alternative explanation is that the ore-bearing granitoids were probably originated from juvenile-crust-derived magmas that were differentiated from the depleted mantle. The TDM2 ages of sample are concentrated between 582 Ma and 1214 Ma, implying a period of crustal accretion during the Neoproterozoic.

It is generally accepted that mantle zircons have a narrow range of $\delta^{18}O$ values averaging 5.3±0.6‰ (2ó; Valley *et al.*, 1998). Zircons with $\delta^{18}O$ values lower than 6.5‰ form from melts that comprise a minor to negligible sedimentary component, whereas zircons with $\delta^{18}O$ values higher than 6.5‰ signify crustal contributions (Hawkesworth & Kemp, 2006). Therefore, the magma source of the ore-bearing granitoids of the porphyry Mo deposits almost has no addition of crustal materials.

Phanerozoic I-type granites are the most abundant intrusions in northeastern China and are characterized by positive $\varepsilon_{Nd}(t)$ values, which suggest the melts were derived from juvenile crust (Wu *et al.*, 2000). The ore-bearing granitoids of the porphyry Mo deposits also exhibit positive $\varepsilon_{Nd}(t)$ values. Furthermore, their young TDM2 ages preclude the possibility of melt derivation from a highly evolved ancient basement. This origin agrees with the conclusion drawn from Hf isotope analytical results for the Mesozoic granitoids in Northeast China. Therefore, it is concluded that the source magma of ore-bearing granitoids of the porphyry Mo deposits in the Lesser Xing'an–Zhangguangcai Ranges was derived from the juvenile crust.

GEOLOGY, ORE MINERALOGY, AND GEOCHRONOLOGY OF THE AKZHAL ORE FIELD, EASTERN KAZAKHSTAN

Evgeny Naumov[1], Yury Kalinin, Konstantin Kovalev, Alexey Travin, Alexander Serdyukov

[1]*V.S. Sobolev Institute of Geology and Mineralogy SB RAS, Novosibirsk and Novosibirsk State University, Novosibirsk, Russia*

naumov@igm.nsc.ru

The Akzhal ore field is located in the southeastern part of the West-Kalba gold belt of East Kazakhstan. Mineralization is controlled by northwestern, sublatitudinal, and northeastern faults. The mineralization is hosted in carbonceous-siliceous aleuropelites of the Arkalyk Formation (S1) with interlayers of basalts. In the central part of the deposit, the diorite- granodiorite massif of the Kunushsky Complex (C3-P1) occurs. Productive gold mineralization is closely associated with the dikes of dacites, rhyodacite, and rhyolite of varying thickness (0.5-10 m).

The rare-earth elements signature in basalts and diorite-granodiorite massif indicates various sources and their different origins. Basalts are characterized by a homogeneous trend of distribution of elements with negative Eu-anomaly, depleted in light REEs. But diorites and dacites have a similar REE patterns, which allows us to suggest a single source for their origin.

The formation of the mineralization in the Akzhal Ore Field is associated with the manifestation of the shear zone. The morphology of ore bodies is determined by structural factors and is characterized by lenticular, platiform, and columnar forms. Gold-sulfide mineralization is represented by mineralized tectonic zones with irregular distribution of sulphides and gold. The main ore bodies are zones of quartz-vein mineralization, accompanied by siliceous, sericite, dolomite, feldspar, albite, and chlorite alteration types.

Two main types of ores are distinguished: carbonaceous schists with impregnated arsenopyrite-pyrite mineralization and quartz-sulfide veins in altered rocks. The main ore minerals of the deposit are pyrite and arsenopyrite, galena, sphalerite, chalcopyrite; vein minerals are represented by quartz of several generations, calcite, plagioclase, chlorite, and muscovite. Minor and rare ore minerals are native gold, fahlore, pierceite, stephanite, schapbachite, and benleonardite. Early gold-bearing arsenopyrite-pyrite and late quartz- gold-polysulfide assemblages are distinguished. The first is represented by fine-grained arsenopyrite-pyrite aggregates with a gold-bearing acicular arsenopyrite, arsenic pyrite with submicroscopic inclusions of gold in siliceous-carbonaceous aleuropelites. The second association is represented by vein and massive quartz-sulphide ores with large-crystal aggregates of pyrite and arsenopyrite. Usually they are brecciated and cemented with galena, chalcopyrite, fahlore, and clayophane. In association with these minerals, gold and a group of rare Ag-Te-Bi-minerals are found. Fine-grained arsenopyrites have low arsenic content (41-42 mol%); for the second group of larger crystalline arsenopyrite, As content is 44-45 mol. %. According to the atomic absorption analysis of monomineralic samples, the fine arsenopyrite contains up to 99.0 ppm Au, and the arsenopyrite of the second type contains 6.7-38.0 ppm Au.

Native gold occurs in association with arsenopyrite-pyrite aggregates and galena-sphalerite- chalcopyrite veinlets. Gold is characterized by the absence of crystalline forms and grain size of 15-20 microns. Gold has different finesse: 700-800 ‰ and 500-600 ‰, corresponding to pyrite-arsenopyrite (Au I) and polysulfide (Au II) associations, respectively. In oxidized ores extremely high finesse gold (900-1000 ‰) is revealed, which is probably supergene.

In the studied quartz samples two clusters of homogenization temperatures of fluid inclusions (250-175 ° C and 440-270 ° C) were established, with the total fluid concentration varying from 17 to 3 wt. %. The bimodal distribution of homogenization temperatures probably corresponds to two stages of ore deposition at the deposit: early arsenopyrite- pyrite with gold-bearing arsenopyrite and late gold-silver-polysulfide.

The spatial confinement of ore zones to the magmatic rocks and the horizontal zoning of mineral parageneses relative to the diorite massif indicate a probable connection between mineralization and magmatism. Based on the results of U-Pb (LA-ICP-MS) analysis, the age of formation of the Akzhal massif is 298-303 Ma (301.1 ± 1.7 and 299 ± 1.1 Ma), the age of the dike is 291.2 - 298.3 Ma. The age of formation of ore mineralization, according to Ar-Ar analysis, is 294.8 ± 4.2 - 298 ± 5.3 Ma (Fig.1). Thus, the obtained age data together with geological observations and mineralogical and geochemical specific features of the ores allow us to attribute this deposit to "intrusion-related" type. Same time, most of gold deposits of the region, such as Bakyrchik, Bolshevik, Suzdal, Zhaima, and others show the age gap (about 10-30 million years) between mineralization and related magmatic rocks (Kovalev *et al.*, 2009, 2016; Naumov *et al.*, 2011; Kalinin *et al.*, 2015).

In eastern Kazakhstan most of the orogenic gold deposits are localized within the West- Kalba metallogenic belt. The largest reserves are the ore cluster of the Kyzyl project, which includes Bakyrchik and Bolshevik deposits and number of minor gold occurrences (joint reserves 7.3 Moz and inferred resources 3.1 Moz, with average grade

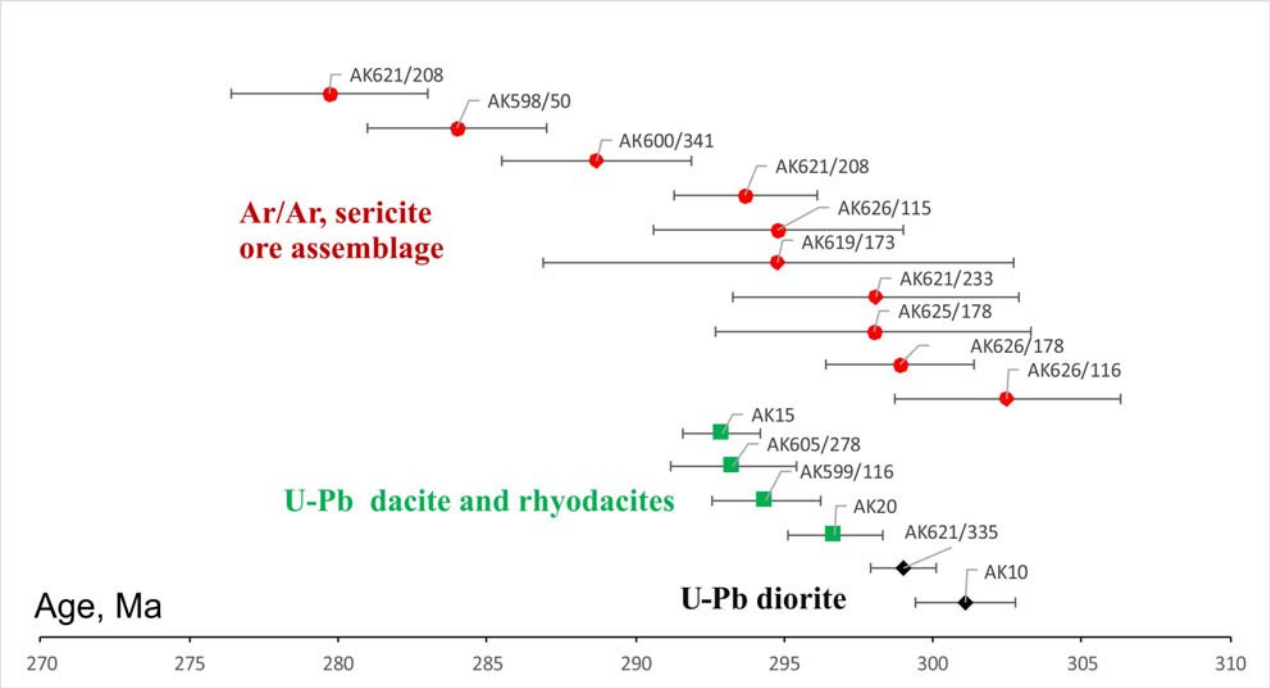

Figure 1. Age of igneous rocks (U-Pb) and hydrothermal mineralization (Ar-Ar, sericite) at Akzhal ore field.

6.8 g/t). Also, the Permian age swere confirmed for Suzdal, Jerek, Zhaima, Balazhal, and Daubai deposits using 40Ar/39Ar (sericite) and U-Pb (SHRIMP) methods for ores and rocks, respectively. The ages of mineralization in Zherek deposit are 287.9±2.8, 286.7±3.4, and 282.5±2.7 Ma. The age of the same type of mineralization of the Bolshevik deposit is 285.6±3.3 Ma, and the age of the main ore stage of Suzdal deposit is 281±3.3 Ma. In the Kuluzhun region (Balazhal gold deposit), the age of the disseminated pyrite-arsenopyrite mineralization in hydrothermally altered gabbro-diorite massif is 276.1 ± 2.7 Ma. In the same area, at the Daubai gold occurrence, quartz-sericite metasomatic gold-bearing rock is dated as 254.3 ± 3.1 Ma. Possibly this younger age is caused by impact of contact metamorphism of Late Permian granitoid intrusion on primary gold-arsenic ores. The Zhaima gold deposit is located in the northwestern part of the West Kalba gold belt and shows Ar/Ar age of three sericite samples from ore veinlets corresponds to the Early Permian: 279 ± 3.3, 275.6 ± 2.9, and 272.2 ± 2.9 Ma. Orogenic gold deposits are accompanied by antimony mineralization separated in time from main gold ore stage. For example, at Suzdal deposit, within a zone of early metasomatic Au-As mineralization, one can observe younger antimony mineralization, which is dated as 248.3±3.4 Ma. This conforms to the time of formation of the trachybasalt-trachyrhyolite association in the Semeitau volcano-plutonic structure (248.2±0.5 Ma), which is in the ore field of this deposit.

Magmatism and metallogeny of the region correlate with similar structures of NW China (Saerbulake (285.9±2.8 Ma), Duolanasayi (263±13 Ma), and others) and other Central Asian provinces, where giant orogenic gold deposits, such as Muruntau, Kumtor, and others, are situated.

REFERENCES

Kalinin Yu., A., Naumov, E.A., Borisenko, A.S., Kovalev, K.R., Antropova A.I., 2015. Spatial–Temporal and Genetic Relationships between Gold and Antimony Mineralization at Gold Sulfide deposits of the Ob–Zaisan Folded Zone. Geology of Ore Deposits 57, 3, 157–171. DOI 10.1134/S1075701515030022

Kovalev, K.R., Kalinin Yu., A., Naumov, E.A., Pirajno, F., Borisenko, A.S., 2009. A mineralogical study of the Suzdal sediment-hosted gold deposit, Kazakhstan: implications for ore genesis. Ore Geology Reviews 35, 2, 186-206. DOI: 10.1016/j.oregeorev.2008.11.007

Kovalev, K.R., Kuzmina, O.N., Dyachkov, B.A., Vladimirov, A.G., Kalinin Yu., A., Naumov, E.A., Kirillov, M.V., Annikova, I.Yu., 2016. Geology of Ore Deposits 58, 2, 116–133. DOI: 10.1134/S1075701516020045

Naumov, E., Borisenko, A., Kovalev, K., Kalinin, Y., Fedoseev, G., Seltmann, R., 2011. Gold deposits of Western Siberia and Eastern Kazakhstan: types and ages of mineralization, correlation with magmatic events. Proceedings of 11 th SGA Biennial Meeting "Let's Talk Ore Deposits", Antofagasta, Chile, 26-29 September 2011, p. 82-84.

NEW EARLY JURASSIC U-Pb AGE IN RHYOLITIC DYKES FROM THE NORTHEASTERN SECTOR OF GASTRE (CHUBUT, ARGENTINA) AND ITS POSSIBLE RELATION TO THE MINERALIZATION OF THE LOS MANANTIALES DISTRICT

Silvia Lagorio[1], Alicia Busteros, Diego Silva Nieto, Raúl Giacosa, Claudia Zaffarana, Marcelo Márquez,

[1]*Instituto de Geología y Recursos Minerales (SEGEMAR). Parque Tecnológico Miguelete, Buenos Aires - silvialagorio@gmail.com*

In this presentation, both stratigraphic and geochronological results are revealed, which were obtained from cartography and regional geology studies carried out in the Gastre region. The area of study is located in the southwestern sector of the North Patagonian Massif, in the vicinity of the Los Manantiales mining district, 12 km to the southwest of the Angela mine, a polymetallic deposit that was active between 1979 and 1992, being during that period the main metal exploitation mine of Chubut.

Lava, pyroclastic rocks and andesitic breccia, as well as volcaniclastic deposits assigned to the Lonco Trapial Formation, crop out in this area. 40Ar/39Ar data from lavas of this region indicated ages of 185.4 ± 2 Ma, 185 ± 1.6 / 184 ± 5 Ma (Zaffarana and Somoza, 2012), corresponding to the Lower Jurassic. A 40Ar/39Ar age of 182.8 ± 0.8 Ma was obtained from ignimbrites at the NW area of the Navidad deposit assigned to the Garamilla Formation, considered equivalent to the Lonco Trapial Formation (Márquez, *et al.* 2016).

These rocks are intruded by numerous WNW, NW, NE, ENE-oriented dykes. The studieddykes are of rhyolitic composition and NE orientation, as well as those from Los Manantiales mining district. They have porphyritic texture, with phenocrysts (2%) of plagioclase and alkali feldspar, with slight sericitic and clay alteration respectively, and minor biotite with zircon inclusions; the groundmass is mainly composed by quartz and feldspar, mostly spherulitic as a devitrification product, with scarce carbonate alteration. These rocks are of subalkaline nature and classify as rhyolites in the TAS diagram as well as using immobile trace element ratios. Besides, they are high-K and peraluminous rhyolites.

The results of a LA-ICPM U-Pb zircon dating carried out in one of these dykes provide evidence of a weighted mean crystallization 206Pb/238U age of 177.26 ± 0.96 Ma, corresponding to the lower Jurassic In Los Manantiales district there is a clear spatial association between mineralization and rhyolitic dykes, which might have provided heat and fluids to the hydrothermal system (Varela, 1994; Márquez, 1999). The main mineralization could have been linked to the final stage of the process, characterized by potassium alteration and conditioned by the uprising circulation of fluids through the fractures and faults that are present in the area (Lafont *et al.*, 2003).

As regards the setting age of these intrusives, Varela (1994) claims that it might be late Cretaceous-early Tertiary, while Márquez (1999) considers that it could be Jurassic in relation to the Lonco Trapial magmatism or Miocene like the volcanism of the Piré Mahuida. Similarly, Dejonghe *et al.* (2002) leave the possibility open even though they are more inclined to a Jurassic genesis. Besides, it should be noted that new LA-ICPM U-Pb zircon dating on volcanic rocks from Cañadón Asfalto Formation from Navidad district yielded ages of 170.8 ± 3.0 and 173.9 ± 1.9 Ma (Bouhier *et al.*, 2017) that are younger than those obtained by Cúneo *et al.* (2013) from tuff levels of the same Formation at Cerro Cóndor and Cerro Bayo Chico (178.76 ± 0.092 Ma and 176.15 ± 0.12 Ma, respectively).

Although no alteration zones associated with these dykes could be recognized at surface levels in the study area as occur in the epithermal polymetallic deposits of the Los Manantiales district, several elements suggest considering the possibility that these dykes might be part of the same intrusive cycle. Apart from the marked lithological similarities, what should be noted is the fact that the studied dykes are part of a NNE- oriented belt of dykes of around 20 km long, being the dykes of the Los Manantiales district located in the northeastern sector of this belt. Therefore, the Early Jurassic age obtained from the analyzed dykes allows the assumption that the genesis of the mineralization of Los Manantiales district might be of that age, related to the posthumous activity of the Lonco Trapial or more probably to the initial volcanism of Cañadón Asfalto Formation.

REFERENCES

Bouhier, V.E., Franchini, M.B., Caffe, P.J., Maydagán, L., Rapela C.W., Paolini, M., 2017. Petrogenesis of volcanic rocks that host the world-class Ag-Pb Navidad District, North Patagonian Massif: Comparison with the Jurassic Chon Aike Volcanic Province of Patagonia, Argentina. Journal of Volcanology and Geothermal Research 338, 101-120.

Cúneo, R., Ramezani, J., Scasso, R., Pol, D., Escapa, I., Zavattieri, A.M., Bowring, S.A., 2013. High-precision U-Pb geochronology and a new chronostratigraphy for the Cañadón Asfalto Basin, Chubut, central Patagonia: Implications for terrestrial faunal and floral evolution in Jurassic. Gondwana Research 24, 1267-1275.

Dejonghe, L., Darras, B., Hughes, G., Muchez, Scoates, J., Weis, D., 2002. Isotopic and fluid-inclusion constraints on the formation of polymetallic vein deposits in the central Argentinian Patagonia. Mineralium Deposita 37, 158–172.

Lafont, D., Strazzere, L., Gregori, D., 2003. Diseños y temperaturas de alteración hidrotermal en Mina Ángela, Comarca Nordpatagónica, Argentina. Revista de la Asociación Geológica Argentina 58(3), 391-402.

Márquez, M.J., 1999. Los sistemas hidrotermales del distrito Los Manantiales, Chubut, in: Zappettini, E.O. (Ed.), Recursos Minerales de la República Argentina. Instituto de Geología y Recursos Minerales SEGEMAR, Anales 35, Buenos Aires, pp. 1167-1175.

Márquez, M.J., Zubia, M.A., Giacosa, R.E., Trevisiol, S.A. y Fernández, M.I., 2016. Características geológicas y metalogenéticas del Depósito Navidad (Ag-Pb-Zn-Cu) Macizo Somún Curá, Chubut, Argentina. Instituto de Recursos Geológico Mineros, Servicio Geológico Minero Argentino. Boletín 40, Buenos Aires. 50 pp.

Varela, M.E., 1994. Silicate-melt and fluid inclusions in rhyolitic dykes, Los Manantiales mining district, Argentina. European Journal of Mineralogy 6, 837-854.

Zaffarana, C.B., Somoza, R., 2012. Paleomagnetism and 40Ar/39Ar dating from Lower Jurassic rocks in Gastre, central Patagonia: further data to explore tectonomagmatic events associated with Gondwana breakup. Journal of the Geological Society of London 169, 371-379.

CHAPTER 9
ORE MINERALOGY

Convenor: Nigel Cook

MOBILITY OF RADIONUCLIDES IN THE OLYMPIC DAM Cu-U-Au-Ag DEPOSIT, SOUTH AUSTRALIA

Mark Rollog[1], Nigel J. Cook, Paul Guagliardo, Cristiana L. Ciobanu, Kathy Ehrig, Matt Kilburn

[1]*School of Chemical Engineering, University of Adelaide, Australia - Mark.rollog@adelaide.edu.au*

BACKGROUND

The Olympic Dam (OD) IOCG-U deposit, South Australia, has a complex history dating back to 1.6 Ga. Discovered under 350 m of sedimentary cover, the deposit contains a resource approximately 80 Mt Cu, 2.6 Mt U_3O_8, 334 Moz t. Ag, and 107 Moz t. Au (Ehrig, *et al.*, 2017). Based on uraninites, at least two stages of mineralization and multiple occurrences of dissolution, mobilization, and recrystallisation have been identified (MacMillan *et al.*, 2016). Coffinite ($USiO_4 \bullet nH_2O$) and brannerite (U^{4+}, REE,Th,Ca)(Ti,Fe^{3+},Nb)$_2$(O,OH)$_6$ are cautiously considered late-stage minerals formed from dissolved uraninite, but may also be the result of U addition (MacMillan *et al.*, 2017).

Radionuclide (RN) daughters of U and Th decay have been dissociated and locally redistributed throughout the orebody

METHODS

Drill cores were sliced and polished as-is. Copper sulfide flotation concentrate (<53 µm) was suspended in 25 mm epoxy resin mounts and polished (~20,000 exposed grains per cm2). Mineral surveys were performed by scanning electron microscopy (SEM), and grains of interest recorded. Isotopic distributions of select grains/regions of interest (ROI) were mapped on a Cameca nanoSIMS 50L. Seven isotopes may be mapped at once, and the standard practice was to map $^{46\text{ or }47}$Ti, $^{54\text{ or }57}$Fe, ^{63}Cu, $^{86\text{ or }87}$Sr, ^{137}Ba, ^{206}Pb, and ^{238}U with a 50 pA beam current (effective spot size ~500 nm), then repeat the same area for $^{54\text{ or }57}$Fe, $^{142\text{ or }144}$Nd, ^{169}Tm, ^{210}RN (dominantly ^{210}Pb), ^{226}Ra, ^{230}Th, and ^{234}U using a 250 pA beam current (effective spot size ~700 nm). All maps are 50x50 Mm, 512x512 pixels. Results were processed by the OpenMIMS plugin (Poczatek *et al.*, 2009) in ImageJ (Fiji) (Schindelin *et al.*, 2012; Schindelin *et al.*, 2015).

Maps could be colorized and overlain on backscattered electron maps for comparison. Figure 1 shows the distribution of six detectable members of the 238U decay chain in an Olympic Dam core sample containing sericite, coffinite, and barite with small inclusions of galena. Variations in ionization potentials for elements in different matrices prevent accurate quantification, but spatial distributions within each map remain true.

RESULTS AND DISCUSSION

Analyses of over 200 grains of interest reveal patterns in radionuclide (RN) distribution. Uraninite tends to contain all members of the ^{238}U decay chain, indicating resistance to dissolution and redistribution – at least within the last few million years but the presence of high concentrations of (exclusively) ^{226}Ra and ^{210}Pb in barites suggests mineral-scale dissociation to some extent in the chain. ^{222}Rn, being a gas, is one speculative source of dissociation; however observed ^{226}Ra and ^{210}Pb distributions almost always correlate, signifying continuity for this section of the decay chain. Coffinite and particularly brannerite are chemically more resistant to dissolution, Ra and Pb are less structurally compatible, and less likely to retain radon within decay-induced transient porosity. The lack of ^{226}Ra and ^{210}Pb in some coffinite and brannerite may indicate either very recent formation or partial dissolution with preferential removal of sulfate-insoluble daughters – possibly through chloride leaching. Figure 1 clearly shows ^{226}Ra and ^{210}Pb preference for barite, while the U and Th species remain in coffinite. ^{206}Pb prefers neither coffinite nor barite but instead forms small inclusions of galena throughout the matrix, suggesting redistribution during an earlier event. These distributions may be the result of one complex dissolution event from one RN source (coffinite), or multiple events from multiple sources. The exceptionally high response on masses 226 and 210 suggest the latter.

Other patterns are present, including an abundance of ^{226}Ra and ^{210}Pb in molybdenite, covellite replacing bornite, and sericite/chlorite (when in proximity to a U-bearing mineral). This, in coordination with spots of RN activity on grain surfaces and at mineral boundaries, suggests that surface features also play an important role in sequestering RN. Basal cleavage planes or charge-imbalanced surfaces may act as filters for RN-bearing fluids or nanoparticles of RN sulfates.

CONCLUSIONS

NanoSIMS isotopic distribution maps show that radionuclides exhibit local scale mobility within the OD deposit. Some mineral groups such as sulfates and phosphates have the ability to scavenge RN – at least from ^{226}Ra down the chain – while many mineral groups remain barren (notably sulfides and most silicates). High surface area minerals and electron-imbalanced surfaces may also act as traps for RN-bearing fluids or nanoparticles.

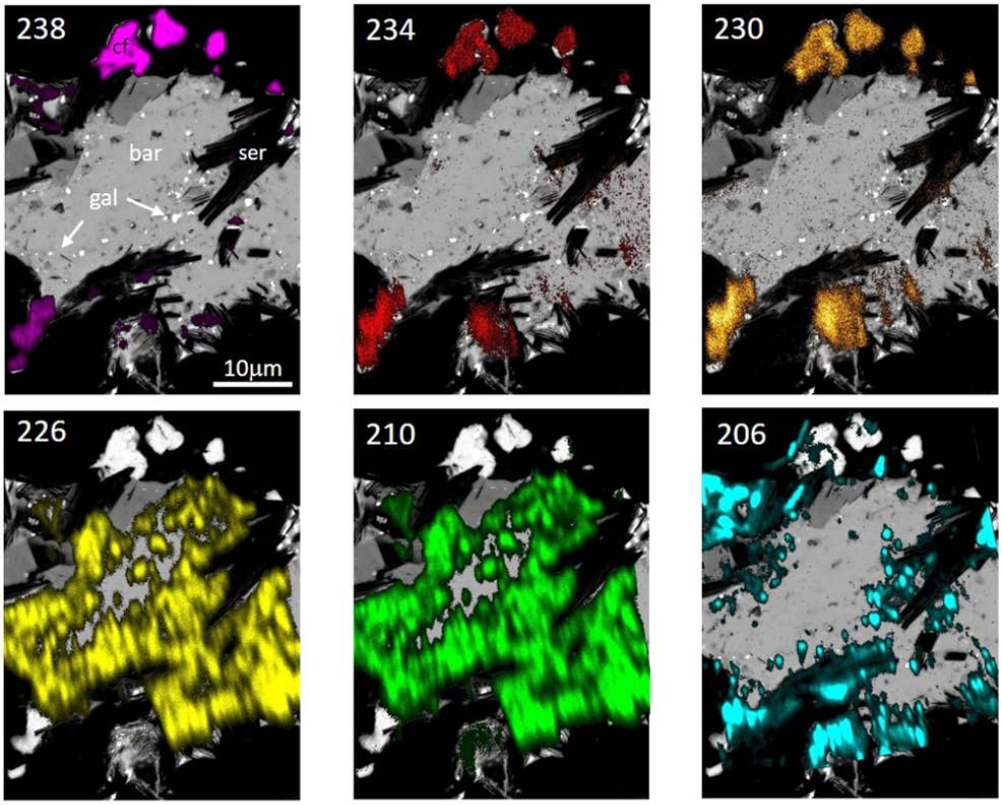

Figure 1. Barite (bar) - coffinite (cf) - sericite (ser) - galena (gal) assemblage from Olympic Dam. Members of the ^{238}U decay chain have dissociated in favor of more compatible mineral hosts.

REFERENCES

Ehrig, K., Kamenetsky, V. S., McPhie, J., Cook, N. J. and Ciobanu, C. L. 2017. Olympic Dam iron oxide Cu-U-Au-Ag deposit. In: Phillips, G.N., ed., Australian Ore Deposits, AusIMM, p: 601-610.

Macmillan, E., Ciobanu, C.L., Ehrig, K., Cook, N. J. and Pring, A., 2016. Chemical zoning and lattice distortion in uraninite from Olympic Dam, South Australia. American Mineralogist 101 (10): 2351-2354.

Macmillan, E., Cook, N. J., Ehrig, K., A., Pring, A., 2017. Chemical and textural interpretation of late-stage coffinite and brannerite from the Olympic Dam IOCG-Ag-U deposit. Mineralogical Magazine 81 (6): 1323-1366. https://doi.org/10.1180/minmag.2017.081.006.

Poczatek, C., Kauman, Z., and Lechene, C.P., 2009. OpenMIMS ImageJ plugin Guide. Harvard Medical School, Boston, Massachusetts, USA.

Schindelin, J., Rueden, C. T., Hiner, M. C. and Eliceiri, K. W., 2015. The ImageJ ecosystem: An open platform for biomedical image analysis. Molecular Reproduction and Development 82, p: 518-529. https://doi.org/10.1002/mrd.22489.

Schindelin,J., Arganda-Carreras, I., Frise, E., Kaynig, V., Longair, M., Pietzsch,T., Preibisch, S., Rueden, C., Saalfeld, S., Schmid, B., Tinevez, J-Y., White, D. J., Hartenstein, V., Eliceiri, K., Tomancak, P. and Cardona, A., 2012. Fiji: an open-source platform for biological-image analysis. Nature Methods volume 9, p: 676–682.

NANOSCALE STUDY OF SILICIAN MAGNETITE FROM IOCG SYSTEMS: EXAMPLES FROM THE OLYMPIC DAM DISTRICT. SOUTH AUSTRALIA

Cristiana L. Ciobanu[1], Max R. Verdugo-Ihl, Ashley Slattery, Nigel J. Cook, Kathy J. Ehrig, Liam Courtney- Davies

[1]*School of Chemical Engineering, University of Adelaide, Adelaide, Australia - cristiana.ciobanu@adelaide.edu.au*

BACKGROUND

'Silician magnetite' (Si-magnetite) refers to magnetite with variable Si (up to ~10 wt.% SiO_2) and occurs in deposits spanning the magmatic-hydrothermal spectrum, low-T metamorphosed BIF ores as well as in mafic and ultramafic rocks (Huberty *et al.*, 2012 and references therein). Definition of Si-magnetite nanoprecipitates as $Si^{IV}[(vacancy)_{0.5}Fe^{2+}_{0.5}]^{VI}[Fe^{3+}]^{VI}O_4$ with maghemite-type vacancy-ordering was only recently possible by using Z-contrast techniques for high-resolution Scanning Transmission Electron Microscopy (STEM) imaging (Xu *et al.*, 2014). Formation of Si-magnetite in hydrothermal systems can be considered as co- precipitation of aqueous silica and Fe-silicate complexes during crystal growth (Xu *et al.*, 2014). It is thus important in modelling deposits where regional/orefield zonation patterns result from fluid evolution. In Iron-Oxide Copper Gold (IOCG) systems, magnetite is associated with early, higher-T, alkali/calcic metasomatism, in turn associated with chalcopyrite-pyrite mineralization in the Olympic Dam District (ODD), South Australia, but not necessarily elsewhere. The Olympic Dam (OD) deposit is hosted within hematite-bearing breccias placed in the central, upper part of the Roxby Downs Granite (RDG) associated with ~1.6 Ga IOCG mineralization and magmatism.

Here we discuss Si-magnetite from 5 locations: 4 from the outer, weakly-mineralised shell of brecciated RDG at OD, and one from the older (~1.85 Ga) Donington granite hosting the Wirrda Well (WW) IOCG prospect, ~17 km SW from OD. These samples are representative of Si-magnetite found in concentrations varying from massive intervals with carbonate gangue at OD to cm-dm-sized nodules or irregular pockets in variably altered granite (OD, WW) and at depths from ~700 m to 2 km. We aim to: (i) characterise; and (ii) explore the petrogenetic significance of Si-magnetite in IOCG systems from terranes with protracted geological histories.

METHODS

Si-magnetite foils prepared for TEM using focused ion beam (FIB)-SEM methods were cut across zonation patterns. Seven foils were analysed using High Angle Annular Dark Field (HAADF) STEM imaging and energy dispersive X-ray spectrometry (EDX)-STEM mapping.

RESULTS

In all samples, magnetite features µm-scale zonation patterns (Fig. 1a) which consists of Si- magnetite nanoprecipitates (Fig. 1b). An eclectic range of other nanomineral inclusions comprising silicates, carbonates, rutile, and U-, and Y±As-bearing nanoparticles (NPs; Fig.1b) were identified using EDX-STEM spot analysis/mapping, and HR-HAADF STEM imaging. Calc-silicates (±rutile) are present in Si-magnetite on the eastern side of OD and at WW, whereas NPs were only identified from the carbonate-hosted Si-magnetite.

Si-magnetite nanoprecipitates occur as darker inclusions on HAADF STEM images (Fig. 1c), varying in size from few to tens of nm, shape and density. Narrower bands (1-2 unit cells wide) of still darker Si-magnetite are stacked along d111 magnetite within the coarser precipitates, or directly in magnetite (Fig. 1c, d). Minor Al and K are measured in Si-magnetite bands from the irregular patches at the location with Fe-oxide nodules in RDG. Although both magnetite and Si-magnetite have very similar crystal structures, intensity line profiles show variation attributable to Si substitution and vacancies comparable with the maghemite model (Xu *et al.*, 2014) (Fig. 1e). Satellite reflections on Fast Fourier Transform (FFT; inset Fig. 1c) are concordant with interpretation of maghemite superstructures.

The strongest overprint is recognised as: (i) abundant lattice-scale defects (twinning, faults), K- and Al-banding, SiO_2-rich inclusion subpopulation and replacement by fluorite in the magnetite from RDG with Fe-oxide nodules; and (ii) conspicuous U, Y and As-enrichment along trails cross-cutting zonation (Fig. 1b and inset), in the carbonate-hosted, massive magnetite occurrence. Calc-silicates are present within Si-magnetite from RDG on the eastern side at OD whereas Ca-Al-bearing amphibole (tschermakite - used as a proxy for the crystal structure model (Abdu and Hawthorne, 2009)) is identified by imaging (Fig. 1f) and mapping of inclusions in magnetite from WW.

DISCUSSION AND CONCLUSIONS

Formation of mineral inclusions in all samples analysed here is attributable to coarsening of Si-magnetite nanoprecipitates during interaction with fluids enriched in elements typical of that evolution stage, e.g., K-Al-

banding and calc-silicates are compatible with early alkali- calcic alteration in IOCGs. Some of these elements can be enriched during early-mineral replacement of granite (Ca, Al, Mg, Ti from plagioclase+mica in RDG). Higher-T for the Ca- Al-amphibole stability may be a response to post-Donington metamorphism. Carbonate- hosted magnetite could be inherited from pre-existing BIF horizons in sediments intruded by RDG but with an IOCG overprint as recognised from the U-Y-As signature. Si-magnetite in samples studied here is distinct from magmatic magnetite in RDG (Cook *et al.*, 2017), or vein-magnetite in volcanics from ODD, both typified by exsolutions of ilmenite±rutile+hercynite. It also differs from occurrences elsewhere studied at the nanoscale, e.g., kin IOCG deposits containing both Ti-spinel and calc-silicates (Deditius *et al.*, 2018), or low-T metamorphosed BIFs (Huberty *et al.*, 2012; Xu *et al.*, 2014). Si-magnetite represents a petrogenetic tool if used in a given context and with the complexity of crystal- chemical phenomena adequately characterised down to the nanoscale.

REFERENCES

Abdu Y.A., Hawthorne F.C., 2009. Crystal structure and Mössbauer spectroscopy of tschermakite from the ruby locality at Fisknaesset, Greenland. Canadian Mineralogist 47, 917-926.

Cook, N.J., Ciobanu, C.L., Ehrig, K., Slattery, A., Verdugo-Ihl, M.R., Courtney-Davies, L. and Gao, W., 2017. Advances and opportunities in ore mineralogy. Minerals 7(12), 233; doi:10.3390/min7120233.

Deditius A.P., Reich, M., Simon, A.C., Suvorova, A., Knipping, J., Roberts, M.R., Rubanov, S., Dodd, A., Saunders, M., 2018. Nanogeochemistry of hydrothermal magnetite. Contributions to Mineralogy and Petrology, 173, 46; https://doi.org/10.1007/s00410-018-1474-1.

Huberty, J.M., Konishi, H., Heck, P.R., Fournette, J.H., Valley, J.W., Xu, H.F., 2012. Silician magnetite from the Dales Gorge Member of the Broc kman Iron Formation, Hamersley Group, Western Australia. American Mineralogist 97, 26–37.

Xu, H., Shen, Z., Konishi, H., 2014. Si-magnetite nano-precipitates in silician magnetite from banded iron formation: Z-contrast imaging and ab initio study. American Mineralogist 99, 2196–2202.

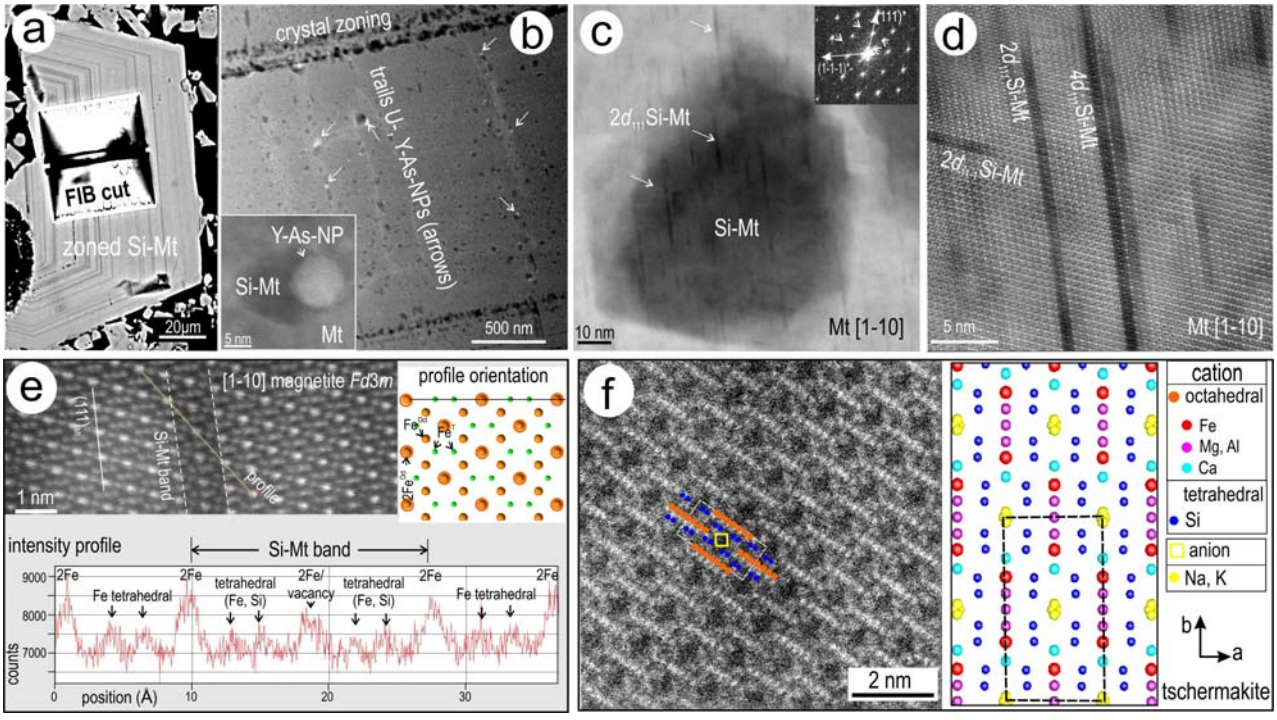

Fig. 1 (a) Back-scatter electron image showing location of FIB-cut across zoning in Si- magnetite. HAADF STEM images of Si-magnetite (b-e) and amphibole (f). Satellite reflections arrowed on FFT (inset) obtained from image in (c). Intensity profile (e) and crystal-structure models (e,f). Tschermakite (Abdu and Hawthorne, 2009) is used as a proxy for the Ca-Al-amphibole. The (Na,K) position has the best fit for the image compared to other potential Ca- amphiboles (e.g., actinolite). Imaging and EDX-STEM at 200 kV (Titan Themis; Adelaide Microscopy).

REE-, Sr- Ca-ARSENATE-PHOSPHATE- SULPHATE MINERALS OF THE WOODHOUSEITE SERIES AND THEIR ROLE AS HOSTS FOR RADIONUCLIDES

Nicholas D Owen[1], Nigel J Cook, Mark Rollog, Kathy J Ehrig, Danielle S Schmandt, Cristiana L Ciobanu

[1]*School of Chemical Engineering, University of Adelaide, Australia - nicholas.owen@adelaide.edu.au*

BACKGROUND

Aluminium-phosphate-sulphate (APS) minerals of the alunite supergroup (Kolitsch and Pring 2001) form in geological environments ranging from sedimentary settings (Tripplehorn *et al.* 1991; Rasmussen 1996; Pe-Piper and Dolansky 2005) to hydrothermal ore deposits such as the giant Olympic Dam [OD] Cu-U-Au-Ag deposit, South Australia (Ehrig *et al.* 2012). Sulphate-free phosphate members and phosphate-free sulphate members (e.g. florencite, jarosite) have been previously identified from OD but the occurrence and composition of mixed phosphate-sulphate members such as those of the woodhouseite series (woodhouseite, svanbergite, etc.) have been inadequately characterised in prior studies. The woodhouseite series represents a broad field of solid solution between florencite, crandallite and goyazite; coupled substitutions between the 'A' and the 'X' sites preserve overall charge balance (Pe-Piper and Dolansky 2005).

Here, we report Sr-Ca-dominant APS minerals of the woodhouseite series from OD with the general formula $AB_3(PO_4)_{1+x}(SO_4)_{1-x}(OH)_6 \cdot n(H_2O)$, where A=Ca, Sr, REE, Pb, and B=Al, Fe, Ga. These phases are of interest for two reasons: the observed replacement relationships with Cu-(Fe)-sulphides that can shed light on ore evolution; and the potential ability of APS minerals in ores and copper concentrates to accommodate, within the 'A' site, ^{238}U decay generated radionuclides (RN), notably ^{226}Ra, ^{222}Rn, ^{210}Po, ^{210}Bi and ^{210}Pb.

METHODS

Samples of Cu-sulphide flotation concentrates (FC) and concentrates following removal of the majority of uranium via sulphuric acid leaching (concentrate leach discharge, CLD) were collected from the Olympic Dam metallurgical processing plant. Backscatter electron (BSE) images were used to document textures and compositional zoning. Quantitative electron microprobe data allowed categorisation of APS minerals present. *In-situ* isotope mapping was attained using a Cameca NanoSIMS 50L (Centre for Microscopy, Characterisation, and Analysis, UWA; methodology described in Rollog *et al.* 2018).

RESULTS

Individual APS mineral grains show significant variation in backscatter contrast on BSE images, consistent with grain-scale compositional zonation. Different zones are variably enriched in REE, Ca and Sr, whereby brighter zones are typically richer in REE. Several species (REE-, Ca-, and Sr-dominant) are present. BSE imaging and EDAX data indicate that different zones also show variation with respect to S and P, suggesting that some are phosphate-dominant, and others are sulphate-dominant. Grains range from finely mottled in appearance through to needle-like grains and then coarsening towards those with tabular morphology, which appear particularly strongly zoned. Coarser subhedral varieties (Figure 1a) can be interpreted as having replaced pre-existing minerals such as bastnäsite (Schmandt *et al.* 2018), florencite or apatite (Stoffregen and Alpers 1987). Sr-Ca-dominant APS minerals (svanbergite, goyazite) are observed to replace Cu-Fe-sulphides (Figure 1b), often showing a modification of grain morphology within the APS minerals along interface boundaries (e.g. a fine-grained replacement zone surrounding coarser grains). Sr-Ca-APS minerals often contain remnants of replaced Cu-Fe-sulphides and gangue including Fe- oxides.

The EPMA dataset shows that REE-phosphate-dominant members are low in total Pb, with Pb concentrations increasing as Ca, Sr and S content rises (Figure 1c). The Pb content also increases with increasing (calculated) H_2O content.

NanoSIMS investigation of FC and CLD samples confirms the presence of RN within Sr-Ca- dominant APS minerals. Within most mapped areas (e.g. Figure 1d-f), there appears to be an excess of daughter ^{226}Ra and ^{210}RN (overwhelmingly ^{210}Pb) compared to the equivalent map for parent ^{238}U. ^{226}Ra and ^{210}RN are also more dispersed throughout the APS minerals than ^{238}U and elevated signals for ^{226}Ra and ^{210}RN do not always coincide with those for ^{238}U. The distribution of ^{210}RN throughout the APS minerals appears to correlate strongly with that of Ca. These qualitative distribution patterns strongly suggest micron-scale migration of ^{226}Ra and ^{210}RN from parent ^{238}U-bearing phases, and possibly diffusion into APS. Although the number of examples mapped by nanoSIMS is currently limited, our mapping also indicates that RN activities are significantly greater within Sr-Ca-APS minerals in the CLD samples

than in the FC samples, suggesting fluid-mineral interaction and sub-solidus diffusion during leaching. The observed difference in 210RN concentrations between FC and CLD samples may also be amplified due to the recycling of Cu-sulphate-rich smelter dust, which is consequently enriched in 210RN, into the leach solution to maximise Cu recovery.

CONCLUSIONS

Textural relationships between Sr-Ca-dominant APS minerals and Cu-(Fe)-sulphides indicate formation at a relatively late stage in the evolution of the deposit. NanoSIMS mapping indicates these minerals carry RN within the processing cycle, especially from ^{226}Ra onwards. Further characterisation of the APS minerals and doping experiments on synthetic analogues are currently in progress to further understand cation (including RN) exchange mechanisms in APS of variable composition.

REFERENCES

Ehrig, K., McPhie, J., Kamenetsky, V.S., 2012. Geology and Mineralogical Zonation of the Olympic Dam Iron Oxide Cu-U-Au-Ag Deposit, South Australia. In: F. Camus, J.W. Hedenquist, M. Harris (eds.), Geology and Genesis of Major Copper Deposits and Districts of the World, a Tribute to Richard Sillitoe, Society of Economic Geology Special Publication, 16, 237–267.

Kolitsch, U., Pring, A., 2001. Crystal chemistry of the crandallite, beudantite and alunite groups: a review and evaluation of the suitability as storage materials for toxic metals. Journal of Mineralogical and Petrological Sciences, 96, 67–78.

Pe-Piper, G., Dolansky, L.M., 2005. Early diagenetic origin of Al phosphate-sulfate minerals (woodhouseite and crandallite series) in terrestrial sandstones, Nova Scotia, Canada. American Mineralogist, 90, 1434–1441.

Rasmussen, B., 1996. Early-diagenetic REE-phosphate minerals (florencite, gorceixite, crandallite, and xenotime) in marine sandstones; a major sink for oceanic phosphorus. American Journal of Science, 296, 601–632.

Rollog, M., Cook, N.J., Gugliardo, P., Ehrig. K., Kilburn, M., 2018. In situ spatial distribution mapping of radionuclides in minerals by nanoSIMS. Geochemistry – Exploration, Environment, Analysis, in press.

Schmandt, D.S., Cook, N.J., Ehrig, K., Ciobanu, C.L., Wade, B.P., Gilbert, S., Kamenetsky, V.S. 2017. Rare earth element fluorocarbonate minerals from the Olympic Dam Cu-U-Au-Ag deposit, South Australia. Minerals, 7(10), 202; doi: 10.3390/min7100202.

Stoffregen, R.E., Alpers, C.N., 1987. Woodhouseite and svanbergite in hydrothermal ore deposits; products of apatite destruction during advanced argillic alteration. *The Canadian Mineralogist* 25, 201–211.

Triplehorn, D.M., Stanton, R.W., Ruppert, L.F., Crowley, S.S., 1991. Volcanic ash dispersed in the Wyodak-Anderson coal bed, Powder River basin, Wyoming. Organic Geochemistry, 17, 567–575.

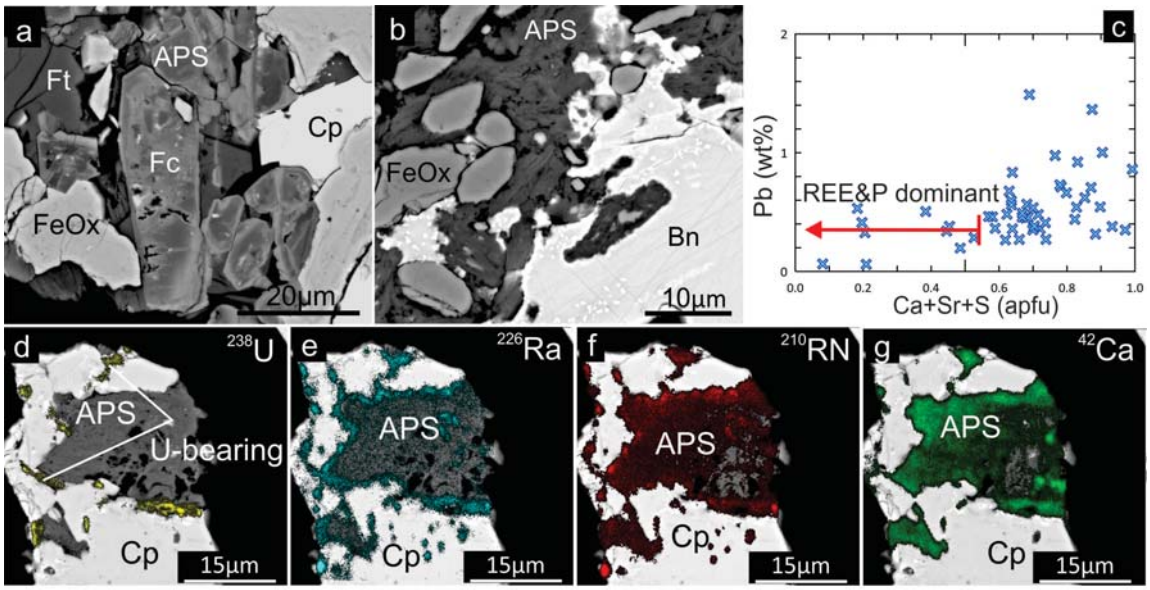

Figure 1: (a,b) BSE images showing APS mineral-bearing assemblages. (c) EPMA data showing the relationship between total Pb (wt%) and (Ca+Sr+S) (apfu). (d-g) NanoSIMS isotope maps of representative area within CLD sample showing distributions of 238U, 226Ra, 210RN and 42Ca within APS. Aluminium-phosphate-sulphate-APS, bornite-Bn, chalcopyrite-Cp, florencite-Fc, Fe-oxide-FeOx, fluorite-Ft.

METAL-BEARING NANOPARTICLES IN HEMATITE

Max R. Verdugo-Ihl, Cristiana L. Ciobanu[1], Nigel J. Cook, Ashley Slattery, Kathy J. Ehrig, Liam Courtney-Davies

[1]*School of Chemical Engineering, The University of Adelaide - max.verdugoihl@adelaide.edu.au*

BACKGROUND

Interaction between minerals and hydrothermal fluids can result in pseudomorphic replacements if dissolution- and (re-)precipitation rates are coupled with one another (CDRR). Such processes are mediated by reaction interfaces along which transient porosity is generated, in which mineral inclusions as products of fluid-mineral interactions can precipitate (Tooth *et al.,* 2011). Hydrothermal hematite from the granite-hosted, iron-oxide-copper-gold deposit at Olympic Dam, South Australia, displays a distinct enrichment in granitophile elements (U-Pb-W-Sn-Mo) (Verdugo-Ihl *et al.*, 2017). These geochemical signatures can be modified within grains featuring partial to complete pseudomorphic replacement of hematite that results in a newly-formed hematite featuring new sets of zonation, porosity, and/or micron-scale inclusion-attached pores. Commonly, the composition of the new hematite differs markedly from that of its precursor.

Among the products of hematite replacement via CDRR discussed in (Verdugo-Ihl *et al.,* 2017), samples from bornite-chalcocite and sulphide-poor intervals represent two unusual cases. These samples, studied here at the nanoscale, originate from the upper mineralised level in the SE-part of the orebody, ~170 m apart from one another. In the first case, a mm-sized hematite grain is partially replaced by hematite depleted in W but preserves some of the other primary elements (e.g., Sn). In the second case, newly-formed oscillatory zonation patterns in hematite are defined by As and Cu-rich bands. Such patterns form overgrowths on the more common U-Pb-W-Sn-Mo oscillatory zoning.

Here, we present evidence for metal-bearing nanoparticles (NPs) occurring along trails of inclusions in such hematites and for the re-precipitation of the host hematite. These observations assist in understanding the behaviour of trace elements during CDRR and, thus, constrain mechanisms of metal remobilisation during superimposed fluid percolation.

METHODS

Foils were prepared for transmission electron microscopy (TEM) by focused ion beam (FIB)- SEM, cut across: (I) a relict U-Pb-W-Sn-Mo zonation pattern showing microfractures/pores, and (II) the unusual Cu-As-rich overgrowths. The foils were analysed using High Angle Annular Dark Field (HAADF) scanning-TEM (STEM) imaging and energy dispersive X-ray spectrometry (EDX)-STEM mapping (Titan Themis instrument operated at 200 kV).

RESULTS

Case-I hematite displays nm-sized inclusions along densely populated, longer trails (Fig. 1a) and shorter sets of splays (Fig. 1b) branching from the main trails. Up to ~200-300 nm sized inclusions occur sporadically along swarms of smaller NPs (1-5 nm). All inclusions along the main trails have comparable contents of Si, Cl, K, Na, and occasionally As (EDX-STEM spot- analysis/mapping). Metal-bearing NPs, mostly W-bearing phases (ferberite and/or WO_3; Fig. 1c) occur attached to silica-bearing inclusions (Fig. 1b).

Case-II hematite displays inclusion trails comparable to *case-I* but also shows As-rich bands of different orientation to the trails, which host As(±Pb)-bearing NPs. As in *case-I*, the trails feature inclusion populations of variable size (from ~5 up to hundreds of nm). However, the coarsest inclusions are multicomponent and often comprise metal-bearing NPs (Cu, As, Mo, W, and Sn; Fig. 1d). As in *case-I*, elements such as K, Na, and Cl are measurable throughout the composite inclusions. The presence of such elements, as well as rounded voids (Fig. 1a, d), suggest that coarser inclusions correspond to fluid inclusions containing a volatile phase that were opened during FIB-milling. The occurrence of clustered Cu-NPs (5-10 nm) is also noted on the walls of voids. High-resolution HAADF-STEM imaging of hematite along the trails displays nanodomains of variable orientation, defects and sets of twinning (Fig. 1e), which differs from the host hematite that consists of a single grain almost devoid of defects. This is evidence that the hematite along the inclusion trails is a fine-grained precipitate formed during interaction between precursor hematite and pervading fluids.

DISCUSSION AND CONCLUSIONS

Metal-bearing NPs along splays branching with fluid inclusion trails are sourced by the release of W and other elements from primarily-zoned domains in host hematite. Evolution of this process led to precipitation of W-depleted

domains adjacent to areas studied here. The antipathetic behaviour of W relative to other granitophile elements (e.g., Sn) may be attributed to their different complexation behaviour during interaction with the pervading fluid at the reaction front. Given the close association between W- and silica-bearing NPs along the splays, we speculate about the reaction of silica-bearing fluids interactive with W but not with other elements.

Results indicate 'open system behaviour' of granitophile elements, including U, in domains that may otherwise be considered reliable for high-precision U-Pb dating (see Courtney-Davies *et al.*, 2018). The presence of metal-bearing fluid inclusions also shows the role played by CDRR in trapping metals released during interaction with fluids. In this case, S-depleted fluids can be invoked to explain precipitation of native elements as NPs, correlating with the presence of Cu-Au alloys, and indeed coarser particles of native copper (Verdugo-Ihl *et al.*, 2017).

REFERENCES

Courtney-Davies, L., Ciobanu, C.L., Tapster, S.R., Cook, N.J., Ehrig, K.J., Kennedy, A.K., Condon, D.J., Verdugo-Ihl, M.R., Wade, B.S., Gilbert, S.E., 2018. The U-Pb systematics of hydrothermal hematite; Insights from the IOCG system at Olympic Dam, South Australia, 15th Quadrennial Symposium of the International Association on the Genesis of Ore Deposits (IAGOD) this volume.

Tooth, B., Ciobanu, C.L., Green, L., O'Neil, B., Brugger, J., 2011. Bi-melt formation and gold scavenging from hydrothermal fluids: An experimental study, Geochimica et Cosmochimica Acta, 75, 5423-5443. doi: 10.1016/j.gca.2011.07.020.

Verdugo-Ihl, M.R., Ciobanu, C.L., Cook, N.J., Ehrig, K.J., Courtney-Davies, L., Gilbert, S., 2017. Textures and U-W-Sn-Mo signatures in hematite from the Olympic Dam Cu-U-Au-Ag deposit, South Australia: Defining the archetype for IOCG deposits, Ore Geology Reviews, 91, 173-195. doi: 10.1016/j.oregeorev.2017.10.007.

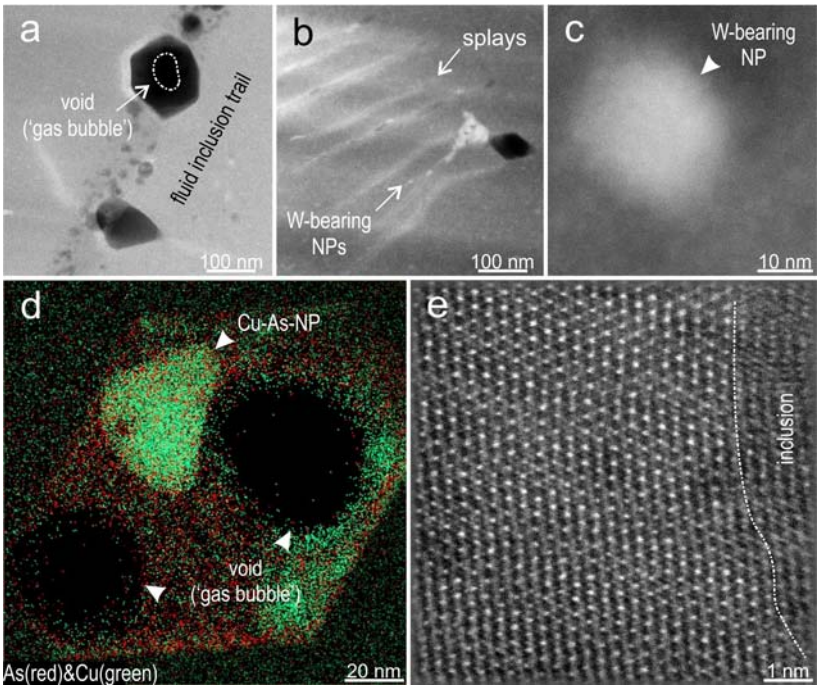

Fig. 1. HAADF-STEM images (a-c, e) and EDX-STEM map (d) showing aspects of inclusions and metal-bearing NPs in recrystallised hematite. See text for further explanations.

GEOLOGICAL SETTING OF BIF ORES, MIDDLEBACK RANGES, SOUTH AUSTRALIA

William Keyser[1], Cristiana L. Ciobanu, Nigel J. Cook, Liam Courtney-Davies, Holly Feltus, Geoff Johnson, Allen Kennedy, Kathy Ehrig

[1]*School of Chemical Engineering, The University of Adelaide - william.keyser@adelaide.edu.au*

INTRODUCTION

The Middleback Ranges form a 60 km-long, N-S striking BIF-hosted iron ore belt in the northeastern Eyre Peninsula, Gawler Craton, South Australia, comprising >20 discrete deposits and prospects (Fig. 1A). The belt is hosted within a granite-gneissic basement terrane considered of Archean to Paleoproterozoic age (Szpunar *et al.,* 2011). Various mafic rocks of debated age are found concordant or discordant to the BIFs along the belt. Iron-oxides from BIFs and ores throughout the belt exhibit textural variation and modification of geochemical signature resulting from overprinting event(s), e.g., interaction with base-metal bearing fluids (As, Sb), or elements attributable to granitic affiliation (Sn, Mo, W, U, REE+Y) (Dmitrijeva *et al.,* 2018, Keyser *et al.,* 2018). The variation of iron-oxide chemistry seen throughout the belt emphasises the need to investigate local deposit settings. One such example is recognized at Iron Count (Fig. 1A) where hematite mineralization shows evidence for interaction with fluids derived from granitic/volcanic rocks emplaced during a ~1790 Ma intracontinental rifting event (Fig. 1B).

Here, we present petrographic and geochronological data for mafic rocks and granitoids associated with several orebodies from the Middleback Ranges with the purpose of better constraining environments of BIF deposition and subsequent tectonomagmatic events that may have impacted on iron-oxide geochemistry.

METHODS

The sample suite for the present study comprises amphibole-bearing mafic rock types and granites. Sensitive high-resolution ion microprobe (SHRIMP) data for zircons separated and concentrated from the samples was obtained using a SHRIMP II at the John De Laeter Centre, (Perth, Western Australia). Uranium-bearing hematite from one deposit was dated by Laser-Ablation Inductively-Coupled Plasma-Mass Spectrometry (LA-ICP-MS) using GJ zircon as internal standard (Adelaide Microscopy).

RESULTS

Granites preserve magmatic alkali-feldspars but display varying degree of alteration whereby magmatic plagioclase (oligoclase) and biotite are rarely observed. Hydrothermal alteration is recognized as calcic (garnet-titanite-calcite-apatite) and potassic (Ba-bearing K- feldspar) in the northern (Iron Monarch) and central (Iron Baron) parts of the belt, respectively. In the south (Iron Magnet), syn-deformational alteration of the granitic basement, thrust onto BIF sequences, is expressed as shears affecting feldspar phenocrysts and comprising new micas, albite and a variety of REE-minerals.

Mafic rocks concordant with BIF sequences at Iron Magnet display a marked schistosity and preserve assemblages recording amphibolite-facies metamorphism (Mg-Fe- and Ca- amphiboles, almandine, biotite, corundum), as well as accessories attributable to an igneous origin (magnetite with trellis-like exsolution of ilmenite). These are nonetheless retrogressed to chlorite facies and locally affected by metasomatism (tourmalinization). In contrast to such lithologies, NW-SE trending mafic dikes crosscutting BIFs are more common throughout the belt. These display doleritic textures consisting of Ca-amphibole and plagioclase and contain Fe-Ti oxides, apatite and baddeleyite as accessories.

SHRIMP U-Pb zircon ages (207Pb/206Pb weighted means) at ~3.1 Ga from granites across the belt are interpreted as the timing of magmatic crystallization (Fig. 1B), whereas the amphibolite at Iron Magnet yields an age of 2670±18 Ma, interpreted as the emplacement age. Zircon from dikes in the central part of the belt produced a spread of ages pointing towards younger emplacement <1.0 Ga. U-Pb dating of hematite from ores from the Iron Knight deposit also yielded young (~650 Ma) ages (Fig. 1B).

DISCUSSION AND CONCLUSIONS

The consistent ages of ~3.1 Ga for the studied granites suggest a more extensive distribution of the ~3.15 Ga Cooyerdoo Granite suite (and other granites ~100 Ma older still, e.g., Sultan) than previously recognised, and support the existence of an Archean basement beneath the entire Middleback Ranges BIF sequence. Although no granite ages attributable to the regionally expansive Donington Magmatic Suite (~1850 Ma) or Hiltaba Suite (~1590 Ma) were found, overprints during post-Archean metamorphism and/or magmatic events (Fig. 1B) are recognizable

from retrograde metamorphism and hydrothermal alteration affecting both granites and amphibolites. These correlate with zircon domains of variable Pb-loss yielding discordant data.

The distribution of mafic rocks throughout the belt suggests intervals of magmatism contemporaneous with BIF deposition, which extended until <1.0 Ga. However, a firm age for dikes requires further constraints. Nonetheless, the present study confirms that dikes were emplaced throughout the belt during younger, tectonothermal events and likely affected BIFs and related ores, e.g. the younger ~650 Ma U-Pb age (Fig. 1B) obtained for Iron Count hematite. Importantly, the 2670±18 Ma age obtained from the dated amphibolite concordant with BIF supports their deposition during the Archean.

REFERENCES

Dmitrijeva, M., Metcalfe, A.V., Ciobanu, C.L., Cook, N.J., Frenzel, M., Keyser, W.M., Johnson, G., Ehrig, K., 2018. Discrimination and variance structure of trace element signatures in hematite: a case study of BIF-mineralization from the Middleback Ranges, South Australia. Mathematical Geosciences (in press). https://doi.org/10.1007/s11004-018-9734-1.

Keyser, W.M., Ciobanu, C.L., Cook, N.J., Johnson, G., Feltus, F., Johnson, S., Dmitrijeva, M., Ehrig, K., Nguyen, P., 2018. Petrography and trace element signatures of iron-oxides in deposits from the Middleback Ranges, South Australia: from banded iron formation to ore. Ore Geology Reviews 93, 337-360.

Szpunar, M., Hand, M., Barovich, K., Jagodzinski, E., Belousova, E., 2011. Isotopic and geochemical constraints on the Paleoproterozoic Hutchison Group, southern Australia: Implications for Paleoproterozoic continental reconstructions. Precambrian Research 187, 99-126.

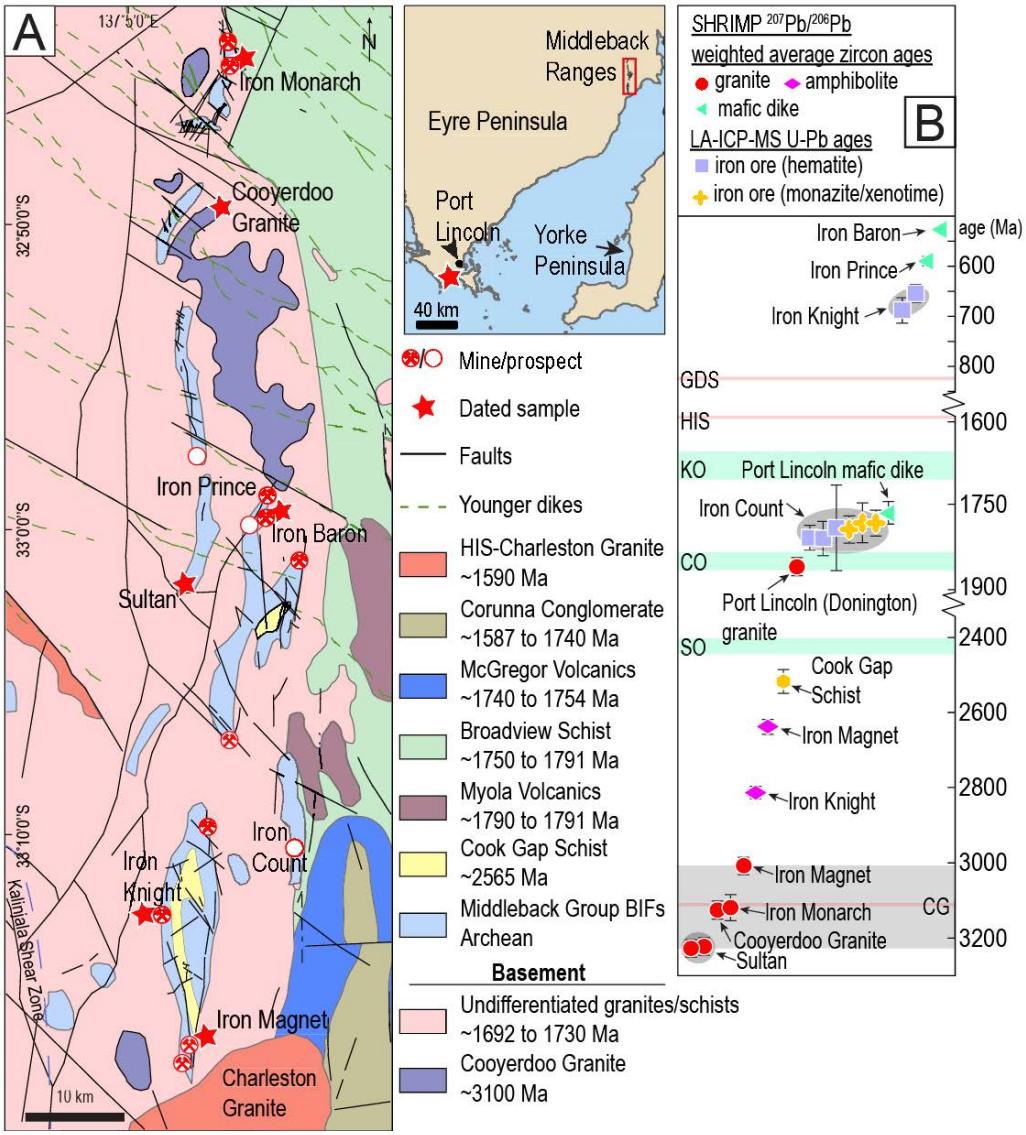

Figure 1. A) Geological map of the Middleback Ranges. B) U-Pb ages for rocks and hematite ores (as marked) in the context of the tectonomagmatic events affecting the eastern Eyre Peninsula. CG-Cooyerdoo Granite; CO-Cornian Orogeny; GSD-

NANO- TO MICRON-PARTICULATE GOLD HOSTED BY MAGNETITE FROM THE BEIYA GIANT GOLD DEPOSIT, SW CHINA: A PRODUCT OF GOLD SCAVENGING BY BISMUTH MELTS

Xiaoming Sun

Sun Yat- sen University, Guangzhou, China - eessxm@mail.sysu.edu.cn

In many hydrothermal deposits, gold always occurs as mineral inclusions and invisible gold hosted by sulphide minerals such as pyrite and arsenopyrite. This is due to the affinity of gold for reduced sulphur. Although oxide minerals such as magnetite have been proposed as important gold host minerals, the occurrence and mechanisms of gold incorporation within magnetite are poorly constrained.

The Beiya gold deposit, located in the southeast Tibetan Plateau, to the east of Jinshajiang- Red River fault zone, is one of the largest gold deposits in China. The deposit is regard as a porphyry-skarn system and is related to a porphyritic alkaline and potassic quartz syenite with zircon U-Pb ages of ~35 Ma. It contains a sizable resource of 125.6 Mt @ 2.42 g/t Au, 169.6 Mt @ 42.56 g /t Ag, 138 Mt @ 33.34 % Fe, 122.9 Mt @ 0.48 % Cu, 131.5 Mt @ 1.84 % Pb, and 145.7 Mt @ 0.35 % Zn. The dominant gold orebodies are skarn-style and are composed of amounts of massive magnetite ores. Here, we demonstrate that abundant nano- to micron-sized gold inclusions are hosted by magnetite from massive magnetite ores. These gold inclusions are present as native gold and electrum 10 nm to 10 Mm in size. They occur in magnetite as randomly disseminated blebs or concentrated in dense patches. Native bismuth was observed within the same assemblage and there is an immediate association between native bismuth and gold.

Native bismuth, when molten is an efficient gold scavenger proven experimentally. Previous study indicated that the prevailing temperatures of magnetite growth in Beiya exceeded the melt point of native bismuth (271°C). We propose that deposition of nano- to micro- particulate gold in magnetite from skarn ores at Beiya can be attributed to Bi melts scavenging gold under the variations of both oxygen and hydrogen sulfide fugacities. The early fluctuation of $O_{2(g)}$ led to pulses of Bi melts, scavenging and refining Au from the hydrothermal fluids, while the drop in $aH_2S_{(aq)}$ eventually terminated it. Therefore, abundant Bi-melts occurred during magnetite growth and subsequently scavenged gold from the hydrothermal fluids is one of the significant mechanisms resulting in enormous Au- enrichment at Beiya. This study also indicates that magnetite-rich systems are also potential targets for Au exploration and extraction.

*This work was jointly supported by the National Natural Science Foundation of China (N° U1302233, 40830425, 40673045, 40873034), the National Key Basic Research Program (N° 2015CB452604, 2009CB421006; Ministry of Science and Technology, China).

NEW CONSTRAINS ON THE GENESIS OF THE DABAOSHAN POLYMETALLIC DEPOSIT, SOUTH CHINA: TEXTURAL, TRACE ELEMENT, AND Re–Os ISOTOPIC ANALYSES OF SULFIDES

Lei Wang

Wuhan Center of Geological Survey, China Geological Survey - cgsleiwang@163.com

BACKGROUND

Massive sulfide deposits that formed in late Paleozoic basins in South China are typically overprinted by porphyry and skarn systems associated with Yanshanian magmatism. This results in the coexistence of various genetic types of mineralization in the same region or even within a single deposit (Xu *et al.*, 1996; Gu *et al.*, 2007; Zaw *et al.*, 2007). The Dabaoshan deposit is a large-sized polymetallic deposit in northern Guangdong province, South China, and consists mainly of porphyry- and skarn-type Mo–W mineralization that is genetically related to Jurassic porphyritic intrusions and adjacent stratabound Cu–Pb–Zn mineralization hosted in mid-Devonian limestone (Liu and Zhou, 1985). It has been debated for a long time whether the stratiform Cu–Pb–Zn mineralization is related to a Jurassic porphyry Cu–Mo system (e.g., Liu and Zhou, 1985; Cai and Liu, 1993; Wang *et al.*, 2011), or, alternatively, to a Devonian exhalative event with Jurassic overprinting (e.g., Ge and Han, 1986; Yang, 1997; Gu *et al.*, 2007; Ye *et al.*, 2011, 2014). In this study, we present textural, and in-situ trace element and Re–Os isotopic data for sulfides to constrain the genesis of the Dabaoshan polymetallic deposit.

METHODS

Sulfide samples and polished sections from the Dabaoshan stratabound Cu–Pb–Zn orebodies were selected for Re–Os isotopic and in-situ LA–ICP–MS trace element analyses, respectively. The analyzed minerals include pyrrhotite, chalcopyrite, pyrite, and sphalerite. Re–Os isotopic analyses (n = 11) were performed at the Re–Os Laboratory of the National Research Center for Geoanalysis, Chinese Academy of Geological Sciences (CAGS), Beijing, China. In-situ trace element analyses (n = 188) were conducted using a 213 nm New Wavelaser coupled to an ELEMENT2 ICP–MS system at the National Research Center for Geoanalysis, CAGS.

RESULTS

ORE TEXTURE

Detailed observations of field outcrops, hand specimens, and thin sections allowed four types of pyrrhotite and three types of chalcopyrite to be identified in the Dabaoshan stratiform Cu–Pb–Zn orebodies. Type 1 pyrrhotite (Po-1) is fine-grained (mainly ≦50 μm), anhedral, disseminated, and is locally intergrown with fine-grained anhedral chalcopyrite (Ccp-1, mainly ≦50 μm). Po-1 shows primary syn-sedimentary textures but has clearly been altered by the later hydrothermal fluids. Type 2 pyrrhotite (Po-2) commonly coexists with Po-1 in single hand specimen or thin section and occurs as veins or blocks with widths of 100 Mm to tens of centimeters. These pyrrhotite crystals locally show ~120° triple-junction grain boundaries in the wider veins and blocks. Po-1 and Ccp-1, which are close to the veins and blocks, show an increase in size. Type 3 pyrrhotite (Po-3) is coarse-grained, massive, shows ~120° triple-junction grain boundaries, and locally coexists with residual Po-1. Po-3 has been replaced by fine-grained anhedral chalcopyrite (Ccp-2) and by K-feldspar, biotite, and quartz as a result of metasomatism by hydrothermal fluid. Type 4 pyrrhotite (Po-4) is coarse-grained, anhedral, and has been replaced by coarse-grained and massive chalcopyrite (Ccp-3); both Po-4 and Ccp-3 have been replaced by anhedral sphalerite (Spl). The mineral associations, crystal textures, and replacement relationships indicate that the sulfides were precipitated in the following order: Po-1 (Ccp-1) → Po-2 → Po-3 → Ccp-2 → Po-4 → Ccp-3 → Spl.

TRACE ELEMENT COMPOSITIONS

There are both similarities and differences among the trace element compositions of the different types of pyrrhotite. From Po-1 to Po-4, Cu contents gradually increase, along with Zn, Cd, and Ag contents, whereas there is no significant change in Pb and Au contents. The extremely high values of Cu and Zn contents may reflect the presence of inclusions of Cu- bearing minerals in Po-2 and Po-4, and of Zn-bearing minerals in Po-4. The Co, Ni, As, Se, and Te contents show only minor differences from Po-1 to Po-4, generally with low Co and high Ni contents. The Co/Ni ratios are <1 and gradually increase as follows: Po-1 (0.001–0.052) → Po-2 (0.006–0.018) → Po-3 (0.001–0.124) → Po-4 (0.002–0.138). These data suggest a primary syn-sedimentary genesis, although the textures of Po-2, Po-3,

and Po-4 indicate overprinting by hydrothermal fluid (e.g., ~120° triple-junction grain boundaries). The S/Se ratios increase as follows: Po-1 (5324–80,708) → Po-2 (5035–83,068) → Po-3 (5575–133,939) → Po-4 (4612–151,516), suggesting that Se, S in pyrrhotite were sourced from deep hydrothermal fluid and seawater sulfate.

Re-Os ISOTOPES

Eight pyrrhotite and three chalcopyrite samples from the Dabaoshan stratiform Cu–Pb–Zn orebodies were examined for Re-Os analysis. Pyrrhotite samples (five samples of Po-3 and three of Po-1) have Re and Os concentrations of 100–1093 ppt and 7–78 ppt, respectively. Combined with seven pyrrhotite samples (Po-3) analyzed by Ying *et al.* (2017), they yield a Devonian Re–Os isochron age of 372 ± 40 Ma (n = 15, MSWD = 287, Os = 0.332 ± 0.074). Three chalcopyrite samples (Ccp-3) have Re and Os concentrations of 70–437 ppt and 5–23 ppt, respectively. Combined with five chalcopyrite samples (Ccp-3) analyzed by Ying *et al.* (2017), they yield a Re–Os isochron age of 240 ± 36 Ma (n = 8, MSWD = 59, Osi = 0.55 ± 0.17). Previously published Re–Os isochron/model ages for molybdenite from porphyry- and skarn-type Mo–W orebodies related to the Jurassic porphyritic intrusions range from 163.2 ± 2.3 to 166.6 ± 0.8 Ma (Wang *et al.*, 2011; Li *et al.*, 2012; Qu *et al.*, 2014).

CONCLUSIONS

Four types of pyrrhotite have been identified in the Dabaoshan stratiform Cu–Pb–Zn orebodies. Textures and trace element compositions indicate that the primary syn- sedimentary genesis at 372 ± 40 Ma has been overprinted by hydrothermal fluid at 240 ± 36 Ma. The Dabaoshan deposit is likely the product of superimposed mineralization events rather than a single event as proposed previously.

REFERENCES

Cai, J.H., Liu, J.Q., 1993. Research and its application of the inclusions characteristics in the Dabaoshan polymetallic deposit, north Guangdong. Journal of Mineralogy and Petrology, 13(1), 33-40 (in Chinese with English abstract).

Ge, C.H., Han, F., 1986. Submarine volcanic hydrothermal sedimentary origin of the Dabaoshan iron and polymetallic sulfide deposit. Mineral Deposits, 5(1), 1-12 (in Chinese with English abstract).

Gu, L.X., Zaw,K., Hu,W.X., Zhang, K.J., Ni, P., He, J.X., Xu, Y.T., Lu, J.J., Lin,C.M., 2007. Distinctive features of Late Palaeozoic massive sulphide deposits in South China. Ore Geology Reviews, 31, 107–138. https://doi.org/10.1016/j.oregeorev2005.01.002.

Li, C.Y., Zhang, H., Wang, F.Y., Liu, J.Q., Sun, Y.L., Hao, X.L., Li, Y.L., and Sun, W., 2012. The formation of the Dabaoshan porphyry molybdenum deposit induced by slab rollback. Lithos, 150, 101–110. https://doi.org/10.1016/j.lithos.2012.04.001.

Liu, X.S., Zhou, S.Z., 1985. On the occurrence of middle ordovician volcanics and analysis of ore-forming mechanism of siderite polymetallic ore deposit from Dabaoshan, Qujiang county, Guandong province. Journal of Nanjing University, 21(2), 348-360 (in Chinese with English abstract).

Qu, H.Y., Chen, M.H., Yang, F.C., Gao, Z.H., Wang, Y.W., Zhao, H.J., Yu, C.F., 2014. Metallogenic chronology of the stratiform Cu orebody in the Dabaoshan polymetallic deposit, northern Guangdong Province and its geological significance. Acta Petrologica Sinica, 30(1), 152-162 (in Chinese with English abstract).

Wang, L., Hu, M., Yang, Z., Qu, W., Xia, J., and Chen, K., 2011. U-Pb and Re-Os geochronology and geodynamic setting of the Dabaoshan polymetallic deposit, northern Guangdong province, South China. Ore Geology Reviews, 43, 40–49. https://doi.org/10.1016/j.oregeorev.2011.06.008.

Xu, K.Q, Wang, H.N., Zhou, J.P., Zhu, J.C., 1996. A discussion on the exhalative sedimentary massive sulfide deposits of South China. Geological Journal of Universities, 2(3), 241–256 (in Chinese with English abstract).

Yang, Z.Q., 1997. Origin of the Dabaoshan massive sulfide deposit: Devonian seafloor thermal events. Geology and Mineral Resources of South China, 1, 7–17 (in Chinese with English abstract).

Ye, L., Cook, N.J., Ciobanu, C.L., Yuping, L., Qian, Z., Tiegeng, L., Wei, G., Yulong, Y., and Danyushevskiy, L., 2011. Trace and minor elements in sphalerite from base metal deposits in South China: A LA-ICPMS study. Ore Geology Reviews, 39, 188–217. https://doi.org/10.1016/j.oregeorev.2011.03.001.

Ye, L., Liu, T., Yang, Y., Gao, W., Pan, Z., and Bao, T., 2014. Petrogenesis of bismuth minerals in the Dabaoshan Pb-Zn polymetallic massive sulfide deposit, northern Guangdong province, China. Journal of Asian Earth Sciences, 82, 1–9. https://doi.org/10.1016/j.jseaes.2013.12.006.

Ying, L.J., Wang, D.H., Li, C., Wang, K., Wang, K.J., Wang, L.G., Wang, Y.W., Zhang, X., Jiang, J.C., 2017. Re-Os dating of sulfides in the north stratiform ore body in Dabaoshan, Guangdong Province and its indication. Earth Science Froniters, 24(5), 31-38 (in Chinese with English abstract).

Zaw, K., Peters, S. G., Cromie, P., Burrett, C., Hou, Z.Q., 2007. Nature, diversity of deposit types and metallogenic relations

THE COPPER ARSENIDES OF THE PICÚN LEUFÚ AREA, PROVINCE OF NEUQUÉN, ARGENTINA

Milka K. de Brodtkorb[1], Juan Carlos Danieli

[1]*Independent Geologist - milkabro@gmail.com*

The first report about the copper ore mine of Picún Leufú was done by Sgrosso (1933), when he presented copper and gold analyses, but without evidence of the presence of gold. Later on, the publication of Malvicini (1963) provided information about the mineralogy of the Kokito II mine. The determination of minerals notably improved in the last 50 years with the application of modern techniques, which are included in this paper, such as microprobe analysis (Paar *et al.*, 2016) and reflectance values, among other methods.

The copper mineralization, occurring as arsenides, sulfides and in oxidized ore within a gangue composed of barite and calcite, is hosted by continental sediments of the Candeleros Formation (Di Paola, 1973), along a E-W trending fault thrust. The dominant lithology of this unit is represented by quartzitic sandstones, graywackic sandstones and graywackes; the latter with abundant muddy matrix (Garrido, 2011).

The main shafts and exploitation works (S39°19'08 "- W69°15'45") are located in the fault fill, which plunges 35° to 42° NNE. The major ore minerals occur in discontinuous aggregates in the fault filling related to calcite and barite. There are also veins in the roof and floor of the structure in the country rock.

The deposit extends over 1.7 to 2 km, presenting a topographic relief constituted by cavernous masses of calcite with subordinated barite and occasional oxidized copper.

The copper "alloy-like" compounds (Ramdohr, 1980) are mostly mixtures of the minerals algodonite, domeykite and "whitneyite". Whitneyite is not considered a real mineral, but an alloy of copper with dissolved As. Actual microprobe analysis gives 1.5-6.6 wt.%.

Contemporary research gives the formula for algodonite as $Cu_{1-x}As_x$, where x=0.15. The mineral is orthorombic, pseudohexagonal, opaque, with a bright white to creamy color and weakly anisotropic. The reflectance value is R1-R2=58.9-62.3 % (540 mm). The microprobe analyses of a sample (in wt.%) gave Cu=84.9, As=15.8, S=0.02, total 100.9 (Paar *et al.*, 2016).

Domeykite is stoichiometric Cu_3As and occurs in two forms: á-domeykite is isometric, while â-domeykite is hexagonal. Heyding and Desfault (in Ramdohr, 1980) prefer the formula $Cu_{15}As_4$ for the hexagonal species. The domeykite inverts above 90 °C to â-domeykite. The color is yellowish white. The reflectance values of á-domeyikite

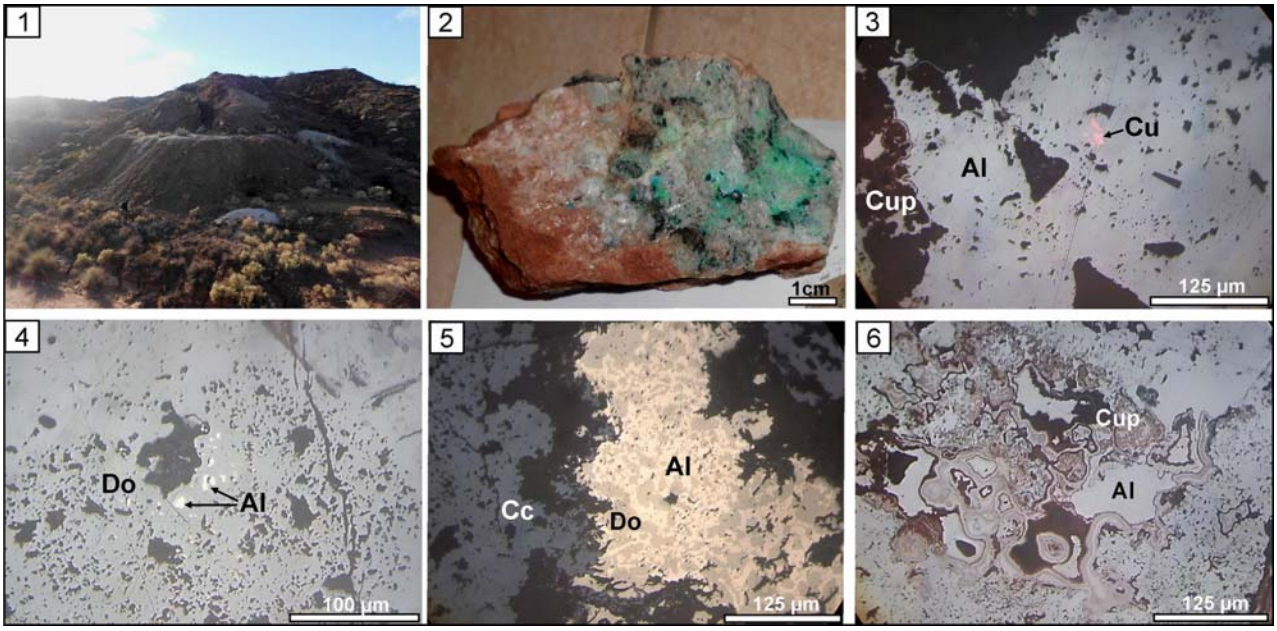

Fig. 1: View of the principal outcrop and mining area (S 39°19´08" and O 69°15'45"). Fig. 2: Hand specimen of the ore, dark grains of algodonite + domeykite surrounded by secondary coper species, in gangue minerals. Fig. 3: Algodonite (Al) with a native copper speck. Fig. 4: Domeykite (Do) with little grains of algodonite (Al). Fig. 5: Algodonite (Al) replacing domeykite (Do); Cc chalcocite. Fig. 6: Algodonite (Al) altered by cuprite (Cup). Fig. 3-6 are microscopic photos, in oil, with uncrossing polars.

is R=50.7 % (540 mm) and for â-domeiykite is R1-R2=45.4-48.6 % (540mm). The microprobe analyses of a sample are in weight % Cu=72.9-73.9, Co=0.01, As=27.1-28.21, Sb=0.01, S=0.01-0.02 (Paar *et al.*, 2016).

Algodonite tarnishes somewhat quicker than domeykite and the last mineral tarnishes iridescent. In the ores of Picún Leufú the gangue minerals are barite and calcite. The primary copper minerals altered to chalcocite, cuprite, tenorite, malachite, azurite, and native copper.

Algodonite and domeykite are frequent in many localities in the world in small amounts but generally in dispersed mode.

Most of the authors believe the ores have a hydrothermal origin. The migration in reducing groundwater in red beds may also precipitate algodonite.

The fault, would have facilitated the circulation of hydrothermal fluids (telethermal deposits sensu Park and MacDiarmid, 1975), which made possible the precipitation of copper arsenides and the incipient alteration of the host rock.

Acknowledgements: to the colleagues of the Neuquen DPM for there help in the field work.

REFERENCES

Di Paola, Elda C., 1973. Caracterización litoestratigráfica de la Formación Neuquén. 5° Congreso Geológico Argentino. Buenos Aires. Actas 3:197-206.

Garrido, A., 2011. El Grupo Neuquén (Cretácico tardío) en la Cuenca Neuquina. Relatorio del 18° Congreso Geológico Argentino, 231-244.

Malvicini, L., 1962. Algodonita en la paragénesis mineralógica de la mina Kokito II, provincia del Neuquén. Revista de la Asociación Geológica Argentina, 17(1-2), 85-95.

Paar, W.H., Brodtkorb, M.K., Putz, H., Martín, R.F., 2016. Atlas of ore minerals: focus on epithermal deposits of Argentina. The Canadian Mineralogist, Special Publication 11, 402 pp.

Park Jr., C.F. and Mac Diarmid, R.A., 1975. Ore Deposits. 1975. Third edition. W.H. Freeman and Company. San Francisco. USA.

Ramdohr, P., 1980. The ore minerals and their intergrowths. Pergamon Press. London.

Sgrosso, P. 1933. Informe sobre las minas de cobre de Picún Leufú. Dirección Nacional de Minería y Geología, Inédito. Buenos Aires.

A | 96

MINERALOGICAL CHARACTERIZATION OF A FLUORITE-BARITE-LEAD DEPOSIT IN DERBYSHIRE, UNITED KINGDOM

Alexandra Gómez Escobar[1], Reimar Seltmann, Alla Dolgopolova

[1]*Universidad Nacional de Colombia - Sede Medellin - alexagomez@gmail.com*

British Fluorspar Ltd (BFL) owns Glebe Mine, a fluorite-barite-lead deposit located in the Peak Lake District (Derbyshire, UK) with fluorspar as main product and barite and lead as by-products. Recent analysis of the CaF2 concentrate showed a high value of deleterious elements such as lead, phosphorous and arsenic, which affect the final quality of the product. The geology of the South Pennine Orefield (SPO) has been widely studied since it overlaps with the limestone outcrop within the Peak District National Park and includes areas of classic limestone geology and geomorphology. There are different styles of mineralization in the SPO deposits mainly categorized by the miners as rakes, scrins, pipes and flats depending on their physical shape. Rakes and scrins are vertical or sub- vertical fissure vein fill structures produced by fracture of the wall rocks. Whereas the last two are stratabound ore deposits comprising a linear series of mineral filled or lined cavities that were formed by wall rock dissolution (karst ores).

The objective of this research was to find the source of the phosphorous found in the final CaF2 concentrate and the mineral associations of different lithologies. The different hypothesis created to define our main objective related with the geology and the mineralogy of the ore were: (i) Fossils in limestones and concretions in the productive horizons make a significant contribution of phosphorous to the mineralized zone, (ii) Presence of lead phosphates (pyromorphite), lead sulfate (anglesite) as source of both Pb and phosphorous, (iii) Rheology of the limestone horizon: permeability (physical) and reactivity (chemical) controls of veins and replacement bodies, (iv) Role of geological and anthropogenic processes (natural karst and mining).

In order to consider the main objective and all the hypothesis, the study performed ore characterization by representative sampling and mineralogical analysis. Energy Dispersive Spectrometry (EDS), Energy Dispersive X-ray spectroscopy (EDX) analysis on Scanning Electron Microscope (SEM) and QEMSCAN analysis were applied for the mineralogical characterization of the F-Ba-Pb deposit as an efficient tool for elemental mapping and for the assessment of different mineral phases and associations; in addition, Lead Isotopes method was utilized to discriminate between barren lithologies and multiple generations of fluid flow causing alteration, providing a new vector to ore deposits formation and generation of mineralizing fluids.

The phosphorous content varies from one lithology to the other. Through chemical analyses could be shown that the highest content of phosphates (P_2O_5) was present in the shale, limestone and replacement areas.

Pipe-vein mineralization comprising dissolution cavity fill with layers of barite and purple to dark purple fluorite is well developed within the wall rock as well as cavities filled with sediments from the Kinder Scout group which contribute with quartz, phosphor bearing minerals and feldspars; it seems it was formed under deep phreatic conditions with slow flows at a time when the local water table was significantly higher than it is today. Mill dam mine has been intersected by late caves development that has enabled the deposition, by fluvial transport processes, of sandy sediments derived from erosion of the Namurian strata (shales and fossiliferous sands) into a pre-existing phreatic cavity. This hypothesis is supported by the lower content of phosphorous at deeper levels in the mine where there is no dissolution in the limestone and less cavities filled with sediments.

Few evidences show the relation between lead and phosphorous as pyromorphite in the samples collected during this study, however, its presence is marked by several authors and by the MLA analysis performed to the flotation feed in 2015, which can be correlated with other ores as those found in the open pit mines. The formation of pyromorphite requires a source of phosphorus. This could be derived from the breakdown of organic material, for example soils containing phosphate, or from the shales that are known to contain high phosphorous from the XRF results which overlie the limestone sequence and productive horizon.

Six isotope ratios including ^{204}Pb, ^{206}Pb, ^{207}Pb, and ^{208}Pb isotopes were calculated for different grains of galena in order to obtain the possible source and to analyze the migration of the fluids. Results obtained show a crustal source of Pb in galena. In a broader context: high values of $^{207}Pb/^{204}Pb$ in samples result in their distribution around Upper Crust (UC) evolution curve and indicate uranium enrichment of the upper crust during mantle-to-crust magma transfer processes.

The different characterization techniques allowed us to go through each of the hypothesis raised at the beginning of this study. Not only one hypothesis was proved, in fact, hypothesis 2 was discarded after mineralogical analysis of all the samples whereas a mix of hypothesis 1, 3 and 4 get close to a better understanding of the mineralization and the source of some deleterious elements in the rocks.

The modal mineralogy of the different lithologies suggested that phosphorus in the samples is not present in mineral forms (such as apatite or pyromorphite), instead it is strictly associated to calcium probably from fossils (debris, shells and fish bones), to the silicon content as proved with the SEM-EDS technique and last but not less important to the cavities in the rocks.

The research is co-funded by the EU Horizon 2020 Project "FAME": Flexible and Mobile Processing Technologies (grant #641650). The authors acknowledge the contributions of the BFL team for sample collection and preparation and scientific discussions that led to the development of this paper. The continued interest in our work by Dr Chris Broadbent (WAI) and Peter Robinson (BFL) is highly acknowledged.

A | 97

REE-Th ENRICHMENTS OF THE ISPARTA TRIANGLE, SOUTHWESTERN TURKEY

M. Sezai Kirikoğlu[1], Emin Ciftci, Murat Budakoğlu, Ali Tuğcan Ünlüer, Zeynep Döner, Mert Terzi, Ilgýn Kursun, Hüseyin Kocatürk

[1]Istanbul Technical University - sezai@itu.edu.tr

METHOD

A series of mineral concentration studies, including gravity separation, magnetic separation and flotation methods, were carried out on samples from the Isparta Triangle (SW Turkey) found to be high in REE content as determined by ICP-MS analyses carried out at ITU – Geochemical Analyses Lab (JAL). Gravity separation was carried out using a shaking table and coarse enrichment, sweeping and cleaning processes. Conditions were 6-8-10° table inclination, 340-400-460 rpm stroke speed and 8-10 L/min operating parameters.

RESULTS

Anomalous concentrations of light rare earth elements (LREE) and Th from the Isparta Triangle region (SW Turkey) occur as pyroclastic deposits closely associated with post- collisional, alkaline-potassic Golcuk volcanism. The trachyandesites, augite trachytes, porphyry trachytes, tephriphonolite dikes, pyroclastic flow deposits and resedimented tuffs of the various eruptive cycles contain significant amounts of incompatible elements. Such anomalous concentrations of LREE and Th can be observed in various locations in Isparta- Burdur province. Geochemical analyzes of the samples from the study area indicates high values for LREE elements such as La (170-300 ppm), Ce (300-630 ppm), and Nd (130-195 ppm). The OREE content of samples are, on average, 820 ppm. Significant amounts of Nb (~50 ppm) and Th (~85 ppm) are also noted. Ore enrichment studies carried out in the pyroclastic flow deposits indicate that the main LREE enrichment can be related to the presence of phosphate-bearing minerals such as fluoroapatite and xenotime. On the other hand, more altered samples of the resedimented tuffs, despite the lack of phosphate minerals, contain similar amounts of REE and Th. By the help of the basic ore enrichment studies, the final REE grade increased to approximately ~%1.5.

REFERENCES

Dilek, Y., & Altunkaynak, ª. (2010). Geochemistry of Neogene–Quaternary alkaline volcanism in western Anatolia, Turkey, and implications for the Aegean mantle. International Geology Review, 52(4-6), 631-655.

HAADF-STEM IMAGING OF SMALL DEFECTS IN NATURAL TUNGSTEN TRIOXIDE, WO_3

Wenyuan Liu[1], Cristiana L. Ciobanu, Nigel J. Cook, Ashley Slattery

[1]*College of Zijin Mining, Fuzhou University, 350108 Fuzhou, China - wenyuan.liu@adelaide.edu.ar*

BACKGROUND

Synthesis and nanoscale analysis of tungsten trioxide (WO_3), a well-known semiconductor with a broad spectrum of applicability, have become prominent with the rapid development of nanotechnology. Three of the five WO_3 polymorphs have stability fields above 0°C with changes in crystal symmetry from monoclinic (P21/n) at 17<T<330°C, to orthorhombic (Pmnb) at 330<T<740°C, and tetragonal (P4/nmm) at 740<T<900°C. The former is the most common structure. The natural mineral analogue has not been identified until now. Apart from polymorphism, various types of defects are inherent to WO_3 phases; these are associated with oxygen deficiency (WO_{3-x}; $x \leq 0.3$), cooling paths or redox conditions, e.g., (Bursill, 1983). For example, a homologous series of MnO_{3n-2} compounds, where M=W,Mo, is derived based upon crystallographic shear planes (CSP) with different periodicities. Such CSP structures and other related compounds are considered a 'route' towards defining anion-deficient perovskites (Abakumov *et al.*, 2006). Apart from the CS-derived planar defects typical of high-T phases, two types of localised, 'small' defects are identified in WO_{3-x}: (i) pentagonal bipyramidal columns (PC); and (ii) hexagonal tunnels (HTB), both attributable to the low-T monoclinic polymorph (Bursill, 1983).

Here we report the first natural occurrence of WO_3 as µm- to nanoscale inclusions in W-Sn- bearing sulphide ores from a depth of 1.5 km in the Zijinshan high-sulfidation Cu-Au deposit, China. This deposit hosts an exquisite assemblage of Sn-, W- minerals, including sulphides and oxides (Liu *et al.*, 2016). Microprobe analysis and micro-Raman spectra rule out the possibility that the WO_3 species studied here at the nanoscale is tungstite, WO_3H_2O. We use High Angle Annular Dark Field (HAADF) Scanning Transmission Electron Microscopy (STEM), a powerful Z-contrast technique, for high-resolution imaging, suitable for identification of atom-scale defects.

METHODS

TEM foils were prepared by focused-ion-beam-SEM technique and were cut across: (I) µm- scale intergrowths between ferberite ($FeWO_3$), WO_3 and kiddcreekite(±mawsonite); and (II) ferberite with sub-µm inclusions of WO_3. Both foils were analysed using HAADF STEM imaging and energy dispersive X-ray spectrometry (EDX)-STEM spot analysis and mapping (Titan Themis instrument operated at 200 kV; Adelaide Microscopy).

RESULTS

The WO_3 phase is identified in both foils as the monoclinic polymorph which could be indexed using space group P21/n. In foil (I) this forms lamellar intergrowths with ferberite and shows no lattice-scale defects whereas in foil (II) this is present as nanoscale (tens-of- nm) inclusions within ferberite. EDX-SEM mapping shows the WO_3 is readily distinguishable from host ferberite by W and Fe contents (Fig. 1a), as well as by less O than ferberite. One of the WO_3 inclusions imaged on [010] zone axis shows defects (Fig. 1b), either along the margins or internally, as short linear strips (~10 nm-long). In detail, host ferberite also displays trails of Al-bearing nanoparticles (Al-NPs) with darker appearance on HAADF STEM images (Fig. 1c). High-resolution imaging of ferberite down to [100] zone axis shows the presence of W (brighter) and Fe atoms (smaller, darker) concordant with crystal- structure models (Fig. 1d and inset). The WO_3 inclusions shows a combination of sharp boundaries and lattice defects consisting of 1-unit pentagonal atom arrangements concordant with small defects of PC type; Fig. 1e). The distribution of PCs along boundaries is either regular, or with jog-like irregular arrangements (Fig. 1f). Marginal PC defects are marked by the presence of darker sites suggesting the presence of vacancies. Defects inside the grain (Fig. 1g) have the same patterns throughout the short-defect alignment with kinked appearance (Fig. 1g). These comprise comparable PC-basic motifs as those along the boundaries but as larger, combinations of 4-unit pentagons (4-PCs) with geometries showing pentagon-sharing corners via a square or triangular motif (Fig. 1g, inset). There are two different pentagonal motifs: with and without an interstitial atom. The interstitial atom is smaller and less bright than W in both internal and marginal PC defects. Additionally, twin planes are observed along the margins with a comparable type of smaller atoms (Fig. 1h).

DISCUSSION AND CONCLUSIONS

Small defects in the natural WO_3 display pentagonal bipyramidal configuration closely resembling those obtained in synthetic $(W,Nb)O_{2.933}$ (Bursill and Smith, 1984). In our case, we can consider substitution of another

transition metal (Sn), available in the assemblage. In addition, non- occupied tunnel sites can be associated with oxygen vacancies as those considered for HTB models (Bursill, 1983). It is likely that WO_3 either within the ferberite matrix or as coarser lamellar intergrowths, was co-precipitated from W-bearing fluids. Pre-existing Sn-W-sulphides (e.g., kiddcreekite) were replaced by W-free, Sn-bearing sulphides (e.g., mawsonite) leading to local W enrichment as ferberite and WO_3. Observed Al-NPs can be attributed to diaspore indicative of acidic fluids typical of high-sulphidation environments. Defect types and symmetry of non-stoichiometric WO_{3-x} indicate T<330°C. Studies of interaction of small and extended defects in non-stoichiometric W- and Ti-oxides show the dependence of individual defects on the relative concentrations of different, locally present small defect types at the time of precipitation rather than a unique and reproducible way of derivation from CSP partial dislocation structures (Bursill and Smith, 1984). The observed variability of natural WO_3 from one location to another at the polished section scale (absence or presence of defects and their configuration) is concordant with this conclusion.

REFERENCES

Abakumov, A.M., Hadermann, J., Bals, S., Nikolaev, I.V., Antipov, E.V., Van Tendeloo, G. (2006) Crystallographic Shear Structures as a Route to Anion-Deficient Perovskites. Angewandte Chemie (International Edition) 45, 6697-6700.

Bursill, L.A. (1983) Structure of small defects in nonstoichiometric WO_{3-x}. Journal of Solid State Chemistry 48, 256-271.

Bursill, L.A., Smith, D.J. (1984) Interaction of small and extended defects in nonstoichiometric oxides. Nature 309, 319-

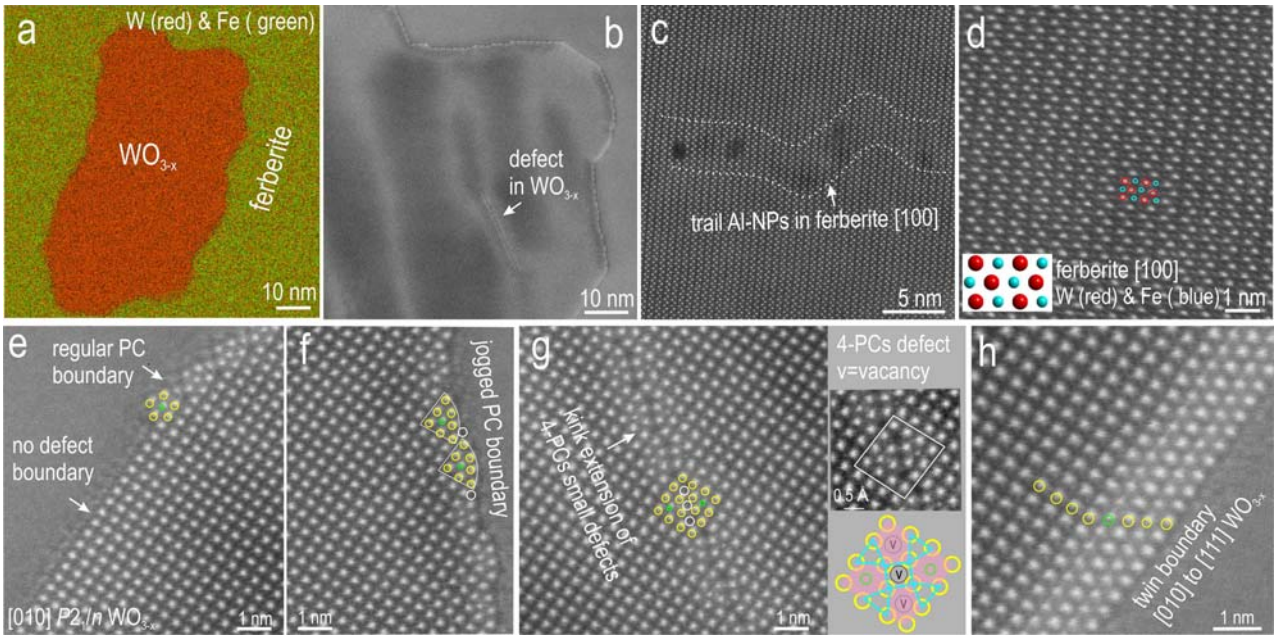

Fig. 1. EDX-STEM map (a) and HAADF STEM images showing internal defect in WO_{3-x} inclusion (b), ferberite (c,d) and small defects in WO_{3-x} (e-h).

URANIUM TRANSPORT FROM MESOPROTEROZOIC BEDROCK GRANITE INDUCED BY TECTONISM: THE BLACKBUSH URANIUM DEPOSIT, SOUTH AUSTRALIA

Urs Domnick[1], Nigel J. Cook, Cristiana L. Ciobanu, Benjamin P. Wade, Russel Bluck, Allen Kennedy

[1]*School of Chemical Engineering, The University of Adelaide, Australia - urs.domnick@adelaide.edu.au*

BACKGROUND

The Blackbush deposit, northern Eyre Peninsula, South Australia, (inferred resource 12,580 tonnes U (UraniumSA, 2007)) is currently the only sediment-hosted U deposit in the Gawler Craton that has been investigated in any detail. Uranium is mainly hosted at the unconformity between Eocene sandstone of the Kanaka Beds and a massive saprolite derived from the subjacent Hiltaba-aged (~1585 Ma) granites, affiliated with the Samphire Pluton (Figure 1).

Basement geology of the Gawler Craton remains poorly constrained. Beneath the Blackbush deposit, three distinct granitoids are recognised (Domnick *et al.*, 2018). The southern part of the pluton features a characteristic green granite (B) whereas the northern part, immediately underlying the Blackbush deposit, is comprised by granite C, characterised by reddened feldspars. These two granites are separated by an arcuate domain of a yellow granite (A), which is significantly less evolved than the other two, as indicated by higher Ca, and lower U. All three granites show complex alteration overprints and textures, as well as crosscutting veins. Alkali feldspar has been replaced by porous K-feldspar and albite, and plagioclase is overprinted by an assemblage of porous albite + sericite ± calc-silicates. In granites A and B, igneous biotite is replaced by calcic garnet. Calc-silicates are indicative of Ca-metasomatism, sourced from the anorthite component of altered plagioclase. Clay alteration of feldspars is present in all samples. Mineral assemblages in veins include quartz+ hematite, hematite + coffinite, fluorite + quartz, and clay minerals. Chlorite and sericite are found in all vein types and overprint other minerals.

Previously published geochronological constraints on the Samphire Pluton are 1584±4 Ma, and 1586±6 Ma for granite B and granite C, respectively (Jagodzinski and Reid, 2017). Here we present new geochronological data for zircon from the underlying granites and for U-minerals in veins within granite, saprolite and overlying sandstone.

METHODS

Sensitive high-resolution ion microprobe (SHRIMP) U-Pb data was obtained for zircons separated and concentrated from the three granites using a SHRIMP II at the John De Laeter Centre, (Perth, Western Australia). Chemical U-Pb ages for coffinite and uraninite were obtained by electron probe microanalysis.

RESULTS

New SHRIMP U-Pb zircon data for all three granites confirms previously published ages (Jagodzinski and Reid, 2017) albeit with minor differences. Granite B yielded an age of 1585±9 Ma, Granite C 1579±9 Ma, and Granite A 1588±9 Ma. The age overlap for granites of distinct appearance and geochemistry indicates either short-lived magmatic activity and/or differences in fractionation due to differences in crustal assimilation. The anomalously high U contents between 10 and 81 ppm in Granite C under the deposit, as well as highly variable Th/U ratios, and the presence of hydrothermal U minerals, like uranothorite and coffinite are clear evidence for mobility of U, which was facilitated by the porosity created during feldspar alteration, and strongly indicate that the granite is the most probable source rock for the uranium (Domnick *et al.*, 2018).

In the deposit, uranium is present as coffinite, $[U(SiO_4)_{1-x}(OH)_{4x}]$, and is hosted mainly in the sandstone, along the unconformity, as well as within a roll front downstream, and to a minor degree also in saprolite (Figure 1). Coffinite and traces of uraninite can also be found in hematite-coffinite-bearing veins that crosscut the underlying granite.

The coffinite in the sandstone and saprolite occurs intergrown with framboidal Fe-sulphides and lignite grains, as well as coatings around grains of quartz. It is poor in trace elements such as REE or Th. In contrast, coffinite within the granite-hosted veins contains a significant amount of Y (11 wt.%) and HREE. Minor uranium also occurs absorbed in lignite, presumably as U^{6+}. Chemical U-Pb dating (582 spot analyses) of coffinite in all three occurrences (sandstone, saprolite and veins) gives a normal distribution with a mean age of 17±1.6 Ma for the whole population. Uraninite in the granite-hosted vein yielded a significantly older age (41±2 Ma).

DISCUSSION AND CONCLUSIONS

Coffinite ages are interpreted as valuable evidence for a single coffinite-forming event during the Miocene. Such an event likely coincided with tectonic movement, indicated by horst and graben structures in the early

Miocene Melton limestone. The latter unit overlies the Eocene sandstone, and, in turn, is overlain by Pliocene Gibbon Beds that show no evidence of tectonism. The significantly older age of granite-vein uraninite indicates this predates sedimentation of the Eocene Kanaka Beds, and likely indicates transport and redeposition of uranium by oxidising fluids within the exposed granite. The ages obtained here on hydrothermal minerals indicate that uraninite formed in granite veins and was subsequently dissolved and reprecipitated as coffinite in younger sediments during tectonic events in the Tertiary. Such data allow interpretation of U-mineralization in the deposit as resulting from U transport out of Mesoproterozoic bedrock granite during tectonic activity.

REFERENCES

Domnick, U, Cook, N.J., Bluck, R., Brown, C., Ciobanu, C.L., 2018. Petrography of granitoids from the Samphire Pluton, South Australia: implications for uranium mineralization in overlying sediments. Lithos 300–301: 1–19.

Jagodzinski, E.A., Reid, A.J. (2017) Project PGC03-01: Geochronology from the Samphire uranium project. PACE Geochronology: Results of Collaborative Geochronology Projects 2013–2015, Report Book 2015/00003, p. 10–28. Department of the Premier and Cabinet, South Australia, Adelaide.

UraniumSA (2007), ASX Release, 12 December 2007, 4 pp.

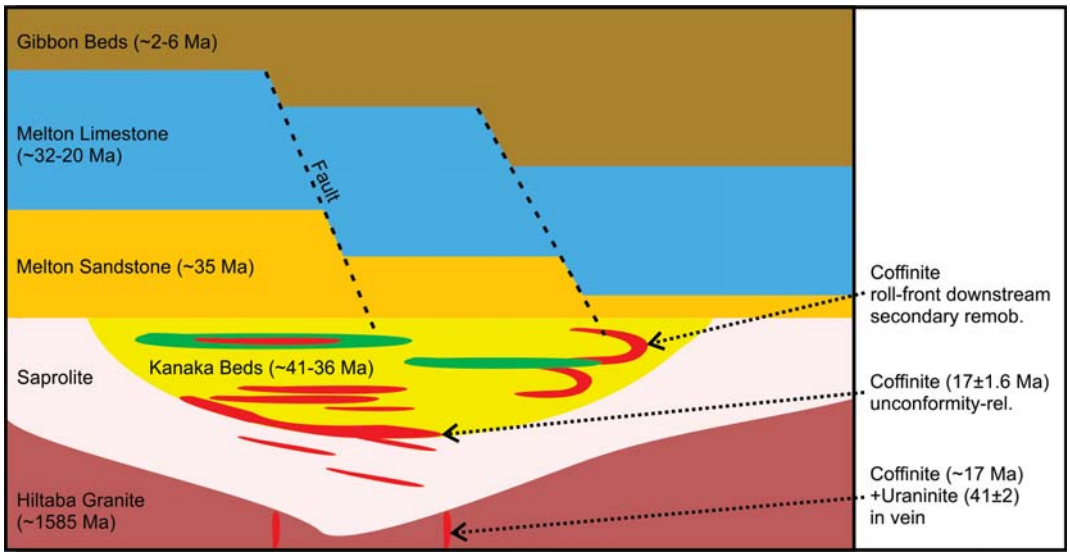

Fig. 1. Schematic cross-section through the Samphire deposit and new chemical ages for U- minerals.

CHAPTER 10
NEW DISCOVERIES AND NEW RESEARCH ON SKARN DEPOSITS

Conveners: Zhaoshan Chang, Larry Meinert

SKARNS REPLACING IGNEOUS ROCKS

Zhaoshan Chang[1], Larry Meinert, David Lawrence, Stephanie Mrozek, Lejun Zhang

[1]*Colorado School of Mines and James Cook University - chang@mines.edu*

Most skarns replace carbonates (limestone-dolostone) and calcareous rocks, therefore the exploration of skarns has been focused on carbonate areas. In recent years several large skarns have been found and they replace intrusive or extrusive igneous rock. This opens new districts for skarn exploration. In this contribution we introduce examples of skarns replacing igneous rocks, summarize their features, identify ways to distinguish such skarns from skarns replacing carbonates, and discuss the exploration implications.

Skarns replacing igneous rocks may have three types of occurrences: Type-1 occurs in purely igneous rocks without any traces of carbonates around, Type-2 skarns dominantly replaces volcanic rocks at and close to its contact with carbonates, rather than the carbonates, and Type-3 replaces intrusions as endoskarns in carbonate area side-by-side with skarns replacing carbonates (exoskarn). Type-1 examples include the Tongon Au skarns in Cote d'Ivoire, containing 3.8 Moz Au @ 2.5 g/t Au and replacing basaltic-andesitic crystal tuffs (Lawrence *et al.*, 2017); Meishan Fe skarn, China, with 334 Mt Fe ores @ 39% Fe (NGAC, 1979), replacing a basalt porphyry intrusion and andesitic volcanic wallrocks; the Nihe Fe skarn, China, containing 184 Mt Fe ores with 21% magnetic Fe (NGAC, 2010), replacing diorite porphyry intrusion and the trachyandesite wallrocks, and the Magnum Bonum, Jumna and Jack-in-a-box Sn skarns replacing metabasalt, plus the Tommy Burns Sn deposit (11,520 t Sn) at metabasalt-chert boundary, NE Queensland, Australia. Type-2 includes the Lake, the Merry Widow, and the Iron Hill Fe skarns where most skarns are in basalt rather than limestone, all in British Columbia, Canada (Meinert, 1984). Type-3 are common, with examples including the giant Antamina Cu-Zn skarn (~2,968 Mt @ 0.89% Cu, 0.77% Zn, 11 g/t Ag and 0.02% Mo; Glencore, 2015) where the endoskarns replace quartz monzonites (Mrozek *et al.*, 2015), the Morelos Au skarn, Mexico (~5.5 Moz Au), where the endoskarns replaces granodiorite, and the Empire Cu-Zn skarn, Idaho, where the endoskarn replaces granite porphyry (Chang and Meinert, 2004, 2008).

The protoliths of skarns replacing igneous rocks are typically mafic to intermediate if there are no carbonates in the vicinity, whereas if there are carbonates, the protolith may be of any composition. Such skarns typically occur as veins when the intensity is weak, and with increasing intensity the skarn veins merge into massive bodies. Or the weak alteration may occur as patches that also grade into massive skarns with increasing alteration intensity. Skarn veins cutting across igneous rocks typically have a garnet-dominant centerline. The mineralogy of the outer part of the vein varies depending on the rock type. In more felsic rocks such as granite porphyry at the Empire skarn, Idaho, and in granodiorite porphyry at the Morelos skarn, Mexico, the outer vein is mostly wollastonite with minor pyroxene, and the vein haloes have disseminated wollastonite alteration (Chang and Meinert, 2008; Chang, unpublished report). In mafic rocks such as basalt, the outer part of the veins are dominated by pyroxene then further out to amphibole, with the vein haloes having disseminated amphibole alteration, e.g., at Lake Fe skarn, British Columbia, Canada (Meinert, 1984). In some skarns there are quartz stockworks with secondary biotite haloes, typical of porphyry deposits, further inside the intrusion, e.g., at Antamina, Peru (Chang *et al.*, 2015). Intrusions related to Fe mineralization, typically dioritic to gabbroic but can be as felsic as quartz monzonite (e.g., Lake, Canada) and granodiorite (e.g., Iron Hill, Canada), tend to have extensive albite alteration beyond skarn; some also have K-alteration (e.g., Nihe; Zhang *et al.*, 2013).

Skarns replacing igneous rocks can be recognized by the residual altered igneous rocks between skarn veins or patches. For massive skarns textures could be misleading in the effort to identify the protolith; it is better done using whole rock geochemistry in some cases (Mrozek *et al.*, 2018).

This study demonstrates that skarns can form in volcanic terranes, particularly in mafic rocks such as basalt and basaltic andesite. Such deposits tend to contain abundant magnetite, although the main economic metal may not be Fe, and therefore magnetic survey could be effective exploration tools.

REFERENCES

Meinert, L.D., 1984, Mineralogy and petrology of iron skarns in western British Columbia, Canada: Economic Geology, v. 79, p. 869-882.

Zhang, L-J., Zhou, T-F., Cooke, D.R., Fan, Y., Chang, Z., and Chen, H-Y., 2013, The Nihe iron deposit, Anhui Province, eastern China: skarn, IOCG or porphyritic iron deposit? Mineral Deposit Research for a High-Tech World – Proceedings of the 12th SGA Biennial Meeting,12-15 August 2013, Uppsala, Sweden, ISBN 978-91-7403-207-9, v. 4, p. 1559-1561.

Chang, Z., and Meinert, L.D., 2004, The magmatic-hydrothermal transition - Evidence from quartz phenocryst textures and endoskarn abundance in Cu-Zn skarns at the Empire Mine, Idaho, USA: Chemical Geology, v. 210, p. 149-171.

Chang, Z., and Meinert, L.D., 2008, The Empire Cu-Zn Mine, Idaho: exploration implications of unusual skarn features related to high fluorine activity: Economic Geology, v. 103, p. 909-938.

Lawrence, D.M., Allibone, A.H., Chang, Z., Meffre, S., Lambert-Smith, J.S., and Treloar, P.J., 2017, The Tongon Au deposit: Northern Cote d'Ivoire: An example of Paleoproterozoic Au skarn mineralization: Economic Geology, v. 112, p. 1571-1593.

Chang, Z., Mrozek, S., Meinert, L.D., and Windle, S., 2015, Skarn-porphyry transition: an example from the Antamina skarn, Peru. In: Proceedings of PACRIM 2015, AusIMM PACRIM 2015 Congress, 18-21 March 2015, Hong Kong, China. p. 409-413.

Mrozek, S., Chang, Z., and Meinert, L.D., 2015, A model for the intrusive sequence and Cu- Zn skarn formation at the Antamina deposit, Peru. In: Proceedings of PACRIM 2015, AusIMM PACRIM 2015 Congress, 18-21 March 2015, Hong Kong, China. p. 423-429.

STRATIFORM-LIKE Cu DEPOSITS IN SOUTH CHINA: SEDEX OR SKARN?

Pei Ni[1], Guo-Guang Wang, Yi-Tao Cai, Xiao-Ting Zhu, Hui Chen, Bai-Sheng Zhang

[1]*Nanjing University - peini@nju.edu.cn*

INTRODUCTION

A group of large stratiform-like Cu deposits is one of the most economically significant ore styles in South China. More than 60% of stratiform-like Cu orebodies are strictly hosted in the Upper Carboniferous Huanglong Formation or temporally equivalent sedimentary sequences (e.g., Outangdi, Zishan formations) limestone, dolomite, sandstone, and shale, and these orebodies show closely spatial relationship with Yanshanian stocks. The unique geologic factors associated with stratiform-like Cu orebodies lead to a hot debate on the ore genesis, regarding Late Carboniferous Sedex or Yanshanian skarn in origin.

Fluid inclusions of original ore-forming fluids trapped in quartz coexisting with ore minerals, are a powerful tool to understand the mineralization characteristics and ore deposit styles. In this presentation, we would present detailed fluid inclusion microthermometric data of the Dongxiang, Jiande, Yongping, and Xinqiao Cu deposits aiming to precisely constrain the ore genesis.

ORE DEPOSIT GEOLOGY

More than 20 Cu deposits in South China have been argued as typical Sedex or skarn type deposits, including Dongxiang, Yongping, Jiande, Chengmenshan, Wushan, Mshan, and Xinqiao, etc.

Yongping: The Upper Carboniferous Outangdi Formation, which is the dominant host rock of stratiform-like Cu ore bodies, is composed of marine carbonates and terrigenous clastic rocks interbedded with siliceous rocks. The intrusions at Yongping are Huoshaogang granite porphyry, Shizitou granite porphyry and quartz porphyritic dikes. Economically, ore zone II is the most important, which accounts for 72% of the Cu reserves of the entire deposit. The stratiform-like Cu bodies were surrounded by skarn alteration, which is associated with the gangue minerals including garnet, pyroxene, scapolite, calcic amphibole, epidote, quartz, sericite, calcite, and chlorite. The stringer mineralization is present in the basement of the Zhoutan Group, which is the footwall of the stratiform-like Cu orebodies. The porphyry style Mo-only mineralization is related to the Late Jurassic Shizitou granite porphyry in the southeastern part of this deposit, but it shows little direct connection with the stratiform- like Cu orebodies.

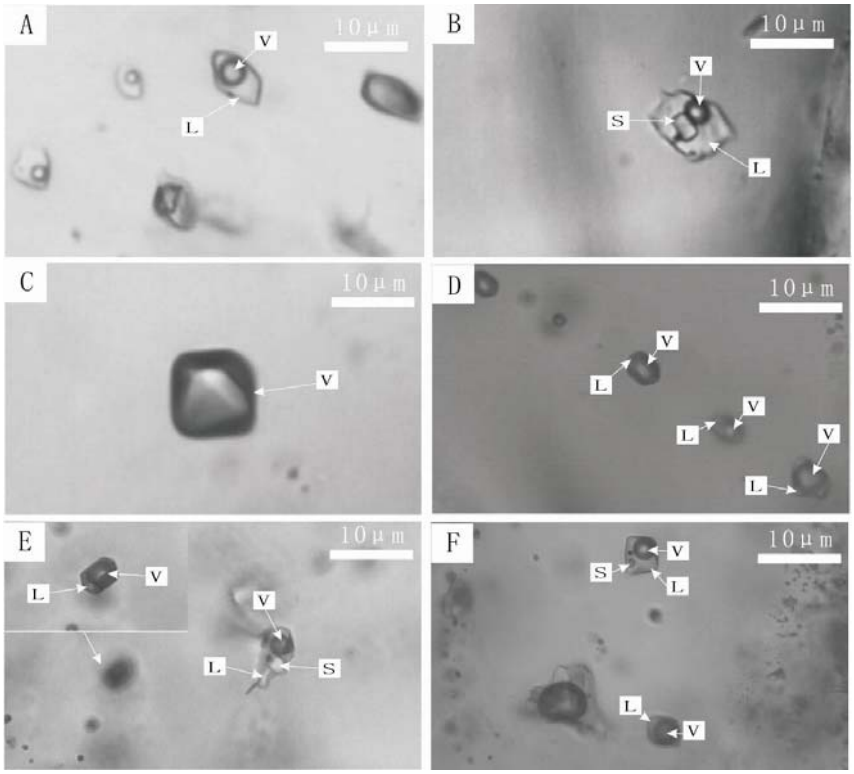

Figure 1. (A) type I inclusions; (B) type II inclusion; (C-D) type III inclusions; (E-F) coexisting type II and type III inclusions in the same region.

Dongxiang: The host rocks are upper Carboniferous Zishan Formation, comprising gray quartz sandstone, sandstone, shale and conglomerate intercalated with marl. The main intrusions are the Jurassic granodiorite porphyries, which are basically controlled by NE- trending faults and cut by NNE- or WNW-trending faults. Field observations show the granodiorite porphyries intrude the Zishan Formation and are closely connencted with the copper ore bodies. The copper ore bodies occur in the sandstone and shale of the upper section of the Zishan Formation occur as stratoid bodies and lenses. These ore bodies are controlled by the same NE–NNE trending faults as the intrusive rocks. Therefore, the ore bodies, faults and intrusive rocks are closely spatially associated and perhaps genetically related. Ore minerals include chalcopyrite, pyrite, bornite and chalcocite. Phyllic alteration and sericitic alteration are generally associated with copper mineralization and commonly observed along the copper ore bodies.

Jiande: The ore hosting Upper Carboniferous Huanglong Formation is composed of grayish- yellow massive limestone, grey dolomite and dolomitic limestone. Intrusive rocks are widely distributed in the mining area, and occur as stocks and dykes. The granodiorite porphyry intruded into dolomites and limestones of the Upper Carboniferous Huanglong Formation. Ore bodies in the Jiande deposit have close spatial relationships with the granodiorite porphyry. The copper ore bodies occur in layer-like form and become thicker in the core of the Songkengwu syncline. The common styles of hydrothermal alteration associated with the orebodies at the Jiande deposit are silicification, marmarization and chloritization. Skarn occurs only locally, close to the granitic intrusion.

Xinqiao: The ore hosting Upper Carboniferous Huanglong Formation in the Xinqiao Cu–S–Fe–Au deposit is composed of limestone and dolomite. The Jitou quartz diorite porphyry is exposed in the Xinqiao deposit with an ellipsoidal surface area of 0.5 km^2. The Jitou stock intruded the Upper Carboniferous and the lower Permian limestone. Weak skarn alteration occurred around the Jitou intrusion. Significant economic metal reserves are predominantly connected to the stratiform-like ore bodies. The stringer mineralization is present in the sandstone of the Wutong Formation, which is the footwall of the stratiform- like Cu orebodies. Skarn type mineralization occurs around the Jitou stock within the alteration zone, but the skarn alteration is very weak.

RESULTS

Three types of fluid inclusions can be identified in these massive sulfide Cu deposits, South China, liquid-rich H_2O-NaCl inclusion (type I), gas-rich H_2O-NaCl inclusion (type II), and halite-bearing inclusion (type III).

Fluid inclusion study on stratiform-like Cu orebodies: In the Yongping deposit, type II and III inclusions yield homogenization temperatures of 250 to 320 °C, and salinity values of 0.7 to 2.7 % wt.% NaCl equivalent and 28.2 to 38.0 % wt.% NaCl equivalent, respectively. In the Dongxiang deposit, homogenization temperatures of type II and III inclusions are 273 to 365 °C, and salinity values of them are 0.4 to 5.9 % wt.% NaCl equivalent and 29.4 to 41.9 % wt.% NaCl equivalent, respectively. In the Jiande deposit, type II and coexisting Type III fluid inclusions in the main stage share similar homogenization temperatures of 293 to 334 °C and 290 to 326 °C, but have two contrasting salinity ranges of 1.2 to 2.2 wt.% and 31.87 to 38.16 wt.% NaCl equiv, respectively.

Fluid inclusion study on stringer mineralization: In the Yongping deposit, type II and III inclusions have analogous homogenization temperatures 292-389 °C and 274-349 °C, but contrasting salinities of 0.4 to 4.5 wt.% and 31.6 to 37.7 wt.% NaCl equivalent, respectively. Type II and III inclusions at Xinqiao have analogous homogenization temperatures of 301-383 °C and 256-370 °C, but contrasting salinities of 0.3 to 2.4 wt.% and 31.7 to 41.1 wt.% NaCl equivalent, respectively.

Our detailed microthermometry and Raman analysis demonstrate that homogenization temperature, salinity, type of fluid inclusions of these deposits are different from typical massive sulfide deposits that formed in submarine environments. Moreover, in each deposit, the range of homogenization temperature of type II inclusions is similar to that of type III inclusions, and they coexist in same quartz grains (Fig. 1), suggesting extensive fluid boiling happened in these deposits. The characteristics of fluid inclusions indicate that even in the strata-like copper orebodies, suggested by some to be generated by submarine exhalation, the fluid inclusions record only the presence of magmatic fluids.

CONCLUSIONS

Stratiform-like Cu deposits are one of the most economically significant ore style in South China.

Abundant boiling fluid inclusion assemblages are preserved in both stratiform-like Cu orebodies and the stringer mineralization veins.

Only the information of magmatic fluid was recorded in the stratiform-like Cu orebodies.

OPTIMIZING SKARN CLASSIFICATION USING GEOCHEMISTRY AND MACHINE LEARNING ALGORITHMS: AN EXAMPLE FROM THE ANTAMINA DEPOSIT, PERU

Stephanie Mrozek[1], Christina Buelow, Zhaoshan Chang, Alberto Paz

[1]*Economic Geology Research Centre (EGRU) and Academic Group of Geosciences, James Cook University, Townsville, QLD, 4811, Australia - stephanie.mrozek@my.jcu.edu.au*

INTRODUCTION

Skarns replace both carbonate wall rocks and igneous rocks, forming exoskarns and endoskarns, respectively (Einaudi *et al.*, 1981; Meinert *et al.*, 2005). Textural inheritance from the precursor (i.e., banding in exoskarns and porphyritic texture or residual patches of igneous rocks in endoskarns) provides the basis for visual classification of skarns in the field. However, some skarns display massive or mottled "indeterminate" textures, which are unreliable for classification. When textures become unreliable, geochemistry can be used to establish a clearer link to the precursor. Accurate classification of indeterminate skarns can refine the deposit geometry and enhance the understanding of ore distribution in different skarn domains. This study aims to provide a workflow for optimizing skarn classification using the giant Antamina deposit (Peru) as an example.

Antamina is located approximately 270 km north of Lima, Peru, at 9°46'S, 77°06'W in the central Peruvian Andes. It is the largest skarn deposit in the world, with a resource of ~2,968 Mt averaging 0.89% Cu, 0.77% Zn, 11 g/t Ag and 0.02% Mo (Glencore, 2015). The deposit is centred on a Miocene porphyry complex (10.95 ± 0.20 to 10.24 ± 0.23 Ma, U-Pb zircon; Mrozek, 2018) that is surrounded by endoskarns and exoskarns. The endoskarns typically contain relict patches of porphyritic rocks, whereas exoskarns (particularly those near the marble front) inherit banded textures from layering in the metasedimentary wall rocks. In between these unequivocal endoskarns and exoskarns are extensive zones of massive and mottled indeterminate skarns, which are difficult to classify.

At Antamina, endoskarn alteration occurs in early trachyandesite porphyries (Mrozek, 2018). Previous workers generally agree that exoskarns are hosted in the Celendín and Jumasha formations; however, the precise location of the contact is poorly constrained (Love *et al.*, 2004; Lipten and Smith, 2005; and Escalante *et al.*, 2010). The Celendín Formation is composed of calcareous shale and marl with lesser impure limestone, whereas the Jumasha Formation is mainly limestone with a minor siliciclastic component (Escalante *et al.*, 2010). It is on this geological basis that we infer two geochemically distinct exoskarn precursors and one endoskarn precursor at Antamina.

Typical protocols for examining geochemical data involve the use of bivariate plots, element ratios, and discrimination diagrams; however manual processing of large data sets is time consuming and interpretation of these results can be subjective. In this study we use a whole rock geochemical data set (217 samples, including marble, hornfels, intrusive rocks, and skarns) from the Antamina deposit to demonstrate how endoskarns and exoskarns can be related to their respective precursors using a combination of unsupervised and supervised machine learning algorithms (MLA). We use R statistical software to analyse our data set, however the process is replicable using other software packages that can run MLAs. Our method uses cluster analysis, a univariate classification tree, and a random forest model to distinguish and classify skarns based on geochemical composition, with reproducible and objective results.

METHODS

All geochemical variables (n = 51) were converted to ppm, then 'opened' using a centred- log ratio transformation and standardised to provide a relative measure of scale. An unsupervised machine learning approach was used to simultaneously consider all geochemical variables and group the rock samples based on their geochemistry. Cluster validation determined that the k-means algorithm with six clusters provided the most homogeneous, stable, and geologically relevant results (Figure 1A). To ensure the geological relevance of the clusters, their classification as either 'metasedimentary' (marble and hornfels), 'igneous', or 'skarn' (endoskarn and exoskarn), was used to inform the cluster analysis.

A random forest model was trained using geochemical data from the precursor rocks, then used to classify the skarns. The probability that each skarn type is derived from one of three precursor types was then quantified (Figure 1B).

Following the geochemical clustering of skarns and precursors, a univariate classification tree was used to determine which chemical variables most effectively partition the data set into the six observed clusters. The tree was pruned based on cross-validation results with the least error (Figure 1C).

RESULTS

K-means cluster analysis identified six clusters representing three types of skarns and three geochemically distinct precursors (Figure 1A). Skarn-1 and Skarn-3 display moderate to high probabilities of classification as endoskarn and exoskarn, respectively, while Skarn-2 displays the lowest probability of classification (Figure 1B). Figure 1C shows the most important variables involved in partitioning the data set into skarns and precursors and provides a geochemical framework for quantitative classification (Figure 1C).

INTERPRETATION

Skarn-1 is derived from igneous rocks (endoskarn), Skarn-3 (exoskarn-1) is derived from Metasedimentary-1 rocks (marl/Celendín Formation, based on composition), and (by elimination) Skarn-2 (exoskarn-2) is derived from Metasedimentary-2 rocks (marble/Jumasha Formation; Figure 1D). The low classification probability of Skarn-2 may stem from difficulty in pairing a relatively pure marble precursor composition with a comparatively complex skarn composition. Our results indicate that skarns derived from compositionally complex precursors (i.e., marl, siltstone, igneous rocks) are more easily related to those precursors than skarns derived from less compositionally complex precursors, such as pure marble.

CONCLUSION

In comparison with texture-based classification of skarns, this method provides a quantitative and objective framework for assessing skarn type using a geochemical data set. As we have demonstrated, this process can relate skarns to their precursors and optimize skarn classification in districts worldwide.

REFERENCES

Einaudi, M.T., Meinert, L.D., and Newberry, R.J., 1981, Skarn deposits, in Skinner, B. J., ed., Economic Geology 75th Anniversary Volume: El Paso, Economic Geology Publishing Co, p. 317-391.

Escalante, A., Dipple, G.M., Barker, S.L.L., and Tosdal, R., 2010, Defining trace-element alteration halos to skarn deposits hosted in heterogeneous carbonate rocks: Case study from the Cu–Zn Antamina skarn deposit, Peru: Journal of Geochemical Exploration, v. 105, p. 117-136.

Glencore, 2015, Annual Report (http://www.glencore.com/assets/investors/doc/ reports_and_results/ 2015/GLEN-2015-Annual-Report.pdf).

Meinert, L.D., Dipple, G.M., and Nicolescu, S., 2005, World skarn deposits, in Hedenquist, J. W., Thompson, J. F. H., Goldfarb, R. J., and Richards, J. P., eds., Economic Geology One Hundredth Anniversary Volume 1905-2005: Littleton, CO, Society of Economic Geologists, p. 299-336.

Mrozek, S.A., 2018, The giant Antamina deposit, Peru: intrusive sequence, skarn formation, and mineralization: PhD thesis, James Cook University, Australia, 173 p.

Lipten, E.J., and Smith, S.W., 2005, The Geology of the Antamina Copper-Zinc Deposit, Peru, South America, in Porter T.M., ed., Super Porphyry Copper & Gold Deposits: A Global Perspective, v. 1: Adelaide, PGC Publishing, p. 189-204.

Love, D.A., Clark, A.H., and Glover, J.K., 2004, The lithologic, stratigraphic, and structural setting of the giant Antamina copper-zinc skarn deposit, Ancash, Peru: Economic Geology, v. 99, pp. 887-916.

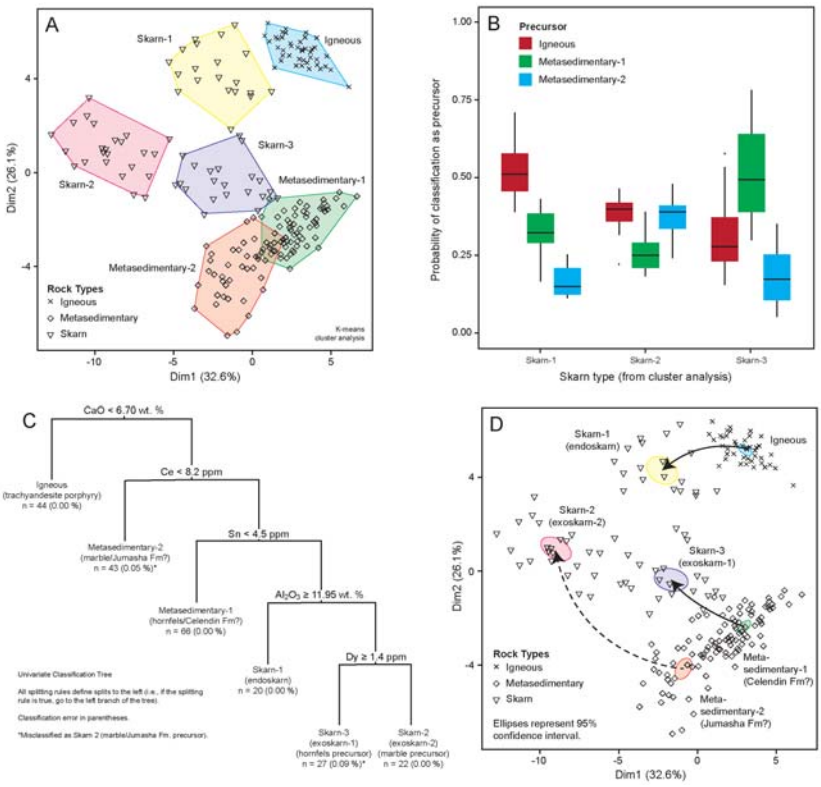

Figure 1. A. Cluster analysis results enveloped by convex hulls; B. Random forest probability model; C. Univariate classification tree; and D. interpretation of cluster analysis results informed from B and C, linking precursors to skarns.

CRITICAL CONSTRAINTS ON LOCALIZATION OFLARGE SKARN OREBODIES: EXAMPLES FROM THE TONGLING-ANQING DISTRICT, CHINA

Liangming Liu

Computational Geoscience Research Center, Central South University - lmliu@csu.edu.cn

BACKGROUND

To understand where and why the large orebodies have formed is very important for mineral exploration. However, it is a large challenge to the exploration geologist because of the complexity of mineralization, especially for skarn ore deposits which generally show extreme irregularity in ore localization and distribution. The Tongling-Anqing is a significant Cu skarn district where the copper skarn ore resources feed the largest copper industry in China. All the ore fields discovered there have gotten intensive exploration and a great deal of data are available to model their 3D architecture for helping us to understand the regularity and mechanism of large orebodies' localization.

The Fenghuangshan ore field is located in the northern east Tongling-Anqing district. In this field, more than 40Mt @ 1.20% Cu ores have been discovered around the Xinwuli intrusion. The orebodies are very unevenly distributed along the contact zone between the Xinwuli intrusion and carbonate rocks of the low Triassic.

The Anqing ore field is located in the southern west Tongling-Anqing district. Hundreds of orebodies discovered in the field are mainly of Cu and Cu-Fe skarns, minor of Fe skarns, with more than 48.8 Mt @ 1.3% Cu ores and 100 Mt @ 48% Fe ores. They mainly occur in the contact zone between the Yueshan intrusion and marble and dolomite marble of the low to mid Tertiary.

3D MODELING AND SPATIAL STATISTICS ANALYSIS

More than 40 km of tunnels and 200 km of drill holes have been completed in the Fenghuangshan ore field since its discovery in 1953. And more than 310 km of drill holes and 60 km of tunnels have also been finished in the Anqing ore field since its discovery in 1959. Applying all the dada from these exploration works, we constructed 3D models of orebodies and ore-controlling intrusions by the surface-based modeling approach (Figs. 1 & 2). Based on these models, we analyze the spatial association of the orebodies with the intrusions and further discuss their genetic relationship by considering their genetic features and the local geodynamic setting.

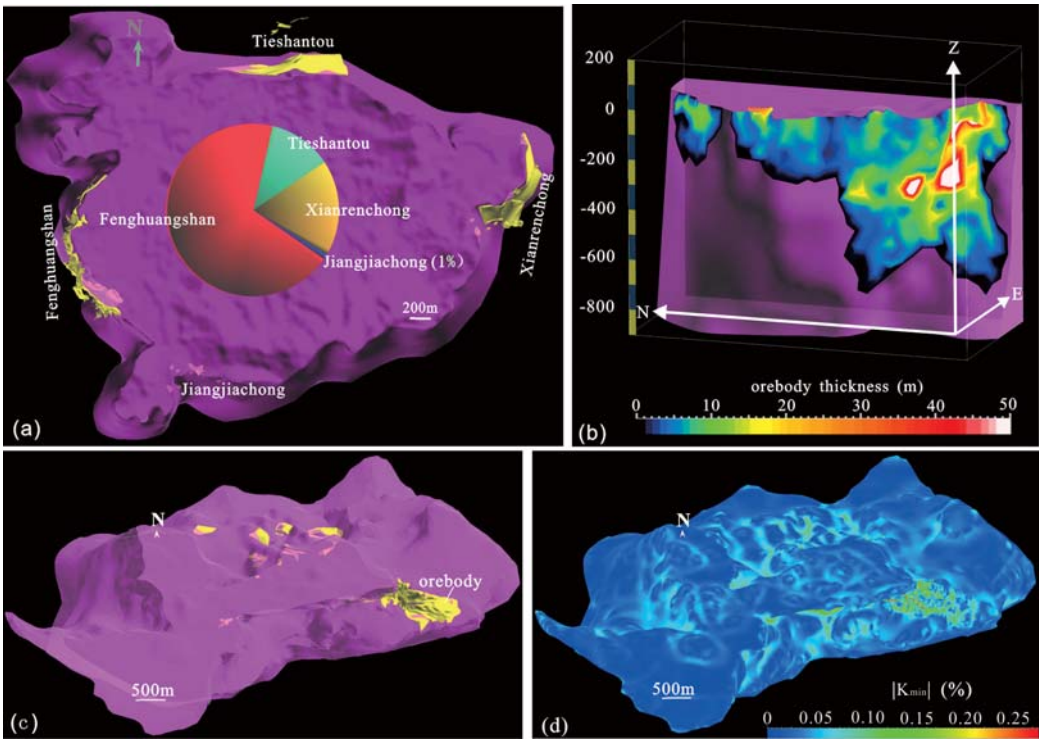

Fig.1: 3D models of intrusions and ore bodies. (a) Xinwuli intrusion and orebodies in Fenghuang ore field; (b) spatial variation of orebody thickness and topography of the western contact zone in Fenghuangshan deposit; (c) Yueshan intrusion and orebodies in Anqing ore field; (d) variation of Gaussian curvature of the Yueshan intrusion's contact surface.

REGULARITY FOR SKARN OREBODIES' LOCALIZATION AND CONTROLLING FACTORS

In the Fenghuangshan ore field, the orebodies are very unevenly localized along the Xinwuli intrusion's contact zone. The largest orebodies and the most voluminous ores are located in the Fenghuangshan deposit along the west contact zone (WCZ) (Fig.1a), where much more voluminous ores are distributed in the southern WCZ than in the northern WCZ (Fig.1b). Such uneven distribution of ores is related to variations in attitude and topography of their hosting contact zone. The main control on genetic origin is in the geodynamic setting and geodynamic processes that affect where and when the mineralization occurred. The NW- trending fault, overlapping with the southern WCZ, led magma intruded initially in the WCZ then moved eastward. The southern WCZ is more perpendicular to the direction of the principal stress s3 of paleo-stress field in early Cretaceous when the mineralization took place. These might have caused the southern WCZ to form more dilatational zones by tensile fracturing, and consequently to host the largest orebodies.

In the Anqing ore field, orebodies are all distributed in both the south and north contact zones that are E-W trending (Fig.2a). About 92% Cu and 42% Fe reserves are in the south contact zone; and 8% Cu and 58% Fe reserves in the north contact zone. The south contact zone, as the host of the large orebodies, has an extremely accidented surface with a wide scope of various dip (Fig.2b). These phenomena suggest that the intrusive topogaphy and E- W trending contact zones are the critical constraints for orebody localization. Such spatial regularity of orebody localization might be related to the emplacement of the intrusion. Its interior structures indicate that the Yueshan intrusion might have intruded initially in the south contact zone and then moved northward.

CONCLUSION

The uneven distribution pattern of skarn orebodies is spatially associated to the attitude and topography of the contact zones. Its genetic origin is in the geodynamic setting and geodynamic processes where and when the mineralization occurred. The contact zone segment where the intrusion was initially emplaced generally has the most irregular topography and are favorable for hosting the large orebody.

SKARN DEPOSITS - USING MINERAL ZONATION IN EXPLORATION

Lawrence Meinert

Meinert Consulting LLC - LDmeinert@gmail.com

Most large skarn deposits are associated with relatively shallow magmatic systems emplaced within or near carbonate rocks. In a simple sense, these deposits form by the transfer of heat and fluid from a cooling magma to the surrounding rocks. This leads, inescapably, to hydrothermal alteration and more importantly, to zoned systems in both space and time. Zonation occurs on scales from km to m to µm and reflects fluid flow, wall rock reaction, temperature changes, and fluid mixing. The most spectacular examples of skarn zonation usually occur at the skarn-marble contact where transitions between monomineralic bands can be knife sharp. Other small scale examples occur in zoned veins and individual mineral crystals. Although, visually striking and scientifically interesting, these small scale variations are less useful in exploration than deposit or district scale zonation.

In most skarns there is a general zonation pattern of proximal garnet, distal pyroxene, and vesuvianite (or a pyroxenoid such as wollastonite, bustamite, or rhodonite) at the contact between skarn and marble. In addition, individual skarn minerals may display systematic color or compositional variations within the larger zonation pattern. For example, proximal garnet is commonly dark red-brown, becoming lighter brown and finally pale green or yellow near the marble front. The change in pyroxene color is less pronounced but typically reflects a progressive increase in iron and/or manganese towards the marble front. Beyond the limit of skarn there is additional evidence for fluid transport in the form of thin, planar to wispy, veinlets generally called fluid escape structures. These represent dissolution surfaces and commonly show geochemical anomalies in the elemental suite characteristic of a particular skarn type.

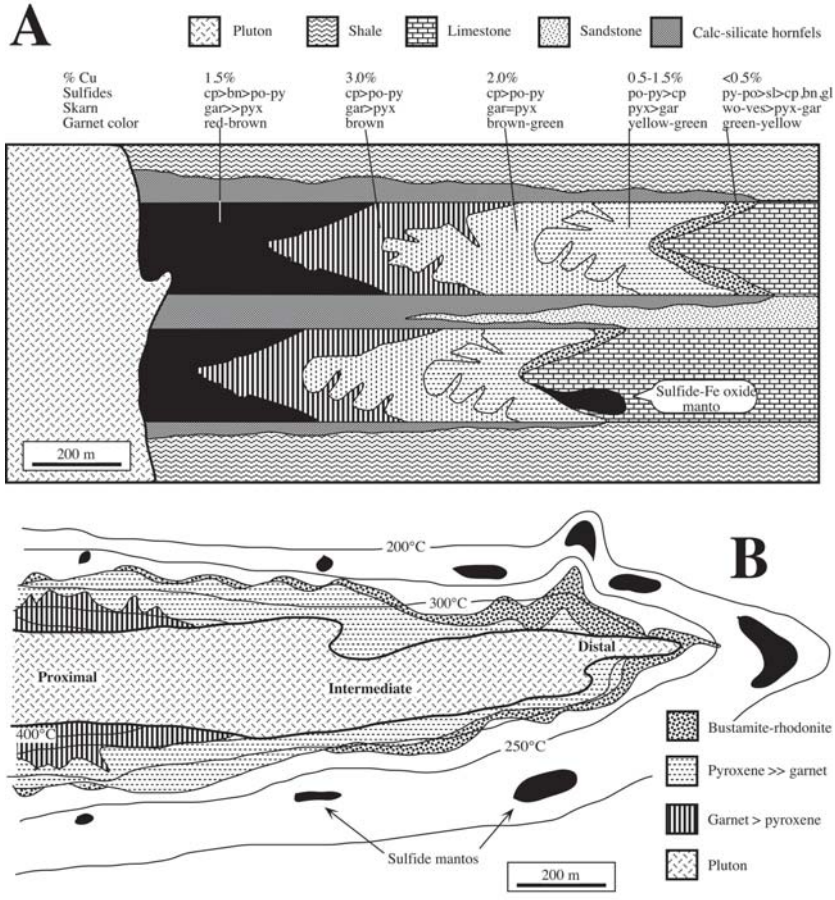

Feature	Proximal	Intermediate	Distal
Garnet:pyroxene	> 1:1	1:20	No garnet
Max Jo in pyroxene	< 25%	25-50%	> 50%
Fe oxides	mt > hm	hm ~ mt	hm > mt
Ore sulfides	sl > gl ~ cp	sl > gl > cp	sl ~ gl > cp
Skarn:manto ore	> 10	1-10	< 1
Temperature	> 400°C	320° - 400°C	< 320°C
Salinity (NaCl eq. wt.%)	> 15 %	7.5-15%	< 7.5%
Zn/Cu	< 10	10-20	> 20
Zn/Pb	> 5	2-5	< 2
Pb/Cu	< 5	5-10	> 10

For some skarn systems, these zonation patterns occur on a scale of kilometers and provide a significant exploration guide. Variations on these general patterns reflect differences in igneous or wall rock oxidation state, depth of formation, protolith and magma compositions, and tectonic setting. Details of skarn mineralogy and zonation can be used to construct deposit-specific exploration models as well as more general models useful in developing grass roots exploration programs or regional syntheses. Reasonably detailed zonation models have been developed for copper, gold, and zinc skarns. The zonation models for Cu and Zn skarns below illustrate the systematic changes in skarn mineralogy, mineral compositions, ore grades, metal ratios, and fluid temperature and salinity.

Zonation patterns for different types of skarn systems have been described by Meinert (1997) and the general characteristics, evolutionary stages, and mineralogy of skarn deposits are summarized by Meinert *et al.* (2005). Application of skarn zonation models has resulted in exploration success in many parts of the world and recent examples from around the world will be illustrated in this presentation.

REFERENCES

Meinert, L.D., 1997. Application of skarn deposit zonation models to mineral exploration: Exploration and Mining Geology, v. 6: 185-208.

Meinert, L.D., Dipple, G. M., and Nicolescu, S., 2005. World Skarn Deposits: in Hedenquist, J.W., Thompson, J.F.H., Goldfarb, R.J., and Richards, J.P., eds., Economic Geology 100th Anniversary Volume, Society of Economic Geologists, Littleton, Colorado, USA, p. 299-336.

PHYSICAL AND CHEMICAL GROWTH PATTERNS OF A DISTAL Pb-Zn SKARN, MADAN, BULGARIA

Aaron Hantsche[1], Kalin Kouzmanov, Stan Sizaret, Georgi Milenkov, Simone Vezzoni, Andrea Dini, Rossitsa Vassileva

[1]*University of Geneva - aaron.hantsche@unige.ch*

BACKGROUND

Distal skarn metasomatism is controlled by fluid transport and chemical interaction with a reactive lithology (Einaudi, 1982; Meinert *et al.*, 2005). These skarn bodies, often found kilometers away from any intrusive source, are pyroxene-rich (>>garnet), have elevated Mn concentrations, and have been associated with Pb-Zn sulfide mineralization. Understanding the physical and chemical evolution of these systems is important recognize the distribution, zonation, and extent of the skarn bodies during resource exploration.

Quantifying skarn growth in a distal pyroxene skarn requires constraining three parameters: 1) skarn front propagation direction, 2) crystal growth direction of skarn silicates, and 3) fluid flow direction of the skarn-forming fluid (Figure 1). These related parameters can often be qualitatively identified using structural field measurements and petrographic analyses of oriented sections. Recent advances in field mapping and magnetic susceptibility, however, have opened the possibility to quantify the relationships between the three parameters (Sizaret *et al.*, 2006; Li *et al.*, 2014).

The Madan ore field in southern Bulgaria is characterized by Pb-Zn sulfide mineralization of distal skarn bodies hosted in marble horizons of the amphibolite grade metamorphic sequence of the Central Rhodope Mountains (Marchev *et al.*, 2005). Distal skarns in the Madan ore field are controlled by the intersection of the marble lenses with a series of northwest trending normal faults (Vassileva *et al.*, 2009). The prograde assemblage is dominated by johansennite (Mn-pyroxene) spheroids, and is replaced by rhodonite, amphibole, quartz, Fe-oxides, and carbonates in the retrograde phase, which precede late-mineralization including galena, sphalerite, pyrite, and chalcopyrite (Vassileva *et al.*, 2005. Replacement mineral growth is structurally controlled by the original pyroxene structure via direct replacement and interstitial crystallization.

At the Petrovitsa deposit, active mining revealed a gallery at the 865m level in which a skarn body extends up to 20m away from a mineralized vein. This gallery was mapped in detail to quantify the skarn distribution, and samples were systematically taken for characterization of skarn silicates. The current project aims to constrain the evolution of distal skarn systems using a combination of field mapping, petrography, anisotropy of magnetic susceptibility (AMS), electron microprobe analyses (EPMA), and mass spectrometry (LA-ICP-MS).

METHODS

Recent work has shown that quantitative measurements of elongate skarn minerals (e.g., pyroxene) can be used relate the skarn silicate growth direction to the skarn front propagation direction (Vezzoni *et al.*, 2016). Mineral lineations were measured in the field and reconstructed on rose diagrams based on location in the outcrop.

AMS measurements were made on oriented samples from the skarn body transect. Cores (2.2 x 2.2 cm) were drilled into skarn, vein, and gneiss samples for measurement by AGICO MFK-1, at the University of Geneva and the Institut des Sciences de la Terre d'Orléans. Thermomagnetic measurements were made using an AGICO CS4 Furnace in order to identify magnetic carrier phases.

Petrographic characterization, in conjunction with backscatter electron imaging, cathodoluminescence, and chemical analyses by Electron Microprobe Analyzer (JEOL 8200), has been done at the University of Geneva. Quantitative pyroxene measurements and element maps were made using at 15 kV using the EPMA. Major element chemistry will be supplemented by LA- ICP-MS analyses of pyroxenes as the study progresses.

RESULTS

Mineral mapping and observation of aggregates of pyroxene growth versors quantify the observed skarn growth direction in the 865m gallery at Petrovitsa. Aggregated data show crystal growth dominated towards the southwest, orthogonal to the local vein. Additionally, clusters of data at the outcrop scale record crystal growth away from contacts between the gneiss and the marble lens.

AMS measurements suggest fluid flow parallel to the contacts between the gneiss and the marble. Data from the vein suggests a nearly vertical magnetic foliation. Thermally induced susceptibility changes at 580°C indicates magnetite as the primary magnetic carrier. Away from the vein, the AMS data suggest fluid flow along lithological boundaries. Whole rock chemical data suggests a general gradient towards more Mn-rich compositions away from the vein. Chemical data from EPMA analyses show that this zonation is controlled by the prograde skarn mineralogy, as pyroxenes are more

hedenbergitic (Fe-rich) near the vein and more johansennitic (Mn-rich) closer to the skarn front. Millimeter-scale pyroxene zonations have variation both chemically and texturally, and cycle between Fe-rich, fine grained pyroxene to Mn-rich, coarse- grained pyroxene. Diopsidic (Mg) compositions are not observed in the prograde skarn.

CONCLUSIONS

Pyroxene growth versors can be used to map the propagation direction of the skarn front during its formation, and serves as a useful tool in distal settings where skarn geometry and zonation is unclear. AMS data, likewise, can be used to reconstruct fluid flow by a proxy of magnetic crystal orientation. It is reasonable to combine crystal growth and fluid flow directions to reconstruct the distribution and growth of distal skarn bodies, and this data can be parlayed into spatial constraints for chemical analyses.

Major element variations show general variations in Fe/Mn with distance from the mineralized vein, allowing for zonation mapping towards more proximal skarn bodies in the Madan system. As future work uncovers information on trace element compositions of these minerals, pyroxene may prove to be a valuable vector pointing towards the heart of mineralized distal skarn systems.

REFERENCES

Einaudi M.T., 1982. Descriptions of skarn associated with porphyry copper plutons, southwestern North America, in Titley, S.R. (Ed.), Advances in geology of the porphyry copper deposits, southwestern North America: University of Arizona Press, Tucson, 139–184.

Li, G., Sizaret, S., Branquet, Y., Barbanson, L., Chen, Y., Wang, B., Wu, G., Gu, L., Shu, L., 2014. Initial geometry and paleoflow reconstruction of the Yamansu skarn-related iron deposit of eastern Tianshan (China) from paleomagnetic and magnetic fabrics investigations. Journal of Asian Earth Sciences, 93, 1–14. https://doi.org/10.1016/j.jseaes.2014.06.009

Marchev, P., Kaiser-Rohrmeier, M., Heinrich, C., Ovtcharova, M., von Quadt, A., & Raicheva, R., 2005. 2: Hydrothermal ore deposits related to post-orogenic extensional magmatism and core complex formation: The Rhodope Massif of Bulgaria and Greece. Ore Geology Reviews, 27(1–4), 53–89. https://doi.org/10.1016/j.oregeorev.2005.07.027

Meinert L., Dipple G., Nicolescu S., 2005, World Skarn Deposits: Economic Geology 100th Anniversary Volume. V. 100, p. 299–336.

Sizaret, S., Chen, Y., Barbanson, L., Henry, B., Camps, P., & Marcoux, E., 2006. Crystallization in flow - I. Palaeocirculation track by texture analysis and magnetic fabrics. Geophysical Journal Internaional, 167(2), 605–612. https://doi.org/10.1111/j.1365-246X.2006.03106.x

Vassileva, R. D., Bonev, I. K., Marchev, P., & Atanassova, R., 2005. Pb-Zn deposits in the Madan ore field, South Bulgaria: Madan District. Ore Geology Reviews, 27(1–4), 90–91. https://doi.org/10.1016/j.oregeorev.2005.07.026

Vassileva R.D., Atanassova R., Bonev I.K., 2009. A review of the morphological varieties of the ore bodies in the Madan Pb-Zn deposits, Central Rhodopes, Bulgaria. Geochemistry, Mineralogy and Petrology 47: 31-49.

Vezzoni, S., Dini, A., & Rocchi, S., 2016. Reverse telescoping in a distal skarn system (Campiglia Marittima, Italy). Ore Geology Reviews, 77, 176–193. https://doi.org/10.1016/j.oregeorev.2016.03.001

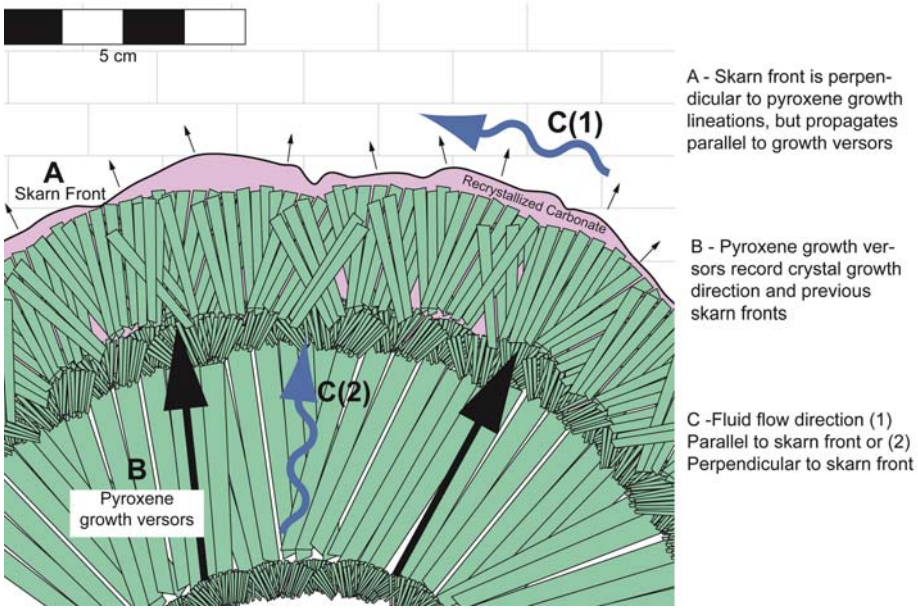

TECTONIC SETTING OF INTRUSIONS ASSOCIATED WITH Fe AND Cu SKARN DEPOSITS IN THE QIMAN TAGH AREA OF QINGHAI PROVINCE, EASTERN KUNLUN OROGEN, CHINA

Zhicheng Lü

Development and Research Center, China Geological Survey - zhichenglv@163.com

BACKGROUND

The Fe and Cu skarn deposits are economically important in China. The Qiman Tahg area of Qinghai Province, located in the western margin of the Eastern Kunlun Orogen, is the most important Fe and Cu skarn belt in western China. The region is characterized by the occurrence of many important Fe and Cu skarn deposits (such as Kaerqueka, Yemaquan and Tawenchahanxi), which are associated with the Triassic magmatism. The common features of these deposits have been extensively summarized by many researchers, but tectonic setting of these Fe and Cu skarn deposits remains unsolved. Combined with regional geology and geochronological data, this study proposes that the Fe and Cu skarn deposits were formed under different tectonic settings.

METHODS

Zircon U–Pb dating of granitoid rocks associated with the Kaerqueka Cu, Yemaquan Fe–Cu–Zn, Hutouya N° II Fe–Cu–Zn–Sn and Tawenchahanxi Fe–Cu–Zn deposits were conducted by laser ablation–inductively coupled plasma source mass spectrometry. Zircons were separated using conventional heavy liquid and magnetic techniques. Zircon grains were handpicked using a binocular microscope, mounted in epoxy resin, and then polished for subsequent cathodoluminescence observation and zircon U–Pb dating. CL images and zircon in situ U–Pb–Hf isotope analyses were acquired using a JEOL JSM–6510 microprobe and a New Wave UP213 laser attached to a Neptune multi–collector ICP–MS at Beijing GeoAnalysis Co., Ltd and the Institute of Mineral Resources of the Chinese Academy of Geological Sciences, respectively.

Zircon U–Pb dating was conducted by laser ablation–inductively coupled plasma source mass spectrometry. Helium was used as a carrier gas to enhance the transport efficiency during ablation. Before entering the ICP–MS, Argon was used as the make-up gas and mixed with helium via a T-connector. Zircon GJ1 standard was applied as an external calibration standard for correcting U–Pb fractionation, and was analyzed twice every 10 analyses during U–Pb dating. Zircon M127 were used as an external standard to determine U, Th and Pb concentrations. U–Pb age calculation and concordia diagram construction were made using ISOPLOT/Ex (v. 3.0).

RESULTS

Spot analyses from 20 grains (sample YM-5) yield concordant results with a weighted mean 206Pb/238U age of 223.5 ± 1.7 Ma, which provides the crystallization age of the monzonite in the Yemaquan Fe–Cu–Zn deposit. All 15 zircons from sample KE49-1 from the Kaerqueka Cu deposit yield a weighted mean 206Pb/238U age of 245.1 ± 1.5 Ma, which represents the crystallization age of the Kaerqueka granodiorite. Analysis results of 17 zircons from the granite in the Hutouya N° II Fe–Cu–Zn–Sn deposit form a coherent group and yield a weighted mean 206Pb/238U age of 231.7 ± 2.1 Ma. A total of 28 zircon U–Pb analyses of the granodiorite porphyry (sample T1-1) in the Tawenchahanxi Fe–Cu–Zn deposit form a coherent group with a concordant weighted mean 206Pb/238U age of 233.5 ± 0.9 Ma.

CONCLUSION

The age obtained in the present study for the Kaerqueka granodiorite (245.1 ± 1.5 Ma) is the same (within error) as the molybdenite Re–Os age (245.5 ± 1.6 Ma) of Gao (2013), obtained from the Cu skarn mineralization at Kaerqueka. For Fe skarn deposits, the LA–ICP–MS zircon U–Pb dating for the monzonite associated with the Yemaquan Fe–Cu–Zn deposit yields the crystallization age of 223.5 ± 1.7 Ma, which is younger than the zircon LA–ICP–MS U–Pb ages for granite (231.7 ± 2.1 Ma) and granodiorite (233.5 ± 0.9 Ma) associated with the Hutouya N° II Fe–Cu–Zn–Sn deposit and Tawenchahanxi Fe–Cu–Zn deposit, respectively. Combined with our new and published data, two discrete suites of the intrusions associated Fe and Cu skarn deposits have been recognized in the region: (1)245.1 ± 1.5 Ma granodiorite related to a Cu skarn deposit; (2) 235–224 Ma granitic rocks associated with Fe skarn deposits. This indicates that intrusions associated with Fe and Cu skarn deposits were associated with different episodes of magmatism.

The Kaerqueka granodiorites are high-K calc-alkaline and metaluminous to slightly peraluminous rocks. They have low Sr/Y and (La/Yb)N ratios and high Y and Yb contents, which show affinity of arc-related magmatism.

However, it is difficult to discriminate high-K calc-alkaline granitoids related to different tectonic environments, because they may have similar geochemical and isotopic compositions. Thus, it has been suggested that granitoids should not be used as a geodynamic indicator alone but in association with structural data. Geological features show that the parallel unconformity developed between Middle Triassic Naocangjiangou Formation (marine facies) and Xilikete Formation (transitional facies from marine to continent) represents Middle Triassic continental uplift event. In addition, 246–242 Ma high-pressure metamorphic rocks are recognized in the EKOB, suggesting that the collision occurred during Middle Triassic. The Kaerqueka granitoids were emplaced contemporaneously in the Middle Triassic which is consistent with the timing of formation of the parallel unconformity in Middle Triassic strata and high-pressure metamorphic rocks, suggesting that the granitoids related to Cu skarn deposit were generated in a syn-collisional setting. Geological features show that the Late Triassic terrestrial volcanic rocks and the contemporaneous A-type granites and mafic–ultramafic rocks were developed in the Qiman Tahg area, suggesting a post-collisional tectonic regime during Late Triassic. As mentioned above, the Fe skarn deposits are associated with the 235–224 Ma granitic rocks. This suggests that the Fe skarn deposits in the Qiman Tahg area were formed under a post- collisional setting.

In summary, combined with geological and geochronological evidence, we propose that the Cu and Fe skarn deposits were formed under syn-collisional and post-collisional settings, respectively.

A REVIEW OF SCHEELITE-BEARING SKARNS IN THE EASTERN SIERRAS PAMPEANAS: MINING RECORDS AND MINERALOGICAL DATA OF LOS GUINDOS MINING GROUP, PAMPA DE OLAEN DISTRICT, CÓRDOBA, ARGENTINA

María José Espeche[1], Raúl Lira

[1]*Consejo Nacional de Investigaciones Científicas y Técnicas (CONICET). Museo de Mineralogía y Geología "Dr. A. Stelzner" - FCEFyN - Universidad Nacional de Córdoba - maru-espeche@hotmail.com*

INTRODUCTION

From 1943 to 1963 Los Guindos mining group (31°10' - 31°12'S / 64°32' - 64°35'W) has been one of the main tungsten (scheelite) producers of Argentina. Between the 40's and 60's, ~20,000 t of ore were mined in an area of 13 km^2, which produced 200 t of scheelite concentrates (69.2 % WO_3).

The mining group is located in Late Proterozoic to Lower Cambrian metasedimentary rocks, ~3 km east of the contact with granites of the Devonian Achala batholith (ca. 2,500 km^2), an anorogenic composite intrusive of A + S mixed petrogenetic signature.

Scheelite ore is found in irregular skarn bodies pseudo concordant with the metasedimentary basement, mainly composed of sillimanite gneisses, schists, amphibolites and marbles, intruded by pegmatites of Lower to Middle Paleozoic ages.

The aim of this contribution is to present an updated review of preexisting petrological and mineralogical studies and new field and mineral chemistry data of on-going research.

RESULTS

The skarns from Los Guindos are coarse grained, isolated, irregular bodies that vary in size from a few up to some hundreds of m2. Contact relations between skarns and country rocks are not easily recognizable due to partial cover with Quaternary sediments and vegetation.

The mined ore was Mo-bearing scheelite, intergrown with calc-silicate minerals, quartz, calcite and fluorite. A preliminary identification of the prograde association related to scheelite mineralization is as follows: Ves+Grt+Ap+Ttn; a late retrograde mineral association (Ep1-Act/Tr-Czo-Chl1-Cal1) replaces prograde paragenesis to different extents. The skarn mineralogy overlaps regional metamorphic mineral associations in marbles and amphibolites and also the border/wall zones of a considerable number of pegmatite bodies. In some mines, Valdez (1984) mentioned the occurrence of helvite crystals associated with garnet and beryl crystals in cavities with vesuvianite. These Be-rich minerals are related to Be-bearing pegmatites. Scheelite mineralization is restricted to the infilling stage associated with Ep2-Chl2-Cal2-Qz-Sp-Ccp-Po-Py-Fl. Garnet exhibits compositions from grossularite (Gr85.9Ad11.6Sp2.5) to grossularite with a high subcalcic component (Gr53.9Sp24.6Ad21.2) and yields F- contents between 0.52 and 1.36 wt. % and 0.17 wt. % ZnO. Vesuvianite F- content varies from 1.85 to 3.17 wt. % and ZnO averages 0.23 wt. %. Sphalerite >> pyrrothite > chalcopyrite > pyrite are common sulfides in the skarn, though of erratic distribution. Other less common sulfosalts and sulfides are gustavite [$PbAgBi_2S_6$], tetradimite [Bi_2Te_2S], bismuthinite [Bi_2S_3], lillianite [$Pb_3Bi_2S_6$], andorite [$PbAgSb_3S_6$], matildite [$AgBiS_2$] and kesterite [$Cu_2(Zn,Fe)SnS_4$], currently restricted to some outcrops (Gamba 1996; Sureda *et al.* 2006); these minerals were interpreted as deposited during a late hydrothermal stage after metasomatism (Sureda *et al.* 2006).

Fluid inclusion microthermometric data in vug-lining gem-quality epidote crystals from two mines yielded homogenization temperatures from 282 °C to 341 °C (n= 26) and 316° to 361 °C (n= 23), with an average of 312 and 339 °C, respectively, and salinities ranged from 6.2 to 12.3% NaCl eq. (n= 8) and 6.2 to 8.2% NaCl eq. (n= 12). These minimum trapping temperatures and salinities represent a late retrograde to infilling stage (Ocanto *et al.* 2001), which is strongly developed in Los Guindos skarns. Despite the clear spatial relation of W and subordinated polymetallic ore with skarn bodies, mineralization stages and the origin of metals are still uncertain. Brodtkorb and Pezzuti (1991) and Gamba (1999a, b) assigned Los Guindos scheelite group to the exhalative syngenetic – synsedimentary deposit type. The main evidence presented by these authors is the stratabound scheelite distribution within conformable units of the basement, and the lens-shaped geometry of the bodies throughout a large areal distribution. Nevertheless, current field and petrographic work does not support such a scheelite-mineralized stratabound pattern. The potential genetic linkage with the neighboring exogreisen quartz-wolframite (±Fe-Cu sulfides) veins hosted within the highly fractionated Achalian Mesa de Mula Muerta muscovite-leucogranite, located ~10 km to the NW, has not been studied yet.

CONCLUSIONS

Garnet compositions fall into the field of the W skarn deposits (Meinert *et al.* 2005). The chemistry of the fluorian garnets, as well as the F-rich vesuvianite in the prograde stage, the anomalous contents of Be (as beryl and helvite group minerals), and the high concentrations of Zn and F, are characteristic of W-Sn-F skarns deposits (e.g., Kwak and White 1982;2 Manning and Bird 1990). Even though Los Guindos scheelite mineralization in skarns is known since early 1900, available published data is still deficient to thoroughly understand the skarn formation, sources of fluids and metals, and evolution of the system. The participation of a magmatic fluid enriched in volatiles (i.e., F- and H O) from the Achalian magmatism and its pegmatitic swarm of hybrid nature (Be-P-F-Nb-Ta-U-Li-enriched), its intra- and perigranitic- wolframite bearing greisen/hydrothermal quartz veins, as well as the contribution of the metamorphic basement as possible source of sulfur and metals to the system, are still subject of study.

REFERENCES

Brodtkorb, M.K. de, Pezzutti, N. 1991. Yacimientos scheelíticos en rocas calcosilicáticas asociadas a anfibolitas, provincias de San Luis y Córdoba, in: Brodtkorb de, M.K. (Ed.) Geología de los depósitos de tungsteno de las provincias de San Luis y Córdoba, Argentina. Publicación del INREMI, Universidad Nacional de La Plata, pp. 169 – 184.

Gamba, M.T., 1996. Minerales de Ag, Bi y Sn en la mina Loma Pajosa, distrito minero scheelítico Los Guindos, Córdoba, Argentina. III Reunión de Mineralogía y Metalogenia. Publicación del INREMI, Universidad Nacional de La Plata 5: 119 – 121.

Gamba, M.T., 1999a. Distrito scheelítico Pampa de Olaen, Córdoba, in: Zappettini, E.O. (Ed.) Recursos Minerales de la República Argentina. SEGEMAR. Anales 35: 251 – 256.

Gamba, M.T., 1999b. Vinculación volcanogénica de los yacimientos de scheelita de Pampa de Olaén, Córdoba, Argentina: interpretación geoquímica de los protolitos metamorfizados. 1° Simposio de Vulcanismo y Ambiente Asociados. p. 96.

Kwak, T.A.P., White, A.J.R., 1982. Contrasting W-Mo-Cu and W-Sn-F Skarn types and related granitoids. Mining Geology 32: 339 – 351.

Manning, C.E., Bird, D.K. 1990. Fluorian garnets from the host rocks of the Skaergaard intrusion: Implications for metamorphic fluid composition. American Mineralogist 75: 859 – 873.

Meinert, L.D., Dipple, G.M., Nicolescu, S. 2005. World skarn deposits. Economic Geology 100th Anniversary Volume: 299-336.

Ocanto, C.A., Gomez, G.M., Lira, R., 2001. Microthermometric data on epidote-clinozoisite from metasomatic-hydrothermal environments, Oriental Pampean Ranges, Argentina, in: Noronha, F., Dória, A., Guedes, A. (Eds) XVI ECROFI European Current Research On Fluid Inclusions. F. Abstracts. Faculdade de Ciencias do Porto, Departamento de Geología 7: 347– 348.

Sureda, R., Lira, R., Colombo, F., 2006. Gustavita, $PbAgBi_3S_6$-P21/c, con los minerales de bismuto y plata en el 'skarn' Los Guindos, Pampa de Olaen, Córdoba, Argentina (31°11'S/64°33'W). Revista Geológica de Chile 33, N° 1: 141 – 160.

Valdez, M.A., 1984. Cartografía geológica y estudio petro-mineralógico del Distrito Minero Los Guindos (Departamento Punilla, Provincia de Córdoba). Escuela de Ciencias Geológicas, FCEFyN. Universidad Nacional de Córdoba. p. 65.

CHAPTER 11

NEW DEVELOPMENTS IN MAGMATIC SULFIDE AND OXIDE DEPOSITS IN SOUTH AMERICA AND WORLDWIDE

Conveners: María Emilia Schutesky Della Giustina, David Holwell

THE VOISEY'S BAY DEPOSIT, CANADA: HOW TWENTY-FIVE YEARS OF RESEARCH REDEFINED GENETIC AND EXPLORATION MODELS FOR MAGMATIC Ni-Cu-Co SULFIDE DEPOSITS

Andrew Kerr[1], Anthonly J. Naldrett

[1]*Memorial University, St. John's, Canada - akerr@mun.ca*

In 1993, exploration program diamonds on the remote coast of Labrador (Canada) led to one of the most significant mineral discoveries of the late 20th century. In late 1993 one of the first holes returned 44 m grading 3% Ni and 1.5% Cu. This generated significant interest, but the true size of the discovery only became apparent when the seventh hole of the program returned over 100 metres of massive sulfides. The hilltop is now known as Discovery Hill, and overlooks an operating mine, where total resources are 141 Mt at around 1.6% Ni. In 2018, Vale announced underground mine construction, and another two decades of production are anticipated. The Voisey's Bay deposit contributes to the economies of Canada, Newfoundland-Labrador and the Inuit Territory of Nunatsiavut, and provides employment and opportunities in a remote region of Canada.

Voisey's Bay had an important impact on our understanding of orthomagmatic Ni-Cu-Co +/- PGE deposits, and also upon exploration models. It is in many respects the new 'type example', and frequently cited in comparative research studies. This influence reflects several factors, including detailed knowledge of the three-dimensional architecture of the deposit and associated magmatic structures, and other research work completed in the decade-long gap between discovery and development. The development of scientific ideas commenced during advanced exploration, and the results were applied directly. Most importantly, early research was jointly funded by Diamond Fields Resources and a public agency, and this collaboration was retained when INCO assumed ownership. The agreement dictated that the results of research could and would be published, and key findings entered the public domain quickly. Later research was in part sponsored by INCO, and led to additional valuable publications and theses. The story of Voisey's Bay and its influence is not just about the science itself, but is also a testament to the importance of open science, where ideas can be assessed and tested by outside interests, leading in turn to new ideas and applications.

The Voisey's Bay discovery drew attention to mafic rocks associated with large-scale magmatic provinces including anorthosite complexes, which had not previously been seen as first-order targets. Although not all discoveries made in the wake of Voisey's Bay proved economic, the research work and testing of ideas involved in these efforts added significantly to our knowledge. Research work at the deposit and elsewhere confirmed many established controls for the development of magmatic sulfide deposits, but prompted rethinking of some key concepts, and ultimately led to a move from closed-system models to open-system models that are more consistent with the dynamic nature of mafic-ultramafic magmatic systems.

The Voisey's Bay Ni-Cu-Co Deposit is hosted by Mesoproterozoic (~ 1333 Ma) mafic rocks that form an early component of the Nain Plutonic Suite (NPS), a vast batholith that also includes anorthosites, intermediate rocks and granites. There is a misconception that the deposit is actually anorthosite-hosted, but this is not so; the most closely associated host rocks are troctolite and olivine gabbro, which likely form part of a much larger (and now eroded) layered mafic intrusion. Compared to mafic and ultramafic host rocks associated with other major Ni deposits, those of the Voisey's Bay Intrusion are compositionally evolved and are not especially metal-rich. The very low PGE contents of these and other NPS mafic magmas imply derivation via sulfur-saturated melting, and/or early separation of sulfide liquid during their ascent, but the relative importance of these effects is difficult to assess. Crustal contamination during ascent of these magmas was multistage and is likewise not easily resolved from isotopic or trace-element data; the quest for a simple 'magic bullet' indicative of magma fertility appears to be naïve. Metasedimentary gneisses are thought to reside at depth, and have been implicated as sources for sulfur to generate immiscible sulfide liquids. However, the stable isotope evidence is inconclusive, and these rocks, which contain only small amounts of pyrrhotite, are poor candidates for such a role. The use of Re isotopes to understand the role of external crustal sulfur versus internal magmatic sulfur proved to be similarly inconclusive. The sulfur in these deposits cannot be assigned entirely as crustal in origin, although there is clear evidence for assimilation of the metasedimentary gneisses by magmas. Unusual xenoliths, containing restite-like assemblages of anorthite, corundum and spinel, are commonly spatially associated with sulphide-rich zones, in heterogeneous rocks that likely formed via interaction of partially crystallized and fully liquid magmas. Such evidence indicates the importance of dynamic, multi-stage magmatic emplacement, rather than more static processes in which the sulfides simply settled out of magmas to accumulate.

The most critical information comes from spatial relationships, which indicate formation in a conduit system that linked two vertically juxtaposed magma chambers. Sulfide liquids, however they might have formed, were concentrated in areas where the conduit system discharged into larger magma reservoirs, or within specific sections of the conduit system. The accumulation of sulfide liquids was governed largely by fluid-dynamic effects related to changes in magmatic flow regimes. The details of these controls are not easily resolved, but the empirical observations from Voisey's Bay have still proven useful in exploration elsewhere. The recognition of the wider 'magmatic conduit' environment soon led to new exploration models based on this premise. Conduit systems facilitate interaction of early- formed sulfide liquids with multiple batches of fresh magma, which eases the physical constraints on metal enrichment. Mineral compositions (notably olivines) at Voisey's Bay suggest the formation of an initial sulfide liquid that had relatively low Ni and Cu contents, followed by progressive upgrading as it interacted with later magma batches. The shift from simple closed systems to more complex open systems also carries other implications. It is likely that any early-formed sulfide liquids would be partially redissolved in this dynamic setting, which further promotes metal enrichment in the remaining sulfides. Numerical modelling suggested that this could have wider consequences, because base metals and PGE behave in very different ways during this dissolution process. Such multistage dissolution-upgrading models inspired by Voisey's Bay may eventually provide us with a route to unified models for sulfide-rich Ni-Cu-dominated deposits and the more problematic sulfide-poor PGE-rich deposits. Finally, the potential for magmatic sulfide accumulations to crystallize as semi-closed systems that form enriched residual liquids has long been understood, but there were few natural examples of it. The large and rich Ovoid deposit at Voisey's Bay indicates the operation of this late-stage process, which concentrated Cu and several other elements into a high-grade core as the sulphide liquid it progressively crystallized, from the outside in.

The recent announcement of underground mining at Voisey's Bay carries much promise for future research. This could add much to our knowledge of local controls on sulfide accumulation, and allow better three-dimensional resolution of the conduit system. Deeper drilling should add to our knowledge of the lower magma subchamber, believed to be where the initial sulfide liquids were formed. The many technological advances since discovery will provide new approaches to tackle remaining questions. This potential is encouraging, but it must be reiterated in closing that the wide influence of research at Voisey's Bay was not just about the science itself, but also about the publication and dissemination of the data and ideas.

SULFIDE INCLUSIONS AS A KEY TO UNDERSTAND ORIGIN OF Ni-Cu-PGE DEPOSITS

Irina Tretiakova[1], Marco Fiorentini, Vlad Malkovets, Laure Martín

[1]*TsNIGRI, Moscow, Russia - iritret@gmail.com*

INTRODUCTION

Mantle-derived silicate minerals such as olivine or garnet often contain droplets of sulfides, which are a unique storage of information about mantle processes leading to Ni-Cu-PGE deposits formation. The significance of these inclusions study is based on their pure mantle origin and absence of interaction with crustal material and alterations due to encapsulation in silicate grains. Sulfide droplets often contain platinum-group elements including Os, which makes them suitable for Re-Os geochronology. Various composition of inclusions, their morphological, geochemical and mineralogical features together with isotopic signatures give us a key for better understanding of processes of sulfide formation, segregation and accumulation in mantle conditions.

SAMPLES AND METHODS

Although olivine is common for Ni-Cu-PGE deposits, in many cases it does not form grains large enough for inclusion study. However, mantle-derived olivine and garnet of suitable grain sizes could be found in other juvenile rocks such as kimberlite, which brings samples of subcontinental lithospheric mantle to the surface. Thirty-eight sulfide inclusions hosted in olivine grains with clear mantle derivation (Mg# - from 90 to 93) have been selected from the heavy mineral concentrate of crushed harzburgite-dunite xenoliths from the Udachnaya pipe, Yakutia, Russia.

Comprehensive study of inclusions and hosting olivine has been done using state-of-art analytical techniques at CMCA and Curtin University (Perth, Australia), Macquarie University (Sydney, Australia) and University of Quebec (Quebec, Canada). At the first stage, reflected light optical microscopy and microprobe elemental mapping were used to reveal mineralogical phases and differences in their composition. Sulphur isotopic composition of sulfides was analyzed using secondary-ion mass-spectrometry (CAMECA 1280). High-resolution investigation of platinum-group phases was done by nanoSIMS technique and atom probe. Sulfide Re-Os geochronology and PGE- distribution study were performed by LA-ICP-MS. Moreover, electron back-scattered diffraction imaging was used to reveal deformations in sulfides and hosting olivine.

RESULTS

Inclusions range from 50 to 250 µm in size. The majority (n=31) of sulfide inclusions are rounded isometric or slightly elongated. However, four show negative crystal shape controlled by the enclosing olivine and other three are isometric but with uneven irregular edges. Reflected light optical microscopy revealed complex internal textures. Most of the sulfide inclusions demonstrate three distinct mineral phases: (i) exsolutions of Fe- and Ni-rich MSS in the central part of inclusion; (ii) pentlandite forming rim or flame-like textures protruding into MSS; (iii) chalcopyrite rim. Back- scattered electron imaging revealed small bright particles in the inner and outer parts of some inclusions, which were later distinguished as platinum-group minerals (PGMs) of different composition.

Imaging using nanoSIMS shows variations in PGM morphology, composition and localization: two types of PGMs were recognized. First type comprises relatively osmium-poor and iridium-rich needle-like particles located in central parts of inclusions (further named needles). They are generally oriented along the exsolution structures of MSS. Second type comprises osmium-richer small globules localized in pentlandite-chalcopyrite rims (globules in following). The occurrence of two types of PGMs within a single sulfide inclusion was observed in at least 8 out of 31 studied samples.

Even more intriguing were results of the atom probe study of PGM phases. Both needles and globules from the same inclusion were sampled for the analyses. It was shown that globules contain 60 at% S, 25 at% Ru, 15 at% PGE (Os+Ir), while needles are composed of 60 at% S, 20 at% Ni, 10 at% Fe and 10% PGE (Ir+Pt+Os).

The distribution of PGEs among sulfides of different phases has been studied using LA-ICP-MS technique. The laser spot size does not allow to ablate the PGM bleb solely, so the results are showing not only composition of PGMs, but admixture of noble metals in sulfides. The main difference between MSS core phase and surrounding pentlandite is the content of palladium, which is one order higher in pentlandite than in MSS. This also was confirmed by nanoSIMS imaging.

Sulfur isotopic compositions of pentlandite rims and MSS cores have been studied separately. In general, across all studied inclusions both main mineral phases (pyrrhotite and pentlandite) demonstrate similar range of $\delta^{34}S$ values: from -0.5 to +3.5‰ and from +0.2 to +3.0‰, respectively. However, comparison of $\delta^{34}S$ of pentlandite

and pyrrhotite within a single inclusion reveals a difference of up to 3‰. Such difference could not be explained by isotopic fractionation between sulfide phases crystallized from the same melt. Moreover, wide range of Re-Os model ages calculated for those inclusions (T(RD) from 0.47 to 3.49 Ga) could reflect mixing of the melts/fluids with different isotopic composition.

CONCLUSIONS

Occurrence of two PGM generations and the clear isotopic disequilibrium of the sulfides in the blebs hosted within a single inclusion suggest that these sulfide phases formed at different times and/or different parts of the mantle.

Three main hypotheses were considered for genesis of these inclusions: alteration by transporting melt, enclosed recrystallization or partial melting, and mixing of different melts before trapping by olivine.

Alteration by transporting melt or enclosed recrystallization could explain some of the features, however both these process would affect hosting olivine. Investigations were done especially to find any signatures of olivine recrystallization, melting or stress effect. Neither zoning or change in olivine composition, no subgrain boundaries or significant misorientation of crystallographic axes were found.

The last hypothesis suggests combining of two sulfide phases before getting them into olivine crystal. This may be a result of mixing of two coexisting sulfide liquids, trapping already existed grains of MSS by ISS melt or partial melting of MSS and its reaction with melt/fluid. Interaction of two sulfide liquids (or crystal and melt) corresponds well to the most of data obtained, however more evidences are still needed for clear understanding of the process.

The heterogenity in PGM distribution also makes use of Re-Os in-situ isotopic dating much more questionable than it was considered.

The results of sulfide inclusions study could be transferred to questions of Ni-Cu-PGE deposits genesis. It was shown for many deposits that ore-bearing intrusion might not be the main phase, but the later portion of melt, which was contaminated by other rocks/melts/fluids. In some cases, crustal contamination is reflected in mineralogical, geochemical and isotopic signatures and is the main factor for ore segregation and concentration. Our study shows that mantle processes also could cause differences in mineralogy, geochemistry and ore specification and content.

Thus, the complex nature of these blebs reflects the chemical and isotopic heterogeneity of the lithospheric mantle of the Siberian Craton, which recorded and stored multiple metasomatic events over a long time. Careful study of such tiny sulfides has huge impact on understanding processes in mantle leading to ore deposits formation.

UNUSUAL NI-SULFIDE DEPOSITS IN THE CARAJÁS IOCG MINERAL SYSTEM: MAGMATIC OR HYDROTHERMAL?

María Emilia Schutesky Della Giustina[1], Claudinei Gouveia de Oliveira, Martín Whitehouse, Victor Garcia, Sérgio Huhn

[1]*Universidade de Brasília - emiliadellagiustina.unb@gmail.com*

BACKGROUND

Ni-sulfide deposits are traditionally linked to mafic-ultramafic intrusions and form due to the crystallization of immiscible, metal-rich sulfide liquids. The first phase to crystallize is the MSS (monosulfide solid solution), an iron-rich sulfide that fractionates Ni and part of PGE from the original magmatic liquid. Under lower temperatures, MSS exsolves to form pyrrhotite + pentlandite (± pyrite). Conversely, hydrothermal Ni-sulfides deposits are scarce and constitute deposits of minor economic importance. They are typically composed of lower-temperature mineral assemblages, such as millerite, gersdorffite, heazlewoodite, vaesite, and bravoite. Additionally, Ni can partition into silicate structures and form Ni-rich chlorite and serpentine. Such deposits occur generally as polymetallic mineralizations, hosted by C-rich metasedimentary rocks, or representing proximal, small-scale remobilization from nearby mafic-ultramafic Ni deposits. Given this, we present new textural and sulfur isotopic data from the Ni-Cu-Fe sulfide assemblages on three Ni-rich deposits within the Carajás IOCG Mineral Province to discuss the nature (magmatic or hydrothermal) of these mineralizations.

METHODS

Drill-core samples from three Ni-sulfide deposits in Carajás – GT-34, Castanha, and Jaguar – were systematically described and detailed mineralogical and textural investigations on the sulfide-oxide assemblages were carried out in the University of Brasilia, Brazil.

RESULTS

The three investigated deposits consist of steeply-dipping elongated ore bodies occurring along or near to regional-scale shear zones, spatially associated with IOCG-deposits of the Southern Copper Belt. They present a lens-shaped geometry, and the mineralization occurs mainly as polymictic, matrix-dominated breccias, as well as veins and replacement-type mineralizations hosted by mylonitic intrusive or subvolcanic felsic rocks. The alteration and ore assemblages present textures suggestive of syn-kinematic crystallization.

Each of the three studied deposits shows particular characteristics. The GT-34 occurrence represents the first description of scapolite-orthopyroxene-bearing rocks formed under hydrothermal conditions, which establishes the temperature estimates for the system to more than 700 °C. The paragenetic sequence is similar to the other Carajás IOCG deposits and is marked by progressive alkali-Fe alteration zones. In the Castanha deposit, such alteration sequence is also observed, but carbonate is an abundant phase occurring in the Ni ore. The Jaguar target, conversely, differs due to its F-rich signature; moreover, it is the only Ni-ore deposit located nearby to a mafic-ultramafic intrusion (the Puma layered complex).

In all cases, however, the primary mineralization is characterized by varying proportions of pyrrhotite+ pentlandite+chalcopyrite (1) forming textures identical to that observed in sulfide ores linked to layered intrusions. Pentlandite represents the primary Ni-ore mineral and occurs forming blocky, individual grains or as flame-like exsolutions in pyrrhotite crystals. Pyrite-millerite-chalcopyrite (2) constitute a secondary assemblage; magnetite and sphalerite are associated with this later alteration, when present. Millerite forms due to pentlandite alteration; it can develop as Pn pseudomorphs or occurs anhedral aggregates associated with euhedral pyrite.

CONCLUSIONS

1) Primary ore textures described in the three deposits are similar to orthomagmatic world- wide examples, thus indicating that Ni-sulfide crystallization occurred under higher temperatures, similar to those observed due to MSS crystallization. 2) Combined mineral alteration sequences, deposit geometry, structural control, as well as spatial and temporal association, suggests that the GT-34, Castanha and Jaguar deposits are part of the IOCG Carajás system. 3) In the literature, nickel is considered as an immobile element, but in these examples, it forms small-scale but high-grade secondary ores. Pentlandite is partial to completely altered to millerite but occurs from the deepest parts of the system (GT-34) to shallower levels (Castanha). This demands a particular fluid-rich transport mechanism, which can be partially achieved in vapor (CO_2-PO_4-rich) conditions. 4) The spatial distribution of the Jaguar deposit, near to a mafic- ultramafic intrusion, may indicate a proximal source to Ni-sulfide. However, the

Puma layered intrusion hosts a Ni-lateritic deposit formed due to silicate weathering and voluminous immiscible sulfide melts are not expected. Thus, nickel, as well as other associated metals, might have a mantle-like filiation. 5) Ni-deposits within the Carajás IOCG system may represent the missing link between orthomagmatic and magmatic-hydrothermal deposits.

THE Ni-Cu-PGE-BEARING MANGABAL COMPLEX: AN EXAMPLE OF SULFIDE CONCENTRATION CAUSED BY METAMORPHISM

Cláudia Tharis Augustin[1], Maria Emília Schutesky Della Giustina

[1]*Universidade de Brasilia - clau.augustin@hotmail.com*

Mangabal Complex is composed of two mafic-ultramafic intrusions located on the south of Goiás Magmatic Arc, Brazil. The rocks of the complex are mainly peridotite and norite, but in fewer proportions, gabbronorite and feldspathic peridotite can exist. Despite the preserved textures and some minerals, the complex was affected by a metamorphism that reached amphibolite facies. This metamorphism had an important role for the remobilization and concentration of the sulfide assemblage, composed mainly of pyrrhotite, pentlandite and chalcopyrite.

INTRODUCTION

Mafic-ultramafic intrusions are known for their association with Ni-Cu(±PGE) deposits. This kind of deposits mostly occurs in extensional tectonic settings (Naldrett, 2004), with only a few examples known from compressional settings (e.g., Aguablanca in Spain, Casquet *et al.*, 2001; Intrusions in Tati and Selebi-Phikwe belts, Maier *et al.*, 2008).

The Arenópolis Arc, located on the Brasilia Belt, contains several small- to medium-sized mafic- ultramafic layered intrusions, being potential for Ni-Cu-(PGE) mineralization. The Mangabal Complex, discussed on this work, is part of these several intrusions and is an example that metamorphism can affect the sulfide mineralization of intrusions. The complex has two intrusions, Northern Mangabal and Southern Mangabal.

GEOLOGICAL SETTING

The Complex is located in the center of Brazil. The Brasilia Belt is a well preserved Neoproterozoic orogenic belt (Fuck *et al.*, 2017) and is one of three orogenic belts formed from the collision of three major continental blocks: The Amazonian to the west, the São Francisco/Congo to the east and the Paranapanema to the south (Pimentel *et al.*, 2000). The Brasilia Belt was developed on the western and southern margin of the São Francisco Craton.

The Goiás Magmatic arc is one of the most important tectonic features of the Brasília belt (Fuck *et al.*, 2017). The evolution of the arc was divided into 2 major cycles: a first one in an intraoceanic island arc setting dated at ca. 890–860 Ma (Fuck *et al.*, 2017). The second cycle of magmatic activity was dated 670 and 600 Ma (Fuck *et al.*, 2017) followed by bi-modal intrusions and accompanied by metamorphism and deformation (Laux *et al.*, 2005). The second event is represented by the emplacement of a cluster of mafic-ultramafic syn-tectonic intrusions (> than 10), being the Mangabal Complex composed of two of these intrusions and located in the centre of the São Luis dos Montes Belos Shear Zone.

THE MANGABAL COMPLEX

The Mangabal Complex is an arc-related Ni-Cu-(PGE)-bearing layered mafic-ultramafic complex that includes two intrusions: northern and southern limb. It is located within the São Luis dos Montes Belos Shear Zone. The geological scenario, consequently, implies an heterogeneous metamorphism overprinting, both on the host rocks and in the Mangabal Complex rocks. Despite that, the complex still partially preserves the original igneous texture and mineralogy.

The northern and the southern limbs are similar and hold the same mineral and textural features. Massive to layered coarse- to medium-grained norite prevaisl in the Mangabal Complex, but dunite and harzburgite also occur on basal portions of the intrusions. The basal ultramafic rocks are predominantly orthocumulates, whereas the mafic rocks are adcumulates or mesocumulates. Commonly, mafic and ultramafic rocks show partially or well-preserved igneous textures with primary olivine, spinel, pyroxene and plagioclase.

Metamorphic assemblages partially replace primary igneous minerals of the Complex. This metamorphic alteration is heterogeneous and characterized by extensive hydration that locally preserves primary textures. However, the transition between igneous phases and metamorphic minerals is documented in different scales and intensity throughout the complex.

The most predominant metamorphic rock of the complex is medium-grained, foliated to non-foliated, pegmatoidal amphibolite that consists of magnesium-hornblende, plagioclase and biotite as the main mineralogy. The proportion of each mineral varies along the complex, but amphibole is always more abundant than plagioclase and biotite. The main texture of the rocks ranges from diablastic to nematoblastic. Quartz, rutile, titanite, apatite and orthoamphibole are common accessory minerals. An important accessory mineral of the amphibolite is kyanite that appears in equilibrium with magnesium-hornblende and plagioclase, indicating that the complex reached a high pressure amphibolite facies.

SULFIDES

The mineralization of Mangabal Complex is here divided into two main groups: igneous and metamorphic alteration. The highest contents of Ni, Cu, Pd and Pt contents are associated with the mafic rocks, and in minor quantity with ultramafic rocks. These highest contents of these metals have a positive correlation with modal sulfides. The principal ore minerals in Mangabal Complex of all rocks are pyrrhotite, pentlandite, pyrite and chalcopyrite. Native silver and nickel-tellurides (±PGE-bearing) are accessory minerals in metamorphic rocks.

The sulfides occur in disseminated, net-textured and massive textures. Disseminated sulfides are mainly present in preserved igneous rocks and in metamorphic rocks where the igneous texture is completely preserved. Massive texture, net-textured and disseminated sulfides are associated with metamorphic assemblages.

On preserved norite and their texture-preserved metamorphic equivalents, the sulfides are disseminated and occur as an interstitial phase among the silicates (mainly plagioclase and bronzite). Pyrrhotite, pentlandite and chalcopyrite are the main sulfides. Hornblendite and other metamorphic rocks evidence a remobilization of the sulfides that show on these rocks massive and net-textured textures. When the hydrous conditions affect the rock, major aggregates of sulfides among recrystallized silicates are observed other than those of directly igneous rocks, as can see in figure 1.

Massive to net-textured textures were only found in a relation with metamorphic assemblages, for example hornblende and garnet (Fig. 2A-B). In these sulfide portions, it is possible to notice porphyroblasts of euhedral pyrite (Fig. 2C), not found in igneous portions.

DISCUSSION

Major Ni-Cu-PGE mineralization is located in the ultramafic rocks and in the basal portion of the mafic rocks. The rocks have textures which exhibit intercumulus disseminated sulfides in igneous and metamorphic rocks and layers of massive sulfide grading to net-textured on shear-zones in rocks under metamorphic conditions.

The igneous composition of the rocks and the presence of the sulfides can indicate that they were formed after the segregation and accumulation of immiscible sulfide liquid from mafic or ultramafic magmas, as a common process described by Naldrett (1997). The presence of the sulfides is common in this kind of rocks. At the Mangabal Complex, the magmatic process was important to indicate the presence of the mineralization, but the metamorphism and deformation overprinted on the complex were important for the remobilization and concentration of sulfides.

REFERENCES

Casquet, C., Galindo, C., Tornos, F., Velasco, F., Canales, A., 2001. The Aguablanca Cu–Ni ore deposit (Extremadura, Spain), a case of synorogenic orthomagmatic mineralization: age and isotope composition of magmas (Sr, Nd) and ore (S). Ore Geology Reviews 18: 237–250.

Fuck R.A., Pimentel M.M., Alvarenga C.J.S., Dantas E.L. 2017. The Northern Brasília Belt. In: Heilbron M., Cordani U., Al kmim F. (eds) São Francisco Craton, Eastern Brazil. Regional Geology Reviews. Springer, Cham.

Laux, J.H., Pimentel, M.M., Dantas, E.L., Armstrong, R., Junges, S.L.. 2005. Two Neoproterozoic crustal accretion events in the Brasília belt, central Brazil. J. South Am. Earth Sci. 18: 183–198.

Maier, W.D., Barnes, SJ., Chinyepi, G. 2008. The composition of magmatic Ni–Cu–(PGE) sulfide deposits in the Tati and Selebi-Phikwe belts of eastern Botswana. Miner. Deposita 43: 373.

Naldrett, A.J. 1997. Key factors in the genesis of Noril'sk, Sudbury, Jinchuan, Voisey's Bay, and other world-class Ni–CuPGE deposits: implications for exploration. Aust J Earth Sci 44: 283–315

Pimentel, M.M., Fuck, R.A., Jost, H., Ferreira Filho, C.F., Araújo, S.M. 2000. The basement of theBrasília Fold Belt and the Goiás Magmatic Arc. Tecton. Evol. South Am. 195–229.

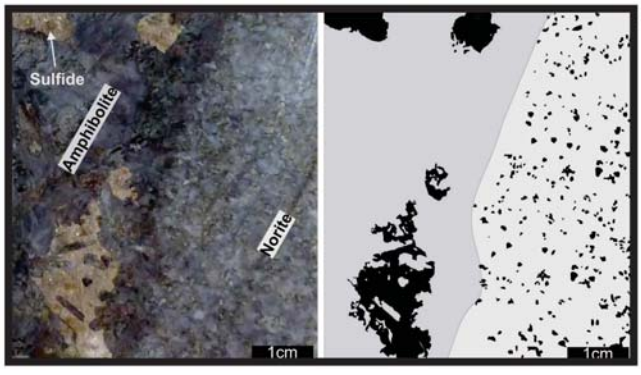

Figure 01

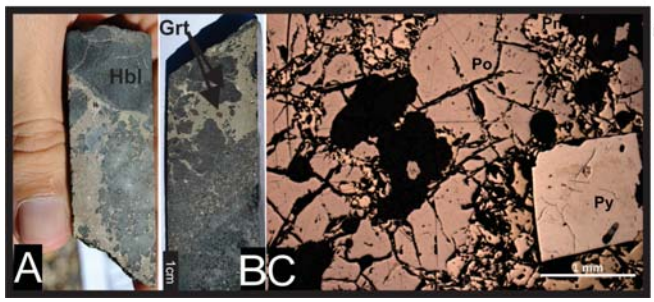

Figure 02

CHROMIUM EXPLORATION TARGETED FOR BOPHI VUM AREA, NORTHWESTERN MYANMAR

Chulho Heo

Korea Institute of Geoscience and Mineral Resources - chheo@kigam.re.kr

In order to grasp the geological characteristics, the occurrence mode of ore body and development potential of Bophi Vum chromium mineralized zone in northwestern Myanmar, Korea Institute of Geoscience and Mineral Resources (KIGAM) and Department of Geological Survey and Mineral Exploration (DGSE) carried out joint exploration from 2013 to 2016. Joint study area is composed of harzburgite, serpentinite and dunite, those are covered by Quaternary alluvium. Chromite ore bodies are developed within dunite and harzburgite bodies, mainly within dunite bodies. Chromite ores are mainly distributed at the elevation range between 200 and 400 m. And, in order to designate the anomaly of Cr and Ni in target area, the geochemical survey using PXRF with ICP-AES was conducted. In this study we measured major element composition of spinels in harzburgite, dunite and chromitite, and examined the hypothesis that spinel Cr can be used as a geochemical indicator in exploration for the Bophi Vum chromitite. The results show that there is a clear correlation between spinel Cr# and distribution of chromitite. The spinel Cr of harzburgite increases with decreasing the distance from the chromitite bodies. The spinel composition is also closely associated with texture and occurrence of spinels. These petrological and geochemical results suggest that the high Cr# spinels have resulted from mantle-melt interaction. To identify the extension of the chromite ore bodies, trench survey were carried out in 5 different sites. Chromite ore bodies have 0.3-1.5 m wide, and several meters of extension, and deformed strongly as a sigmoid and a boudin shapes with dunite and harzburgite bodies by ductile deformation. Ductile deformation have a top-to-the-west shear sense, indicating the existence of a westward thrusting. The NW-SE trending distribution of ore bodies is related to the dextral ductile shearing and/or to the block rotation as a book- shelf structure by dextral strike-slip movement. And, to analyze the distribution of chromite, magnetic survey was also carried out. As a result, the magnetic susceptibility of chromite was lower than those of dunite and harzburgite. Also, the locations of low magnetic anomaly zone and low magnetic susceptibility models of 3D magnetic inversion result are spatially well matched with those of chromite occurrences confirmed by the surface geological survey and trench survey. Some of low magnetic effects are expanded to the periphery area of chromite occurrences. Considering the magnetic susceptibility characteristics of various rocks in this area, the expanded low magnetic anomaly zones are estimated as the high potential areas bearing chromite. These results will be helpful to construct 3D model to predict the hidden ore body in the future.

CHAPTER 12
MAGMATIC-HYDROTHERMAL SYSTEMS AND THE FORMATION OF ORE DEPOSITS

Conveners: Fernando Tornos, David Lentz

THE ANATOMY OF A MODERN SUBMARINE ARC VOLCANO: MAGMATIC-HYDROTHERMAL ACTIVITY AND THE TRANSPORT OF METALS

Cornel E. J. de Ronde

GNS Science, 1 Fairway Drive, Avalon, Lower Hutt 5010, New Zealand - Cornel.deronde@gns.cri.nz

Brothers volcano is a caldera volcano that lies ~400 km NE of the North Island of New Zealand, and is one of ~32 distinct volcanic centers that mark the active arc front of the Kermadec arc. It forms an elongate edifice 13 km long by 8 km across that strikes NW-SE. The volcano has a caldera with a basal diameter of ~3 km and a floor at 1,850 m below sea level, surrounded by 290 to 530 m high walls (de Ronde *et al.*, 2005). Lavas recovered from the NE caldera walls are predominantly dacitic in composition, as is the volcanic cone that rises 350 m from the caldera floor and partially coalesces with the southern caldera wall.

Plume mapping surveys, followed by manned submersible, AUV (autonomous underwater vehicle) and ROV (remotely operated vehicle) surveys, have delineated five active vent sites and one inactive site, namely; Upper Caldera, NW Caldera, West Caldera, Upper Cone and Lower Cone that are all active, and the SE Caldera site that is inactive. The NW Caldera site is the largest of all the active sites; its boundaries were distinguished by a high-resolution, near seafloor (~70 m altitude) AUV survey of water column measurements (Baker *et al.*, 2012) and seafloor magnetics (Caratori Tontini *et al.*, 2012) that defined a magnetic 'low' traversing up to 1300 m of the caldera walls in a SW-NE direction, and ~300 m in elevation, between the caldera rim (~1450 m) and base of the caldera walls (~1750 m). Subsequent ROV surveys in January 2017 and March 2018 show that the NW Caldera vent field is connected to the recently discovered active vent field of the Upper Caldera, itself perched on caldera walls above the caldera rim that separates this field from that of the NW Caldera.

The NW Caldera and Upper Caldera vent fields are both host to numerous black smoker chimneys, both active and inactive, that reach heights of ~12-14 and 20 m, respectively. Maximum temperatures recorded for hydrothermal fluid discharging from the chimneys is 320 °C from the NW Caldera vent field (Humphris *et al.*, 2018) and 311 °C from the Upper Caldera vent field (Koschinsky *et al.*, 2017). Abundant sulfide talus, partially buried massive sulfides and hydrothermally altered volcanic rocks are also seen amongst the chimneys; ^{226}Ra/Ba dating of the active chimneys indicates ages up to 40 years (from time of sampling) and 1,200 years for inactive chimneys and other mineralization (de Ronde *et al.*, 2005; 2011). Two main types of chimney predominate: Cu-rich (up to 28.5 wt.% Cu; including up to 91 ppm Au) and more commonly, Zn-rich (up to 43.8 wt.% Zn). An anastomosing array of stockwork veins were seen to lie immediately beneath some inactive chimneys at the NW Caldera vent field, where exposed by faulting (Koschinsky *et al.*, 2017). These veins are dominated by massive pyrite with lesser chalcopyrite and are hosted by intensely altered volcanics.

Over both NW Caldera, SE Caldera and Cone sites, the alteration minerals identified include silicates, silica polymorphs, sulfates, sulfides, Fe and Mn oxide/oxyhydroxides and native sulfur, which are consistent with precipitation at a range of temperatures from fluids of different compositions. The NW Caldera and Upper Caldera vent sites are parts of a long- term hydrothermal system that is today dominated by evolved seawater, but which has witnessed episodic injections of magmatic fluid.

An advanced argillic assemblage of illite + amorphous silica + natroalunite + pyrite + native S at the Cone site, the occurrence of chalcocite + covellite + bornite + iss + chalcopyrite + pyrite in sulfide samples from the SE Caldera site, and veins of enargite in a rhyodacitic sample from the NW caldera site (de Ronde *et al.*, 2005) are indicative of high sulfidation conditions similar to those of subaerial magmatic-hydrothermal systems. Drilling of both NW Caldera and Cone sites by IODP in May-June 2018 will elucidate the sub- seafloor distribution of base and precious metals and metalloids, and the reactions that have taken place along pathways to the seafloor. Drilling will also characterize any sub-volcano, magma chamber-derived volatile phase to test model-based predictions that there is either a single-phase gas, or two-phase brine-vapor beneath the Cone site (de Ronde *et al.* 2017).

REFERENCES

Baker, E.T., Walker, S.L., Embley, R.W., de Ronde, C.E.J., 2012. High-resolution hydrothermal mapping of Brothers caldera, Kermadec arc. Economic Geology 107, 1583-1593.

Caratori Tontini, F., Davy, B., de Ronde, C.E.J., Embley, R.W., Leybourne, M.I. and Tivey, M.A., 2012. Crustal magnetization of Brothers volcano, New Zealand, measured by autonomous underwater vehicles: geophysical expression of a submarine hydrothermal system. Economic Geology 107, 1571-1581.

de Ronde, C.E.J., Hannington, M.D., Stoffers, P., Wright, I.C., Ditchburn, R.G., Reyes, A.G., Baker, E.T., Massoth, G.J., Lupton, J.E., Walker, S.L., Greene, R.R., Soong, C.W.R., Ishibashi, J., Lebon, G.T., Bray, C.J. and Resing, J.A., 2005. Evolution of a submarine magmatic- hydrothermal system: Brothers volcano, southern Kermadec arc, New Zealand. Economic Geology 100, 1097-1133.

de Ronde, C.E.J., Massoth, G.J., Butterfield, D.A., Christenson, B.W., Ishibashi, J., Ditchburn, R.G., Hannington, M.D., Brathwaite, R.L., Lupton, J.E., Kamenetsky, V.S., Graham, I.J., Zellmer, G.F., Dziak, R.P., Embley, R.W., Dekov, V.M., Munnik, F., Lahr, J., Evans, L.J. and Takai, K., 2011. Submarine hydrothermal activity and gold-rich mineralization at Brothers volcano, Kermadec arc, New Zealand. Mineralium Deposita 46, 541-584. DOI 10.1007/s00126-011-0345-8.

de Ronde, C.E.J., Humphris, S.E. and Höfig, T.W., 2017. Expedition 376 Scientific Prospectus: Brothers Arc Flux. International Ocean Discovery Program. https://doi.org/10.14379/iodp.sp.376.2017.

Humphris, S., Reysenbach, A. L., Tivey, M., de Ronde, C. and Caratori Tontini, F., 2018. Brothers volcano, R/V Thomas Thompson, ROV Jason II cruise, March 6- 26, 2018, TN 350 Cruise Report, 32 pp.

Koschinsky, A., Shipboard Scientific Party, 2017. $SO_2$53-HYDROTHERMADEC, Noumea-Auckland 22 December 2016 to 21 January 2017, R/V Sonne 253 Cruise Report, 183 pp.

APATITE (U-Th)/HE THERMOCHRONOLOGY IN THE CENTRAL ANDES (31°30'S), MAIN CORDILLERA SAN JUAN, ARGENTINA: IMPLICATIONS FOR PORPHYRY TYPE Cu (Au) MINERALIZATION

Laura Maydagán[1], Massimiliano Zattin, Marta Franchini

[1]*CONICET - lauramaydagan@yahoo.com.ar*

BACKGROUND

The study region (31°30' S, 70° 15' W) is located in the southwestern sector of San Juan Province (Argentina), in the southern portion of the Pampean flat-slab segment and northeast end of the la Ramada fold and thrust belt of the Andes Main Cordillera. This region is a continuation of the Miocene and Pliocene porphyry copper belt of Chile that hosts three of the largest copper deposits in the world (El Teniente, Río Blanco - Los Bronces and Los Pelambres). Numerous Cu (Au) prospects with high mining potential have been discovered in this area. Some of them show the overlap between porphyry-type and high sulfidation epithermal deposits, indicating a high degree of uplift during their formation.

The Altar deposit is a large porphyry Cu (Au-Mo) with associated high sulfidation epithermal veins (measured resources of 995 Mt @ 0.35% Cu and 0.083 g/t Au, Maydagán *et al.*, 2014). The basement of the area is characterized by a late Carboniferous tonalitic batholith (~ 297 Ma, U-Pb, Maydagán, 2012) that crops out to the east of the Altar district. Cretaceous volcanic rocks outcrop to the west, in the Chile-Argentina border, between the Pantanosa Fault to the east and Tres Quebradas Fault to the west (Bergoeing, 2016).

Early Miocene volcanic rocks that crop out in the study area (Lower Volcanic Complex, Maydagán *et al.*, 2011) were intruded by porphyritic stocks of andesitic-dacitic composition in the middle to late Miocene (Maydagán *et al.*, 2011, 2014) that contains most of the Cu-Au mineralization.

Igneous rocks of Altar region were grouped in the lower Miocene early volcanic complex (21.6 ± 1.2 Ma to 20.8 ± 0.3 Ma, U-Pb zircon, Maydagán *et al.*, 2014), that consist of an intercalation of basaltic andesite and porphyritic andesite-dacite lavas, levels of andesitic- dacitic lapilli tuff, and pyroclastic breccia that grade upwards to an upper unit of compacted and thick rhyolitic tuff, and the upper subvolcanic suite of middle-late Miocene age (11.75 ± 0.24 Ma, 8.9 ± 0.4 Ma, U-Pb zircon, Maydagán *et al.*, 2014) that consists of a series of porphyritic intrusions, dykes, and magmatic-hydrothermal breccias.

LA-ICPMS U-Pb zircon ages from the Altar porphyries indicate four discrete events of intrusions over an extended magmatic life time of ca. 3 m.y. It comprises a pre- mineralization porphyry (11.75 ±0.24 Ma), three mineralized porphyries (11.62 ± 0.21 and 11.68 ± 0.27 Ma, 11.13 ± 0.26 Ma, 10.35 ± 0.32 Ma) related to hydrothermal breccias, two post-mineralization intrusions, and a post-mineralization breccia (8.9 ± 0.4 Ma, Maydagán *et al.*, 2011, 2014).

In this study we present new apatite (U-Th)/He data (AHe) in order to quantify the extent of tectonic-related exhumation in the Andes Main Cordillera in Argentina and compare the results with the exhumation patterns from the Coastal, Frontal and Main Cordilleras at similar latitudes in Chile. The aim of our research is to identify possible pulses of tectonic exhumation in the region given their importance to emplacement of subvolcanic intrusions related to Cu (Au) mineralization.

METHODS

We present preliminary U-Th/He ages of apatite from 7 igneous rock samples obtained in the Altar region. The preparation of the samples for U-Th/He analysis of apatites was done in the laboratory of the University of Padova (Italy) and the U-Th/He ages were obtained in the University of Arizona, Tucson (USA). Three apatite crystals (euhedral shape, width greater than 90 Mm and without inclusions) were selected per sample. The ages that are presented correspond to the average of apatite crystals analyzed in each sample.

RESULTS

AHe ages present a broad distribution ranging from 9.96 to 56.83 Ma, but the majority of them show middle Miocene ages. Two samples from the tonalitic batholith of Late Carboniferous age (~ 297 Ma dating U-Pb in zircons, Maydagán, 2012) showed AHe ages of 14.3 and 11.87 Ma. AHe ages from the subvolcanic stocks from the middle to late Miocene showed ages between 13.45 and 11.17 Ma.

CONCLUSIONS

The U-Th/He ages ranging between 14.3 and 11.17 Ma obtained for the late Carboniferous tonalite and for the subvolcanic stocks indicate an exhumation pulse of the region during the middle Miocene. This lapse of time

partially overlaps with the period of emplacement of the subvolcanic porphyries in the Altar deposit, which have U-Pb crystallization ages between 12.0-10.3 Ma (Maydagán *et al.*, 2011, 2014). Therefore, thermochronological data indicate that the intrusion of subvolcanic bodies in the study region coincide with the final stage of the regional exhumation event.

In the study area, Triassic and Jurassic sedimentary rocks are tectonically overlain by the late Carboniferous tonalite along the E-vergent Mondaquita reverse fault (Perelló *et al.*, 2012). U-Th/He ages obtained in the tonalite could be therefore related to vertical displacements associated to the Mondaquita Fault. To the west, the Pachón Fault brings the Miocene sequence (early volcanic rocks and middle-late Miocene subvolcanic stocks) on the late Carboniferous tonalite. As the AHe ages obtained from both sides of the Pachon Fault are similar we can hypothesize that the entire area (irrespective of the Pachon Fault) was exhuming between 14 and 11 Ma.

The overlap of U-Pb and AHe ages recognized in the samples of the middle Miocene porphyritic intrusions analyzed (Altar North and Altar East) suggests that these AHe ages are related not to exhumation, but rather to igneous cooling and, thus, that the intrusion depth of these porphyritic stocks was shallow, probably in the upper ~2-3 km.

In the Frontal Cordillera of Chile, to the west, Rodríguez Montecinos (2013) obtained fission-track ages significantly older than AHe ages in Late Cretaceous, Paleocene, and Eocene intrusions, therefore demonstrating that these magmatic bodies were intruded at deeper levels. However, the AHe ages obtained by these authors are Miocene (18.1-6.9 Ma) reflecting a similar time of exhumation in the Frontal Cordillera of Chile and the study area.

The period of exhumation reflected by AHe ages also coincide with the collision and passage of the Juan Fernández Ridge below the flat-slab segment at these latitudes. The new data confirm a temporal connection between ridge arrival, exhumation, and porphyry copper formation in the study region.

REFERENCES

Bergoeing, J.P., 2016. Evolución geoquímica del magmatismo de la región de los Pelambres (31°S). Unpublished Ph.D. thesis, Universidad de Chile, 137 p.

Maydagán, L., Franchini, M., Chiaradia, M., Pons, J., Impiccini, A., Toohey, J., Rey, R., 2011. Petrology of the Miocene igneous rocks in the Altar Region, Main Cordillera of San Juan, Argentina: a geodynamic model within the context of the Andean flat-slab segment and metallogenesis. Journal of South American Earth Sciences, 32, 30–48.

Maydagán, L., 2012. El Prospecto de Cu-(Au-Mo) Altar (31°292 LS, 70°282 LO). Unpublished Ph.D thesis, Universidad Nacional del Sur, Argentina, 340 p.

Maydagán, L., Franchini, M., Chiaradia, M., Dilles, J., Rey, R., 2014. The Altar porphyry Cu- (Au-Mo) deposit (Argentina): a complex magmatic-hydrothermal system with evidence of recharge processes. Economic Geology, 109 (3), 621-641.

Perelló, J., Sillitoe, R.H., Mpodozis,C., Brockway, H., Posso, H., 2012. Geologic setting and evolution of the porphyry copper-molybdenum and copper-gold deposits at Los Pelambres, central Chile. Society of Economic Geologists, Special Publications, 19, 79-104.

Rodríguez Montecinos, M.P., 2013. Cenozoic uplift and exhumation above the southern part of the flat slab subduction segment of Chile (28.5-32°S). Unpublished Ph.D thesis, Universidad de Chile, 220 p.

GOLD IN PORPHYRY GOLD SYSTEMS: DISTRIBUTION AND COMPOSITION OF GOLD AT THE BIELY VRCH DEPOSIT, SLOVAKIA

Peter Kodera[1], Jaroslav Kozák, Jana Brèeková, Martín Chovan, Jaroslav Lexa, Michal Jánošík, Adrián Biroò, Peter Uhlík, František Bakos

[1]*Department of Economic Geology, Faculty of Natural Sciences, Comenius University in Bratislava, Slovakia*

peter.kodera@gmail.com

INTRODUCTION

Porphyry gold deposits represent a distinct type of porphyry gold ore, known from only a few global ore provinces. Despite their increasing importance, little is known about factors governing the gold distribution and chemistry. The Biely Vrch deposit in the Western Carpathians belongs to the shallow, sulfide-poor porphyry gold deposit type. This contribution documents the diversity of gold assemblages at Biely Vrch as a potential aid to the exploration and mining of porphyry gold deposits elsewhere.

BIELY VRCH DEPOSIT

This deposit is hosted by the Javorie stratovolcano in the NE part of the Central Slovakia Volcanic Field. It is centered on a diorite porphyry stock, emplaced into pre-mineralization andesite. Paleovolcanic reconstruction indicates that the top of the porphyry intrusion attained a depth of ~500 m below the paleosurface (Kodìra *et al.*, 2014). Hydrothermal alteration includes early, high-temperature K-silicate and Ca-Na-silicate alteration types, with the latter present only in deeper parts of the deposit (>500 m). Intermediate argillic alteration occurs mostly in the upper parts of the deposit. The central part of the deposit (from surface to 400 m) is affected by advanced argillic alteration, which is the youngest alteration type.

Quartz veinlets are the dominant type of veining, forming an intense stockwork from surface to >750 m depth. The quartz stockwork coincides with the Au mineralization, which has an exceptionally low Cu/Au ratio (0.018 wt% Cu/ppm Au). Fluid inclusion data in quartz veinlets showed that the high-temperature alteration and gold mineralization formed from nearly anhydrous Fe-K-Na-Cl salt melt, coexisting with hydrous vapor of very low density (Kodìra *et al.*, 2014). Based on LA-ICPMS microanalytical data, the salt melt inclusions contain up to ~10 ppm Au, whereas the concentration of Cu is only ~100x higher. The low sulphur fugacity, resulting from fluid expansion, suppressed the precipitation of sulfides, which explains the gold-only style of this deposit.

METHODS

Distribution of gold, copper, sulphur and intensity of quartz veinlets were modelled using drill hole data provided by EMED Mining Plc. and the LeapfrogGeo software (52 holes, assayed for 37 elements at 1 or 2 m intervals). Identification and chemical composition of gold and associated alteration minerals are based on WDS, EDS, and XRD analyses. SEM-CL imaging was used in combination with precise electron microprobe analyses of Ti for the application of the TitaniQ geothermometer.

DISTRIBUTION OF GOLD, COPPER, SULPHUR, AND QUARTZ VEINLETS

According to 3-D geochemical models, gold grades are elevated in the centre of the system (>0.5 ppm Au) and continue from surface to a depth of >700 m. Increased copper concentrations (>150 ppm Cu) are limited to intermediate depths in the central part of the system. The highest intensity of quartz veining is present in the central part of the system and continues from surface to depth. Elevated sulphur contents (>0.5 wt% S) are limited to the upper marginal part of the deposit and fade out below ~400 m depth.

In the deepest part of the system (below 600 m), gold grades correlate with potassium content and quartz veinlet intensity, while in zones of maximum veining and K content, they reach >1 ppm Au. In higher levels of the deposit, gold concentrations become more scattered and the close correlation with K-silicate alteration and quartz veining is lost.

MINERAL ASSEMBLAGES WITH GOLD

Most of the gold is present near quartz veinlets in various alteration minerals representing different alteration types. Typically, the gold grains have anhedral shapes and small sizes (~2 - 5 µm, locally up to 60 µm), but a significant proportion of gold is submicroscopic (<2 Mm), as observed in detailed SEM images and X-ray maps. Based on the

minerals hosting the gold grains, three types of mineral assemblages were defined. K- and Ca-Na silicate gold assemblage occurs in deepest parts of the system, where gold grains usually occur in hydrothermal plagioclase, K-feldspar, magnetite or in infill of quartz veins. Locally, gold is attached to ferro-actinolite or clinopyroxene. The intermediate argillic gold assemblage is the most widespread, with gold hosted mostly by chlorite, illite-smectite, illite and quartz. Gold is also intergrown with sulphides and Fe-Ti oxides. In the advanced argillic gold assemblage gold is hosted by kaolinite, uncommonly by pyrophyllite.

CHEMISTRY OF NATIVE GOLD

The highest gold fineness is for samples displaying advanced argillic alteration (mean value 994), whereas the lowest (mean value 914) is for samples hosted by K-silicate alteration. However, samples affected by Ca-Na silicate alteration contain significantly higher fineness gold. In the intermediate argillic gold assemblage, the fineness is mostly variable (875-990), probably inherited from the former gold mineral assemblages. Samples with exceptionally high grades come from roots of the advanced argillic zone that penetrate downward to the boundary between the K- and Ca-Na silicate alteration zones.

DISCUSSION

The limited spatial correlation between Au and Cu probably results from primary introduction of gold by salt melt and Cu by low-density vapor, as indicated by fluid inclusion LA ICPMS data (Kodìra *et al.*, 2014). Most of the gold was transported as chloride complexes and the observed decrease in fineness in direction to surface is probably related to cooling of ascending fluids in the absence of silver-bearing minerals.

The low Ti content (<8 ppm) of the vein quartz, associated with or hosting the gold, indicates that the temperature of gold precipitation was <380 °C. However, due to low- pressures, quartz exhibits retrograde solubility during isobaric cooling (Fournier, 1985), which can explain the predominance of gold in altered rock rather than vein quartz. The lower temperature limit for gold precipitation can be deduced from final solidification of salt melts at eutectic temperatures in the $FeCl_2$-KCl-NaCl salt system, which occurs at 330 or 309 °C and corresponds to first melting of salt melt inclusions at Biely Vrch (Kodìra *et al.*, 2014).

Gold hosted by advanced argillic alteration has probably experienced at least partial dissolution and reprecipitation due to elevated gold solubility in low-pH hydrothermal fluids, as indicated by increasing fineness with increasing intensity of this alteration. Gold hosted in intermediate argillic minerals has probably just experienced replacement of the former high-temperature host minerals by intermediate argillic minerals, because in near-neutral pH fluids Au solubility is at minimum.

CONCLUSIONS

The origin and fate of gold at the Biely Vrch deposit is predominantly controlled by the unusually shallow setting of the porphyry system, resulting in two contrasting types of fluids. Primary precipitation of gold occurred during ascent and cooling of salt melts at 450° to 309 °C, mostly during retrograde quartz solubility, with higher fineness associated with deeper, probably higher temperature fluids forming K- and Ca-Na silicate alteration. Appreciable gold was later affected by remobilization in the clay mineral stability fields, which resulted in its irregular distribution and enrichment in upper parts of the deposit. The extremely high fineness results from gold remobilization by fluids, responsible for the advanced argillic alteration.

Support by grants APVV-15-0083, 0537-10 and VEGA-1/0560/15 is acknowledged.

REFERENCES

Fournier, R.O., 1985. The behavior of silica in hydrothermal solutions, in: Berger, B.R., Bethke, P.M. (Eds.), Geology and Geochemistry of Epithermal Systems. Reviews in Economic Geology, 2, pp. 45–61.

Kodìra, P., Heinrich, C.A., Wδlle, M., Lexa, J., 2014. Magmatic salt melt and vapor: Extreme fluids forming porphyry gold deposits in shallow volcanic settings. Geology, 42, 495-498.

SEEKING THE MANTLE AS A SOURCE FOR PRECIOUS METALS IN MAGMATIC-HYDROTHERMAL DEPOSITS

José María González-Jiménez

Departamento de Mineralogía y Petrología,Universidad de Granada, Facultad de Ciencias, Fuentnueva s/n 18002, Granada, España - jmgonzj@ugr.es

INTRODUCTION

The potential endowment of precious metal (Au, Ag, platinum-group elements (PGE): Os, Ir, Ru, Rh, Pt, Pd and Re) in subduction zones (SZ) is enormous, with a large proportion of their resources confined in a variety of ore deposits hosted in either oceanic or continental crust, clustered in either provinces or metallogenic belts. In subduction zone settings, several types of ore deposits enriched in precious metals, with a wide range of sizes, usually develop in different restricted epochs. It is currently debated whether a given metal deposits has a unique mode of formation, or it represent a case within a spectrum of mineralization style, formed by an optimum convergence of common geological processes. The traditional notion of metal endowment in a given metallogenic province is that metal accumulated by highly efficient magmatic-hydrothermal enrichment processes operating in a chemically "average" crust. However, many recent frontline studies suggest that metal endowment requires the possible existence of anomalously enriched sources and/or magmas. It is now under debate whether these metal-rich reservoirs exist in the mantle, the mantle-crust transition or the crust. In this scenario, our research efforts must be tailored to determine the fundamental factors that control precious metal transfer from a deep mantle or lower crustal source to the shallow crust where the ore deposits accessible to mining are found. In this communication I will provide key evidence about how noble metals are transferred from the subducting slab to the sub-arc mantle and lower continental crust where metal-rich magmas parental of magmatic-hydrothermal deposits are formed.

TRANSFER OF METALS FROM SUBDUCTING SLAB TO MANTLE WEDGES

During subduction, drifting associated with corner flow may produce downwards movement of the sub-arc peridotitic rocks, while large volumes of fluid can be released by dehydration of the subducting oceanic crust. The main dewatering takes place at temperatures between 300 and 600 °C and pressures lower than 15 kbar. The upward percolation of these fluids may induce hydration of the overlying peridotite wedge beneath the crust of continental or oceanic arcs. Hydration reaction may produce the partial or total transformation of the peridotite to serpentinites, which act as sponges for a wide suite of elements such as semimetals (As, Sb, Se), and base (Fe, Zn, Cu) and precious metals (Au, Pd, Pt). The anomalously high contents of these suite of elements are directly associated with the formation of Ni-As-Sb-S rich minerals, including sulfides, arsenides and sulfarsenides. Particular enrichment of these minerals is observed in serpentinite shear zones that act as a preferential pathway for fluid movement. In some subduction channel serpentinites high contents of precious metals are also related with the Ni-As-Sb mineralization. A direct window to these processes are mantle wedge serpentinites that have been exhumed through subduction channels now preserved in the accretionary prism of some active subduction zones from the Andean subduction zone.

METAL-RICH RESERVOIRS IN THE MANTLE AND MANTLE-CRUST TRANSITION

Continued movement downward of the already hydrated sub-arc lithosphere promotes burial of these serpentinites while they are progressively heated (i.e., prograde metamorphism). As result minerals carrying the metals are destabilized while liberating metal-leaden fluids that may infiltrate deeper regions of the sub-arc mantle. The infiltration of these metal-rich fluids through specific regions of the sub-arc mantle may produce metal- fertile domains, which may be the source region for the generation of metal-rich magmas. The analyses of xenolith that have sampled these regions of the mantle underlying ore- productive crust confirm this hypothesis. Thus, significantly high concentrations of gold and other metals have been detected in both whole-rock and base-metal sulfides in ultramafic xenoliths that have sampled these regions of sub-arc mantle infiltrated by dehydration- related fluids. Additionally metal-rich melts topping the upper mantle may accumulate at the mantle-crust transition zone or lower crust of the magmatic arcs, giving rise to mafic cumulate rich in base-metal sulphides. These may also act as a source of metal-rich magmas. In this communication I will provide good examples of these processes in the continental margins of the North American Cordillera, the Andes and North China, as well as from the island arc of Papua New Guinea. The example of the Deseado Massif where o metal-refertilization of the upper mantle was related to plume-melts, and the later generation of metal-rich melts parental to Au-Ag deposits to partial melting triggered by subduction-related fluids is also presented in this communication.

A | 117

TRACE ELEMENT DEPORTMENT ACROSS PORPHYRY DIKE GENERATIONS IN THE BINGHAM CANYON PORPHYRY Cu-Mo-Au DEPOSIT

Maurice Brodbeck[1], P. Redmond, B. S. Kamber, S. McClenaghan

[1]*Department of Geology, Museum Building, Trinity College Dublin, Dublin 2, Ireland - brodbecm@tcd.ie*

INTRODUCTION

For fertile porphyry systems with large metal endowments, major commodities such as Cu, Mo, Au, Ag are well constrained, however the distribution of energy critical elements (ECE's) are poorly understood. These can potentially be recovered as by-products and thus add value to the primary commodities. Approximately 90% of the total Te currently produced worldwide, for example, is recovered from anode slimes during the Cu refining process (Schuyler Anderson, 2016). However, the mineralogy and substitution mechanisms responsible for the deportation of trace ECE's in Cu ores is not fully understood and may limit their effective recovery. Furthermore, there is insufficient knowledge on the mineral scale distribution of deleterious elements (e.g., Se, As, Cd) that may result in refining penalties and represent an environmental hazard. For best recovery, ore that is extracted from a part of a deposit yielding high trace metal potential should not accidentally be diluted with ore of a lesser content. Characterization of sulphide phases in terms of trace metal signatures (penalty vs. credit) may add value to ore resources, improve recovery, and help mitigate environmental effects of metal dispersion in the environment.

Historical Bingham Canyon Cu-Mo-Au samples, collected from the northwestern side of the deposit (Redmond and Einaudi, 2010), have been characterised for their ECE endowment and potential use as a discriminator of hydrothermal processes. In this section, the volumetrically largest porphyry intrusion at Bingham, quartz-monzonite porphyry (QMP), is hosting most of the high-grade copper-gold ore with grades in excess of 1.0% Cu and 1.0 g/t Au. The Bingham stock comprises equigranular monzonite and a series of mineralization-related porphyry dikes. At least five distinct crosscutting porphyry phases have been recognised at Bingham (Stringham, 1953; Bray, 1969; Moore, 1970; Moore and Czamanske, 1973; Lanier *et al.*, 1978; Babcock *et al.*, 1995; Phillips *et al.*, 1998) culminating in Redmond and Einaudi (2010) formally defining the genetic sequence as follows: (1) quartz monzonite porphyry (QMP); (2) latite porphyry (LP); (3) biotite porphyry (BP); (4) quartz latite porphyry breccia (QLPbx); and (5) quartz latite porphyry (QLP). Each porphyry phase has an associated sequence of quartz veins, sulphide mineralization, and potassic alteration halo. Vein-hosted sulphides consist of chalcopyrite, bornite, and digenite with minor molybdenite and rare pyrite. Variability in metal content, sulphide ratios and potassic alteration indicate a progressive decrease in Cu and Au over the porphyry sequence. This has been interpreted as an effect of metal depletion and loss of volatiles in the underlying magma source (Redmond and Einaudi, 2010). In the present study, analyses of sulphide mineral phases were investigated to test the effectiveness of trace-element (ECE's) signatures as a fingerprint of hydrothermal processes and metal behaviour linked to the evolution of the porphyry sequence.

TRACE ELEMENT DEPORTMENT

Vein-hosted sulphides in 17 polished thin sections were examined on a Tescan TIGER MIRA3 FEG-SEM equipped with two Oxford Instruments EDX detectors allowing for the determination of major element compositions of ore phases. The trace element compositions of bornite, chalcopyrite, and digenite were determined by Laser Ablation ICP-MS. In situ spot analyses were carried out on a Photon machines G2 193 nm UV laser with a Helex two- volume cell coupled to a Thermo iCAPQ ICP-MS. Spot analyses used a beam size of 30 µm, whereas element mapping of complexly zoned minerals was carried out using a beam size of 12 µm.

Petrography of sulphide phases has shown that the modal abundance of chalcopyrite, bornite, and digenite is variable across five distinct vein generations. Chalcopyrite is ubiquitous, while bornite is abundant in all but one of the porphyry generations; the QLP contains only chalcopyrite. Digenite is associated with bornite and most abundant in the QMP, but rare in the LP, BP, QLPbx phases and absent in the youngest QLP intrusion. Linking sulphide mineralogy and trace element inventory, some of the clearest findings are as follows. Trace element maps (Fig. 1) illustrate the broad distribution of ECE's and penalty elements between the major sulphide mineral phases. Where grating textured digenite is associated with bornite, digenite contains the majority of Ag and Au among the base-metal sulphides. Bornite is a major host of Bi and Te, and in the absence of digenite also for Ag. Chalcopyrite is the primary host for Co, Ge, In, and Ga. Apart from base-metal sulphides, extremely rare telluride, electrum, native gold, and wittichenite grains contain high concentrations (tens of wt. %) of Te, Ag, Au, and Bi. Lead contents of bornite seem to be most prone to the presence of sub-micron scale inclusions of galena or sulphosalts. This is indicated by frequent Pb spikes in time-resolved bornite ablation profiles, which, in contrast, are absent in respective chalcopyrite profiles. Among

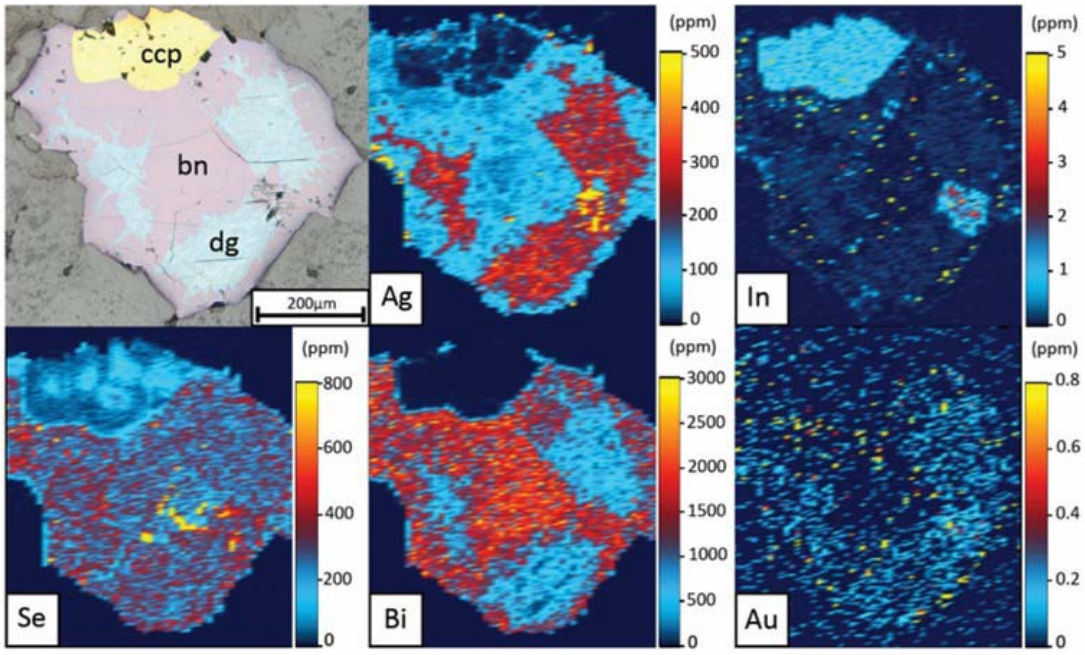

Figure 1: Semi-quantitative LA-ICP-MS trace element maps of a chalcopyrite-bornite-digenite intergrowth from the Bingham Canyon deposit. Data collected using a 12 µm beam diameter at a 40 Hz repetition rate, fluence of 1.2 J/cm^2, and a scan speed of 20 µm/sec. USGS MASS-1 (Wilson et al., 2002) was used as a calibration standard.

the penalty elements, Se is elevated in samples, yielding highest concentrations in galena micro-inclusions (up to 5 wt.% Se) and bornite (up to 800 ppm Se), followed by digenite (up to 600 ppm) and chalcopyrite (up to 400 ppm); concentrations of As and Cd are commonly below 5 ppm.

Laser Ablation ICP-MS analyses of major sulphide minerals was successful at elucidating the trace element deportment across the sequence of porphyry intrusions. A continuous sequential change in trace metal contents of chalcopyrite and bornite is not apparent; however, a decline in the modal abundance of Cu-Fe-sulphide host phases confirms the decrease in overall ECE contents along with Cu grades. As this decline is more pronounced for digenite and bornite, the overall amount of contained metals (Te, Bi, Ag, and Au) seems to diminish more intensely than for chalcopyrite-hosted metals (Co, Ge, In, and Ga) over the intrusive sequence. This further implies the absence of notable Te, Bi, Ag, and Au contents in the youngest intrusive phase, QLP. These observations are potentially linked to a non- uniform depletion of different ECE's in the magma source.

REFERENCES

Babcock, R.C., Jr., Ballantyne, G.H., Phillips, C.H., Bolm, J.G., 1995. Summary of the geology of the Bingham district, Utah. Arizona Geological Society Digest, 20, 316–335.

Bray, R.E., 1969. Igneous rocks and hydrothermal alteration at Bingham, Utah. Economic Geology, 64 (1), 34–49.

Lanier, G., John, E.C., Swensen, A.J., Reid, J., Bard, C.E., Caddey, S.W., Wilson, J.C., 1978. General geology of Bingham mine, Bingham Canyon, Utah. Economic Geology, 73 (7),
1228–1241.

Moore, W.J., 1970. Igneous rocks in Bingham mining district, Utah. Unpublished Ph.D. thesis, Stanford University, 184 p.

Moore, W.J., Czamanske, G.K., 1973. Compositions of biotites from unaltered and altered monzonitic rocks in the Bingham mining district, Utah. Economic Geology, 68 (2), 269–274.

Phillips, C.H., Smith, T.W., Harrison, E.D., 1998. Alteration, metal zoning, and ore controls in the Bingham Canyon porphyry copper deposit, Utah. Society of Economic Geologists, Guidebook Series, 29, 133–145.

Redmond, P.B., Einaudi, M.T., 2010. The Bingham Canyon porphyry Cu-Mo-Au deposit. I. Sequence of intrusions, vein formation, and sulfide deposition. Economic Geology, 105 (1), 43-68.

Schuyler Anderson, C., 2016. Tellurium. In USGS Mineral Commodity Summaries.

Stringham, B.F., 1953. Granitization and hydrothermal alteration, at Bingham, Utah. Geological Society of America Bulletin 64 (8), 945–991.

A | 118

DEFINING IOCG SIGNATURES THROUGH COMPOSITIONAL DATA ANALYSIS: A CASE STUDY OF LITHOGEOCHEMICAL ZONING AT OLYMOIC DAM, SOUTH AUSTRALIA

Marija Dmitrijeva

University of Adelaide - marija.dmitrijeva@adelaide.edu.au

BACKGROUND

Iron-oxide–Cu-Au (IOCG) comprises a diverse clan of ore deposits that are found in a wide spectrum of geological settings spanning the Archean to Tertiary (Groves *et al.*, 2010). These deposits are inherently associated with zoned alteration assemblages represented by distal alkali-rich, and proximal hydrolytic alteration, with respect to the main Fe-oxide (±Cu-Au) mineralization (Barton, 2014). This zonation is observed at different scales, from regional down to individual orebodies, and results from the circulation and evolution of hydrothermal fluids. Understanding the spatio-temporal distribution of metals and minerals relative to fluid sources is thus crucial to constrain genetic models and develop exploration strategies.

The Olympic Dam (OD) deposit, South Australia, shows a regional and deposit-scale zoning with respect to alteration assemblages. The sulphide-zonation is roughly concentric, displaying a deeper-to-shallower transition from pyrite-chalcopyrite (Py-Cp) through chalcopyrite-bornite (Cp-Bn) to bornite-chalcocite (Bn-Cc) (Ehrig *et al.*, 2012). The deposit is hosted within the Olympic Dam Breccia Complex (ODBC), itself within the ~1.59 Ga Roxby Downs Granite and is predominantly derived from progressive brecciation and increasing Fe-metasomatism of the host granite. This relatively simple geological setting and mineralogical zonation make OD a prime target to investigate geochemical patterns potentially associated with zoning and concentration gradients relative to metal source(s). As a first step towards constraining zoning within the ODBC, principal component analysis (PCA) was performed to derive lithogeochemical zonation and identify key elements defining IOCG signatures.

METHODS

The whole-rock dataset consists of 10,546 samples from 533 drillholes and forms a dense grid in the south-eastern part of ODBC. Each sample represents a 15 m-long drillhole interval, which was assayed for 39 elements (as on Fig. 1). The PCA was performed on the centred logratio transformed data containing all elements, and the PC1 interpolated in Leapfrog3D software (Fig. 1a).

We present only the first principal component (PC1), which governs the greatest variability (~32%) within the dataset and represents an interpretable geological process. As an example, the NW-SE partial cross-section (Fig. 1b) represents the majority of lithologies/alteration types documented in the ODBC. The combination of multivariate statistics, i.e. PCA/hierarchical clustering, with a large whole-rock dataset, allows a comparison of empirical lithological/alteration and sulphide and gangue mineralogical zonation (obtained from Cu:S ratios and supported by modal mineralogy data), with an IOCG geochemical signature represented as the PC1, and provides data-driven decisions for element groupings.

RESULTS AND DISCUSSION

Relationships among elements within whole-rock geochemical datasets are governed by the mixture of minerals and their stoichiometries. The PCA transforms data into a set of linear combinations of elements or PCs, whereby the dominant PC1 reflects mineralogy and describes geological processes, which are mirrored by a relative increase or decrease of elements. The resulting PC1 and dendrogram shows two main element groups (Fig. 1c), defined as Class 1, and an antithetic association represented by Classes 2, 3 and 4. These two distinct groups represent the inverse relationship between (i) trace elements in host rocks (unmineralized granite, mafic and carbonate units), and (ii) elements typifying an IOCG geochemical signature within the ODBC. Notably, the highest loadings on PC1 are given by Class 3 elements Au-W-As-Mo-Sb (Fig. 1d).

If compared with the lithological/alteration cross-section (Fig. 1b), the distribution of positive PC1 values only partially overlaps with the distribution of >20 wt% Fe hematite breccias and vice versa. This may suggest that: (i) in some areas mineralization may not be associated with the Fe-metasomatism; and (ii) the presence of some Fe-rich lithologies may pre- or postdate IOCG mineralization.

The Cu(-Fe)-sulphide zone interfaces represent a complex but mappable feature. However, when compared to the significant correlation between PC1 and lithological/alteration zones, no pattern can be observed. This mismatch may be attributed to the low-resolution sampling and/or pervasive distribution of abundant Cu(-Fe)-

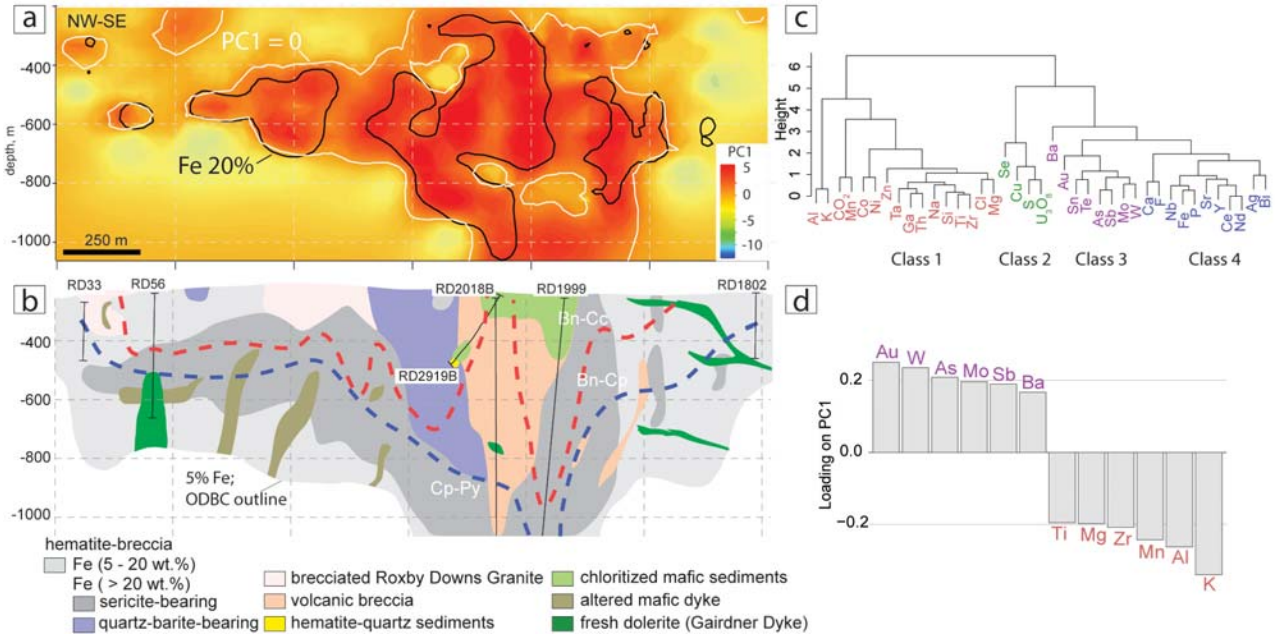

Figure 1. (a) NW-SE cross-section showing interpolated values of PC1 scores; (b) corresponding geological sketch; (c) dendrogram of analysed elements; (d) highest absolute element loadings on PC1.

sulphides and Fe-oxides that host trace elements. The latter stresses the necessity for investigation of individual metal gradients with emphasis on statistically defined classes, such as the Au-W-As-Mo-Sb signature.

CONCLUSIONS

The PCA has implications for delineation of the ODBC from the enclosing granite by deriving groups of elements representing IOCG mineralization. Although PC1 overlaps with Fe- metasomatism, it neither gives solid gradients nor defines zonation. This may signify that data-driven grouping of elements is the next step for further metal zonation investigation with a potential to detect primary/replacement patterns. However, given the complexity of ore assemblages in response to multiple episodes of mineral dissolution and (re)precipitation, trace element signatures in individual minerals (e.g. Cu(-Fe)-sulphides, Fe- oxides) may prove better at constraining the spatiotemporal evolution of the ODBC.

REFERENCES

Groves, D.I., Bierlein, F.P., Meinert, L.D., and Hitzman, M.W., 2010. Iron oxide copper- gold (IOCG) deposits through Earth history: Implications for origin, lithospheric setting, and distinction from other epigenetic iron oxide deposits: Economic Geology, 105, 641–654.

Barton, M.D., 2014. Iron Oxide (–Cu–Au–REE–P–Ag–U–Co) Systems, in: Treatise on Geochemistry. Elsevier, 13, pp. 515–541.

Ehrig, K., McPhie, J., Kamenetsky, V., 2012. Geology and Mineralogical Zonation of the Olympic Dam Iron Oxide Cu-U-Au-Ag Deposit, South Australia, in: Hedenquist, J.W., Harris, M., Camus, F. (Eds.), Geology and Genesis of Major Copper Deposits and Districts of the World: A Tribute to Richard H. Sillitoe. Society of Economic Geologists, Special Publication 16, pp. 237–267.

A | 119

HIGH RESOLUTION X-RAY COMPUTED TOMOGRAPHY STUDIES OF GOLD–Cu SULFIDE RELATIONSHIPS IN THE GRASBERG PORPHYRY Cu-Au DEPOSIT, PAPUA, INDONESIA

J. Richard Kyle[1], Kylie A. Wright, Richard A. Ketcham, Nathan R. Miller

[1]University of Texas at Austin - rkyle@jsg.utexas.edu

The Grasberg porphyry Cu-Au deposit is one of the world's largest intrusion-related Cu-Au orebodies with 3.2 Gt of ore averaging 0.9% Cu and 0.9g/t Au. The orebody is hosted within the ~3-Ma Grasberg Intrusive Complex within the Central Range of New Guinea. Grasberg Cu ore consists principally of veinlets of chalcopyrite and bornite, with native gold generally occurring within or along boundaries of Cu sulfides. The consistent Cu:Au ratio of the ore and spatial association of native gold with Cu sulfides is the rationale for our investigation of the genetic causes of these relationships using volumetric analysis and trace element geochemistry.

Experimental studies by other researchers have shown that at ore-forming temperatures (~300-700°C) and elevated sulfur activity, bornite and chalcopyrite can host 1000s of ppm Au within the sulfide lattice or as nano-inclusions. Upon retrograde cooling of the hydrothermal system, the capacity of the Cu-Fe sulfides to host Au significantly decreases to ~10 ppm, suggesting that the Au becomes unstable within the Cu-Fe sulfide matrix and could passively migrate out of the sulfides and coalesce to form native gold grains. These data suggest that Cu-Fe sulfides could exert a strong control on the nature and distribution of gold in porphyry deposits.

To assess the role of Au-bearing Cu-Fe sulfides in the concentration of native gold in this setting, High Resolution X-ray Computed Tomography (HRXCT) was used to measure the size, shape, texture, and occurrence of native gold grains, and to map the extent of contiguous Cu-sulfides in Grasberg ore. HRXCT data were used to construct 3D modified Voronoi regions, as a measure of the diffusional domains that may have provided Au to gold grains during cooling. Modified Voronoi volumes are defined for each gold grain as the set of points within the Cu-sulfide network that are closer to that gold grain than any other, when measured along a path through the Cu sulfides. In all, 16 linear correlation values between modified Voronoi volumes and gold grain volumes were produced. Complementary

Laser Ablation Inductively Coupled Plasma Mass Spectrometry (LA-ICP-MS), along with earlier microbeam analysis, was used to assess and compare trace element variation within the Cu-Fe sulfides and to constrain spatial variation of Au within Cu-Fe sulfides that contain native gold grains.

A number of previous petrographic studies have provided information on the nature and relationships of gold in the Grasberg ores; all of these have limitations, including the inherent difficulty of locating a significant number of any component that is present in average concentrations of less than 1 g/t. Traditional petrography is limited further by the two-dimensional nature of the studied surface which may suggest misleading, or at least incomplete, associations. The general conclusion of traditional petrographic studies of Grasberg copper ores is that the native gold commonly occurs near the margins of the copper sulfide concentrations, with lesser occurrences of "free" gold in matrix or in association with other metallic minerals. HRXCT also has limitations but is able to determine the in-situ 3D nature of gold grains and their associations. We have assessed more than 600 in-situ native gold grains from Grasberg ores, using Blob3D analysis of HRXCT data to calculate sizes and best fit ellipsoid radii of grain shapes. Based on best fit ellipsoid radii for these native gold grains, 58.9% were elongate or rod-shaped, 22.9% were platy or disc-shaped, and 18.2% were compact or spherical. Grain sizes based on maximum dimension range from >2 mm to ~50 µm; earlier studies had imaged gold grains to ~10 µm in small scan volumes. The mean aspect ratio of the best fit ellipsoid for all native gold grains was 1.85 ± 0.66; grain size and aspect ratio have a moderate positive correlation. Gold grains in chalcopyrite appear smaller, more equant, and less angular, whereas gold near bornite appears less regular in shape. However, the aspect ratios of gold hosted in bornite and in chalcopyrite are similar in the HRXCT data. Gold grains primarily form equant inclusions when they are contained entirely within chalcopyrite, whereas grains associated with bornite typically occur along boundaries of chalcopyrite-bornite intergrowths. Morphologies of gold grains associated with bornite were varied, although grains typically appeared larger and less symmetrical than those in chalcopyrite. In a well- characterized high grade Grasberg sample, gold grains occurred near Cu-Fe sulfide phases 99% of the time; of these, 91% occurred near chalcopyrite while 8% occurred near bornite. Thirty-eight percent of grains occurred on the edges of Cu-Fe sulfides, while 53% occurred as inclusions within bornite or chalcopyrite. Only 9% of grains were found in matrix material.

However, in evaluating the hypothesis of dispersed gold becoming aggregated to form the existing gold grains, the correlation coefficients for modified Voronoi region and gold grain volumes were consistently low. The poor correlations could be due to the simplifying assumptions of the model not accurately accounting for the

complexity of the physical system. If Au mobility is based on the presence of "excess Au" diffusing out of Cu-Fe sulfides, rates of cooling could have a dramatic effect on the ability of Au to exsolve from sulfides and then move an appreciable distance. The modified Voronoi model assumes a uniform distribution of gold throughout both major Cu-Fe sulfides, and that gold diffuses equally well through both minerals. Because intergrowths of these minerals were common in our samples, chalcopyrite and bornite were treated as one Cu-Fe-S mineral phase for Voronoi calculations. Chalcopyrite has been shown to accommodate significantly smaller concentrations of gold, thus bornite is more capable of exsolving the volume of gold necessary to form a large gold grain. The modified Voronoi calculations also presume that all growing gold grains are larger than the detection limit, which depends on scan resolution. Our correlation values only provide a minimum estimate of the correlation between Cu-Fe sulfides and boundary gold grains, suggesting that there is, especially in high grade porphyry samples, some correlation between the volume of copper sulfide minerals and the volume of gold present in a sample. Another common issue encountered is that calculated drainage regions commonly extend to the physical edge of the samples, rendering their actual volumes ambiguous and the correlations associated with them uninterpretable.

Electron microbeam analyses of native gold reveal high fineness compositions ranging from 930 to 986 (ave. 964). Silver is the main trace element in native gold ranging up to 7 wt%, with Pd and Bi detected in many analyses, with maximum concentrations of 0.35 and 0.38 wt%, respectively. Pd telluride inclusions have been documented in copper sulfides, but Te was not detected in the native gold with high Pd analyses. LA-ICP-MS analyses of copper sulfides reveal a strong positive correlation between Bi and Ag, and a moderate positive correlation between Bi and Au.The "patchy" distribution of Au in Cu sulfides may imply that the majority of non-visible gold exists in Au nanoparticles, rather than solid solution with the Cu-Fe sulfides. Spot analyses and 2D maps indicate the presence of an "enrichment halo" of elevated Au contents in Cu-Fe sulfides surrounding the gold grains. This "enrichment halo" can be interpreted as evidence in support of a hybrid Ostwald-type ripening process that coarsens gold inclusions in chalcopyrite at high-temperatures in porphyry-skarn systems.

A | 120

AN INTEGRAL MODEL FOR THE FORMATION OF MAGNETITE-(APATITE) DEPOSITS

Fernando Tornos[1], John M Hanchar, Francisco Velasco

[1]Instituto de Geociencias (CSIC-UCM), Madrid, Spain - f.tornos@csic.es

INTRODUCTION

Magnetite-(apatite) deposits form an enigmatic style of mineralization best represented by the clusters of the American Cordillera (Chile, Peru and Mexico), the Norrbotten region (Sweden), Mexico, the Great Bear Zone (Canada), the Adirondacks (USA), and the Bafq area (Iran). They share common geological and geochemical features and, despite included into the IOCG clan, they are only loosely related to IOCG deposits. Genetic models for these deposits include the hydrothermal replacement of host rocks by basinal- or magmatic- hydrothermal brines, crystallization of iron-rich melts, separation and upward movement of magnetite phenocrysts by an aqueous fluid that separated from a crystallizing mafic melt, and the evolution of a magmatic-hydrothermal system related to a crystallizing iron melt. Combined geological, geochemical, and mineralogical data suggest that only the last model accounts for all the observed features.

GEOLOGY AND GEOCHEMISTRY OF MAGNETITE-(APATITE) DEPOSITS

Magnetite-(apatite) deposits share features that are uncommon in other styles of mineralization such as the presence of a core of, sometimes vesicular, massive magnetite with variable but small proportions of fluorapatite and actinolite. This massive ore is often capped, or surrounded by, a rock characterized by the presence of coarse-grained actinolite and/or apatite with interstitial magnetite. Zoned around this core there is commonly a large area of zoned hydrothermal alteration with a conspicuous assemblage that consists of K- feldspar/albite, actinolite/diopside and scapolite (alkali-calcic alteration), with the proportion of the late crystallizing minerals increasing towards the centre of the system. The hydrothermal mineralization includes an internal zone of stockwork-like magnetite and an outer zone with disseminated magnetite. Breccia bodies with fragments of altered host rock supported by actinolite, scapolite, and magnetite are often abundant. There is an external aureole of propylitic alteration. In shallow systems, the zone of alkali-calcic alteration is overprinted by a steam-heated sulfate-rich alteration that can be responsible of the transformation of magnetite to hematite. Other major features of this style of mineralization are the almost complete lack of coeval quartz and sulphides.

DISCUSSION AND CONCLUSIONS

Stable isotope, melt/fluid inclusion data, and experimental results suggest that the internal zone of massive magnetite is the product of the crystallization of a water-bearing iron-rich melt. These melts are thought to intrude along small dilatational zones in overall compressive settings, such as pull-apart structures. Especially important are the significant amounts of water, phosphorous, fluorine and sometimes boron, which seem to strongly fractionate into the iron-rich phase. These late P, F and B act as fluxing elements, decreasing the solidus temperature of the magnetite from nearly 1650 °C to ca. 950 °C and decrease the already low viscosity of these melts. Degassing of the water-rich melts during their upward movement and crystallization exsolves large amounts of magmatic-hydrothermal fluids. The concomitant loss of the fluxing elements would lead to an increase of the solidus, quenching of the melts and produce the extreme temperature gradients recorded in these rocks as well as large magmatic-hydrothermal systems formed at temperatures well above those related with silicate melts. Such dewatering is probably responsible for the formation of the coarse grained magnetite-actinolite-apatite rocks that are interpreted as equivalent to pegmatites. In shallow systems, vigorous dewatering dominantly in the form of gas produces diatremes of very variable size and pyroclastic eruptions that accompany low-viscosity flows similar to those of Mid-ocean Ridge (MOR) basalts.

The low proportion of silica in the systems inhibits the crystallization of major amounts of silicates, which only precipitate in the form of actinolite. Later lack of silica and the high amount of phosphorous and fluorine should promote the stabilization of fluorapatite and fluorite as the product of the crystallization from the residual melts.

The iron-rich melts have variable amounts of silica, alkalis, Ca and Mg. Their exact composition is poorly known but it seems to strongly depend on the composition of the parental melt and the extent of the immiscibility with the felsic silica- and aluminium-rich conjugate melt. The more evolved the melts are, the less silica and more iron oxide is present in the system; it is likely that magnetite-apatite deposits crystallize in highly evolved systems.

The addition of large amounts of fluxing elements likely makes the immiscibility field more complex and several other types of melts appear. The conjugate silica-rich melt, with a composition close to that of rhyolite-rhyodacite, should quench immediately after the separation of the less viscous water-bearing iron-rich melt. However, there are multiple lines of evidence for the existence of these coeval magmas in many magnetite-apatite deposits.

The formation of these melts must be related to a chemical modification of a primitive magma generated in the sub-continental lithospheric mantle (SCLM). At El Laco, there are direct lines of evidence for contamination by underlying shallow marine to continental sediments that occur beneath the volcano; however, this model cannot be easily extrapolated to other districts. A systematic increase in the $^{87}Sr/^{86}Sr$ ratios found in many deposits globally, suggests that the addition of marine sediments from a subducting slab could add enough amounts of contaminant material to promote melt immiscibility.

A | 121

CHARACTERISATION OF SERICITIC ALTERATION AT THE TACA TACA BAJO PORPHYRY CU DEPOSIT, ARGENTINA

Sebastian Benavides

First Quantum Minerals Ltd. - sebastian.benavides@fqml.com

INTRODUCTION

The Taca Taca Bajo porphyry Cu deposit, Salta province, northwestern Argentina has a calculated resource of 2,165 Mt at 0.57% Cu eq. It was emplaced in the back-arc of the central Andean Eocene-Oligocene magmatic arc, and is hosted by a structurally-bound block of local crystalline basement. Multiple phases of syn-mineralization Oligocene (29.30 ± 0.57Ma) rhyodacite porphyritic intrusions have been recognized in association with the deposit, although most of the mineralization is within the hosting batholithic Silurian Taca Taca granite and is closely related to sericitic alteration.

At Taca Taca Bajo a green sericite facies has been described coexisting with a white sericite facies, and both occur as an overprint on potassic alteration. The deposit is characterised by a barren potassic core, with the vast majority of Cu ore related to 'green' and 'white' sericite alteration outboard of the causative porphyritic intrusions. The aim of this study is to understand the compositional and textural differences between the types of sericite reported in Taca Taca Bajo, as well as their relationship with potassic alteration and main stage mineralization. This information will also be used to extrapolate this material classification to a deposit scale to aid speciation of ore and gangue mineralogy for metallurgical analysis.

METHODS

Twenty-four samples were collected from the Taca Taca Bajo porphyry Cu deposit, three background fresh granite, three background potassic altered porphyry, and nineteen samples of green and white sericite in varying proportions. Twenty-five laser mounts were produced from these samples.

Short wave infrared (SWIR) measurements were collected and interpreted from each mount. The sericite samples were then classified by different scalars derived from the SWIR spectra such as the wavelength of the absorption feature near 2200 nm (w2200). Reflected light microscopy was conducted on the laser mounts to characterise textural relationships and sulfide species.

The mounts were investigated under scanning electron microprobe (SEM), where textural relationships of sericite sites were described, and a total of 665 electron microprobe analyses were conducted. This information was used to select points for LA-ICPMS ablation analysis to provide detailed trace element chemistry for a range of sericite colour and morphological classes. A total of 318 laser spots on sericite sites were analysed by LA- ICPMS.

Samples not used for microanalysis were used for potassium staining and quartz textural study by cathodoluminescence, so as to provide some constraints on other aspects of the silicate paragenesis.

RESULTS

Three main associations were distinguished between the sericite classes as logged and observed sulfides. There is a strong correlation between green sericite occurrence and chalcopyrite. White sericite is always present to some degree where pyrite has replaced chalcopyrite. White sericite is always present in samples where pyrite is the only observed sulfide and white sericite has a strong correlation with a late, acid overprint of chalcopyrite by pyrite-bornite-chalcocite-covellite.

SEM textural characterisation revealed two distinct morphologies of sericite. The dominant sericite type is relatively coarse-grained, comprises euhedral tabular crystals and was observed in most samples as pervasive alteration. A much finer grained, 'shreddy' style composed of patches of anhedral to subhedral, sericite was consistently observed in samples described as green sericite or mixed green-white sericite, and sericite with this morphology is uncommon in white sericite samples. This finer grained sericite morphology resembles the texture of hydrothermal biotite formed in the potassic zone of porphyry copper deposits, and likewise seems to have nucleated on mafic sites of the potassic altered protolith.

SEM analytical data showed that the coarse, bladed sericite has a muscovitic composition, whereas the shreddy sericite is elevated in Fe and Mg, i.e., phengitic, and plots on compositional trend towards biotite. The more precise analysis by LA-ICPMS confirmed the coarser sericite is muscovite, and that the shreddy sericite is phengite. When comparing analytical results with macroscopic logging of sericite types, it becomes apparent that rocks described during logging as 'white sericite' are dominated by the coarse bladed muscovite, while those logged as

'green sericite' contain abundant patchy, shreddy phengite. This conclusion is supported by the SWIR spectral data, for which the wavelength of the absorption feature near 2200 nm is known to respond to substitution of Fe-Mg for Al in white micas. Among our sample set there is a clear trend from shorter 'aluminous' wavelengths of this feature among 'white' sericite to longer 'phengitic' wavelengths among 'green' sericite.

In relation to ore, samples with phengite show elevated Cu grades, suggesting than phengite was either intimately associated with Cu deposition or, at the very least, was not ore destructive. In contrast, white, muscovite-bearing samples contain < 0.1% Cu and the petrographic analysis clearly shows that the muscovite event was ore-destructive with pyrite replacing chalcopyrite. The trace element chemistry of sericites is also distinct. Whereas the muscovite contains low levels of most trace elements, phengite at Taca Taca Bajo is commonly enriched in Li, Zn, Mn, and Ni, and exhibits bimodal behaviour with V, Ba and to a lesser degree Sn and Sr. The enrichments are interpreted to be due to hydrothermal input, whereas the bimodal behaviour could be related to partial geochemical conservation of the pre-existing biotite (V) or feldspar (Ba, Sr). Potassium staining revealed that samples with predominant muscovite-pyrite assemblages contain minor or no relict orthoclase, whereas samples with the phengite-chalcopyrite assemblage preserve moderate to intense relict orthoclase flooding. There is an intimate relationship between potassic alteration, ore deposition, and phengite alteration.

Taken together, the macroscopic textures and relationships, microscopic textures and associations, and the microanalytical data lead to the interpretation 'green sericite' is phengite that formed as replacement of other silicates, at a higher T and under less acid conditions than the muscovitic 'white sericite'.

CONCLUSIONS

At Taca Taca Bajo, copper ore was not deposited during the main-stage phyllic alteration event as previously thought. Potassic alteration extended well beyond the preserved barren core, and occupied the entire mineralised volume. The outer parts of this greater potassic zone were overprinted by an early stage sericitic alteration, characterised by quartz- chalcopyrite and chalcopyrite only veins with phengite-chalcopyrite selvages. Phengite replaced hydrothermal biotite that had altered primary ferromagnesian minerals and, to a lesser extent, phengite also replaced the orthoclase flooded groundmass. This suggests that the chalcopyrite was deposited during the phengite overprint, although commencement of mineralization during potassic alteration cannot be ruled out. This phengite assemblage is analogous, in paragenetic terms, to sericite-chlorite alteration with the difference in phyllosilicate mineralogy perhaps due to the felsic nature of the host rock or the depth of emplacement of Taca Taca Bajo. Then, as the system cooled a more acidic fluid caused the replacement of pre-existing silicate alteration by muscovite, and chalcopyrite by pyrite. The ore zone at Taca Taca Bajo is constrained to the region where this late muscovitic alteration was weaker or at the very least transitional from phengite alteration. The cooler, more acid, late stage of muscovitic alteration displays an increase in sulfidation state, replacing chalcopyrite by pyrite-bornite-chalcocite.

Taca Taca Bajo is a rare example of a porphyry copper deposit with abundant phengite alteration directly associated with hypogene mineralization. Exploration models for porphyry copper deposits therefore must permit the occurrence of phengite, *sensu strictu*, as a transitional phase between potassic and muscovitic phyllic alteration. This alteration facies is distinguished from the more common description of phengitic illite as an extreme distal expression of phyllic alteration.

Cu-BEARING VEIN AND ALTERATION IN GRANITIC ROCKS IN TSOGTTSETSII AREA, MONGOLIA: POTENTIAL FOR PORPHYRY-Cu MINERALIZATION

In Joon Kim[1], Sanggun No

[1]KIGAM - ijkim@kigam.re.kr

Chalcopyrite- and malachite-bearing veins are discovered at eight points in granitic rock in the Tsogttsetssi, Mongolia. The veins have NW-SE, NE-SW trending directions. Feldspar grains in the host-rock show pinkish color at the contact with veins. The width of pinkish part increases with increasing the width of veins. The veins are subdivided into four types (1) magnetite + hematite + chalcopyrite + quartz; (2) quartz + hornblende + chalcopyrite + chalcocite + magnetite + hematite + orthoclase + epidote + chlorite; (3) quartz + epidote + chlorite + chalcopyrite + pyrite; and (4) chlorite + pyrite + quartz + chalcopyrite. These veins occurred along the fracture with the above mineral assemblages.

The host-rock alteration is recognized in three alteration types. The alteration type is subdivided into two types by color of feldspars, such as white and pinkish parts occurred with vein type (1), (2), and (4). Hornblende and biotite are partly altered to chlorite, and plagioclase is partly altered to sericite in white part. Hornblende and biotite are mostly altered to chlorite and magnetite, and plagioclase is partly altered to sericite or epidote in pinkish part. Shredded hornblende grains are entirely altered to chlorite, in this part were observed. Hornblende and biotite are altered to epidote and chlorite, and plagioclase is altered to albite and calcite in the host-rock which bears vein type. Cu contents are 500 to 3,000 ppm in the veins bearing chalcopyrite.

We compare mineral assemblages of veins and alteration characteristics with porphyry-type Cu mineralization. The characteristics of Cu-bearing veins in the study area are similar to typical porphyry Cu-Au deposit developed in calc-alkaline series suite. The alteration occurred in host-rock match the propylitic and potassic alteration types overprinted by chlorite-sericite alteration. The discrimination diagram of SiO_2 vs Na_2O+K_2O shows that host-rocks are plotted in porphyry Cu-Au(-Mo) area. Furthermore, Sr/Y and V/Sc ratios that can divided into fertile (Sr/Y >40, V/Sc >10) or infertile porphyry suites are 36.2 to 62.9 and 10.0 to 18.1, respectively, indicating that the parental magma was fertile.

In conclusion, mineral assemblages of veins and host-rock alteration characteristics show that the study area has the potential for porphyry Cu-Au mineralization.

THE LINDERO PORPHYRY GOLD DEPOSIT, NORTHWESTERN ARGENTINA

Jorge Kesting[1], K. Brock Riedell, Eric N. Chapman and David Volkert

[1]*Fortuna Silver Inc. - ikesting@mansfieldmin.com*

The Lindero and the nearby Arizaro deposits are located 260 km west of Salta, Argentina, and hosted by a Miocene (16.8-15.2 Ma) intrusive-volcanic complex that crosscuts a granitic basement of Ordovician age and Paleogene redbeds. Surface mapping and core-logging show that the Lindero complex flares upward and consists of multiple, mostly concentric intrusions of plagioclase + hornblende ± biotite ± quartz-phyric porphyries. There are four mineralized zones that form an annular orebody 600 m in diameter and extending to at least 600 m depth. Early- to syn-mineral quartz-diorite intrusions (FPD and CPD1) ring the complex and host the highest Au and Cu grades, followed by an inter-mineral PBFD quartz- diorite. Monzodiorite to quartz monzodiorite porphyries of late-mineral (CPD2 and DDP) to post-mineral (PMI) age form the barren to low-grade core of the system. The presence of breccias, layers of pyroclasticrocks and of flow-dome shapes indicate the PMI phase was subvolcanic and locally vented out. Narrow bodies of magmatic-hydrothermal breccias with matrices of quartz + sulphide ± sulphates or magnetite ± chlorite were synchronous with CPD1. Crosscutting relations indicate CPD1 is the principal source of metals. There are abundant steeply dipping faults with northwest-southeast strike, and minor post-mineral strike-slip to oblique-slip offset.

Gold-copper mineralization at Lindero is related to moderate to strong biotite-K feldspar- magnetite alteration of the igneous hosts, and quartz + biotite ± sericite ± K-feldspar alteration in the redbeds. Potassic-altered rocks typically contain $\leqq$10% quartz-sulfide and magnetite-sulfide veins, which strongly influence the Au and Cu grades. Primary mineralization is subequal chalcopyrite and pyrite, with far subordinate bornite, molybdenite, covellite, galena and sphalerite. Free gold grains 20-70 Mm are associated with chalcopyrite and/or magnetite. Partial to complete oxidation ranges from <10 m in the margins of the deposit to over 200 m in its center; Cu sulfides are replaced by neotocite and chrysocolla.

The Lindero deposit is similar to the Miocene porphyry Au(-Cu) deposits of the Maricunga belt ~200 km to the south-southwest due to its size, tectonic setting, the presence of quartz- dioritic intrusions, an important biotitic alteration, and the high magnetite contents. However, it differs from them in the relative lack of sericitic and argillic alteration zones and the absence of the banded quartz veins. that are typical of Maricunga These differences are probably related to a deeper level of emplacement and/or erosion.

Fortuna Silver Mines Inc. initiated the construction of an open-pit, heap leach operation at Lindero in late 2017. The feasibility study projects a 15-year operation producing an average 96,000 ounces gold per year starting in mid-2019.

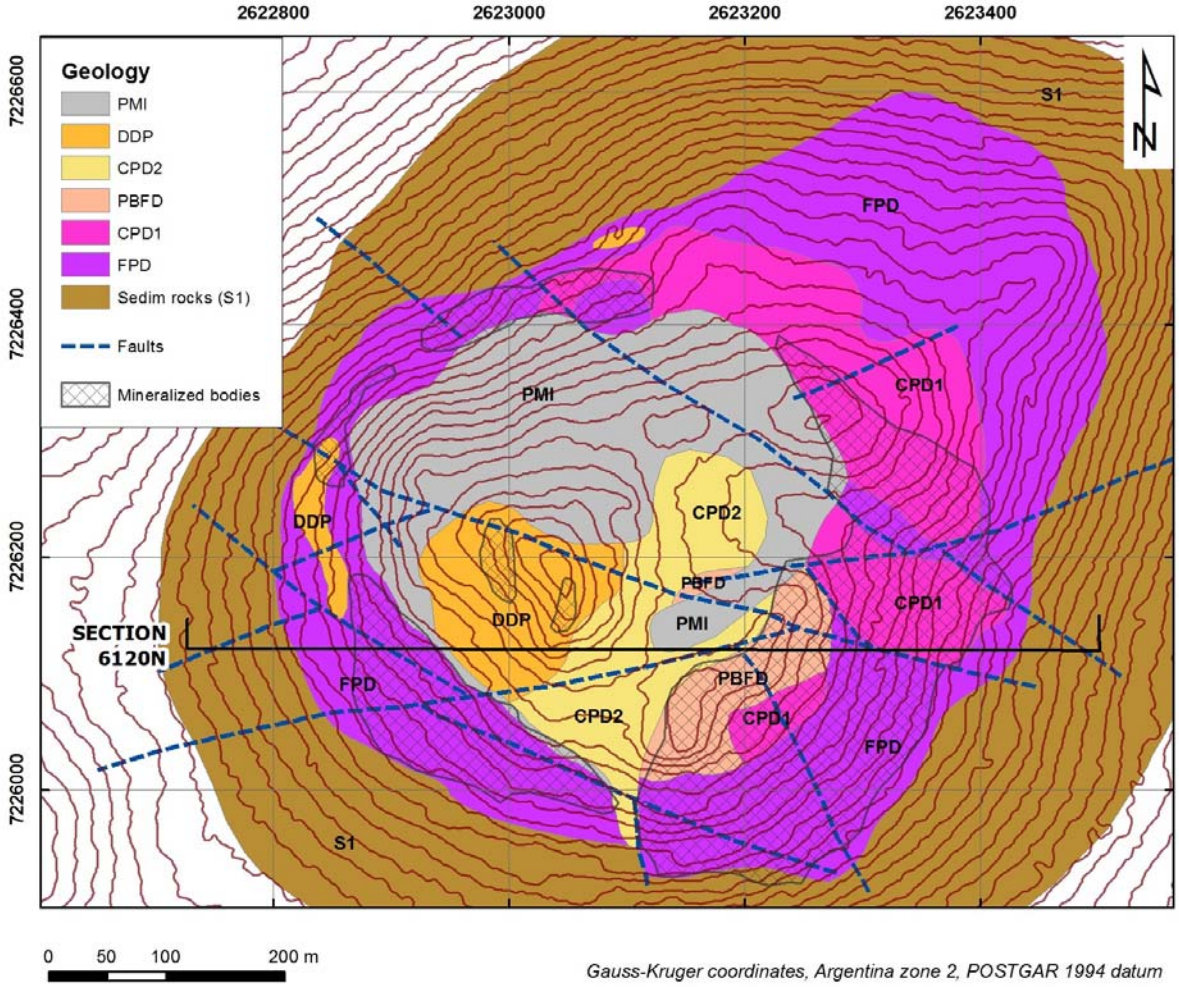

Gauss-Kruger coordinates, Argentina zone 2, POSTGAR 1994 datum

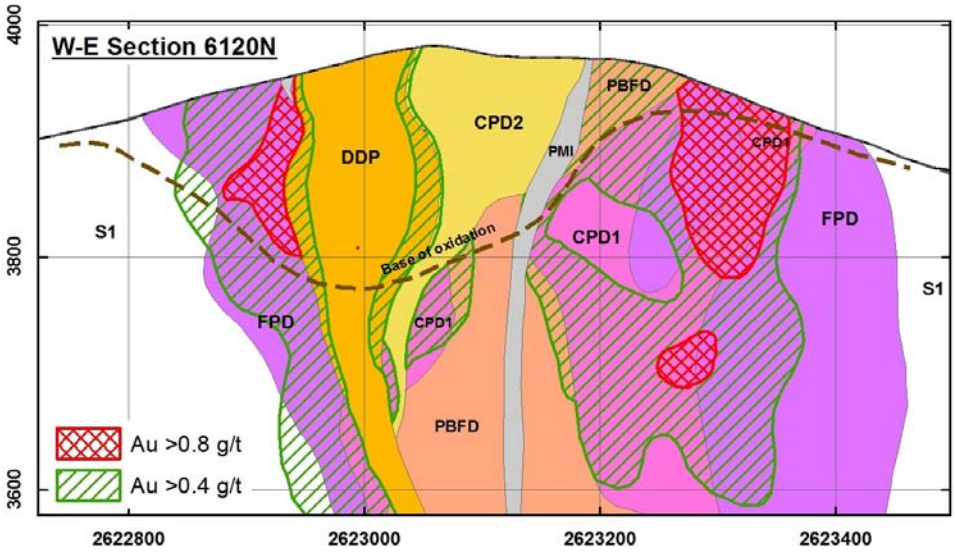

THE BORON ISOTOPIC GEOCHEMISTRY OF HYDROTHERMAL TOURMALINE FROM THE IOCG OCCURRENCES OF THE GREAT BEAR MAGMATIC ZONE, NWT, CANADA

Colter Kelly[1], William Davis, Eric Potter, Louise Corriveau

[1]*Geological Survey of Canada, 601 Booth Street Complex, Ottawa, ON K1A 0E8, Canada - colter.kelly@canada.ca*

The Great Bear magmatic zone (GBmz) is host to the only iron oxide-copper-gold (IOCG) deposits in Canada with known or indicated resources. The GBmz is a continental margin magmatic belt that formed at the western edge of the Wopmay orogen following the accretion of the Hottah terrane to the Archean Slave craton (Hilderbrand *et al.*, 2010). Many of the polymetallic deposits and occurrences of the GBmz fall within the IOCG continuum (Corriveau *et al.*, 2016) and represent a significant U resource. The source(s) of the ore- forming fluids in IOCG systems remains contentious. Current models invoke either dominantly magmatic (Tornos *et al.*, 2012) or non-magmatic (marine or terrestrial brine component; Barton and Johnston, 1996) fluid sources. Alternatively, there are hybrid models, which propose a magmatic-hydrothermal event followed by the interaction with non-magmatic brines.

Boron isotopes can be a valuable tool for evaluating the origin of fluids in IOCG hydrothermal systems, and in particular identifying contributions from marine or evaporate derived fluids. Boron is a fluid-mobile, moderately volatile lithophile element with a low atomic mass. It has two stable isotopes 10B and 11B with isotopic abundances of 19.8 and 80.2 %, respectively in nature. The large relative mass difference between the two isotopes (~10%) and the physiochemical properties of boron result in large isotopic fractionations between slightly alkaline fluids and the solid phases interacting or derived from them. The global 11B/10B ratio varies by several tens of per mil in surficial environments with non- marine evaporites having δ11B values of -27‰ whereas marine brines can be up to +55‰. Typical magmatic rocks, including arc-related magmas typically have lower δ11B values while higher δ11B values indicate a marine contribution. The strong enrichment of B in the crust and its affinity for fluid phases coupled with the significant difference in the δ11B of different geologic reservoirs make B a powerful tool for tracing hydrothermal fluids in metasomatic and ore forming processes when tourmaline (a B sink) is present as a gangue mineral (Slack and Trumbell, 2011).

Tourmaline ($XY_3Z_6(T_6O_{18})(BO_3)_3V_3W$) is chemically complex borosilicate that stoichiometrically contain 3 wt% B. The principle prerequisite for the growth of tourmaline is a source of B, therefore tourmaline often forms in chemical sedimentary and metasedimentary rocks, as well as granites derived from the melting of deeply-buried sedimentary rocks. Tourmaline can also form in crustal rocks due to the infiltration of B- bearing metasomatic fluids (Henry and Dutrow, 1996). Depending on the occurrence of the crystal and the degree of fluid rock interaction, the chemistry of tourmaline can be either rock or fluid buffered. Tourmaline is resistant to chemical diffusion and isotope homogenization, even at high pressures and temperatures, meaning that chemical and isotopic heterogeneities may be preserved up to upper amphibolite facies conditions (van Hinsberg *et al.*, 2011). The fractionation factors between tourmaline and water at high temperature, which dominate in magmatic-hydrothermal systems, are less than -2 ‰ units. Therefore, it is possible to derive robust estimates of the B-composition of the fluid from the B isotopic composition of tourmaline.

Boron isotopes in hydrothermal tourmaline from IOCG deposits has been underutilized due to the inconsistent presence of tourmaline in this deposit type. In the GBmz, hydrothermal tourmaline is present as small (>10 micron) grains in texture-preserving metasomatic alteration, breccia cement in the magmatic-hydrothermal Southern Breccia corridor, or as 10 cm to 1 m wide tourmaline-biotite-quartz-K-feldspar veins as seen at the Nori occurrences at DeVries Lake. We present data from three IOCG occurrences that represent texturally different tourmaline that formed prior to, synchronous with, and following the IOCG-related mineralization. The Tourmaline do not show significant chemical zonation and vary from schorl-dravite within samples from the Southern Breccia and DeVries Lake, with significant uvite and feruvite components around the Contact Lake showing.

Boron isotopic compositions were determined using a sensitive high-resolution ion microprobe (SHRIMP II) at the Geological Survey of Canada (Ottawa, Canada) operated at a mass resolution of ~1500, adequate to resolve BH peaks. IMF was calibrated relative to Harvard reference materials. The δ11B composition of hydrothermal tourmaline from IOCG occurrences within the GBmz is consistently between –15 and –11‰, with no major differences among the occurrences suggesting a common genetic mechanism across the belt. The δ11B values are significantly lower than seawater or marine evaporates, suggesting minimal contributions from carbonate sequences within the local stratigraphy of the Treasure Lake Group that hosts the occurrences. The negative δ11B are consistent with volcanic and plutonic sequences globally, indicating that the B within the GBmz alteration systems lacks a significant marine

component. These data contrast with data reported for tourmaline in the world class IOCG systems of the Coastal Cordillera (Chile), and the Dahongshan group (China) which have δ11B values between –10‰ and +6‰ (Tornos *et al.*, 2012) and –14‰ and +6 (Su *et al.*, 2016), respectively, as well as the Carajas Mineral Province (Brazil) which has δ11B values between +14‰ to +26‰, +6‰ to +9‰, and –8‰ to +11‰ depending on the deposit (Xavier *et al.*, 2008) Differences between deposits globally suggests that cordilleran type IOCG deposits may not form by a unique mechanism requiring exclusively a marine or evaporate derived fluid vs. a magmatic derived fluid source.

REFERENCES

Barton, M.D., Johnson, D.A., 1996. Evaporitic-source model for igneous-related Fe oxide–(REE-Cu-Au-U) mineralization. Geology, 24 (3), 259-262.

Corriveau, L., Montreuil, J.F., Potter, E.G., 2016. Alteration facies linkages among iron oxide copper-gold, iron oxide-apatite, and affiliated deposits in the Great Bear magmatic zone, Northwest Territories, Canada. Economic Geology, 111(8), 2045-2072.

Henry, D.J., Dutrow, B.L., 1996. Metamorphic tourmaline and its petrologic applications. Reviews in Mineralogy and Geochemistry, 33 (1), 503-557.

Hildebrand, R.S., Hoffman, P.F., Housh, T., Bowring, S.A., 2010. The nature of volcano- plutonic relations and the shapes of epizonal plutons of continental arcs as revealed in the Great Bear magmatic zone, northwestern Canada. Geosphere, 6 (6), 812-839.

Slack, J.F., Trumbull, R.B., 2011. Tourmaline as a recorder of ore-forming processes. Elements, 7 (5), 321-326.

Su, Z.K., Zhao, X.F., Li, X.C., Zhou, M.F., 2016. Using elemental and boron isotopic compositions of tourmaline to trace fluid evolutions of IOCG systems: The worldclass Dahongshan FeCu deposit in SW China. Chemical Geology, 441, 265-279.

Tornos, F., Wiedenbeck, M., Velasco, F., 2012. The boron isotope geochemistry of tourmaline-rich alteration in the IOCG systems of northern Chile: implications for a magmatic-hydrothermal origin. Mineralium Deposita, 47 (5), 483-499.

van Hinsberg, V.J., Henry, D.J., Marschall, H.R., 2011. Tourmaline: an ideal indicator of its host environment. The Canadian Mineralogist, 49 (1), 1-16.

Xavier, R.P., Wiedenbeck, M., Trumbull, R.B., Dreher, A.M., Monteiro, L.V., Rhede, D., Torresi, I., 2008. Tourmaline B-isotopes fingerprint marine evaporites as the source of high-salinity ore fluids in iron oxide copper-gold deposits, Carajas Mineral Province (Brazil). Geology, 36 (9), 743-746.

PB-ISOTOPE AND TRACE ELEMENTS ANALYSIS BY LA-Q-ICPMS OF GALENA FROM ARGENTINIAN EPITHERMAL DEPOSITS: A PRELIMINARY ANALYSIS

Laura Maydagán[1], Christopher McFarlane, David Lentz, Verónica Bouhier, Pablo Caffe, Ana Laura Rainoldi, Josefina Pons, María Lis Fernández, Marta Franchini, Geraldine Luna

[1]*INGEOSUR-CONICET, Departamento de Geología, Universidad Nacional del Sur, Argentina - lauramaydagan@yahoo.com.ar*

BACKGROUND

In situ laser ablation quadrupole inductively coupled plasma-mass spectrometry (LA-Q- ICPMS) allows us to obtain rapid, accurate, and precise Pb isotope measurements together with trace elements in galena (McFarlane *et al.*, 2016). Recent investigations have shown that galena can host a broader range of elements than previously recognized, many of them (e.g., Ag, Bi, Se, Te) can be extracted as by-products of an ore containing galena and others (Sb, Cd, Tl) existas impurities (George *et al.*, 2015).

Pb isotopic studies have been applied as a tool in exploration of metallogenic terrains based on comparing the isotopic compositions of existing deposits within a district to prospective showings. Bouhier *et al.* (2017) presented Pb isotopic data of the Navidad Ag world class epithermal deposit. These authors indicated that the Pb isotopic ratios of Jurassic volcanic rocks and ore minerals from epithermal deposits of Patagonia have distinctive signatures in the North Patagonian Massif, the Deseado Massif, and the Andean region that vary with time in the volcanic events of the Chon Aike Volcanic Province.

The objective of this contribution is to present new Pb isotopic data and trace elements obtained with the method LA-Q-ICPMS in galena from epithermal deposits in Argentina in order to identify patterns at regional and local scales that may be useful in exploration or exploitation.

METHODS

Samples of galena were selected from epithermal deposits of Argentina: Navidad mining district (Loma Galena, Loma La Plata and Valle Esperanza deposits, hosted by Jurassic volcanic rocks, Chubut Province, North Patagonian Massif) Virginia and La Paloma (hosted by Jurassic volcanic rocks, Santa Cruz Province, El Deseado Massif), Chinchillas (hosted by Miocene volcanic rocks, Jujuy Province, Northern Puna), and Andacollo deposit (hosted by Carboniferous and Permian volcanic rocks, Neuquén Province). Polished thin sections of galena were analyzed by the quadrupole LA-ICP-MS facility at the Department of Earth Sciences of the University of New Brunswick, Fredericton, Canada (McFarlane *et al.*, 2016).

RESULTS

Galena from Chinchillas and Andacollo yields the highest $^{207}Pb/^{204}Pb$ ratios (average values 15.631 and 15.642 Chinchillas; 15.651 Andacollo), whereas the less radiogenic $^{207}Pb/^{204}Pb$ ratios are recognized in galena from Patagonia: Virginia (15.587) and Loma La Plata (15.571-15.627).

The $^{206}Pb/^{204}Pb$ results are highest in galena crystals from Chinchillas (18.583-18.618) and Andacollo (18.497) and lowest in galena from the Navidad mining district (18.231-18.262), whereas galena from La Paloma and Virginia yield intermediate $^{206}Pb/^{204}Pb$ ratios.

Galena crystals from Andacollo and Chinchillas deposits show higher $^{206}Pb/^{204}Pb$ and $^{208}Pb/^{204}Pb$ ratios than samples of galena from Patagonia (North Patagonian and Deseado Massifs). Samples of galena of epithermal deposits from the Deseado Massif (La Paloma and Virginia) yield higher $^{206}Pb/^{204}Pb$ ratios than samples from the North Patagonian Massif (Navidad mining district).

The $^{208}Pb/^{204}Pb$ ratio is highest in galena from the Chinchillas deposit (average values of 38.750 and 38.827) and lowest in the samples from the Navidad mining district (average values of 38.203 and 38.311).

Silver is the most abundant trace element in the crystals analyzed. The highest mean concentrations of Ag were recorded in samples from epithermal Ag-rich deposits from Patagonia (e.g., Navidad 9958 ppm, Virginia 5901 ppm). In La Paloma deposit, galena has average contents of 127 ppm Ag. Samples from Andacollo deposit have mean values of Ag of 895 ppm, and two samples of galena from Chinchillas have average values of 3510 and 4471 ppm Ag.

Mean Sb concentrations in galena crystals show a wide range, from 2.7 ppm in a sample from Navidad deposit to 4412 ppm in galena from Chinchillas deposit. The highest concentrations of Bi were obtained in galena from the Andacollo deposit (mean value of 92 ppm).

Selenium concentrations vary over 3 orders of magnitude in the studied samples. Galena from La Paloma shows the highest Se contents. The highest mean Cd concentrations were obtained in galena crystals from Navidad

(262 ppm) and La Paloma (190 pmm) deposits. In Virginia, Andacollo, and Chinchillas, Cd values are very low, with mean concentrations ranging from 17 to 23 ppm. Tellurium concentrations in galena from the Andacollo deposit show a wide range of values (26 to 1060 ppm) with a mean of 150 ppm Te.

CONCLUSIONS

We present new Pb isotopic data and trace elements in galena from Argentinian epithermal deposits. The Pb isotopic data obtained allow correlate galena to geological provinces and ages. Within the Patagonia it is possible to differentiate galena from the Deseado Massif and the North Patagonian Massif according to their isotopic signatures, especially their $^{206}Pb/^{204}Pb$ and $^{208}Pb/^{204}Pb$ ratios. We suggest that these analyses could be useful to identify metallogenetic events in Patagonia and could be applied in regional mining exploration complemented with conventional exploration techniques.

Pb isotopes in galena from Chinchillas have the same signatures as the Eastern Cordillera basement domain defined by Aitcheson *et al.* (1995) and the Antofalla domain of Mamani *et al.* (2010). The similarity in isotope ratios with host volcanic rocks and regional volcanism (e.g., Caffe *et al.* 2002) suggests that Pb isotope compositions of Chinchillas ores were inherited from magmas in which the basement participates through different mechanisms (mixing of crustal and arc melts or as contaminants in AFC processes) that affect Puna backarc magma evolution (Caffe *et al.*, 2002; Kay *et al.*, 2010).

Regarding trace elements, large standard deviations recognized in Ag and Sb contents in Navidad, Virginia and La Paloma samples, are interpreted as the result of nano-inclusions of Ag mineral phases and Sb-sulfosalts in galena. The relative low standard deviations recognized in Andacollo and Chinchillas samples suggest that Ag and Sb in these crystals could be present as solid solution.

Similarly, low standard deviations in Se from La Paloma galena crystals suggests its presence in solid solution. Bismuth values show high standard deviations in all the samples consistent with the presence of sub-micron-size Bi-bearing phases. The wide range of values of Te in Andacollo deposit suggests microinclusions of telluride minerals.

REFERENCES

Aitcheson, S.J., Harmon, R.S., Moorbath, S., Schneider,A., Soler,P., Soria-Escalante, E., Worner, G., 1995. Pb isotopes define basement domains of the Altiplano, Central Andes. Geology, 23 (6), 555-558.

Bouhier,V.E., Franchini,M.B., Caffe,P.J., Maydagán,L., Rapela,C.W., Paolini,M., 2017. Petrogenesis of volcanic rocks that host the world-class Ag-Pb Navidad District, North Patagonian Massif: Comparison with the Jurassic Chon Aike Volcanic Province of Patagonia, Argentina. Journal of Volcanology and Geothermal Research, 338, 101-120.

Caffe, P.J., Trumbull, R.B., Coira, B.L., Romer, R.L., 2002. Petrogenesis of Early Neogene magmatism in the Northern Puna; implications for magma genesis and crustal processes in the Central Andean Plateau. Journal of Petrology, 43 (5), 907-942.

George, L., Cook, N.J., Ciobanu, C.L., Wade, B.P.,2015. Trace and minor elements in galena: A reconnaissance LA-ICP-MS study. American Mineralogist, 100 (2-3), 548-569.

Kay, S.M., Coira, B.L., Caffe, P.J., Chen, C.H., 2010. Regional chemical diversity, crustal and mantle sources and evolution of central Andean Puna plateau ignimbrites. Journal of Volcanology and Geothermal Research, 198 (1), 81-111.

Mamani, M., Wörner, G., Sempere, T., 2010. Geochemical variations in igneous rocks of the Central Andean orocline (13S to 18S): Tracing crustal thickening and magma generation through time and space. Geological Society of America Bulletin, 122 (1-2), 162-182.

McFarlane, C.R., Soltani Dehnavi, A., Lentz, D.R., 2016. Pb-isotopic study of galena by LA-Q- ICP-MS: Testing a new methodology with applications to base-metal sulphide deposits. Minerals, 6 (3), 96.

MAFIC MAGMA SIGNATURE FROM Co-Ni-Cu SULFIDE ON PORPHYRY Cu-Au MINERALIZATION AT THE GRASBERG DEPOSIT, PAPUA, INDONESIA

Kotaro Yonezu[1], Katsuhito Terashima, Thomas Tindell, Benny Bensaman, Mega Fatimah Rosana

[1]*Kyushu University - yone@mine.kyushu-u.ac.jp*

BACKGROUND

The Grasberg-Ertsberg district of Papua, Indonesia, hosts numerous porphyry- and skarn- type Cu-Au deposits, including the Grasberg deposit, which is one of the largest porphyry Cu-Au deposits in the world. The exposed Cu-Au mineralization at the Ertsberg, the first discovery site, was firstly recognized by a Dutch geologist in 1936 during his expedition to climb the peak of Papua (Dozy, 1939). Freeport assessed the mineralization in the 1960s, and operations commenced in 1973 (Mealey, 1996). Since then, exploration drilling identified other Cu-Au deposits in the area. The Grasberg deposit, one of the largest porphyry Cu-Au deposits in the world, was discovered at 2 km northwest of Ertsberg in 1988, and ore production at the deposit began in 1989 (Mealey, 1996). As of the end of 2011, 1062.8 million tons of ore were produced at a grade of 1.09% Cu, 1.32 g/t Au and 2.21 g/t Ag with 1331.6 million tons of remaining reserves at a grade of 0.95% Cu, 0.80 g/t Au and 3.07 g/t Ag (summarized by Leys *et al.*, 2012). Though economical open pit reserves of the deposit have generally been exhausted, there are still huge underlying Cu-Au reserves, to be mined by the block caving method from 2018. Though the world-class Cu-Au reserves of the Grasberg deposit has been paid considerable attention, the factors contributing to the huge reserves are not fully understood. As minerals suggesting presence of mafic magma, which contains a significant amount of siderophile-chalcophile elements and sulfur, were newly identified at the deposit, this study aims to examine mafic magma contributions to Cu- Au mineralization.

Samples analyzed in this study were mainly collected from two drill cores: AM30-03H-05, which cuts complex intrusive rock phases in the central part of the Grasberg igneous complex (GIC), and GRD38-09, which cuts through the GIC from the center to the surrounding limestone of the Faumai Formation in the New Guinea Limestone Group. This study focuses on the samples collected from the central part of the GIC, where porphyry Cu- Au mineralization associated with potassic alteration is dominant even though there are confirmed several different types of mineralization around outer part of GIC.

METHODOLOGY

Applied methodology in this research is microscopic observation of polished sections and double-polished thin sections to identify mineral assemblage and fluid inclusions using a polarizing microscope (NIKON ECLIPSE LV100 POL) at the Department of Earth Resources Engineering, Kyushu University. After fluid inclusion petrography using a microscope, heating and cooling experiment of the fluid inclusions for microthermometry was conducted using a Linkam heating-cooling stage (10002L) at the Department of Earth Resources Engineering, Kyushu University.

Scanning electron microscopy – energy dispersive X-ray spectroscopy (SEM-EDX) was conducted to determine chemical composition of minerals using SEM (SHIMADZU SS-550) – EDX (Genesis 2000) at the Center of Advanced Instrumental Analysis, Kyushu University. Laser ablation – inductively coupled plasma – mass spectrometry (LA-ICP-MS) is used for elemental mapping, line and spot analysis to reveal trace element distribution in Cu-Au ore and fluid inclusions using Agilent 7900 (ICP-MS) equipped with a NWR193UC laser system at the Department of Earth Resources Engineering, Kyushu University. IQuant2 was used to process the line analysis results into 2D images for elemental mapping.

RESULTS

The porphyry Cu-Au mineralization in the Grasberg Deposit is hosted by the Pliocene intrusive rocks, which intrude the Jurassic-Cretaceous siliciclastic dominated Kembelangan Group and the Lower to Middle Cenozoic carbonate dominated New Guinea Limestone Group. The central ore zone of the Grasberg deposit commonly consists of chalcopyrite, bornite, present as veinlets and disseminations, with minor covellite, digenite, rare native gold, and molybdenite. In addition to these ore minerals, merenskyite ($(Pd, Pt)(Te, Bi)_2$) and Co-Ni-Cu sulfides ($(Co, Ni, Cu)_3S_4$) were newly identified with Cu(-Fe) sulfides and native gold in this study. Though Pd, Co, and Ni mineralization is synonymous with mafic magmas, such as associated with Ni-Cu-PGE deposits, it has been known that Pd can concentrate at porphyry Cu deposits as a result of high oxygen fugacity of magma during fractional crystallization. In contrast, Co and Ni are strongly partitioned into mafic minerals in the early stage of fractional crystallization, and Co-Ni-Cu sulfides clearly indicate the presence of components directly derived from primitive mafic magma in the

ore-forming fluid. Elemental mapping and line analysis revealed that Co and Ni are concentrated in magnetite and rare siderite, which precipitated before Cu-Au mineralization, by replacing Fe. Therefore, Co and Ni are likely to be removed from hydrothermal fluid before Cu-Au mineralization. This suggests additional mafic magma between quartz-magnetite(-siderite) precipitation and later Cu-Au mineralization. Fluid inclusion petrography, microthermometry and determination results indicate the following facts: 1) Cu is contained in hydrothermal fluid since the early stage of hydrothermal activity; 2) temperature of hydrothermal fluid significantly decreased before Cu-Au mineralization from that of early hydrothermal fluid; 3) sulfur is possibly richer in late hydrothermal fluid than in early hydrothermal fluid. These results suggest the following two possible mafic magma contributions for Cu-Au mineralization at the Grasberg deposit: A) Additional mafic magma supplied sulfur and metals to the system, in which Cu could not precipitate due to lack of sulfur, and triggered Cu(-Fe) sulfide mineralization. B) Mafic magma was added to a magma chamber and triggered sulfur- and metal-rich magmatic activity forming the main Grasberg Intrusion. Cu-Au mineralization occurred as the temperature of the hydrothermal fluid decreased. Mafic magma was added to the system even during evolution of the hydrothermal fluid, supplying additional sulfur and metals.

CONCLUSION

In both scenarios, the presence of primitive mafic magma is clear, and the mafic magma must have contributed, at least partly, to the world-class Cu-Au and sulfur (as sulfide) reserves of the Grasberg deposit, Papua, Indonesia.

REFERENCES

Dozy, J.J., Erdman, D.A., Jong, W.J., Krol, G.L., Schouten, C., 1939. Geological results of the Carstensz expedition 1936. Leidse Geologische Mededelingen, 11 (1), 68-131.

Mealey, G. A., 1996. Grasberg: Mining the richest and most remote deposit of copper and gold in the world, in the mountains of Irian Jaya, Indonesia. Freeport-McMoRan Copper & Gold.

Leys, C.A., Cloos, M., New, B.T., MacDonald, G.D., 2012. Copper-gold±molybdenum deposits of the Ertsberg-Grasberg District. Papua, Indonesia: Society of Economic Geologists, Special Publication, 16, 215-235.

CHAPTER 13

HIGH-TECH CRITICAL METALS: EVALUATION AND DEPOSIT MODELS. MEETING THE RESOURCE DEMANDS OF THE LOW

Conveners: Kenzo Sanematsu, Yasushi Watanabe, Jens C. Andersen, Reimar Seltmann

THE ZINNWALD – CINOVEC Sn-Li DEPOSIT: CONSTRAINTS FOR METAL RECOVERY

Alla Dolgopolova[1], Reimar Seltmann, Robin Armstrong, Chris Stanley, Jens Andersen, Gavyn Rollinson, Beth Simons, Mirko Martín, Pavel Reichl, Vojtek Sesulka, Fernando Noronha, Violeta Ramos, Chris Broadbent, Axel Müller, Vitaly Shatov

[1]*NHM London, UK - a.dolgopolova@nhm.ac.uk*

The Zinnwald-Cínovec deposit is located in the eastern Erzgebirge/Krušne Hory area and extends across the Czech and German state border. Both parts of the deposit are currently being explored by drilling for Sn-Li vein and greisen ores, accompanied by advanced ore processing tests.

The Zinnwald-Cínovec granite hosting the world-class Sn-W-Li deposit forms an elliptical granite cupola outcropping 1.3 km in N-S direction. The W contact of the intrusion is steep, whereas the S, SE and E contact plunges with 10 to 30°. The upper part of the intrusion is formed by lithium-albite granite that is underlain by medium-grained protolithionite granite at a depth of 730 m (beneath Cínovec; Štemprok and Šulcek, 1969; Rub *et al.*, 1983). In the cupola, the lithium-albite granite consists of two textural varieties: an older porphyritic granite and a younger medium-grained seriate granite, which encloses the relicts of the porphyritic granite. Zinnwaldite is the predominant mica in the lithium-albite granite.

The lithium-albite granites (alkali feldspar granites) contain on average 0.11 wt.% $L_{i2}O$ and 4.62 wt.% K_2O. Plagioclase is absent, sodium feldspars are represented by albite with a low (<3 wt.%) anorthite content. Main accessories are cassiterite, fluorite, topaz, columbite- tantalite in addition to rare bastnaesite, uranpyrochlor, uranmicrolite, strueverite, synchisite (Johan and Johan, 1993; Rub *et al.*, 1998).

The protolithionite granite contains on average 0.05 wt.% Li_2O and 5.34 wt.% K_2O. Main accessories are zircon, columbite, monazite, xenotime and rutile. Apatite is very rare.

The low-grade Li ore is confined to zinnwaldite with substantial Rb and Cs contents. In addition, the ore contains Sn and W in cassiterite, wolframite and scheelite. Apart from this, the Sn and W concentrates contain considerable contents of Nb, Ta, and especially Sc.

The large petrographic and mineralogical variability of magmatic rocks and their alteration products is shown in Figure 1; with quartz, potassic feldspar, albite, topaz, di-/ trioctahedral micas, clays, and accessory minerals having main impact on metal recovery.

As key challenges for an optimised ore processing the following geological (petrographic, mineralogical, geochemical) and geometallurgical constraints have been identified:

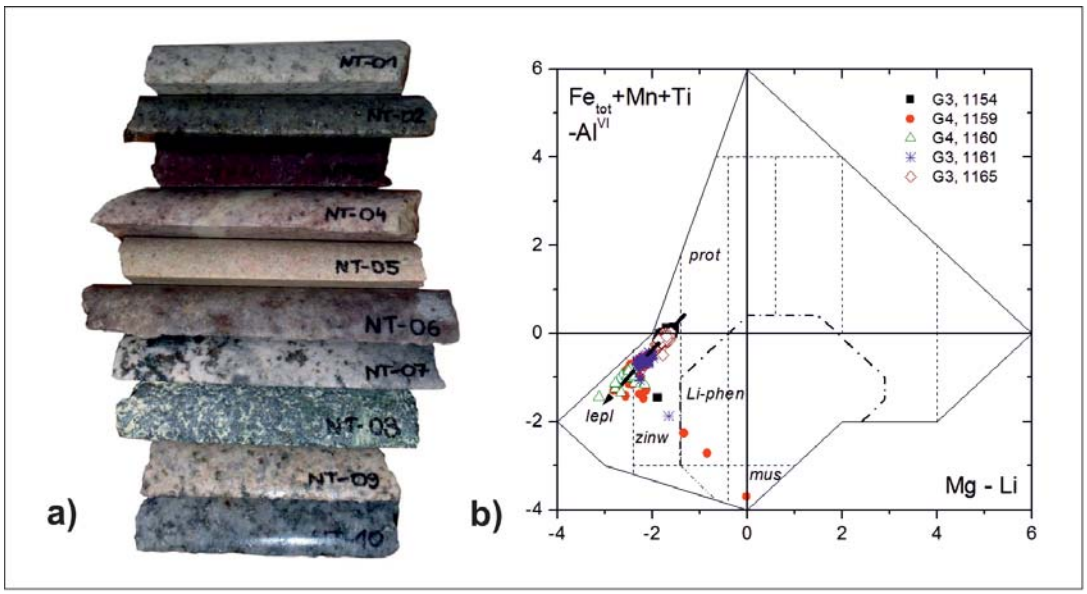

Figure 1. a) Mineralogical and petrographic variability of granites and greisens from Cínovec drill core (scale: NT-06 half core sample is 10 cm long). b) Mineralogical variability of lithium mica from Zinnwald-Cínovec: Li-Phengite - Zinnwaldite - Lepidolite (plot after Tischendorf *et al.*, 1997).

- Subhorizontal thin-layered anatomy (sheeted laccolite, alteration zones, flat ore bodies)
- Strong petrographic-mineralogical variability
- Contrasting magnetic properties of mica phases
- Variable grain size and strong Li zonation of mica

A previously neglected mineralogical parameter but important for increased by-product recovery are the elevated contents of Nb and Ta in the alkali feldspar granites (outside the Li-Sn cut-off of the greisen ore bodies). Besides that, low-temperature clayey alteration hosted in the intergranular space may potentially cause loss of Li in slimes.

The research is co-funded by the EU Horizon 2020 Project "FAME": Flexible and Mobile Processing Technologies (grant #641650). The authors acknowledge the contributions of the whole FAME project team for sample collection and preparation and scientific discussions that led to the development of this paper.

REFERENCES

Johan, V., Johan, Z., 1993. Accessory minerals of the Cínovec (Zinnwald) granite cupola, Czech Republic, part 1. Nb-, Ta, and Ti-bearing oxides. Mineralogy and Petrology, 49, 1-21.

Rub, M. G., Pavlov, V.A., Rub, A. K., Štemprok, M., Drábek, M., Drábková, E., 1983. Elements of vertical zoning in the Cinovec massif of lithium fluorine granites (Czechoslovakia), in: Correlation of magmatic rocks of Czechoslovakia and some districts of the USSR Izd. Nauka, Moskva (in Russian), pp: 108-137.

Rub, A.K., Štemprok, M., Rub, M.G., 1998. Tantalum mineralization in the apical part of the Cínovec (Zinnwald) granite stock. Mineralogy and Petrology, 63, 199-222.

Štemprok, M., Šulcek. Z., 1969. Geochemical profile through an ore-bearing lithium granite. Economic Geology, 64, 392-404.

Tischendorf, G., Gottesmann, B., Förster, H.-J., Trumbull, R.B., 1997. On Li-bearing micas: estimating Li from electron microprobe analysis and an improved diagram for graphical representation. Mineralogical Magazine, 61, 809-834.

DATA MINING FOR CRITICAL MINERALS: GERMANIUM, GALLIUM, AND INDIUM

Jane M. Hammarstrom[1], Alan Koenig, Robert R. Seal, Erin Marsh

[1]*USGS - jhammars@usgs.gov*

BACKGROUND

Germanium (Ge), gallium (Ga), and indium (In) are three mineral commodities that appear on most lists of critical minerals. Demand is expected to increase as they become more essential for advanced technologies such as manufacturing of fiber optics (Ge), integrated circuits and solar cells (Ga), and liquid crystal displays (In). As a prelude to developing assessment strategies for these by product critical minerals, several databases were examined for distributions of Ge, Ga, and In by deposit type in ore samples, tailings and mine waste, and in mineral assemblages.

Ge is produced from sedimentary zinc-lead (Zn-Pb) deposits and coal. Ga is mainly produced from bauxite and Zn ores, and In is a byproduct of copper, zinc, and tin extraction. Few minerals contain these elements as primary constituents. The enigmatic carbonate-hosted Kipushi-type deposits in Africa produced Ge in the past and host the type localities for many of these rare minerals. However, Ge, Ga, and In are all known to substitute in sphalerite and some other minerals.

In 2017, Ge was recovered from zinc concentrates at two Mississippi-Valley type deposits (MVT) at Gordonsville, Tennessee, and Pend Oreille, Washington, and at the sedimentary- exhalative (SEDEX deposit) at Red Dog, Alaska. Neither In nor Ga is produced in the U.S. currently. In the 1980s, the oxidized Kipushi-type Apex deposit in Utah produced Ge and Ga as primary products. The other Kipushi-type deposit recognized in the U.S. to date is the Ruby Creek deposit in Alaska. Indium occurs in chalcopyrite in some porphyry copper deposits in the western U.S. (Bingham, Santa Rita, Hanover) and an advanced exploration project is targeting the West Desert Zn-Cu-Fe-In skarn deposit in Utah (33 g/t In). Mineral occurrence databases for the U.S. list fewer than 50 occurrences each for Ge, Ga, or In; however, there are thousands of zinc deposits and prospects. Typical rock and ore analysis rarely report these elements, all of which can pose analytical challenges and have low average crustal abundances—Ge (1.4 mg/kg), Ga (17.5 mg/kg), and In (0.056 mg/kg) — compared with Zn (67 mg/kg). Key questions include (1) is there something special about the geologic sources in some parts of the world; (2) have we simply not analyzed deposits for these commodities; (3) do potentially economic concentrations of these commodities reside in unexpected deposit types or in tailings; and (4) are there certain zinc deposits that are more likely to host these commodities?

An understanding of the nature of critical minerals associated with zinc ores and mine wastes is important because these commodities are produced almost exclusively as byproducts. Therefore, increased production will require extraction from currently non- producing sites that have an unrecognized potential or by reprocessing existing mine waste.

METHODS

Ore sample geochemistry was compiled from the Australian Center of Exploration Targeting OSNACA database (http://www.cet.edu.au/projects/osnaca-ore-samples-normalised-to-average-crustal-abundan ce) and new USGS data for historical ore sample collections. Both datasets used internally consistent methods and represent a variety of different deposit types globally. Chemical analyses for a suite of tailings samples were collected from different deposits around the world; altered rock and soil samples associated with mineralized systems were screened for anomalous Ge, Ga, and In concentrations (https://pubs.usgs.gov/ds/433/).

A mineralogy database for ~1,400 zinc-bearing mineral deposits classified by deposit type was compiled using the crowd-sourced mineralogy database MINDAT (https://www.mindat.org/), the Mineral Resources Data System (https://mrdata.usgs.gov/), and compilations of mineralogy for individual types of mineral deposits. MINDAT contains information for nearly 300,000 localities, many of which are mine sites of known deposit type.

RESULTS AND CONCLUSIONS

For ore samples, median element concentrations for Ga, Ge, and In normalized by average crustal abundance (CA) for each element show that Gad CA for all deposit types considered. Median Ge values exceed CA for all types (> 9 times CA for MVT deposits). Median values for In exceed CA for all deposit types by a factor of 3 or more (See Figure). Other anomalous ore samples include those from the Blackbird cobalt deposit in Idaho that average about 85 mg/kg Ga; carbonatites (Zn>100 kg/mg) are enriched in Ga, Ge, and In relative to CA. Mine tailings from a diverse suite of deposit types showed similar trends where In exceeds CA for most samples but Ga and Ge values typically do not. Zn-rich mine waste soils from VMS deposits in Vermont average about 0.3 mg/kg In. Eighty-two soil samples

associated with the undeveloped Pebble porphyry copper deposit in Alaska have average concentrations of Ga (17 mg/kg), Ge (1.6 mg/kg), and In (0.06 mg/kg), or are essentially at CA.

Of the mineralogy sites that report Ge, about half of the epithermal deposits contain argyrodite (Ag_8GeS_6). Germanite ($Cu_{13}Fe_2Ge_2S_{16}$) group minerals occur in some VMS deposits; mostly in the felsic (Kuroko) subtype. Some Ge-bearing MVT deposits report the presence of bitumen or pyrobitumen. Given that Ge is an element that exhibits organophile behavior and is known to concentrate in coal, the presence of organic material may provide a clue to Ge-rich MVT deposits. Bitumen is reported in Ge-rich MVT deposits at Pine Point, Canada; Central Tennessee; SE Missouri; and many Chinese deposits. These general trends suggest that Zn-bearing deposits warrant further investigation for future critical resources.

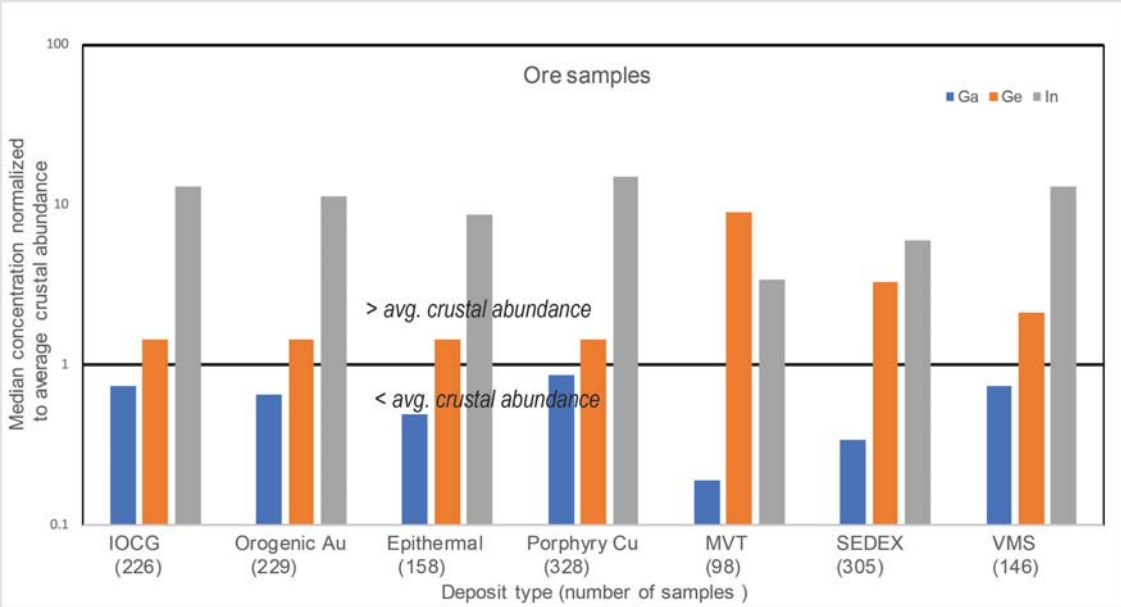

KEY ROLE IN THE FORMATION OF LITHIUM-RICH BRINE DEPOSITS: A CONSTRAINTS FROM LITHIUM ISOTOPE RATIOS

Daisuke Araoka

Geological Survey of Japan, AIST - d-araoka@aist.go.jp

Lithium (Li) is one of the critical metals and industrially important for many purposes. Especially, rapid increase of the demand for Li-ion battery leads the recent increase of production and market price of Li. There are 3 major types of Li deposits: brine, pegmatite, and sedimentary deposits. Among them, brine deposits account for more than half of identified worldwide Li resources and worldwide Li production because of low production cost. Although the origin and formation process of Li-rich brines have been studied, few studies have used Li isotope ratios to examine the ore genesis of Li-rich brine deposits.

Li isotope ratios in natural samples have been widely used for investigating various geochemical processes because the large mass differences between the isotopes of Li (16%, 6Li and 7Li) result in large isotopic variations in natural systems. Especially, Li isotopic systematics is a powerful tool for investigating water-rock interactions because of strong temperature dependence of Li isotopic fractionation between aqueous fluid and solid. For example, in the submarine hydrothermal systems, seawater-basalt interactions at high temperature condition result in light isotopic values (δ7Li: < +7‰, Araoka *et al.*, 2016) in Li- rich hydrothermal fluids because of effective leaching of Li from basalts together with little isotopic fractionation. In contrast, in the river systems, although there are large changes in Li isotopic values both over downstream and with the seasons, Li in river water is poor and isotopically heavy (δ7Li: mainly from +10 to +35‰, Manaka and Araoka *et al.*, 2017). Therefore, Li isotopes have a potential as a tool for constraining not only origin of Li but also formation process of Li-rich brine deposits. Moreover, analysis of Li isotope ratios in natural samples has become easy using automated separation of Li by ion chromatography equipped with fraction collector system (Yoshimura and Araoka *et al.*, 2018). Here, we studied two types of Li-rich brine deposits in the United States by the use of Li isotopes: one is evaporite deposit in the playas near Silver Peak Li mine, the other is geothermal brine deposit located in Salton Sea region.

There are numerous playas consisting of Li-rich salts and clay beds in the region east of Sierra Nevada. Araoka *et al.* (2014) has already reported Li isotopic compositions of evaporites and clay samples collected from 4 playas in Nevada. The results show light isotopic values (δ7Li: -1.0 to +7.9‰), which is close to the values of upper continental crusts (UCC δ7Li: +4 ± 2‰, Teng *et al.*, 2004). These results indicate that Li in these playas was supplied mainly by continental hydrothermal fluids resulting from local (e.g. Clayton Valley) geothermal activity. Moreover, preferential uptake of 6Li in clay minerals cause isotopic differences between evaporite and clay samples.

In the Salton Sea region, there are many geothermal plants and Li-rich geothermal brines have been reported. Most Sr in geothermal brine is acquired from associated sediments of ancient Colorado River, which is supported by Sr isotopic compositions of brine and sediments (Doe *et al.*, 1966). As is the case with Sr, we analyzed Li and Sr isotopic composition of 1 geothermal brine sample for tracing origin of Li. The Sr isotopic composition ($^{87}Sr/^{86}Sr$: 0.71150) is within the range of previously reported values of geothermal brine and Li isotopic composition (δ7Li: +4.0‰) shows extremely light value, indicating that most Li in geothermal brine is also derived from fluid-sediment interaction at high temperature.

In both cases, the effective leaching from rocks caused by high-temperature fluid-rock interaction results in light isotopic composition in fluid phase because the leaching of Li from rocks is strongly temperature dependent and UCC has relatively-uniform isotopic signature. Local/regional geothermal systems which prompt effective leaching from rocks can be a one of the key roles that Li-rich brine has been formed in the deposits. In fact, geothermal activities have been reported around economic Li-rich brine mines (e.g. Salar de Atacama). High content of Li in brine is preserved due to large aqueous solubility of Li even at low temperature. However, evaporation and accumulation modified contents of Li and other elements in the brine. In contrast, Li isotopic signature can be preserved in evaporite and brine in the deposits because most Li has remained in the deposits and little isotopic fractionation is expected during evaporative enrichment. Therefore, Li isotopic fingerprint is possibly good indicator for economically-important Li-rich brine deposits associated with local geothermal activity.

REFERENCES

Araoka, D., Kawahata, H., Takagi, T., Watanabe, Y., Nishimura, K., Nishio, Y., 2014. Lithium and strontium isotopic systematics in playas in Nevada, USA: constraints on the origin of lithium. Mineralium Deposita, 49, 371–379.

Araoka, D., Nishio, Y., Gamo, T., Yamaoka, Y., Kawahata, H., 2016. Lithium isotopic systematics of submarine vent fluids

from arc and back-arc hydrothermal systems in the western Pacific. Geochemistry, Geophysics, Geosystems, 17, 3835–3853.

Doe, B.R., Hedge, C.E., White, D.E., 1996. Preliminary investigation of the source of lead and strontium in deep geothermal brines underlying the Salton Sea. Economic Geology, 61, 462–483.

Manaka, T., Araoka, D., Yoshimura, T., Hossain H.M.Z., Suzuki, A., Nishio, Y., Kawahata, H., 2017. Downstream and seasonal changes of lithium isotope ratios in the Ganges–Brahmaputra river system. Geochemistry, Geophysics, Geosystems, 18, 3003–3015.

Teng, F.Z., McDonough, W.F., Rudnick, R.L., Dalpe, C., Tomascak, P.B., Chappell, B.W., Gao, S., 2004. Lithium isotopic composition and concentration of the upper continental crust. Geochimica Cosmochimica Acta, 68, 4167–4178.

Yoshimura, T., Araoka, D., Tamenori, Y., Kuroda, J., Kawahata, H., Ohkouchi, N., 2018. Lithium, magnesium, and sulfur purification from seawater using an ion chromatograph with a fraction collector system for stable isotope measurements. Journal of Chromatography A, 1531, 157–162.

THE WORLD-CLASS STRANGE LAKE REE DEPOSITS, CANADA: RADIOGENIC ISOTOPE EVIDENCE FOR THE ORIGIN OF MAGMAS AND METALS

Andrew Kerr[1], Jeff C. Pollock

[1]*Memorial University, St. John's, Canada - akerr@mun.ca*

INTRODUCTION AND SUMMARY

The Strange Lake deposits in northern Labrador and adjacent Québec in northern Canada (Figure 1) represent one of the largest potential sources for REE outside China, and are noted for strong enrichment in the heavy REE and yttrium (Y). Near-surface resources are ~60 Mt at ~ 0.9% total REE oxides in Labrador, and ~ 20 Mt at ~ 1.4% total REE oxides in Québec, and the deposits also contain substantial Zr, Nb and Be. The total resource in Québec is estimated to be > 250 Mt, but most of this is at depth and at lower grades. The depth extent of mineralization in Labrador remains undefined. Despite such favourable attributes, two attempts to develop these unique deposits have to date failed, but this in part reflects non-geological factors such as the remote location and related land-use issues. Strange Lake remains an important future contributor to global supplies of REE. Previous investigations of these deposits and their unique peralkaline granite host rocks have focused on mineralogy, and the relative roles of orthomagmatic and hydrothermal processes. This contribution assesses geochemical and radiogenic isotope data (Sm-Nd and Lu-Hf) that may constrain the origins of magmas and metals. Data imply that the main economic commodities (REE, Zr) are to a large extent of mantle origin, and that magmatic fractionation (sensu lato) dominated enrichment and ore-forming processes.

GEOLOGY AND GEOCHEMISTRY

The ca. 1240 Ma Strange Lake Intrusion (Figure 1) is a small, circular body within which three units of peralkaline granite show progressive increases in the levels of Zr, REE and other incompatible elements with the inferred intrusive sequence. The most strongly- enriched granite is associated with complex pegmatite-aplite zones that contain high-grade mineralization. The most important REE mineral is an endemic Ca-Y-REE silicate named gerenite. The mineralized granite is petrologically distinct from the other granite types, suggesting that it is not simply an altered variant of one of them. REE are correlated with other incompatible elements, consistent with expectations for magmatic differentiation processes. The similarity of REE patterns amongst granitic units is striking, but aplites and pegmatites have more varied patterns. Fine-grained, rounded melanocratic inclusions in some units resemble those commonly interpreted by petrologists to indicate physical interaction of coexisting mafic and silicic magmas.

Many evolved granites in the Strange Lake Intrusion have > 0.5% REE oxides, but the highest REE grades (locally 5% oxides or more) are in pegmatites and aplites that generally have intrusive contacts with all but the most evolved granite. The grade envelopes for economic mineralization reflect the relative proportions of pegmatite-aplite and host granite, and the background REE content of the latter. Pegmatites can be strongly enriched in heavy REE and/or depleted in the light REE, but locally may be enriched in light REE. However, mineralogical heterogeneity, large crystals and poor core recovery complicate the interpretation of pegmatite geochemistry, and the aplitic rocks generally indicate increased heavy REE contents in the late-stage magmas.

RADIOGENIC ISOTOPE DATA

Sm-Nd and Lu-Hf istopic studies used archived drill core samples of host rocks and mineralization from Strange Lake, coupled with drill-core and outcrop material from the surrounding Archean gneisses and an adjoining quartz monzonite intrusion defined by field relationships to be an older Mesoproterozoic plutonic complex.

Nd and Hf isotopic patterns are consistent with the interpreted age differences and geological relationships. The Strange Lake Intrusion and its related mineralization define a Sm-Nd age of 1248 ± 48 Ma, consistent with the 1240 ± 2 Ma U-Pb zircon age. Lu-Hf data yield a similar age estimate, but have greater uncertainty. No age information can be obtained from older rock types, in part because of limited variation in Sm/Nd or Lu/Hf. Samples from Strange Lake show greater ranges in Sm/Nd and Lu/Hf, but this is not necessarily indicative of disturbance, as the most Nd- or Sm-enriched samples are typically coarse-grained pegmatites. The consistency of pseudo-isochron behaviour argues against later disturbance of either system.

Neodymium isotope geochemistry is summarized in Figure 2. Archean gneisses have strongly negative epsilon Nd signatures (below -12) at ~ 1240 Ma, and their depleted- mantle model ages approach 2400 Ma. Samples from the older quartz monzonite unit also have negative epsilon Nd (-9) at ~ 1240 Ma, but do not overlap Archean

gneisses at the assumed time of their emplacement (~ 1420 Ma), or at any other time. Samples from Strange Lake have epsilon Nd values that range from -1.5 to -5.5 at ~ 1240 Ma, but most samples have epsilon Nd between -2.0 and -3.0 at this time. Some mineralized samples have high $^{147}Sm/^{144}Nd$, such that they yield very young model ages (50 Ma to 950 Ma) and one sample defies model-age calculation because it evolves subparallel to the depleted mantle. Despite these complications, the consistent isotopic data argue against hydrothermal disturbance of Sm-Nd isotopic systematics. The Lu-Hf isotopic system shows similar results, but epsilon Hf is less consistent.

DISCUSSION AND CONCLUSIONS

The Strange Lake deposits and their host rocks have primitive Nd and Hf isotopic signatures compared to metamorphic rocks that best represent potential deep source regions, and are also more juvenile than older Mesoproterozoic intrusive rocks. All such potential sources would have had epsilon Nd from -9 to -12 (or lower) at ~ 1240 Ma, when the Strange Lake Intrusion was emplaced. The Strange Lake parental magmas cannot be derived entirely by anatexis of older crustal rocks, and must instead contain significant juvenile, mantle-derived material. A subordinate contribution of Nd from older rocks is possible, but this is severely limited by their low REE contents. World-class REE resources hosted by the Strange Lake Intrusion are dominantly of mantle origin, although crustal sources may have contributed more of the Zr, based on some divergence in the results from Sm-Nd and Lu-Hf systems. These unusual rocks and deposits have a wealth of potential for mineralogical and geochemical research.

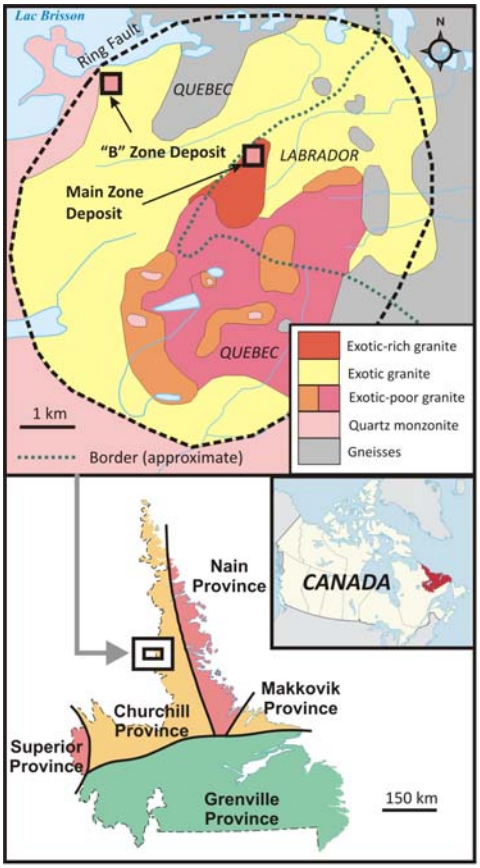

Figure 1. Location and general geology of the Strange Lake Intrusion and adjacent area, showing the main REE-Zr-Nb deposits defined to date by exploration.

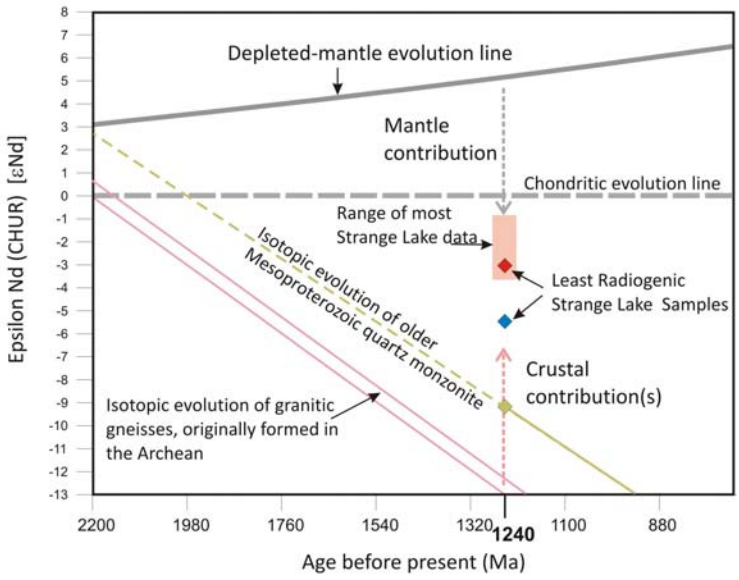

Figure 2. Summary of Sm-Nd istopic data and Nd isotope evolution for the Strange Lake Intrusion and associated REE-Zr-Nb deposits.

LITHIUM AND STRONTIUM ISOTOPE COMPOSITION OF TYPICAL SALAR DEPOSITS FROM THE SALAR DE POZUELOS, ARGENTINE PUNA: IMPLICATION FOR THE SOURCE OF LITHIUM

Simone Kasemann[1], Anette Meixner, Ricardo Alonso, Friedrich Lucassen

[1]*Faculty of Geosciences and MARUM-Center for Marine Environmental Sciences, University of Bremen, Germany*

asemann@uni-bremen.de

BACKGROUND

Evaporite basins (salars) of the Lithium Triangle in NE Chile, NW Argentina, and south of Bolivia are the host of world-class lithium-brine deposits and are an important supply for the world's rapidly increasing demand of lithium (Li). The sources of Li are the abundant Cenozoic volcanic rocks of the active magmatic arc in the Central Andes, which receive substantial amounts of their Li contents during assimilation of the Palaeozoic basement, and potentially the basement itself. Leaching of Li into aqueous fluids occurs during weathering and/or hydrothermal activity driven by arc magmatism. Fluids collect from restricted catchment areas in endorheic basins and the associated evaporitic deposits are preserved in the longstanding arid climate of the Puna-Altiplano Plateau. The Li isotope composition of the host rock is substantially changed in the course of weathering and formation of secondary minerals, whereas the strontium (Sr) isotope composition of a certain host rock type stays unchanged and provides direct information on the source, e.g. of a brine. The catchment of the Salar de Pozuelos (SdP) comprises abundant Ordovician and younger, Eocene to Miocene and Quaternary sedimentary rocks; continuous outcrops of volcanic rocks are comparable rare. The SdP is classified as a mature, halite salar. Drill cores from Li-prospection show ~90 m of halite above a more siliciclastic filling, dominated by weakly solidified clay – silt – fine sand traced down to ~180 m. We studied lithium brine and salt deposits from the SdPs' surface, and salt and clastic sediments from the drill holes for their Li and Sr isotope composition.

METHODS

Lithium isotope composition and concentration were analysed by Multi Collector Inductive Plasma Source Mass Spectrometry (MC-ICP-MS), and Sr isotope ratios by thermal ionization mass spectrometry both at the MARUM, University of Bremen, Germany. Li isotope values are given relative to NIST RM 8545 in the conventional δ^7Li (‰) notation. The sample set from SdP comprises (1) brine and salt from from the surface at different locations near the borders of the salar, salt-brine pairs from brine pools, and a hydrothermal spring with related travertine deposits, and (2) two drill cores close to the centre of the salar with salt down to ~90 m and siliciclastic sediments below ~90 m down to ~180 m, which were separated into a water soluble fraction (mainly halite 6 to 17 wt%), a clay to silt fraction, and the fine sand fraction.

RESULTS

The surface deposits compositional ranges are: brines δ^7Li 15.4 to 19.3 ‰, Li 1 to 173 µg/g, $^{87}Sr/^{86}Sr$ 0.7108 to 0.7125; salts δ^7Li 16.5 to 17.3 ‰, Li 8 to 150 µg/g, $^{87}Sr/^{86}Sr$ 0.7119 to 0.7125; hydrothermal spring δ^7Li 11.4 ‰, Li 9 µg/g, $^{87}Sr/^{86}Sr$ 0.7197 and related travertine δ^7Li 0.0 to 1.4 ‰, Li 3 to 17 µg/g, $^{87}Sr/^{86}Sr$Sr 0.7168 to 0.7247. The drill cores are: halite down to 90 m δ^7Li 16.0 to 17.0 ‰, Li 6 to 63 µg/g, $^{87}Sr/^{86}Sr$0.7139 to 0.7151; leachates (salt) 90 m to 180 m δ^7Li 16.0 to 17.6 ‰, Li 248 to 935 µg/g, $^{87}Sr/^{86}Sr$ 0.7119 to 0.7125; washed clay and silt δ^7Li -0.6 to -3.7 ‰, Li 193 to 370 µg/g, $^{87}Sr/^{86}Sr$ 0.7127 to 0.7238; washed fine sand δ^7Li -0.1 to -2.3 ‰, Li 63 to 322 µg/g, $^{87}Sr/^{86}Sr$ 0.7123 to 0.7157.

CONCLUSIONS

The large rock reservoirs at and near the outcrop level, i.e. the potential source rocks of Li in the salars, include Palaeozoic metamorphic, magmatic and sedimentary basement, the Cenozoic large volume (lv-) ignimbrite, and the Cenozoic andesite with δ^7Li and $^{87}Sr/^{86}Sr$ whole rock signatures between -4 and +2 ‰ and >0.73 up to 0.79, -4.7 and +4.7 ‰ and closely around 0.71, and -3.5 and +6 ‰ and >0.705 up to 0.708, respectively. A related study shows that the Cenozoic volcanic rocks recycle variable amounts of Palaeozoic basement and incorporate also substantial Li from this basement. The isotopic composition of the SdP's surface deposits, especially near the borders, should reflect differences related to the spatial distribution of different source rocks. During weathering (hydrothermal leaching) of silicate rocks, the heavy 7Li preferentially enters the fluid whereas light 6Li remains in the silicate minerals, e.g. secondary clay minerals, leading to higher 'heavy' respectively lower 'lighter' δ^7Li values compared to

the source rocks. All salt and brine deposits show high δ^7Li values >15 ‰ while the siliciclastic sediments, clay and silt and fine sand show all negative δ^7Li and may comprise secondary clay minerals, i.e. these signature are in accordance with the invoked process. The largest variability in δ^7Li of about 4 ‰ occurs indeed in brines and salts near the borders of SdP and may reflect differences in the source rocks or activation process of the Li from the source. In contrast, δ^7Li of salt from the halite section and leachate (water soluble fraction mainly halite) from the siliciclastic section below the halite section are very similar and uniform with a variability of 1 ‰. This indicates a homogenization of δ^7Li signatures in the long term evolution of the mobile material in SdP. The time represented by the drill core section is unknown, but should be >100 ka from comparison with dated strata from other salars (Hombre Muerto, Atacama). The contributions of the diverse source rocks to the mobile material (brine, salts) and the silicate sediments of the SdP are traced by the $^{87}Sr/^{86}Sr$. The geology of the catchment area of SdP suggests a potentially high contribution of the Ordovician sedimentary rocks with $^{87}Sr/^{86}Sr$ >0.73, but the highest contribution from his source restricts to the hydrothermal spring and related travertine. The $^{87}Sr/^{86}Sr$ of salt and brine is between 0.711 and 0.715, which points to a considerable amount of Sr from andesite and lv-ignimbrite. The lower values of this compositional range can be explained solely by a lv-ignimbrite source and the somewhat higher ratios by some Ordovician additions. The $^{87}Sr/^{86}Sr$ composition of the clay and silt fraction of the SdP sedimentary rocks supports the idea of low contributions from the Ordovician. The $^{87}Sr/^{86}Sr$ of the clay and silt fraction is somewhat higher as in the fine sand fraction of the same sample, which is expected from the enrichment of detrital mica. However, Early Palaeozoic micas have high $^{87}Sr/^{86}Sr$ >>0.73 (the lower whole rock ratio) and even small additions have a large effect on Sr isotope signatures, which is not seen. We conclude that the dominant source of all SdP deposits is lv-ignimbrite.

THE LITHIUM TRIANGLE OF THE CENTRAL ANDES: A VIEW FROM LITHIUM CONCENTRATIONS AND ISOTOPIC COMPOSITION OF POTENTIAL SOURCE ROCKS

Friedrich Lucassen[1], Anette Meixner, Raul Becchio, Carisa Sarchi, Simone Kasemenn

[1]*Faculty of Geosciences and MARUM-Center for Marine Environmental Sciences University of Bremen, Germany*

lucassen@uni-bremen.de

BACKGROUND

Lithium has rapidly advanced to a strategic commodity for energy storage in all kind of mobile devices and growing electro mobility, contributing to future low carbon societies. The Central Andes host world-class Li-deposits in endorheic evaporite basins (salars). The deposits are geographically bound to the so called Li-Triangle between the southern Bolivian Altiplano, the Argentine Puna, and its western slope in Chile. Lithium is mobilized from its host rocks during weathering or hydrothermal leaching, preferentially from igneous rocks and possibly from Li-enrichments in melt inclusions. In the (semi) arid climate, the run off collects and concentrates in the evaporite basins. The reasons for the restriction of the Li-anomaly to the Lithium-Triangle remain largely unknown. We investigate the Li concentration and Li isotope composition in mainly Early Palaeozoic metamorphic and sedimentary rocks (hereafter the basement) of the Central Andes and follow the trace of the Li in the hybrid Cenozoic magmatic rocks, which recycle variable amounts of the basement. The protoliths of the basement in the Argentine Puna are Neoproterozoic to Early Cambrian rocks, regionally known as the sedimentary Puncoviscana Formation, which origins from Proterozoic protoliths.

METHODS

Lithium isotope composition and concentration were analysed by Multi Collector Inductive Plasma Source Mass Spectrometry (MC-ICP-MS) at the MARUM, University of Bremen, Germany on previously published and geochemically well characterized whole rock sample sets of the metamorphic and magmatic basement, Cenozoic andesite and large volume ignimbrite, and Cenozoic basaltic andesite from the current back arc. The samples cover the Puna - Altiplano plateau between ~26.5 and 21.5° S. Li isotope values are given relative to NIST RM 8545 in the conventional δ^7Li (‰) notation.

RESULTS

The basement rocks show δ^7Li values between -4 and +2 ‰ (n=13) with 9 samples < 0.0 ‰ and Li concentrations mainly between 20 and 50 µg/g. The average Li signature of the basement is thus slightly higher in concentration and lighter in isotope composition compared to the general upper continental crust. The $^{87}Sr/^{86}Sr$ of the basement is mainly >0.73 up to 0.79. The Cenozoic volcanic rocks show variable assimilation of basement in their $^{87}Sr/^{86}Sr$ isotope signatures, which is highest in the large volume ignimbrite and much lower but similar in both, andesite and basaltic andesite. The different types of volcanic rocks comprise some samples with δ^7Li of +4 to +5 ‰, which is within the compositional range of average Mid Ocean Ridge Basalts (MORB). Li concentrations (~10 to 20 µg/g) of these samples are, however, higher than average MORB. We define an empirical baseline composition for Cenozoic volcanic rocks at δ^7Li of +4 to +5 ‰ and a Li concentration of 10 µg/g. The baseline represents the composition of the magma from the subduction system without substantial addition of the basement. The andesite younger than 1.5 Ma, large volume ignimbrite, and basaltic andesite evolve from this baseline composition and show a negative linear covariation between Li concentrations and δ^7Li towards and into the field of basement compositions. Large volume ignimbrite and basaltic andesite show also a covariation of increasing $^{87}Sr/^{86}Sr$, as an indicator of crustal assimilation, and decreasing δ^7Li.

CONCLUSIONS

The Cenozoic volcanic rocks of the Central Volcanic Zone (CVZ) that cover vast areas in the studied section of the Andean arc show a clear relationship between Li contents and δ^7Li towards the composition of the basement. A comparison of Li contents of the CVZ volcanic rocks with Li contents of volcanic rocks from the Southern Volcanic (SVZ) and Northern Volcanic Zones (NVZ) shows that the Li contents in the CVZ is higher. Furthermore, Li enrichment in the SVZ and NVZ volcanic rocks is related to magmatic fractionation, starting from basalts with low Li contents toward rhyolites with high Li contents. In contrast, Li enrichment in the CVZ is related to assimilation of basement which blurs the fractionation trend. We hypothesize that the regional Li-anomaly of the Lithium Triangle is fostered by the recycling of basement by the abundant young volcanic rocks. These rocks make the Li easily accessible to leaching, e.g. during weathering of Li-rich melt inclusions described from such rocks. The extent of the Lithium

Triangle is limited (1) by the extent of the specific basement that includes several periods of reworking in its long history; the western extent of this basement coincides roughly with the western border of the Plateau, but it extents east and south of the Puna Plateau, and (2) by the distribution of favourable conditions for evaporite formation such as arid climate and endorheic basins, and Li- enrichment of brines from leaching (weathering) of young, Li-rich volcanic material. If one of the conditions is not met, evaporites are not enriched in Li (e.g. in the Chilean Pre- and Coastal Cordillera).

EVALUATION OF CRITICAL METAL COMPOSITION OF GEOLOGICAL SAMPLES USING LASER ABLATION ICP-MS

Yoshiaki Kon[1], Takaomi D. Yokoyama

[1]*Geological Survey of Japan, AIST - yoshiaki-kon@aist.go.jp*

One of the basic petrological descriptions is the determination of major and trace element abundance as whole-rock chemical composition, as well as the analysis of mineral modal composition. The whole rock chemical composition provides important key information to understand petrogenesis of igneous rocks. Because of its rapidness and simplicity in analytical procedures for igneous rock samples, X-ray fluorescence (XRF) analysis of glassbeads have been widely used to determine whole-rock chemical composition of major elements. For the linearity of calibration lines, and to ensure complete sample decomposition, 1:10 (rock: flux) glassbeads are commonly used.

For trace element analysis, XRF analysis using pressed powder-pellets or low dilution-ratio (c.a. 1:2 to 1:5) glassbeads has commonly been employed. In this case, however, it takes long time for the analysis (c.a. 20 min/sample), and also need to take time for making another glassbeads or powder pellets. Furthermore, the analytical accuracy for rare earth element (REE) is generally unacceptable for geochemical studies, because of insufficient analytical sensitivity.

In order to achieve precise elemental analysis of trace elements including REE, more sensitive analytical methods such as solution ICP-MS technique have to be used. The measurements by solution ICP-MS is highly accurate, and the auto-sampler provides us rapid analysis (c.a. 2 min/sample). However, highly complicated and time consuming procedures for chemical decomposition and separation are required. Oxide interference causes problems for the analysis of several elements, such as Sc, Zn and Eu. Moreover, great care must be given for incomplete decomposition of refractory minerals.

To overcome the issues above, laser-ablation sample introduction technique has been employed for the geochemical analysis of trace elements. Previous studies have reported that whole-rock chemical analysis by laser-ablation ICP-MS (LA-ICPMS), using powder pellets, fused glass and low dilution-ratio (c.a. 1:2 to 1:5) glassbeads. In case of powder pellets, the analytical uncertainty in REE abundance of an igneous rock is up to 20% (RSD) caused by the effect of elemental inhomogeneity in a powder pellet. Since the fused glasses, which are entirely made of rock powder, are intrinsically more homogeneous in mafic rocks, erroneous measurements caused by possible sample heterogeneity can be minimized. However, the inhomogeneity of felsic-rock samples are still remains in this fused-glass method, because felsic rocks commonly include refractory minerals such as zircon and monazite, and their melt is highly viscous. The low dilution-ratio glassbeads, which are made of lithium tetraborate flux and rock powder, can easily be homogenized even in the felsic rocks. However, these methods still require additional sample preparation only for the trace-element analysis. Abundances of the internal standardization elements (e.g., Si, Ca, or Sr) are separately measured by XRF analysis. Thus, the precision and accuracy of the abundance values of the analytes can be affected by the reliability of the abundance data for the internal standardization elements obtained by XRF.

In this study, we employed a different internal standardization correction technique. We calibrated the abundance values of the analytes based on internal standardization with Li, obviating the use of internal standardization elements whose abundance values are separately obtained by another analytical technique. By using both an internal standardization protocol with Li and fused glass bead laser-ablation with femtosecond lasers, we then successfully determined abundances of 10 major and 34 trace elements in 34 GSJ geochemical reference samples. The data presented here demonstrate clearly that the combination of Li normalization and the femtosecond-LA-ICP-MS (fsLA-ICP-MS) technique has potential as a powerful and rapid analytical tool for simultaneous measurement of major and trace elements present in concentrations ranging from wt% to ppb.

Before the elemental analysis, glass beads were prepared by mixing each sample with a high-purity alkali flux with a 1:10 mixing ratio. The abundances of the major and trace elements were externally calibrated by using glass beads containing the major and trace elements prepared from six geochemical reference materials (AGV-1, AGV-2, BCR-1, BCR-2, BHVO-2 and DTS-1) distributed by the United States Geological Survey (USGS).

Abundances of most major elements in the 34 GSJ geochemical reference samples were consistent with previously reported values. We rigorously tested the reliability of the trace- element abundance data against the data obtained from JB-1, JB-1a, JA-1, and JA-2, because the trace-element abundances of these reference samples were recently re-compiled. All trace-element compositions of these reference samples were consistent with the reference values, suggesting high reliability of the fsLA-ICP-MS analytical technique. Typical analysis repeatabilities for the GSJ geochemical reference samples were better than 3% for SiO_2, Al_2O_3, Na_2O, and K_2O; <5% for TiO_2, total Fe_2O_3, MnO, MgO, CaO, P_2O_5, V, Cr, Co, Ni, Rb, Sr, Y, Zr, Nb, Cs, Ba, La, Ce, Pr, Nd, Sm, Eu, Gd, Tb, Dy, Ho, Er, Tm, Lu, Hf, Ta, Th, and U; and <9% for Sc, Cu, Zn, Sn, Yb, and Pb. These data clearly demonstrate that high analytical

A | 134

DO GEOTHERMAL SYSTEMS PLAY A ROLE IN LITHIUM BRINE ENRICHMENT IN PLAYA ENVIRONMENTS?

Catherine Hickson[1], Mark Coolbaugh, Beatriz Coira

[1]Dajin Resources Corp. - cathie@dajin.ca

Exploration for economic deposits of lithium to be processed for use in batteries to power electric vehicles has become supercharged in the past few years. Numerous companies have entered the race to identify resources and many are focused on potential brine deposits within the internally drained basins that make up the Andean Puna (Altiplano) region of Argentina, Bolivia, and Chile, as well as the Basin and Range region of the western United States (Nevada and Utah in particular). It was at Albemarle's Silver Peak mine in Clayton Valley, Nevada where the evaporation pond technology to extract lithium was developed, and where lithium values during initial phases of production were as high as 600 mg/l. In South America the concentrations in various salars varies significantly. Values range from less than 100 mg/l to over 1,500 mg/l, with a similar variability in the concentration of magnesium and other contaminants. The question remains as to why such a variability exists. In general, lithium brine deposits require a specific set of geological and climatological factors: 1) a source of lithium, 2) a natural extraction mechanism, 3) a transport mechanism, 4) a trap (closed basin), 5) a suitable solar evaporation rate, and 6) scale (mass flux of lithium and limited dissolved salt competition).

Geothermal fluids are spatially associated with many lithium brine resources around the world (e.g., Clayton Valley, Nevada; Quaidam Basin, China; Atacama Salar, Chile; Salinas Grandes, Argentina). Thermal groundwater may contribute to more efficient and selective extraction of lithium from basin sediments and basement rocks; they may help transport the enriched fluids due to thermal upwelling; and finally provide long term mass flux that over sufficient time leads to significant endowment in basins. The basins of western Nevada have many of these prerequisites, but are dominated by clastic sediments and have relatively high subsidence and sedimentation rates. For these reasons it is likely that lithium-enriched brines are deeper than in the mature basins of South America. Since few basins in Nevada have had deep drilling, paleo-brines may remain to be discovered at depths not yet investigated by exploration companies. The variability in lithium endowment between basins in South America is likely related to the first three factors listed above – source, extraction and transport, with additional variability related to the robustness of the geothermal systems in the various basins.

GEOCHEMICAL CHARACTERISTICS OF ION-ADSORPTION REE ORES IN ASIA: IMPLICATIONS FOR EXPLORATION

Kenzo Sanematsu[1], Yoshiaki Kon

[1]*Geological Survey of Japan, AIST - k-sanematsu@aist.go.jp*

BACKGROUND

Rare earth elements (REE) consist of light REE (La – Eu) and heavy REE (Gd – Lu plus Y), and they are mined from carbonatite-related deposits and ion-adsorption type deposits, respectively. The ion-adsorption type deposits typically consist of weathered granites on calcalkaline granite or alkali granite and REE grades are much lower (up to 6500 ppm REE) than carbonatite ores. However, ion-adsorption ores typically contain more than 50 % ion-exchangeable REE relative to whole-rock REE content (Bao and Zhao, 2008; Sanematsu and Watanabe, 2016). Because of the REE extractable by dilute electrolyte solution and enrichment of HREE, the low-grade ores can be economically mined.

Ion-adsorption ores are found in presently temperate or tropical regions and they are weathered enough to break down the primary REE-bearing minerals and to produce clays (e.g., kaolinite) that can be adsorbent of REE^{3+} ions. The occurrence of weatherable REE- bearing minerals is important because the resistance to chemical weathering is variable between different minerals. The weatherable minerals including REE fluorocarbonates, allanite and titanite are considered the source for ion-exchangeable REE.

In a weathering profile, REE^{3+} ions move downward and are adsorbed on the surface of clays. Near the surface of the weathering profile, Ce^{3+} is mostly oxidized into Ce^{4+} due to oxidizing conditions and is incorporated into cerianite (CeO_2) and Mn oxides. As a result, the weathering profile of the deposits can be divided into a REE-leached zone in the upper part of the profile with a positive Ce anomaly, and a REE-accumulation zone including ion-adsorption ores in the lower part of the profile with a negative Ce anomaly (Sanematsu and Watanabe, 2016).

Weathered granites with Ce anomalies are not uncommon in the temperate and tropical regions, however, promising ion-adsorption type ore bodies are rarely found outside of southern China. We analyzed whole-rock chemical compositions of weathered granites and ion-exchangeable REE concentrations in order to constrain geochemical characteristics of ion-adsorption REE ores.

METHODS

Weathered granite samples were collected from outcrops of granite areas of Thailand, Laos, eastern Myanmar and southern China (Dingnan County). Parent rocks are mostly biotite granite and muscovite-biotite granite and are characterized by ilmenite-series I-type and S- type features. The samples were dried at room temperatures and crushed by a jaw crusher. Individual ~50 g fractions of the crushed samples were pulverized using a rod mill with alumina containers and rods for 3 min. Pulverized samples were mixed with lithium tetraborate flux for whole-rock chemical analyses. The sample mixture was fused at 1250°C in a Pt crucible using a high-frequency fusion instrument, and cooled on a Pt disk. Major elements in the glasses were analyzed by X-ray fluorescence Spectrometer. Calibration curves were established using the GSJ geochemical reference samples of igneous rock series.

Trace elements and fluorine were analyzed by ALS and Activation Laboratories Ltd., Canada. The powdered samples were mixed with a flux of lithium metaborate and/or tetraborate and fused in an induction furnace. The fused sample was poured into a NHO_3 solution with an internal standard and they mixed until completely dissolved. Element concentrations of the sample solution were analyzed by inductively coupled plasma mass spectrometry (ICP-MS).

The REE extraction experiments and solution ICP-MS analysis were conducted to determine concentrations of ion-exchangeable REE. A 1 g powder of weathered granite was soaked in 40 ml volume of 0.5 mol/l ammonium sulfate [$(NH_4)_2SO_4$] solution of pH = ~5.7 in a 50 ml centrifuge tube. The tubes were mechanically shaken at room temperature for 24 h. The extract is separated from the solid samples by centrifugation. The supernatant solution was filtered by using a membrane filter (ö = 0.22 Mm), and the filtered solution was acidified using HNO_3 and kept in a polypropylene container. Ultra-pure water and internal standard were added to the sample solutions.

Element concentrations were determined by Agilent Technologies 7500cx ICP-MS. Flow rates of carrier gas and the ion-lens setting of the ICP-MS were optimized to maximize the signal intensity of Ce and to minimize the oxide production rate ($^{232}Th16O/^{232}Th < 0.01$). Calibration lines were made by multi-element standard solutions including REE.

RESULTS AND DISCUSSIONS

Results of chemical analyses show that REE contents of weathered granites range from 30 to 3828 ppm and concentrations of ion-exchangeable REE range from 0.2 to 1339 ppm (Sanematsu *et al.*, 2009; 2015; 2016). A wide range of these values result from REE contents of parent granites controlled by the degree of partial melting of magma and from the degree of chemical weathering (these weathered granites were sampled both from REE-leached zones and REE-accumulation zones). Percentages of ion-exchangeable REE concentrations relative to whole-rock REE contents range widely from 1 to 93.7 % and have a negative positive correlation with Ce anomalies of weathered granites (Fig. 1a). This correlation is explained by removal of REE^{3+} ions (depleted in Ce^{3+}) from REE-leached zones and subsequent adsorption of REE^{3+} ions onto clays in REE-accumulation zones. Weathered granites with a negative Ce anomaly less than 0.4 may have sufficient ion-exchangeable REE (Fig. 1a). Thus, Ce depletion indicated by whole-rock Ce anomaly is a good indicator of ion- adsorption ores.

Whole-rock P_2O_5 contents of weathered granites are considered most available between major elements because REE are generally contained in phosphate minerals (e.g., monazite, rhabdophane and florencite) in weathered granites. In this study, we compared ion- exchangeable REE of P_2O_5-poor granite area dominated by I-type granites and P_2O_5-rich granite area dominated by S-type granites.

Weathered granites underlain by P_2O_5-poor granites tend to have higher percentages of ion- exchangeable REE (Fig. 1b). Weathered granites with more than 50 % of ion-exchangeable REE are characterized by low P_2O_5 contents (<~0.1 %). In the P_2O_5-rich weathered granites, REE are presumably contained in phosphate minerals resistant to chemical weathering. This result suggests that whole-rock P_2O_5 content of weathered granites can be used as a geochemical indicator of ion-adsorption ores.

REFERENCES

Bao, Z., Zhao, Z., 2008. Geochemistry of mineralization with exchangeable REY in the weathering crusts of granitic rocks in South China. Ore Geology Review, 33, 519–535.

Sanematsu, K. Watanabe, Y., 2016. Characteristics and Genesis of Ion-Adsorption Type REE Deposits, in: Rare and Critical Elements in Ore Deposits, Reviews in Economic Geology, 18, pp. 55-79.

Sanematsu, K., Murakami, H., Watanabe, Y., Duangsurigna, S., Vilayhack, S., 2009. Enrichment of rare earth elements (REE) in granitic rocks and their weathered crusts in central and southern Laos. Bulletin of Geological Survey of Japan, 60, 527–558.

Sanematsu, K., Kon, Y., Imai, A., 2015. Influence of phosphate on mobility and adsorption of REEs during weathering of granites in Thailand. Journal of Asian Earth Sciences, 111, 14-30.

Sanematsu, K., Ejima, T., Kon, Y., Manaka, T., Zaw, K., Morita, S. Seo, Y., 2016. Fractionation of rare-earth elements during magmatic differentiation and weathering of calc-alkaline granites in southern Myanmar. Mineralogical Magazine, 80, 77-102.

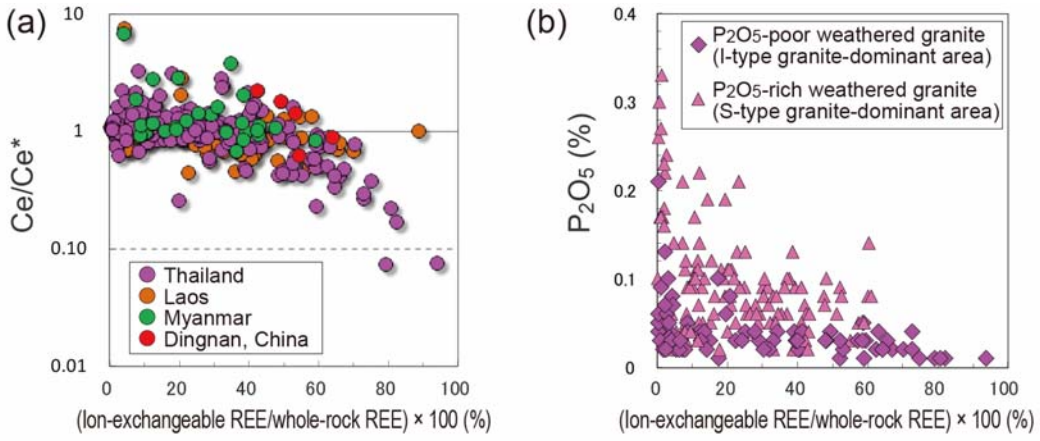

Fig 1 (a) Plots of Ce anomaly ($Ce/Ce^* = Ce_N/(La_N \cdot Pr_N)^{1/2}$) versus percentage of ion-exchangeable REE relative to whole-rock REE of weathered granites (Sanematsu and Kon, 2013; Sanematsu et al, 2009; 2015; 2016). (b) Plots of P_2O_5 content vursus percentage of ion-exchangeable REE relative to whole-rock REE of P_2O_5-rich and -poor weathered granites in Thailand (Sanematsu et al., 2015). Subscript of N indicates normalization by chondrite values.

MULTI-STAGE ALTERATION AND MULTIPLE FLUID INPUTS FOR THE PALEOPROTEROZOIC JUOMASUO, HANGASLAMPI AND HAARAKUMPU COBALT (-Au-REE) DEPOSITS OF THE KUUSAMO SCHIST BELT, FINLAND

Walter K. Witt[1], A. Davies, S. G. Hagemann

[1]*Centre for Exploration Targeting, University of Western Australia - wittww@iinet.net.au*

The Juomasuo, Hangaslampi and Haarakumpu Co-Au(-REE) deposits are advanced to preliminary resources in the Paleoproterozoic metasedimentary rock-dominated Kuusamo Schist Belt, in Finland. Previous geochronological data from Juomasuo and Hangaslampi indicate that hydrothermal monazite formed in these deposits at ca 1.8 Ga, coincident with the 1.9-1.8 Ga Svecofennian Orogeny and formation of the Central Lapland Granitoid Complex, although no felsic to intermediate intrusions are known in the deposit areas. The regional metamorphic setting is mid- to upper greenschist facies, based on regional and local petrological studies. The syn-metamorphic mineral deposits are flattened pipe-like structures in fold hinges related to the F2 Kayla-Konttiaho Antiform. However, the diverse mineralization is the product of several successive hydrothermal events: pre-metamorphic albitisation (+uranium?), F1 biotite-albite alteration controlled by F1 fold hinges (+REE), F2 chlorite alteration (+Co) controlled by F2 fold hinges, and late-F2 muscovite alteration (+Au) controlled by ductile shear zones in axial planes of the F2 fold hinge. Late-to post-F2 static metamorphic recrystallization produced neoblastic amphibole and may have produced CO_2 and S resulting from decarbonation and desulfidation reactions, especially in the central parts of the ore bodies.

The main stage of cobalt enrichment was during chlorite alteration, the products of which typically contain 5-30% sulfides, predominantly pyrrhotite, accompanied by minor chalcopyrite, diagenetic pyrite and idioblastic pyrite. The hydrothermal ore fluid leached Co from altered and metamorphosed ultramafic rocks, which are interleaved with altered albitites, and deposited it in chlorite alteration zones as minor components of Fe sulfides. Microprobe analyses show that pyrrhotite contains 0.2-0.6% Co, and idioblastic pyrite contains up to 3% Co. Gold mineralization associated with muscovite alteration is concentrated in ductile shear zones and resembles orogenic gold, except for the low carbonate component of the alteration assemblage. Cobalt is depleted in the ductile shear zones. Muscovite alteration extends beyond the ductile shear zones into adjacent, typically chlorite-altered wallrocks. Cobalt from the ductile shear zones was mobilised into the adjacent wallrocks to combine with As from the auriferous hydrothermal fluid and form cobaltite. Cobaltite is also found in chlorite-altered rocks that lack muscovite but, because of proximity to auriferous ductile shear zones, were also exposed to the auriferous fluid through addition of As and Co.

Possible sources of the successive hydrothermal fluids at Juomasuo and Hangaslampi are basinal fluids exposed to evaporitic sedimentary rocks (albitisation), magmatic fluids related to intrusions of the Central Lapland Granitoid Complex (biotite alteration and REE mineralization), metamorphic fluids (chloritisation and main introduction of sulfides and cobalt), and a deeply-sourced orogenic fluid (gold, arsenic and upgrading of pre-existing cobalt concentrations), but further studies are required to better constrain these sources. The Haarakumpu (Co-Cu) deposit, located 30 km northwest of Juomasuo and Hangaslampi, is hosted by mid to upper amphibolite facies metasedimentary rocks. The Co-Cu lode is a shallowly-dipping structure interpreted as a metamorphosed shear zone (the granofels unit in Figure 1). The interpreted pre-metamorphic hydrothermal alteration zoning at Haarakumpu displays some similarities to that observed at Juomasuo and Hangaslampi, although Au and REE mineralization is relatively minor at Haarakumpu. The proximal mineral assemblage at Haarakumpu typically contains K-feldspar (microcline) and sulfides (mainly pyrrhotite and chalcopyrite), with variations in the abundance of biotite, diopside and actinolite. Ore textures include a well-developed granoblastic fabric with widespread 120° triple point grain boundaries and sulfides interstitial to silicate minerals. Metamorphic olivine-bearing units locally indicate the presence of ultramafic rocks in the ore environment.

Metamorphosed distal alteration at Haarakumpu extends for tens to hundreds of meters around the lodes and comprises biotite-plagioclase (albite?) and biotite-actinolite (±plagioclase) gneiss (Figure 1). These assemblages may represent metamorphosed equivalents of biotite and chlorite alteration at Juomasuo and Hangaslampi. Widespread calc-silicate gneiss with abundant diopside is interleaved with the biotite (±actinolite) gneisses, particularly in the hanging wall, and may represent a metamorphosed quartz- dolomite alteration halo. These rocks are cut by numerous late-stage, but variably deformed, granitic to pegmatitic dikes, many with accessory specular hematite, that probably formed by partial melting of the sequence under oxidising conditions. Hematite dusting of the biotite-actinolite gneiss unit appears to be spatially related to these dikes.

Tremolite and talc are strongly oriented in retrograde shear zones, within both the lode and its hydrothermally altered country rocks.

Despite the low Cu content of the Juomasuo and Hangaslampi deposits, they display many characteristic features of the sediment-hosted Co-Cu-Au class, for which proximity to mafic –ultramafic rocks (as a source of cobalt) may be a critical component. A critical difference with the classic example of sediment-hosted Co-Cu-Au, the Idaho Cobalt Belt (ICB), is that cobalt is associated with hydrothermal biotite in the ICB. Other examples with many similarities to Juomasuo and Hangaslampi include Mount Cobalt and Mount Elliot in the Eastern Succession of the Mt Isa region, Australia, the Scadding and Cobalt Hill deposits, Ontario, and the NICO district of the Great Bear Magmatic Zone, both in Canada, and the Bou Azzir deposit, Morocco. The amphibolite-hosted Sin Quyen IOCG deposit in Vietnam may be an analogue of Haarakumpu. In this class of deposit, the overprinting gold event may be critical in upgrading cobalt concentrations to economic values, as at Juomasuo and Hangaslampi. District-scale albitisation is a common feature of these deposits and may be critical in providing a rheological contrast with metamorphosed mafic-ultramafic rocks and focussing hydrothermal fluids into sites of low mean stress such as fold hinges.

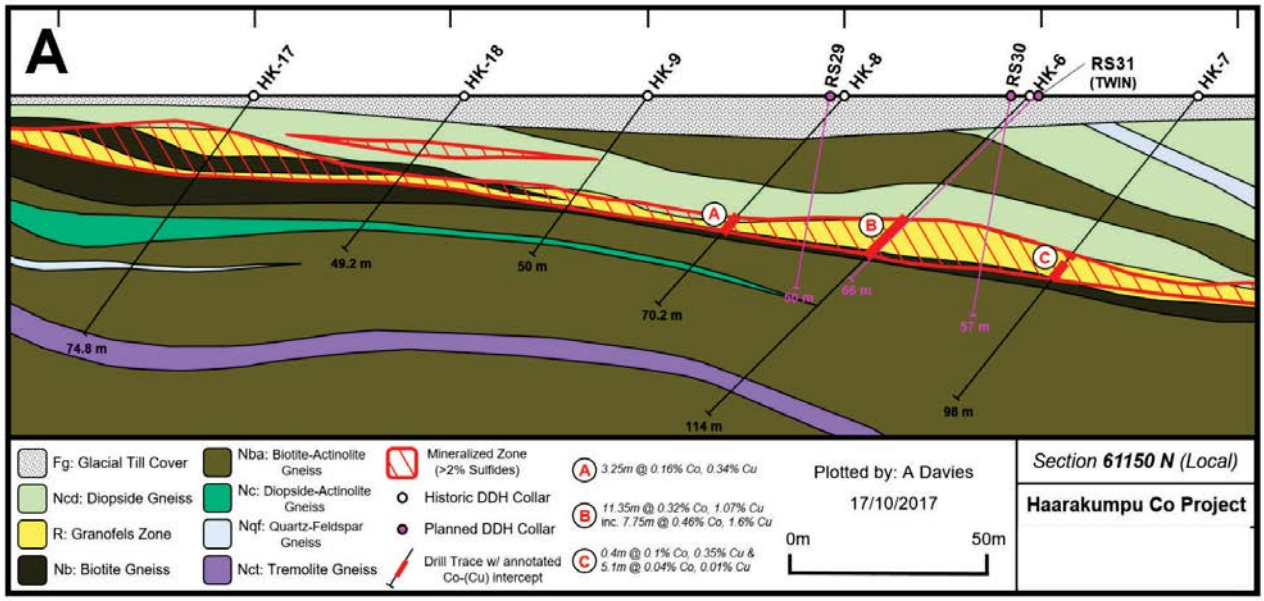

Figure 1. Schematic model of hydrothermal alteration zoning, and metal grades, around the Juomasuo and Hangaslampi Co-Au(-REE) deposits.

COBALT: PERSPECTIVES ON FUTURE RESOURCE SUPPLY

Richard Herrington[1], The CoG3 Research Team

[1]*Natural History Museum - r.herrington@nhm.ac.uk*

Cobalt is a metal associated with modern technologies with the Li-ion battery industry using around 42 percent of global cobalt production ("No Cobalt, No Tesla"). Of the battery metals, Co appears to have the tightest supply and demand fundamentals. Over 95 percent of the world's primary cobalt comes as a by-product of nickel or copper mining. Furthermore, 55% of that by-product production is located in the DRC, some of which is linked to unethical mining practices.

The recent price hike for cobalt suggests that we are already witnessing an increased scarcity of cobalt supply. Mines producing complex arsenide ores in Morocco are the only primary cobalt producers so an added pressure to supply may be that the price of copper and nickel has been dropping to their current six-year lows, making some of the mines traditionally supplying by-product cobalt uneconomic. In the short term at least, with a growing cobalt market, new resources are needed to secure the supply.

In absolute terms, the planet's cobalt resources are more than adequate, for example the deep ocean manganese nodules are estimated to contain more than 120 million tonnes of cobalt, yet imminent supply from these sources is unlikely. As a result, industry has turned to seeking terrestrial cobalt in a range of neglected deposit types such as those related to arsenides. There is also the realization that by changing recovery strategies in existing operations, by-product cobalt production could be increased.

This talk will highlight the ongoing results of a research project CoG_3, funded through the UK's NERC SoS Minerals programme that is focused on the geology, geomicrobiology and geometallurgy of cobalt deposits with the aim of increasing recovery of cobalt from the diversity of natural deposits http://www.nhm.ac. uk /our-science/our-work/sustainability/cog3-cobalt-project.html. This talk will integrate results emerging from this research with work by other groups where it is shown that, simple changes to processing methods could extract more cobalt currently lost at existing or dormant operations, often close to where the metal is needed. For other scenarios with more complex ores, implementation of innovative technology could be the game-changer needed to stimulate a diversity of supply of primary cobalt needed for the growing green economy.

A | 138

COBALT-BEARING NICKEL DEPOSITS: SULFIDE DEPOSITS VERSUS LATERITIC DEPOSITS

Kenzo Sanematsu[1], Yoshiaki Kon, Daisuke Araoka, Takaomi D. Yokoyama

[1]*Geological Survey of Japan, AIST - k-sanematsu@aist.go.jp*

Tight demand and supply of cobalt will be a concern in the near future with increasing demand of lithium-ion rechargeable battery for hybrid electric vehicles and electric vehicles in the world. Because the Copperbelt in Democratic Republic of the Congo and Zambia accounts for the majority of mine production of cobalt in the world, cobalt is susceptible to a change of price and supply. Magmatic sulfide Cu-Ni±(PGE) deposits and lateritic Ni deposits account for the remaining cobalt production and Co is extracted as a by-product of these main commodities in refinery plants. Cobalt grades of these deposits are somewhat lower than those of the Copperbelt. However, the sulfide and lateritic Ni deposits can potentially decrease the supply risk of cobalt because they are distributed in different regions of the world. This study reviews and compare Co mineralization, grade and ore reserves (resources) of the two different deposit types: sulfide Ni and lateritic Ni deposits.

Magmatic sulfide Ni deposits are hosted in Archean to Paleozoic komatiite and ultramafic to mafic plutonic rocks and they have different ore genesis. Valuable metals including Ni, Cu, Co and PGE are concentrated in sulfide minerals due to the immiscibility of sulfide and silicate melts. Cobalt minerals consist mainly of cobaltite, linnaeite, carrollite, safflorite, sketterudite and erythrite. Pentlandite and pyrite, which commonly occur in the sulfide Ni deposits, may contain a small amount of cobalt. Average Ni and Co grades typically range from 0.2 to 3.2 % and up to 0.25 %, approximately. The Ni/Co ratio of the sulfide deposits range from 10 to 55, approximately.

Lateritic Ni deposits are composed of laterite formed by weathering of exposed serpentinite and peridotite of ophiolite in tropical regions. Laterite consists mainly of limonite and saprolite and they are characterized by oxide and silicate minerals, respectively. Typical Co- bearing minerals are asbolane, lithiophorite and goethite, and these oxide minerals are commonly found in limonite ores. Saprolite ores characterized by garnierite are relatively low in Co. Average Ni and Co grades of lateritic ores typically range from 0.7 to 2.4 % and up to 0.25 %, approximately. The Ni/Co ratio of the laterite deposits range from 10 to 55, approximately. However, this ratio may range more widely between limonite and saprolite ores because of the occurrence of Co-bearing minerals is common in limonite ores. Nickel is presumably more immobile than Co in the process of lateritic weathering.

The data suggest that the Co grades are not largely different and Ni/Co ratios are comparable between sulfide and lateritic ores. In the lateritic deposits, limonite ores potentially become the more important cobalt source in the world.

PETROLOGY AND GEOMETALLURGY OF THE TABUAÇO SCHEELITE DEPOSIT, PORTUGAL

Liene Spruzeniece[1], Beth Simons, Jens C. Andersen, Gavyn K. Rollinson, Violeta Ramos, Fernando Noronha,

[1]*Camborne School of Mines, University of Exeter - L.Spruzeniece@exeter.ac.uk*

The Tabuaço deposit is located in the Douro province of Northern Portugal around 80 km to the East of Porto (Fig.1A). The deposit comprises two major skarn bands that developed in the metamorphic host of the Paredes da Beira-Tabuaço massif. The deposit was recently under licence by Colt Resources who carried out an initial drilling programme in 2009-2011. Initial evaluations suggest indicated mineral resources of 1,495 kt with 0.55 wt.% WO_3 and inferred mineral resources of 1,230 kt with 0.59 wt.% WO_3 (Colt Resources, 2012). The aims of this study are to explore the origin of the deposit and determine the mineralogical constraints on scheelite processing by froth flotation.

The Tabuaço deposit is located in the Central Iberian Zone, which comprises a succession of folded Pre-Cambrian to Lower Palaeozoic metasediments that have been intruded by Variscan granites. The skarns occur in the Schist-Greywacke Complex (Douro Group, Bateiras Formation) Lower Cambrian in age, about 100 m from the contact with the synorogenic peraluminous Tabuaço granite (311±7 Ma) (Cerejo *et al.*, 2014) (Fig. 1B). Exploration by Colt Resources (2012) identified two principal units of scheelite skarn: the "Upper Skarn" and the "Lower Skarn" (Fig.1C). They occur below a barren carbonate-rich unit and are separated by schist. Smaller lenses of W and Sn-bearing skarn are found above and below the two main bands.

Samples from the Tabuaço deposit were examined by optical and scanning electron microscopy and analysed using QEMSCAN and electron-probe microanalysis. The skarns comprise two principal mineralogical types: (1) L-type skarns (Fig. 2A) display fine banding, and are dominated by strongly zoned pyroxene, grossular and epidote group minerals (Fig. 2B). Domains of vesuvianite, quartz and albite locally replace the primary foliation. The L- type skarn carries minor titanite, mica, amphibole and scheelite. The scheelite is typically associated with fluorvesuvianite (Fig 2C). (2) M-type skarns (Fig. 2D) mainly consist of vesuvianite, fluorite and apatite and locally display foliation. Minor amounts of epidote, albite, mica, chlorite, quartz, garnet, titanite and scheelite are also present. Scheelite commonly surrounds or replaces fluorite grains (Fig. 2E, F). Other, rare skarns include the Sn-rich F-type- skarns that are rich in vesuvianite and fluorite, and contain malayaite, cassiterite and stokesite. While all skarn types can be found in both stratigraphic units, M- type is dominant in the "Upper Skarn" while L-type is predominant in the "Lower Skarn". F-type skarn typically occurs as straight bands associated with the M-type skarn.

The primary target mineral at Tabuaço is high-purity scheelite (only trace amounts of molybdenum). Minor tin is also present as cassiterite, malayaite and stokesite. QEMSCAN analysis of ten representative thin sections demonstrate that scheelite is most abundant in the M-type skarns (0.31 - 3.65 area%). Scheelite grains most often have boundaries with vesuvianite and fluorite grains. L-type skarns have less scheelite, in most samples <0.01 area%, with the exception of one sample, where scheelite comprises 2.31 area%. F-type skarns have the lowest amounts of scheelite (0.65 area% on average), but the highest amounts of Sn-minerals (0.37 area% of cassiterite and 0.68 area% of malayaite + stokesite). Scheelite occurs as crystals with different grain sizes: very fine-grained (< 60 µm) and fine (60 to 250 µm) individual crystals; poorly rounded medium (250 to 500 µm) and coarse- grained (> 500 µm) assemblages. The coarse grain assemblages occur both scattered and/or as clusters of fine grained crystals.

The variability of skarn types at the Tabuaço deposit can be attributed partly to heterogeneity of the original protolith and partly to differences in the fluid-rock interaction at a local scale. Textural and

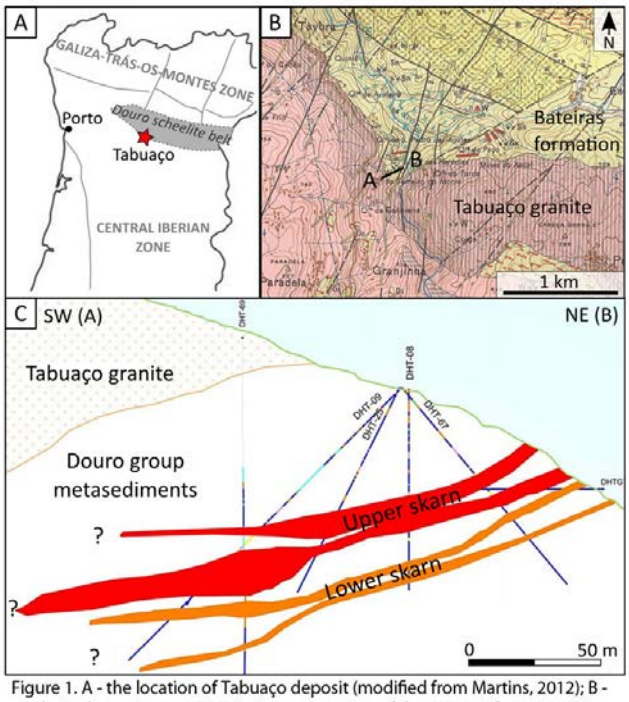

Figure 1. A - the location of Tabuaço deposit (modified from Martins, 2012); B - geological map (source: LNEG); C - cross section of the transect from A to B in Fig.1B, showing the drill core sites and interpreted skarn geometry (modified from Colt Resources, 2012).

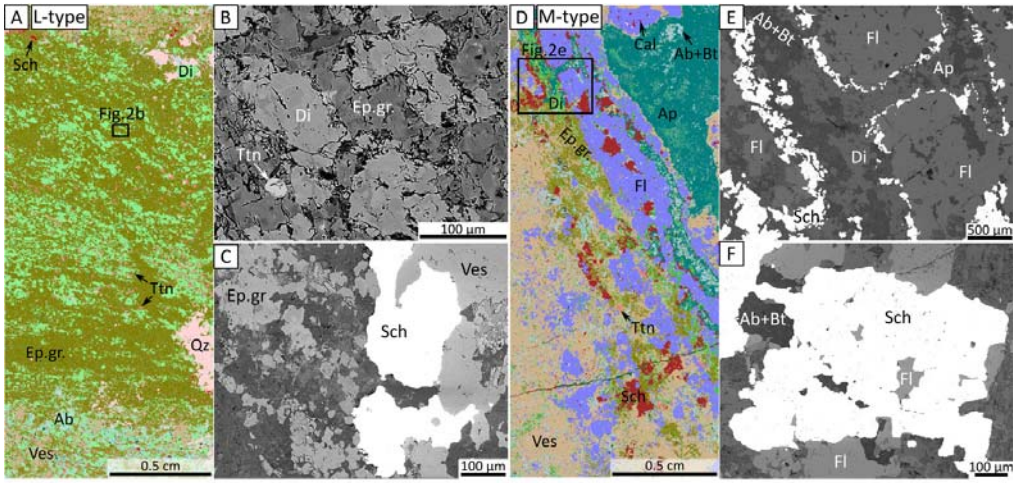

Figure 2. A, D - skarn types in the Tabuaço deposit; B, C - BSE images of typical mineral relationships in L-type skarn; E, F - BSE images of typical mineral relationships in M-type skarn. Note the relation between scheelite and vesuvianite in Fig. 2C and scheelite and fluorite in Fig.2F. Mineral abbreviations after Whitney and Evans (2010).

petrological evidence indicates at least three distinct stages during the skarn formation. The earliest stage (I) is characterized firstly by the formation of diopside, plagioclase, grossular, titanite, K-feldspar and malayaite (Ia) followed by vesuvianite, cassiterite and apatite (Ib). The second stage begins with fluorite formation (IIa), followed by scheelite and quartz (IIb). During the final stage (III) skarns underwent extensive fracturing with subsequent precipitation of calcite, feldspars, quartz, epidote group minerals, chlorite, sericite and stokesite.

The formation of scheelite in the Tabuaço deposit is strongly correlated with fluorine- bearing minerals. Scheelite replaces fluorite and titanite in M-type skarns, and fluorvesuvianite in L-type skarns. These relationships are similar to other W-deposits in the world (e.g. Guo *et al.*, 2016). We suggest that fluorine in the percolating fluids exerted a significant control on scheelite precipitation. Textural relations suggest that the L-type and M-type mineralogies may be related to the evolving fluid-rock interaction. The F-type appears as a specifity of this skarn deposit, in association with M-type skarn.

Although scheelite grades at Tabuaço are promising, the close association between scheelite and fluorite presents a challenge for its recovery using standard flotation techniques (Kupka and Rudolph, 2018). As suggested by Foucaud *et al.* (2018), minimisation of fluorite grade in the final concentrate and tailoring of flotation reagents is required for efficient scheelite extraction.

The Tabuaço deposit is an excellent illustration of the skarn evolution in a heterogeneous host as it progressively reacted with granite-related fluids. The deposition of scheelite appears to have been strongly controlled by fluorine. Tabuaço represents a well-developed example of metasomatic mass transfer in ore systems that can be used to develop a better global understanding of these valuable mineral resources.

Research for this presentation was carried out as part of the FAME project (Flexible and Mobile Economic Processing Technologies) funded by the European Union Horizon 2020 programme (grant number 641650).

REFERENCES

Cerejo, T., Santos, J.F., Sousa, J.C., Castanho, N., Sérgio, G., Ribeiro, F., 2014. Geochronology and isotope geochemistry of granitoids and metasediments of São Pedro das Águias area (Tabuaço W project). Comunicações Geológicas, 101, Especial I, 61-64.

Colt Resources, 2012. Tabuaco tungsten project, Portugal. NI 43-101 technical report. Prepared by SRK Exploration. Released: October 3, 2012, Filed on SEDAR, November 15, 2012. http://coltresources.com/Tabuaço/ (accessed on 12th June 2018).

Foucaud, Y., Lechenard, B., Marion, P., Filippova, I., Filippov, L., 2018. Geology, Textural Study, Ore Genesis and Processing of the Tabuaço Tungsten Deposit (Northern Portugal), in: Al-Juboury, A. (Eds.): Contributions to Mineralization. InTech Open, pp. 134–146.

Guo, S., Chen, Y., Liu, C. Z., Wang, J. G., Su, B., Gao, Y. J., Mao, Q., 2016. Scheelite and coexisting F-rich zoned garnet, vesuvianite, fluorite, and apatite in calc-silicate rocks from the Mogok metamorphic belt, Myanmar: Implications for metasomatism in marble and the role of halogens in W mobilization and mineralization. Journal of Asian Earth Sciences, 117, 82–106.

Kupka N., Rudolph M., 2018. Froth flotation of scheelite – A review. International Journal of Mining Science and Technology, 28, 373-384.

A HIGH-TECH CRITICAL METALS AND TRACE ELEMENTS IN SELECTED ORE DEPOSITS IN POLAND – PRELIMINARY DATA

Mikulski Stanislaw Z.[1], Sadlowska Katarzyna, Chmielewski Andrzej, Malek Rafal, Oszczepalski Slawomir

[1]*Polish Geological Institute-National Research Institute - stanislaw.mikulski@pgi.gov.pl*

INTRODUCTION

In Poland in different metalogenic ore formation were documented 42 deposits with anticipated economic resources of Cu, Zn, Pb, Ag, Mo, W, Ni, Sn, Au, Fe-Ti, V and As. Among them to the most valuable deposits are those from the Kupferschiefer formation with the Lubin – Sieroszowice Cu-Ag mining district, which ranks as one of the largest in the world. In 2017 anticipated economic resources of copper and silver ores from this sediment- hosted deposits amounted to 1,931.9 Mt, whereby metallic copper and silver amounted to 34.59 Mt and 104.47 kt, respectively (acc. to The balance of mineral resources deposits in Poland as of 31 XII 2017). Important are also Zn-Pb deposits related to Triassic carbonate rock formation of the MVT with anticipated economic resources of Zn-Pb ores at 84.42 Mt of ore yielding 3.62 Mt of zinc and 1.48 Mt of lead. Besides, were documented: Fe-Ti-V oxide deposits related to Mesoproterozoic AMCG complex, and in the Variscan orogenic belt – the Myszków Cu-Mo(-W) porphyry type deposit, stratiform Sn deposits, Au-As skarn deposit and weathered deposits of Ni (saprolitic type). Only the Cu-Ag and Zn-Pb deposits are under exploitation, now. The technological and metallurgical processing of sulfide ores from these deposits allowed for production not only base metals (Cu, Zn, Pb) but also noble, critical and trace elements. As an example in 2017 the KGHM Polish Copper Combine S.A. produced from own concentrates 358.9 kt of electrolytic copper, 1,218 kt of silver, 571.7 kg of gold, 39.2 kg of Pt-Pd concentrate, 73.90 t of selenium and 9.31 t of rhenium. Other metals recovered from copper ores include Pb (26.0 kt) and nickel sulfate (1.79 kt) and sulfuric acid and copper sulfate.

In 2017 from Zn-Pb Polish mines extracted 1,711 kt of ores yielding 50 kt of zinc and 13 kt of lead. Besides, zinc and lead ores contained admixture of cadmium (0.01-0.05 % Cd; estimate resources – e.r. 22.10 kt), gallium (e.r. 130 t), germanium (e.r. 30 t), thallium (e.t. 150 t) and silver (e.r. 950 t). However, beside Zn, Pb and S only Cd and Ag are presently recovered from MVT deposits in Poland. Some of the other critical elements – which often have a high market value – are not recovered during the processing of these ores.

METHODS AND RESULTS OF TRACE ELEMENTS INVESTIGATION

Over three hundred samples with economic ore mineralization representing variable type of Cu-Ag, Zn-Pb, Fe-Ti-V, Sn, Cu-Mo-W, Au-As and Ni documented deposits in Poland were subject of modern complex geochemical (ICP-QMS, ICP-OES, WD-XRF, GF AAS and ETA- AAS) and mineralogical (EPMA, CAMECA-SX100) studies. Samples were collected mostly from the archive core material of boreholes drilled during deposits documentation as well as from the underground operating mines. The analyses were performed in the presence of an international and internal standard. In the case of chemical measurement the quality control included double digestion selected samples and double samples measurement.

In sphalerite-galena-pyrite/marcasite ores of MVT the average contents of trace elements, such as Cd (arithmetic average = 440 ppm), Ga (51.3 ppm), and Hf (25 ppm) are high. Silver occurs from 0.9 to 102.7 ppm (an average = 13.4 ppm). A strong positive correlation has been recognized between Zn and Cg, Ag, Cu and Ga and between Pb and Hf, Nb, Rb, U, Y, Zr, Cr and Ga. Microprobe (EPMA) investigation revealed a high admixtures of cadmium ($\leqq$2.6 wt. %) and silver ($\leqq$0.33 wt. %) in sphalerite and of gold (up to 0.17 wt. %), silver ($\leqq$0.1 wt. %), and antimony ($\leqq$1.8 wt. %) in galena.

In the Fe-Ti-V deposits dominate vanadium-bearing magnetite-ilmenite ores with minor sulfides (pyrrhotite, pentlandite, and chalcopyrite). A strong positive correlation has been recognized between Fe-Ti and Cd, Ge, In, Ga, V, Ni, Co and Br. An average content of vanadium for Fe-Ti oxide ores from the Krzemianka deposit is 0.1 % and of nickel and gallium – 400.6 ppm and 43.1 ppm, respectively. EPMA investigation shows that magnetite contained vanadium admixture up to 0.6 wt. % and ilmenite up to 0.22 wt. % V. Besides, bismuth and tellurium minerals were found in sulfides ores. On the basis of the new criteria, ore resources of these deposits were classified as sub-economic due to low content of metals, especially vanadium (from 0.26% to 0.31% V_2O_5 at the average) and occurrence at large depths. However, the presences of co-occurring minerals in these deposits (including REE in carbonates) increase their potential of mineral resources.

In the core samples from the nickel saprolitic type deposit were recognized very interesting concentration of co-occurring elements, such as cobalt and chromium. In Ni-bearing ore samples an average Cr is of 0.33 % and Co of

220 ppm. Make notice enrichments in Pt (up to 150 ppb). A strong geochemical correlation was found not only between distribution of Ni and Co and Cr but also between Co and Cd, V, Sc and Pt.

Several samples were collected from the archive boreholes, which documented the Myszków Mo-W-Cu porphyry type deposit. Its ore mineralization is of the stockwork type, forming a system of quartz veins with ore minerals, sulfides and oxides related to Variscan igneous activity. Anticipated economic resources of the deposit were estimated at about 0.295 Mt of Mo, 0.238 Mt of W and 0.8 Mt of Cu. The Myszków ores have not yet been exploited. Our data revealed some increased in content of Bi. According to available data, there are high chances for discovery of other deposits of Mo-Cu porphyry type as well as hydrothermal Au- Ag and/or polymetallic skarn deposits related to Variscan felsic magmatism.

It is also interesting to investigate Sn oxide ores collected from the archive boreholes, which documented tin deposits in Krobica and Gierczyn in the Lower Palaeozoic Schist Belt in Sudetes, on the NE margin of the Bohemian Massif. Tin resources of the considering deposits were classified as anticipated sub-economic and were estimated at 4.6 Mt of ore with Sn content of about 0.5% at the average. However, perspective resources of tin ore in the entire area were estimated at about 20 Mt, with content of metallic tin of about 100,000 t. With cassiterite ores are associated sulfides with co-occurring elements such as Bi and Co (up to 0.02 %), Au and Pt. Te-, Bi-, Sb-, Se-, and In-bearing minerals were also found by microscopic observation.

CONCLUSIONS

The application of complex geochemical and mineralogical investigation with use of modern analytical instruments allowed for identification of critical and trace elements distribution in the documented different ore deposits in Poland. Microscopic and EPMA investigation revealed that with the main ore minerals are associated rare minerals, which might carry different trace elements. Accumulations of some of these elements were poorly covered by prospecting and exploration that rarely resulted in evaluations of their indicated/inferred resources. On occasion, their resources were documented.

IMPORTANCE OF BEDROCK FOR CONCENTRATION OF SC IN A NICKEL LÑATERITE DEPOSIT, CENTRAL DINAGAT ISLAND, PHILIPPINES

Tomiyuki Yamada

Kyushu University - yamada-tomiyuki@mine.kyushu-u.ac.jp

BACKGROUND

The Rare Earth Elements consist of lanthanides (Ln: La-Lu), scandium (Sc) and yttrium (Y). REE are elements with special chemical and physical properties needed for sophisticated technical applications associated with renewable energy, reduction of greenhouse gasses and energy efficiency (green technologies)(Aiglsperger *et al.*, 2015). The importance of heat-resist magnet materials increase with the spread hybrid vehicles. Scandium also finds applications in Al-Sc superalloys, increasing tensile strength and improving weldability while maintaining light weight, an energy-saving factor in aerospace and automotive industries. In solid oxide fuel cells, the addition of Sc to the electrolyte improves conductivity and lowers the operating temperature, extending fuel cell life (Chasse, 2017). However, as the demand is driven by energy issues (Emsley, 2014) and scandium rarely produces it as a main component, the mine development only for it is difficult. Therefore it is small production as the by-products. Wang *et al.* (2011) introduced the collection method as the by-products of scandium in various smelting processes and mentioned that nickel laterite was the most promising as a scandium ore (Sanematsu *et al.*, 2012). The ion- adsorption type REE deposits have been economically mined in South China. The deposit show the high concentration of REE. This time, study area in Philippines is not REE deposits, but it is expected to find concentrations of Sc and REE with Ni.

METHODS

Geochemical analyses were conducted to understand how Sc and the other REE concentrate and the influence of bedrock for enrichment of Sc. The research area, Central Dinagat Island is mainly composed of mafic and ultramafic rocks collectively known as the Dinagat Ophiolite Complex. Samples used in this study were taken from two drill cores (P11, AA and DH) in Central Dinagat Island. P11, AA and DH were drilled up to 21.5m, 30.7m and 54.41m in depth, respectively. XRD analysis revealed that the bedrock in this study area is harzburgite consisting of olivine, orthopyroxene, spinel and serpentine and gabbro consiting of orthopyroxene, amphibole and plagioclase. In this study, laterite samples are classified as limonite (FeO>60%), earthy saprolite (30%<FeO<60%) and rocky saprolite (FeO<30%). The samples were dried in an oven at 40° for 24 hours. Rock samples were roughly crushed by a hammer. The crushed rock samples and laterite samples were ground by vibration mill. Powder samples crust by mill used for XRF, XRD and ICP-MS analysis.

Loss of ignition (LOI) in the samples was measured based on the loss of weight after ignition prior to XRF analysis. Bulk geochemical composition of major and minor elements of the rock and soil samples were determined by XRF (X-Ray Fluorescence Spectroscopy Rigaku RIX-3100) at the Department of Earth Resources Engineering, Kyushu University, operating under conditions of 50kV and 50mA. For XRF analysis, pulverized samples were pressed to form pellets. Mineral composition of the samples was identified by XRD (X-Ray Diffraction Rigaku Ultima IV) at the Department of Earth Resources Engineering, Kyushu University, operating under the conditions of 40kV, 20mA and scan speed at 2.0°/minute. The samples were pressed in the sample holder. Chemical composition of trace elements including REE in the samples was analyzed by Inductively-Coupled Plasma Mass Spectrometer (ICP-MS) at ALS Chemex, Canada. The analytical code applied was «ME-MS81» and «ME-4ACD81» for determination of Y, Ln and Sc, respectively. Polished thin sections were prepared for petrographic analysis. Microscopic observation of the thin sections was conducted by using a NIKON E6TP-M61 in order to identify the mineral assemblages.

RESULTS

Geochemical analyses of laterite profile revealed that there are no apparent correlation between nickel, which is the main product of Ni laterite deposit, and scandium, which is investigated as by-product of nickel laterite deposits. It can be said that nickel mineralization is not similar to Sc concentration. On the other hand, Sc shows clear positive correlation with Fe, which is regarded to be one of the immobile elements during weathering. The geochemical behavior of Sc is similar to Fe^{3+} during weathering, so that Sc^{3+} replaces the Fe^{3+} site because almost all the iron in laterite would be iron oxide and hydroxide as Fe^{3+} (Sanematsu *et al.*, 2012). Al also shows positive correlation with Sc. It is because Al is also regarded to be an immobile element during weathering. Therefore Sc exhibits positive correlation with immobile elements such as Fe and Al, resulting in Sc enrichment (up to 108ppm) mainly from limonite to upper part of earthy saprolite. However, red soil profiles were irregularly observed in

limonite zone. XRD analysis revealed that the red soils were mainly composed of gibbsite which is mainly contained in bauxite. Therefore red soils were identified as bauxite samples. Some bauxite samples do not obey the correlation as same as Sc-Fe and show high content of Al whereas they show low content of Sc. Therefore it can be considered that bauxite samples, which are taken from P11, AA and DH, were derived from gabbro because the color of bauxite samples are red and they show high Al content. And gabbro generally contains more Sc than harzburgite in bedrock. Hartzburgite mainly contain olivine (50%) and Sc is hard to be distributed between bedrock of harzburgite (8ppm). On the other hand, gabbro is composed of amphibole and orthopyroxene, which shows high distribution coefficient. Therefore gabbro (OC2) generally contains more Sc than harzburgite (P11L, AAO and OC1) in bedrock. However, some bauxite samples considered to be derived from gabbro showed lower Sc content than laterite samples derived from harzburgite after weathering.

CONCLUSIONS

Olivine and orthopyroxene in harzburgite are changed to goethite or hematite and Fe3+ is replaced by Sc3+ during weathering process. It results in the high content of Sc in samples derived from harzburgite. On the other hand, in gabbro, plagioclase, which is poor in Sc, is mainly contained in gabbro (65%) and changed to gibbsite, which is rich in Al and poor in Sc whereas olivine and orthopyroxene are changed to goethite as same as harzburgite. As a result, the high Al content reduce Sc content relatively and bauxite samples show lower Sc content than samples derived from harzburgite after weathering. Therefore the bauxite samples show high Al content and can be considered that bauxite samples in gabbro layer in ophiolite sequence reduce dignity of Sc relatively as same as other some elements, for example Ni which is main product of Ni laterite deposit. Therefore gabbro layer in ophiolite sequence can reduce dignity of Sc on Ni laterite deposit.

REFERENCES

Aiglsperger, T., Proenza, J.A., Zaccarini, F., Lewis, J.F., Garuti, G., Labrador, M., Longo, F., 2015. Platinum group minerals (PGM) in the Falcondo Ni-laterite deposit, Loma Caribe peridotite (Dominican Republic). Mineralium Deposita, 50 (1), 105-123.

Sanematsu, K., Hoshino, M., Watanabe, Y., 2012. Lateritic scandium-bearing deposits. Shigen Chishitsu 62, 17-26.

Wang, W., Pranolo, Y., Cheng, C.Y., 2011. Metallurgical processes for scandium recovery from various resources: A review. Hydrometallurgy, 108 (1), 100-108.

MINERALOGICAL AND GEOCHEMICAL CONSTRAINTS OF THE ZUDONG REGOLITH-HOSTED HREE DEPOSIT IN SOUTH CHINA

Martín Yan Hei Li

The University of Hong Kong - martinli@hku.hk

The Zudong heavy rare earth element (HREE) deposit in South China is the largest regolith- hosted HREE deposit in the world with a resource of ~17,600 t of REO, at an average grade of ~0.1 wt. % REO. Despite its importance in current global HREE production, comprehensive investigations are lacking. In this study, we focused on the mineralogical and geochemical characteristics to constrain the ore genesis of the Zudong HREE deposit. The deposit develops from subtropical weathering of an A-type alkaline granite. Consequent weathering crust is developed on the hillsides of a deeply incised landscape (relief ~ 150m) and could be up to 70 m thick, while mostly are of 10 – 30 m thick. Thickness of the ore bodies varies from a few meters to up to 10 m and they are hosted mainly within the lower B to upper C horizons of the weathering profiles (i.e. the transition zone between the semi- weathered and completely weathered horizons).

The parent alkaline granite contains quartz, albite, K-feldspar, and muscovite as the major minerals, and has an accessory mineral assemblage of synchysite-(Y), yttrian fluorite, gadolinite-(Y), hingganite-(Y), yttrialite-(Y), zircon, euxenite-(Y), fergusonite-(Y), polycrase- (Y), xenotime-(Y), columbite, and thorite. Major REE minerals, such as synchysite-(Y) and yttrialite-(Y), as well as muscovite are of hydrothermal origin and grew preferentially along cleavages of feldspar. With progressive weathering, the abundance of albite, K-feldspar and muscovite decrease from the lower C to the A horizons, whereas those of the kaolinite and halloysite, the major clay minerals in the deposit, are relatively consistent from the C to the B horizons but increase dramatically in the A horizon. Smectite and illite are minor and their occurrence are limited to the C horizon. Abundance of Fe-Mn oxyhydroxides also gradually increases from the C to the A horizons. Several supergene REE minerals occur in the weathering crust, including chernovite [$YAsO_4$], being more frequently observed in the lower B to the upper C horizons; and cerianite [CeO_2], being more abundant in the upper part of the weathering profile with a close spatial association with Fe-Mn oxyhydroxides. Remaining REE minerals in the weathering profiles comprises residual euxenite-(Y), fergusonite-(Y), polycrase-(Y), xenotime-(Y), zircon, and thorite.

In term of geochemistry, REE contents of the parent granite vary from ~200 to ~450 ppm. The parent granite is also HREE-enriched. In the weathering crust, rare earth element concentrations increase from the A horizon to the maximum in the lower B to upper C horizons and decrease with further depth in the profile. The entire soil profile is HREE- enriched with (La/Yb)N values <1, but the REE-enriched lower B horizon is less HREE- enriched (i.e. higher (La/Yb)Nvalues) than the underlying C horizon. Exchangeable REE, representing REE that are adsorbed in the deposit, comprises 25 to 75% of the bulk REE contents. The main minerals adsorbing the REE are kaolinite and halloysite; the proportions of REE adsorbed to Fe-Mn oxyhdyroxides and organic matter are negligible.

The Zudong deposit formed from weathering of a HREE-enriched A-type granite, containing abundant REE minerals, such as synchysite-(Y), gadolinite-(Y), hingganite-(Y), and yttrialite- (Y) which are susceptible to chemical weathering. Decomposition of these minerals released REE to the weathering fluid, and the interaction between alkali feldspar, muscovite and the weathering fluid produced abundant clay minerals. With progressive weathering, these minerals accumulated together with quartz, refractory zircon, xenotime-(Y) and euxenite- (Y). In upper parts of the soil profile, at where conditions were acidic, REE tends to remain in dissolved forms. Deeper in the profile, conditions become less acidic leading to adsorption of the REE on the surface of various clay minerals. Ongoing operation of this eluviation-illuviation process at Zudong gradually enriched the soils in HREE to form such a giant deposit.

A | 143

INTRA-GRANULAR DISTRIBUTION OF ENERGY CRITICAL ELEMENTS IN SULPHIDE MINERALS: RESOLVING PARAGENESIS AND RESOURCE POTENTIAL THROUGH LASER ABLATION ICP-MS

Sean H. McClenaghan

Trinity College Dublin - mcclens@tcd.ie

INTRODUCTION

The occurrence of Energy Critical Elements (ECE) in primary ore minerals and their subsequent enrichment in waste tailings is of great metallurgical interest. Recovery of many ECEs, in particular In, Ge, and Ga have come chiefly as a by-product of base-metal production (smelting and refining). As the ECEs become more important for a growing number of technological applications, it is critical to map the distribution of these elements in ore and waste (gangue) minerals to optimize their recovery and remediation.

Sphalerite is found in a wide-range of ore forming conditions including sedimentary and volcanogenic massive sulphides, as well as mineralization associated with intrusive settings such as porphyries, skarns and epithermal veins. Sphalerite is a known host for In, Sn, Ge, Te, and Ga (Cook *et al.*, 2009); these represent valuable commodities, increasing the value of Zn production worldwide. These elements along with their deleterious counterparts Se, Hg, Tl, and Cd can reveal much about the genesis of a mineralizing system; in particular, the accommodation of trace elements in the sphalerite structure is an ideal proxy for comparing both inter- and intra-deposit variations in hydrothermal geochemistry as well as enabling broad comparisons across a wide spectrum of deposit types. This study investigates the distribution of ECEs in epigenetic base-metal veins associated with Devonian granite plutons within Irish Caledonian terrains, based on known associations of Sn, In, Ge, and Ga in intrusion-related polymetallic veins (Sinclair *et al.*, 2006; Murakami and Ishihara, 2013; Anderson *et al.*, 2016).

LASER ABLATION ICP-MS

Laser ablation ICP-MS is ideal for the quantitative measurement of trace elements in ore minerals as well as associated gangue materials. Improvements in spatial resolution and detection limits has effectively decreased the amount of ablated material required for analysis, permitting micro-chemical mapping at scales smaller than 10 microns. Minimizing the transfer volume between the ablation cell and the ICP-MS torch with a Teledyne Cetac Aerosol Rapid Introduction System (ARIS) (Van Acker *et al.*, 2016) provides faster washout of the sample aerosol and allows for scan speeds in excess of 50Mm/sec, while resolving pulses of 50 Hz.

Laser ablation ICP-MS analyses of sphalerite were performed using a Teledyne PhotonMachines G2 193 nm Excimer ArF laser with a HelEx II 2-volume cell coupled via the ARIS to a Thermo Elemental iCapQs mass spectrometer at Trinity College Dublin. Analyses were performed by ablating lines using a 10 Mm beam diameter, proceeding as a continuous profile at 60 Mm/sec with a repetition rate of 50 Hz and a fluence of 1.5 J/cm2. Data were calibrated with line analyses of MASS-1 (Wilson *et al.*, 2002) and MUL-ZnS-1 (Onuk *et al.*, 2016) standards.

MINERALIZATION

The large Leinster batholith in southeast Ireland consists of a series of granitic plutons intruding between 417 and 405 Ma (Fritschle *et al.*, 2018) into Cambro-Ordovician turbiditic shale and wacke of the Ribband Group. The occurrence of the cross-cutting Pb-Zn veins within the granite and metamorphic aureole, as well as metal anomalies within metablastic mineral growths indicate a genetic link to the granite pluton. Nevertheless, numerous base-metal veins and volcanic-hosted stratiform massive sulphides occur across southeast Ireland and are unrelated to the emplacement of the Leinster batholith.

Epigenetic Pb-Zn mineralization in the Glendalough region consists of vein networks and breccias comprising quartz, barite, gypsum-anhydrite, carbonate, fluorite and variable contents of sphalerite, galena as well as lesser chalcopyrite and pyrite. Sphalerite exhibits marked zonation with broad variations in Fe and Cd, corresponding to its appearance under transmitted light varying from honey brown to crimson red and black. Distinct oscillatory zonation reflects variations in hydrothermal fluid chemistry with sphalerite growth. Later fracturing of veins led to the precipitation of sphalerite along discrete fractures and stepped triangular features formed as crystallographic oriented growths or as an etching feature. Overall, the protracted growth history of sphalerite is further supported by the extensive crack-seal textures exhibited by the host vein quartz and sulphides observed at the hand specimen and microscopic scale.

INTRA-GRANULAR ECE VARIATIONS

Laser-ablation ICP-MS analyses of sphalerite in epigenetic veins at Glendalough reveal anomalous levels of In (2400 ppm), Ga (1400 ppm) and Ge (350 ppm) supporting the influence of the intruding granite on the ECE endowment around the Leinster Batholith. Sphalerite analyses from regional vein and stratiform massive sulphides do not exhibit distinct In-Ga-Ge signatures with relatively minor contents of ECEs. Element mapping (LA-ICP-MS) of sphalerite (Figure 1) reveals strong zonation of ECEs at the mineralogical scale, displaying features consistent with oriented crystal growth and selective substitution along crystal faces and broadly corresponding to observed zonation and variations in Fe and Cd contents. Correlative behavior between Cu, Sn, and In, is consistent with coupled substitution mechanisms invoked for In-bearing polymetallic veins (Murakami and Ishihara, 2013), and with negligible influence from discrete mineral inclusions. Furthermore, distinct trace-element signatures are exhibited for several phases of sphalerite showing an evolution of ECE contents and relative proportions in response to varying hydrothermal conditions.

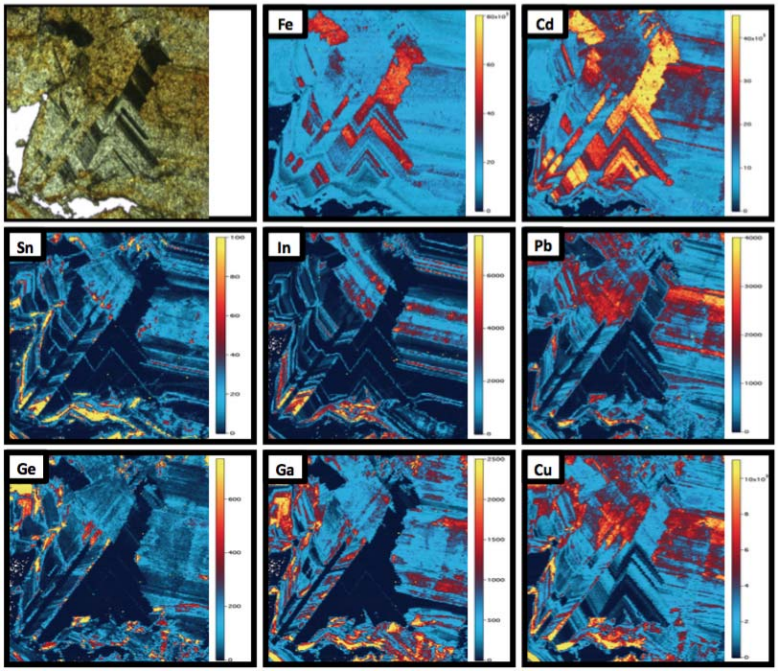

Figure 1: Semi-quantitative LA-ICP-MS trace-element maps of sphalerite in epigenetic veins associated with the Leinster Batholith, Glendalough mining district. Field of view is 500 microns; pre-ablated grains are shown in transmitted light; all concentrations in ppm.

CONCLUSION

While sphalerite grains exhibit locally high contents of energy critical elements (In-Ga-Ge), their overall concentration in sphalerite is low, due to the high intra-granular variability. It is important to note that while bulk analyses remain a good estimate of bulk metal contents, they do not portray the heterogeneous nature of trace elements in epigenetic vein systems; Assessing this trace-element variability could indicate fertility in a system and the delineation of phases enriched in ECE's.

REFERENCES

Andersen, J.C.O., Stickland, R.J., Rollinson, G.K., Shail, R.K., 2016. Indium mineralization in SW England: Host parageneses and mineralogical relations. Ore Geology Reviews, 78, 213-238.

Cook, N.J., Ciobanu, C.L., Pring, A., Skinner, W., Shimizu, M., Danyushevsky, L., Saini- Eidukat, B., Melcher, F., 2009. Trace and minor elements in sphalerite: a LA-ICP- MS study. Geochimica Cosmochimica Acta, 73, 4761-4791.

Fritschle, T., Daly, S.J., Whitehouse, M.J., McConnell, B., Buhre, S., 2018. Multiple intrusive phases in the Leinster Batholith, Ireland: Geochronology, isotope geochemistry and constraints on the deformation history. Journal of the Geological Society, 175 (2), 229-246.

Murakami, H., Ishihara, S., 2013. Trace elements of Indium-bearing sphalerite from tin- polymetallic deposits in Bolivia, China and Japan: A femto-second LA-ICPMS study. Ore Geology Reviews, 53, 223-243.

Onuk, P., Melcher, F., Mertz-Kraus, R., Gäbler, H-E., Goldmann, S., 2016. Development of a Matrix-Matched Sphalerite Reference Material (MUL-ZnS-1) for Calibration of In Situ Trace Element Measurements by Laser Ablation-Inductively Coupled Plasma-Mass Spectrometry. Geostandards and Geoanalytical Research, 41 (2), 263-272.

Sinclair, W.D., Kooiman, G.J.A., Martín, D.A., Kjarsgaaard, I.M., 2006. Geology, geochemistry and mineralogy of indium resources at Mount Pleasant, New Brunswick, Canada. Ore Geology Reviews, 28, 123-145.

Van Acker, T., Van Malderen, S., Van Heerden, M., McDuffie, E.J. Cuyckens, F., Vanhaecke, F., 2016. High-Resolution Laser Ablation-Inductively Coupled Plasma-Mass Spectrometry Imaging of Cisplatin-Induced Nephrotoxic Side Effects. Analytica Chimica Acta, 945, 23-30.

Wilson, S.A., Ridley, W.I., Koenig, A. E., 2002. Development of sulfide calibration standards for the laser ablation inductively-coupled plasma mass spectrometry technique. Journal of Analytical Atomic Spectrometry, 17 (4), 406-409.

COBALT MINERALIZATION IN ARGENTINA

Martín R. Gozalvez[1], Lidia I. Korzeniewski, Samuel Gregorat

[1]Servicio Geológico Minero Argentino - Martín.golzalvez@segemar.gov.ar

Cobalt in Argentina is present in several ore deposit types including Au-quartz orogenic veins (e.g., King Tut, La Rioja province), five-element deposits (e.g., La Niquelina, Esperanza, Purísima Rumicruz, Salta and Jujuy provinces) and Ni-Cu-Co-PGE (-Cr) associated with stratified intrusions (e.g., Las Águilas, San Luis province; Fiambalá, Catamarca province; Salamanca, Mendoza province).

KING TUT

The King Tut deposit is located 58 km northeast of the town of Vinchina, Famatina Range, La Rioja province. The mine produced gold for two years (1901-1902). The geological setting is constituted by Ordovician low-grade metamorphic rocks with acidic and basic interlayered volcanic rocks. The volcano-sedimentary sequence is intruded by Ordovician mafic dikes and granitic-tonalitic batholith. Finally, andesitic volcanism extruded during Paleogene. To the southeast, other Co-Au occurrences (La Alumbrera and Quebrada del Hoyo) are recognized in an area of 2x10 km. Estimated resources for a block of 220m x 50m x 0.8m are 20,000 t with 0.91% Co and 3.7 g / t Au. Quartz-veins are hosted in the volcanosedimentary sequence and ore minerals are glaucodot, pyrite, cobaltite, pyrrhotite, marcasite, chalcopyrite, bornite, native gold, native bismuth and tetradymite.

LA NIQUELINA

The mineral occurrence is located 73 km southeast of La Quiaca city, Santa Victoria Range, Salta province. The outcrops are dominated by Cambrian quarzitic sandstones and Ordovician shales. The deposit is emplaced in a tectonic block limited by reverse faults. Several veins and breccias are recognized in an area of 0.32 km^2 with pitchblende, gersdorffite, nickeline, chalcopyrite, sphalerite, galena, tetrahedrite and pyrite in gangue of quartz and minor siderite. Grades of selected samples are 0.47% to 1.76% Co, 20% to 24% Ni and 27% to 31% As.

ESPERANZA MINE

It is located approximately 100 km northeast of the town of Iturbe, Salta province. Historically, it has produced a few tons of copper and lead. The mine is located on the eastern hillside of the Zenta range. Grades of the ore range from 0.14% to 0.3% U_2O_3, 9.75% to 10.3% Zn, 10% to 21% Pb and 19% to 23% Cu. The mineral deposit consists of fault- controlled veins hosted in deformed and metamorphosed rocks of Neoproterozoic to Paleozoic age. There are copper-bearing and lead-bearing veins with thickness varying from 0.5 to 1 m, lengths of 100 to 250 m, and a vertical extent of 50 to 125 m. Ore minerals are galena in a gangue of barite and chalcocite, sphalerite, tetrahedrite in a gangue of dolomite.

PURÍSIMA-RUMICRUZ MINES

The extension of the district is 30 km^2 and it is located approximately 20 km southeast of the town of Abra Pampa, Jujuy province. Various mines in the district produced copper and lead. The geology of the region consists of folded Ordovician sandstones, greywackes and pelites. In some sectors of the district fault density is 50 faults per km^2, with east-west faults controlling the mineralization. Grades are 5.5% Cu, 7% Pb, 0.01-0.3% Ni and 270 g / ton Ag; there is no data for Co content. The ore bodies are tectonic breccias of 2,000 m length and 1.5 m thickness. Ore minerals are galena, pyrite, chalcopyrite, tetrahedrite-tennantite, chalcocite, nickeline, Co-rich gersdorffite, pitchblende, bornite, digenite in gangue of barite and quartz.

FIAMBALÁ

This area is located approximately 30 km northwest of the city of Tinogasta, Catamarca province. In this region, schists and gneisses, partly migmatizated during the Ordovician, were intruded by a syntectonic, concordant and stratified gabbronorite pluton. The pluton consists of two layers of ultramafic rocks of dunites (79-100 ppm Co), lherzolites (59-130 ppm Co), wherlites, websterites and norites (46-59 ppm Co). Ore minerals in the ultramafic rocks are as follows: chromite, magnetite, ilmenite, awaruite, heazlewoodite and gold in the dunites; chromite, magnetite, ilmenite, pyrrhotite, pentlandite and gold in the lherzolites and webstarites; pyrrhotite, pentlandite, chalcopyrite, sphalerite, ilmenite, magnetite, mackinawite, gold, pyrite, violarite, covellite and digenite in the norites.

LA SALAMANCA DISTRICT

The district is located approximately 30 km west of the city of Tunuyán, Mendoza province. The deposit consists of several lensoid peridotitic bodies in an area of 900 m x 100 meters. The complete serpentinization of peridotites result in chlorite, talc, serpentine, actinolite, calcite, dolomite, magnesite and quartz. Ore minerals in mineralized veins consist of pyrrhotite, chalcopyrite, sphalerite, pyrite, pentlandite, Co-pentlandite, mackinawite, cubanite, molybdenite, valleriite, Ag-pentlandite and cobaltite. The ultramafic rocks of the Salamanca area have <3400 ppm Cr, 2500 ppm Ni, 500 ppm Co, 400 ppm Cu, 600 ppm Zn, 6-12 ppb Os, 0.2-3.3 ppb Ir, 2-5 ppb Ru, 2-4 ppb Rh, 2-7 ppb Pt, 8-55 ppb Pd and 2-1800 ppb Au.

LAS ÁGUILAS

The deposit is located approximately 40 km north of the city of San Luis, San Luis province, in the southern part of the San Luis Ranges constituted by a Neoproterozoic-Cambrian igneous-metamorphic basement that involves sedimentary rocks, granitoids and ultramafic rocks, deformed and affected by regional metamophism grading from greenschist to granulite facies. Ultramafic rocks are lenticular bodies and occur along a belt of approximately 100 km. The ultramafic rocks outcrops in an area of 3 km^2 and are form a synclinal system with dunites and hazburgites in the core and pyroxenites, norites and gabbros on the edges. Two orebodies were defined, one of conical geometry with an elliptical base of approximately 100 m x 75 m; the other orebody is tabular with a length of 200 m and a thickness of 10 meters. Total resources reach 4.6 million tonnes with 0.41% Ni, 0.41% Cu, 0.03% Co with non-quantified precious metals (PGM-Au-Ag) content (grades of mineral concentrate are 6 g/t Pt+Pd, 3 g/t Au, 9 g/t Ag).

The Argentinian cobalt districts were explored and mined for gold, copper and lead, however, the cobalt potential remains, in some districts possibly as primary ore (King Tut, Las Águilas), in others as a potential byproduct. The highest cobalt potential is related to the ultramafic rocks, emplaced in the Paleozoic Orogenic Belts. Other exploration targets are the deposits that formed in Mesozoic back-arc extensional environment (five-element deposits type) as well as copper-gold deposits hosted in volcanic and Mesozoic sedimentary rocks (e.g, IOCG and IOA) in the Puna region and the Neuquina Basin.

CHAPTER 14

TECHNICAL DEVELOPMENTS AND GEOLOGICAL APPLICATIONS IN REMOTE SENSING: FROM SATELLITES TO UNMANNED AERIAL VEHICLES (UAV)

Conveners: Valery Bondur, Sergey Cherkasov

NEW REMOTE SENSING TOOLS FOR THE EXPLORATION AND MINING LIFECYCLE

Dan Taranik

Exploration Mapping group, Inc - dtaranik@explorationmapping.com

This talk presents the latest developments in geological remote sensing for mineral exploration and mining and covers a broad variety of remote sensing technologies from satellites to UAVs. The technologies are transforming the technical approach to the mining lifecycle from exploration, mine planning, production and related environmental monitoring.

We are still find and exploit mineral resources that outcrop at the surface although these are increasingly rare. Exploration is often conducted in difficult and challenging environments including extreme climates, exotic modes of transport and hostile environments with short field seasons. Even in developed mining districts exploration mapping, sampling and survey work are physically demanding. Field operations can be time-consuming and expensive, in many cases the singular most expensive component of an exploration budget. Most companies find and use the best information available before going to the field and plan their field operations wisely.

Satellite optical remote sensing is used extensively as a tool for exploration to identify features of geological interest before and during field operations. Satellite imagery provides important fact-based information on geology, lithology, alteration, structure, site access, survey planning and in rare cases direct discovery of mineralization. There are many remote sensing options available for country, district, project and even outcrop scales. Specific systems highlighted will include the American DigitalGlobe WorldView-3 satellite, European Copernicus missions, the rapidly growing number of global 'Small Sats', plus hyperspectral satellites on the horizon being developed by the German, French and Chinese governments. These new technologies are successors to a long line of resource satellites which create an opportunity to search the globe for what previous resource satellites have missed. Examples will be shown with satellite data worldwide and include Argentina and Chile precious and base metal deposits.

Satellite radar systems are becoming increasingly important in cloudy and vegetated terrains where a remote sensing approach is not normally considered notably the jungle regions of Ecuador and Brazil. New multipolarization and multi-frequency radar is being used to produce color composites with geological content in dense vegetation. New radar systems have the ability to see minute elevation changes on the order of millimeters to detect active and recently-active fault systems that may be clues to finding mineral systems where other geoscientific data is scarce. The advantages of cloud penetration, vegetation canopy penetration and day and night data acquisition not dependent on good weather make satellite radar an increasingly useful tool for the exploration geologist in difficult regions.

Unmanned Aerial Vehicle (UAV) technology platforms have seen amazing growth in recent years and are being used to significantly improve the profitability of active mining operations. A large number of UAV platforms are available - fixed wing, multi-rotor and helicopters with detector systems including natural color, thermal infrared, hyperspectral and radar/lidar. The choice depends on the type of terrain you are planning to fly, the materials you want to detect and the wind conditions typical of the project area. One example shows UAV-based stockpile volume

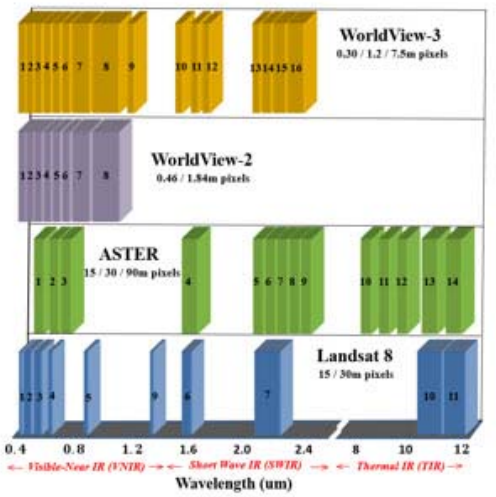

Relative Spectral Coverage of WorldView-3, WorldView-2, ASTER and Landsat

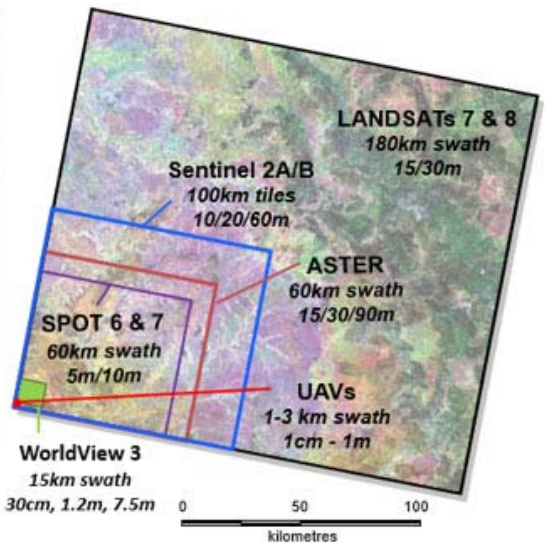

measurements have 15% greater accuracy than traditional ground survey techniques used as the basis for grade/tonnage calculations. Examples are also shown of accurate UAV ground measurements made in dangerous no-go areas with toxic mine tailings, busy haul truck routes and the measurement of pit wall slump or failures.

Geobotanical remote sensing as an exploration tool has become a reality with the deployment of the WorldView-3 satellite less than three years ago. With seventeen spectral bands and pixel sizes of 30cm the WorldView-3 satellite has the world's highest spatial and spectral resolution of any commercial satellite. A variety of vegetation health parameters, e.g., leaf pigment concentration, plant and cell structures, biochemical nutrients and water content show discreet areas with poor vegetation health which can be measured and mapped directly in a highly accurate and consistent approach across a scene. The impacts of direct metal stress, the health of individual bushes and trees, mine leakage and petroleum seepage effects will be shown with examples from an arid region, a boreal forest and dense tropical jungle.

Remote sensing in all its forms is an indispensable technology across the entire mining lifecycle. This talk explains how mining companies are leveraging remote sensing technology to explore, mine and monitor their mining operations with unprecedented accuracy and reliability. You will learn the latest technology developments with satellite imagery, UAVs and ground based spectrometry and see examples of various ore deposit styles, lithologies and alteration minerals that may be of interest for your exploration and mining operations.

HYDROTHERMAL ALTERATION MAPPING USING ASTER DATA IN THE IGLESIA DEPARTMENT, SAN JUAN PROVINCE, ARGENTINA

Diego Azcurra[1], Fernando Ganem, Dolores Álvarez, Diego Rodríguez, Silvia Chávez, Leda Moser, Javier Benítez

[1]*SEGEMAR - diego.azcurra@segemar.gov.ar*

This study is part of a project carried out under the Framework Agreement for Cooperation and Technical Assistance between the Argentine Mining Geological Service (SEGEMAR) and the Ministry of Mining of San Juan Province (MMSJ). Its objective is to contribute to the mining development of the province, generating new data to increase geological-mining knowledge on areas with a high potential discovery, related to gold, silver, copper, molybdenum and base metals mineralization, which serve as basic information for future research and investments in prospecting and mining exploration.

The study area includes the department of Iglesia, which is located in the San Juan province, Argentina, and is characterized by two geological settings, Frontal Cordillera and Precordillera.

Metallogenetically, the projects are related to the Andean and Gondwanic cycles, and correspond to different deposit models, including the famours Maricunga and El Indio belt, standing out for their abundance of gold + silver + copper low/ high sulphidation epithermal, polymetallic and porphyries types deposits, such us the world class Josemaría project in the Macho Muerto district, and the Veladero and Lama-Pascua in the Valle del Cura district.

ASTER data consists of measurements of the solar radiation reflected and emitted from the Earth's surface from three Sensors, VNIR, SWIR and TIR. The first consists of three bands in the visible wavelength and near infrared (NIR) region of 0.52 to 0.86 micrometers (Mm). The second subsystem consists of six bands in the short-wave infrared wavelength region (SWIR) from 1.6 to 2.43 Mm. While the third subsystem is characterized by five bands that capture the terrestrial radiation emitted in the wavelength region of the thermal infrared (TIR) from 8.125 to 11.65 Mm. The VNIR subsystem presents 15 meters of spatial resolution, 30 meters the VNIR and 90 meters the TIR (Fujisada, 1995).

Twenty-nine ASTER L1T images obtained from the United States Geological Survey (USGS) were processed. The images obtained were calibrated to radiance and then converted to reflectance from the FLAASH module of the ENVI program. This module uses the MODTRAN model to make atmospheric corrections to images. The selection of the atmospheric model was made based on water vapor data obtained from MODIS data.

The bands 10 to 14, corresponding to the thermal infrared region, were converted to emissivity by the Normalization method, which consists of calculating the surface temperature for each band using the same reference emissivity value.

Argillic, phyllic, silica-rich rocks and propillitic hydrothermal alterations were calculated based on their spectral characteristics by means of band ratios, logical relations between bands (Mars and Rowan, 2006) (Mars, 2013) and threshold determination with the ENVI software.

Hydrothermally altered phyllic and argillic rocks were mapped using ASTER VNIR and SWIR data at 30-m spatial resolution. SWIR band ratios were used to enhance Al-O-H spectral absorption features at 2.165-Mm and 2.2-Mm that are associated to alunite, kaolinite, and sericite-muscovite.

Hydrothermal silica-rich rocks were mapped using ASTER SWIR and TIR band ratios at 90- m resolution. TIR band ratio of band13/band 12 enhance the 9.09-Mm quartz absorption feature and SWIR band ratio of band 4/band 7 is higher for hydrothermal silica-rich rocks.

Hydrothermally altered propilitic rocks were mapped using ASTER SWIR and TIR band ratios at 90-m spatial resolution. Calcite, dolomite, epidote, and chlorite exhibit CO_3 and Fe, Mg-O-H spectral absorption features at 2.31 to 2.33 Mm in the SWIR region. However, in the TIR spectral region calcite and dolomite exhibit an 11.2-Mm spectral absorption feature . Thus, TIR calcite-dolomite spectra exhibit higher ASTER band-13 emissivity and lower ASTER band-14 emissivity.

The analysis of hydrothermal alteration from ASTER data together with geology, structural lineaments, geophysics (magnetometry), satellite images (LANDSAT) and Metallic Domains, allowed defining sixty-five (65) new exploration targets without previous information, similar to the large deposits located in the Macho Muerto and Valle del Cura districts.

REFERENCES

Fujisada, H., 1995. Design and performance of ASTER instrument: Proceedings of the International Society for Optical Engineering, 2583, 16"25.

Mars, J.C., and Rowan, L.C., 2006. Regional mapping of phyllic- and argillic-altered rocks in the Zagros magmatic arc, Iran, using Advanced Spaceborne Thermal Emission and Reflection Radiometer (ASTER) data and logical operator algorithms. Geosphere, 2, 161–186, 2 plates, doi:10.1130/GES00044.1.

Mars, J.C., 2013, Hydrothermal alteration maps of the central and southern Basin and Range province of the United States compiled from Advanced Spaceborne Thermal Emission and Reflection Radiometer (ASTER) data (ver 1.1, April 8, 2014: U.S. Geological Survey Open-File Report 2013–1139, 6 p., 13 plates, scale 1:1,300,000, http://dx.doi.org/10.3133/ofr20131139.

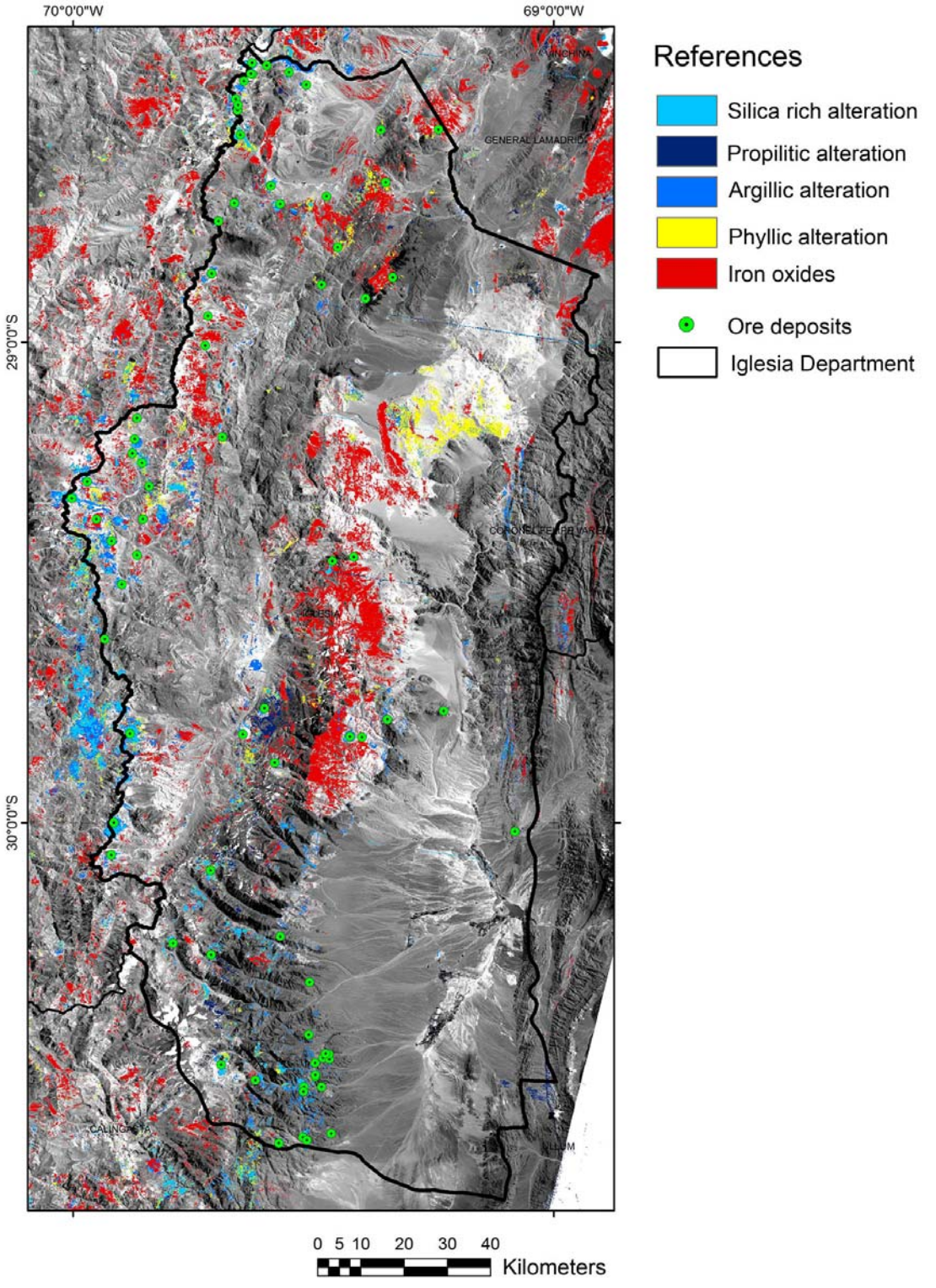

AEROMAGNETIC DATA INTERPRETATION FOR MINING EXPLORATION TARGETS DETECTION IN SAN JUAN PROVINCE, ARGENTINA

Dolores Alvarez[1], Diego Rodríguez, Fernando Ganem, Diego Azcurra, Leda Moser, Javier Peroni

[1]*SEGEMAR - dolores.alvarez@segemar.gov.ar*

Between 1999 and 2001 Geological and Mining Survey of Argentina (Servicio Geológico Minero Argentino, SEGEMAR) carried out 26 magnetic and gamma ray airborne surveys, covering mainly the relief areas of Cordillera de Los Andes, Pre-cordillera and part of Sierras Pampeanas in the north and center of the country.

In 2017, within the framework of an agreement between SEGEMAR and the Mining Ministry of San Juan Province was carried out a project for the updating and characterization of known mineral deposits, and the generation of new exploration targets, involving the update of the mining projects database and the reviewing and reinterpretation of geological, geophysical and remote sensing data already owned by SEGEMAR.

The San Juan province is recognized for having world class deposits, related to the famous Maricunga and El Indio belts, shared with the neighboring country of Chile, such as Lama, Veladero, Josemaría and Filo low/ high sulfidation epithermal and porphyries type deposits, as well as Altar, Azules and Pachón latest discoveries of porphyries in the Calingasta sector, and the skarn deposit of Gualcamayo, in the Precordillera. Also, a varied amount of polymetallic deposits, simple and complex, can be found. For this project were individually studied the Departments of Iglesia, Calingasta, Jáchal, Valle Fértil and Caucete.

The airborne magnetic data involving San Juan Province is divided into six blocks that were surveyed by different contractors. To be able to interpret the data it was necessary to join and level the total magnetic field grids, to process what is known as "stitching" that was done using Oasis Montaj 7.1 by Geosoft. With the stitched grids, several processings were performed on the total magnetic field grid to help with the interpretation of the data and enhance the lineaments. The applied processing methods were: reduction to the pole (RTP), analytical signal amplitude (AS), first derivative of the total magnetic field reduced to the pole (1DV) and the tilt derivative (TILT). Using these grids to characterize the known mineral deposits, highly relevant geophysical patterns were defined, identifying magnetic lineaments and individual anomalies that seem significant in the geophysical interpretation.

For target detection were analyzed, along with magnetic lineaments and anomalies, the geology at 1:250.000 scale for which nine geological charts were joined and their formations grouped in tectonostratigraphic units, emphasizing those ones related with the metallogenic cycles that hosted mineral deposits in San Juan Province. More than 120 ASTER images were processed for the identification of hydrothermal alteration, obtaining maps of argillic, phyllic, propylitic and sillic alteration. Terrain lineaments were determined using digital terrain models (DEM) generated through ASTER Global DEM and SRTM models, and this features were used together with faults and folds mapped in 1:250.000 scale geological charts and the magnetic lineaments obtained for this project. The nearness to known mining projects or mineralized areas was considered too as factor for target evaluation, for which was necessary the update of the database of mining prospects of San Juan Province.

The data obtained through the processing of the aeromagnetic surveys were especially important for the detection of NW-SE lineaments, oblique to the main N-S strike of the Andean structures, which control a large part of the world class deposits. These lineaments, generally difficult to see in the field, are strongly related to mineralization and in severals cases are a continuation of metallogenic domains in Chile, and the mining projects are always aligned with them.

From this study 261 new targets were detected; 76 of them with high potential, 100 with intermediate potential and 85 with low potential. The mining potential maps that resulted from this project are a new way of applying regional geophysics that relates the patterns of hydrothermal alteration, igneous intrusions and structural controls, and can help to promote the mining potential of our country.

1. a) Stitching of six differents blocks of aeromagnetic data. b) An example of Iglesia Department of magnetic data interpretation and the resulting targets map.

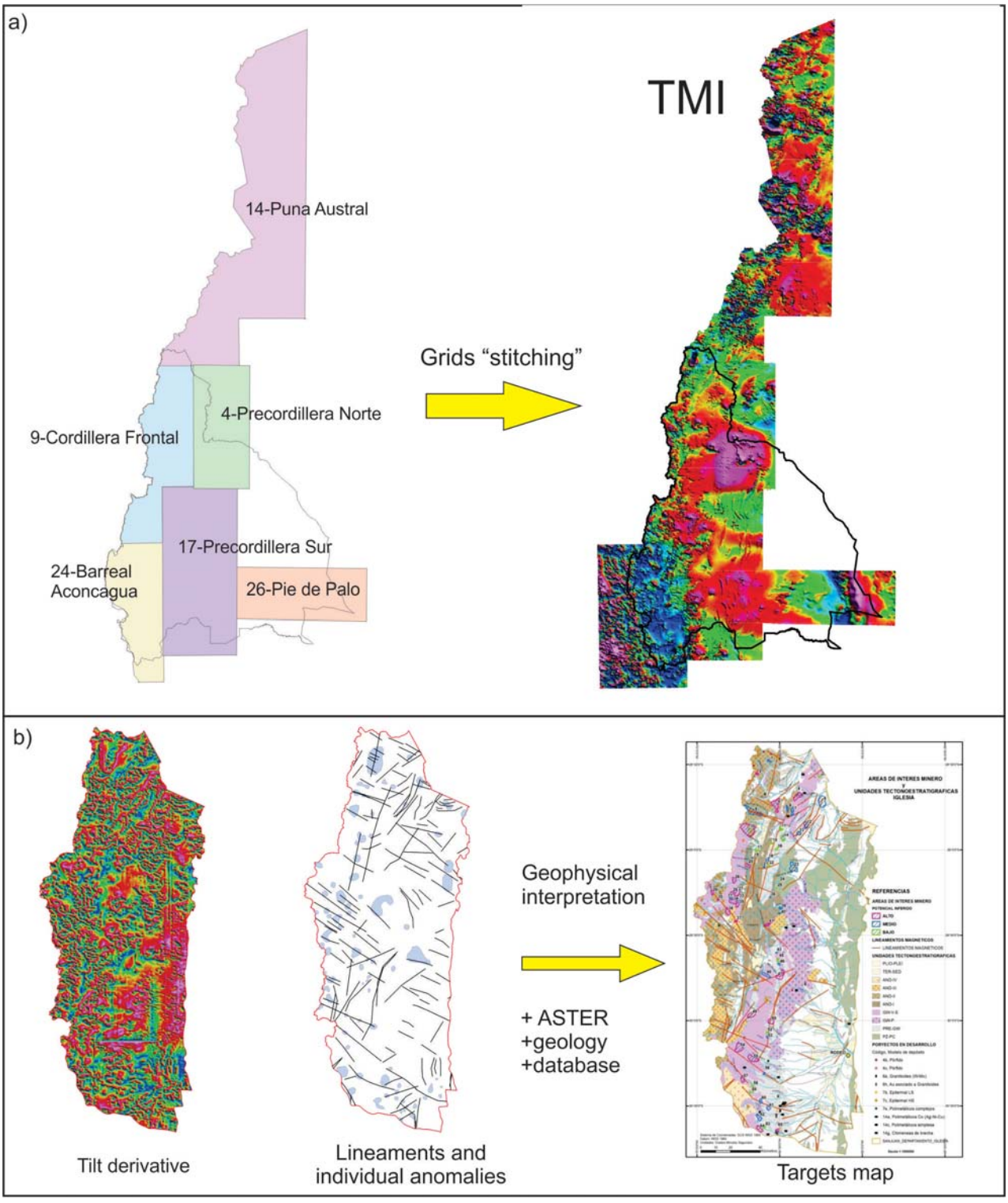
a)
14-Puna Austral
4-Precordillera Norte
9-Cordillera Frontal
17-Precordillera Sur
24-Barreal
Aconcagua
26-Pie de Palo
Grids "stitching"
TMI
b)
Tilt derivative
Lineaments and
individual anomalies
Geophysical
interpretation
+ ASTER
+geology
+database
Targets map

EVALUATION OF A PROTOCOL FOR RAPID CHARACTERIZATION OF THE MAGNETIC SIGNATURE OF COMMERCIAL UAV MULTICOPTERS AS PLATFORMS FOR SCIENTIFIC MAGNETIC SURVEYS

Ruy Sanz[1], Francisco Javier de Frutos, Miguel Angel Rivero, Sergio Fernández Romero, Maria Parrondo, Eduardo De Diego, Francisco Ocaña, Emanuel Ramírez-Catapano, Enrico Fini, Javier Isabel Hernández, Aitor Ibarra Ibaibarriaga, David Gonzalez, María Ramírez-Nicolás, Francisco Rios, Rolf Kilian, Marina Díaz Michelena
Instituto Nacional de Técnica Aeroespacial, INTA. Departamento de Cargas útiles y Ciencias del Espacio.
[1]*sanzgr@inta.es - Background*

Traditionally, airborne magnetic surveys are performed with manned aircrafts. However, such platforms are a source of strong magnetic signals and this magnetic contamination represents an important drawback of this method. An effective solution, in order to mitigate its effects on the magnetic payload is to include booms of several meters length even though compromising the aerial operations. In addition, limitations arise when detailed magnetic surveys are demanded, due to the minimum altitude at which they have to be performed. Thus, when detailed and precise measurements are needed, land-based methods are preferred, with their corresponding longer times, higher risk and limitations by the orography. The use of Unmanned Aerial Vehicles (UAV's) as survey platforms seems to be an optimal solution to close the gap between airborne and land-based magnetic surveys. Multicopters UAV's are more appropriate for detailed surveys on areas of limited or difficult access, thanks to vertical take-off and landing, and hovering. However, the traditional mitigation strategies of large booms are not implementable in small UAV platforms, therefore the magnetic characterization of the platform is of critical importance.

In this contribution, we present the preliminary work done to adapt vector magnetometers to two multicopter platforms: DJI Matrice600pro and DJI S1000+, and we report on the systematic measurements performed in laboratory environment as well as in well-known magnetic signature set-ups. The final objective of these characterizations and performance tests is to carry out vector geomagnetic surveys based on UAV multicopters, with real time data link.

METHODS

The methodology followed can be summarized as follows: Firstly, a magnetic characterization of the magnetic signature of the drones has been done in INTA Space Magnetism Laboratory testing facility. Secondly, the distance of the needed boom has been calculated and validated experimentally through tests in the laboratory with different operational modes and interpreting the magnetic signature of a well-known configuration of magnets. Thirdly, a field campaign has been done with combined terrestrial and drone-based measurements over another reference configuration of magnets in an area of 2500 m2 where the natural surface magnetic anomalies are lower than 0.5 µT.

The characterization of the magnetic signature of the UAV was performed indoor at the magnetic testing facility at INTA, following adapted aerospace standardized tests (ECSS-E-ST-20-07C) which enable to simulate different maneuvers (take-off, hovering, pitch, roll, etc…), but can be performed at a stationary position (Fig.1a).

Based on the obtained magnetic signatures by those tests and combined with mechanical and aerodynamics analysis, a sensor boom was designed which enables to achieve a resolution lower than 1 nT after a modeled noise compensation.

For an experimental validation of the proposed configuration, the UAV has been placed in a bench at INTA Space Magnetism Laboratory facility which provides a simulating set up with the sensor payload at well-determined distances from the UAV. These experiments consisted in the measurement of a known configuration with three reference permanent magnets (170 mA·m2) at 1 m distance below the sensors position, displaced horizontally at 0.3 m/s. The measured vector magnetic field components have been compared to the calculated field magnetic field strength above the magnets (Fig.1b).

Afterwards an experimental validating campaign was performed in a relatively flat area with low magnetic anomalies. At first the natural magnetic anomalies of this area has been mapped with a high resolution on ground magnetometer system developed ad hoc by INTA and UT teams .This system enabled precisely oriented vector measurements. After this, several magnets have been displayed over the area with different special configurations and flight surveys have been done with a commercial FGM-3 fluxgate on a 90 cm boom attached to a DJI S1000+ UAV with a real time data link at different altitudes. Finally, the data have been post-processed.

RESULTS

The resulting magnetic dipole moment of the drones were: mx= -82±13 my= 24±13 mz=-0.14±0.06 (mAm2). From the obtained results, the optimal position for the magnetic sensor at less than 1 meter from the gravity center of the UAV was determined considering the general aim to obtain a magnetic noise below 1 nT. This position allows the use of a boom that did not limit the flight performance of the platform. The second indoor test revealed that the magnetic payload at this position, even in worst-case scenario (motors at max. power), is able to reproduce the magnetic profiles predicted by theoretical models (Fig.1b). Finally, the results of the field campaign verified that: the flight performance of the UAV was kept almost unaltered, that it was possible to detect and locate the reference magnets at real time by data link between the payload and ground controlling station. This configuration enables an appropriate in-flight data visualization and processing (Fig.1c).

CONCLUSIONS

The application of aerospace standardized testing methods has been employed to characterize the magnetic signature of two UAVs. This information allowed an appropriate implementation of magnetic payloads at a short boom, which able to minimize the effects of the magnetic contamination while keeping the UAV flight capacities. The performed preliminary field tests with the proposed assembly configuration also confirmed a successful in situ transmission and processing of the magnetic and attitude data.

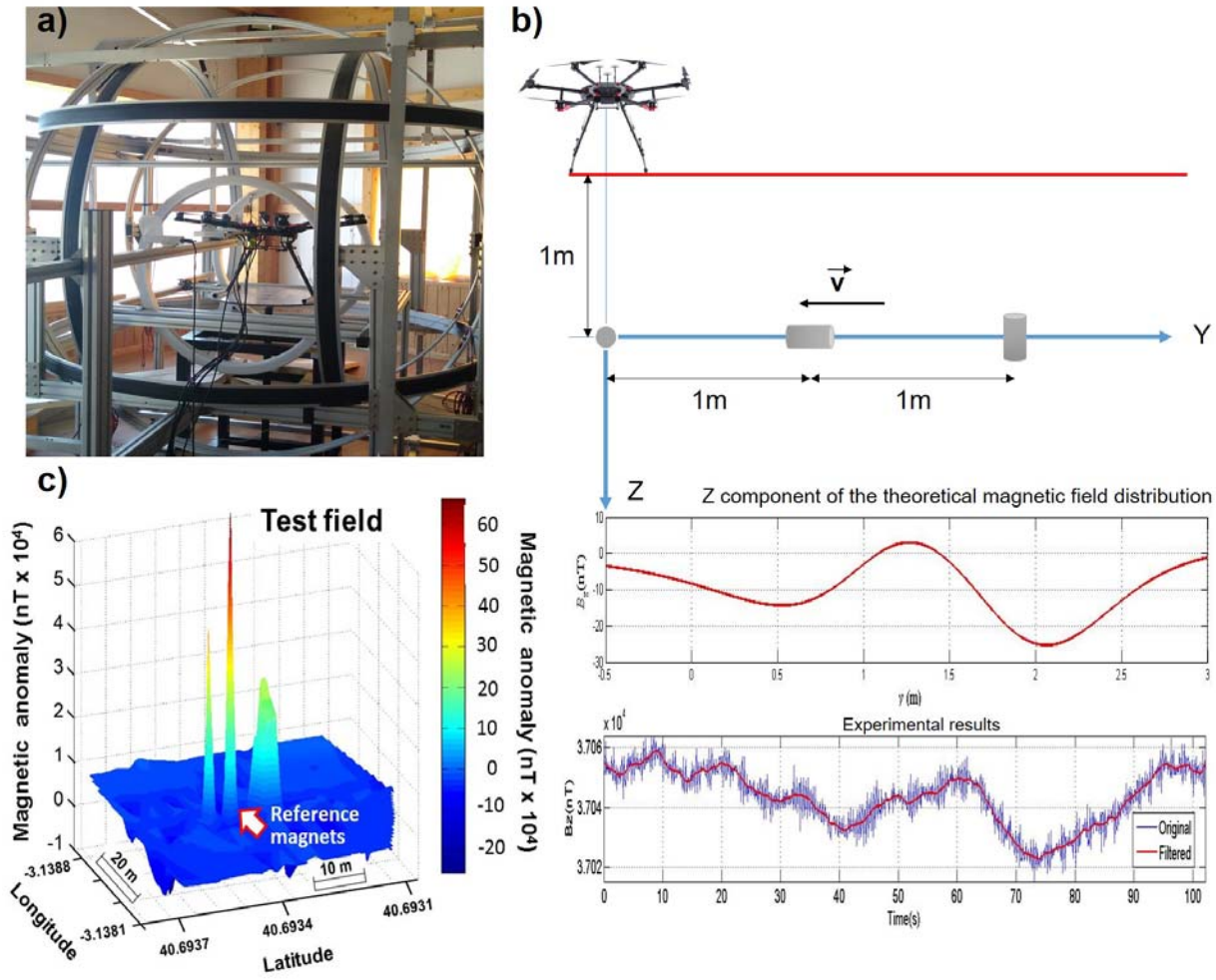

REMOTE SENSING FOR GEOLOGY IN THE XXI CENTURY

Bondur, Valery G.[1], Cherkasov, Sergey V.

[1]*Russian Academy of Sciences - vgbondur@aerocosmos.info*

Everybody agrees that *remote sensing* means an acquisition of information about an object or phenomenon without making physical contact with the object. For geologists, the term is connected rather with satellite imagery, including multi- and hyperspectral techniques. Sometimes the same kind of survey is being carried out using an aircraft platform.

At the same time, from the initial definition, remote sensing in geology should embrace every method registering any natural field(s) influenced by geological objects, which includes the whole electromagnetic spectrum, potential fields, namely - magnetic and gravity, and radioactive radiation. The sensors for these measurements can be installed at a satellite as well as at any aircraft, including unmanned aerial vehicles (UAV). To select a method (or a set of methods) for resolving a specific geological task, one has to take into account all these remote sensing opportunities along with characteristics of the environment under consideration.

Most of the remote sensing methods can be used with different types of the carriers (Table 1), excluding gravimetric survey and ã-methods.

It is also necessary to note that the same method for different carriers has different characteristics, and, consequently, resolves different geological tasks. For instance, both, magnetic and gravimetric surveys in satellite version can be used for planetary-scale tasks; traditional aeromagnetic and aero-gravimetric surveys are really useful for geological mapping of large (over 200-300 sq. km) areas, and UAV-based magnetometry provides the best results for geological prospecting of mineral deposits in the areas under 200 sq. km. Modern technologies cannot facilitate the use of small UAV for gravimetric survey because of the gravimeter's weight. By the same reason, a γ-spectrometry can be conducted by a traditional aircraft or by really heavyweight UAV only.

For all kinds of imagery, the key factor defining the method's capacity is resolution. The best from the satellite imagery at the moment is WorldView-4 with resolution of 25 cm. Surely, imagery received with both, traditional aircraft, and UAV, can do much better, but at higher price per sq. km. Also, recent research on use of visual photo for 3D modeling of the Earth surface demonstrate advantages of small UAV in comparison with satellite when the territory under study is characterized by inclinations over 15°.

The biggest issue for use of any imagery for geology is a non-direct relation of an image and the geological elements under study. It is complicated even for territories without soil cover, and once we think of forestry, it becomes a very difficult, and often – an unresolvable task.

For potential fields, the fields' properties define limitations of different methods rather than the methods capacities or the sensor's characteristics. The response of magnetic field lowers as r^3, and of the gravity field – as g^2, where *r* is a distance from the source. Besides of that, the anomalies from different sources get superimposed, and quality of their interpretation diminishes with height position of a sensor. Thus, the closer to the surface we move the sensor, the better. In fact, from the space we can register the Earth gravity and magnetic fields, but the interpretation will be either a point of mass, or a magnetic dipole representing our planet. No useful information for geology can be obtained this way. The most promising for measurements of the magnetic field looks an unmanned aeromagnetic system (UAMS), which can fly as low as first tens of meters. UAMS can nearly compete with the ground magnetic survey in terms of the survey quality, and is minimum 10 times more productive than the latest.

Carrier	Visual Photo	Infrared	Multi- and hyper-spectral	Magnetic survey	Gravimetric survey	γ and γ-spectrometry
Satellite	+	+	+	+	+	-
Aircraft and UAV over 20kg	+	+	+	+	+	+
UAV (up to 20 kg)	+	+	+	+	-	-

Table 1. Methods of remote sensing for geology by carriers

CONCLUSIONS

In the XXI century, the remote sensing methods for geology are represented by imagery, including infrared and hyperspectral ones, and by the potential fields' measurements. Besides of that, ã-spectrometry is a well-established method in the traditional aerogeophysics.

For all kinds of imagery, as well as for magnetic survey, UAV-based technologies become competitive with traditional aerial survey. Still, such methods as gravimetry and ã-spectrometry cannot be used with the small UAV because of the sensors' characteristics, and, thus, stay with traditional aerogeophysics. Consequently, when a specific geological task requests these methods, a traditional aircraft capable of simultaneous execution of magnetic, gravity, ã-spectrometry, and imagery would be a logical choice.

The set of the remote sensing technologies should be decided upon detailed consideration of the geological task as well as capacities of different methods on different carriers.

PORPHYRY EXPLORATION SUPPORTED BY AIRBORNE HYPERSPECTRAL IN THE PERUVIAN ANDES

Alexander Farrar

First Quantum Minerals - alex.farrar@fqml.com

BACKGROUND

Central and southern Peru is home to numerous world-class porphyry copper deposits that occur within multiple metalogenic belts. Contained copper of the known deposits in these two regions exceeds 140 Mt, with the major deposits being Toquepala, Cerro Verde, Cuajone, Antamina, and Toromocho.

Prospectivity maps applying the mineral systems approach (e.g. Wyborn *et al.*, 1994; McCuaig *et al.*, 2010) were created using geologic, geophysical and geochemical based inputs and were combined with multispectral datasets such as ASTER and LANDSAT to create a fully integrated, ranked 'prospectivity map' for porphyry copper exploration in southern and central Peru. The geologic and geophysical datasets were used to create a favorable structural 'architecture' map, whilst the geochemistry and multispectral datasets were used to directly target potential hydrothermal systems and combined into one product.

'Areas of Interest' (AOIs), occur where multiple favorable factors come together in one location and is thus deemed a favorable location to explore for a porphyry copper deposit. Added confidence in the validity of the prospectivity map product is that all of the known major deposits are associated with a high ranking AOI. In total there were roughly 330 AOIs deemed necessary for follow up fieldwork in the original products.

METHODS

FIELDWORK

The terrain of the work area varies from relatively flat desert within the coastal Jurassic belt, to steep, rugged terrain in the Paleocene-Eocene and Miocene bets of the *Cordillera Occidental* where altitudes range from 2000-5000m asl. The majority of the high ranking AOIs occur within the *Cordillera Occidental* - most of which don't have direct road access.

As a result a lot of field time is devoted to trying to gain vehicle access as close as possible to each AOI, and then hiking to field truth each AOI. Approximately 20% of the time it was found impossible to reach the AOI on foot due to extreme terrain, with an average of two days to vet each AOI. After the first year of fieldwork, based on the rate of AOI verification, it was anticipated that it would take 8-10 years to field check all of the AOIs with the personnel resources on hand.

MULTISPECTRAL SHORTFALLS

Due to the multispectral nature of ASTER, it is only possible to confidently map mineral groups, not species, within the 1900-2500nm range for clays and white micas. These mineral groups contain some of the key indicator minerals associated with porphyry hydrothermal systems, and can represent hydrothermal alteration associated to phyllic, argillic and advanced argillic alteration zones. However in the field it was found that the vast majority of the AOIs that were being visited (>80%) were not actually hydrothermal in origin, rather simply due to surficial weathering of existing geology.

It was also found that the 30m ASTER pixel size was not sufficient to identify some true hydrothermal anomalies which were variably covered by Quaternary ash, but had hydrothermal alteration outcropping in creeks which incise the thin ash layer.

RESULTS

EXAMPLES OF FALSE POSITIVES FROM MULTI-SPECTRAL DATASETS

It was found that Jurassic-Cretaceous marine and continental sediments which occur throughout the region were yeilding 'argillic' and 'advanced argillic' false positive anomalies owing to the surficial weathering of shale to produce kaolin. Additionally, weathering of the sediments liberates detrital white micas which can yield 'sericite' anomalies though are non- hydrothermal in origin and therefore also produce false positive anomalies.

Voluminous dacitic – andesitic lavas occur throughout the study region and often have a porphyritic texture, with 2-10mm phenocrysts of feldspar common. When these units are weathered, the feldspar converts to kaolin and yields a false positive argillic /advanced argillic signal.

Weathering of units with an andesitic composition liberates iron from the mafic minerals within the rock. The iron is often remobilized and forms secondary iron oxide coatings on the outside surfaces of the rock, which causes broad hematite and goethite anomalies, though which are not associated to a hydrothermal alteration cell.

It is a common phenomenon for mafic units that have undergone regional metamorphism to form epidote and chlorite veins which yield a false 'propylitic' signal.

AIRBORNE HYPERSPECTRAL ACQUISTION

In order to speed up field validations of the AOIs, and in an attempt to reduce the number of false positive anomalies being visited, FQM decided to trial an airborne hyperspectral survey in southern Peru. A novel survey design allowed for all priority AOIs to be overflown as well as all eight of the known deposits within the survey area within budget constraints.

Being able to accurately distinguish the hydrothermal minerals of alunite, pyrophyllite and dickite from kaolinite was key to be able to downgrade the AOIs that exhibit just kaolinite – which were deemed to have formed from solely from surficial weathering processes.

The ability to accurately map the wavelength differences of the sericite 2200nm absorption feature in the airborne hyperspectral data allowed the calculation of illite chemistry and crystallinity, which assisted with distinguishing true hydrothermal sericite vs detrital micas liberated from weathered sediment which further helped to filter spurious anomalies

In total roughly 25% of the AOIs were able to be filtered out in this manner, saving 2-3 years of fieldwork, a further 50% more were ranked as low priority for field visits due to different alteration intensities or non-favorable erosional levels.

The specific hydrothermal mineral mapping of the AlOH group as well as the sericite 2200nm absorption feature and crystallinity both of which are particularly useful in quartzite packages, allowed FQM to immediately re-rank the existing AOIs based on their favorable mineralogy. This meant that the truly high priority AOIs could be flagged for immediate field validation.

The 6X smaller pixel size of the airborne hyperspectral survey relative to the ASTER pixel allowed for previously subtle multispectral anomalies (i.e. concealed by ash cover) to properly reveal themselves in creeks and gullies. It also enabled the desktop vetting of the inaccessible AOIs, which previously would have had to be visited via helicopter, both costly and a safety risk in the Andes.Iron oxide species are better mapped and subtle jarosite anomalies (resulting from the oxidation of sulfides) were revealed at several AOIs.Additionally FQM was able to take the mineralogical fingerprint of all the known deposits in the region and use it as a training dataset for favorable spectral characteristics to our AOIs.

Field validations have been made more efficient because the team can go directly to the anomalous outcrops to verify the size and intensity of hydrothermal alteration, on average visiting 1 AOI per day, twice as fast as pre-hyperspectral.

CONCLUSIONS

Conducting hyperspectral surveys has reduced what would have been an 8-10 year generative program to a 4-5 year program. By being able to re-rank the existing AOIs based on their hyperspectral characteristics, FQM was able to prioritize field visits to the most exciting AOIs earlier than would have occurred if the survey was never acquired. This has been especially important in the current exploration climate where large tracts of free exploration ground are becoming available in Peru. This has resulted in the identification of four large porphyry alteration zones, three of which were able to be fully staked by FQM. Additionally, in two of FQM´s current projects, the survey has assisted by defining the limits of alteration as well as highlighting the areas of interest and assisting with mineral identification.

REFERENCES

McCuaig, T.C., Beresford, S., Hronsky, J., 2010. Translating the mineral systems approach into an effective exploration targeting system. Ore Geol. Rev. 38, 128

Wyborn, L.A.I., Heinrich C.A., Jaques A.L., 1994. Australian Proterozoic mineral systems: essential ingredients and mappable criteria: Australian Institute of Mining and Metallurgy Annual Conference, Melbourne, Proceedings, p. 109-115.

EXPRESS INTERPRETATION OF MULTI-LEVEL UNMANNED AERIAL MAGNETIC SURVEY. CASE STUDY

Sergey Cherkasov[1], Dmtry Goglev, Dmitry Kapshtan

[1]*SGM RAS - s.cherkasov@sgm.ru*

Different researchers developed the theory of multi-level magnetic survey in the 50th-60th of last century. But, the cost of aeromagnetic survey made multi-level measurements too expensive. Some attempts to apply the theory to practice have been made on the basis of using regular aeromagnetic and ground data together. This approach is still being used for magnetic anomalies' interpretation, but, in fact, it lacks most part of advantages the multi- level survey can provide to the geologists. The use of unmanned aircraft magnetometric system (UAMS) with lightweight unmanned aerial vehicle as a platform makes a multi-level magnetic survey economically efficient.

As an example of UAMS' capacities, an express interpretation of 3-level magnetic survey can define the depth of magnetic masses using a system of simple equations:

$$\Delta T_2/\Delta T_1 = x^3/(x+a^3), \text{ and } \Delta T_3/\Delta T_1 = x^3/(x+b^3) \quad (1)$$

where ΔT_n – an amplitude of magnetic anomaly measured at the level n, x – unknown vertical distance from magnetic masses to the level 1, *a* and *b*–relative height of levels 2 and 3 (to the level 1), correspondingly. The solution of such system comes to a simple quadratic equation.

An experimental 3-level UAMS survey has been executed nearby Hautoovara village, 450 km from Sankt-Petersburg in June, 2018. The UAMS' platform (Geoscan-401 copter) and rubidium atomic magnetometer are being produced by Geoscan, Ltd. since 2016, and demonstrate stable and precise magnetic measurements.

Geological environment is represented by Hautovaara series of Archean volcanic and volcanic-sedimentary rocks overlaid by relatively thin sedimentary (glacial) cover. Some of the crystalline complexes contain phenocrysts of pyrrhotite causing magnetic anomalies with amplitudes up to n x 1000 nT.

The results of the three-level survey correspond to 40 m, 70 m, and 120 m height above the surface (fig. 1).

After applying to (1) ΔT_1= 3000 nT, ΔT_2= 2300 nT, ΔT_1= 1150 nT, *a*=30 m, and *b*=80 m, we receive a quadratic equation $102{,}5x^2-5021{,}5x-162659=0$ with roots 71 (m) and -23 (m). Neglecting the second root as irrelevant, and taking into account 40 m-height of flight, we can estimate the depth of magnetic mass as 30 m from the surface. The thickness of sedimentary cover in the area varies from 3 to 10 m with rare outcrops of the basement rocks. The difference between 30 and 3-to-10 meters reflects, from one side, inaccuracy of the express interpretation (the shape of the magnetic body was not taken into count as well as its magnetic properties), and from another side – highly probable uneven distribution of magnetic properties with depth. Also, the wind speed during the flights achieved over 15 m/sec, which had complicated the survey.

The most peculiar fact about the UAMS survey is its efficiency. In our case, all fieldwork (by a team of two) including 450 km drive, 12 flights 25-35 minutes each, 130 km in total, and driving back has taken one day. It was just 7,5 hours from the first takeoff to the last landing.

The capacities of the multi-level UAMS survey are not limited by the express evaluations. Multi-level measurements have great potential as for geological mapping so for geological prospecting on the basis of 3D modeling of magnetic bodies from 3D magnetic anomalies.

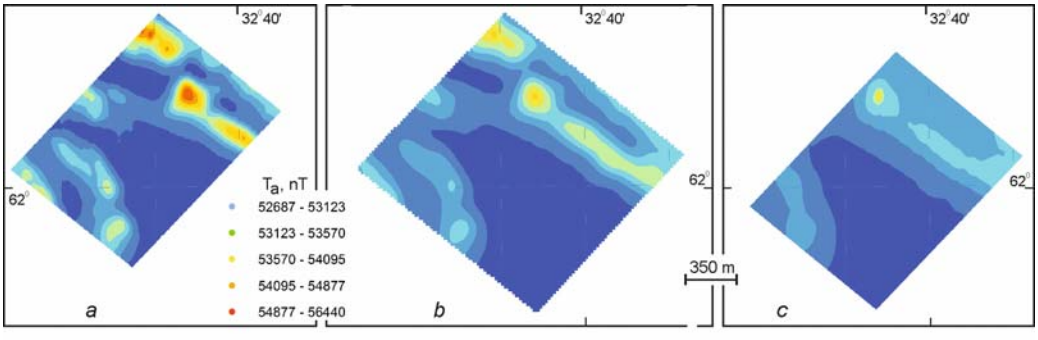

Fig. 1. Magnetic field map at altitudes: 40 m (a), 70 m (b), and 120 m (c).

A | 152

HIDROTHERMAL ALTERATION MAPPING WITH ASTER IN PANCHO ARIAS, NW SALTA, ARGENTINA

Silvia Castro Godoy[1], Víctor Bercheni

[1]Geological Survey of Argentina (SEGEMAR) - silvia.castro@segemar.gov.ar

BACKGROUND

Advance Spaceborne and Reflection Radiometer (ASTER) was designed to identify hydrothermal alteration areas, among other, with its 3 bands in the visible and near infrared region (VNIR), 6 in the shortwave infrared (SWIR) and 5 bands in thermal infrared, with 15m, 30m and 90 m of spatial resolution respectively.

Economic deposits such as gold and copper are associated with hydrothermally altered rocks which have hydrous zones of alteration minerals that exhibit diagnostic spectral absorption features in the VNIR -SWIR and TIR regions.

From Remote Sensing area of Geological Survey of Argentina, hydrothermal alteration mineral mapping is systematically carried out by applying logical operator algorithms (Mars 2013) that identify mineral groups from argillic, phyllic, propylitic and siliceous alteration zones. In this context, the results of applying this methodology in Pancho Arias (S24°15´46", W65°50´50") are presented here.

Pancho Arias is a mining district located in the northwest of Salta Province, approximately 100 km to the northwest of Salta city. It is considered as a molybdenum deposit in stockwork and disseminated porphyry type and as a porphyry copper.

This district gathers cenozoic igneous rocks whose location was favored by the faults parallel to the Calama-Olacapato-El Toro lineament (Figure 1A). Martín *et al.* (2008) described the miocene hydrothermal alteration with symmetric spatial distribution with a potassium core, surrounded by the phyllic alteration area and an outer halo with propylitic alteration.

METHODS

ASTER L1T orthorectified image (14 bands per scene) downloaded from the Geological Survey of the United States (https://earthexplorer.usgs.gov/) was procesed. It was calibrated to radiance and then VNIR-SWIR bands were converted to reflectance by FLAASH module of ENVI. Thermal bands were converted to emissivity by the normalization method (Guillespie, 1985).

The hydrothermal alteration minerals were detected by logical operators using together band thresholds and band ratios (Mars and Rowan, 2006 and Mars, 2013) in order to map the following absorption characteristics:

- Argillic alteration: Minerals as kaolinite have absorption at 2.20 microns (SWIR, band 6).
- Advanced argillic alteration: Detects alunite/pyrophyllite due to absorption in 2,169 microns (SWIR, band 5).
- Phyllic alteration:This type of alteration, dominated by illite/muscovite/sericite, has a strong absorption at 2.20 microns (SWIR, band 6) and at 2.38 microns (SWIR, band 8).
- Siliceous alteration: Silica-rich rocks (quartz, chalcedony,opal, amorphous silica) have an absorption feature at 9.09 microns (TIR, band 12). To differentiate hydrothermal silica, there were SWIR bands used because they have a lower reflectance value in the range 2.26 to 2.4 than non-hydrothermal silica.
- Propylitic alteration: Minerals such as calcite, chlorite and epidote are present in this type of alteration and have absorption features at 2.31 to 2.33 microns (SWIR, band 8). To differentiate chlorites and epidote from carbonates, bands of the thermal range are used, where carbonates show a characteristic strong absorption in band 14, unlike epidote and chlorites that have absorption in band 13.

The main objective is to apply these algorithms in known and accessible areas to validate methodology and to extrapolate it to another areas as a prospective tool.

RESULTS

Hidrothermal alteration was detected in Pancho Arias including argillic, phyllic and hydrothermal silica zones in a typically circular pattern for this porphyry system (Figure 1, B).

The propylitic alteration described by Martín *et al.* (2008) was not detected by the algorithm. This could be due to several reasons: because it is not an extended area; because the area is covered by other units; or because

the outcrops are in vertical walls. It should be considered that in this algorithm thermal bands of 90m special resolution are used.

A positive response was obtained for siliceous alteration algorithm overlapping phyllic and argillic zones.

CONCLUSIONS

Hydrothermal alteration units were successfully detected in Pancho Arias by using logical operator algorithms applied to ASTER VNIR, SWIR and TIR bands. There were mapped argillic, phillic and silica alteration zones.

It would be important to check them, especially propillitic halo, by field control to understand the origin of differences between ASTER mapping and descriptions from compiled information in order to adjust the methodology if necessary.

REFERENCES

Martín, F.A., J.M. Arnosio and P.J. Caffe. 2008. "Caracterización Petrográfica y Relaciones de Intrusión en un Sistema de Pórfido de Cu-Mo: El Prospecto Pancho Arias". XVII Congreso Geológico Argentino, San Salvador de Jujuy, Actas I: 223-224

Gillespie, A. R. 1985. "Lithologic mapping of silicate rocks using TIMS". InThe TIMS data User\'s Workshop, Jet Propulsion Laboratory Publication 86-38, 1985: 29–44

Mars, J.C., and L.C.Rowan. 2006. "Regional mapping of phyllic- and argillic-altered rocks in the Zagros magmatic arc, Iran, using Advanced Spaceborne Thermal Emission and Reflection Radiometer (ASTER) data and logical operator algorithms". Geosphere, 2, 161–186, 2 plates, doi:10.1130/GES00044.1.

Mars, J.C. 2013. "Hydrothermal alteration maps of the central and southern Basin and Range province of the United States compiled from Advanced Spaceborne Thermal Emission and Reflection Radiometer (ASTER) data". Ver 1.1, April 8, 2014: U.S. Geological Survey Open-File Report 2013–1139, 6 p., 13 plates, scale 1:1,300,000, http://dx.doi.org/10.3133/ofr20131139.

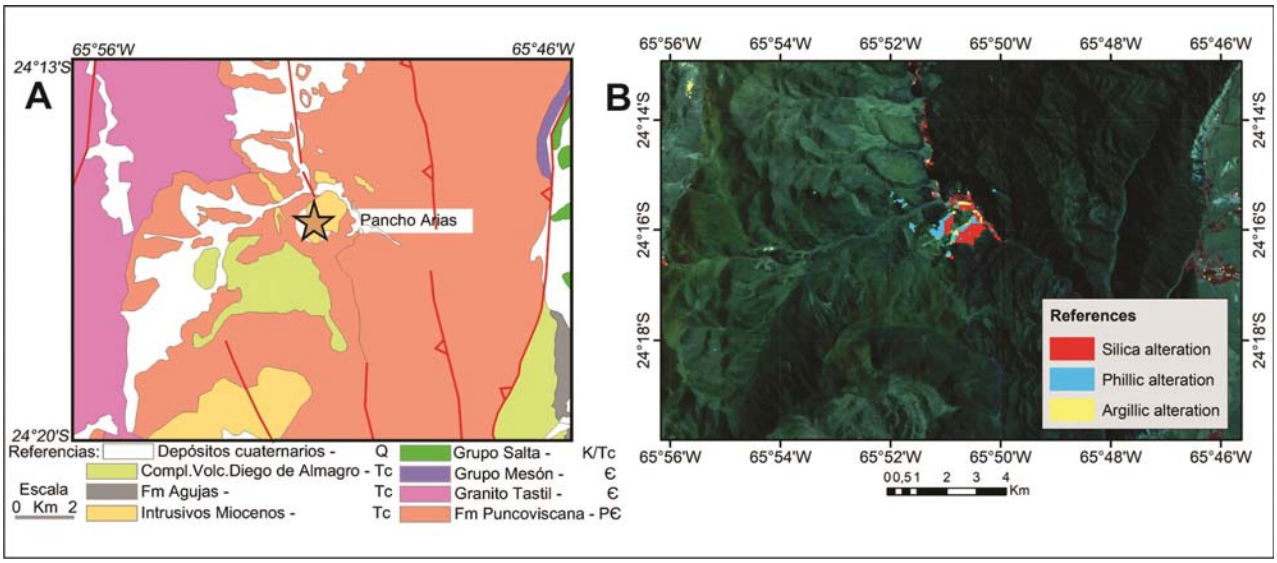

Figure 1. Pancho Arias - A. Geological map B. Hidrothermal alteration map.

CHAPTER 15
URANIUM DEPOSITS AND RESOURCES

Conveners: Luis López, Michel Cuney, Mostafa Fajek

THE CURRENT SITUATION AND FUTURES PERSPECTIVES OF THE FLUID EVOLUTION IN THE LAGOA REAL URANIUM PROVINCE, BRAZIL

Tiago H. DeFerreira[1], Ariela C. Diniz, Lucilia A. Ramos de Oliveira, Lucas E. D. Amorim, Francisco J. Rios, Kazuo Fuzikawa

[1]*CDTN/CNEN - deferreirat@gmail.com*

Currently, Brazil has the seventh largest uranium reserve in the world, being the sole U producer in South America. The Lagoa Real Uranium Province is located in the central- south part of the Bahia State, within the São Francisco Craton. It consists of a variety of Paleoproterozoic albitite, gneissic rocks and metagranitic bodies that intruded the Archean basement of migmatitic rocks. The uranium mineralization is restricted to albitite. The Cachoeira Mine accounts for all uranium production in Brazil. Besides this deposit, thirty- seven uranium anomalies are dispersed along a 33 kilometers long, north-south trending helical structure.

The Lagoa Real Uranium Province has largely been studied over the last decades in order to understand the uranium mineralization, particularly the correlation between albitization and mineralization. Nine studies have used fluid inclusions as a tool to assess the characteristics of the fluids involved in metasomatic and mineralizing processes. Only few of them attempted to correlate fluid-inclusion data from different authors. Here, we compare such data to provide an overview of the fluids involved in the geological evolution of the Province.

We have compiled and revised microthermometric results carried out by previous researchers. This is presented in the Figure as a diagram of salinity vs. homogenization temperatures. Numerous measurements were disregarded because of ambiguous results. The Figure suggests the existence of at least four distinct fluids: (i) aqueous carbonic, trapped in plagioclase of microcline gneiss and in quartz of the Monsenhor Bastos granite, with a wide range of homogenization temperatures (220 °C - 530 °C) and moderate salinity; (ii) aqueous saline brine, recorded in pyroxene, garnet and epidote; (iii) low to intermediary- salinity fluid responsible by the crystallization of albite and late plagioclase; (iv) later fluid containing CO_2+CH_4, found in calcite from carbonate veins, showing the highest salinities and lowest homogenization temperatures.

Previous workers characterized pyroxene, garnet and epidote as hedenbergite ($CaFeSi_2O_6$), andradite ($Ca_3Fe_2(SiO_4)3$) and Ca-rich epidote ($Ca_2(Al,Fe)3(SiO_4)3(OH)$ respectively.

At least two hypotheses can be advanced from the Figure: i) the fluid involved in the albite formation is that trapped in garnet, pyroxene and epidote or ii) the latter minerals and the albite formation are unrelated to each other. According to the first hypothesis, as Na cannot be incorporated into andradite, hedenbergite and epidote, the fluid phase had its Na+ concentration increased. It promoted enough content of sodium to enable formation of albite from K-feldspar. Therefore, Na content on fluid phase decreased and albite trapped less saline fluid. The second hypothesis implies low salinity and Na metasomatism, but garnet, pyroxene and epidote would have formed in a metamorphic process, characterized by higher salinity fluids.

The different types of fluid inclusions found in the albitites and in granites, suggest that those rocks underwent for complexes and distinct processes of metasomatism and metamorphism. Even the fluid inclusions from epidote

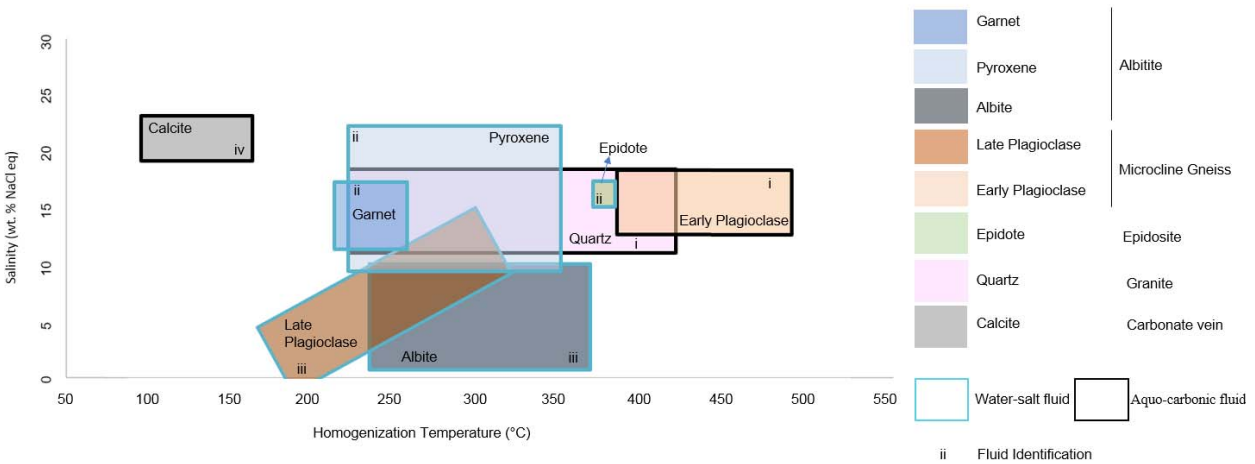

could be formed from a different fluid. As argued by some researchers, epidosites could be associated with a second metamorphic stage, following the formation of albitites. Hence, their fluid inclusions had a distinct origin from those observed in garnet and pyroxene.

More than 30 years after the first researches in the the Lagoa Real Uranium Province and new data continue to be found. Several new isotopic, dating and geochemical data are being obtained in attempt to elucidate the characteristics of the several and complexes events that the area went to. The data and analysis in this work will provide a substrate for those future studies related to the origin, evolution and mineralization in Lagoa Real Uranium Province.

INTEGRATED GEOCHRONOLOGICAL, GEOPHYSICAL AND ISOTOPIC INVESTIGATION INTO THE PATTERSON LAKE CORRIDOR OF THE SOUTHWESTERN ATHABASCA BASIN, CANADA

Jeremy W. Powell[1], Victoria Tschirhart, Eric G. Potter, Colin Card, Dinu I. Pana, Kenneth Wheatley, Cameron MacKay

[1]*Natural Resources Canada - Geological Survey of Canada - jeremy.powell@canada.ca*

Present-day uranium exploration in Canada is focused on the Athabasca Basin, where more than 30 high-grade deposits (average of 1.97 % U) have been discovered in association with the unconformity between Paleo – Mesoproterozoic sedimentary strata of the Athabasca Supergroup and the underlying crystalline basement (Figure 1)[1]. The majority of these deposits are located in eastern Athabasca Basin where the unconformity is intersected by crustal-scale faults rooted in graphitic gneisses and schist. However, the recently discovered Patterson Lake Corridor (PLC), which hosts uranium deposits (e.g. Triple R and Arrow) and occurrences (e.g. Spitfire) outside and along the southwestern margin of the Athabasca Basin, is projected to be a world class uranium district. Known ore lenses along the PLC occur well below the regional unconformity and are hosted in altered mafic to ultramafic intrusions and orthogneisses belonging to the Taltson Domain of the southwest Rae Province[2]. These host rocks are atypical when compared to the basement of unconformity-related uranium deposits east of the Snowbird Tectonic zone. Although hosted in reactivated fault structures, the location and magnitude of these recent discoveries in the west challenge the standard unconformity-related deposit model and thus warrant further investigation.

The Geological Survey of Canada's (GSC) Target Geoscience Initiative uranium fluid pathways activity (TGI-U) is a collaborative government-industry-academia research program that is examining the role of long-lived reactivation of crustal-scale shear zones in driving fluid flow to sites of uranium mineralization. The TGI-U research is integrating geochronological, geochemical and geophysical studies to both constrain the multi-phase deformational and alteration histories of the PLC basement, and quantify the expressions of fertile alteration along the reactivated fluid pathways that span the southwestern Athabasca Basin.

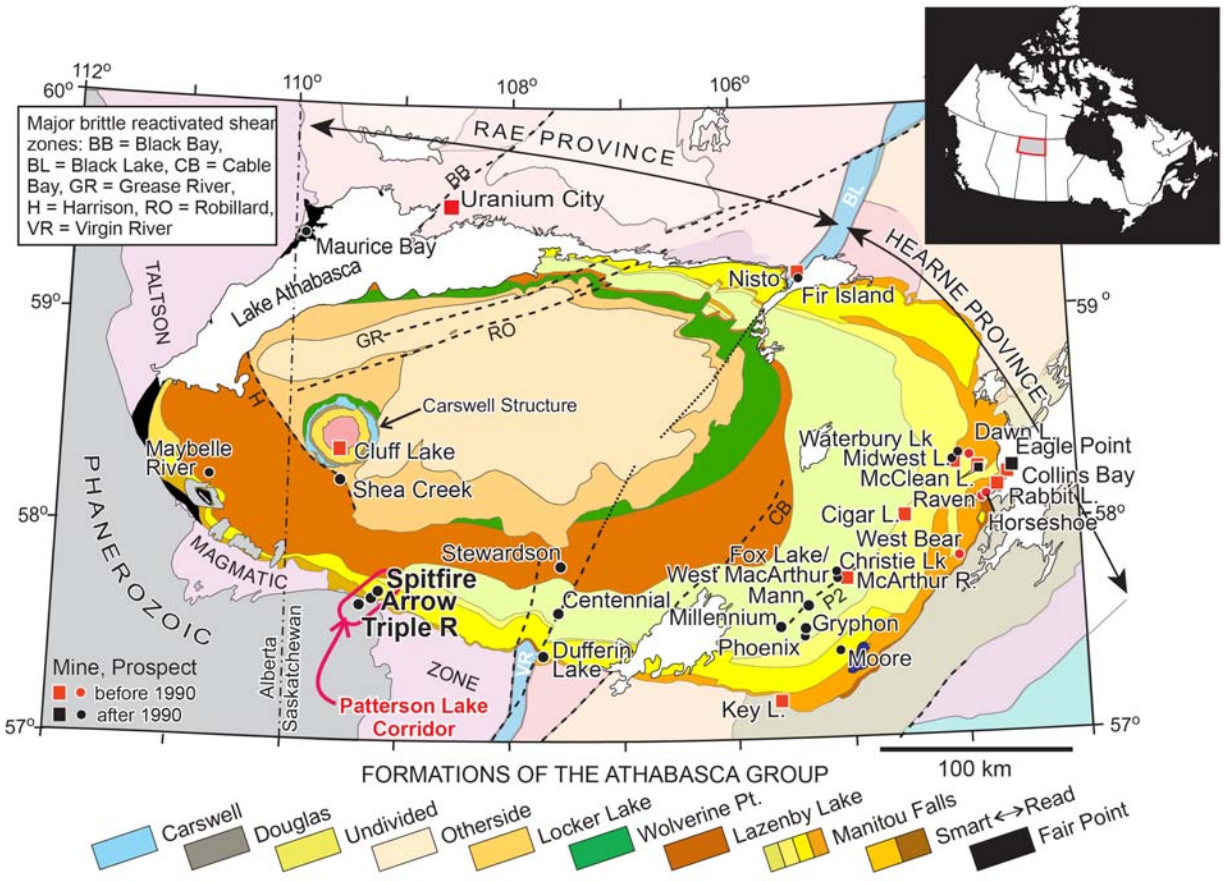

Figure 1. Geological map of the Athabasca Basin, highlighting the location of unconformity-related uranium deposits. Modified after Jefferson et al., 2007[1]

In 2017, an aeromagnetic survey was flown over the PLC stretching into northeastern Alberta, where only low-resolution, legacy aeromagnetic data was previously available. Additionally, zircon U-Pb ages from a suite of bedrock samples from northwestern Alberta and northern Saskatchewan were measured at the GSC Sensitive High-Resolution Ion Microprobe (SHRIMP) laboratory to determine crystallization ages of basement protoliths and their subsequent metamorphic history[3].The new survey provides the first modern aeromagnetic dataset over the region to shed light into the tectonic history of the region and the regional architecture to help inform on-going exploration activities in this understudied area of the Canadian Shield. Discrete magnetic-lithologic domains below Phanerozoic sedimentary cover were identified, including characteristic linear to curvilinear anomalies along the PLC that are truncated by the magnetic high–gravity low north-south trending Clearwater Domain intrusions. Whereas previous studies speculated the continuity of the Taltson Domain across either side of the Clearwater Domain[4][5], the new aeromagnetic data reinforces these interpretations and zircon U-Pb SHRIMP ages between 1968 ± 7.9 Ma and 1977.5 ± 4.4 Ma confirm a western extension of the Taltson Domain orthogneisses.. At the local scale, when interpreted along-side rock property and geological data, the new survey identified discrete magnetic anomalies associated with mafic- ultramafic intrusive rocks and carbonatite intrusions.

Zircon U-Pb data from a granitic gneiss south of the PLC indicate crystallization at 2422 ± 28 Ma and metamorphism at 1923.0 ± 7.3 Ma[3], both of which are typical for rocks of the Proterozoic Taltson Basement Complex. Although rocks outcropping in the region commonly retain evidence of >1.90 Ga events, major corridors of heterogeneous, ductile high strain better preserve the region's younger history. Drill core samples from the PLC exhibit a range of textures that span the brittle to ductile transition, and hydrothermal – metasomatic mineral assemblages that predate uranium mineralization[2]. To understand the long-term reuse of these high-strain corridors, micaceous and clay-rich samples were collected for geo-thermochronology and isotope studies. Presently, in situ and step heating 40Ar/39Ar analyses of muscovite are being conducted at the GSC noble gas laboratory to constrain the age of ductile structures, regional quartz flooding events, and subsequent brittle recrystallization. Samples from clay halos proximal to mineralized horizons are being dated via the K-Ar method to determine the timing of hydrothermal alteration related to uranium mineralization. Additionally, the Fe and Mg isotopic signatures of clay-rich alteration are being investigated to determine whether they record fluid-rock interactions along the fault/fluid conduit. These small variations may provide a means of identifying fertile fault corridors and vectoring to ore within established districts.

Ongoing TGI-U activities include a 2018 field season targeting Triple R and Arrow deposits, and planned gravity and magnetotelluric geophysical surveys over the PLC and Clearwater domain. Although data collection are in preliminary stages, the integrated and multidisciplinary nature of TGI-U research will provide valuable information for informing future exploration efforts and understanding the broader litho-structural setting of the region.

REFERENCES

Card, C.D., 2017. Geol. Surv. Sask. Misc. Rep. 2014-4.1, Paper A-11, 19 p.

Jefferson, C.W., Thomas, D.J., Gandhi, S.S., Ramaekers, P., Delaney, G., Brisbin, D., Cutts, C., Portella, P., Olson, R.A., 2007. Unconformity-associated uranium deposits of the Athabasca Basin, Saskatchewan and Alberta. Bulletin 588: Geological Survey of Canada. 588, 23-68.

Lewry, J.F., and Sibbald, T.I.I., 1977. Variation in lithology and tectonometamorphic relationships in the Precambrian basement of northern Saskatchewan. Can. J. Earth Sci. 14, 1453-1467.

Powell, J.W., Pana, D.I., Card, C.D., Potter E.G., Tschirhart, V., Joyce, N., 2018. New geochronological insights into the Taltson Domain of northern Alberta and Saskatchewan. Geological Survey of Canada. Open File 8373, 43–56.

Wallis, R.H., 1970. A geological interpretation of gravity and magnetic data, northwest Saskatchewan. Canadian Journal of Earth Sciences. 7, 858-868.

GEOLOGICAL AND GEOCHEMICAL CHARACTERISTICS OF THE JILING NA- METASOMATISM URANIUM DEPOSIT, GANSU, CHINA

Xiao Dong Liu[1], Wen Heng Liu, Jia Yong Pan

[1]*State Key Laboratory Breeding Base of Nuclear Resources and Environment, East China University of Technology, Nanchang, Jiangxi, 330013, China - liuoff99@163.com*

BACKGROUND

The metasomatite-related uranium deposit hosts the second largest uranium resource repository in all deposit types. It widespread distributes in Australia, Brazil, Russian, and Ukraine, but rarely presents in China. The Longshoushan-Qilianshan area is an important Paleozoic uranium mineralized belt in China, hosts the most typical sodium metasomatic uranium deposit. The purpose of this study was to increase our knowledge of the Jiling sodium metasomatic uranium deposit geochemically and mineralogically, to determine the relative and absolute timing, conditions of formation, source of uranium, and source of alteration and mineralizing fluids, and to suggest a possible formation model.

METHOD

Zircon geochronology was carried out using LA-ICP-MS in State Key Laboratory for Mineral Deposits Research, Nanjing University. Major elements and trace elements were analyzed in ALS Mineral-ALS Chemex using XRF and ICP-MS, respectively. Sr isotope compositions were analyzed using TIMS and Nd isotopic composition was analyzed using LA-MC-ICP-MS.

RESULT

Petrographic features illustrate that the Jiling pluton is a complex, with granitic samples and syenites. Meanwhile, both the granitic samples and the syenites contain abundant microgranular mafic enclaves (MMEs). Zircon geochronology reveals that the Jiling granitic samples, syenite and the MMEs were emplaced during the Paleozoic periods, their crystallized ages were 440-441 Ma, 427 Ma, and 440 Ma. Geographic and geochemical features reveal that the granitic samples and syenites belong to A-type magmas and were formed by magma mixing/mingling between crustal-derived and mantle-derived magmas. The high Th/U ratios (2.76 to 10.63) of the Jiling granitoids can provide uranium for mineralization.

Uranium minerals in the Jiling sodium-metasomatic uranium deposit contain pitchblende, uraninite, and brannerite. The pitchblende is the main uranium mineral. Alteration is intensive in the Jiling uranium deposit, including albitization, chloritization, thematization, carbonatation, and siliconization. Petrological features indicate that a large number of uranium minerals occur in fractures in the newly formed albite, indicating the main mineralization stage occurred later than albitization. The uranium mineralization is related to chloritization and carbonatation. Two morphologies of chlorite, hematite, and calcite were identified. The chlorite contains foliated and disseminated ones, the hematite contains veined and disseminated ones, and the calcite contains veined and flake-like. Uranium- related chlorite is the disseminated one. Compared to the fresh granitoids, the mineralized granitoids display high Na, U, low K, Si contents, and LREE/HREE ratios. H, O and C isotope reveal that the CO_2 originated from the mantle, and H_2O in hydrothermal fluid from mixing between magmatic hydrothermal and meteoric water. Pb isotope reveals that the uranium may derive from the host granitoids.

Finally, a diagenetic model was given. Mixing/mingling between the mantle-derived and crustal-derived magmas generated the Jiling granitic samples and syenite. The alkali-rich fluid which was formed by differentiation of syenite magmas altered the Jiling granitic samples generated sodium metasomatic rocks. Meanwhile, the ore-forming fluids which mixed by the meteoric and water with the alkali-rich fluid, leached uranium from the Jiling granitic samples to form the uranium-rich fluids. These uranium-rich fluids were reduced by the reductive materials in the sodium-metasomatic rocks, and generated the Jiling sodium- metasomatic uranium deposit.

CONCLUSION

1 Both the Jiling granitic samples, syenite, and enclave were formed by magma mixing between crust-derived and mantle-derived magmas during the Paleozoic period. High Th/U ratios indicate that the Jiling granitic samples can provide uranium for mineralization.
2 Uranium mineralization in the Jiling sodium metasomatic uranium deposit accompanied by chlorite and calcite.

3 H and O isotopic composition reveal that the ore-forming fluids were formed by the mixing between the magmatic fluid and meteoric water.
4 A diagenetic model was proposed to illustrate the genesis of Jiling sodium metasomatic uranium deposit.

URANIUM IN ARGENTINA: DEPOSITS, RESOURCES AND NUCLEAR SUPPLY

Luis López

National Atomic Energy Commission (CNEA) - lopez@cnea.gov.ar

Despite the apparent growth prospects of the use of nuclear energy for the generation of electricity in the country, which would lead to double the uranium needs by 2030, there are no immediate prospects for the provision of nuclear raw material for fuel fabrication from the local production of uranium oxide concentrates at Argentine deposits. In 1992, due to the low prices in the international market, the import of uranium concentrates began from South Africa, a situation that gradually led to the closure of local production in 1997. Since then, there has been no production of uranium in the country, while the uranium needs from operating nuclear power plants have been met with raw materials imports from abroad (*i.e.,* Uzbekistan, Czech Republic, Kazakhstan and Canada). Despite the fact that international uranium market has been depressed in recent years, the Free On Board (FOB) prices that the country has paid for the purchase of yellowcake in the spot market have not necessarily been trivial, mainly due to the increases in transportation charges, insurance premium and taxes. Furthermore, to define the economic feasibility of the Comisión Nacional de Energía Atómica projects, uranium prices in the international market should be taken as a reference, not as a determining factor, considering that the raw material has a bearing of 5 to 7 per cent in the total cost of nuclear energy in the country, which is USD 80–100/MWh. In Argentina, more than 37,000 tU have been reported as identified domestic resources at the production cost category lower than USD $130/ kgU in the Red Book classification scheme. It would be economically viable to put into production in the short term the identified resources evaluated in the country, notably the uranium available from the Cerro Solo (sandstone type), Laguna Salada (surficial type), Sierra Pintada (volcanic-related type), Amarillo Grande (sandstone/ surficial type?) and Meseta Central (sandstone type) projects. One main concern is that the identified uranium resources in Argentina are mostly located in the provinces of Chubut and Mendoza. These are areas where no metallic mineral mining projects are in operation, and also, the provincial legislations markedly restrict uranium production. These factors need to be taken into account when studying the social viability of the projects. However, it could also be assumed that the mining laws could be amended as necessary if a requirement of uranium and other critical materials for clean energy projects becomes very important to Argentina. Also, projects with a higher degree of maturity must complete technical feasibility studies for the recovery of uranium. In the case of possible future production of U, other valuable materials such as V and Mo, can be assumed to be produced as a by- or co-product, contributing to the mineral sector development in Argentina. While U is used for nuclear fuel, V and Mo have critical applications, especially in the renewable energy and steel industry sectors. At the exploration level, there are several projects within the basins of great interest in the country that are carried out by both the private sector and the government. However, as a general rule, the integral exploration at basin level has not been carried out, and the evaluated resources are meager compared to the country's uranium potential. Also, these resources have generally been evaluated with a low level of confidence. The most advanced exploration projects, such as Golfo San Jorge (sandstone), Amarillo Grande (sandstone/ surficial?), Alipan (granite-related), Mina Franca (granite-related) and Laguna Sirven (surficial), have a high potential of transforming to a higher degree of maturity as classified in the UNFC system. Initially, it will be necessary to advance the delineation of resources and raise their level of confidence through preliminary economic assessments of these projects. In sedimentary environments, particular attention should be given to those sandstone-type deposits that are amenable to in situ leaching to recover uranium. Also there are some unconventional sources of uranium that could provide sustainable alternatives for nuclear supply in the foreseeable future, such as rare earth projects, phosphates, and lake and sea waters. Currently, uranium is imported for domestic use in Argentina, which has implications for supply and energy security. For this reason, different possibilities for the sustainable domestic production of uranium are outlined, especially considering the world situation of the uranium market where the commodity- driven model seems to be weakening.

MANTLE-DERIVED NOBLE GASES IN ORE- FORMING FLUIDS OF THE URANIUM DEPOSITS IN SOUTH CHINA

Rui-Zhong Hu[1], Jin-Cheng Luo, You-Wei Chen, Xian-Wu Bi

[1]State Key Laboratory of Ore Deposit Geochemistry, Institute of Geochemistry, Chinese Academy of Sciences, Guiyang 550081, China - huruizhong@vip.gyig.ac.cn

INSTRODUCTION

Despite uranium's incompatible behavior in silicate magmas, uranium deposits resulting directly from magmatic processes are quite rare in the world. It was confirmed that uranium is mobilized by hydrothermal fluids well after the emplacement of felsic rocks in most uranium deposits (Cuney, 2014; Hu *et al.*, 2008). However, the mobilized mechanism of uranium from the felsic rocks is still a matter of debate.

South China is rich in vein-type uranium deposits which are hosted dominantly in granitic and rhyolitic volcanic rocks. Previous studies (Hu *et al.*, 2008) have shown that there was a large time gap between the ages of the host igneous rocks and the mineralization (20 Ma to>700Ma). Cretaceous mantle-derived mafic dikes intruded in an extensional regime correspond to the major episode of uranium mineralization. These deposits formed from meteoric fluids at temperatures about 150-250!, and the uranium in the ore-forming fluids was likely extracted from uranium-rich felsic igneous rocks. The important question remains about why the deposits were directly followed the intrusion of the mantle-derived mafic dikes.

Involvement of mantle-derived components in ore deposits can be sensitively traced using the isotopic composition of the noble gases as the large differences between crustal and mantle noble gas isotopic compositions mean noble gases are ideal tracers in systems where mantle volatiles are added to crustal fluids (Stuart *et al.*, 1995; Hu *et al.*, 2004). This paper presents He and Ar isotopic analyses, and discusses the origin of the gaseous components in the ore-forming fluids and their implications for the relationship between uranium mineralization and mafic dikes in south China.

GEOLOGICAL BACKGROUND

South China, located in the southeastern part of the euro-asian continent, was formed by amalgamation of the Yangtze and Cathaysia Blocks during the Neoproterozoic (Fig. 1). The Precambrian strata, tightly folded but only weakly metamorphosed, are considered to represent the basement. The sedimentary cover in this region consists mainly of folded Paleozoic and Lower Mesozoic strata of shallow marine. Jurassic, Cretaceous and Cenozoic strata are entirely continental sequences. Farther to the southeast lies a large granitic province of >1000 km wide across the whole Cathaysia Block. The granitoids (including granites and rhyolitic volcanic rocks) in the province formed dominantly in Jurassic, although there are also relatively minor granitoids of Indosinian, Caledonian and Grenvillian age. In the Cretaceous, the lithospheric extension resulted in the formation of numerous NE-SW-trending grabens and the emplacement of mantle-derived mafic dikes. This region has been named the Cathaysian rift system.

Abundant vein-type hydrothermal uranium deposits in the Cathaysian Block are hosted in uranium-rich granites and felsic volcanic rocks (usually more than 10 ppm U) which are highly variable in age, ranging from Precambrian to Jurassic. Ore-hosting granites are mainly Jurassic and Triassic and rarely Caledonian and Grenvillian in age. They are typically two-mica, biotite and muscovite granites. Ore-hosting volcanic rocks consist mainly of Jurassic rhyolites, rhyodacites and tuffs. There was a large time gap between the ages of the host igneous rocks and the mineralization (20 Ma to >700Ma). Cretaceous mantle-derived mafic dikes intruded in an extensional regime correspond to the major episode of uranium mineralization.

The uranium deposits are epigenetic concentrations of hydrothermal minerals in open 2 33 spaces such as fractures, fissures and breccias in granitic rocks. Regardless of their host rocks, they have similar mineral assemblages, typically including pitchblende, pyrite, quartz and calcite. The ore-forming fluids have low salinity (1.3-8.9 wt% NaCl eq.) with temperatures about 150-250. Gas chromatographic analyses of the fluid inclusions have shown that carbonic phases (including CO, CO_2- and HCO^{-3}) are the most important constituents in the ore-forming fluids.

RESULTS AND DISCUSSIONS

Ore samples from representative U-bearing hydrothermal veins were collected from underground workings in three uranium deposits as shown in Fig. 1 where the Xiangshan deposit is hosted by felsic volcanic rocks, and the Xiazhuang and Zhuguang deposits are hosted by granites. After the samples were crushed, pyrite associated with pitchblende were hand-picked under a binocular microscope, then cleaned ultrasonically in alcohol and dried for He and Ar isotopic analyses. He and Ar in fluid inclusions trapped by pyrite grains were released into an all-metal

extraction system by sequentially crushing in modified Nupro type valves, and then measured by a GV5400 noble gas mass spectrometer at Institute of Geochemistry, Chinese Academy of Sciences.

The results show that the 3He/4He ratios in inclusion fluids of pyrites from the Xiangshan deposit are 0.10-3.37Ra (Ra represents the 3He/4He ratio of air, 1.39×10-6) and 40Ar/36Ar ratios are 299-664, 0.02-1.04Ra and 298-547 from the Xiazhuang deposit, and 0.03-0.57Ra and 294-577 from the Zhuguang deposit. Moreover, there are excellent correlations between He and Ar isotopic compositions. The results suggest that the ore-forming fluids are a mixture between a crustal fluid containing atmospheric Ar and crustal 4He and a fluid containing mantle components. It is likely that the former is a low temperature meteoric fluid, and the latter is a mantle-derived fluid which was controlled by Cretaceous lithospheric extension. Carbon isotopic analyses of calcite deposited in the main-stage mineralization in the veins from these uranium deposits yield $\delta^{13}C$ values of ore-forming fluids mainly from -4 to -8‰, which are permissive of a mantle origin for the CO_2 in the ore-forming fluids. Therefore, the mantle-derived fluid should a CO - and 3He-rich end-member.

It was confirmed that uranium in ore-forming fluids of these deposits is present dominantly in the form of $UO_2(CO_3)22-$ and $UO_2(CO_3)34-$, suggesting that CO_2 in fluids is critical for mineralization (Hu *et al.*, 2008) . We speculate that the incorporation of dominantly mantle- derived CO_2 in the hydrothermal fluids was responsible for remobilization of uranium from the granitic source rocks and eventual deposition in the veins.

CONCLUSIONS

The Cretaceous lithospheric extension and associated mafic magmatism in South China allowed CO_2-rich mantle-derived fluids to migrate upward and to mix with CO_2-poor meteoric water. The mixed CO_2-rich hydrothermal fluids mobilized uranium from the U-rich felsic rocks, and then formed the uranium deposits.

REFERENCES

Cuney, M., 2014. Felsic magmatism and uranium deposits. Bulletin De La Societe Geologique De France, 185, 75-92.

Hu R.Z., Burnard P.G., Bi X.W., Zhou M.F., Peng J.T., Su W.C., Wu K.X., 2004. Helium and argon isotope geochemistry of alkaline intrusion-associated gold and copper deposits along the Red River- Jingshajiang fault belt, SW China. Chemical Geology. 203, 305-317.

Hu R.Z., Bi X.W., Zhou M.F., Peng J.T., Su W.C., Liu S., Qi H.W., 2008. Uranium metallogenesis in South China and its relationship to crustal extension during the Cretaceous to Tertiary. Economic Geology. 103, 583-598.

Stuart F.M., Burnard P.G., Taylor R.P., Turner G., 1995. Resolving mantle and crustal contributions to ancient hydrothermal fluids: He-Ar isotopes in fluid inclusions from Dae Hwa W-Mo mineralization, South Korea. Geochimica et Cosmochimica Acta. 59, 4663-4673.

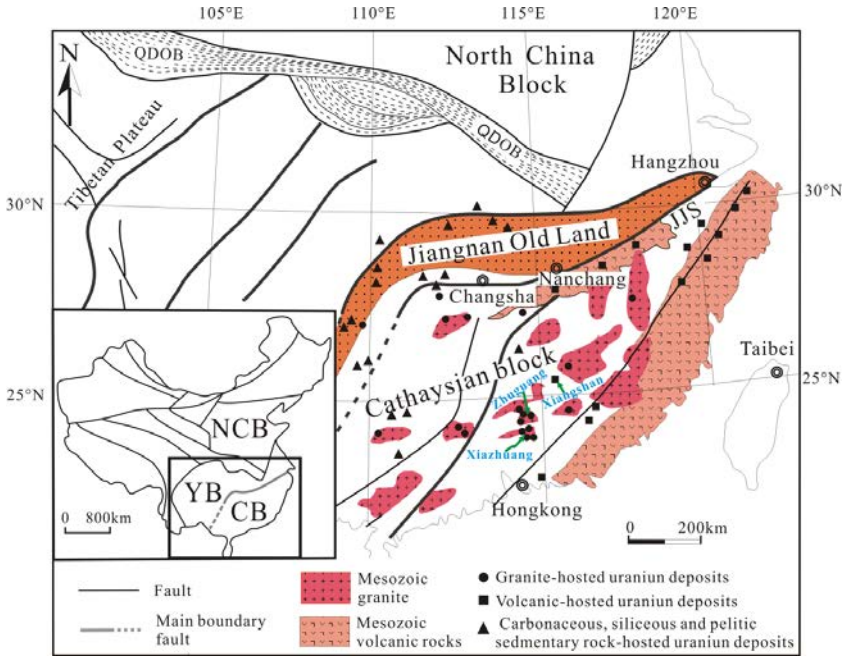

Fig. 1 Map showing the tectonic units and distribution of uranium deposits in South China (modified from Hu *et al.*, 2008). NCB-North China Block, YB-Yangtze Block, CB-Cathaynian Block, QDOB-Qinling-Dabie Orogenic Belt.

A | 158

THE ORIGIN OF PYRITE FROM THE KIGGAVIK URANIUM DEPOSIT, NUNAVUT, CANADÁ

Brandi M. Shabaga[1], Mostafa Fayek, David Quirt, Patrick Ledru

[1]University of Manitoba - Brandi.Shabaga@umanitoba.ca

INTRODUCTION

Proterozoic unconformity-related deposits produce ~30% of the world's uranium. These deposits occur in marginal or intracratonic basins such as the Athabasca and McArthur basins in Canada and Australia, respectively. The Thelon Basin, which is located in the Nunavut territory, Canada, is similar in size and geology to the Athabasca Basin. It has been suggested that uranium deposits located adjacent to the Thelon Basin, in the Kiggavik region, are also unconformity-related deposits. However, while the Athabasca Basin has been thoroughly studied in terms of its stratigraphic, sedimentological, diagenetic, fluid, and metallogenic histories, the Thelon Basin has a much smaller body of literature documenting such characteristics.

Uranium mineralizing processes are generally associated with complex hydrothermal and fault systems. Consequently, understanding fluid movement through structures within these terrains and the source of U is of great importance for mineral exploration. It is necessary to use different isotopic methods to characterize the minerals filling the structures because host rocks, fluid composition, and possibly temperature, may have varied over time and space thus precipitating different types of minerals. Use of different isotopic systems will provide necessary information such as age and fluid composition from different minerals.

A growing number of specialized techniques (e.g., Re-Os geochronology of sulfides) and *in situ* micro-analytical techniques (e.g., secondary ion mass spectrometry (SIMS) U-Pb dating of U minerals, *in situ* Ar-Ar geochronology) are now available and can be used to date a wide range of fault-hosted minerals. Although a number of studies have used SIMS to date uranium minerals using the U-Pb method, establishing the timing of initial U emplacement and subsequent alteration history of U deposits have been challenging. It is often uncommon to obtain concordant U-Pb data from uraninite and the degree of discordance is often much greater than 5%, leading to uncertainty in the interpretation of the U-Pb values. The observed uncertainty in age highlights the intrinsic limitations of the methods used and underscores both the susceptibility of U deposits to alteration and the mobility of U and Pb during these alteration events.

Geochronology of sulphide minerals associated with U mineralization using the Re-Os method may provide information regarding the age of the deposit because the Re-Os chronometer in sulphide minerals is more difficult to reset at low temperatures (Creaser and Stasiuk, 2007). However, prior to Re-Os analysis of sulphides, detailed characterization is necessary to avoid analysis of pyrites that are not associated with U mineralization. Here we use petrography in combination with the sulphur isotopic composition of pyrite from the Kiggavik deposit to determine the origins of pyrite.

GEOLOGY OF THE KIGGAVIK DEPOSIT

The Kiggavik Project area is located approximately 80 km west of Baker Lake, Nunavut, and 2 km south of the Thelon Fault. This area is dominated by metamorphosed and polydeformed ultramafic to felsic volcanic, volcaniclastic, and metasedimentary rocks of the Neoarchean Woodburn Lake Group (WLG) Pipedream assemblage, Pukiq Lake Formation rhyolite, Paleoproterozoic Ketyet River Group quartzite, and Paleoproterozoic granitic rocks of the Schultz Lake Intrusive Complex (SLIC). Within the Kiggavik Project area, several U deposits and showings occur along a ~30 km long NE–SW structural trend, informally termed the Kiggavik–Andrew Lake structural trend; the Kiggavik deposit is the northernmost deposit in this trend. The Kiggavik deposit is comprised of three separate mineralized zones: the Main, Centre, and East Zones. The Main Zone occurs at the contact between the WLG and SLIC, with U mineralization occurring in both the metasediments and granite. The Centre and East Zones occur within the WLG and epiclastics of the Pukiq Lake Formation, and are spatially associated with and likely structurally controlled by the contacts with overlying quartzite lenses.

RESULTS

Based on $\delta^{34}S$ and $\delta^{33}S$ values, isotopically distinct groups for pyrite are observed for each sample. From the Main Zone, hydrothermal pyrite occurring in veins associated with altered uraninite has average $\delta^{34}S$ and $\delta^{33}S$ values of 6.6 ± 0.6‰ and 3.7 ± 1.0‰, respectively, and an average $\Delta^{33}S$ value of 0.3 ± 1.2‰. Subhedral grains of galena (200-300µm) in the same sample are associated with corroded calcite veins and uranyl minerals that are devoid of

lead, and have an average $\delta^{34}S$ value of -11.2 ± 2.9‰. In another sample from the Main Zone, pyrite with subhedral and framboidal morphologies display a pitted texture, and are associated with altered U minerals also displaying biogenic textures, have average values of $\delta^{34}S$ = 35.3 ± 1.2‰, $\delta^{33}S$ = 19.1 ± 0.6‰, and $\Delta^{33}S$ = 0.6 ± 0.8‰. Large (≤1mm) euhedral pyrite from the East Zone has an average $\delta^{34}S$ value of 0.6 ± 0.6‰, $\delta^{33}S$ value of 0.6 ± 0.3‰ and a $\Delta^{33}S$ value of 0.2 ± 0.3‰. Euhedral pyrite from the Center Zone displays very low $\delta^{34}S$ and $\delta^{33}S$ values averaging -37.6 ± 3.1‰ and -18.8 ± 1.7‰, respectively, with an average $\delta^{33}S$ = 0.9 ± 0.7‰. Altered subhedral grains of pyrite from the same sample have a higher $\delta^{34}S$ value of 0.3 ± 0.3‰.

A | 159

IVANA URANIUM-VANADIUM DEPOSIT, A NEW RESOURCE FOR ARGENTINA

Guillermo Pensado[1], Ariel Testi, Jorge Berizzo, Jon Thorson

[1]*Blue Sky Uranium Corp. - amtesti@yahoo.com.ar*

The Ivana uranium-vanadium deposit contains an initial mineral inferred resource of 19.1 million pounds of U_3O_8, and 10.2 million pounds of V_2O_5, contained in 23.9 million tonnes of ore with a grade of 0.036% U3O8 & 0.019% V_2O_5, calculated using a cut-off grade of 100 ppm U. The Ivana deposit contains the first mineral resource announced for the Amarillo Grande Project, a uranium-vanadium exploration trend stretching for about 140 km, within which Blue Sky Uranium has claimed more than 280,000 hectares of mineral exploration rights. The Amarillo Grande Project contains two additional advanced prospect areas, Anit and Santa Barbara.

The Ivana deposit is located about 25 km north of the town of Valcheta, in a sparsely populated, semi-arid area of flat topography. Access can be made by paved Provincial Highway #4 to within 10 km of the deposit, then by dirt ranch roads. Blue Sky Uranium has been exploring the greater Amarillo Grande Project since 2006; the Ivana area and Ivana deposit are the most advanced part of that project.

The Ivana deposit occurs in Eocene Chichinales Formation at the distal, thin, southeastern edge of Neuquen Basin sedimentary sequences. The Chichinales is composed of conglomerate, tuffaceous sandstone, siltstone and mudstone, deposited unconformably on older basement rocks. The Ivana deposit contains mineralization of two types; oxide mineralization and primary mineralization. Oxide mineralization is composed of carnotite and variable limonitic iron oxides coating pebbles and sand grains, and disseminated in fine-grained poorly-consolidated sedimentary rocks. Primary mineralization is composed of coffinite and minor uraninite in pyritic and carbonaceous gray-colored poorly-consolidated sedimentary rocks. A variant of the primary mineralization is dark brown to black in color from impregnation by vitreous "non-woody" carbonaceous organic matter.

Four alteration styles have been recognized at the Ivana Deposit; reduced alteration, reduced carbonaceous alteration, oxidized alteration and hematitic alteration. These alteration types appear to relate to an oxidation-reduction boundary with a complex geometry that is not yet completely understood, but appears to be a controlling factor in the deposition of the primary uranium-vanadium mineralization.

The Ivana uranium-vanadium deposit has some similarities to the surficial uranium deposits of Australia and Namibia in that the oxide uranium mineralization consists of carnotite coating pebbles and sand grains, and as disseminations, in poorly-consolidated sediment. Ivana, however, lacks the well-developed calcrete layers generally associated with surficial uranium deposits in semi-arid to arid climates. The primary uranium mineralization at Ivana has considerable similarities to sandstone-hosted uranium deposits in other locations, particularly basal-channel sandstone-hosted uranium deposits, and appears to be related to a redox boundary of possible regional extent. Thus, the Ivana uranium-vanadium deposit should be considered a hybrid deposit, in part a surficial deposit, and in part a sandstone- hosted deposit, requiring its own unique genetic model. That model is maturing as exploration of the deposit progresses.

Exploration of the Ivana uranium-vanadium deposit, resulting in the inferred mineral resource estimate, has been largely conducted through a shallow geophysical technique called electrical tomography (ET) and drilling. The ET surveys were particularly designed to identify and map shallow paleochannels incised into basement rocks, which control the location of uranium mineralization. Drilling comprised 427 Reverse Circulation (RC) drill holes for a total of 6577 meters drilled; average drill hole depth was 15.4 m. Exploration drilling was carried out with track-mounted RC rigs for ease and rapidity of movement between shallow drill holes, and to minimize environmental impact. Samples were collected for each meter drilled, logged, and transported for assay preparation in Mendoza, Argentina. Assays were completed at Bureau Veritas Commodities Canada Ltd., Vancouver, BC, Canada and reported in parts per million uranium (U ppm) and vanadium (V ppm). The inferred resource estimate supported by this report is entirely based on chemical assays of uranium and vanadium; no equivalent-uranium (eU or U_3O_8) data has been used in the calculations.

The resource estimate calculation was performed on two layers of mineralization, an upper zone that is largely oxide mineralization, and a lower zone that contains both primary mineralization and oxide mineralization. For the base case estimation, the mean uranium grade in the upper layer is 103 ppm U within a range between 4.4 ppm U and 6440 ppm U. The lower layer of mineralization has a mean uranium grade of 293 ppm U within a range of 6 ppm U to 17,780 ppm U. The inferred mineral resource is not constrained by a pit shell, due to the shallow depths of mineralization, less than 25 meters below surface.

The Ivana uranium-vanadium deposit has potential to be developed into a low-cost uranium- vanadium producing mine. Planning for mineralogical, metallurgical, and mining studies is underway to advance towards development. Potential also exists for continuing exploration of the Amarillo Grande Project to delineate additional uranium-vanadium resources, similar to the Ivana deposit, including possible deposits related to regional redox systems.

		Average Grade				Contained Metal	Contained Metal
Zone	Tonnes (t)	Uranium (ppm)	U_3O_8 (%)	Vanadium (ppm)	V_2O_5 (%)	U_3O_8 (lbs)	V_2O_5 (lbs)
Upper	3,200,000	132	0.016	131	0.023	1,100,000	1,600,000
Lower	20,700,000	335	0.040	105	0.019	18,000,000	8,600,000
U + L	23,900,000	308	0.036	109	0.019	19,100,000	10,200,000

Table 1, Ivana Deposit, Estimate of Inferred Mineral Resource, reported at 100 ppm Uranium Cut-off

A | 160

REDUCING MECHANISMS IN THE PRECIPITATION OF UNCONFORMITY-RELATED URANIUM DEPOSITS: INSIGHTS FROM FLUID FLOW MODELING

Jianwen Yang

University of Windsor - jianweny@uwindsor.ca

A 2-D conceptual model is developed to address possible reducing mechanisms in the precipitation of unconformity-related uraninite deposits in sedimentary basins. A series of numerical scenarios are investigated using TOUGHREACT to examine the role of graphite zone and Fe-rich chlorite as the reducing agents in the ore genesis. It is revealed that graphite is more efficient in reducing oxidized uranium than Fe-rich chlorite, though both the reducing mechanisms can lead to the precipitation of uraninite. A uranium deposit forms in the basement either away from the fault zone or along it, and its locale appears to be controlled by a dominant downwelling convective flow and the resultant temperature and pH regimes, which is determined in turn by the orientation and hydraulic properties of the fault zone. Uraninite precipitates simultaneously with hematite in the areas experiencing the reduction of oxygen fugacity and having a temperature of 180-200 °C and a pH of 2.5-4.5. Wide-spread alteration halos in the basement and around the deposit include hematite, chlorite and muscovite accompanied by minor amounts of pyrite and K-feldspar alteration.

CHARACTERIZATION OF RARE EARTH MINERALS IN LAGOA REAL URANIUM PROVINCE, BAHIA, BRAZIL

Lucas E. D. Amorim[1], Lucilia A. R. Oliveira, Ariela Costa Diniz, Tiago De Ferreira, Camila Marques dos Santos, Francisco Javier Ríos, Mônica Elizetti de Freitas, Evando Carele de Matos

[1]*CDTN/CNEN Brazil - ledamorim@cdtn.br*

The Lagoa Real Uranium Province is located at the central portion of São Francisco Craton, south of Bahia State (Brazil). This province has as reserve of 110 mil tons of U distributed in 38 anomalies. The main lithologies that constitute its structure are paleoproterozoic granites, orthogneisses and albitites. The first is the protolith of the two other lithologies. The latter is the host of U mineralization, which occurs mainly as uraninite associated to pyroxene, garnet, and amphibole.

This province is known for having undergone metassomatic, metamorphic and hydrothermal processes. That would have culminated in the alteration and rework of the present lithologies and in the uranium mineralization.

The literature reports the existence of a correlation between the occurrence of rare earth elements bearing minerals with hydrothermal or epithermal fluids related. Those process could have evolved alkaline granites, pegmatites, skarns and/or syenites.

One of the goals of the recent studies carried at Lagoa Real has been to identify and characterize the occurrence of those rare earth elements bearing minerals. The relationship between the rare earth minerals crystallization processes with the U mineralization could be the key to explain the province evolution. In addition, the presence of these minerals, under the economic point of view, may represent an important byproduct of the U exploration and beneficiation at the Lagoa Real province.

In this work it was performed the identification and chemical characterization of rare earth minerals using scanning electron microscope and Electron microprobe. The samples were from: (i) Lagoa do Barro (1.77Ga) and São Timoteo (1.74Ga) granites;(ii) Cercadinho and Morro da Contagem albite-gneiss; (iii) pegmatoid pockets related to São Timoteo granite; and (iv) representative barren albitite from the 34 anomalies.

Several minerals were identified, but their composition varies greatly depending on the lithology. The rare earth elements are mainly hosted by silicates such as titanite and allanite or phosphates as monazite and xenotime. However, they also occur as more complex minerals such as F-bearing carbonates and silicates.

Lagoa do Barro granite has mainly titanite containing La, Ce, Y, F and V as major constituents (Figure A and B). This mineral exhibit granular and corona texture and do not show a homogeneous composition. A thin layer of rare earth F-carbonates occur at its edges and interstices. In the São Timóteo granite, there are titanite, allanite and F-carbonates, (Figure C and D), in an agglomeration of concentric minerals. It appear with ilmenite and overgrows hastingsite and/or biotite or in fractures. These rare earth minerals always present corona texture and fractures.

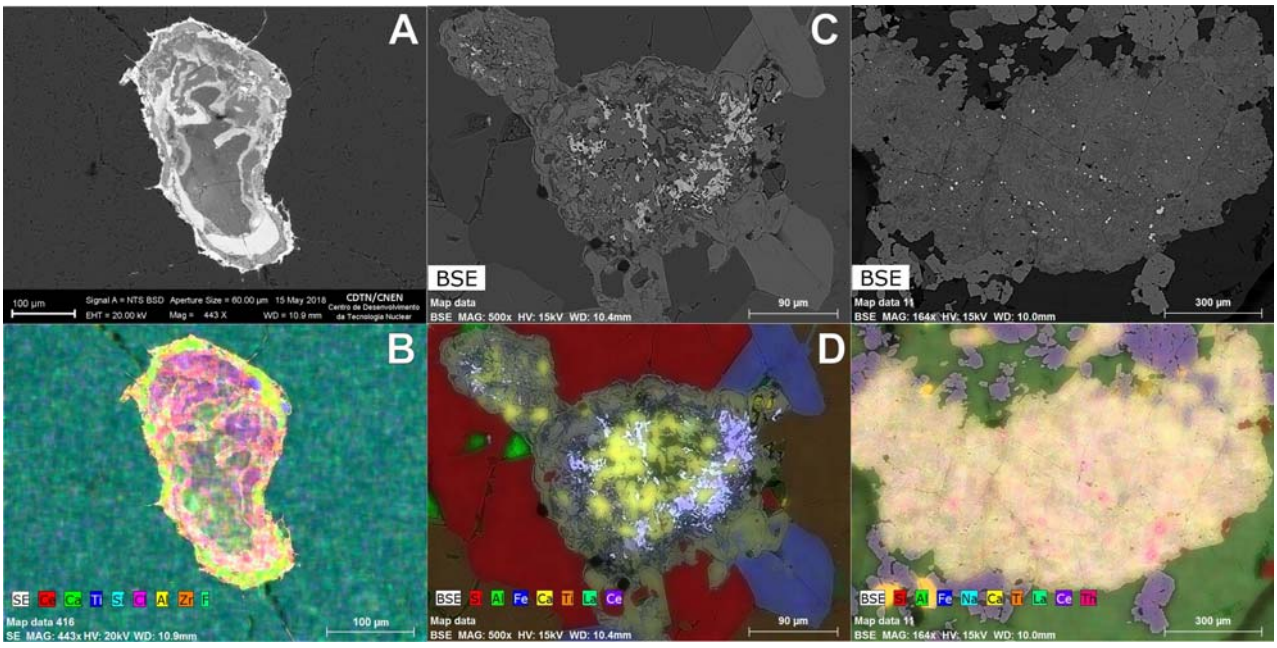

They have mainly Ce, La and F/CO_3 as major constituent in their structure and sometimes-present thorite and zircon crystals in the coronitic intergrowth.

The pegmatoid pockets of the São Timóteo granites have a wide occurrence of rare earth minerals. The main of them is (Ce,La)-monazite and Gd-xenotime which occurs in heterogeneous agglomerates overgrowing quartz and alkali-feldspars. (Ce,Y,La)-allanite displays replacement and coronitic textures with titanite. They occur commonly in fractures terminations associate with ilmenite. Some complex (Y,Yb,Dy,Nd)-silicates overgrow feldspars and quartz. Thorite occurs as inclusions in all this rare earth minerals.

In the albite-gneiss the main rare earth mineral is represented by (Th,La,Ce)-allanite (Figure E and F). It also does not present compositional homogeneity, having variation from the edges to core. The edge has higher rare earth concentration than the core and contains a rare earth F-carbonate layer. This mineral occurs overgrowing the other minerals from the assemblage, and have a lot of thorite little crystals.

Similarly to the albite-gneiss, the non-mineralized albitites contain mainly (Ce,La)-allanite. Many are also composed by some Th. At the allanite core often appears Nb-rich titanite, poor in rare earth elements, which shows replacement textures with allanite. Zircon and thorite inclusions are common in both allanite and titanite. Again, this agglomerate occurs overgrowing the other minerals from the rock, such as quartz, plagioclase, garnet and pyroxene and surrounded by radial fractures.

According to collected data, we observe a great variation in rare earth minerals composition. This could be due to the different mineralogical assemblages found at each studied lithology. Thus, the same event that originated the rare earth minerals, when interacting with the different assemblages, generated different minerals.

The results show that La, Ce and F mainly compose the rare earth minerals occurring at Lagoa Real Uranium Province. The textures observed shown that those minerals are related to a late process as they overgrow the original minerals or communicate via fractures. In this way, the presented data suggests that the event, which gave rise to these minerals, is more recent than the granitic intrusions, the metamorphism and the sodium albitite-related metassomatism.

It is important to add that the study and characterization of the rare earth minerals in Lagoa Real continues to be developed. In this way, it is likewise intended to characterize the fluids related to the formation of these minerals, as well as its the source. It is so being characterized the mineral waste of U beneficiation and extraction, in order to evaluate it as a by-product.

TITANITE AS AN IMPORTANT PETROLOGIC INDICATOR FROM GAMELEIRA I U-DEPOSIT (ANOMALY 35) LAGOA REAL URANIUM PROVINCE (LRUP), BAHIA, BRAZIL

Camila Marques dos Santos[1], Francisco Javier Rios, Lucas E. Dias Amorim, Helena Leonhardt Palmieri, Evando Carele de Matos

[1]*Programa de Pós-Graduação em Ciência e Tecnologia dos Minerais e Meio Ambiente*

Centro de Desenvolvimento da Tecnologia Nuclear (CDTN/CNEN) - camisgeo@gmail.com

The Lagoa Real Uranium Province (LRUP) is located in northwest of Bahia state and is the major uranium producing target of South America. It has approximately extension of 35 km, where contain 38 uraniferous anomalies along three semi-arched lineaments. The orebodies contain a total reserve of ca. 112,000 metric tons and 0.2 to 0.5 grade of U3O8. Uranium production started in 1999 by the Indústrias Nucleares do Brasil (INB) and 300 tons per year of uranium concentrate was produced from seven ore bodies of the Cachoeira mine (Anomalia 13).

The uranium deposits are associated to albitites, what comprise sodium-enriched rocks dominated by plagioclase (albite±oligoclase). Albitite rocks commonly contain calcic-sodic to sodic-calcic assemblage. The main characteristics of the protolith were lost due to recrystallization during the Brasiliano event, but in general, they are though product of intense metasomatic alteration of granitic-gneissic rocks from Lagoa Real Intrusive Suite (LRIS) (1746 ± 5 Ma) that produced in these rocks sodium enrichment and silica depletion. Uranium mineralization is highly concentrated in the most oxidised zones mainly in garnet- hedenbergite-rich rocks. Recent published geochronological data based on U-Pb in titanite suggests that mineralizing and hydrothermal alteration event are Tonian (956 ± 49 Ma).

The studied deposit, called Gameleira I, is located in northwest area of LRUP and is mainly composed by gneissic-granitic rocks and albitites. Albitite rocks were classified in this work according to main mafic mineral abundance, they are: magnetite-, garnet-, pyroxene- and biotite albitite. Ore assemblage, represented by uraninite, titanite and zircon, occurs as centimetric lenses in micro shear-zones hosted mainly by pyroxene and biotite albitites.

Titanite is a common accessory mineral in granitic-gneissic rocks from LRIS and albitites. The close relationship with ore assemblage and the possibility of providing geochronological data to elucidate the age of the mineralizing event indicate that titanite is an important mineral in this context, but chemical data obtained in recent literature is scarce. "Uranium- rich titanite" was already described by some authors in LRUP, but in relation to uranium content this term is not well defined and the interpretation has been controversial. In order to understand titanite occurrence and significance in LRUP context we executed petrographic and chemical characterization of that mineral. These studies are important to support future geochronological and petrologic interpretation. In addition, titanite is a known carrier of trace elements what makes it an important petrogenetic indicator.

For this study, thirty-three polished thin sections of 35 anomaly F-10 drill-hole located in northwest of LRUP were petrographically studied. Selected mineralized samples were analysed by SEM in order to understand uraninite and titanite relationship. Fifteen representative samples were studied in electron probe micro-analyzer at *LMA-Federal University of Minas Gerais* to measure major elements. Compositional data for trace elements were obtained in four samples by laser ablation inductively coupled plasma mass spectrometry (LA-ICPMS) at Nuclear Technology Development Center using mass spectrometer inductively coupled ELAN-6100DRC-e, Perkin Elmer/SciexTM, and ESI, NWR213 model. Calibration was made using NIST-610 and NIST-612 glasses. For internal standardization we used the Ca contents obtained by electron microprobe. Data acquisition, drift corrections and final data reduction were done using SILLs software.

According to petrographic association two titanite groups, granular and prismatic, were observed. Granular colourless titanite corone type-texture with ilmenite occurs in granitic- gneissic rocks and magnetite albitite. Prismatic, brownish shoals of well-formed linked crystals titanite with euhedral, rhomboid to elongate, rounded outlines associate with garnet or pyroxene in garnet and pyroxene albitite. In mineralized levels, the most common group is prismatic brownish to red coloured what occurs as single crystal together with very fine rounded uraninite and zircon crystal (~5 µm). Semi-quantitative (energy-dispersive espectometry analysis) data shows that uraninite contain high Y content.

Major elements content does not showed significant differences in relation to titanite textures, but the main differences are among its host rock. Variations are related to Al, Ti and Fe contents, as granitic rocks are more enriched in Al and Fe, and has lower Ti than albitite rocks. The Ca and Si contents are nearly constant, ranging from 0.96 to 1.00 and 0,95 to 1,05 a.p.f.u., respectively. On the other hand, when titanite is together with ore paragenesis

constantly shows the lowest Fe and Al contents. According to literature, oxygen fugacity controls Fe^{+3} abundance through coupled substitution (Al, Fe^{+3}) + (F, $OH)^{-} \longleftrightarrow Ti^{+4} + O^{2}$. As such, Fe+Al – Ti diagram draws a oxygen fugacity trend of granitic rocks, barren albitites towards mineralized one.

Titanite shows very similar rare-earth element contents (sum = 0,5 to 1,2%). It is slightly impoverished in light rare-earth element and enriched in heavy rare-earth element, and titanite related to mineralization has subhorizontal pattern. All groups have positive Eu anomaly (Eu/Eu*>1). On the other hand, they show Ce negative anomaly (Ce/Ce*>1). These data show that magmatic titanite has recrystallized without modification in rare-earth element pattern.

Some trace elements discriminate titanite according texture. Consistently, granular titanite has higher V, Zr/Hf, U, HREE+Y and lower V than prismatic titanite. Zirconium and hafnium show fracionating behavior in Zr/Hf vs Zr diagram. The relationship of Zr and Hf published in literature indicates that Zr/Hf and Y/Ho ratio can be good tracers of aqueous fluids interaction since these elements have an ionic radius and charge similar to which results in similar behavior. Our data shows that in prismatic titanite there is a decrease mainly in the Hf content in relation to Zr, which results in the increase of the Zr/Hf ratio. The hafnium loss may be related to new zircon crystallization since this element is strongly partitioned to this mineral and evidence of hydrothermal zircon is indicated by presence of fine zircon crystal included in titanite.

The presented data shows that magmatic rocks evolved to hydrothermal paragenesis in less oxygen fugacity condition. Ilmenite consums and the low oxygen condition turns titanite enriched in Ti. Hydrothermal alteration did not modified rare-earth elements pattern in titanite, but changed some contents of elements like U, Th, Pb, HREE+Y, Hf and V. Mineralizing fluids were able to remove U, HREE+Y and Hf from titanite to precipitate hydrotermal zircon and uraninite in reduced conditions. Trace element presented data diverges of literature as we show that, at least in anomaly 35, uraninite-related titanite has the lowest uranium contents (<6 ppm). In addition to these elements mobility, the closer relationship between titanite and uraninite sugests that titanite may has acted as metal source to uranium mineralization, at least locally.

U, Th AND RARE EARTH ELEMENTS MOBILITY IN TITANITE FROM MAGMATIC/ METAMORPHIC PARAGENESIS IN THE LAGOA REAL U- PROVINCE, BAHIA, BRAZIL

Nilo H. B. Lopes[1], Lucilia A. Ramos de Oliveira, Francisco J. Rios, Lucas E. D. Amorim, Evando C. de Matos

[1]*CDTN/CNEN - balzanilo@live.com*

The Lagoa Real Province is located in the central-south of the São Francisco craton, Bahia State, Brazil. It contains 110 thousand tons of uranium reserves distributed in 38 anomalies. The Province is comprised of granite, orthogneiss and albitite. Uranium occurs mainly as uraninite dispersed at the albitite. Relevant concentrations of rare earth elements however mainly occur in titanite, allanite, F-bearing carbonate and phosphate.

Uranium and rare earth elements could occur associated due their similar ionic radius when in an eightfold coordination. The mutual incorporation of these elements in the crystalline structure of the mineral is controlled by temperature and chemical availability. Furthermore, the presence of rare earth elements is described as an important tool to define the geological provenience of uranium minerals, such as uraninite.

Titanite is a common accessory mineral in magmatic and metamorphic rocks, and also could be found in hydrothermal environment. In its crystalline structure, the Ca can be occasionally substituted by other ions such as the rare earth elements, U, Th and Pb. Thereby, it is considered important to geochemical studies since it can be used to comprehend the effects of the distribution of those elements at the crystalline structure what consequently helps with the characterization of different geological environments.

In this work we seek to verify the occurrence of U, Th, Pb and rare earth elements at different titanite textures found in different bodies of granite, gneiss and amphibolite trying to establish geochemical trends and correlations. For that, *in-situ* laser ablation-inductive coupled plasma-mass spectrometry was performed at the different titanite textures found in: (i) the contact between microcline-gneiss and amphibolite (Rabicha deposit); (ii) granite (Lagoa do Barro and São Timóteo); (iii) albite-gneiss (Morro da Contagem and Fazenda Cercadinho).

The studies in titanite from microcline-gneiss (Rabicha deposit) were performed at the Swiss Federal Institute of Tecnology, Zurich. All the other samples were studied at the Nuclear Technology Development Center, Brazil.

Considering all the analyzed lithologies, both textures of titanite from Lagoa do Barro granite (granular and corona) show the highest mean concentrations of rare earth elements. They present values higher than 1000ppm for La, Ce, Nd, Sm and Lu, higher than 15000ppm for Yb and above 150000ppm for Y. It would be expected that the highest uranium concentration would also be found at this titanite crystals, due to the similar radius/charge with the rare earth elements. But, this is not observed. Uranium is detected with highest mean concentrations (~200ppm) in the granular titanite found at microcline- gneiss and amphibolite (Rabicha). Considering Th and Pb, Lagoa do Barro titanite once again shows the highest concentration (~4000ppm).

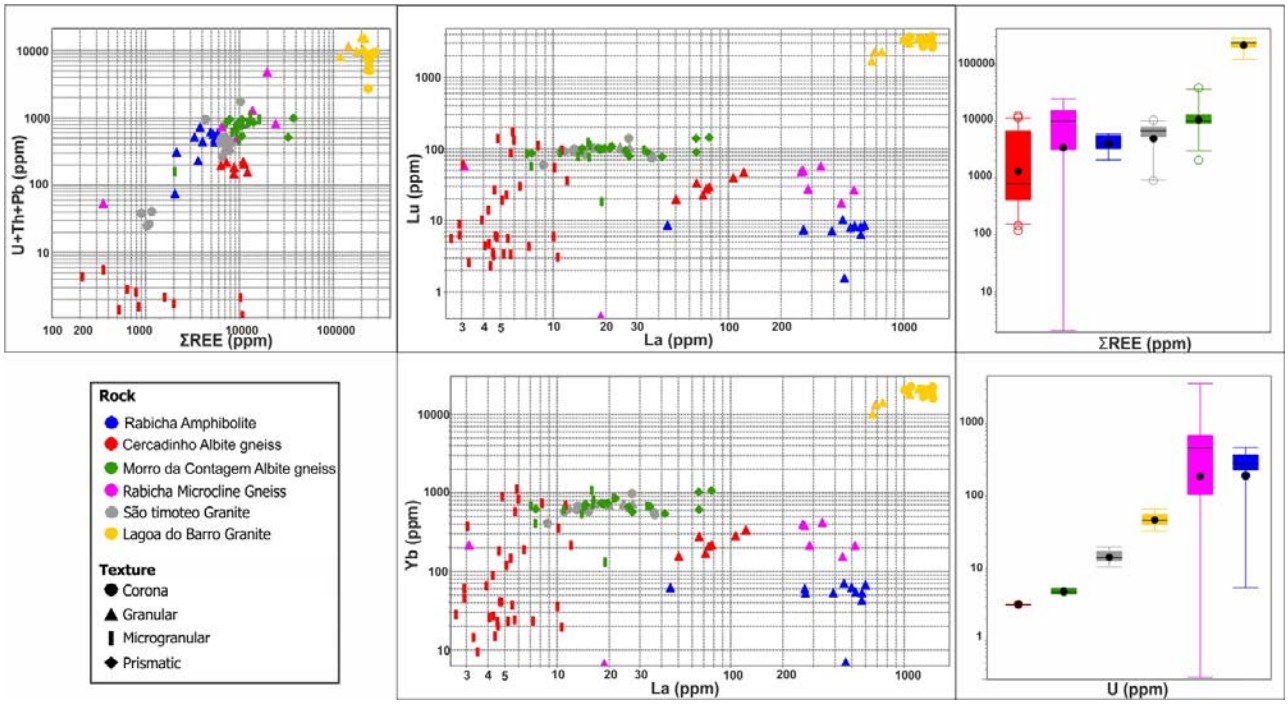

Regarding the total concentrations of rare earth elements at all the different titanite generations, we conclude that they present anomalously high values (always above 1000ppm). Granular titanite from the amphibolite and microcline-gneiss (Rabicha) are enriched in light rare earth, as seen in La *versus* Lu and La *versus* Yb diagrams.

The obtained results for the total amount of U, Th and Pb are not so similar, with the microgranular titanite from albite-gneiss (Cercadinho) showing mean concentration of 14ppm and from both textures of granite (Lagoa do Barro) next to 8000ppm. Meanwhile, all titanite textures from São Timóteo granite, Morro da Contagem albite-gneiss, Rabicha microcline-gneiss and amphibolite present approximately 500ppm.

The titanite crystals from Cercadinho albite-gneiss were divided in two distinct textural groups: (i) microgranular texture, aligned with the structural foliation; (ii) granular texture, intercepting the foliation planes. The first group is poorer in rare earth elements, U, Th and Pb, when compared with the second one. The microgranular titanite presents the lowest concentrations of the studied elements considering all the analyses and samples.

Regarding the titanite grains from the Cercadinho albite-gneiss, it can be said that the microgranular crystals have a pre-deformational genesis, while the granular ones were crystalized after the deformation. As they differ in rare earth elements concentrations, it can be affirmed that these elements are coming from a source active during a post- deformational hydrothermal event.

Comparing the U and rare earth elements, it is observed that the highest concentrations are found in different titanite generation (Rabicha and Lagoa do Barro, respectively). This could indicate distinct origin for U and rare earth elements, with sources that could have come from at least two different events. These events would have had distinct physicochemical characteristics, capable of affecting relatively similar elements in such differentiated ways.

In that context it is important to indicate that, in addition to this preliminary work, and several others already concluded, few researches are being accomplished. All of them seeking out the better explanations regard the mobility of these chemical elements, their origin and relation with the complexes events that have affected that economically important area.

CHAPTER 16
BASE METALS IN SEDIMENTARY SEQUENCES

Conveners: Thierry Bineli-Betsi, Josefina Pons, Joseph Zulu

BASE METAL MINERALIZATION IN THE DAIRI Zn-Pb±Ag DEPOSIT, NORTH SUMATRA, INDONESIA

Tomy Alvin Rivai

Department of Earth Resources Engineering, Kyushu University, Japan - tomyalvinrivai@mine.kyushu-u.ac.jp

INTRODUCTION

The Dairi Zn-Pb±Ag deposit is situated in North Sumatra, Indonesia, approximately 65 km to the northwest of Lake Toba. This deposit is estimated to have 25.1 Mt of ore at 10.2 wt.% Zn, 6.0 wt.% Pb, and 8.4 g/t Ag. The mineralization is hosted by sedimentary rocks of the Permo-Carboniferous Tapanuli Group, which is the oldest known rock unit in Sumatra. This sequence is considered as a sag-phase basin-filling unit related to the separation of Sibumasu and Gondwana. At present, the Dairi deposit is the only giant sediment-hosted Zn- Pb±Ag deposit that has been discovered in Indonesia. Therefore, a thorough study is essential to reveal its nature and to determine potentially useful characteristics for exploration of sediment-hosted Zn-Pb±Ag deposits in Indonesia.

METHODS

Standard petrography of approximately 100 samples was carried out to examine textural relationship, deformation, and metamorphism of rock-forming and ore-gangue minerals. X- ray fluorescence spectrometry analyses were applied to determine bulk geochemical composition of host rocks from nearly 60 samples. The sulfur isotope ratio of sulfides in more than 40 samples was analyzed to deduce sources of sulfur and mechanism of supply of reduced sulfur. Lastly, fluid inclusion microthermometry was carried to obtain the likely formation temperature.

RESULTS

The Tapanuli Group in the Dairi deposit is divided into three units from top downward: Dagang, Julu, and Jehe. The Dagang unit consists of interbedded dolomitic siltstone and sandstone with minor carbonaceous shale. The Julu unit is defined by interbedded carbonaceous shale and dolomitic siltstone. Fine-grained, subhedral to euhedral pyrite and anhedral sphalerite are occasionally present in these units while framboidal pyrite is rare. Concordant quartz veins containing large euhedral pyrite, sphalerite, galena, chalcopyrite, and pyrrhotite were identified in the Julu unit. The Jehe unit is characterized by massive sandy dolostone. This massive dolostone has been partially brecciated in some locations, and subsequently cemented by quartz. Wide distribution of muscovite foliation in the Dagang and Julu units suggests that the basin had undergone low-grade metamorphism.

The orebody hosted by the Julu unit is concordant and stratiform. Three mineralized strata have been identified: lower, main, and upper horizons. The lower and main horizons are continuous while the upper horizon is composed of lenses. Principal ore minerals are sphalerite and galena. Iron sulfide is predominantly pyrite, except in the lower horizon where pyrrhotite is the principle sulfide. Chalcopyrite, bournonite, and tetrahedrite occur in trace and minor amounts. Gangue minerals consist of quartz, dolomite, hyalophane, zeolites as well as trace barite and calcite. Sphalerite, galena, hyalophane, zeolites, and barite decrease toward northwest while quartz, dolomite, and calcite increase. In the same direction, framboidal pyrite is more abundant and overgrown by cubic pyrite. These trends suggest that ore-forming fluid was supplied into seafloor and sub-seafloor environments from presumed Permo-Carboniferous syn-sedimentary faults in the southeastern part of the deposit.

In contrast to the orebody hosted in the Julu unit, the orebody hosted in the Jehe unit is discordant, despite its stratabound distribution in deposit-scale. Sphalerite and galena are the main ore minerals along with tetrahedrite and tennantite. Other sulfosalts and sulfides (pyrargyrite, acanthite, freieslebenite, boulangerite, and diaphorite) are locally present in the disseminated ore type. Chalcopyrite occurs in minor amount as disease in sphalerite while arsenopyrite coexists with tennantite. As this orebody is present beneath the ore hosted in the Julu unit, the ore hosted in the Jehe unit is considered as a feeder zone for the stratiform ore in the Julu unit.

In terms of precipitation sequence, framboidal pyrite preceded the other ore minerals (diagenetic stage). Precipitation of cubic pyrite in the Julu and Jehe units was concurrent with that of other ore minerals (hydrothermal stage), although some portion of corroded, cubic pyrite appears to have formed earlier. Hydrothermal pyrite was recrystallized, deformed, disaggregated, and metamorphosed to pyrrhotite prior to regrowth of pyrite from pyrrhotite in retrograde phase (metamorphism stage). The last stage was also featured by remobilization of sphalerite, galena, chalcopyrite, tetrahedrite, and bournonite into pyrite fractures as well as sphalerite, galena, and pyrrhotite re-precipitation into piercement veins.

Geochemical characteristics of the host rocks in the Julu unit show an enrichment trend of MnO, Ba, and Sr toward the orebody as well as a depletion trend of MgO. Toward the orebody, 10MnO/10MnO+MgO(AI1) and $10MnO+10^{-4}Ba+10^{-2}Sr/10MnO+10^{-4}Ba+10^{-2}Sr+MgO$ (AI2) exceed 0.2 and 0.3, respectively. The elevated zone of AI1 and AI2 in the southeastern portion of the deposit extends to the contact with the Jehe unit while in the northwestern portion it is limited to a-five-meter- thick rock around the orebody. The decrease in thickness of the zone suggests that the ore- forming fluid flowed from southeast to northwest.

$\delta^{34}S$ of diagenetic pyrite in the host rock ranges from -4.1‰ to +18.6‰ indicating bacteriogenic reduction of contemporaneous seawater sulfate. In the ore hosted by the Jehe unit, $\delta^{34}S$ of sulfides ranges from +3.5‰ to +8.0‰. Homogenization temperature of fluid inclusions in sphalerite is of 160-170p C. $\delta^{34}S$ of sulfides in the lower horizon ranges from +4.9‰ to +18.1‰ while that in the main and upper horizons from +13.5‰ to +28.8‰. The trend of increased $\delta^{34}S$ in an upward stratigraphy and homogenization temperature suggests thermochemical reduction of sulfate from an underlying evaporite as the main mechanism involved in economic mineralization. The presence of a Silurian evaporite in the Sibumasu mirror image in Australia and $\delta^{34}S$ of sulfides in the ore hosted in the Jehe unit suggest the Silurian evaporite as a possible source of sulfur responsible for mineralization.

CONCLUSIONS

The Dairi Zn-Pb±Ag deposit is hosted in a sag-phase basin sequence which had undergone low-grade metamorphism. Economic mineralization occurred in the hydrothermal stage with reduced sulfur supplied by thermochemical sulfate reduction of an underlying Silurian evaporite. Ore-forming fluids were channeled through presumed Permo-Carboniferous syn- sedimentary faults in the southeastern portion of the deposit and flowed from southeast to northwest within the Julu unit.

COBALT IN SEDIMENTARY BASINS

Richard Herrington[1], Steve Roberts

[1]*The Natural History Museum, Cromwell Road, London SW7 5BD - r.herrington@nhm.ac.uk*

BACKGROUND

The majority of cobalt is produced as a by-product of copper and nickel production. Despite a very significant association of cobalt with magmatic nickel-copper and unusual five- element type deposits, more than 60 % percent of primary cobalt production comes from the Central African Copperbelt (CAC), particularly from mines in the Democratic Republic of Congo. Copper-cobalt deposits in the CAC represent the only clastic sediment-hosted copper district where significant cobalt is currently recovered. Similar sediment-hosted copper districts of the world (Fig 1.) are not know for cobalt although this could partly be a function of historical priorities. Cobalt is also recorded from a range of carbonate- hosted lead-zinc and copper districts but is likewise rarely recovered. Siliciclastic sequences in other rift environments are known to host cobalt-enriched massive sulfides. The cobalt-rich Windy Craggy deposit in Canada and the previously mined Kilembe deposit in Uganda are both considered to be Besshi-type systems formed in arc settings. New exploration is now focusing on cobalt in a range of other sedimentary associations like central Idaho, iron oxide-copper-gold deposits in a range of settings, and the five-element vein deposit types typified by those in the Cobalt region of Ontario.

DISCUSSION

Cobalt behavior in sedimentary-hosted ore systems is poorly documented; much is published on the origin of the largely copper-dominated mineralization but there is little published on cobalt deportment. The observation that significant cobalt is only recovered from the Congolese and western parts of the Zambian Copper Belts within the CAC is quite remarkable. In the DRC, the most cobalt-rich deposit, Kisanfu, has primary grades that are economic, supporting primary cobalt production. The hypogene mineral host in the CAC is largely carrollite but a more important part of the cobalt production in the belt comes from the overlying oxidized zones where cobalt is largely hosted in secondary phases like heterogenite. The close association of the deposits in the CAC with large volumes of mafic and ultramafic igneous suites could be a factor in the primary cobalt endowment of the potential source rocks in the basin. However, what is also clear is that the CAC has had a more protracted history of diagenesis, deformation and hydrothermal fluid flow which may account for the range of mineralization styles and mineralogical associations. Evidence is emerging that redox and temperature may be important factors in decoupling copper and cobalt behavior in such settings and these factors may account for the inhomogeneous distribution of primary cobalt through the CAC. The implications on the cobalt deportment in other sediment-hosted settings through Europe, Asia and the Americas will be discussed in light of these findings.

REFERENCE

Hitzman, M.W., Kirkham, R., Broughton, D., Thorson, J., and Selley, D., 2005, The sediment- hosted stratiform copper ore system. in Hedenquist, J.W., Thompson, J.F.H., Goldfarb, R.J., and Richards, J.P, eds., Economic Geology – 100th Anniversary Volume, p. 609-642.

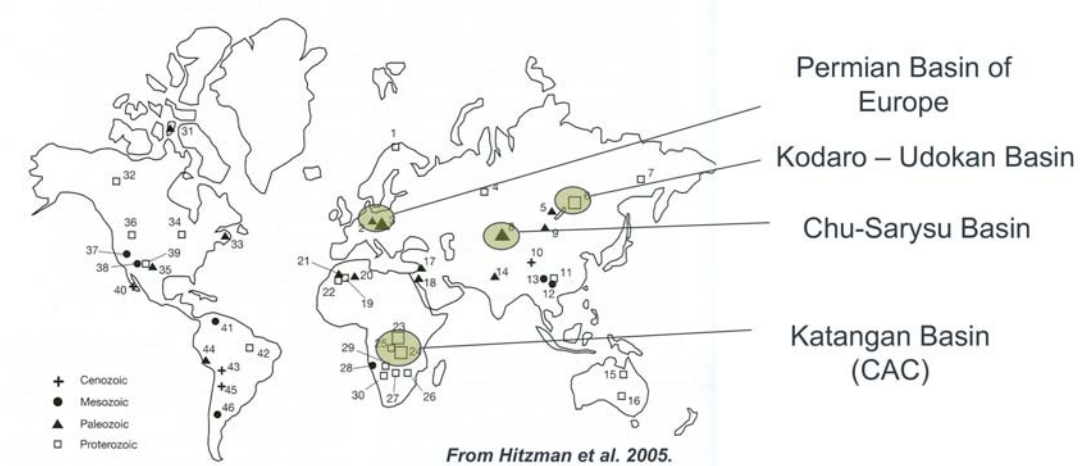

Figure 1. World map showing key sediment-hosted copper basins with significant mine production of copper (modified from Hitzman *et al.* 2005)

A | 166

THE DISTRIBUTION AND PARTITIONING OF SILVER IN THE BANANA ZONE SEDIMENT-HOSTED Cu- Ag DEPOSIT IN THE GHANZI-CHOBE CU BELT PORTION OF THE KALAHARI Cu BELT: CONSTRAINTS FROM LA-ICP-MS STUDY

Tebogo Kelepile[1], Thierry Bineli Betsi, Fulvio Franchi, Elisha Shemang

[1]*Department of Earth & Environmental Sciences, Botswana International University of Science & Technology, Private Bag 16, Palapye, Botswana - kelepilet@biust.ac.bw*

BACKGROUND

The Banana Zone Cu-Ag Deposit (hereafter Banana Zone), in north-western Botswana, is within the Kalahari Copper Belt. The Banana Zone (Kelepile *et al.*, 2017 and references therein), a simple doubly plunging folded structure with no major faulting includes five mineralised subzones namely; the Chalcocite (CC), New Discovery (ND), North Limb (NL), North East Fold (NEF), and South Limb Definition (SLD).

The NEF is located at the northeastern end and sits at the fold closure of this doubly plunging folded structure. The mineralization style at the NEF is veinlet-controlled and stratabounded in the grey sedimentary beds. The main ore phases include bornite, chalcocite, and chalcopyrite, with minor sphalerite, galena, covellite, tennantite-tetrahedrite, as well as rare occurrences of silver-bearing minerals consisting of fine- grained (< 60 Mm) native silver and stromeyerite.

Despite the rare occurrences of Ag-bearing minerals, Ag grades up to 0.1 wt. % locally. The distribution of Ag correlates best with those of Cu, implying that Cu-(Fe)-S minerals may contain traces of Ag. Such occurrences of silver in Cu-minerals have been reported in various deposits elsewhere (e.g. Walraven and Borg, 1992; Dewaele *et al.*, 2006; Cook *et al.*, 2011; Kozub, 2014).

The objectives of this study are, therefore: (i) to track the distribution and the partitioning of Ag in the spatially associated sulphide phases (ii) to constrain the mode of occurrence (i.e. nanoparticle-hosted and lattice-bound) of Ag in these phases.

METHOD

LA-ICP-MS spots analysis and elemental mapping of coexisting sulphide phases from NEF were conducted in the Department of Earth Sciences of the University of New Brunswick, Canada. A Resonetics M-50-LR 193-nm Excimer laser ablation system coupled to an Agilent 7700x ICP-MS was employed.

Sulphide analyses were carried out using a 33-micron spot running at 3 Hz and on-sample energy (fluence) of 1.3 J/cm2, with 40-second ablations and 30-second gas backgrounds between each ablation. Carrier gasses were ultra-pure helium (300 ml/min), ultra-pure nitrogen (2 ml/min), and standard Argon (930 ml/min). The second rotary pump was also used which increases sensitivities of heavy isotope by almost double. The standards used were MASS-1 (sulphide precipitate) and NIST610 (glass standard). The data were reduced using Cu as an internal standard for Cu-phases (bornite, chalcopyrite, and chalcocite) and Zn for sphalerite. The ICP-MS was tuned for a full suite of elements (7, 47, 118, and 207; monitored during tuning) to ensure maximum sensitivity over the range of analysed masses while keeping doubly charged ions and oxides at a maintainable level (Â 0.3% for each).

RESULTS

Preliminary results identify chalcocite, bornite, wittichenite, and galena as the major Ag- carrier in this deposit. Silver concentration ranges from 175 to 539 ppm in chalcocite, 131 to 1390 ppm in bornite, 1220 to 2660 ppm in wittichenite, and 407 to 511 ppm in galena. In the coexistence of Cu-(Fe)-S minerals, Ag is preferentially partitioned into a more Cu-rich phase (Fig. 1). In the chalcopyrite-bornite assemblage, almost all the Ag is partitioned into bornite (96% of Ag) over chalcopyrite. Equally, in the bornite-chalcocite assemblage, chalcocite has almost 60% of the Ag. This is consistent with the previously observed geochemical assay data indicating a positive correlation between Cu and Ag. Of note is the contrasting relationship between Ag and Bi in coexisting phases as demonstrated by a positive correlation in the chalcopyrite-bornite pair (Fig. 1b, c) and a negative correlation in the bornite-chalcocite couple (Fig. 1e, f). In galena Ag positively correlates Sb, suggesting the presence of Ag-Sb-bearing phases either in the form of inclusions or solid solution.

The homogeneous distribution of Ag (Fig. 1) and small to medium standard deviations averaging 3 to 44% of the mean suggest that Ag is most likely in solid solution in the structures of these sulphides (George *et al.*, 2015). It is also observed from these maps that there are at least two Ag mineralizing events as demonstrated by an Ag-rich veinlet that crosscut both the chalcocite and the bornite (Fig. 1e). Our results highlight the variation in Ag and Bi

contents between chalcocite grains from the same sample and within a single chalcocite grain, with the latter demonstrating compositional zoning at grain scale. These contentions may indicate a change in the composition of the mineralizing fluid through time.

CONCLUSIONS

This study shows that:

Chalcocite, bornite, wittichenite, and galena are the main hosts of Ag in the Banana Zone;
Silver preferentially partitions into chalcocite than bornite and bornite than chalcopyrite;
Silver occurs as a solid solution in the structure of sulphide phases;
At least two precipitation events of Ag occurred;
The composition of the mineralizing fluid changed over time.

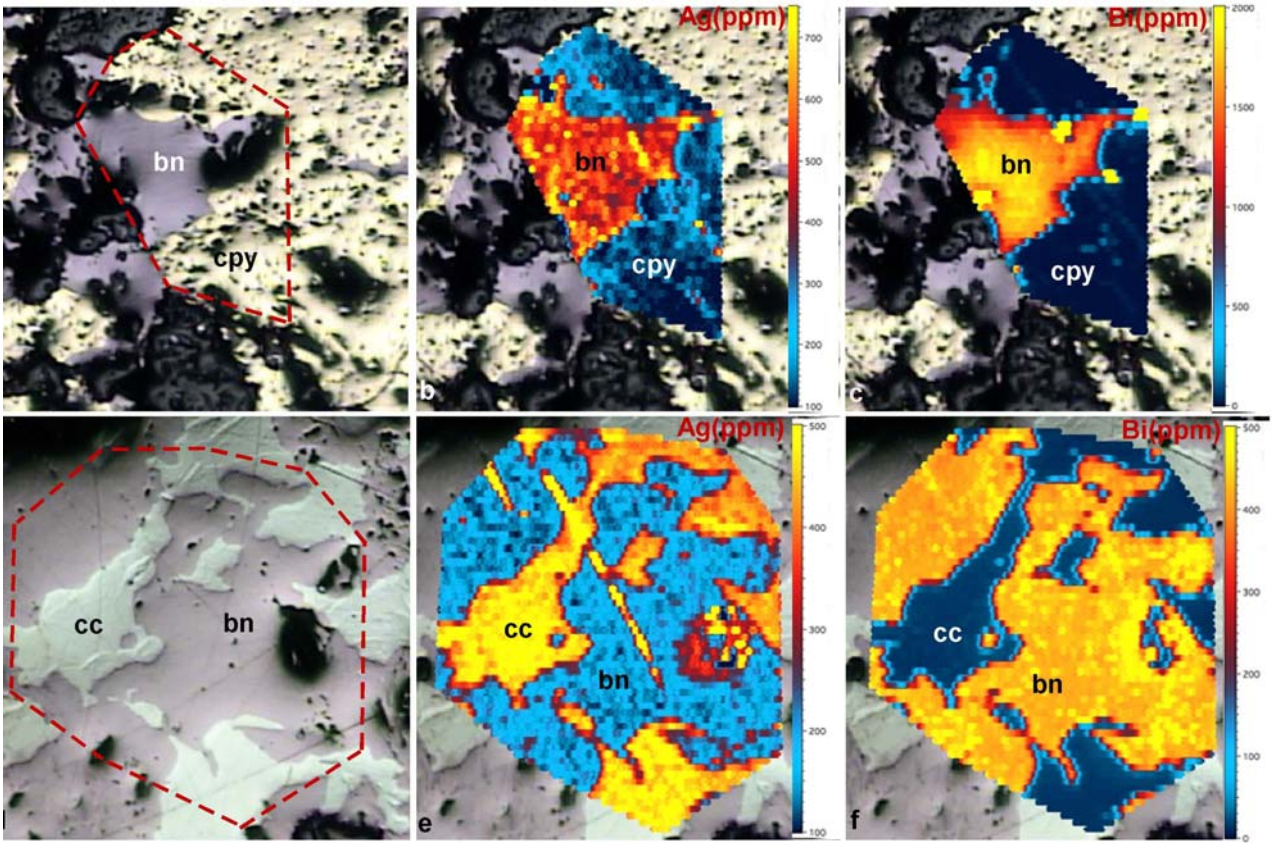

Fig. 1: (a) Photomicrograph of a bornite-chalcopyrite assemblage of the mapped area (polygon). (b) LA-ICP-MS maps showing the distribution of Ag in bornite (bn) and chalcopyrite (cpy). (c) LA-ICP-MS maps showing the distribution of Bi in bn and cpy. (d) Photomicrograph of a bornite-chalcocite assemblage of the mapped area (polygon). (e) LA- ICP-MS maps showing the distribution of Ag in bn and chalcocite (cc). (f) LA-ICP-MS maps showing the distribution of Bi in bn and cc.

A | 167

HYDROCARBONS LINKED TO STRATIFORM SEDIMENT HOSTED LEAD, ZINC AND COPPER MINERALIZATION IN LAJAS FORMATION, NEUQUÉN BASIN ARGENTINA

María Josefina Pons[1], Ana Laura Rainoldi, Marta Franchini, Adolfo Giusiano.

[1]Centro Patagónico de Estudios Metalogenéticos, CONICET, Instituto de Paleobiología y Geología Universidad Nacional de Río Negro - jpons@unrn.edu.ar

BACKGROUND

Rocks mineralized with lead, zinc and copper sulfides were discovered at ~1000 m depth below the Barda González and La Cuprosa stratiform sandstone-hosted copper deposits (SSHCD) at Aguada Baguales oil field, Neuquén Basin. Mineralized rocks occur in fluvio- deltaic sandstones of Lajas Formation (Aalenian-Bajocian) which is a current oil and gas reservoir rock. The zinc and lead sulfides were first reported by Garrido *et al.* (2000), in dolomitic facies of the Lajas Formation outcrops, 200 km SW of the study area (Puesto Gregor) and they were attributed an epigenetic origin.

The Neuquén Basin is a complex retroarc-foreland basin, developed in the eastward of the Andean Cordillera (Argentina). The basin initially formed as a rift system during the Late Triassic-Early Jurassic followed by several episodes of structural inversion during the Tertiary. Tectonic evolution is reflected in the stratigraphic record with 220 Myrs of basin subsidence with 7,000 m of Upper Triassic-Cenozoic preserved basin infill and the development of source and reservoir hydrocarbon rocks, as well as evaporates and several red beds sequences.

This contribution presents new petrographic description of diagenetic and ore minerals and sulfide stable isotope geochemistry from the fluvial-deltaic rocks from Lajas Formation, in order to understand the role of diagenetic processes, hydrocarbons and metal-charged basinal brines in the mineralization of Zn-Pb-Cu.

METHODS

Representative samples of mineralized rocks from selected drill holes were collected for laboratory analysis. Polished thin sections were examined with a polarization-fluorescence microscope. Sulfur stable isotope analyses were carried in sulfide at the Servicio de Isótopos Estables, Universidad de Salamanca (Spain), using two SIRA-II gaseous source dual inlet mass spectrometers. Samples were prepared by handpicking and isotopic results are reported in δ notation relative to Canyon Diablo Troilite (CDT).

RESULTS

Mineralized rocks have been intersected by drill core AB-1010 in Aguada Baguales oilfield (973-1088 mbsl). Zinc, lead and copper minerals fill the porosity of coarse-grained facies from bed-load deposits irregularly distributed in the upper, middle, and lower section of the Lajas Formation. They consist of lithic feldspathic conglomerate and sandstone with quartz (40-35%), feldspar (15-20%), lithics (45-39%) and zircon as accessory. The porosity varies from 3 to 15%, depending on the amount of diagenetic minerals. These rocks show moderate and high proportion of hydrocarbon impregnations with yellow fluorescence. Six stages of porosity infill were recognized: 1) early quartz overgrowths 10-100 µm thick, 2) interstitial gypsum, 3) marcasite±illite (illite-smectite), 4) siderite, 5) Fe, Zn, Cu and Pb sulfides and, 6) late well-crystallized kaolinite.

Quartz overgrowths and detrital quartz are partially dissolved and covered by bitumen impregnations, early marcasite fills the pores and illite + illite-smectite mixed layers rim detrital grains. Locally, marcasite replaces previous gypsum cement. Mn-bearing siderite (MnO up to 10%) fills the remained porosity and is replaced by patches of galena, iron-poor sphalerite (< 1% Fe) and traces of chalcopyrite. Sphalerite is the most abundant sulfide, occurs as yellow, anhedral grains or as fibro radial crystals sourrounding black spots of solid hydrocarbons or previous marcasite. Probably, this fibro radial habit resulted as pseudomorphs of early fibro radial marcasite. Late kaolinite and calcite seal the remaining porous spaces.

Isotopic sulfur values from marcasite varies between -3.5 to -2.2‰ (n=2), sphalerite presents heavier and homogenous values between +10.4 to +10.8‰ (n=3) and galena shows an intermediate value with +5‰ (n=1). The equilibrium isotopic temperature calculated for sphalerite and galena was 120-130 °C using the equation of Liu *et al.* (2015).

At Aguada Baguales oil field, Lajas Formation shows textural evidence that marcasite ± illlite and illite-smectite mixed layers are epigenetic, precipitated after quartz overgrowths and formed in contact with liquid hydrocarbons. Marcasite shows a maximum sulfur isotope fractionation δ34S ~19.2 to 33.5‰, considering, that the main sulfur source could be the dissolution of evaporate layers of the basin with a δ34S between 17 to 30‰ (Lo Forte

et al., 2005, Cavallaro *et al.*, 2007). This fractionation range is just between the values obtained from biogenic sulfate reduction -BSR- (>20‰) and those from thermochemical sulfate reduction -TSR- (<20‰) with a lower and upper thermal limits for BSR between ~80 °C and ~100 °C respectively (Machel *et al.*, 1987). If we consider the estimated temperature ~ 90 to 100 °C in base of the burial depth of Lajas Formation, BSR could have been taken place during the precipitation of marcasite.

Textural evidence indicates that siderite and Pb, Zn, Cu, and Fe sulfides precipitated after marcasite ± illite and illite-smectite cements, filling the remaining porosity as a consequence of a new input of chloride-bearing oxides brines (SO_4>H_2S), capable of transporting Pb, Zn, Cu, and Fe (Cooke *et al.*, 2000). In consequence, siderite represents the first product of the brines-hydrocarbons interactions at temperatures lower than 150 °C and pH between 5 to 7 (Cooke *et al.*, 2000). The continue interaction of these oxides fluids with interstitial hydrocarbons produce additional decrease in oxygen fugacity and the precipitation of Zn, Pb and Cu sulfides after siderite formation (Cooke *et al.*, 2000). Possibly, sulfur source of these later sulfides could be previous marcasite and the sulfate-bearing brines. In consequence lower isotopic fractionation (6.7 to 24‰) occurred during Zn, Pb, Cu mineralization (galena, sphalerite and traces of chalcopyrite) via TSR at slightly higher temperature than the previous marcasite (Machel *et al.*, 1987). It is consistent with isotopic equilibrium temperature of 120-130 °C calculated for galena-sphalerite. This temperature is coherent with the temperature (140 °C) obtained by Gómez *et al.* (2008) from microthermometric analyses of fluid inclusions hosted in saddle dolomite from Lajas Formation in Puesto Gregor area. In consequence, the main factor to produce an abrupt change in solubility of these base metals was a decrease in oxygen fugacity when metal-bearing oxidizing brines arrived into the oil reservoir rocks.

CONCLUSION

New mineralogical, textural and analytical evidences indicate that Cu, Zn and Pb mineralization was epigenetic and results from the interaction of hydrocarbons with host rocks and metal-charged basinal brines via TSR, and mark the potentiality of Neuquén basin to host SSH-metal deposits of economic interest.

REFERENCES

Cavallaro, A., Alberdi, M. I., Galliano G. R., 2007. Overview of H2S souring Cases in Argentina Reservoirs: Origin and mitigations sceneries. In Society of Petroleum Engineers, SPE 107376, 1-7.

Cooke, D.R., Bull, S.W., Large, R.S., McGoldrick, P.J., 2000.The importance of Oxidized brines for the formation of Australian proterozoic stratiform sediment-hosted PbZn (Sedex) deposits. Econ. Geol. 95, 1–18.

Garrido, M., E. Domínguez, M.C. Gómez, N. Cesaretti y G. Aliotta, 2000. Una mineralización de Zn-Pb de tipo MVT en la Cuenca Neuquina. In proceedings of 5° Congreso de Mineralogía y Metalogenia, La Plata, 164-170.

Gómez C., Garrido M., Cesaretti N., Dominguez E., 2008. Petrografía y geoquímica de la dolomita hospedante de la mineralización de Zn y Pb Puesto Gregor Neuquén, Argentina. Lat. Am. J. of Sedimentol. and Basin Analyses,15 (1), 27-36.

Liu S, Li Y, Liu J, Shi Y 2015. First-principles study of sulfur isotope fractionation in pyrite- type disulfides. American Mineralogist 100, 203-208.

Lo Forte GL, Orti F, Rosell L 2005. Isotopic characterization of Jurassic evaporites. Aconcagua-Neuquén Basin, Argentina. Geológica Acta 3, 155–161.

Machel H. G. 1987. Some aspects of diagenetic sulphate- hydrocarbon redox-reactions. In: Marshall J.D., (Ed), Diagenesis of Sedimentary Sequences, Geologist Society Special Publication 36, pp. 15-28.

A | 168

VOLCANIC SHALE-HOSTED MASSIVE SULPHIDES IN THE BATHURST MINING CAMP, CANADA: A SEDIMENTARY PERSPECTIVE

Sean H. McClenaghan

Trinity College Dubin - mcclens@tcd.ie

BACKGROUND

Volcanic shale-hosted massive sulphide (VSHMS) deposits of the Bathurst Mining Camp (BMC) are syngenetic in origin, precipitating from exhalative activity along sedimentary horizons within rifted ensialic segments of the Tetagouche-Exploits back-arc basin. For siliciclastic dominant back-arc environments, hydrothermal precipitates can be modified by pelagic, volcaniclastic and terrigenous contributions, which complicate the geochemistry of exhalites and mask primary hydrothermal signatures. Furthermore, exhalative systems in the Tetagouche-Exploits back-arc were active within several distinct basins floored by Cambro-Ordovician sedimentary rocks and para-autochthonous volcano-sedimentary sequences, namely the Tetagouche, California Lake and Sheephouse Brook Groups. Despite the complexity, sulphide mineralization across the tectonostratigraphic framework of the BMC yields mineralogical and geochemical variations, as well as distinct variations in $\delta^{34}S$ signatures, owing to these differing basin conditions.

METHODS

Representative sulphides from 34 massive sulphide deposits in the BMC were subjected to geochemical and isotopic analysis. Bulk lithogeochemistry was carried out using total- digestion fusion methods and analyzed for a full suite of major and trace elements. For sulfur isotope analyses, prepared samples were transferred to a column maintained at 1,000 °C, and material flash-combusted at 1,800 °C in the presence of oxygen. The purified SO_2 gas was passed through an EA1110 gas chromatograph column and transferred to a triple collector VG SIRA 12 mass spectrometer for isotopic mass separation, counting and quantification. The technique was accurate to within 1.0 to 1.5‰ of standard reference materials with analytical precision of +/- 0.2‰.

RESULTS

The largest sulphide tonnage in the BMC is associated with the Brunswick Horizon (>350 Mt) hosted by the Tetagouche Group. Algoma-type iron formation in the BMC (see Peter and Goodfellow, 1996) marks a hiatus in volcanism that is punctuated by numerous massive sulphide occurrences including the world class Brunswick N°12 deposit. Along the Brunswick Horizon, strong inter-element correlations among Zr, Ti, Nb, V, Cr, Th, Y and rare earth elements (REE) in massive sulphides are due primarily to the intercalation of volcaniclastic material and define an overall trend indicative of tuffaceous material. Iron formation in the immediate hanging wall to massive sulphide mineralization displays a geochemical shift towards terrigenous signatures consistent with passive margin sedimentation. Chondrite normalized REE patterns for massive sulphides exhibit prominent fractionation signatures consistent with mixing of high temperature hydrothermal fluids with seawater; however, these anomalies are commonly masked by the effects of intercalated sedimentary material complicating the geochemistry of exhalative horizons.

On a regional scale, variations in sedimentary environment have affected the bulk composition of massive sulphides with lower "REE contents exhibited overall for the Caribou Horizon (19.4 ppm) relative to massive sulphides of the Tetagouche Group (40.6 ppm), and largely reflect varying aluminosilicate contributions. REE profiles for massive sulfides exhibit systematic variation amongst exhalative horizons, with massive sulfides of the Tetagouche Group exhibiting higher LREE enrichment (LaN/LuN, 30.5) than California Lake Group exhalites averaging 6.85. Similarly, positive Eu anomalies are significantly larger in the Tetagouche Group (Eu/Eu*, 7.68), relative to the California Lake Group (2.54).

Overall, $\delta^{34}S$ for massive sulfides of the BMC average +11.4‰ (n=217), reflective of seawater sulfur sources,and signatures evolving towards progressively heavier values of $\delta^{34}S$ through Rayleigh fractionation. These signatures are similar to contemporaneous sedimentary pyrite from the Selwyn Basin, which records a detailed record of ocean redox conditions for the Ordovician and conforms to $\delta^{34}S$signatures for pyrite in sedimentary basins worldwide (Goodfellow, 1987). Deviations from the secular curve likely represent a mixture of bacterially reduced (heavy) signatures with isotopically lighter igneous, volcanic and/or sedimentary signatures; values of $\delta^{34}S$ for Cambro-Ordovician black shale of the Miramichi Highlands is highly variable, ranging from -17.3 to 27.6‰, and reflecting fluctuating redox conditions in the Tetagouche–Exploits back-arc basin (Goodfellow *et al.*, 2003). Rare occurrences of barite in the Louvicourt and Brunswick N°12 deposits (McClenaghan *et al.* 2006) exhibit similar values (Avg., 28.8‰), and are consistent with secular variations in $\delta^{34}S$ signatures for sulfates in Ordovician evaporate sequences (Claypool *et al.*, 1980).

Regionally, $\delta^{34}S$ signatures exhibit a distinctly bimodal distribution (Figure 1) that is broadly consistent with the setting of massive sulfides within volcano-sedimentary rocks of the California Lake and Tetagouche Groups. Deposits hosted by the Tetagouche Group exhibit heavier isotopic signatures with $\delta^{34}S$ values averaging +12.7‰ and ranging from +7.4 to +16.7‰, whereas deposits of the California Lake Group exhibit relatively light signatures with deposits averaging +7.1‰ and ranging from +4.6 to +11.3‰. These variations may represent systematic variations in seawater anoxia within sub-basins of the Tetagouche–Exploits back-arc basin and/or mixing of different S sources. Broad similarities in δ34Svalues throughout the Tetagouche Group indicate deposition within related anoxic bottom waters of the stratified Tetagouche–Exploits back-arc basin (Peter and Goodfellow, 1996).

Isotopically lighter massive sulphides of the California Lake Group exhibit considerable variability ranging from +1.1 to +14.0‰. The 70.0 Mt Caribou deposit exhibits the lightest signatures in the BMC with $\delta^{34}S$ values for massive sulfides ranging from +1.1 to +9.7‰. Given the setting of the Caribou Horizon at the base of the California Lake Group and preceding felsic volcanism of the Spruce Lake Formation, the lighter isotopic signatures could, in part result from differing basin signatures evidenced by their lower stratigraphic setting and older age.

CONCLUSIONS

Back-arc basin dynamics have exerted significant controls on the geochemistry of massive sulphides in the BMC. This has resulted in varied signatures across the tectonostratigraphic framework of the region, and further accentuates key differences in VSHMS deposit settings. Sulfur isotope signatures tend to support temporal and/or spatial separation of exhalative horizons in the BMC. An overall increase in $\delta^{34}S$ values over time has resulted from increased bacterial reduction of sulfate and progressively heavier isotopic conditions within a closed basin.

REFERENCES

Claypool, G.E., Holser, W.T., Kaplan, I.R., Sakai, H., and Zak, I., 1980, The age curves of sulfur and oxygen isotopes in marine sulfate and their mutual interpretation. Chemical Geology, 28, 3-4.

Goodfellow, W.D., 1987, Anoxic stratified oceans as a source of sulphur in sediment-hosted stratiform Zn–Pb deposits (Selwyn basin, Yukon, Canada). Chemical Geology, 65, 359-382.

Goodfellow, W.D., and Peter, J.M., 1996, Sulphur isotope composition of the Brunswick N°12 massive sulphide deposit, Bathurst Mining Camp, N.B.: Implications for ambient environment, sulphur source and ore genesis. Canadian Journal of Earth Sciences, 33, 231-251.

Goodfellow, W.D., Peter, J.M., Winchester, J.A., and van Staal, C.R., 2003, Ambient marine environment and sediment provenance during formation of massive sulfide deposits of the Bathurst Mining Camp: Importance of reduced bottom waters to sulfide precipitation and preservation. Economic Geology Monograph, 11, 129-156.

McClenaghan, S.H., Lentz, D.R., and Beaumont-Smith, C.J., 2006, The gold-rich Louvicourt volcanogenic massive sulfide deposit, New Brunswick: a Kuroko analogue in the Bathurst Mining Camp. Exploration and Mining Geology, 15, 127-154.

Peter, J.M., and Goodfellow, W.D., 1996, Mineralogy, bulk and rare earth element geochemistry of massive sulphide-associated hydrothermal sediments in the Bathurst Mining Camp, New Brunswick. Canadian Journal of Earth Sciences, 33, 252-283.

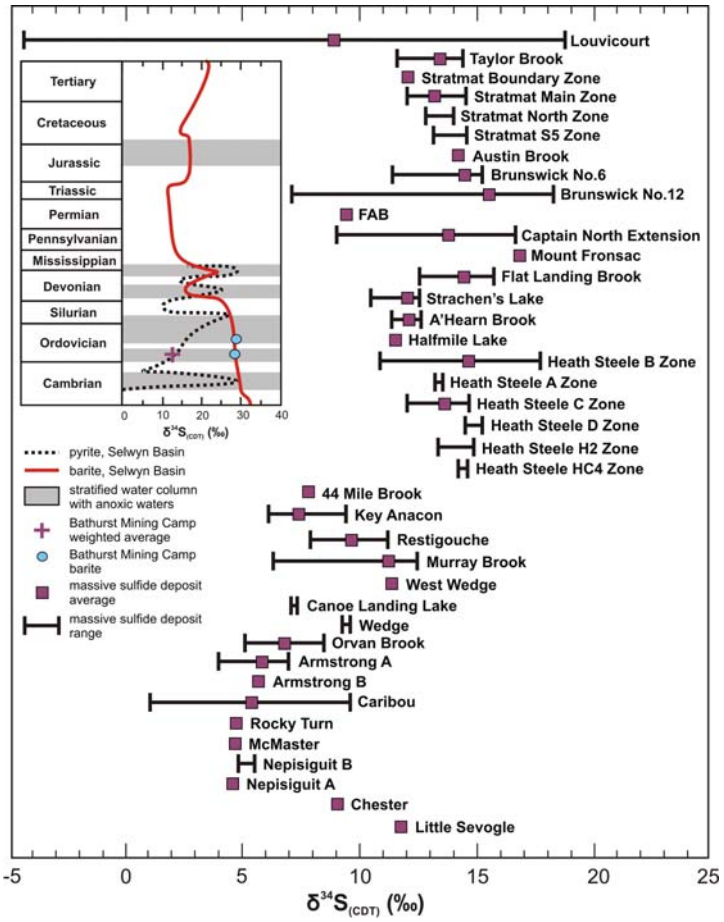

A | 169

THE UPPER PENINSULA COPPER PROVINCE, MICHIGAN: GEOLOGIC OBSERVATIONS AND GENETIC IMPLICATIONS

José Perelló[1], Richard H. Sillitoe

[1]Antofagasta Minerals, Apoquindo 4001, Piso 18, Santiago, Chile - jperello@aminerals.cl

BACKGROUND

The Upper Peninsula of northern Michigan lies within the 1150-1080 Ma Midcontinent Rift (MCR) of the Lake Superior region. The rift comprises ~20-25 km of subaerial basaltic lava flows and lesser interbedded siliciclastic rocks overlain by a 5-8-km siliciclastic sequence (Keweenawan Supergroup; Fig. 1). The syn-rift Portage Lake Lava Series (PLLS) comprises >200 basalt flows, characterized by vesicular and brecciated flow tops, and interbedded red-bed conglomerate. Rhyolite and felsic tuff occur in the lower and upper parts of the Keweenawan Supergroup (e.g., Porcupine Volcanics). The overlying Oronto Group, deposited during post-rift thermal subsidence, comprises: a basal, red-bed fluvial sequence (Copper Harbor Conglomerate; CHC), with locally interbedded stromatolites and basaltic flows; a sequence of grayish-black shale and carbonate laminates (Nonesuch Formation) deposited under anoxic lacustrine conditions; and an upper unit of reddish-brown sandstone, siltstone, and mudstone (Freda Sandstone), representing a return to fluvial conditions.

The MCR evolved within Laurentia, although rifting ceased prior to complete continental separation. Extension lasted from ~1110-1093 Ma, with volcanism continuing to ~1086 Ma during post-rift fluviatile sedimentation. The PLLS formed during main-stage MCR magmatism, from ~1098-1093 Ma. Far-field compression resulting from continental collision along the Grenville front at ~1060 Ma caused ~30 km of shortening, thick-skinned deformation, and inversion of the rift-bounding normal faults, including the >200-km-long Keweenaw fault (Fig. 1).

Copper mineralization in the Upper Peninsula comprises two principal styles: native copper in syn-rift basaltic lavas and intercalated siliciclastics of the PLLS and stratiform, sediment-hosted chalcocite in Nonesuch shale (Fig. 1). Minor native copper also occurs in the CHC and stratiform, chalcocite-bearing sediment-hosted mineralization is contained in the uppermost Nonesuch Formation.

The native copper (+ silver) deposits produced ~5 Mt of copper averaging 1.8%, ~60% from a stacked series of brecciated and amygdaloidal flow tops and the remainder from interflow clastic rocks and fissure veins. Individual bodies were tabular and 3-5 m thick, with strike lengths of up to 12 km and locally >2 km down dip, whereas the steep fissure veins cut >1000 m of stratigraphy. K-feldspar, chlorite, epidote, calcite, quartz, hematite, pumpellyite, and prehnite are typical associated minerals. Chalcocite veins commonly crosscut the native copper lodes but did not contribute to production. Chalcocite in lower Keweenawan basalt flow tops and in fractures near andesite sills locally formed deposits <2 km from the Keweenaw fault (Fig. 1). These deposits also contain minor amounts of native copper, typically overprinted by chalcocite.

The main chalcocite deposits are White Pine and Copperwood, the former producing ~2 Mt of copper at 1.14% plus 8 g/t Ag, ~80% as fine-grained, bedding-parallel disseminations in the 5-m-thick basal Nonesuch shale. Chalcocite sheets are also present along faults, and native copper occurs at the top of the underlying CHC and in the White Pine fault zone that offsets the deposit. Mineralization is vertically zoned from basal chalcocite through other chalcocite-group minerals plus bornite and chalcopyrite to upper pyritic shale, with the zones transgressing stratigraphy. Various types of veinlets and seams occur and contain the same sulfide assemblages as the adjoining disseminated mineralization.

METHODS

Underground inspection of unmined portions at White Pine and core logging of selected drill holes from White Pine, Copperwood, and other sediment- and volcanic-hosted sulfide and native copper prospects in the Upper Peninsula.

RESULTS

Mutually crosscutting relationships between native copper and chalcocite are evident in all mineralization styles: native copper veinlets cut finely disseminated chalcocite mineralization and chalcocite rims native copper grains. This is considered unambiguous evidence for precipitation of native copper both before and after chalcocite.

CONCLUSIONS

Current models support two copper mineralizing events in the Upper Peninsula: chalcocite deposition during diagenesis of the Nonesuch Formation and native copper mineralization during the deformation that accompanied

rift-basin inversion. The observed relationships between chalcocite and native copper mineralization in the two principal deposit styles together with the brittle nature of both chalcocite- and native copper-dominant fissure veins throughout the region suggest an alternative model: mineralization during a single, protracted event triggered by rift-basin inversion. The 1060±5 Ma age of hematite pigmentation and magnetization in the CHC confirms that large-scale flow of oxidized fluids was initiated during basin inversion and, furthermore, that the copper mineralization in the Upper Peninsula accompanied the advanced stages of Grenvillian deformation during Rodinia construction.

Precipitation of either chalcocite or native copper were likely controlled by local redox conditions rather than by chemically and temporally distinct basinal fluids. Thus, much of the PLLS, lacking an obvious reductant, was mineralized with native copper, although chalcocite was locally important. At White Pine, relatively oxidized fluid also precipitated native copper in the White Pine fault and CHC. In contrast, chalcocite formed in the more- reduced, diagenetic pyrite- and organic carbon-rich Nonesuch shale. The mutually crosscutting relationships between native copper and chalcocite imply local evolution and/or fluctuation of redox conditions, while the bedding-parallel and -transverse, chalcocite- bearing veinlets suggest post-diagenetic chalcocite introduction at White Pine and elsewhere in the region.

The copper signature of the Upper Peninsula province was likely attained in the Paleoproterozoic, when sediment-hosted copper mineralization in the Animikie basin (Kona; Fig. 1) formed in response to 1.9-1.8 Ga Penokean basin inversion during Columbia assembly.

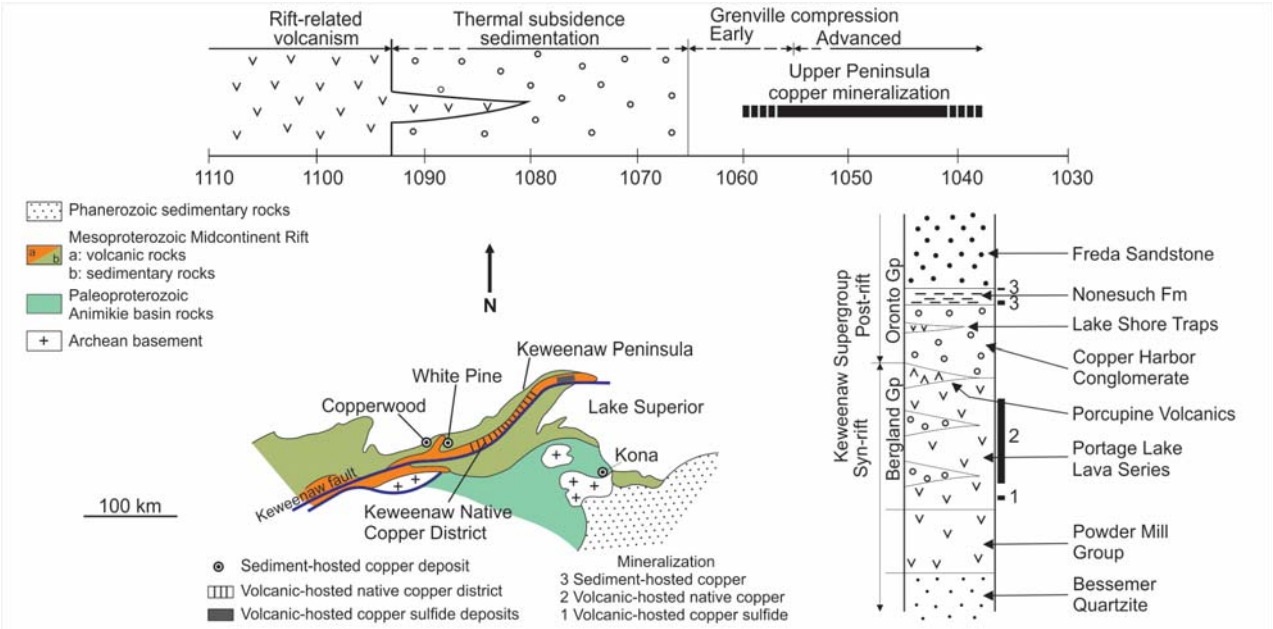

Figure 1. Upper Peninsula province, Michigan: geology and timing of copper mineralization.

A | 170

ROLE OF THERMOCHEMICAL AND BIOGENIC SULFATE REDUCTION IN THE FORMATION OF THE EL PORVENIR SEDIMENT-HOSTED STRATIFORM COPPER DEPOSIT, NEUQUÉN, ARGENTINA

Ana Laura Rainoldi[1], Marta Franchini, Adrian J. Boyce, Adolfo Giusiano, Nora Cesaretti, María Josefina Pons, Francisco Javier Ríos.

[1]*Centro Patagónico de Estudios Metalogenéticos, CONICET, Departamento de Geología, Universidad Nacional del Sur, San Juan 670, 8000 Bahía Blanca, Argentina - ana.rainold@gmail.com*

BACKGROUND

The El Porvenir deposit is one of the numerous sediment-hosted stratiform copper (SSC) occurrences and deposits of the Neuquén Basin (Argentina). It is located in the west sector of the Huincul High structure, near hydrocarbon fields, and is hosted in the Huincul Formation (Late Cenomanian-Early Turonian) of the Neuquén Group. The mineralization at El Porvenir occurs in bleached sandstone, associated with bitumen, whereas fine-grained sandstone and siltstone remain red, reflecting a strong control of porosity and permeability in both alteration and ore formation. In the last decades, several hypotheses on the formation of these SSC deposits have been proposed, however, a comprehensive genetic model for the deposits of the Neuquén Basin is currently lacking. In this contribution, we present the summary of a petrographic and geochemical study of the El Porvenir deposit and discuss the processes responsible for the copper mineralization.

METHODS

Representative samples of fresh, altered and mineralized rocks from selected profiles and drillholes were collected for laboratory analysis. Polished thin sections were examined with a polarization-fluorescence microscope for fluid inclusion petrography and identification of trapped hydrocarbons. Microthermometric analysis were performed in fluid inclusions host in analcime and calcite cements using a Linkam MDS 600 (-180°/+600 °C) fluid inclusion cooling-heating stage at the Universidad Nacional del Sur and a Linkam FTIR600 stage at the Centro de Desenvolvimento da Tecnologia Nuclear. Sulfur, carbon and oxygen isotope analyses were carried out in sulfide and calcite at the Scottish Universities Environmental Research Centre, Scotland. For sulfide, purified gases were analyzed on a VG Isotech SIRA II mass spectrometer and for carbon isotope analyses, carbon dioxide was produced from calcite by reaction with 100% phosphoric acid and analyses were performed on an AP 2003 mass spectrometer. Oxygen, carbon and sulfur data are reported relative to the V-SMOW, V- PDB and V-CDT, respectively.

RESULTS

The Huincul Formation consists of well sorted and texturally immature feldspatic litharenite that was originally red. However, at the site of mineralization, this rock is now bleached. It contains lithic fragments (with predominance of basic and mesosilicic volcanic fragments), quartz, feldspar and accessory minerals. In the red sandstone, diagenetic minerals include hematite coatings, Na-rich corrensite, microquartz envelopes and quartz overgrowths, calcite I and analcime. Analcime hosts primary, two-phase fluid inclusions with Na-Mg-Cl- H_2O fluids with salinities between 10.5 and 21.3 wt % NaCl equiv. that homogenize at an average temperature of 100 °C.

In the white sandstone, hematite coatings are absent but remained preserved below quartz overgrowths. The interlayer charge of corrensite is compensated by Ca instead of Na, calcite I and analcime are dissolved, and pyrite ($\delta^{34}S$ +10.2‰) and calcite II ($\delta^{13}C$ -12.9 to -8.3‰ and $\delta^{18}O$ +18.6 to +22.2‰) precipitated. Calcite II hosts aqueous fluid inclusions with Mg-Ca-Na-Cl-H_2O fluids with salinities between 1.6 and 5.9 wt % NaCl equiv. that homogenize at an average Th of 133 °C. Aqueous fluid inclusions coexist with hydrocarbon- bearing fluid inclusions where the liquid shows blue fluorescence under UV light and formation of clathrates indicate the presence of carbonic species.

Hypogene ore consists of chalcopyrite and bornite ($\delta^{34}S$ +12.3‰) after pyrite accompanied by coarse-grained calcite IIIa ($\delta^{34}C$ -19 to -10.1‰ and δ^{34} O +18.5 to +24.3‰). Microthermometric studies in primary fluid inclusions from calcite IIIa indicate the presence of Na-Ca-Mg-Cl-H_2O fluids with salinities between 10.1 and 21.3 wt % NaCl equiv. that homogenize at an average Th of 145 °C. Minerals from the chalcocite series ($\delta^{34}S$ -11.7 to +4.1‰) replace previous Fe-Cu sulfides and precipitated in the pore space with fine- grained calcite IIIb ($\delta^{13}C$ -31.4 to -29.9‰ and $\delta^{18}O$ of +17.7 to +20.6‰). Fluid inclusions in calcite IIIb indicate the presence of Na-Ca-Mg-Cl-H_2O fluids with

salinities between 17.5 to 19 wt % NaCl equiv. that homogenize around 90 °C; aqueous inclusions coexist with one-phase fluid inclusions filled with oil, which shows a yellow fluorescence under UV light.

CONCLUSIONS

The sedimentary rocks from the Huincul Formation were subject to several stages of fluid- rock interaction. The spatial relationships between red, bleached and mineralized sandstones together with petrographic and geochemical evidence point to three distinctive episodes: diagenesis of red bed, bleaching of red bed and ore precipitation.

The Huincul Formation was deposited in a fluvial system under oxidizing conditions, promoting the precipitation of hematite coating, which resulted in the reddening of sandstone. Arid climatic conditions likely favored the precipitation of Mg-rich smectite from alkaline water. With increasing temperature, Mg-rich pore water continued reacting with sediments transforming the smectite into corrensite with Na in interlayer position. Diagenetic quartz was deposited as microquartz envelopes or quartz overgrowths, covering the hematite coatings. Late cementing minerals like calcite I and analcime precipitated at higher temperature (~100 °C) from Mg and Na-rich saline connate fluids.

During the Tertiary Andean tectonism, reactivation of faults promoted the migration of hydrocarbons, organic acids and formation water from the deeper source or reservoir rocks up to the Huincul Formation. These fluids reacted with the sandstone and oxidizing formation water causing the dissolution of early cements, including hematite. Ferric iron was reduced and precipitated as pyrite, bleaching the host rocks, whereas hydrocarbons were oxidized. Calcite II precipitated as by-product of the redox reaction from carbon sourced by oxidized hydrocarbons and extraformational saline (Na-Ca-Mg-Cl), warm and isotopically evolved oilfield fluids ($\delta^{18}O$ of +3.5 to +8.2‰), which also promoted the exchange of Na by Ca in corrensite.

During subsequent uplift stages, incoming of metal-charged basinal brines precipitated sulfides characterized by an overall progressive and marked lowering of $\delta^{34}S$ and $\delta^{13}C$ from chalcopyrite-bornite ($\delta^{34}S$ +12.3‰) and calcite IIIa ($\delta^{13}C$ -12.9 to -8.3‰) to chalcocite- spionkopite ($\delta^{34}S$ -11.7 to +4.1‰) and calcite IIIb ($\delta^{13}C$-31.4 to -29.9‰). The temperature also decreased from the formation of chalcopyrite-bornite-calcite IIIa (145 °C) to the formation of chalcocite-spionkopite-calcite IIIb (90 °C).

Based on the isotopic and fluid inclusion data, ore precipitation was characterized by a Fe- Cu ore stage generated by thermochemical sulfate reduction and a final Cu stage dominated by biogenic reduction, using hydrocarbon as a reducing agent. The $\delta^{18}O$ (+5.6 to +11.4‰) of the fluids in equilibrium with calcite IIIa are similar to oilfield and basinal brines whereas fluids in equilibrium with calcite IIIb show a significantly lower $\delta^{18}O$ (-0.6 to +2.3‰). Lowering of $\delta^{18}O$ in calcite IIIb, could be related to the incoming of cooler, metal-charged fluids and/or due to the infiltration of meteoric water during the Tertiary Andean uplift, facilitating bacterial activity. The results show that Cu ore was deposited - and refined - during a series of events that developed in an evolving basin, involving multistage reducing fluids, Cu-sulfate-bearing brine, and meteoric water penetrating through the Cretaceous red beds in response to Andean tectonism.

A | 171

PORTABLE X-RAY FLUORESCENCE SPECTROSCOPY AS EXPLORATION TOOL AND ITS APPLICATION ON CORE SAMPLES IN THE MURRAY BROOK VOLCANOGENIC MASSIVE SULPHIDE DEPOSIT, BATHURST MINING CAMP, NEW BRUNSWICK, CANADA

Maiara Toniazzo[1], Braga David R Lentz

[1]*University of New Brunswick - maiatbraga@gmail.com*

BACKGROUND

The Portable X-ray Fluorescence spectrometry analysers (pXRF) are a beneficial tool for exploration as they are portable, simple to use, non-destructive, can rapidly and simultaneously analyze *in situ* over 30 elements at low cost (Lemière, 2018). Using this tool during the geochemical prospecting phase can be extremely useful since the samples will undergo a prior assays evaluation before being sent to the laboratory. The use of the pXRF is not intended to replace the others analytical methods carried out in laboratories, but rather to complement them by selective sampling. This real-time evaluation tool can be an essential ally in quick decision-making, can assist in identifying several types of mineralization and alteration, especially those that are not easy to be identified with the naked eye. pXRF can evaluate, for example, if a drill has crossed a mineralized zone or an area with Cu, Ni, Co, Zn, Pb or Au (Chapman *et al.*, 2010; Peter *et al.*, 2010).

The main idea of this study is to build a more robust pXRF database with analytical data obtained by the analysis of the massive sulphide (ore) and host sequence, and then the results were compared with the results obtained by other analytical methods via laboratory (average pXRF value versus laboratory geochemistry). These accurate determinations can be immensely helpful during exploration and future phases of the project (Piercey and Devine 2014).

The Murray Brook Volcanogenic Massive Sulphide (VMS) deposit occurs in the Bathurst Mining Camp (BMC) in New Brunswick (Canada) and was the first geochemical discovery in the BMC (Rennick and Burton, 1992). In 1956, a drill hole intersected 89 m of massive sulphides under cover of 16 m of gossan. By 1958, Kennco had completed sufficient drilling to allow an estimated reserve of 21.5 million tonnes of 2.81% combined Pb-Zn (Rennick, 1990). Similarly, Perusse (1957) estimated a resource of 23.6 million tonnes in 1958. The current measured and indicated mineral resource is 5.28 million tonnes with a grade of 5.24% Zn, 1.80% Pb, 0.46% Cu, 68.9 g/t Ag, and 0.65 g/t gold (PUMA-TSXV 2018). The Murray Brook Volcanogenic Massive Sulphide (VMS) deposit is hosted within sedimentary rocks of the Charlotte Brook Member, in the lower part of the Mount Brittain Formation in the California Lake Group. At the deposit scale, the sulphides are distinctly zoned in two structural lenses: an eastern copper-rich lens and a western zinc-rich lens. The sulphide ore is dominantly fine-grained, massive, laminated pyrite, with disseminated or banded sphalerite, chalcopyrite, and galena (McCutcheon, 2012). The alteration in the surrounding sedimentary rocks is variable, as well as the distribution of sulphide mineralization. The common alteration assemblages observed in representative drill core are chloritic, sericitic, silicic, carbonate, and potassic.

METHODS

The samples used in this study were selected from hole named as MB-2012-90 that was chosen because it cuts through a significant part of the hanging wall, the deposit, and the footwall. Fifty-seven samples were selected for analysis with an Olympus VANTA pXRF in the 50k benchtop configuration. Five certified reference materials, selected based on similar ore contents (CRM: OREAS-620; OREAS-622; OREAS-146; MP-1b; CZN-4) were analysed to determine correction factors (calibration), and one silica blank was used to monitor instrument contamination. The Vanta analysed the five CRMs under eight integration time settings: 60, 70, 120, 180, 240, 360, 480, and 720 seconds and the upper integration time limits (720 sec.) were chosen based on proximity to certified values and because the Low Elements (LE) are only detectable with this set up time. To increase accuracy during the pXRF analyses, the round samples were stabilised with a piece of wood. No contamination was identified from it after several tests using the silica blank.

The instrument was operated in 'Soil-Extra mode' and 'GeoChem REE(2) mode'. The 'Soil- Extra mode' sequentially utilises three different X-ray beam energies to determine a wide range of elements (see Garcelon *et al.*, 2016). For every analysis, each of the three beams was integrated over 240 seconds, for a total analysis time of 720 seconds. The 'GeoChem REE(2) mode', which best determine the concentrations of Si, Al, and Mg, utilises two different X-ray beam energies, and the total analysis time was set-up for 70 seconds. For every tenth analysis, a calibration check was performed analysing a silica blank and one of the CRMs.

The sampling and analyses were conducted in two different intervals of the hole. Localized alteration features such as quartz, carbonate, and sulfide veins were avoided during sampling. The first interval consisted of 58 analysis

on 29 samples (each one was analysed by 'Soil-Extra mode' and 'GeoChem REE 2 mode') over 63 m. Half of the analyses were on the round side and the other half on the flat side. A more concentrated approach was used for the second interval and consisted of 118 analysis on 28 samples (also analysed by 'Soil- Extra mode' and 'GeoChem REE 2 mode') in the interval of 208 m to 212 m (4m). Half of the analysis were on the round side and the other half on the flat side. The interval was chosen for its apparent mineralogical homogeneity.

The accuracy of measurements on core samples was estimated by comparing pXRF data with traditional laboratory assays. Each core sample was measured by pXRF six or 8 times, according to the sample length (4-10 cm was used between analyzes) then averaged for each sample to yield a representative pXRF composition, which can be compared with traditional assays. In general, accuracy and precision was then classified using %RD and %RSD as excellent (0 to ≤3%), very good (>3 to ≤7%), good (>7 to ≤10%), or inaccurate/imprecise (>10%) (see Jenner, 1996).

RESULTS

The element that presented the best result was Pb with a relative standard deviation (RSD) of 3.27%. The results obtained for the Cu, Zn, and Ag showed imprecise results (>10%), i.e., the most significant difference when compared to the values determined by the laboratory although still quite useful. This behaviour can be explained by the heterogeneity of the sulphide cores as those elements typically contained in sulphides disseminated in the rock, in other words, the results can be affected by the percentage of sulphide grains (coarse- grained) were analysed (Bourke and Ross, 2016).

CONCLUSIONS

The scattering effects can theoretically be reduced by performing more *in situ* measurements (close to each other) and averaging the obtained results. The pXRF shows to be an excellent geological tool, allowing real-time acquisition of geochemical data that could directly assist in several steps of an exploration program. Selecting CRMs appropriate for the material is key, with at least 5 covering the range of compositions is best. However, care must be taken to evaluate if its data presents sufficient quality for the purpose, or an incorrect interpretation of its results can occur. The most indicated approach is using this equipment associated with others analytical methods.

REFERENCES

Bourke, A., Ross, P-S., 2016. Portable X-ray fluorescence measurements on exploration drill cores: comparing performance on unprepared cores and powders for "whole-rock" analysis. Geochemistry: Exploration, Environment, Analysis 16,147-157.

Garcelon, E.A., Lentz, D.R., Walker, J.A., 2016. Portable X-ray fluorescence spectroscopy applied to volcanic rocks hosting VMS deposits of the California Lake Group, Bathurst Mining Camp, New Brunswick. New Brunswick Dept. Resource Development, Geological Surveys Branch, Geoscience Report 2016-5 (Online), 25 p.

Jenner, G.A., 1996. Trace element geochemistry of igneous rocks: geochemical nomenclature and analytical geochemistry. In Trace Element Geochemistry of Volcanic Rocks: Applications for Massive Sulphide Exploration. Edited by D.A. Wyman. Geological Association of Canada, Short Course Notes 12, pp. 51–77.

Lemière, B., 2018. A review of pXRF (field portable X-ray fluorescence) applications for applied geochemistry. Journal of Geochemical Exploration 188, 350-363.

McCutcheon, S.R., 2012. Geology of the Murray Brook – Camel Back Area (Claim 4925) - Gloucester & Restigouche Counties NTS 21O/09 .,Assessement File Report number 477318

Perusse, J., 1957. Final Report on Murray Brook Project 1956. Unpub. Kennco Explorations (Canada) Limited, Internal Report, NovaGold Resources Inc.

Peter, J.M., Chapman, J.B., Mercier-Langevin, P., LaytonMatthews, D., Thiessen, E., McClenaghan, M.B., 2010. Use of portable x-ray fluorescence spectrometry in vectoring for base metal sulfide exploration; Program and Abstracts Volume, Targeted Geoscience Initiative 3 Workshop, Vancouver, B.C., pp. 3–6.

Piercey, S.J., Devine, M.C., 2014. Analysis of powdered reference materials and known samples with a benchtop, field portable X-ray fluorescence (pXRF) spectrometer: evaluation of performance and potential applications for exploration lithogeochemistry. Geochemistry: Exploration, Environment, Analysis 14, 2, 139 – 148.

Rennick, M.P., 1990. Murray Brook sulphide deposit study, Restigouche County, New Brunswick. In Project Summaries for 1989, Fourteenth Annual Review of Activities. Edited by S.A. Abbott. New Brunswick Department of Natural Resources and Energy, Minerals and Energy, Minerals and Energy Division, Information Circular 89-2 (Second Edition), pp. 80–86.

A | 172

COMPARATIVE GEOLOGY AND GEOCHEMISTRY OF SEDIMENTARY ROCK-HOSTED GOLD DEPOSITS OF YOUJIANG BASIN, SW CHINA AND CHAUVAI ORE FIELD, SW KYRGYZSTAN

A.A Zhaanbaeva
orogeny.geo@mail.ru

The Youjiang basin is the southwestern margin of giant Yangtze Craton and is located between Yunnan-Guizhou-Guanxi provinces, South China. It bounded by the deep-seated Mile-Shizong, Shuicheng-Ziyun-Bama and Red River regional faults which are major tectonic features of the basin (Cai and Zhang, 2009; Yang *et al.*, 2012). The basin is an important region of South China low-temperature metallogenic domain and includes Au-As- Sb-Tl-Hg hydrothermal deposits. These multi-type deposits characterized by the low temperature (typically below 200-250°C), shallow depth and commonly hosted by sedimentary rocks from Cambrian to Triassic age (Hu *et al.*, 2002; 2017).

Gold deposits of Youjiang basin quoted as the classic examples of world-class «Carlin-type Au deposits». With more than 200 gold deposits and occurrences and 800 t of gold reserves (Hu *et al.*, 2017), the Youjiang basin becomes the second largest Carlin-type gold mineralized area after Nevada and play important role in in the world's gold production. The Carlin-type gold deposits of the basin characterized by micro-disseminated gold in arsenian pyrite rims, enriched with the Au-As-Tl-Hg-Sb elements association, hosted by carbonaceous and calcareous sedimentary rocks and have typical alteration assemblages as: silicification, decalcification, argillization.

A lot of successful works were done focused on understanding the origin of the deposits of Youjiang basin,that used as an exploration model and applied to Chauvai Au-As-Sb-Hg ore field of SW Kyrgyzstan, which have many characteristics of Carlin-type deposits.

Historically the Chauvai ore field («COF» further) was identified and mined for the mercury and antimony only. The potential for «Carlin-like» deposits in the ore field had been suggested by Rogalskiy *et al.* 1988, Yakubchuk *et al.* 2002, Seltmann *et al.* 2004 and Kirwin *et al.* 2017, further a new deposit style for the area and the potential for a new gold district was identified. The COF is represented by a series of similar sites which are hosted by carbonaceous sedimentary rocks. Rocks in the limestone and shale contact zone was subjected to selective silicification for more than 20 km. Those silicified zones are the most favorable area for ore localization.

Valuable data gleaned from geochemical and isotopic studies of arsenian pyrite and stibnite, that used as a potentially important tool to understand ore genesis and ore source processes. In this regard, here we report the element concentration, S and Pb isotopic compositions of selected deposits of Youjiang basin and COF.

SEM and EPMA analyzing methods document the mineral assemblages, textures, element composition of arsenian pyrite from the COF and show similarities with the Carlin-type gold deposits of Youjiang basin. The results of inductively coupled plasma mass spectrometry (ICP-MS) was used to detect element concentration in stibnite and demonstrated wide range of values with considerable intersystem variability between two areas. Nano-SIMS was used to determine element distribution and sulfur isotopic composition of arsenian pyrite from two sites of COF, where elevated gold concentrations correlate mainly with elevated concentrations of As and sulfur isotopic composition of the samples present in a high variable values that range from +4 to +21‰, with the lower sulfur values in the As-rich rim than in core. According to Shaun *et al.*, 2009, samples from the Carlin Trend, and Getchell Trend, located in northern Nevada, show similar results with the lower sulfur values in the rim and higher in the core of gold bearing pyrites. Sulfur values of stibnite also show broad variabilities ranging from -14 to +20 ‰. The Pb isotopic compositions were obtained from stibnite samples, analyzed by MC-ICP-MS, which represents narrow range of 206Pb/204Pb, 207Pb/204Pb and 208Pb/204Pb values and suggest the upper crustal source of lead for both areas.

Based on this data, geological features, and results of a large number of previous works we suggest that Chauvai ore field, that located in the SW part of Kyrgyzstan include important «Carlin-like» deposits on its territory, and have quite similar geological and geochemical characteristics with the well-known Carlin-type gold deposits of Youjiang basin, SW China.

VANADIUM MINERALIZATION AT LOS CHIHUIDOS SEDIMENT-HOSTED STRATIFORM CU DEPOSIT

Ana Laura Rainoldi[1], Daniel Beaufort, Patricia Patrier, Adolfo Giusiano, María Josefina Pons, Nora Cesaretti.

[1]Centro Patagónico de Estudios Metalogenéticos, CONICET, Departamento de Geología, Universidad Nacional del Sur, San Juan 670, 8000 Bahía Blanca, Argentina - ana.rainold@gmail.com

BACKGROUND

Sediment-hosted stratiform copper (SSC) deposits represent the main metalliferous resource of the Neuquén Basin (Argentina). These deposits are spatially linked to oil and gas reservoirs and contain minor amounts of V, U and Ag. Los Chihuidos deposit outstands because contains major amounts of vanadium compared with the other SSC deposits of the basin. The Los Chihuidos deposit (37°50'30"S; 69°27'W) is located in the central part of the Neuquén Basin, near the Sierra Chata gas reservoir, and it is hosted in the Huincul Formation (Late Cenomanian-Early Turonian) of the Neuquén Group. The Neuquén Group represents a red bed sequence, but at the site of mineralization, the rocks are bleached. Bleaching resulted in colorful outcrops variations with the original red sandstone interbedded with white sandstone, whereas gray and brown sandstones are subordinated to the contact between the formers. The highest anomalies of V are always located below zones with high Cu grades, but at regional-scale, V is always present at the contact between the red and the overlying bleached sandstone, where gray sandstones occur. Uranium anomalies are more erratic, always associated with vanadium anomalies and characterized by the presence of U-V supergene minerals (i.e. carnotite group). The main differences between the sandstones with different colors are due to variations in the porosity and in the mineralogy of the authigenic minerals. This contribution presents the first mineralogical study of the vanadium-rich zones at Los Chihuidos, and discusses plausible sources of vanadium and the mechanisms for the metal precipitation, which has important implications for understanding the formation of vanadium mineralization in the SSC deposits of the Neuquén Basin.

METHODS

Representative samples of diagenetic facies from selected profiles were collected for laboratory analysis. Samples were analyzed first with a binocular polarizing microscope under transmitted and reflected light. Clay minerals were identified using a Bruker D8 Advance diffractometer. Representative samples were selected for SEM observations; paragenesis and chemical composition of mineral assemblage were studied with a JEOL® 5600 electron microscope equipped with a Bruker energy dispersive X-ray spectroscopy detector (EDS).

RESULTS

Red sandstone of the Huincul Formation consists of feldspathic litharenite cemented by hematite coatings, pore-filling kaolinite, quartz and albite overgrowths, calcite I and minor barite and anhydrite. The red color of the sandstone is due to hematite coatings.

White sandstone is characterized by a notorious porosity enhancement and abundant bitumen impregnations. Hematite coatings are lacking, only present below quartz and albite overgrowths. Previous kaolinite, calcite I, barite and anhydrite are locally to pervasively dissolved and new authigenic minerals include pyrite, calcite II and minor V-Cu-rich montmorillonite. Copper mineralization occurs in white sandstone in contact with bitumen impregnations and consists of chalcocite-djurleite with traces of very fine-grained pyrite replaced by supergene chrysocolla > malachite > covellite > brochantite > cuprite.

Gray sandstone contains abundant bitumen impregnations, authigenic V±Cu-bearing clay minerals (montmorillonite, interstratified illite-smectite and subordinated chlorite-corrensite mixed-layers) and V-bearing hematite. Hematite can be also found in detrital martitized titanomagnetite, where Ti concentrations occur in magnetite and V in hematite. When Cu±V-rich chlorite-corrensite mixed-layers predominate over montmorillonite, the sandstone turns to brown color, defining the brown sandstone. Rarely, a secondary mineral enriched in Mn has been identified replacing chlorite-corrensite mixed-layers. Supergene volborthite and Cu-V-U minerals with high amount of V-rich clays are located at the contact between the gray and white sandstones, where copper mineralization occurs. Vanadium-rich montmorillonite, interstratified illite-smectite and hematite in the gray sandstone represent more oxidizing conditions, whereas Cu-rich chlorite-corrensite mixed-layers indicate chloritization of montmorillonite under more reducing conditions. Vanadium could have been carried by hydrocarbons and incorporated in clay and oxide minerals. The occurrence of vanadium has been observed previously in the Neuquén Basin in whole rock analysis from the Vaca Muerta Formation (Spaletti *et al.*, 2014) but also worldwide in oil fields

and hydrocarbon source rocks (Breit and Wanti, 1991; Parnell and Carey, 1995). The analyses of bitumen infill of veins (asphaltites) from the La Escondida deposit located 60 km east of Los Chihuidos, yielded up to 0.2 wt.% vanadium (Parnell and Carey, 1995).

CONCLUSION

Reddening of the sandstone took place during early-diagenesis when infiltration of meteoric water promoted hematite coating precipitation. With burial increases, kaolinite, quartz and albite overgrowths and calcite I precipitated. During the Andean tectonism, upflow of hydrocarbon-bearing fluids up to the red beds of the Huincul Formation promoted the development of a redox system where most cements including hematite were dissolved, iron was reduced and precipitated as pyrite, promoting the discoloration of the previous red sandstone. Hydrocarbons were oxidized and calcite II precipitated as by-product of the redox reaction. Vanadium-rich montmorillonite precipitated with pyrite and calcite II.

Hydrocarbon-bearing solutions reached intermediate redox conditions at the contact zone with the white (reduced) and red (oxidized) sandstones. In this zone, abundant V-Cu-rich clay minerals (montmorillonite, illite-smectite and chlorite-corrensite) with V-bearing hematite and a Mn-rich mineral precipitated, defining the redox front. This mechanism could favored the destabilization of the soluble complexes generated during bleaching of the sandstone, precipitating the highest concentrations of V-rich montmorillonite, interstratified illite-smectite and interstratified chlorite-corrensite along the redox front, where the oxidizing-reducing conditions promote precipitation of such metallic elements whose speciation is very sensible to Eh conditions.

A new stage of fluids migration resulted in copper mineralization in the white sandstone in contact with hydrocarbons. Minor copper was also incorporated in the gray and brown sandstones minerals like montmorillonite, illite/smectite and chlorite-corrensite mixed- layers. During the Andean uplift, infiltration of meteoric water promoted supergene alteration with precipitation of volborthite as oxidizing product of the vanadium ore at the redox front and, covellite, cuprite, brochantite, malachite/azurite and chrysocolla in the reduced white sandstone.

REFERENCES

Breit, G.N., Wanty, R.B., 1991. Vanadium accumulation in carbonaceous rocks: a review of geochemical controls during deposition and diagenesis. Chemical Geology, 91, 83–97.

Parnell, J., Carey, P.F., 1995. Emplacement of bitumen (asphaltite) veins in the Neuquén Basin, Argentina. American Association of Petroleum Geologists, 79, 1798–1816.

Spalletti, L.A., Schwarz, E., Veiga, G.D., 2014. Geoquímica inorgánica como indicador de procedencia y ambiente sedimentario en sucesiones de lutitas negras: los depósitos
transgresivos titonianos (Formación Vaca Muerta) de la Cuenca Neuquina, Argentina. Andean Geology, 41, 401–435.

PLENARY LECTURES

METALLOGENIC POTENTIAL OF ARGENTINA

Eduardo O. Zappettini

Servicio Geológico Minero Argentino - Eduardo.zappettini@segemar.gov.ar

The geotectonic evolution of Argentina provides an appropriate frame of reference to understand the processes that are responsible for the location of the known mineralization. They are, as well, an adequate foundation to establish metallogenic belts, outlining permissive areas for the localization of mineralization with a typology closely related to the involved processes.

The Argentine territory consists of a cratonic nucleus (the Río de la Plata Craton) to the east of the country, mostly covered by Phanerozoic sediments, an Upper Precambrian-Lower Cambrian belt (Pampia), in the central part of Argentina, consisting of metamorphic rocks affected by mostly Paleozoic intrusions, and the Andean Orogen, developed to the West. The basement of this Orogen as well as the southern part of the country consists of a mosaic of parauthoctonous and allochtonous terranes, including Patagonia, Cuyania, Chilenia and Antofalla main blocks. These main geotectonic features are at the origin of the metallogenic characteristics of Argentina.

The Rio de la Plata Craton, with main outcrops in Uruguay and Paraguay, is exposed in Argentina in the Buenos Aires province. The Paleo- to Neo-Proterozic basement has been the site of important historic exploitations of industrial minerals and dimensional stones. Neo-Proterozoic sequences carry Rapitan-type BIF deposits.

The Lower Paleozoic basement in the Northwest involves polymetallic sedex deposits (Aguilar, La Colorada) and saddle reef Au-Sb veins that are part of a belt of continental extension. Paleozoic foreland basin deposits in the North and platform deposits in northern Patagonia involve Clinton-type Fe deposits (Zapla and Sierra Grande, respectively).

The old mining activity in Argentina, mainly developed during the first half of the XX century, involves numerous W-Sn vein and greisen deposits mostly related to Upper Carboniferous anorogenic granites and Be-Li-Nb Paleozoic pegmatites emplaced in the Pampean Orogen. This area has not been the target of further detailed exploration and it deserves a re-evaluation.

The Upper Paleozoic Gondwanan Orogen involves arc-related porphyry type mineralization (San Jorge, la Voluntad), as well as polymetallic veins (Pb-Ag-Zn) (Castaño Viejo, Paramillos de Uspallata) and F veins (San Rafael district), related to the Orogen collapse during the Triassic.

During the Mesozoic, a generalized extension occured to the east of the Andean Orogen mainly developed in the Chilean territory. In Patagonia, a terrane of controversial origin that collided with Gondwana during the upper Paleozoic, an extensional mostly acid volcanism developed during the Jurassic, related to the opening of the Atlantic Ocean. Main metallogenic models related to this environment are low to high sulfidation Au-Ag epithermal deposits (Cerro Vanguardia, San José, Cerro Negro, Cerro Moro, El Pingüino) and epithermal Pb-Ag polymetallic deposits (Navidad). Identified resources reach 19 Moz Au and 1150 Moz Ag.

The Mesozoic extension was also at the origin of five-element veins (La Niquelina, Esperanza, Rumicruz), REE deposits related to alkaline magmatism involving locally carbonatites (Rangel district, Rodeo de los Molles), and stratabound Cu-U-V deposits located in an intraractonic rift-related sedimentatry sequence (Juramento, Martín Bronce).

During the Jurassic-Lower Cretaceous, arc-back-arc magmatism developed in southern- central Andes with associated manto-type Cu deposits (San José-Las Cuevas and El Burrero districts) and in Tierra del Fuego province where polymetallic syntectonic epithermal veins are located in shear zones (Sargent, Arroyo Rojo).

In the Neuquén basin, the Mesozoic back-arc sedimentary sequence contains one of the richest KCl concentrations in the world, reaching 2.5 Bt (Río Colorado), as well as stratabound Cu and Cu-U deposits (Tordillos, Porvenir, Sauzal Bonito, etc.) and Ba-Sr beds and veins.

The Andean Orogen contains some of the richest metallogenic belts in the world related to the Cenozoic magmatic arc. In the Northwest, it includes some world-class clusters of porphyry Cu and porphyry Cu-Au deposits, such as Taca Taca and Lindero and, in a back arc position, Bajo de la Alumbrera and Agua Rica. Epithermal polymetallic deposits related to calderas and domes, are part of the southern extension of the Bolivian Tin Belt (Pirquitas and Chinchillas). In this region identified resources reach 46 Moz Au, 875 Moz Ag and 58 Blbs Cu.

The south-central Andean region include: high-sulfidation Au-Ag deposits (Pascua-Lama, Veladero), at least four porphyry Cu clusters (Los Helados-Josemaria; Pachón-Altar-Los Azules; Famatina in a back arc position; and the southern continuation of the El Teniente belt). This region has identified resources of 78 Moz Au, 1550 Moz Ag and 122 Blbs Cu.

Cenozoic sedimentary basins in the Puna region are rich in industrial minerals. They involve one of the most important concentrations of Li in salt lakes in the world (Salar del Hombre Muerto, Rincón, Olaroz, Cauchari) with measured resources reaching 51 Mt $LiCO_3$ and 134 Mt K as a by-product. Argentina also hosts the fifth world largest borate province with 127 Mt B2O5 resources included in salt lakes as well as layers related to a Tertiary continental volcano-sedimentary sequence. Both Li and B are genetically related to the volcanic activity that surrounds the salt lakes (lixiviation from volcanic glass and geothermal springs).

Quantitative assessment of undiscovered porphyry copper deposits of the Andes and similar evaluations for other deposit models, allowed to define a geologic potential for the Argentine territory of up to 500 Mt of Cu, 6 Mt Mo, 10,000 t Au, 300,000 t Ag, 10 Mt Zn, 10 Mt Pb, 100 Mt $LiCO_3$ and 250 Mt $B2O_5$.

The comparison of mineral resources of Argentina in terms of economic weight by commodity, deposit models and deposit ages, allow highlighting interesting features of the metallogenic potential of Argentina. Almost 50% of resources are present in porphyry type deposits and 40% in sediment-hosted deposits. Copper represents a 40% of the total economic resources value, KCl a 20%, $LiCO_3$ a 16% and Au 11%. Finally, 50% of the considered resources constitute mineral deposits of Neogene age, 20% of Mesozoic age and 20% of Quaternary age.

Finally, it should be noted that the analysis of the evolution of total mineral resources in Argentina shows that they are related to an initial epoch of regional exploration programs carried out by the Argentine Government. This activity led to the identification of porphyry copper deposits (Bajo de la Alumbrera, Paramillos, etc.), epithermal deposits and prospective districts (Cerro Vanguardia, Macizo del Deseado, Valle del Cura) and Li-rich brines in salt lakes (Salar del Hombre Muerto). This stage was succeded by successful exploration programs developed by mining companies since the 90' thanks to a favorable legal framework that promotes the mining investment as well as the opening of more than 20 mines.

SINGULARITY OF LITHOSPHERE PHASE TRANSITION AND ORIGINATION OF PORPHYRY MINERALIZATION

Qiuming Cheng

State Key lab of Geological Processes and Mineral Resources, China University of Geosciences - qiuming.cheng@iugs.org

Porphyry mineral deposits are associated with igneous activities which are either originated from lower crust or upper mantle or from mantle with contributions of crust during evolution of continental crust especially in association with convergent and divergent plates. These igneous activities are often formed episodically depicting intermittency with anomalous high magmatic addition rate (MAR) and pulses of high-volume magmatic flare- ups caused by plate subduction or collision. The mechanical behavior of the Moho as a transition zone with discontinuity of lithosphere separating the crust and the mantle is not only characterized by remarkable change of seismic wave velocity and lithosphere density but also closely associated with the formation and distribution of earthquakes, origination of magmatism as well as other extreme events. Phase transition may occur at the boundary of deeply subducted slabs. Due to subduction of oceanic lithosphere underneath the continental lithosphere, solid phase lithosphere can be partially melted to facilitate formation of magma. During the progress of subduction, water and other volatile components contained in the rocks are progressively released from the slab at different depths. Fluids or melts released at greater depths will be in supercritical fluid phase which hydrates the mantle and causes partial mantle melting. This eventually leads to deeply rooted magma which provides the source for porphyry mineralization. Partial melting in lower crust and mantle also causes strain rate change of the lithosphere which facilitates formation of intermediate and deep earthquakes. Due to the great depth of subduction the fluid released may be in supercritical condition with fractal density with strong solvent strength facilitating the hydration and metasomatism of mantle rocks. When the pressure and temperature are reduced to around the critical point, the system goes through a great reduction of gradient of density, accordingly increasing the specific volume which further enlarges porous space and fractures rocks thus in turn facilitating the formation of magma, mineralization and earthquakes through positive feedback processes. Porphyry mineralization associated igneous activities in Circum Pacific subduction belt and in Tethys collisional belt were investigated and compared in this paper with focuses on influence of phase transition on porphyry mineralization systems.

A | 176

NATIONAL STRATEGIC ACTION PLAN OF MINERAL EXPLORATION - APPLICATION OF METALLOGENIC THEORY AND EXPLORATION TECHNOLOGY IN CHINA

Li Jinfa

Vice President of China Geological Survey and Executive Vice President of Chinese Academy of Geological Sciences, 45 Fuwai Street, Xicheng District, Beijing, P. R. China

The Chinese government launched a 10-year Strategic Action Plan of Mineral Exploration in 2011, which has provided sufficient resource supply and industrial support for the smooth and fast development of the economy. The objectives of this Action Plan include:

1) To guide exploration work into wider areas and more minerals types by devoting more efforts into basic geological studies and technological innovation, and thus strengthening the capabilities of deep-earth, deep-sea exploration and airborne geophysical exploration;
2) To enhance basic geological survey and provide basic information for mineral exploration, and
3) To carry out nationwide resource potential assessment and metallogenic prediction for improvement of mineral exploration efficiency.

The Action Plan has proved fruitful over the past 7 years since its launching. Most minerals have reached or exceeded their goals, with exceptions of only a few minerals such as coal- bed methane and tin. In the cases of gold, lead, zinc, nickel, tungsten and molybdenum, their 10-year prospecting targets have been completed in advance.

In this presentation, a systematic summary is made in terms of typical ore deposit theories and exploration technology, application cases during its implementation, including the metallogenic system theory, the metallogenic series theory, the "Three in One" exploration target prediction theory, and the wide-field electromagnetic method (WFEM).

Eight theories and technology application cases have been studied by means of theoretical analysis, field application and engineering verification, including the three theories regarding natural gas hydrate, multi-island-arc-basin continental hyperplasia theory (mineralization of Qinghai-Tibet Plateau), subvolcanic type of Three in One prediction theory (Zhijiadi silver-lead-zinc mine). The experiences from the Strategic Action Plan was summed up. It should be highlighted that the support of the Government, the establishment of a Mineral Exploration Technical Guidance Center of the Ministry of Natural Resources, and the innovative prospecting mechanism are crucial for ensuring rapid and substantial progress.

On this basis, the report proposes future plans for the Strategic Action Plan of Mineral Exploration on six aspects, including Continuous Promotion of the Strategic Action Plan, Innovative Metallogenic Theory and Exploration Technologies, Strengthening Deep Mineral Exploration, Promoting Green Exploration, Focusing on Comprehensive Investigation and Assessment.

MINERAL EXPLORATION MODELS FROM SIMPLE FICTION TO COMPLEX REALITY

Reimar Seltmann

Natural History Museum, Centre for Russian and Central Eurasian Mineral Studies, London - r.seltmann@nhm.ac.uk

Refining mineral exploration models and how to get them "from fiction to reality" may significantly increase the resource, leading to discovery of new ore bodies and deposits and reduce exploration costs. This presentation will feature examples from several case studies:

VHMS DEPOSITS AND OROGENIC GOLD MINERALIZATION

Some of the profitable gold mined in the Devonian Cu-Zn-Pb (Ag-Au) deposits of the Rudny Altai (Eastern Kazakhstan / Russia border region) is supposedly related to overprinting mineralization of orogenic style of Permian age, related to monzonitic dikes and intersecting shear zones. Rather than following the massive sulphide seams, tracking the gold credit requires a paradigm shift towards understanding the kinematic controls of emplacement of late- to post-collisional dikes, stocks and crosscutting structures.

CONTINUUM MODEL FOR RARE METAL DEPOSITS

Aspects of case studies from Zinnwald / Cinovec and Eibenstock, Gottesberg and Podlesi in the Erzgebirge / Krusne hory (Germany / Czech Republic border region) and from Mount Pleasant (New Brunswick, Canada) are discussed. Whereas timing of fluid-buffered greisen formation is structurally controlled by ductile / brittle transition and brittle failure (sudden decompression, focused fluid flow), the earlier melt-buffered ore-bearing system may enrich dispersed ore elements (HFSE such as Nb, Ta,..) to economic levels in the evolved host granite – historically often neglected and only realised by smelter credits.

Other mineral systems show in space and time the development of several interconnected deposit types where a single exploration model would not lead to success: the Mount Pleasant deposits combine features of Sn-W-base metal sulfide mineralization of porphyry breccia type, followed by greisen stockwork and rare metal granite intrusions at depth.

The (plutonic) 325 Ma Eibenstock tin granite in Western Erzgebirge (Germany) got assigned a historic 300 kt tin potential. This is reflected by the vast Sn resource related to the mineralised aureole of skarn and schist ores enveloping the Eibenstock granite massif (Breitenbrunn - Pöhla-Globenstein – Hδmmerlein – Tellerhδuser – Zlate kopec). Latest geochronological data establish strong context of coeval intrusion and mineralization ages. But there is ongoing ambiguity that in parts the Eibenstock granite massif may represent largely also just a Sn host where a substantial portion of the tin mineralization is related to rapid uplift of the crustal block, its fracturing to tap residual fluid-melt sources at depth and fluid-channelling connected with 310-315 Ma porphyry stocks & pipes (Bolivian style) intruding into the Eibenstock granite massif, but remaining hidden at subvolcanic depth. If that scenario can be proven, a revised exploration model is required and paradigm change means that a previously 300m productive extension of tin potential related to the immediate exo-/endocontact of the evolved plutonic granites is now open at depth with a vertical extension of up to 4000m if considering the concealed subvolcanic bodies!

MAIN COMMODITY VERSUS BY-PRODUCT CREDIT

Speculative descriptive genetic models historically assigned one of the largest undeveloped tin deposits in the world to "metamorphogenic remobilisation of stratabound / stratiform Riphean massif sulphides". Field surveys and assessment of documentation, however, revealed that there is a controlling shear zone that exhibits an alteration halo of granitophile elements (topaz, Rb, Cs, Be, W, Nb, Ta) and at depth a transition into a greisen stockwork in the surrounding of a tin granite. A verification attempt of drill core logs referring vaguely to "metasomatites" turned out to contain relic features and shadow textures of intersecting tin porphyries (that were reportedly drilled at depth). Assays and resource calculations of the latest exploration campaign focused on a very limited number of main elements but ignored a by-product potential doubling the expected ROI of the deposit.

A | 178

COPPER DEPOSITS IN BRAZIL: GEOLOGICAL SETTING, PROCESSES AND EVOLUTION OF MINERAL SYSTEMS

Lena Virgínia Soares Monteiro[1], Caetano Juliani, Carlos Marcello Dias Fernandes, University of São Paulo
[1]*lena.monteiro@usp.br*

The copper metallogeny in Brazil is mainly related to evolution of Precambrian terrains. Brazilian copper production (1.5% of world production) is concentrated in few mines (e.g., Sossego and Salobo, in Carajás – IOCG; Chapada, in Goiás – porphyry copper; and Caraíba, Niquelândia, Fortaleza de Minas and Americano do Brasil – magmatic sulfide deposits). However, the development of metallogetic potential related to magmatic-hydrothermal copper–gold systems and VHMS in older terrains, and their recognition after a complex tectonic-metamorphic evolution, represent a current challenge in Brazil.

MAGMATIC COPPER DEPOSITS

Among the magmatic deposits, the Caraíba Mine, located in the Curaçá River Valley district, stands out. It is inserted in the Itabuna–Salvador–Curaçá Orogen, a Paleoproterozoic orogenic belt located at the eastern border of the São Francisco Craton.

The main copper orebodies in the Caraíba mine (Pilar: 24.64; Mt 1.8 % Cu; Surubim: 8.72Mt; 0.88% Cu; Vermelhos: 51.41 Mt: 0.91 % Cu) are hosted by pyroxenites, norites and glimmerites associated with mafic-ultramafic intrusions. These intrusions underwent granulite and amphibolite facies metamorphism, migmatization, and intrusion of granitic and syenitic rocks.

Intercumulus sulfides (chalcopyrite–bornite–covelite–cubanite–digenite–pyrrhotite– pentlandite) are product of the ca. 2.6 Ga orthomagmatic copper mineralization. This was overprinted by structurally-controlled epigenetic mineralization represented by chalcopyrite–bornite–magnetite veins and breccias. Incipient sodic (albite–andesine), intense potassic (microcline–phlogopite), chlorite, and hydrolytic (sericite–hematite–barite) alteration is also recognized. According to Garcia *et al.* (2018), the evolution of the Curaçá River Valley deposits points to: (i) primary magmatic mineralization; (ii) construction of the Itabuna-Salvador-Curaçá orogen, with high-grade metamorphism and associated granitogenesis (ca. 2.08 Ga); (iii) hydrothermal mineralization during orogenic collapse (ca.2.04 Ga); and (iv) orogenic uplift and late metasomatism.

THE ARCHEAN–PALEOPROTEROZOIC CARAJÁS COPPER SYSTEM

The Carajás Province, located in the Amazonian Craton, contains world-class iron oxide–copper–gold deposits (IOCG with resources > 2 billion tons at 0.77–1.4 wt. % Cu; 0.28 – 0.86 g/t Au). Clusters of IOCG deposits occur within regional E–W shear zones. These deposits are mainly hosted by Mesoarchean (ca. 3.07–2.96 Ga TTG orthogneisses, ca. 2.97 Ga greenstone belts, and ca. 2.87–2.84 Ga granites) and Neoarchean units (e.g., 2.76–2.74 Ga metavolcanosedimentary sequences, gabbros, charnockites and post-colisional A2-type granites).

The older IOCG-forming event (ca. 2.70-2.68 Ga) at Carajás was identified in the Southern Copper Belt, in the Sequeirinho orebody (Sossego Mine) nd Cristalino deposit. These deposits are characterized by regional sodic (albite) and sodic-calcic (albite–actinolite) alteration and associated massive magnetite–apatite bodies. In the Castanha and Jatobá deposits, an early stage of structure-controlled nickel mineralization (Ni-pyrrhotite–Ni- pyrite–Co-chalcopyrite–Co-pentlandite) precedes the bulk of copper (chalcopyrite) mineralization. The isotopic and chemical (Cu–Au–Fe–LREE–Ni–Co–Pd) ore signatures reveal deep-seated magmatic components and inheritance of the ultramafic and mafic rocks through fluid-rock interaction.

In the Northern Copper Belt, the ca. 2.76–2.74 Ga metavolcanosedimentary sequences underwent intense deformation along shear zones and were intercepted by ca. 2.74 Ga and ca. 2.57 F-rich peralkaline granites (e.g., Old Salobo granite). Older VHMS copper-zinc mineralization (e.g., Pojuca) is associated with anthophyllite–cordierite schist, which was interpreted as the metamorphic product of chlorite alteration zones. A protracted tectono-thermal event (ca. 2.58–2.45 Ga) has been related to IOCG mineralization (magnetite–bornite–chalcocite–chalcopyrite) accompanied by high-temperature hydrothermal alteration (e.g., Salobo, Alemão) with grunerite–almandine–biotite.

Paleoproterozoic copper deposits (ca. 1.90–1.88 Ga; e.g., 118 deposit) at Carajás were broadly coeval with widespread ca. 1.88 Ga A2 -type granites. The ore signature (U–Nb–Sn–Y–Be–HREE–F) and higher d^{34}Scpy values (up >7.5‰) are consistent with IOCG formation after the Great Oxygenation Event.

PALEOPROTEROZOIC PORPHYRY Cu–Mo–(Au) DEPOSITS

In the Amazonian craton, very well-preserved magmatic-hydrothermal systems are associated with extensive Paleoproterozoic volcano-plutonic events in immature (greenfield) areas. In the Tapajós Province, volcanic rocks, porphyries and granites were formed in multiple magmatic events. Cu–Mo ± Au porphyry-type and high- and intermediate-sulfidation epithermal Au and base metal mineralization is associated with ca. 2.0–1.95 Ga and 1.89–1.87 Ga high-K I-type calc-alkaline sub-volcanic and volcanic rocks, formed in continental magmatic arcs. Hydrothermal alteration zones are mainly characterized by K- feldspar–biotite, sericite and propylitic assemblages. High temperature (> 450 °C) and salinity (up to 69 wt% eq. NaCl) fluids associated with potassic alteration are similar to those of magmatic fluids.

In the Alta Floresta Gold Province, magmatic-hydrothermal Au ± Cu and Au+ base metal deposits are hosted by ca. 1.98 Ga, 1.90 Ga, and 1.87 calc-alkaline I-type granitic intrusions (Ga) and ca. 1.77 Ga quartz-feldspar porphyries. The latter were coeval to the post- collisional Juruena arc felsic magmatism and mineralization (e.g., Colíder and Teles Pires suites; Assis *et al.*, 2017).

NEOPROTEROZOIC Cu-Au PORPHYRY DEPOSITS

The Chapada Cu–Au–(Zn–Mo–Pb) deposit (479.84 Mt; 0.25 g/t Au and 0.29 % Cu) is associated with ca. 867±884 Ma porphyritic metadiorites of the Neoproterozoic Mara Rosa Magmatic Arc and associated metavolcanosedimentary units. Host and mineralized rocks underwent amphibolite (ca. 760±730 Ma) and greenschist (610±600 Ma) facies metamorphism during the Brasiliano collisional event. Quartz–feldspar–biotite, epidote–amphibolite, and kyanite (kyanite–rutile–corundum–lazulite–anhydrite–roscoelite–tourmaline–gold) schists were interpreted as the metamorphic products of hydrothermal potassic, propylitic and argillic alteration in a porphyry copper system (Oliveira *et al.*, 2016).

NEOPROTEROZOIC TO EARLY PALEOZOIC COPPER DEPOSITS

In the Camaquã copper mine, chalcopyrite–bornite–chalcocite–covellite–pyrite occur as disseminated sulfides, replacement zones, fracture filling, and veins in sandstones and conglomerates of the Neoproterozoic to Early Paleozoic Camaquã basin. Hydrothermal alteration encompasses chlorite, carbonate, barite and illite–kaolinite formation. Low temperature epithermal deposits have been associated with a distal magmatic-hydrothermal system related to the post-collisional volcanism (Bongiolo *et al.*, 2011).

The Pedra Verde Copper Mine, in the Borborema Province, is hosted by carbonaceous phyllite of the Neoproterozoic Martinópole Group. The Pedra Verde deposit has upwards ore zoning with marcasite/pyrite, native silver, chalcopyrite, bornite, chalcocite, native copper and hematite, close to contact with oxidized conglomerates. Dextral transcurrent shear zone (ca. 590±570 Ma) exercised important structural control. The Pedra Verde Copper Mine represents an epigenetic syn-orogenic deposit likely formed late during the Gondwana amalgamation (Matos *et al.*, 2017).

PHANEROZOIC COPPER OCCURENCES

In the Paraná Basin, a Devonian to Cretaceous intracratonic sedimentary basin that covers the entire central-eastern portion of South America, copper–(gold–silver) occurrences are associated with hydrothermal breccias in basalts of the Cretaceous Serra Geral Formation. These have been considered linked to epigenetic hydrothermal systems related to the Guaraní aquifer, representing new prospective frontiers (Arena *et al.*, 2014).

REFERENCES

Arena, K.R.; Hartmann, L.A.; Baggio, S.B., 2014. Geological controls of copper, gold and silver in the Serra Geral Group, Realeza region, Paraná, Brazil. Ore Geology Reviews, 63: 178–200.

Assis, R.R., Xavier, R.P., Creaser, R. 2017. Linking the Timing of Disseminated Granite-Hosted Gold-Rich Deposits to Paleoproterozoic Felsic Magmatism at Alta Floresta Gold Province, Amazon Craton, Brazil: Insights from Pyrite and Molybdenite Re-Os Geochronology. Economic Geology, 112: 1937–1957.

Bongiolo, M. E., Renac, C., Sampaio Mexia, A., Boscato Gomes, M. E., Ronchi, L.H., Patrier-Mas, P., 2011. Evidence of Ediacaran glaciation in southernmost Brazil through magmatic to meteoric fluid circulation in the porphyry–epithermal Au–Cu deposits of Lavras do Sul. Precambrian Research, 189: 404–419.

Garcia, P.M.P., Teixeira, J.B.G., Misi, A., Sá, J.H.S., Silva, M.G. 2018. Tectonic and metallogenic evolution of the Curaçá Valley Copper Province, Bahia, Brazil: A review based on new SHRIMP zircon U-Pb dating and sulfur isotope geochemistry. Ore Geology Reviews, 93: 361–381.

Matos, J.H.S.N., Santos, T.J.S., Monteiro, L.V.S. 2017. The carbonaceous phyllite rock-hosted Pedra Verde copper mine, Borborema Province, Brazil: Stable isotope constraints, structural controls and metallogenic evolution. Journal of South American Earth Sciences, 80: 422–443.

Oliveira, C.G., Oliveira, F.B., Della Giustina, M.E.S., Marques, G.C., Dantas, E.L., Pimentel, M.M., Buhn, B.M. 2016. The Chapada Cu–Au deposit, Mara Rosa magmatic arc, Central Brazil: Constraints on the metallogenesis of a Neoproterozoic large porphyry-type deposit Ore Geology Reviews, 72:1–21.

CHARACTERISTIC FEATURES OF THE EPITHERMAL ENVIRONMENT THAT HAVE IMPLICATIONS FOR EXPLORATION

Jeffrey W. Hedenquist

University of Ottawa - jhedenquist@gmail.com

Epithermal precious (± base) metal deposits are largely hosted by volcanic rocks, and the tops of ore bodies formed within 10s to a few 100s m of the paleosurface (Lindgren, 1933) in hydrothermal systems driven by magmatic intrusions. There is a large variation in the style of epithermal deposits, including the associated alteration minerals, that is related to tectonic setting, magmatic affiliation, lithologic and structural features, and other potential variables (Sillitoe, 1977; Hedenquist *et al.*, 2000; Sillitoe and Hedenquist, 2003). The active equivalents include geothermal systems with near-neutral pH hot springs at the surface (Sillitoe and Hedenquist, 2003), as well as highly reactive fluids associated with the condensates of volcanic fumaroles (Arribas, 1995; Sillitoe, 1999), although alteration related to the latter is barren, formed prior to ascent of the potential mineralizing liquid (Hedenquist and Taran, 2013).

The features developed at the paleosurface, including silica sinters and steam-heated alteration (Sillitoe, 2015) as well as at relatively shallow depths, to a few 100s m, provide indications that are useful during exploration. This includes evidence for the level (depth) of erosion, zonation toward channels of fluid ascent, and style of deposit, aspects that can improve the efficiency and effectiveness of mineral exploration.

ADVANCED ARGILLIC ALTERATION

Shallow alteration in the epithermal environment commonly indicates mineralogic evidence for acidic conditions, and these minerals as a group are referred to as advanced argillic; this represents extreme hydrolytic base leaching and formation of aluminum-rich phases (Meyer and Hemley, 1967). The minerals (and their temperature of formation) may include: kaolinite (<200 °C), dickite (~200-250 °C) and pyrophyllite (~250-350 °C; Hedenquist *et al.*, 2000), alunite (<300 °C, although natroalunite tends to form at temperatures higher than alunite), diaspore (~250-320 °C), and alkali-deficient white mica (sericite is commonly used as a textural term; ~300-400 °C). These minerals can locally and variably be accompanied by andalusite (~300-400 °C), tourmaline (in a B-rich environment), and topaz and zunyite (in a F-rich environment; ~250-350 °C). Residual quartz, formed where the pH is <2 (<250 °C) and most components (including Al) are leached from the rock is not included in the term advanced argillic (Meyer and Hemley, 1967). An appropriate term for residual quartz is silicic, in contrast to silicification, which involves silica being precipitated from solution.

These minerals are commonly reported as advanced argillic (on maps and in logging and on cross sections), but since they can form in four distincly different environments, with each having different implications for exploration, the original mineralogy (plus texture and morphology of alteration) should be retained. This is particularly relevant to exploration, both in the interpretion of erosion level as well as zonation (Arribas, 1995). These four environments and their characteristic mineral assemblages are:

1) Hypogene (magmatic) vapor condensation, pH ~1, in active volcanic environments, with acidity caused by SO_2 disproportionation to H 2 SO_4 as well as the presence of HCl (Hedenquist and Taran, 2013). Typical minerals include: alunite, dickite and kaolinite, with decreasing temperature (to <150 °C); roots of dickite, diaspore and pyrophyllite at higher temperature (to >300 °C) (Arribas, 1995).
2) Steam-heated horizon above the vadose zone, pH ~2.5 at $\leqq$100 °C, over boiling liquids, with acidity caused by H_2S oxidation by atmospheric O_2 to H_2SO_4 (Schoen *et al.*, 1974). Typical minerals include: kaolinite, alunite, dickite, and at the base of the vadose zone, a layer of cristobalite (or opal) that precipitates at the paleogroundwater table.
3) Supergene horizon, also formed above the vadose zone, pH potentially very low (equal to acid mine drainage) at ambient temperature of ~20 ±20 °C, where acidity is caused by oxidation of pyrite by atmospheric O_2 to H_2SO_4, after hydrothermal activity (Sillitoe, 1993). Typical minerals include: kaolinite, alunite, allophane (amorphous clays), plus iron hydroxides.
4) Deep pyrophyllite zone forms a) within the high-temperature (~300 °C) feeders of residual quartz, at paleodepths of ~300-500+ m, or b) above a deep zone of white mica due to cooling (<350 °C) of white mica at depths of 1 km or more (Watanabe and Hedenquist, 2001). Typical minerals include: pyrophyllite, dickite and diaspore in the feeder structures of residual quartz, or pyrophyllite and white mica at the base of the epithermal environment, i.e., at the transition upward from depths of porphyry deposits.

ZONED ALTERATION MINERALOGY

Within the epithermal environment, clay minerals tend to be abundant at shallow depths, including the kaolinite group (kaolinite, dickite, nacrite and halloysite), smectite and illite. Kaolinite (stable up to ~200 °C, vs halloysite up to ~100 °C) and dickite (~200-250 °C) can be present variably in the shallow steam-heated and supergene environments (kaolinite), as well as deeper hypogene (dickite). Thus mineralogy must be used with other observations of features to interpret the environment(s) of formation as well as pH and temperature.

Smectite (<150 °C), interstratified illite-smectite (I/S; ~150-200 °C) and illite (~200-250 °C), with higher temperatures favoring compositions and crystallinity that approach muscovite) form at near-neutral pH, typically as halos to epithermal veins in which the paleotemperature decreased both vertically but also laterally with distance from the vein (Hedenquist *et al.*, 2000). As such, zonation of smectite to I/S to illite on the surface or in a drill hole indicates an increase in paleotemperature and thus the approach to a fluid channel, possibly one hosting an epithermal quartz vein that may be mineralized. Adularia commonly occurs proximal to a flow channel, replacing wall rock, with chlorite in intermediate-composition (andesitic) wall rocks.

DISCUSSION

The clay minerals have characteristics that allow them to be recognized by hand lens, although confirmation initially by SWIR (short wave infrared) increases confidence and improves reliability. Mapping or logging these minerals simply as clay alteration results in a loss of the information that mineral assemblages as well as their zoning can indicate. Similarly, lumping minerals that formed in acidic conditions with the term advanced argillic results in much information and insight being lost. These minerals, determined from hand lens and confirmed by the now-widespread use of SWIR equipment, provide information on environment, i.e., syn-hydrothermal hypogene or near-surface steam-heated, vs pyrophyllite at higher temperature (deeper), and post-hydrothermal supergene, the latter as an overprint. Many of these minerals also indicate temperature of formation, indicating paleodepth and thus degree of erosion.

REFERENCES

Arribas, A., Jr., 1995. Characteristics of high-sulfidation epithermal deposits, and their relation to magmatic fluid: Mineralogical Association of Canada Short Course 23: 419–454.

Schoen, R., White, D.E. and Hemley, J.J., 1974. Argillization by descending acid at Steamboat Springs, Nevada. Clay and Clay Minerals 22: 1–22.

Hedenquist, J. W., Arribas, A., Jr., and Gonzalez-Urien, E., 2000, Exploration for epithermal gold deposits. Reviews in Economic Geology 13: 245–277.

Hedenquist, J.W. and Taran Y.A., 2013. Modeling the formation of advanced argillic lithocaps: Volcanic vapor condensation above porphyry intrusions. Economic Geology 108: 1523–1540.

Lindgren, W., 1933. Mineral deposits, 4th Ed. New York and London, McGraw-Hill BookCompany. 930 p.

Sillitoe, R.H., 1977. Metallic mineralization affiliated to subaerial volcanism: Geological Society Special Publication 7: 99–116.

Sillitoe, R.H., 1993. Epithermal models: genetic types, geometrical controls and shallow features. Geological Association Canada Special Paper 40: 403–417.

Sillitoe, R.H., 2015. Epithermal paleosurfaces. Mineralium Deposita 50: 767–793

Sillitoe, R.H., Hedenquist, J.W., 2003. Linkages between volcanotectonic settings, ore - fluid compositions, and epithermal precious-metal deposits. Society of Economic Geologists Special Publication 10: 315"343.

PALAEOZOIC PORPHYRY Cu (Mo, Au) SYSTEMS – LESSONS FROM THE URALS

Olga Y. Plotinskaya[1], Anatoly I. Grabezhev, Reimar Seltmann

[1]*Institute of Geology of Ore Deposits, Petrography, Mineralogy and Geochemistry, Russian Academy of Sciences (IGEM RAS), Moscow, Rusia - plotin-olga@ya.ru*

The Urals hosts dozens of porphyry and porphyry related deposits and occurrences (including epithermal and skarn types). Most important ones are located in the Middle and South Urals and some are currently under exploration. Most of the porphyry Cu (±Mo,Au) deposits of the Urals can be subdivided into the following groups according to subduction zones of different ages (Plotinskaya *et al.*, 2017):

1) Deposits related to Silurian intra-oceanic subduction: porphyry Cu deposits of the Birgilda-Tomino ore cluster (Birgilda, Tomino, and Kalinovskoe) and the Zeleny Dol porphyry Cu deposit. These deposits are associated with Na-K calc-alkaline diorites with moderate LREE to HREE enrichment (La_n/Yb_n = 6.50).
2) Deposits linked to the Magnitogorsk intra-oceanic arc, which was active from Early Devonian (Emsian) and collided to the East European plate in the Late Devonian (Famennian). Porphyry-style mineralization of the Magnitogorsk megaterrane shows an evolving relationship from gabbro-diorite-quartz diorite in the Middle Devonian (Salavat and Voznesenskoe porphyry Cu deposits) to granodiorite-plagiogranodiorite (Yubileinoe porphyry Au deposit) and syenite (Verkhneuralskoe porphyry Mo occurrence) in the Late Devonian with an increase in the mean Lan/Ybn ratio (2.97 to 14.29).
3) Deposits located in the Trans-Uralian megaterrane and linked to the Late-Devonian to Carboniferous subduction. This includes the Late Devonian to Early Carboniferous Mikheevskoe porphyry Cu deposit linked to an intra-oceanic arc, Late Carboniferous deposits of the Alexandrov volcanic arc terrane (Bataly porphyry Cu deposit) and Early Carboniferous deposits formed due to eastward Andean-type subduction under the Kazakh continent (Benkala porphyry Cu deposit). The REE patterns of the Mikheevskoe (Lan /Ybn = 3.10). Benkala and Bataly deposits have significant LREE enrichment (La_n/Yb_n = 11.01 and 17.01 respectively).
4) Continent-continent collision of the East European plate and the Kazakh continent in the Late Carboniferous produced the Talitsa porphyry Mo deposit located in the East Uralian megaterrane. It is related to sub-alkaline granodiorite to granite and establishes the highest LREE to HREE enrichment (La_n/Yb_n = 42.01).

This study was supported by the Presidium of the Russian Academy of Sciences, Program N° 48; RS acknowledges funding under NERC Grant NE/P017452/1 "From arc magmas to ores (FAMOS): A mineral systems approach.

REFERENCES

Grabezhev, Anatoly I., Shardakova, G. Y., Ronkin, Y. L., Azovskova, O. B., 2017. Systematization of U-Pb zircon ages of granitoids from the copper porphyry deposits on the Urals. Lithosphere (Russia) 17 (5), 113–126 (in Russian).

Ivanov, A. I., Vartanyan, S. S., Chernykh, A. I., *et al.*, 2016. State and prospects of the Russian diamond, gold, copper, lead and zinc mineral base development (based on work results of FSUE TsNIGRI for 2012–2015). Otechestvennaya geologia, 5, 1–52 (in Russian).

Plotinskaya, O.Y., Grabezhev, A. I., Tessalina, S., Seltmann, R., Groznova, E. O., Abramov, S. S., 2017. Porphyry Deposits of the Urals: Geological Framework and Metallogeny. Ore Geology Reviews, 85, 153–173.

Smirnov V. N., Ivanov, K. S., Shokalsky, S. P., Ronkin, Y. L., 2017. The results of U-Pb SHRIMP-II dating of zircon from granitoids of Talitsky molybdenum-bearing massif (eastern slope of the Middle Urals). Lithosphere (Russia) 17 (3), 145–150 (in Russian).

Deposit/current status	**Major associated intrusions**	**Age**	**Tonnage, grade**
EAST-URALIAN VOLACNIC TERRENE			
Tomino / Under operation	quartz diorite porphyry	427±6 (U-Pb) 430.7±1.3 (Re-Os)	1.54 Mt Cu (331 Mt@ 0.47Cu), Au 0.12 ppm[1]
MAGNITOGORSK TERRANE			
Salavat / occurrence	diorite, quartz diorite porphyry	Devonian	Inferred: 993Mt Cu @0.48%)[1]
Voznesenskoe/ occurrence	quartz-diorite-diorite-gabbrodiorite pre-ore pluton, diorite porphyry dykes	381±5 Ma (U-Pb)	Unknown, Cu/Mo= 250
Yubileinoe / Under operation	diorite-granodiorite pluton plagiogranite porphyry stock	374±3Ma (U-Pb)	85.2 Mt @2.07ppm Au and 0.16%Cu[2]
Verkhneuralskoe/ occurrence	gabbro-granodiorite-syenite pluton; quartz-diorite, granodiorite porphyry	Late Devonian to Early Carboniferous, (Geol); 341±1 (Rb-Sr)	Unknown, Cu/Mo= 15
TRANS-URALIAN TERRANE			
Mikheevskoe / Under operation	diorite porphyries, plagiogranodiorite porphyry	356±6 (U-Pb) 357.8±1.8 and 356.1±1.4 (Re-Os)	629 Mt @ 0.41% Cu (2.6 Mt Cu)[3]
Benkala / Under operation	diorite-granite pluton; dykes of granite porphyry	334.7±2.9 (U-Pb)	1.56 Mt Cu @ 0.42%Cu[4]
Bataly / occurrence	breccia, granodiorite, granodiorite porphyry, diorite porphyry	309.1 ±0.7 (U-Pb)	Unknown, 0.52% Cu,0.001%Mo, 0.18ppm Au
EAST-URALIAN TERRANE			
Talitsa / occurrence	diorite-granodiorite pluton, granodiorite and granite porphyry stocks	297.4±2.3 Ma (UPb) 5; 298.3 ± 1.3 Ma (Re-Os)	Unknown, 0.04-0.34% Mo, 0.09-0.47% Cu, 0.1-0.4 ppm Au

Source: [1] Ivanov *et al.*, 2016; [2] http://kase.kz/files/emitters/ATEC/atecp_2015_rus.pdf; [3] http://rmk-group.ru; [4] http://www.frontiermining.com; [5] Smirnov *et al.*, 2017

Table 1. A selection of key porphyry deposits of the South and Middle Urals, updated from (Plotinskaya *et al.*, 2017; Grabezhev *et al.*, 2017)

WHY DETAILED MINERALOGY IS IMPORTANT: UNDERSTANDING EVOLUTION OF THE OLYMPIC DAM IRON-OXIDE COPPER-GOLD SYSTEM, SOUTH AUSTRALIA

Nigel Cook[1], Kathy Ehrig, Cristiana Ciobanu, Liam Courtney-Davies, Max Verdugo-Ihl, Mark Rollog, Danielle Schmandt, Nicholas Owen, Edeltraud Macmillan, Alkiviadis Kontonikas-Charos, Sasha Krneta, Marija Dmitrijeva

[1]*School of Chemical Engineering, University of Adelaide, Australia - nigel.cook@adelaide.edu.au*

Olympic Dam is one of the largest deposits on Earth and a significant producer of copper, uranium, gold and silver (Ehrig, *et al.*, 2013). Uranium-Pb geochronology using undisturbed magmatic and hydrothermal minerals allows interpretation of the initial and major hydrothermal ore- forming event at ~1593 Ma, associated with emplacement of the Gawler Silicic Large Igneous Province. The >10 billion-tonne resource is heterogeneous and contained within a breccia complex, itself confined to the ~1593 Ma Roxby Downs Granite. Ore textures suggest multiple episodes of replacement, remobilization and recrystallization and are supported by (radio) isotope data yielding a range of younger ages. Conceptual models for ore formation, necessary for exploration in the region, and optimised processing of complex fine-grained ores characterised by enrichment in an extraordinarily wide variety of elements are dependent on an exceptionally thorough understanding of mineralogy and geochemistry underpinned by high-quality, high-resolution assay data, extensive MLA datasets, and deportment models for multiple elements.

Micron - to nanoscale studies of feldspars and accessory phases within the alteration envelope, and of Fe-oxides, Cu-(Fe)-sulphides, sulphates, U- and REE-bearing minerals within the deposit all point to common mechanisms involved in formation of the mineral assemblages as observed today, the prevailing Mm-scale mineral textures, and measured variations in mineral compositions. Detailed mineralogical investigation has proven pivotal in establishing a framework for ore evolution.

Each of the 100 minerals in the Olympic Dam deposit has a story to tell. The complex fine- grained, intergrown, heterogeneous assemblages necessitate ultra-careful investigation on multiple representative samples and with compositional data requiring verification by examination at the nanoscale. We therefore use a combination of whole rock assay, optical and scanning electron microscopy, electron probe microanalysis (EPMA), laser-ablation inductively-coupled plasma mass spectrometry, complemented by imaging and nanoscale compositional analysis by transmission electron microscopy (TEM) on foils extracted *in-situ* by focussed ion beam SEM methods.

Investigation of feldspars from within and outside the deposit allows an understanding of the magmatic to hydrothermal transition and early Fe-metasomatism (Kontonikas-Charos, *et al.*, 2017). Nanoscale characterization of feldspars undergoing transformation from early post-magmatic (deuteric) to hydrothermal stages in granites hosting the deposit reveals complex perthitic textures, anomalously Ba, Fe, or REE-rich compositions, and REE-fluorocarbonate+molybdenite assemblages that pseudomorph feldspars (Kontonikas-Charos, *et al.*, 2018). Epitaxial orientations between (igneous) cryptoperthite, (deuteric) patch and albite replacive within vein perthite support interface-mediated reactions between pre-existing alkali-feldspars and pervading fluid, irrespective of micron-scale crystal morphology. Such observations are consistent with coupled dissolution-replacement reactions (CDRR), indicating that albitization enhances rock permeability via the generation of transient pores which facilitate grain-scale element remobilization and trap elements as nanoscale inclusions. These inclusions represent the earliest stage of REE remobilization at the grain-scale, and reflect the significant role feldspar replacement reactions play in concentrating REE during hydrothermal alteration.

Hematite is by far the most abundant hydrothermal mineral and preserves oscillatory and sectorial zoning and incorporation of U, W, Mo, Sn and other trace elements, including REE (Verdugo-Ihl, *et al.*, 2017). The presence of U and Pb allows application of hematite U-Pb geochronology [e.g., Courtney-Davies, *et al.*, 2018]. These primary textures give way to repeated processes of brecciation, fluid-assisted reworking, element redistribution, recrystallization and overprinting. CDRR permits release of trace elements from the lattice to be trapped as nm- to Mm-scale inclusions (e.g., uraninite), or to form discrete minerals (e.g., scheelite molybdenite) in the near vicinity.

EPMA-scale compositional data combined with TEM investigation of chalcocite-group minerals, bornite and chalcopyrite has shown that Cu-Fe-sulphides from different ore zones feature nanoscale intergrowths, lattice defects, superstructure domains and antiphase boundary domains (Ciobanu, *et al.*, 2017). Such features can be interpreted as having originated via a combination of exsolution, coarsening, and phase transformation during cooling from high-T solid solutions (e"400°C) in the system Cu-Fe-S and sub-systems. A scenario of 'exsolution from primary solid-solution, corroborated by the consistency in phase relations within each zone across different scales of observation from deposit- to nanoscale, supports a model of primary hypogene ore precipitation rather than replacement, and

accounts for the observed zoning patterns at OD. Nonetheless, evidence for CDRR, replacement, phase transformation and local (Mm- to tens m-wide) remobilization is evident.

Uraninite, coffinite, brannerite and hematite are the dominant U hosts [Courtney-Davies, *et al.*, 2018, Macmillan, *et al.*, 2016, Macmillan, *et al.,* 2017). Although some uraninite and hematite retain U and daughter isotopes, breakdown and replacement can lead to release, remobilization and redistribution of radionuclides (RN) at scales from nm upwards. New minerals may be formed (late uraninite, coffinite) and U and Pb can also be incorporated into existing minerals (barite, svanbergite-woodhouseite). RN are, however, also concentrated as sub-microscopic particles within pores, microfractures and at grain boundaries in the near vicinity of altered or replaced U-bearing mineral grains (Rollog, *et al.*, 2018) attesting to fluid-mediated processes. Such redistribution carries implications for ore processing and, potentially also for the interpretation of geochronological data.

Three groups of REE-minerals are observed: REE-fluorocarbonates (bastnosite and subordinate synchysite (Schmandt, *et al.*, 2017), which appear paragenetically early; REE-phosphates (dominantly florencite of variable age and association but also minor xenotime, the main carrier of HREE); and Ca-, Sr-, REE-bearing phosphate-sulphates (svanbergite- woodhouseite], which are generally late and replace earlier-formed minerals (Owen, *et al.,* 2018). Minor REE are also contained in apatite, which displays evolving chondrite-normalized REE fractionation trends that can be explained in terms of changes in fluid parameters and speciation of REY in ore-forming fluids (Krneta, *et al.,* 2017). Under hydrothermal conditions typical of iron- oxide copper gold mineralization, a decrease in salinity, pH and temperature is associated with hematite-sericite alteration sufficient to produce a characteristic MREE-enriched apatite. However, anomalous high-pH (~7) fluids at 300 °C may account for high-grade Cu ores as modelled from apatite with strong positive Eu anomalies (Krneta, *et al.,* 2017).

Although primary assemblages are identified, a persistent narrative is offered by multiple episodes of fluid-assisted replacement, phase transition, remobilization, migration, and re- precipitation of all ore components. These processes played a major role in the modification of textural and geochemical patterns in many minerals. However, more refractory minerals, notably hematite, apatite, pyrite, some REE-minerals, and some sub-types of U-minerals, can preserve primary geochemical signatures and can also record and retain evidence of evolving and overprinting fluid signatures. Fluid regimes were likel heterogeneous given observations of texturally and geochemically distinct generations of the same mineral within single samples.

REFERENCES

Ehrig, K., McPhie, J., Kamenetsky, V., 2013. Geology and mineralogical zonation of the Olympic Dam iron oxide Cu-U-Au-Ag deposit, South Australia. In: Hedenquist, J.W., Harris, M., Camus, F. (Eds), Geology and Genesis of Major Copper Deposits and Districts of the World, a Tribute to Richard Sillitoe. SEG Special Publication 16, pp. 237-268.

Kontonikas-Charos, A., Ciobanu, C.L., Cook, N.J., Ehrig, K., Krneta, S., Kamenetsky, V.S., 2017. Feldspar evolution in the Roxby Downs Granite, host to Fe-oxide Cu-Au-(U) mineralization at Olympic Dam, South Australia. Ore Geology Reviews, 80, 838-859.

Kontonikas-Charos, A., Ciobanu, C.L., Cook, N.J., Ehrig, K., Ismail, R., Krneta, S., Basak, A., 2018. Feldspar mineralogy and rare earth element (re)mobilization in iron-oxide copper gold systems from South Australia: a nanoscale study. Mineralogical Magazine 82 (S1), S173–S197.

Verdugo-Ihl, M.R., Ciobanu, C.L., Cook, N.J., Ehrig, K., Courtney-Davies, L., Gilbert, S., 2017. Textures and U-W-Sn-Mo signatures in hematite from the Cu-U-Au-Ag orebody at Olympic Dam, South Australia: defining the archetype for IOCG deposits. Ore Geology Reviews 91, 173–195.

Courtney-Davies, L., Ciobanu, C.L., Tapster, S.R., Cook, N.J., Ehrig, K.J., Kennedy, A.K., Condon, D.J., Verdugo-Ihl, M.R., Wade, B.S., Gilbert, S.E., 2018. The U-Pb systematics of hydrothermal hematite; insights from the IOCG system at Olympic Dam, South Australia. IAGOD Symposium, Salta (this volume).

Ciobanu, C.L., Cook, N.J., Ehrig, K., 2017. Ore minerals down to the nanoscale: Cu-(Fe)- sulphides from the iron oxide copper gold deposit at Olympic Dam, South Australia. Ore Geology Reviews 81, 1218-1235.

Macmillan, E., Cook, N.J., Ciobanu, C.L., Ehrig, E., Pring, A., 2016. Uraninite from the Olympic Dam IOCG-U-Ag deposit: linking textural and compositional variation to temporal evolution. American Mineralogist 101, 1295–1320.

Macmillan, E., Cook, N.J., Ehrig, K., Pring, A., 2017. Chemical and textural interpretation of late-stage coffinite and brannerite from the Olympic Dam IOCG-Ag-U deposit. Mineralogical Magazine 81, 1323-1366.

Rollog, M., Cook, N.J., Gugliardo, P., Ehrig. K., Kilburn, M., 2018. In situ spatial distribution mapping of radionuclides in minerals by nanoSIMS. Geochemistry – Exploration, Environment, Analysis (in press).

Schmandt, D.S., Cook, N.J., Ciobanu, C.L., Ehrig, K., Wade, B.P., Gilbert, S., Kamenetsky, V.S., 2017. Rare earth element fluorocarbonate minerals from the Olympic Dam Cu-U-Au-Ag deposit, South Australia. Minerals 7(10), 202; doi: 10.3390/min7100202.

Owen, N.D., Ciobanu, C.L., Cook, N.J., Slattery, A., Basak, A., 2018. Nanoscale study of clausthalite-bearing symplectites in Cu-Au-(U) ores: Implications for ore genesis. Minerals, 8(2), 67; doi:10.3390/min8020067.

Krneta, S., Ciobanu, C.L., Cook, N.J., Ehrig, K., Kontonikas-Charos, A., 2017. Rare earth element behaviour in apatite from the Olympic Dam Cu-U-Au-Ag deposit, South Australia. Minerals 7(8), 135; doi:10.3390/min7080135.

IRON OXIDE COPPER-GOLD (IOCG) SYSTEMS: EXAMINATION OF END-MEMBER MODELS, PHYSIOCHEMICAL PROCESSES, AND POSSIBLE MODERN ANALOGIES

David R Lentz

Department of Earth Sciences, University of New Brunswick, Fredericton, NB E3B3A3 Canada - dlentz@unb.ca

INTRODUCTION

Many perspectives have been given on the subject, including quite divergent views on the same material as we have seen most recently with the El Laco debate, let alone Kiruna and many others. The focus will be on the iron oxide (& apatite, or IOA) part of the system and less so on the copper, gold, uranium, and rare earth elements, although aspects of these enrichments will also be examined. Magmatic iron oxide (apatite) melt (immiscible from silicate melts) and magmatic hydrothermal (volatile exsolution from silicate melts) and hydrothermal (fluid circulation) are clearly the endmember hypotheses that will be examined. For the most part, all hypotheses involved magmas and many involve diorite magmatic systems, which will be explored further on. It is important to realize that magnetite and apatite are both highly susceptible to near surface fluid reaction processes (dissolution-reprecipitation processes), which can modify mineral compositions and reset or modify geochronometers with minimal visual effects, except with petrographic and chemical analysis. Few robust minerals are associated with these systems, except monazite that can commonly exsolve from apatite upon cooling or fluid induced reactions. Zircon is extremely rare. End-member models will be reviewed as noted above, physiochemical processes will be explored, including those beyond the scope of the current literature. Some theoretical models have been proposed to reconcile the high T assemblages, but only a few experiments done and a few more most recently that build on the immiscibility hypothesis. There are experiments on the solubility of magnetite in magmatic hydrothermal systems and hydrothermal systems.

EL LACO OBSERVATIONS AND INTERPRETATIONS

This is a logical system to start with as it is become the fulcrum for the debate on the origin of IOA systems. With Park's 1961 observations of magnetite-dominated flows crosscutting tuffs, the debate began in this part of the world with other evidence presented like textures, and mineral assemblages and fluids and helped reignited debate, in particular for Kiruna. Sillitoe and Burrows in 2002 reexamined the evidence at El Laco noting a hydrothermal origin, for which there was a quick rebuttal. In 2003 Dick Sillitoe followed up with a timely systematic analysis of IOCG throughout the Andes noting the empirical structural and dioritic and andesitic igneous associations in many of these systems. In 2015 Sare Dare did a mineral-chemical study of magnetites and showed they were similar to magmatic hydrothermal systems. Others have recently used physical evidence (crystalized melt inclusions) and stable isotopic evidence to show that the assemblages are equilibrated to high temperatures. In 2018 Jim Mungall and others have demonstrated a magmatic origin, although is skeptical of immiscibility. Are there other explanations that can help reconcile these two divergent hypotheses.

OTHER IOA-IOCG SYSTEMS

My initiation to these systems was working in the Great Bear Magmatic Zone (Canada) with Sunil Gandhi who was a proponent of the immiscible melt model, based on his work in Canada, although he recognized the issues coming out of the work by Robert Hildebrand in 1986. Both researchers acknowledge the close empirical association with monzonitic intrusions and their spatial and temporal relation to Cu-Co-Ni-Ag-Au (U, REE) vein systems (Five element veins). Since the 2000s, much has been done in that region mostly building on the magmatic hydrothermal hypothesis culminating recently in a magmatic hydrothermal hypothesis that is akin to porphyry Cu-Au systems that was completed by Jeremy Richards and Hamid Mumin in 2013; this hypothesis is quite compelling as are the

hydrothermal models intersecting evaporates. It is well known that the solubility of Fe, is dominantly as a divalent ion or complex ligand (i.e., FeCl+, $FeCl_2$, etc), but the stability of magnetite is large relative so saturation of Fe under depositional conditions is commonly magnetite. Even studies of the solubility of magnetite note the overall salinity or chlorinity of the system, pH, T, etc., although the hydrothermal hypothesis falls short of evaporate syntexis. However, open system reaction of saline fluids, including circulation around igneous systems can drive them to brines and salt melts, which are ionic melts, so can dissolve more high field strength elements (HFSE), like ionic carbonatite liquids, with a P association.

The carbonatite associations for these deposits have yet to be noted, e.g., Phalabowra by David Groves, but they do have merit discussing as significant titaniferous magnetite is associated with that unique deposit. Similarly the Bayan Obo iron ore, which is dominantly magnetite, is also rich in P & REEs. In both cases it is possible that ferroan carbonatites (sideritic) maybe involved in their genesis. Patrick Williams *et al.* in 2005 and then Groves *et al.* in 2010 have grouped these separately, as they have the other subdivisions of IOA deposits they noted, but there are valuable lesson in these comparison. The lesson from this is that what we see now as a ferroan carbonatite association is touched on later, but these ionic liquids can dissolve HFSEs.

GAPS IN KNOWLEDGE

Interest in magnetite petrogenesis has been led by mineral-chemical data. This new data has been empirically examined to relate to different magmatic, magmatic hydrothermal, hydrothermal, including exhalative hydrothermal systems. Interestingly this has been used to try to help discriminate between IOA-IOCGs, skarns, porphyries, etc. With magnetite compositions, Knipping et al in 2015 recently postulated that magnetite flotation in a magmatic system was a good way to maintain the high temperature signatures of magnetite, but still be associated with the vapor phase. Although challenging, it does point out that in some IO systems that the Ti content is important to reconcile and shows these are forming at a very high temperatures. In 2018 Hou and other just demonstrated that increasing either a H_2O and fO_2 can enhance immiscibility, although at quite high temperatures, yielding intermediate to silicic melts, with coexisting Fe-Ti-Ca-P liquid. Therefore processes that can enhance water saturation, i.e., fractionation of anhydrous phases or changing oxygen fugacity can enhance immiscibility. The link with volatiles, especially water in reducing solidi in magmatic systems, has long been known, but changing redox has not. I did mention that sideritic magmas may have been the systems that were associated with two reknown carbonatites and one of the main hypotheses of carbonatites is a liquid immiscibility hypothesis. Also, carbonatite's main flux is water as well. Hypothetically water and evolution of H_2 from a system at shallow levels could cause oxidation. However assimilation of evaporates can increase magmas salt content, but would invariably assimilate limestones, which was long thought to be challenging. The derivative product of limestone syntexis is a carbonated peralkalic silicate melt and immiscible carbonate (& salt) melt, and CO_2. CO_2 can act as an oxidant to the magmatic system as well as increase overall ÄV of the system, causing brecciation. Similarly ascending carbonatites can react with silicate rocks or associated silicate melts to evolve CO_2 as well such that they form diatremes that envelope the carbonatite and probably autooxidize it as well to destabilize $FeCO_3$ of the fractionated carbonate melt to form magnetite.

THE CONTINUUM MODEL

Is it possible that oxidation of $FeCl_2$-rich salt melts or $FeCO_3$ components of ferroan carbonate melts, which both have ionic melt behavior, and can dissolved HFSE? The ephemeral nature of these highly reactive and unstable ferrous iron-rich systems, which would undoubtedly be water bearing, could transport Fe, with P, Ti, REE, etc. The diorite, ferroan diorite to ferroan andesite-basalt association to IOAs and IOCGs could be related to oxidation induced by limestone assimilation (syntexis) and (or) evaporate assimilation (syntexis) to enhance immiscible ionic melt formation that would immediately oxidize to form magnetite as dikes or flows. The subsequence fluid circulation systems associated with upper crustal emplacement of dioritic magmatic systems could also generate further $FeCl_2$-rich hypersaline brines to salt melts that would be somewhat similar to their higher temperature syntectic derivatives, i.e., part of a continuum from magma immiscibility to magmatic hydrothermal, to hydrothermal systems (to exhalative). I will point out a few comparable systems that highlight the continuum similarities that I noted some of with are active modern systems. Usually the best hypothesis is one simplest one that explains all the evidence (Occam's Razor).

MICROBIOLOGY AND THE FORMATION OF ORE DEPOSITS

Fernando Tornos

Instituto de Geociencias (CSIC-UCM), Madrid, España - f.tornos@csic.es

INTRODUCTION

Metabolism of prokaryotes in the deep biosphere is controlled by the different redox reactions taking place in the presence of liquid water. At temperatures above *ca.*120-150 °C, these reactions are spontaneous but at low temperatures most of them are kinetically inhibited and only enzymes are able to catalyse them. Thus, from the geochemical point of view, life is the key mechanism that controls redox at low temperatures. Thus, is not surprising that ore deposits that are enriched in elements having variable valences, such as Fe, Mn, or Cu, and specially carbon and sulphur, can be formed or modified by biogenic activity.

In fact, direct or indirect evidence of microbial activity has been described in very different ore forming environments such as volcanogenic and sediment-hosted massive sulphide deposits, banded iron formations, gossans or cementation zones and seems to play also a major role in the formation of alluvial gold, platinum and silver deposits. However, detection of such a biogenic activity is not always easy. In ancient systems, preservation and interpretation of microbial fossils or biomarkers is always controversial and most putative biogenic activity is based in the carbon and sulphur isotopes. In recent systems and where microbes are active, selection of samples or contamination can hamper a correct determination of the microbial ecosystems.

SULPHATE-REDUCTION AND FORMATION OF MASSIVE SULPHIDES

Perhaps the best known role of microbial metabolism in ore forming processes is its control in the formation of many sediment -or volcanic- hosted massive sulphides. Oxygen-free bottoms can form either due to the lack of seawater convection in confined basins or due to the accumulation of anoxic brines on the seafloor (brine pools). In these environments, the reduction of seawater sulphate combined with the oxidation of electron donors such as hydrocarbons, methane or H_2, can lead to the formation of an almost infinite reservoir of H_2S_{aq}. Here, the biogenically -controlled mineralization can form when these fluids enriched in reduced sulphur mix with (deep) reduced sulphur-deficient hydrothermal fluids carrying large amounts of base metals. This mechanism leads to the quick (super-) saturation of pyrite and other sulphides that precipitate in the anoxic bottoms and the immediate sub-seafloor; these environments are also ideal for the preservation of the mineralization since they inhibit later oxidation and destruction of the already precipitated sulphides.

BANDED IRON FORMATIONS

Iron oxidizing bacteria have been interpreted as being the major inducers of the formation of banded iron formations. The consortium of photoferrophs and cyanobacteria uses soluble Fe^{2+} as reductant during photosynthesis, producing insoluble Fe^{3+}, which precipitated as hematite. This process is 60 times faster than the abiotic oxidation of Fe^{2+} and is perhaps responsible of the formation of large amounts of banded iron formations.

THE ROLE OF MICROBES DURING OXIDATION

Now it is clearly established that microbial activity is critical for the oxidation of pyrite-rich cropping out mineralization. The formation of gossans is directly related with the microbial oxidation of pyrite to goethite via the combined oxidation of Fe^{2+} into Fe^{3+} and oxidation of the reduced sulphur in a process that is 105 faster than the abiotic equivalent. These reactions release large amounts of $^{H+}$ leading to the formation of acid waters that, in turn, are able to remobilize large amounts of leached copper and zinc.

MICROBES AND SECONDARY COPPER DEPOSITS

The role of microbes in cementation zones is controversial. Despite it has been argued that the formation of covellite -and chalcocite- rich rocks must be biogenic and there are descriptions of putative microbes, their role has been minimised by the dominance of presumed abiotic processes involving the replacement of silicates and pyrite by copper sulphides. However, a recent microbiological study at Las Cruces deposit (Spain) has shown that the cementation zone hosts a complex and biologically diverse anaerobic ecosystem dominated by sulphate-reducer bacteria accompanied by methanogenic archaea and many other microbial consortiums. Copper sulphides form due to the biogenic increase of $a H_2S_{aq}$, first nucleating on the extrapolymeric substance (EPS) hosting the bacteria and later infilling massive veins and cavities.

THE MICROBIAL CONTROL ON SECONDARY REDUCTION

Sulphate-reducing bacteria also control the formation of sulphides in subaerial but anaerobic environments, such as in aquifers or even reducing earlier and buried oxidized assemblages. In these systems, goethite, hematite and lead-bearing sulphates and carbonates are biogenically reduced to iron polymorphs (greigite and smythite) and galena. Here, methanotrophic archaea symbiotically associated with sulphate-reducing bacteria produces large amounts of CO_2 and makes carbonates stable.

PRECIOUS AND TOXIC METALS AND MICROBIAL ACTIVITY

Gold and probably other precious metals can be corroded and placed in solution by specific groups of bacteria. However, there is a second group of bacteria that detoxifies water by reduction of Au^{3+} into Au0. This leads to the formation of the, sometimes large, nuggets that are found in placers. Along with gold, these bacteria are thought to be able to precipitate platinum, native silver and As-Sb-Ag-Hg sulphosalts.

CONCLUSIONS

Biologic activity is intuitively one of the major processes leading to ore formation at low temperatures. However, tracing it is not always easy since there are few remnants of biomarkers and microbes do not easily fossilize. The precipitation of the neoformed minerals is not directly controlled by the microbial activity but is a consequence of the chemical changes produced by this metabolism. They seem to preferentially precipitated in the EPS enclosing the microbes or even far away from the microbial consortiums.

The most widely used technique is the isotope geochemistry of sulphur and carbon but these tracers cannot detect if the biogenic activity was in situ or away from the place of ore deposition. In general, highly negative sulphur and carbon isotopes reflect the presence of biogenically-derived reduced sulphur or oxidized carbon. Despite, this is generally true for carbon, high $\delta^{34}S$ values can be also of biogenic origin when the system is depleted in electron donors.

RARE EARTH MINERAL SYSTEMS ASSOCIATED WITH ANOROGENIC ALKALINE INTRUSIONS AND CARBONATITES

Franco Pirajno

Centre for Exploration Targeting, The University of Western Australia - franco.pirajno39@gmail.com

In the last decade or so, the REE market has become critically very important due to an ever increasing demand for innovative digital technology, fibre optics, hybrid vehicles, wind turbines, lightweight devices, cell phones, etc. The main consumers are: China, USA, Japan and Korea. REE minerals can be extracted from ion-adsorption clays, laterites, bauxites, heavy mineral sands, phosphorites, pegmatites and even magnetite-apatite mineral systems (IOA). However, perhaps by far more important especially from the geological, economic and environmental aspects, are the REE ores associated with intracontinental anorogenic alkaline intrusions and carbonatites. It is estimated that carbonatite-hosted REE deposits contribute some 50% of the global production. Alkaline and carbonatite magmatism are generally associated, in space and time, with extensional tectonics and more specifically with rifting events. Magma genesis in rift environments is thought to be related to the ascent of mantle melts and their interaction with the subcontinental lithospheric materials. The main products of rift magmatism are fissure-fed tholeiitic flood basalts, mafic-ultramafic intrusions and intracontinental alkaline provinces, which are part and parcel of large igneous provinces (LIPs). Anorogenic intracontinental magmatism, includes alkaline ring complexes, carbonatites, kimberlites, and monogenetic volcanism (Pirajno, 2015). Here I focus on intracontinental anorogenic alkaline magmatism and carbonatites. Most primary alkaline magmas are mafic, rather than ultramafic, and in many cases, prolonged lithospheric and/or crustal residence time results in a wide range of rock types, including felsic derivatives far removed from compositions in equilibrium with mantle olivine. The rock types considered here range from mafic to felsic and usually contain feldspathoids (e.g. nepheline, sodalite) and/or alkali-pyroxene and alkali-amphibole. The silica-oversaturated rock types range from monzonite to syenite, alkali-syenite and alkali-granite, and their volcanic equivalents. On the other hand the nomenclature for the silica-undersaturated rock types (generally feldspathoid-bearing) can be confusing and plagued by locality-based names (see Le Maitre, 2002, for a classification). From the stand point of economic mineralization, important rock associations of alkaline magmatism are: kimberlites, mafic ultrapotassic rocks, syenite-pyroxenite-ijolite-carbonatite complexes, carbonatite plugs and dykes, alkali basalts, peralkaline granite-syenite-gabbro assemblages. These rocks occur as dykes, pipes, hypabyssal and subvolcanic intrusions and as central volcano-plutonic structures, many of which form ring complexes. Anorogenic alkaline complexes are generally characterised by unusual concentrations of non-hydrous volatiles (CO_2, B, F), REE and LILE incompatible elements (P, Zr, Ba, Nb, U, Th, Sn, Ta and W). Carbonatites are especially significant because they constitute a major source of Nb, P, Zr, Ti, Th, Sr and REE. Most economic mineral deposits occur associated with central vent-type complexes of which two main groups are recognised: 1) alkali-granite-syenite (saturated-oversaturated); and 2) ijolite-carbonatite (undersaturated). It is important to bear in mind the level of erosion, and hence age, in terms of the preservation potential of the contained mineral deposits. The origin of carbonatite magma is still controversial, and at the heart of the controversy is the relationship between carbonatites and the silica-undersaturated rocks with which they are commonly associated.

MINERALIZATION IN ANOROGENIC ALKALINE INTRUSIONS

Mineralization in alkaline rocks is formed through at least three principal ore-forming processes, namely: 1) primary magmatic, in which the ore minerals are precipitated from residual fluids in the subsolidus range of temperature and pressure; 2) hydrothermal, from late-stage fluids evolved from (1) and their mixing with heated meteoric waters, this hydrothermal mineralization commonly overprints the primary magmatic; 3) supergene, usually developed in the weathering profiles of carbonatite in tropical climates and under conditions of high Eh and low pH. Good examples are provided by the Mount Weld laterite- hosted P-La-Nb-Ta deposit in Western Australia and its "twin" ~87 Ma Araxá in Minas Gerais in Brazil. It is important to point out that the age of the Mount Weld laterite (Late Cretaceous-Cenozoic?) does not coincide with the age of the primary carbonatite (~2025 Ma).

The mineralizing fluids associated with alkaline complexes develop during the late stages of crystallisation and differentiation of the melts. These late-stage fluids have an alkaline to peralkaline chemistry. Depending on the permeability of the country rocks (porosity, fractures, faults, shear zones), they are expelled from the cooling magma inducing metasomatic changes from a few hundred metres to several kilometres away from the complex. Thus, we may distinguish mineralization associated with: 1) saturated- oversaturated complexes); and 2) undersaturated complexes. The saturated-oversaturated complexes tend to be enriched in Sn, W, U, Mo, Bi, As, Y, Li, Ta, Zr, La, Ce and Nb (pyrochlore), the undersaturated complexes in Sr, Ba, Th, Nb, Ti, Fe (magnetite) and P

(apatite). Good examples of mineralised anorogenic alkaline complexes can be found in Namibia (Damaraland Alkaline Province), in Nigeria (e. g. Jos Plateau), in the Nubian Province of the Arabian Shield and in central Asia.

MINERALIZATION IN CARBONATITES

Carbonatites are the main host of Nb-Ta, Fe-apatite, Nb-REE and fluorite mineralization, both magmatic and hydrothermal. Of these, the largest include Bayan Obo (China), Mountain Pass (USA) and Palabora (also spelled Phalaborwa, South Africa) (see Pirajno 2015 and references therein). Carbonatite-related Fe-apatite, Nb-Ta, Nb-REE deposits (e. g. Tomtor, Karasug, Beloziminskoe) are numerous in the Siberian Craton and surrounding orogenic belts (Seltmann *et al.* 2010). The Mountain Pass carbonatite typically contains bastnaesite-parisite as primary magmatic minerals, albeit in a late-stage carbonatite. Hydrothermal REE minerals are more common, forming polycrystalline aggregates, veinlets and interstitial fillings, and are usually associated with barite, fluorite and monazite in varying amounts, which may or may not be economic. Most hydrothermal carbonatite- hosted REE deposits are small and uneconomic, although it is possible that a Bayan Obo style mineral system could be found in rift-related tectonic settings (Yang *et al.* 2017). Weathering of carbonatite complexes results in dissolution of carbonate minerals, leaving residual and/or supergene monazite, apatite and REE minerals, such as bastnaesite, parisite and florencite, ilmenite, rutile, monazite and synchysite in the carbonatite rocks. Apatite is one of the principal accessory minerals in both carbonatite and alkaline complexes. This is the case for both the above mentioned Mount Weld and Araxá primary carbonatites, resulting in the apatite enrichment in their lateritic caps.

The Bayan Obo world-class REE deposit, located on the northern margin of the North China Craton (NCC), is an extremely complex, hydrothermal, stratabound mineral system hosted in carbonate rocks of the Mesoproterozoic Bayan Obo Group. The Bayan Obo carbonatite contains, apart from calcite and dolomite, benstonite [$(Ca,Sr)_6Ba_6Mg(CO_3)_{13}$], norsethite [$BaMg(CO_3)_2$], barytocalcite ($BaCaCO_3)_2$ and strontianite ($SrCO_3$). The age of the Bayan Obo mineralization is controversial and uncertain, with various age data from K-Ar, Sm-Nd, Re- Os, show ages ranging from 1400 Ma, 1340 Ma, 1250 Ma, 900±800 Ma, 555±474 Ma, 430±420 Ma (Pirajno 2015 and references therein).

An interesting and perhaps somewhat novel mineralised carbonatite system is the Gifford Creek ferrocarbonatite complex (Mesoproterozoic Gascoyne Province, Capricorn Orogen, Western Australia) (Pirajno *et al.* 2017). One of the main features of this ferrocarbonatite complex is the widespread occurrence of ironstone (mainly magnetite, hematite and goethite) veins that are spatially associated with the ferrocarbonatite intrusions. These are surrounded by relatively narrow haloes of fenitic alteration interpreted to have formed during post-magmatic alteration processes. In situ U-Pb age by LA-ICP-MS of apatite and U- Pb-Th of monazite, yielded ages ranging from 1075 Ma to 1050 Ma, respectively. These ages fit well with the age range of the Warakurna Large Igneous province (Wingate *et al.* 2004), therefore a link with a mantle plume that may have generated the Warakurna LIP is considered possible (Pirajno *et al.* 2017).

CONCLUDING REMARKS

Anorogenic and intraplate alkaline magmatism and carbonatites are gaining ever increasing attention due to their potential to host economically viable critical and rare metals. The products of intraplate and rift-related magmatism are volumetrically small when compared to the large granitic batholiths formed at plate margins. Nevertheless, in spite of this, rift- related alkaline magmas and carbonatites provide excellent and most useful insights into mantle and sub-continental lithospheric mantle dynamics. Therefore, intraplate alkaline magmatism typically with syenitic-nephelinitic melts and associated carbonatites are dominantly emplaced in rift structures formed by the impingement of mantle plumes at the base of the sub-continental mantle lithosphere. This is well shown in the geological record as well as present-day intracontinental rifts.

REFERENCES

Le Maitre, R.W. (Ed), 2002. Igneous rocks – A classification and glossary of terms. Cambridge University Press, Cambridge, 236pp.

Pirajno, F., 2015. Intracontinental anorogenic alkaline magmatism and carbonatites, associated mineral systems and the mantle plume connection. Gondwana Research 27: 1181-1216.

Pirajno, F., González-Álvarez I., Border, A., Porter, M. 2017. Mount Weld and Gifford Creek rare elements carbonatites. The Australasian Institute of Mining and Metallurgy Monograph 32: 163-166.

Seltmann, R., Soloviev, S., Shatov, V., Pirajno, F., Naumov, E., Cherkasov, S., 2010. Metallogeny of Siberia: tectonic, geologic and metallogenic settings of selected significant deposits. Australian Journal of Earth Sciences 57: 655-706.

Wingate, M.T.D., Pirajno, F., Morris, P.A., 2004. The Warakurna large igneous province: a new Mesoproterozoic large igneous province in west-central Australia. Geology 32, 105-108. Yang X. Y., Lai, X. D., Pirajno, F. Liu Y. L., Mingxing, L., Sun, W. D., 2017. Genesis of the Bayan Obo Fe-REE-Nb formation in Inner Mongolia, North China Craton: A perspective review. Precambrian Research 288: 39-71.

ABSTRACTS INDEX

ABSTRACT #	TITLE
28	Gold deposits of the Altay-Sayan fold area (Russia) related to Cambrian and Ordovician granitoids A.I. Chernykh, E.V. Vetrov
29	Highly evolved Xianghualing A-type granitic rocks: Insights into multi-stage Sn-polymetallic mineralization in South China Huan Li
30	Genesis of the Mount Pleasant W-Mo-Bi (Fire Tower Zone) and Sn-Zn-Cu-In (North Zone) deposits, NB Canada: examination of contrasting mineralization types possibly linked to redox evolution during episodic devolatilization of an extremely fractionated leucogranite David R. Lentz
31	The contribution of bismuth (tellurium) melts to gold mineralization: a case study from the Baolun gold ore deposit in Hainan Province of South China Deru Xu
32	Geology and Metallogeny of Tungsten and Tin Deposits in China: An Overview Jingwen Mao, Hegen Ouyang, Shiwei Song, Santosh M., Shunda Yuan, Zhenhua Zhou, Wei Zheng, Huan Liu, Yanbo Cheng, Maohong Chen, Junfeng Xiang
33	Trace-element composition of Li-bearing micas from Jianfengling W-Nb-Ta bearing granite, Hunan province, South China: implication of magmatic-hydrothermal process in highly fractionated granite (Under review) Xu Zhao, Jianjun Lu
34	Ore genesis of the giant Shapinggou porphyry Mo deposit: Constraints from the ore-related granite porphyry, fluid inclusion, H-O-S-Pb isotopes and molybdenite Re-Os geochronology Guo-Guang Wang, Pei Ni, Yu Wen, Hui Chen
35	Tin and Tungsten Deposits in Northeast Queensland, Australia: Past, Present, and Prospectivity Yanbo Cheng
36	New granite-related tungsten deposits in northern Jiangxi Province of south China: Ore-forming process and genetic model Shao-Yong Jiang, Ning-Jun Peng, Suo-Fei Xiong, Dao-Hui Pi
37	W-Nb-Pb-Zn mineralization in Early Cretaceous I-type granitoids in the Lizikeng volcanic basin of Jiangxi Province, South China Hui-Min Su, Shao-Yong Jiang, Ming-Yu Cao
38	Age and geochemistry of the ore-bearing granitoids of the porphyry Mo deposits in the Lesser Xing'an–Zhangguangcai Range metallogenic belt, NE China: Petrogenesis and tectonic implications Xiaofei Yu
39	Study on the exploration and resources estimation of rare earth elements, Northern Vietnam Jaeho Lee
40	Implications of Sn isotope fractionation in ores and rocks associated with Sn mineral deposit Ryan Mathur, Wayne Powell
41	Ta-Sn-Nb paragenesis in complex pegmatites: A case study from Presqueira Dyke (Galicia, Nw Spain) Mercedes Fuertes-Fuente, Antonia Cepedal, Ana Roza Llera, Agustín Martin-Izard
42	Skarn Evolution of A Giant Sangdong W-Mo Deposit, South Korea:Genetic Implications Jeonggeuk Kang, Seon-Gyu Choi, Jieun Seo, Sang-Tae Kim, Gyoo-bo Kim, Jonghyun Lee, Chang Seong Kim
43	The geochemistry of the Cretaceous granitoids suites associated with the tungsten polymetallic deposits in the Hwanggangri Province, South Korea Jonghyun Lee, Seon-Gyu Choi, Chang Seong Kim, Jieun Seo
44	Fertile Magma Generation During the Orosirian on the Southern Amazonian Craton: An Example From the Tapajós Mineral Province, Northern Brazil Lucas Villela Cassini, Jean-François Moyen, Caetano Juliani
45	Copper-Gold-Silver Mineralized Tourmaline Breccia Pipes at Soledad, Per Steven Park
46	A new hydrothermal alteration area associated to neogene magmatism in Valle Hermoso District, Central Andes (35° S) Martín Gozalvez, Patricia Sruoga, Cintia Marquetti, Angel Jara, Marta Godeas, Mario Rosas
47	Hydrothermal alteration and mineralization in Santa Clara porphyry cu-mo deposit, Argentina Feliciano Pagnanini, Nora Rubinstein, Eduardo Zappettini, Susana Segal
48	A Mio-Pliocene Li-bearing ignimbrite in the Ratones endorheic basin, Puna Plateau, Salta, Argentina Walter Rojas, Manfred Strecker, Heiko Pingel, Ricardo Alonso
49	Distribution of the hydrothermal alteration in the Morro del Cobre porphyry deposit, Argentina María Verónica Bastías Torres, Nora A. Rubinstein
50	Characterization of the mineralizing fluids of the Quebrada del Diablo Lower West epithermal gold deposit, Argentina María Celeste D'Annunzio, Nora A. Rubinstein
51	Permian magmatism related to Palaeozoic porphyry and epithermal mineralisation in an early Andean metallogenic belt, Cordillera Frontal, Argentina Gregory Poole, Steffen Hagemann, Anthony Kemp, Marco Fiorentini, Eduardo Zappettini, Heejin Jeon, Ian Williams, Nora Rubinstein
52	The Casposo Gold-Silver Deposit: Evidence for Permian, Low Sulfidation Epithermal Mineralization in the Cordillera Frontal, San Juan Province, Argentina Sebastian Grignola, Steffen Hagemann, Ana Fogliata, John Miller, Fred Jourdan, Arianne Ford, Joao O. Santos, Gustavo Sotarello, Irma Belvideri
53	Magma oxidation conditions related to gold and copper mineralization in the Hualgayoc mining district, Peru Martin Viala, Keiko Hattori
54	Alkali Element Mobility Associated With Gold Mineralization In The Pilar De Goiás Greenstone Belt, Central Brazil Rafael Rachid Barbieri Bacha, Catarina Labouré Bemfica Toledo, Adalene Moreira Silva
55	Precambrian conglomerate-hosted gold deposits in Brazil: a review Evandro Klein

ABSTRACT #	TITLE
56	Lithological and structural characterization of the Almas Volcanic Sedimentary Sequence Caio Bussaglia Ress, André Gomes Walczuk, Tiago Angelo Valim, Henrique Araujo Lopes, Felipe Henrique Teles Faria Souza
57	Ediacaran quartz-gold vein mineralization in the Paleoproterozoic basement, «El Tarumán», Pirarajá, Uruguay Felipe Paullier, Graciela Sosa, Klaus Wemmer, Alfons van den Kerkhof, Julio Jorge Spoturno, Pedro Oyhantcabal
58	Paleoproterozoic (2.0 to 1.88 Ga) Paleo-magmatic–hydrothermal Systems in the Tapajonic Magmatic Arcs and the Potential Cu–Mo–Au Porphyry and Au Epithermal Mineralization in the Amazonian Craton, Brazil Caetano Juliani, Carlos Marcello Dias Fernandes, Lena Virgínia Soares Monteiro, Cleyton de Carvalho Carneiro, Carlos Mario Echeverri-Misas, Diego Felipe Gómez-Gutierrez, Lucas Villela Cassini
59	New Petrogenetic Model for Mid-Miocene Adakitic Magmatism in Patagonia and its implications on Porphyry-Copper Deposits Fertility Indicators Gonzalo J. Henriquez, Robert R. Loucks, Marco L. Fiorentini
60	Volcanogenic Massive Sulfide (VMS) Deposits of Turkey Emin Ciftci, Cahit Dönmez, Kurtuluº Günay, Nail Yildrim
61	Structural evolution of the Pataz region, Eastern Andean Cordillera, northern Perú, and implications for the formation of a Carboniferous granitoid-hosted quartz-sulphide-gold vein-system Daniel Wiemer, Steffen G. Hagemann, Nicolas Thébaud, Carlos Villanes
62	The geodynamic setting of the Bushveld Igneous Complex John Paul Hunt
63	An Overview of Flake Graphite – an example from the Lindi Jumbo Graphite Project, Tanzania Michael Cunningham, Andrew Cunningham
64	Probabilistic Mineral Resource Assessment of U.S. Territories of the Caribbean Basin and Adjacent Areas: Progress Report Lukas Zurcher, Floyd Gray, Steve Ludington, Frederic Wilson, Greta Orris, Mark Cocker, Mark Gettings, Tim Hayes
65	The formation of the Sora porphyry Mo-Cu deposit in the Kuznetsk Alatau terrane, Russia: zircon U–Pb age, geochemistry and Sr–Nd isotopic results Anita N. Berzina, Adel P. Berzina, Victor O. Gimon
66	White mica mineral vectors to ore obtained by SWIR spectroscopy mapping in the Altar Porphyry Cu-(Au) deposit, San Juan, Argentina Luciano Matias Bocanegra
67	Distinctive Chemical Characteristics, Geodynamic Settings and Petrogenesis of Gold Ore Forming Arc Magmas Robert Loucks
68	The metallogenic map of Central America and the Caribbean Eduardo O. Zappettini, Natalia Amezcua, Gloria Prieto Rincón, Santiago Muñoz Tapia, Xiomara Cazañas Díaz, David Jara Carolina Maldonado, Fernando Erazo
69	Cartography, petrograpgy, geochemistry of the Maloung mega-quartz vein (West-Cameroun): implication on its economic interest Kevin Igor Azeuda Ndonfack, Jean Pierre Tchouankoue, Josiane Sonmo, Yuling Xie
70	Metallogenic implications of redefining the Upper Paleozoic Magmatism in Argentina: Tectonic Settings and related Deposit Models Eduardo O. Zappettini, Carlos J. Chernicoff
71	Metallogeny of the western part of the Yana-Kolyma gold-bearing belt, Northeast Russia Valery Fridovsky, Gennady Gamyanin, Maxim Kudrin
72	The Portas deposit (Lugo, nw of Spain): an orogenic gold deposit related to Paleozoic ironstones Antonia Cepedal, Mercedes Fuertes-Fuente, Agustín Martin-Izard, Daniel Arias, David Aragón
73	Geochronology of the Sarekoubu gold deposit, southern Altaides, China: Ar-Ar ages of fluid inclusions in vein quartz Jiuhua Xu, Hui Zhang, Xihui Cheng, Chunjing Bian
74	3d modeling of structural controlled ore-shoots in a high sulfidation epithermal deposit. Guanaco, northern Chile Luciano Lopez, Sebastián Jovic, Conrado Permuy Vidal, Diego Guido, Matias Galina
75	Sulphur & oxygen isotope characteritics of Turkish Vms Deposits Emin Ciftci, Yýlmaz Demir, Abdurrahman Lermi, Gülcan Bozkaya, Nurullah Hanilçi
76	Fluid inclusions from active and fossil hydrothermal system in Chile Daniel Moncada
77	Fluid Inclusions Characteritics Of Turkish Vms Deposits Emin Ciftci, Gülcan Bozkaya, Nurullah Hanilçi, Yýlmaz Demir, Abdurrahman Lermi, David Banks
78	Geochemical characteristics of Rare Earth Elements in the Changpingzi Pb-Zn Deposit, Guizhou Province Ziyong Wang
79	Stable isotopes and fluid inclusion data from ba-sr ore deposits of the Neuquén basin, West Argentina Raúl E. de Barrio, Rodrigo I. Escobar, Melisa A. Salvioli, Clemente Recio, Miguel A. Del Blanco, Ricardo O. Etcheverry
80	Characteristics of deep-sea mound ore forming fluids in the Izena Hole site, Okinawa Trough, Japan Thomas Tindell, Nobuhiro Mukae, Junro Ishibashi, Tatsuo Nozaki and Kotaro Yonezu
81	Similarities and differences between fluid inclusions hosted by Colombian emeralds Javier García Toloza, Andrés Felipe Gónzalez Duran
82	Geothermal fluids and mineral scales at Irrupputuncu and Olca, Chile; searching for strategic minerals Daniel Moncada, Gregory De Pascale, Cristian M. Sprohnle, Rodrigo Castagno
83	The U- Pb systematics of hydrothermal hematite: Insights from the IOCG system at Olympic Dam, South Australia Liam Courtney-Davies, Cristiana L. Ciobanu, Simon R. Tapster, Nigel J. Cook, Kathy J. Ehrig, Allen K. Kennedy, Daniel J. Condon, Max R. Verdugo-Ihl, Benjamin S. Wade, Sarah E. Gilbert

ABSTRACT #	TITLE
84	*Re- Os and Ur Pb geochronology of Cu-Mo(-W) porphyry-style, ore-forming processes - an example from the foreland, Variscan orogenic belt, Poland* *Stanislaw Z. Mikulski, Holly J. Stein, Ian S. Stein, Marek Markowiak*
85	*Magma source of the ore-bearing granitoids of the porphyry Mo deposits in the Lesser Xing'an–Zhangguangcai Range metallogenic belt, NE China: in situ zircon Hf-O isotopic constraints* *Xiaofei Yu*
86	*Geology, Ore Mineralogy, and Geochronology of the Akzhal Ore Field, eastern Kazakhstan (Under Review)* *Evgeny Naumov, Yury Kalinin, Konstantin Kovalev, Alexey Travin, Alexander Serdyukov*
87	*New Early Jurassic U-Pb age in Rhyolitic Dykes from the Northeastern Sector of Gastre (Chubut, Argentina) and its possible relation to the mineralization of Los Manantiales district* *Silvia Leonor Lagorio, Alicia Busteros, Diego Silva Nieto, Raúl Giacosa, Claudia Zaffarana, Marcelo Márquez*
88	*Mobility of radionuclides in the Olympic Dam Cu-U-Au-Ag deposit, South Australia* *Mark Rollog, Nigel J. Cook, Paul Guagliardo, Cristiana L. Ciobanu, Kathy J. Ehrig, Matt Kilburn*
89	*Nanoscale study of silician magnetite from IOCG systems: examples from the Olympic Dam District (South Australia)* *Cristiana L. Ciobanu, Max R. Verdugo-Ihl, Ashley Slattery, Nigel J. Cook, Kathy J. Ehrig, Liam Courtney-Davies*
90	*REE-, Sr- Ca arsenate-phosphate-sulphate minerals of the woodhouseite series and their role as hosts for radionuclides* *Nicholas D. Owen, Nigel J. Cook, Mark Rollog, Kathy J. Ehrig, Danielle S Schmandt, Cristiana L. Ciobanu*
91	*Metal bearing nanoparticles in hematite* *Max R. Verdugo-Ihl, Cristiana L. Ciobanu, Nigel J. Cook, Ashley Slattery, Kathy J. Ehrig, Liam Courtney-Davies*
92	*Geological setting of BIF ores, Middleback Ranges, South Australia* *William Keyser, Cristiana L. Ciobanu, Nigel J. Cook, Liam Courtney-Davies, Holly Feltus, Geoff Johnson, Allen Kennedy, Kathy Ehrig*
93	*Nano - to micron-particulate gold hosted by magnetite from the Beiya giant gold deposit, SW China: a product of gold scavenging by bismuth melts* *Xiaoming Sun*
94	*New constrains on the genesis of the Dabaoshan polymetallic deposit, South China: Textural, trace element, and Re–Os isotopic analyses of sulfides* *Lei Wang*
95	*The copper arsenides of the Picún Leufú area, province of Neuquén, Argentina* *Milka K. de Brodtkorb, Juan Carlos Danieli*
96	*Mineralogical characterization of a fluorite-barite-lead deposit in Derbyshire, United Kingdom* *Alexandra Gomez Escobar, Reimar Seltmann, Alla Dolgopolova*
97	*Ree-Th enrichments of the Isparta Triangle, Southwestern Turkey* *M. Sezai Kirikoğlu, Emin Ciftci, Murat Budakoğlu, Ali Tuğcan Ünlüer, Zeynep Döner, Mert Terzi, Ilgýn Kursun, Hüseyin Kocatürk*
98	*HAADF-STEM imaging of small defects in natural tungsten trioxide, WO3 Wenyuan Liu, Cristiana L. Ciobanu, Nigel J. Cook, Ashley Slattery*
99	*Uranium transport from mesoproterozoic bedrock granite induced by tectonism: the Blackbush Uranium deposit, South Australia* *Urs Domnick, Nigel J. Cook, Cristiana L. Ciobanu, Benjamin P. Wade, Russel Bluck, Allen Kennedy*
100	*Skarn replacing igneous rocks* *Zhaoshan Chang, Larry Meinert, David Lawrence, Stephanie Mrozek, Lejun Zhang*
101	*Stratiform-like Cu deposits in South China: Sedex or Skarn?* *Pei Ni, Guo-Guang Wang, Yi-Tao Cai, Xiao-Ting Zhu, Hui Chen, Bai-Sheng Zhang*
102	*Optimizing skarn classification using geochemistry and machine learning algorithms: an example from the Antamina deposit, Peru* *Stephanie Mrozek, Christina Buelow, Zhaoshan Chang, Alberto Paz*
103	*Critical constraints on localization of large skarn orebodies: Examples from the Tongling-Anqing district, China* *Liangming Liu*
104	*Skarn Deposit- Using mineral zonation in exploration* *Lawrence Meinert*
105	*Physical and Chemical Growth Patterns of a Distal Pb-Zn Skarn, Madan, Bulgaria* *Aaron Hantsche, Kalin Kouzmanov, Stan Sizaret, Georgi Milenkov, Simone Vezzoni, Andrea Dini, Rossitsa Vassileva*
106	*Tectonic setting of intrusions associated with Fe and Cu skarn deposits in the Qiman Tagh area of Qinghai Province, Eastern Kunlun Orogen, China Zhicheng Lü*
107	*A review of scheelite-bearing skarns in the Eastern Sierras Pampeanas: mining records and mineralogical data of Los Guindos mining group, Pampa de Olaen district, Córdoba, Argentina* *María José Espeche, Raúl Lira*
108	*The Voicey's Bay Deposit, Canada: How Twenty-Five Years of Research Redefined Genetic and Exploration Models for Magmatic Ni-Cu-Co Sulfide Deposits* *Andrew Kerr, Anthonly J. Naldrett*
109	*Sulfide inclusion as a key to understand origin of Ni-Cu-PGE deposits* *Irina Tretiakova, Marco Fiorentini, Vlad Malkovets, Laure Martina*
110	*Unusual Ni-sulfide deposits in the Carajás IOCG mineral system: magmatic or hydrothermal?* *Emilia Schutesky Della Giustina, Claudinei Gouveia de Oliveira, Martin Whitehouse, Victor Garcia, Sergio Huhn*
111	*The Ni-Cu-PGE-bearing Mangabal Complex: an example of sulfide concentration caused by Metamorphism* *Cláudia Tharis Augustin, Maria Emília Schutesky Della Giustina*
112	*Chromium exploration targeted for Bophi Vum area, northwestern Myanmar* *Chulho Heo*
113	*The anatomy of a modern submarine arc volcano: magmatic-hydrothermal activity and the transport of metals* *Cornel E. J. de Ronde*

ABSTRACT #	TITLE
114	Apatite (U-Th)/He Thermochronology in the Central Andes (31°30'S), Main Cordillera San Juan, Argentina: Implications for porphyry type Cu (Au) mineralization Laura Maydagán, Massimiliano Zattin, Marta Franchini
115	Gold Porphyry Gold Systems: distribution and composition of gold at the Biely Vrch deposit, Slovakia Peter Kodera
116	Seeking the mantle as a source for precious metals in magmatic-hydrothermal deposits José María González-Jiménez
117	Trace Elements Deportment across Porphyry Dike Generations in the Bingham Canyon Porphyry Cu-Mo-Au Deposit Maurice Brodbeck, P. Redmond, B. S. Kamber, S. McClenaghan
118	Defining IOCG signatures through compositional data analysis: A case study of lithogeochemical zoning at Olympic Dam, South Australia Marija Dmitrijeva
119	High resolution X-ray Computed Tomography Studies of Gold–Cu Sulfide Relationships in the Grasberg Porphyry Cu-Au Deposit, Papua, IndonesiaJ. Richard Kyle, Kylie A. Wright, Richard A. Ketcham, Nathan R. Miller
120	An integral model for the formation of magnetite-(apatite) deposits Fernando Tornos, John M. Hanchar, Francisco Velasco
121	Characterization of Sericitic Alteration at the Taca Taca Bajo Porphyry Cu deposit, Argentina Sebastian Benavides
122	Cu-bearing Vein and Alteration in Granitic Rocks in Tsogttsetsii area, Mongolia: Potential for Porphyry-Cu Mineralization In Joon Kim, Sanggun No
123	The Lindero porphyry gold deposit, Northwestern ArgentinaJorge Kesting, K. Brock Riedell, Eric N. Chapman, David Volkert
124	The Boron Isotopic Geochemistry of Hydrothermal Tourmaline from the IOCG Occurrences of the Great Bear Magmatic Zone, NWT, Canada Colter Kelly, William Davis, Eric Potter, Louise Corriveau
125	Pb-isotope and trace elements analysis by LA-Q-ICPMS of galena from Argentinian epithermal deposits: a preliminary analysis Laura Maydagán, Christopher McFarlane, David Lentz, Verónica Bouhier, Pablo Caffe, Ana Laura Rainoldi, Josefina Pons, María Lis Fernández, Marta Franchini, Geraldine Luna
126	Mafic Magma Signature from Co-Ni-Cu Sulfide on Porphyry Cu-Au Mineralization at the Grasberg Deposit, Papua, Indonesia Kotaro Yonezu, Katsuhito Terashima, Thomas Tindell, Benny Bensaman, Mega Fatimah Rosana
127	The Zinnwald Cinovec Sn-Li deposit: Constraints for metal recovery Alla Dolgopolova, Reimar Seltmann, Robin Armstrong, Chris Stanley, Jens Andersen, Gavyn Rollinson, Beth Simons, Mirko Martin, Pavel Reichl, Vojtek Sesulka, Fernando Noronha, Violeta Ramos, Chris Broadbent, Axel Müller, Vitaly Shatov
128	Data mining from critical minerals: Germanium, gallium, and indium Jane M. Hammarstrom, Alan Koenig, Robert R. Seal, Erin Marsh
129	Key role in the formation of lithium-rich brine deposits: A constraints from lithium isotope ratios Daisuke Araoka
130	The world-class Strange Lake REE deposits, Canada: Radiogenic isotope evidence for the origin of magmas and metals Andrew Kerr
131	Lithium and strontium isotope composition of typical salar deposits from the Salar de Pozuelos, Argentine Puna: Implication for the source of lithium Simone Kasemann, Anette Meixner, Ricardo Alonso, Friedrich Lucassen
132	The Lithium Triangle of the Central Andes: A view from Lithium concentrations and isotopic composition of potential source rocks Friedich Lucassen, Anette Meixner, Raul Becchio, Carisa Sarchi, Simone Kasemenn
133	Evaluation of critical metal composition of geological samples using laser ablation Yoshiaki Kon, Takaomi D. Yokoyama
134	Do Geothermal Systems Play a Role in Lithium Brine Enrichment in Playa Environments? Caterine Hickson, Mark Coolbaugh, Beatrice Coira
135	Geochemical characteristics of ion-adsorption REE ores in Asia: Implications for exploration Kenso Sanematsu, Yoshiaki Kon
136	Multi stage alteration and multiple fluid inputs for the Paleoproterozoic Juomasuo, Hangaslampi and Haarakumpu Cobalt (-Au-REE) deposits of the Kuusamo Schist Belt, Finland Walter Witt
137	Cobalt: perspectives on future resource supply Richard Herrington, The CoG3 Research Team
138	Cobalt-bearing nickel deposits: Sulfide deposits versus lateritic deposits Kenzo Sanematsu, Yoshiaki Kon, Daisuke Araoka, Takaomi D. Yokoyama
139	Petrology and geometallurgy of the Tabuaço scheelite deposit, Portugal Liene Spruzeniece, Beth Simons, Jens C Andersen, Gavyn K Rollinson, Violeta Ramos, Fernando Noronha
140	A high-tech critical metals and trace elements in selected ore deposits in Poland – preliminary data Stanislaw Z. Mikulski, Katarzyna Sad³owska, Andrzej Chmielewski, Rafa³ Ma³ek, S³awomir Oszczepalski
141	Importance of bedrock for concentration of Sc in a nickel laterite deposit, Central Dinagat Island, Philippines Tomiyuki Yamada
142	Mineralogical and geochemical constraints of the Zudong regolith-hosted HREE deposit in South China Martin Yan Hei Li
143	Intra-Granular Distribution of Energy Critical Elements in Sulphide Minerals: Resolving Paragenesis and Resource Potential Through Laser Ablation ICP-MS Sean H. McClenaghan
144	Cobalt mineralization in Argentina Martín R. Gozalvez, Lidia I. Korzeniewski, Samuel Gregorat
145	New remote Sensing Tools for the Exploration and Mining Lifecycle Dan Taranik

ABSTRACT #	TITLE
146	Hydrothermal alteration mapping using ASTER data in the Iglesia department, San Juan province, Argentina Diego Azcurra, Fernando Ganem, Dolores Álvarez, Diego Rodríguez, Silvia Chávez, Leda Moser, Javier Benítez
147	Aeromagnetic data interpretation for mining exploration targets detection in San Juan Province, Argentina Dolores Alvarez, Diego Rodriguez, Fernando Ganem, Diego Azcurra, Leda Moser, Javier Peroni
148	Evaluation of a protocol for rapid characterization of the magnetic signature of commercial UAV multicopters as platforms for scientific magnetic surveys Ruy Sanz, Francisco Javier de Frutos, Miguel Angel Rivero, Sergio Fernández Romero, Maria Parrondo, Eduardo De Diego, Francisco Ocaña, Emanuel Ramírez-Catapano, Enrico Fini, Javier Isabel Hernández, Aitor Ibarra Ibaibarriaga, David Gonzalez, María Ramírez-Nicolás, Francisco Rios, Rolf Kilian, Marina Díaz Michelena
149	Remote Sensing For Geology In The XXI Century Valery G. Bondur, Sergey Cherkasov
150	Porphyry exploration supported by airborne hyperspectral in the Peruvian Andes Alexander Farrar
151	Express interpretation of multi-level unmanned aerial magnetic survey. Case study Sergey Cherkasov, Dmitry Goglev, Dmitry Kapshtan
152	Hidrothermal alteration mapping with Aster in Pancho Arias, NW Salta, Argentina Silvia Castro Godoy
153	The Current Situation and Futures Perspectives of the Fluid Evolution in the Lagoa Real Uranium Province, Brazil Tiago H. DeFerreira, Ariela C. Diniz, Lucilia A. Ramos de Oliveira, Lucas E. D. Amorim, Francisco J. Rios, Kazuo Fuzikawa
154	Integrated Geochronological, Geophysical and Isotopic Investigation into the Patterson Lake Corridor of the Southwestern Athabasca Basin, Canada Jeremy W. Powell, Victoria Tschirhart, Eric G. Potter, Colin Card, Dinu I. Pana, Kenneth Wheatley, Cameron MacKay
155	Geological and geochemical characteristics of the Jiling Na-metasomatism uranium deposit, Gansu, China Xiao-Dong Liu, Wen-Heng Liu, Jia-Yong Pan
156	Uranium in Argentina: Deposits, Resources and Nuclear Supply Luis López
	The ultimate origin of uranium deposits Michel Cuney
157	Mantle -derives noble gases in ore-forming fluids of the uranium deposits in south China Rui-Zhong Hu, Jin-Cheng Luo, You-Wei Chen, Xian-Wu Bi
158	The origin of pyrite from the Kiggavik Uranium Deposit, Nunavut, Canada Brandi M. Shabaga, Mostafa Fayek, David Quirt, Patrick Ledru
159	Ivana Uranium Vanadium Deposit, a New Resource for Argentina Guillermo Pensado, Ariel Testi, Jorge Berizzo, Jon Thorson

ABSTRACT #	TITLE
160	Reducing Mechanisms in the Precipitation of Unconformity-related Uranium DepositsÿInsights from Fluid Flow Modeling Jianwen Yang
161	Characterization of rare earth minerals in Lagoa Real Uranium Province, Bahia (Brazil) Lucas E. D. Amorim, Lucilia A. R. Oliveira, Ariela Costa Diniz, Tiago De Ferreira, Camila Marques dos Santos, Francisco Javier Rios, Mônica Elizetti de Freitas, Evando Carele de Matos
162	Titanite as an important petrologic indicator from Gameleira I U-Deposit (Anomaly 35) Lagoa Real Uranium Province (LRUP), Bahia, Brazil Camila Marques dos Santos, Francisco Javier Rios, Lucas E. Dias Amorim, Helena Leonhardt Palmieri, Evando Carele de Matos
163	U, Th and rare earth elements mobility in titanite from magmatic/metamorphic paragenesis in the Lagoa Real U-Province, Bahia, Brazil Nilo H. B. Lopes, Lucilia A. Ramos de Oliveira, Francisco J. Rios, Lucas E. D. Amorim, Evando C. de Matos
164	Base metal mineralization in the Dairi Zn-Pb±Ag deposit, North Sumatra, Indonesia Tomy Alvin Rivai
165	Cobalt in sediment-hosted ore systems Richard Herrington, Steve Roberts
166	The dsitribution and partitioning of silver in the Banana Zone sediment-hosted Cu-Ag deposit in the Ghanzi-Chobe Cu Belt portion of the Kalahari Cu Belt: Constraints from LA-ICP-MS study Tebogo Kelepile, Thierry Bineli Betsi, Fulvio Franchi, Elisha Shemang
167	Volcanic Shale Hosted Massive Sulphides in the Bathurst Mining Camp, Canada: A Sedimentary Perspective A. A. Zhaanbaeva
168	Comparative geology and geochemistry of sedimentary rock-hosted gold deposits of Youjiang basin, SW China and Chauvai ore field, SW Kyrgyzstan (Pending) A. A. Zhaanbaeva
169	The Upper Peninsula Copper Province, Michigan: Geologic observations and genetic implications José Perelló, Richard H. Sillitoe
170	Role of thermochemical and biogenic sulfate reduction in the formation of the El Porvenir sediment-hosted stratiform copper deposit, Neuquén, Argentina Ana Laura Rainoldi, Marta Franchini, Adrian j. Boyce, Adolfo Giusiano, Nora Cesaretti, María Josefina Pons, Francisco Javier Ríos
171	Portable X-ray Fluorescence Spectroscopy as exploration tool and its application on core samples in the Murray Brook Volcanogenic Massive Sulphide Deposit, Bathurst Mining Camp, New Brunswick, Canada Maiara Toniazzo Braga, David R. Lentz
172	Hydrocarbons linked to stratiform sediment hosted lead, zinc and copper mineralization in Lajas Formation, Neuquén Basin Argentina Maria Josefina Pons, Ana Laura Rainoldi, Marta Franchini, Adolfo Giusiano
173	Vanadium mineralization at Los Chihuidos sediment-hosted stratiform Cu deposit Ana Laura Rainoldi, Marta Franchini, Daniel Beaufort, Patricia Patrier, Adolfo Giusiano, María Josefina Pons, Nora Cesaretti

ABSTRACT #	TITLE
174	*Metallogenic Potential of Argentina* *Eduardo Zappettini (Geological and Mining Survey of Argentina - President of IAGOD)*
175	*Singularity of Lithosphere Phase Transition and Origination of Porphyry Mineralization* *Qiuming Cheng (China University of Geosciences - President of the International Union of Geological Sciences – IUGS)*
176	*National Mineral Exploration Strategic Action Plan-Application of Metallogenic Theory and Exploration in China* *Li Jinfa (Deputy President, China Geological Survey)*
177	*Mineral exploration models from simple fiction to complex reality* *Reimar Seltmann (Natural History Museum, London - IAGOD Distinguished Lecturer)*
178	*Copper deposits in Brazil: geological setting, process and evolution of mineral systems* *Lena Virginia Soares Monteiro (SEG Regional VP Lecturer)*
179	*Near-surface features of the epithermal environment: Formation, characteristics and contrasting implications for exploration* *Jeffrey Hedenquist (University of Ottawa)*
180	*Paleozoic porphyry Cu (Mo, Au) systems from the Urals* *Olga Plotinskaya*
181	*Why detailed mineralogy is important: understanding evolution of the Olympic Dam iron-oxide copper-gold system, South Australia* *Nigel Cook (University of Adelaide)*
182	*Iron Oxide Copper-Gold (IOCG) Systems: examination of end-member models, physicochemical processes, and possible modern analogues* *David Lentz (University of New Brunswick)*
183	*Microbiology and the formation of ore deposits* *Fernando Tornos*
184	*Rare Earth mineral systems associated with alkaline Intrusions and carbonatites* *Franco Pirajno*

AUTHORS INDEX